NASA CP-2010

ERDA/NASA-1022/76/10

# Terrestrial Photovoltaic Measurements - II

A workshop held at
Baton Rouge, Louisiana
November 10-12, 1976


NASA CP-2010

ERDA/NASA-1022/76/10

Distribution Category UC-63

# Terrestrial Photovoltaic Measurements - II

A workshop sponsored by
Energy Research and
Development Administration

and organized by
NASA Lewis Research Center

and held at Baton Rouge, Louisiana
November 10-12, 1976

For sale by the National Technical Information Service
Springfield, Virginia 22161
Price: $11.00

## FOREWORD

The second ERDA/NASA Workshop on Terrestrial Photovoltaic Measurement Procedures was held in Baton Rouge, Louisiana, November 10-12, 1976. The organization of this meeting was similar to that of the first Workshop, which was held at the NASA Lewis Research Center March 19-21, 1975. The purpose and agenda of the second Workshop were designed to accommodate the accumulated experience gained in the interim and to define and explore the additional measurement needs of the photovoltaic community.

The Workshop was structured around three topics that were considered to be of major import to the overall subject of terrestrial photovoltaic measurement procedures. A full day was devoted to each of the topics:

- Terrestrial Solar Irradiance
- Solar Simulation and Reference Cell Calibration
- Cell and Array Measurement Procedures

In turn, these major topic areas were further explored by working groups - each organized to discuss subtopics of the primary theme.

In the mornings, short papers were presented at a general session attended by all participants. In the afternoons, the working groups convened to discuss various subtopics related to the general subject matter of the day. At the conclusion of the deliberations of the working groups, the general session was once again assembled to hear reports of the working group sessions and to further consider related matters through a question and answer period.

The papers presented and the reports of the working groups are included in this Proceedings. In order to expedite the issuance of the Proceedings, the papers included are precisely as submitted by the authors. A measurement Procedures Manual will be prepared based on the findings of the Workshop and will be issued by mid 1977.

The Workshop was conducted under the general chairmanship of Henry W. Brandhorst (Head, Photovoltaic Research and Technology Section, NASA-Lewis Research Center).

CONTENTS

## CELL AND ARRAY MEASUREMENT PROCEDURES

### Eugene L. Ralph, Chairman

# MONITORING SOLAR RADIATION: THE ERDA PROGRAM

FREDERICK A. KOOMANOFF AND MICHAEL R. RICHES

Energy Research and Development Administration

Division of Solar Energy

20 Massachusetts Avenue, NW.

Washington, D.C. 20545

## ABSTRACT

An overview of the Energy Research and Development Administration planned insolation data network is described. The design of this network is predicated on an analysis and definition of user requirements. Research and analysis projects covering data collection, forecasting and extrapolation are presented.

## INTRODUCTION

Prior to monitoring the solar resource, a series of fundamental questions must be considered:

- What meterological parameters must be measured?
- What must be the data quality (where quality includes accuracy, precision, frequency and format)?
- What geographic network is required (including instrumentation)?

Answers to these questions are seriously effected by definition of user and the user is the forcing function, as it were, as to how these questions should be answered.

## CLASSIFICATION OF USERS

In a preliminary analysis, two solar radiation data user categories were considered:

1. Classification according to the operational roles of users in the solar energy community.

2. Classification according to the types of data, analyses, and output information required by users.

The first mode, classification of users by operational roles, relates uses and users, corresponding to the three solar energy applications (specific technology requirements such as photovoltaic and biomass, energy generation-network requirements and (individual) independent unit application). An example of such a classification is thermal users by temperature range and application. This was proposed by Hoffman and Rapp of the American Technology University in Texas. It is a unique method to classify users in relation to the temperature range required for the solar application. This approach might be better labeled technological matching and is shown on Exhibit 1. The optical technology required to produce the required temperature indicates the solar radiation measurement needed.

The second mode of classifying users appears to have the attributes of simplicity and direct linkage to resource data needs. This classification consists of two users categories: forecasters and scientists. Users of solar radiation data from a routine network are defined as forecasters; the users of the data from a research network, as scientists. The users of a routine network are assumed to be interested primarily in data as input parameters to problems of design, reliability and performance of solar systems. The users of research network are interested primarily in obtaining a better understanding of the physical and biological laws associated with solar climatology.

Although one must recognize that it is impossible to be all things to all men, it is possible, however, to design an insolation data network which collects, records and archives data to that degree which attempts to supply information to the forecaster and researcher and also considers the operational roles of user organizations in the solar energy community.

## DATA NETWORKS

The National Oceanic and Atmospheric Administration (NOAA) is working closely with ERDA in expanding the insolation data available. NOAA's National Weather Service (NWS), plus cooperative agencies, operates approximately 60 sites which record global solar radiation

data. Only five sites presently measure direct, or what is termed normal incident radiation. Two-thirds of the stations record daily global values only, the remainder record hourly values. Cooperative sites are operated by other Federal agencies, the states, universities and a few private industries. Recording and measuring equipment of these cooperatives is calibrated and checked to assure compatibility with NWS network data.

An improved NWS network will soon be commissioned. The 35-site network will have new pyranometers and recorder integrators. Ten of the 35 sites will measure diffuse radiation as well a global radiation (direct plus diffuse). Additionally, funds have been transferred to NOAA's calibration center in Boulder, Colorado, to equip the entire 35-station network with pyrheliometers. These sites are at NWS stations so complete weather observations will be available. The sites are shown in Exhibit 2. Thus the ERDA-NOAA basic solar radiation network will report global, diffuse, and direct solar irradiance. To this network, ERDA is planning to add from four to six research sites. These insolation research sites will be specialized facilities and will be equipped to accurately measure in excess of 45 meteorological and atmospheric parameters. They also may serve as regional calibration and training centers for solar energy related meteorological measurements.

The future network concept is shown graphically on Exhibit 3. This network will consist of a small number of sites with limited geographical coverage but highly sophisticated measuring capabilities such as shown in Table 1.

Table 1. Possible Meteorological Variables to be measured at the Solar Energy Meteorological Research Sites.

RADIATION

- o Direct Irradiance
- o Global Irradiance
- o Diffuse Irradiance
- o Spectral Composition
  - Direct
  - Global
  - Diffuse
- o Ultra Violet Irradiance
- o Infrared Irradiance
- o Distribution of Diffuse over sky
- o Circumsolar
- o Turbidity
- o Polarization
- o Global Radiation at various angles
- o Reflected Irradiance
- o Minutes of Sunshine

OTHER ATMOSPHERIC VARIABLES

- o Tower Wind Velocities
- o Tower Temperatures
- o Tower Dew Points
- o Precipitation
- o Cloud cover and distribution relative to the sun
- o Pressure
- o Water Vapor
- o Total Ozone
- o Dust fall
- o Gaseous pollutants
- o Current Weather

The basic 35-station network provides hourly global and direct insolation data and all standard weather data. This then will be further augmented by the cooperative network where, as a minimum, daily global insolation data will be available on a continuous basis. We plan to include the insolation and other meteorological data recorded by the present Canadian network, thus supplying the northern United States with additional data.

The University of Alabama at Huntsville is compiling an inventory of solar radiation monitoring sites in the United States. From this inventory, data sets of special interest to the solar energy community will be archived. Additionally, selected data sets will be analyzed to fill short fall by climatic zone.

Another interesting data set will be the solar and meteorological data measured at the approximately 100 solar heating and cooling demonstration projects. This one to two year data set will take solar radiation data at the angle and the aperature of the collector. Ambient temperature, relative humidity and wind velocity will also be measured. These mini-weather stations will aid in generating high quality, additional data sets for both the forecaster and the scientist.

In addition to the network of fixed stations, a number of mobile instrument sets will be acquired to permit data collection at specific locations as required. The device for photovoltaic applications measures direct and diffuse in seven wavelength regions plus gives the distribution of diffuse over the sky. The sensor is described in detail by Kleckner et. al.

However, we must not only look at the future but we must look at the past and the present in developing a sound data base from which to proceed. Accordingly, a major project is underway to rehabilitate hourly solar radiation data. All hourly solar radiation at 26 sites is being rehabilitated, based upon engineering analysis and the development of regression models to fill in insolation data which is missing. The hourly insolation data will be integrated with other meteorological data onto a single (standardized format) magnetic tape. This is shown in Exhibit 4. Accordingly, 24 years of a station's historical hourly insolation data, as well as corresponding standard meteorological data,

will be on magnetic tape compatible for normal computer proceeding. All future data will be archived in the SOLMET format. Additionally, 25 sites with daily insolation totals are being rehabilitated. These daily insolation totals will be combined in a meteorological summary and archived in a special format similar to SOLMET. These projects are under the direction of Dr. Lester Machta and Mr. Frank Quinlan of NOAA.

To insure the quality of the new isolation data so future reanalysis of it is not necessary, NOAA and ERDA have established a master calibration center at Boulder, Colorado. This center, under the excellent direction of Mr. Edwin C. Flowers, will act as a master calibration and data quality control center. Current projects include the testing of pyranometers in inclined positions and development of the future pyrheliometer network.

RESEARCH PROGRAM

To meet future needs and clarify the present ones, a set of research projects will be started in FY 1977. Several special data sets will be developed. These will include analyses of the solar radiation differences in a urban-rural area, in a coastal-inland region, and in a mountain-valley system. Also, a unique data set relating aerosol and cloud effects on solar radiation data will be compiled using a special mobile sensor package developed by Drs. Vernon Derr and Gordon Lerfald of NOAA.

As solar energy applications grow, solar radiation forecasts will be required as a part of the standard meteorological forecast. We will begin examining some possible techniques to provide forecasts of the principle solar radiation variables. Both "now" casting and long-range forecast techniques will be considered.

The special data sets and the forecast techniques research will help define user solar radiation data requirements. Thus, these research projects will feed into our network development as well as provide needed basic data.

Our progam plan has as its major goal the development of a continuing network for collection of solar and other meteorological data; the processing, recording and archiving with effective dissemination those data required by the user (no matter how the user is classified); and, through selected goal directed research and analysis, filling in some of the gaps in our knowledge of insolation and other key meteorological relationships.

REFERENCES:

Hoffman, A.A.J., and Rapp, D., "A Classification of Solar Energy Techniques and Uses by Temperature Range", (Draft Paper, March 31, 1976).

Machta, L., "Monitoring Solar Radiation for Solar Energy." To be Published by WMO-UNESCO. Jefcoat, I.A., "Impact of Air Quality Degradation on Solar Insolation, Solar Energy Efficiency and Costs," prepared for the Industrial Environmental Research Laboratory, Environmental Protection Agency, January, 1976.

Report and Recommendations of Solar Energy Data Workshop, Prepared for the National Science Foundation Research Applied to National Needs (RANN), by the National Oceanic and Atmospheric Administration, Environmental Research Laboratories, Air Resource Laboratories, Silver Spring, Md., NSF-RA-N-74-062 (September 1974).

Development of Proposed Standards for Testing Solar Collectors and Thermal Storage Devices, prepared for the Energy Research and Development Administration, by the U.S. Department of Commerce/National Bureau of Standards (NBS Technical Note 899), issued February 1976.

Terrestrial Photovoltaic Measurements, Workshop Proceedings, organized by Lewis Research Center, National Aeronautics and

Space Administration sponsored by Energy Research and Development Administration, March 19-21, 1975, in Cleveland, Ohio.

Solar Data Verification Project, SAI-76-176-WA, prepared by Science Applications, Inc.

A preliminary Investigation of User Requirements for Solar Radiation Data, prepared by Battelle Columbus Laboratories for the Energy Research and Development Administration (a working paper).

Kleckner, E.W., Smith, L.L., and Hoch, R.J. The Design and Construction of a Multipurpose Instrument for Solar Radiation Measurements. Proceedings of the Society of Photo-optical Instrument Engineers, Vol. 68, 1975.

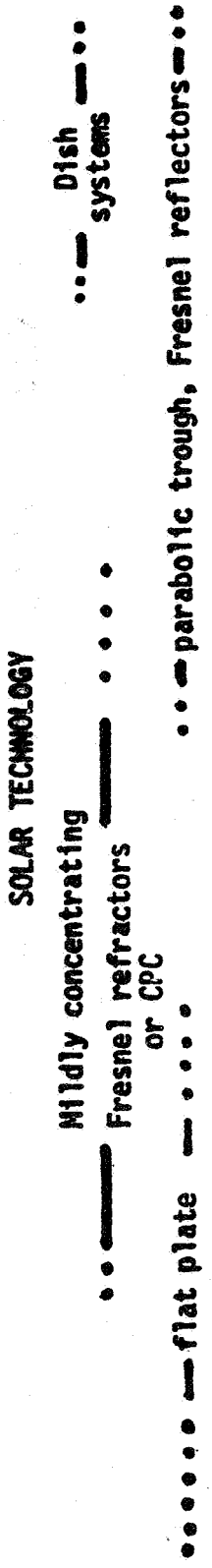


| Temperature °F | APPLICATIONS |
|---|---|
| 500 - | |
| // | Production of electrical power |
| 400 - | Process steam |
| | - Evaporation in various processes |
| | - Digestion in paper pulp, kraft |
| | - Drying diatomaceous earth |
| | - Drying fishmeal, lumber |
| 300 - | Alumina via Bayer's process |
| | - Drying farm products; canning of food |
| | - Evaporation in sugar refining |
| | - Fresh water by distillation |
| | - Drying of cement slabs |
| | - Most food drying |
| 200 - | Space cooling by absorption refrigeration (lower limit) |
| | - Food drying (lower limit) |
| | - Space heating |
| | - Animal husbandry |
| | - Greenhouses (lower limit) |
| | - Mushroom growing |
| 100 - | Hot baths |
| | - Swimming pools, biodegradation, fermentation |
| | - Fish hatching, fish farming |

Required temperatures for various applications

EXHIBIT 1

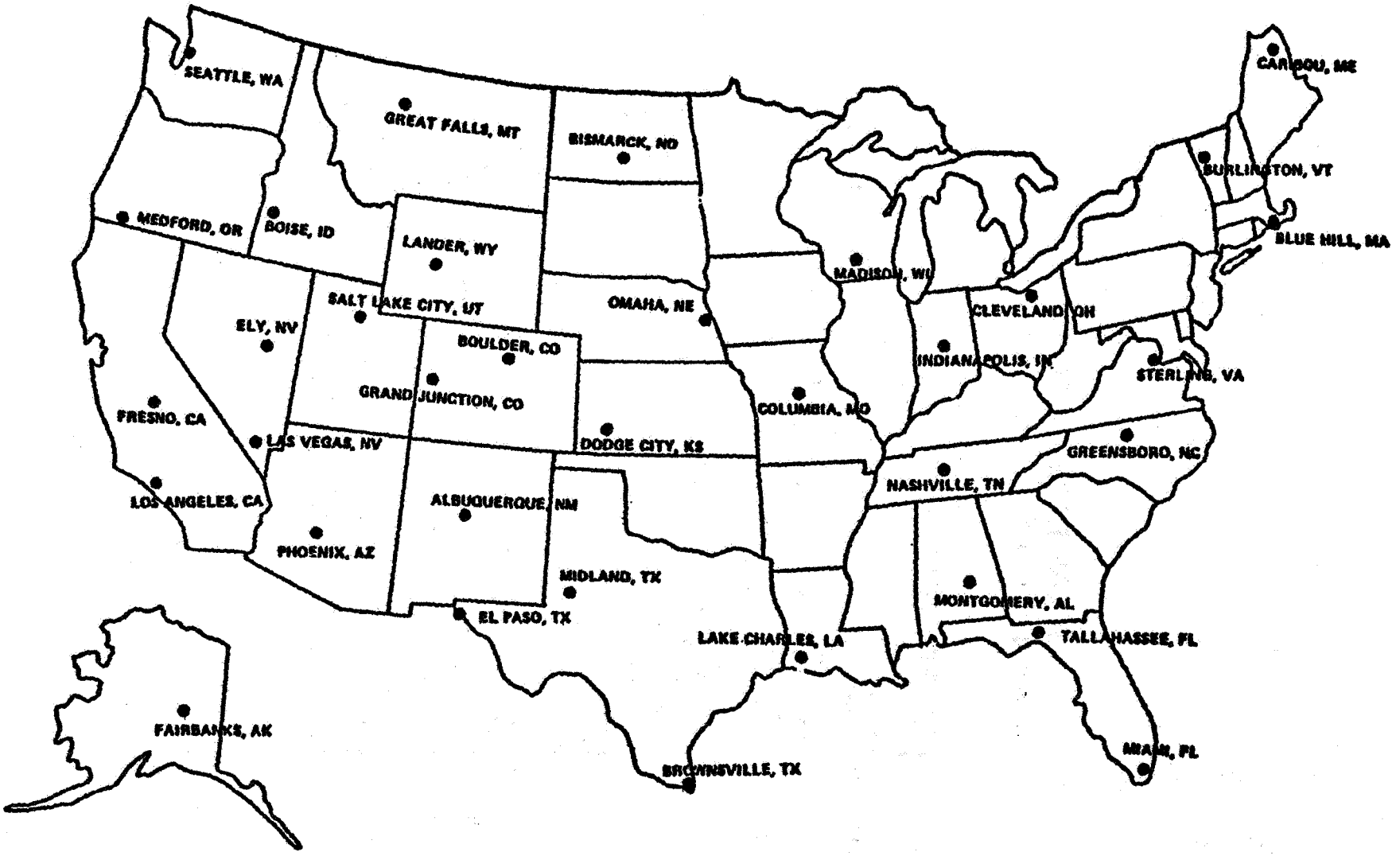


# NEW NOAA NATIONAL WEATHER SERVICE NETWORK

EXHIBIT 2

## SOLAR RADIATION
### MONITORING SYSTEM CONCEPT

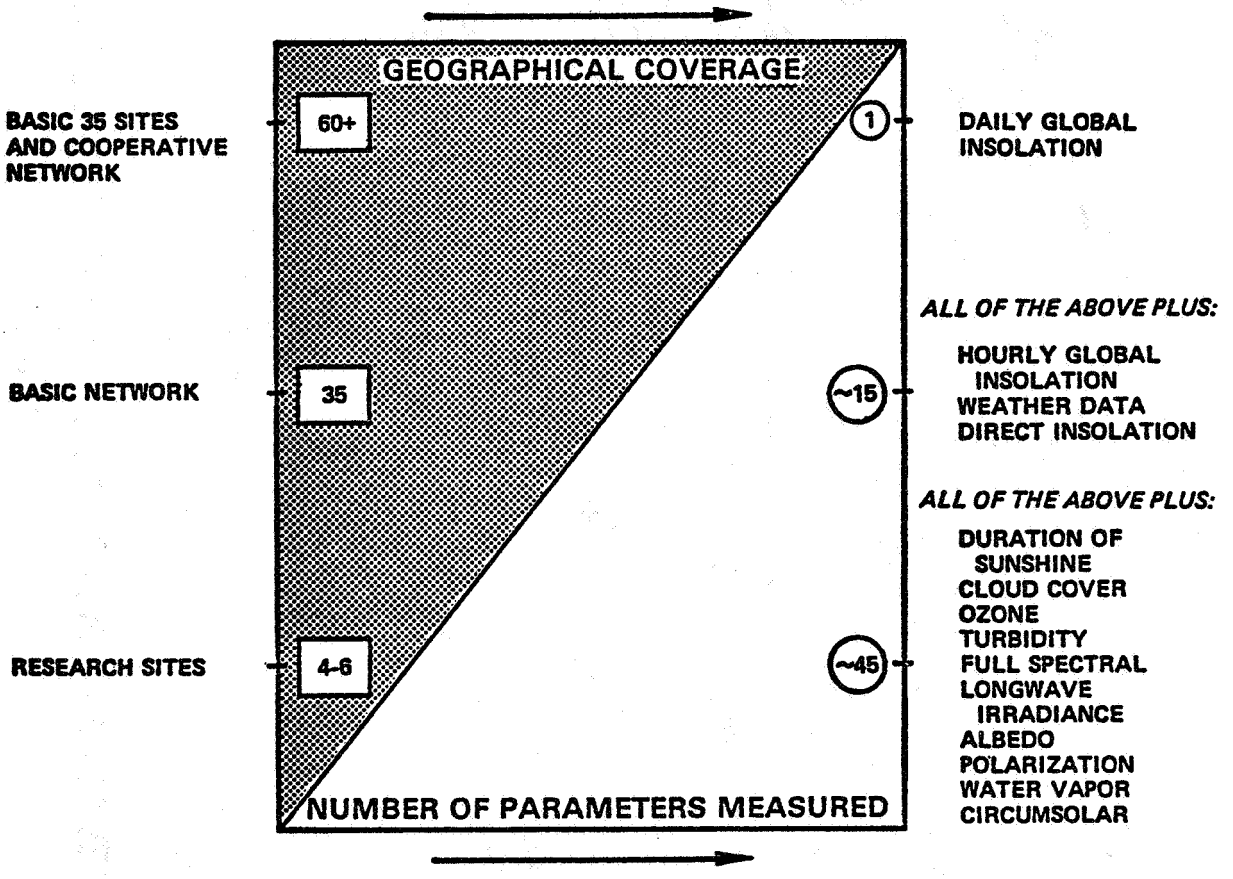


EXHIBIT 3

# SOLMET

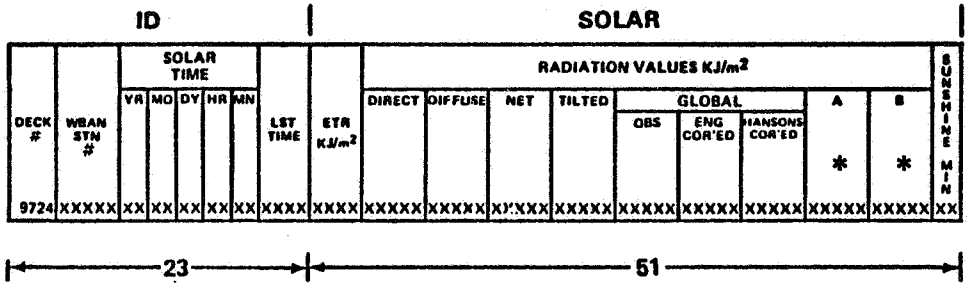


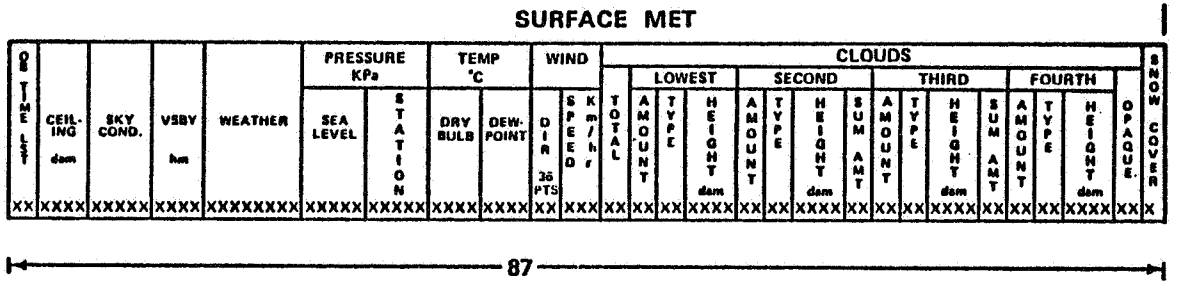


161 BYTES/RECORD, BLOCKED 24 (3864 BYTES)

14 yrs. per reel at 800 bpi
24 yrs. per reel at 1600 bpi

FORMAT IS FORTRAN COMPATIBLE – NO OVERPUNCHES
– MISSINGS CODED – "9's"

ESTIMATED RADIATION VALUES INDICATED BY ADDING 80,000
ESTIMATION FROM SUNSHINE MODEL INDICATED BY ADDING 60,000
ESTIMATION FROM CLOUD MODEL INDICATED BY ADDING 40,000

* 'A' AND 'B' ARE SUPPLEMENTAL FIELDS FOR ADDITIONAL RADIATION MEASUREMENTS; I.E., ULTRAVIOLET, TILTED, ETC.

| LEGEND | |
|---|---|
| YR | YEAR |
| MO | MONTH |
| DY | DAY |
| HR | HOUR |
| MN | MINUTE |
| LST | LOCAL STANDARD TIME |
| ETR | EXTRATERRESTRIAL RADIATION |
| $KJ/m^2$ | KILOJOULES PER SQUARE METER |
| OBS | OBSERVED |
| ENG COR'ED | ENGINEER CORRECTED |
| HANSONS COR'ED | HANSONS CORRECTED |
| MIN | MINUTES |
| dam | DEKAMETERS ($M \times 10^1$) |
| hm | HECTOMETERS ($M \times 10^2$) |
| KPa | KILOPASCALS (NEWTONS PER SQUARE METER) |
| °C | DEGREES CELSIUS |
| DIR | DIRECTION (TO NEAREST TEN DEGREES) |
| Km/hr | KILOMETERS PER HOUR |
| SUM AMT | SUMMARY AMOUNT |

## FORMAT FOR SOLAR RADIATION/METEOROLOGY DATA

EXHIBIT 4

# THE SOLAR SPECTRUM AT TYPICAL CLEAR WEATHER DAYS+*

K. W. Böer
Institute of Energy Conversion
University of Delaware

And

SES, Incorporated
Newark, Delaware 19711

The solar spectrum in the range of $300<\lambda<1500$nm is given for five typical clear weather days. These days are selected to represent typical seasonal conditions in respect to airmass water vapor, ozone, and turbidity. Present data are reviewed, and specific conditions are selected. The spectral distribution of the irradiance is given for the direct component, the scattered skylight, the total flux on a horizontal surface, and the flux on an inclined surface normal to the direct beam.

## 1. Introduction

Clear weather days are often used to calibrate the operational parameters of solar collectors. For a number of applications, not only the total energy but the spectral distribution of the sunlight is important. For instance, solar cells are very sensitive[1] to changes in the solar spectrum. Changes of almost 30% in conversion efficiency have been observed[2] with seasonal periodicity for "clear day insolation" of $CdS/Cu_2S$ solar cell panels.

The knowledge of the spectral distribution of sunlight as it passes through each active layer of such a cell, hence of the generation rate of photocarriers in each layer, is key to any quantitative analysis of the cell performance.

---

+Sponsored by SES, Inc.

*An Appendix to this paper contains the computer printout of the typical clear weather spectra.

Unlike a calibrated light source, the solar spectrum, as received on terrestrial surfaces, is variable, dependent on variations in solar emission, the earth-sun distance, the thickness and composition of the earth atmosphere and the angle between the sun, observer, and zenith. Compared to the first three contributions*, only the last two are of major importance. (Only "clear" days are considered for this paper.) For non-horizontal collector surfaces, also, reflection from other surfaces must be considered.

These variations control total intensity and spectral distribution. Therefore, the electrical output of solar cells will depend on specific insolation conditions and usually cannot be normalized by adjusting only the total intensity, say to 100mW/cm$^2$, a value often used as norm for sea level/zenith/insolation (usually referred to as airmass one - AM1 insolation).

The purpose of this paper is to describe a number of typical clear sky conditions which can be used for calibration and general testing purposes and to give the spectral distribution of a number of solar flux conditions for these typical days.

The direct solar component is difficult to measure with sufficient accuracy. The highest degree of reproducibility can be expected for the direct solar plus forward scattered Mie component, hence we have chosen this component, excluding scattered global sky radiation, for calibration purposes. Measurements related to this type of illumination have the solar cell normal to the solar beam and require a collimation tube of proper length/diameter ratio (see below).

When the scattered global skylight is included, the solar cell is positioned on an elevated horizontal surface in order to exclude any reflected light from terrestrial surfaces**.

---

* Variations due to sun-spot activities are important in the radio wavelength range; integral variations are negligible. Variations due to earth-sun distance periodicity[3] are less than ± 3.4% (from 130.9 to 139.9mW/cm$^2$). Barometric (thickness) variations from 950 to 1050 mbar amount to changes of 1% in the total insolation and can be considered as ± 5% change in airmass (see Fig. 18 for an estimate of the influence on the spectral distribution).

** This, however, does not exclude light reflected from such surfaces and then backscattered from the atmosphere onto the solar cell. At higher atmospheric turbidity, this may be a substantial fraction.

Mostly, collector surfaces are inclined and, consequently, are also exposed to light reflected from terrestrial surfaces. However, the sky radiation is partially obstructed by the inclined collector surface.

All four spectral distributions of the impinging light onto a collector surface are given for each of five typical clear weather conditions.

## 2. Selection of Typical Atmospheric Conditions

Most of the changes in the spectral distribution of the impinging light are due to changes in the earth atmosphere. These changes are substantial even for clear sky conditions. We will, therefore, discuss the relevant parameters in more detail with the goal to identify five combinations which are typical for certain clear weather days and cover a wide variety of conditions. These typical clear weather days are chosen so that, with high probability, similar conditions can be observed throughout the year to provide convenient testing opportunities. However, they will include days close to extreme conditions in order to provide also the means for a sensitivity analysis.

### 2.1 AMO Solar Spectrum

The spectral distribution of sunlight above the earth atmosphere (airmass zero, AMO) was first derived by Johnson[3,5] and more recently by Thekaekara[24]. The latter is based on GSFC Measurements[25] from CV990 and is used for all further computation*. An average solar constant of 135.3mW/cm$^2$ is assumed[4,24,26].

The Thekaekara curve is shown as curve 0 in Fig. 1.

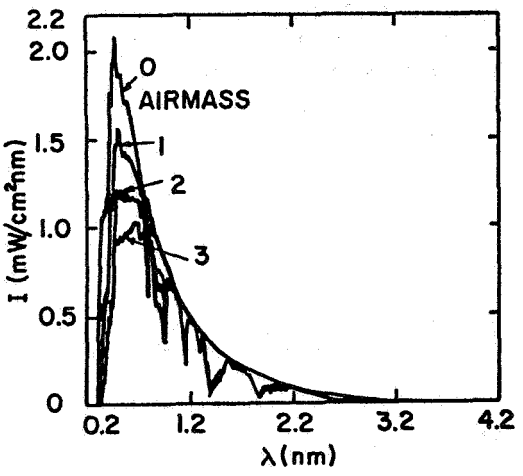


Fig. 1. Spectral Distribution of direct component of sunlight for different airmasses (family parameter) and for $O_3$=0.34cm, $H_2O$=0.3 cm, $\alpha$=1.5, and $\beta$=0.03.

* The original of the card deck used was obtained from a computer program developed by D. Hoyt of NCAR and R. Mitchell of GSFC at request of M. P. Thekaekara[6].

The relative energy contribution in selected spectral bands is given[6] in Table 1.

| Spectral Range μm | Intensity mW/cm$^2$ | Fraction of Total Intensity % | |
|---|---|---|---|
| 0.3 | 1.63 | 1.21 | |
| 0.3 - 0.35 | 4.47 | 3.31 | 85.2 in range |
| 0.35 - 1.2 | 108.29 | 70.4 | covered in |
| 1.2 - 1.5 | 16.2 | 12.0 | this paper. |
| 1.5 | 18.2 | 13.5 | |

TABLE 1

The wavelength range of interest for this paper is limited at lower wavelength by the optical absorption of ozone (Fig. 2) and of the transparent solar cell cover, and at longer wavelength by the relevant optical absorption of the active solar cell layer yielding a range of $300<\lambda<1500$nm.

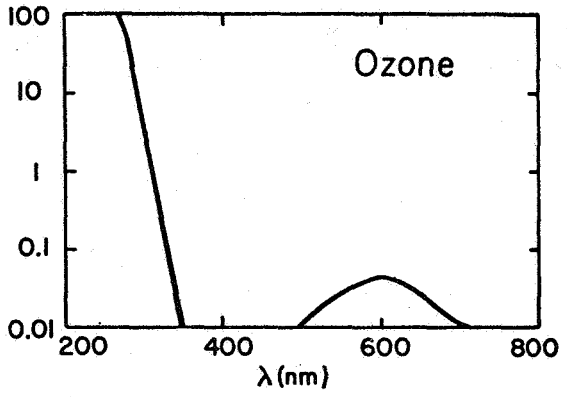


Fig. 2. Absorption spectrum of ozone in $250<\lambda<800$nm.

## 2.2 Influence of the Earth Atmosphere

The intensity of the direct component of the sunlight is given by

$$I_D(\lambda) = I_o(\lambda) \exp(-K_m m) \quad (1)$$

with

$$K_m(\lambda) = \sum_i \{K_{ia}(\lambda) + K_{is}(\lambda)\} \quad (1a)$$

the attenuation coefficient (normalized to airmass 1) which is composed of numerous components (see below) depending on scattering, s,

and absorption, a, of a variety of molecules and larger particles and m is the airmass:

$$m = 1/\cos(\phi - \pi/2) \tag{1b}$$

and $\phi$ the angle between the sun and the horizontal (solar elevation).

The extinction is due to a number of absorption and scattering mechanisms. In the range of interest, these are:

a) Rayleigh Scattering
b) Mie Scattering
c) Absorption by ozone, and
d) Absorption by water vapor.

There is also absorption by $O_2$, $CO_2$, and $CH_4$ (See Fig. 3) in this range, however these contribute little to the total extinction since the absorption bands are either very narrow or not very intense.

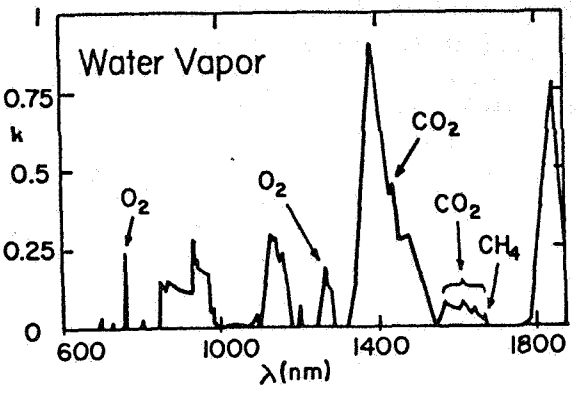


Fig. 3. Absorption spectrum of molecules in air, except ozone in $600<\lambda<1800$nm.

We will first review the present knowledge about the different extinction phenomena and then develop the arguments for defining the typical atmospheres.

### 2.2.1. Rayleigh Scattering

Molecular scattering in air[7] can be described by an extinction constant

$$\eta_1 = \frac{8\pi^3}{3} \cdot \frac{(n-1)^2}{N \cdot \rho} \cdot \frac{1}{\lambda^4} \tag{2}$$

with the parameters (for air) of $N=2.28.10^{25}$/kg, $\rho=1.29$kg/m$^3$, $n=1.00063$ yielding $\eta_1 \cdot \lambda^4 = 1.13.10^{-30}$ m$^3$. For airmass 1 (using normal conditions: p=1013mbar), one obtains from $K_1 = \eta_1 p/\rho$ :

$$K_1 = 8.9 \cdot 10^{-3} \lambda^{-4} \ (\mu m^{-4}) \tag{3}$$

Equ. 3 holds within $\pm$ 3% if anisotropic molecules are considered[7].

Table 2 shows the transmission of a normal atmosphere at sea level for Rayleigh Scattering*. The total extinction from Rayleigh Scattering is given in Table 2.

The angular distribution is essentially isotropic as shown in Fig. 5 (molecular). The fraction scattered from the primary beam is given by 1-exp ($-K_1 m$) (See Fig. 4), half of which contributes to the skylight (the rest is back scattered and contributes to the albedo).

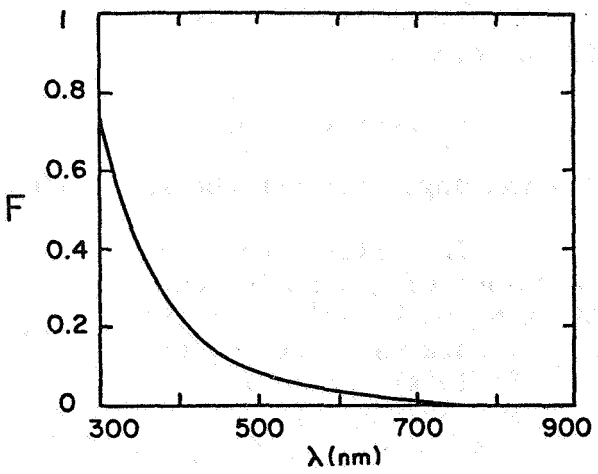


Fig. 4. Ratio of total Rayleigh Scattering[16] to transmitted light.

| solar elevation | 90° | 60° | 30° | 10° |
|---|---|---|---|---|
| airmass | 1 | 1.25 | 2 | 5.76 |
| extinction | 9.4% | 10.5% | 16.3% | 32% |

TABLE 2

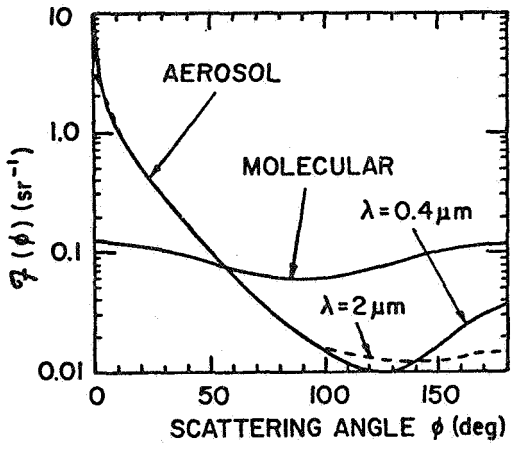


Fig. 5. Angular distribution of scattering[8]. $F(\phi)$ is defined by $I_s(\phi,\lambda)=I_s(\lambda)F(\phi)$.

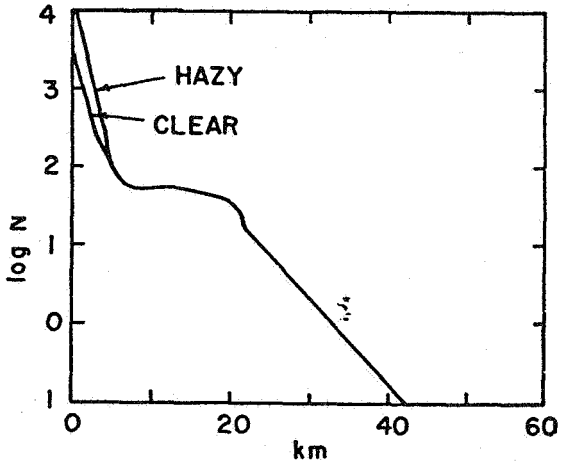


Fig. 6. Particle density for typical cases[8] as function of altitude.

* The program used employs the Elterman values[27] of Rayleigh and ozone optical depth.

### 2.2.2. Mie Scattering

Scattering at aerosols is much more complex. It depends on the size, shape and optical constant of the particles and their density.

There are a wide variety of aerosols suspended[8] in the atmosphere (dust, water droplets, etc.) up to altitudes of 100km (See Fig. 6).

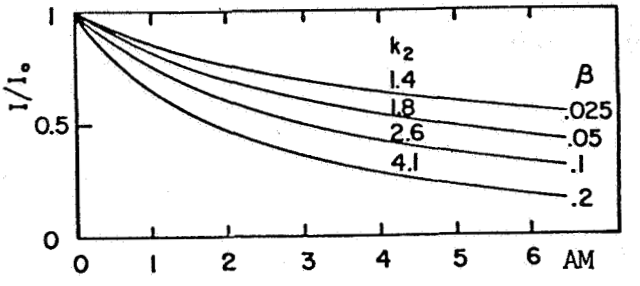


Fig. 7. Attenuation of the direct solar component as a function of the airmass (AM) for different turbidity.

The particle size is characterized by $2\pi r/\lambda$ with r the particle radius. For $2\pi r/\lambda<0.1$, the scattering is similar to the Rayleigh $\lambda^{-4}$ law. The larger the particle, the less dependent is the scattering on wavelength. Typically, particles from $<0.1\mu$ to $\gtrsim 10\mu$ are suspended. The scattering of particles of different size and refractive index was computed by Penndorf[7] and shows oscillatory spectral distribution with a tendency to flatten out for larger particles. With a wide distribution of particles, the scattering may be described by

$$K_2 = \beta/\lambda^{\alpha} \qquad (4)$$

with the empirical Ångström[9] parameters $\alpha$ and $\beta$*($\lambda$ in $\mu$m) (See Fig. 8).

The total attenuation due to the scattering for $\alpha\simeq 1.3$ and various $\beta$ values (or various $K_2$ values - approximative) as a function of the airmass is given in Fig. 7.

The solar spectrum for a variety of values for $\alpha$ and $\beta$ is shown in Figs. 9 and 10.

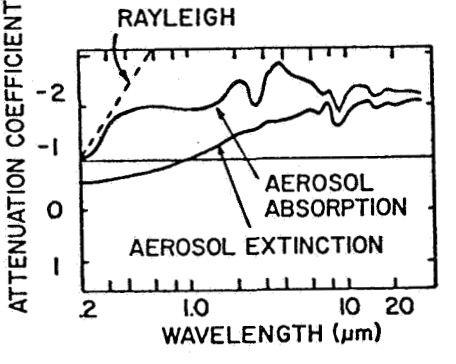


Fig. 8. Attenuation coefficient for aerosol transmittance (Absorption and Total Extinction)[8].

* Often the turbidity parameter $T(=K_2)$ is used instead of $\beta/\lambda^{\alpha}$ (Linke[11]).

The visibility* may be used as some measure of atmospheric turbidity. At sea level, a total particle density of 3000 $cm^{-3}$ corresponds to 23km visibility, 14000 $cm^{-3}$ to a 5km visibility[8], with an assumed seize distribution of

$$\frac{n(r)}{\Delta r} = 0.883 \cdot 10^{-3} \begin{cases} r^{-4} & \text{for } 0.1<r<10\mu m \\ 10^{-4} & \text{for } 0.02<r<0.1\mu m \end{cases} \qquad (5)$$

and $\Delta r=1\mu m$.

An example of the spectral distribution of the attenuation coefficients of such aerosols is given[8] in Fig. 8.

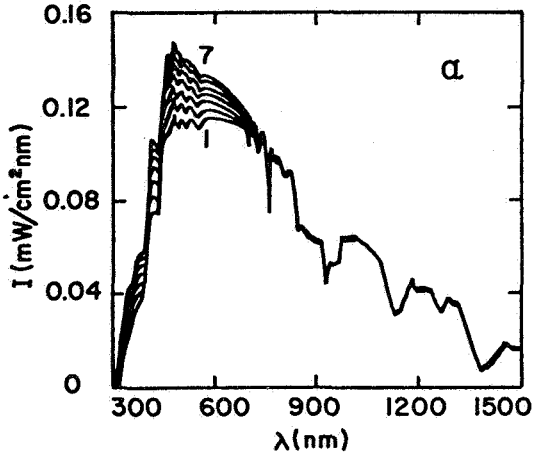


Fig. 9. Spectral distribution of direct component of sunlight for different values of α (family parameter α changes from 0.5 to 2.0 in steps of 0.25 for curves 1 through 7 airmass 1.2, β=0.07, other parameters as in Fig. 1).

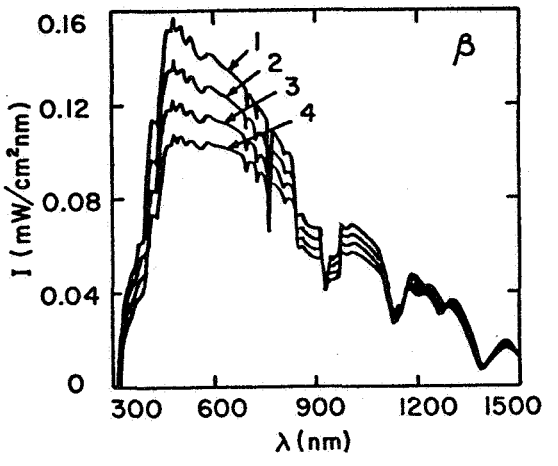


Fig. 10. Spectral distribution of the direct component of sunlight for different values of β (family parameter β changes from 0.02 to 0.17 in steps of 0.05 for curves 1-4) for α=1, other parameters as in Fig. 1.

---

* Attention must be given to the layer-like distribution of aerosols in which often the low layer visibility is considerably reduced without changing the solar radiation accordingly.

The Mie Scattering is highly anisotropic, with a large fraction of the light being forward scattered (See Fig. 5), most of it within an angle of $10^{o}$.

Extensive data are collected[10] and indicate a variation of $\beta$ between 0.02 and 0.5 and of $\alpha$ between 1.5 and 0.5 for exceptionally clear and very hazy days respectively. A measure of the turbidity is the whiteness of the sky: The higher the turbidity, the larger are the long wavelength components of the scattered sky radiation.

### 2.2.3 Ozone Absorption

The major ozone absorption bands are in the UV (Hartley band) from 180-340nm and a very weak Cappius band from 440 to 740nm (See Fig. 2), both with little structure. Ozone is non-uniformly distributed in the atmosphere, and is contained mainly in a 10-15km thick layer, with its middle approximately 23 to 30km above the earth surface[8,12].

The total ozone content averages 0.38cm in the upper latitudes and 0.24cm over the equator[12], here it is nearly constant throughout the year. In upper latitudes, it varies with an amplitude at polar regions of 0.2cm, the maximum in the fall, the minimum in the spring. Irregular daily variation can be as high as 25%. Maximum observed changes over the globe are from 0.07 to 0.7cm. Variation of the solar spectrum with different ozone content is shown in Fig. 11 for AM1.2 and in Fig. 12 for AM2.3.

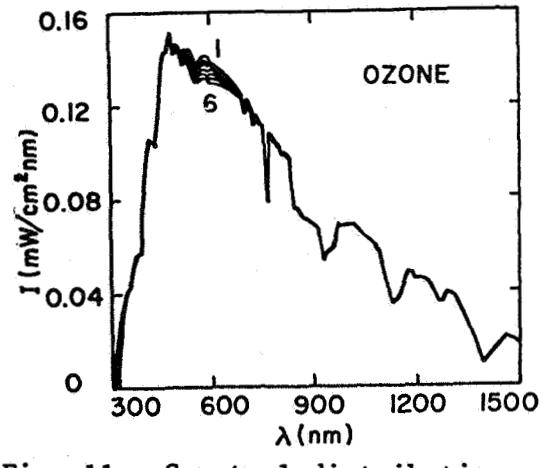


Fig. 11. Spectral distribution of the direct component of sunlight for different ozone concentrations (family parameter changes from 0.1 to 0.6cm in steps of 0.1cm for curves 1-6) airmass 1.2, other parameters as in Fig. 1.

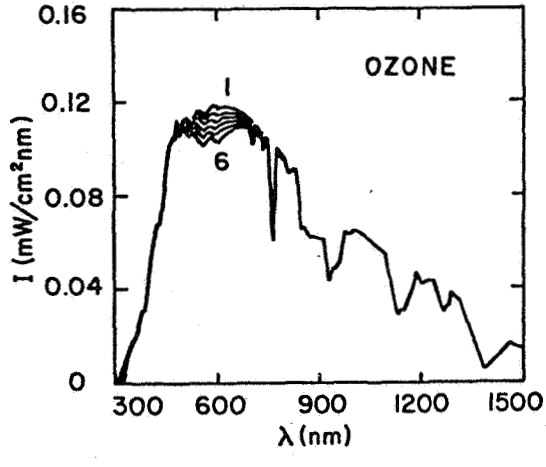


Fig. 12. As Fig. 11, however, for airmass 2.3.

A median value for 40° latitude seems to be[6] 0.35cm.

### 2.2.4. Water Vapor

There are several water vapor bands in the wavelength range of interest (See Fig. 3). The most intense band lies between 1320 and 1540 nm, with its maximum absorption close to 1400nm. Two other water bands extend from 850 to 980nm and from 1100 to 1180nm.

The transmission function, t, for numerous absorption lines within each band is well approximated by a random model[13] with

$$t(\bar{\alpha},w) = \exp\{-kw/2\pi\delta\ (1+kw/\pi\bar{\alpha})^{1/2}\} \qquad (6)$$

with w the quantity of water vapor along the path, k the average line intensity, $\bar{\alpha}$ the half width, and $\delta$ the mean line spacing. Equ. 6 usually is approximated[14] by a square root, a linear and a quadratic branch dependent on $kw/\pi\bar{\alpha} \gtrless 1$. This approximation[16] is used for the computation in this paper.

The water vapor in the atmosphere is non-homogeneously distributed. It is high in low altitudes and decreases rapidly. The total precipitable water content of the atmosphere in the optical path varies widely between cold, very dry winter days, where it may be as low[14] as 0.2cm to hot, very humid summer days with up to 5cm (without cloud formation). Though both extremes may be rare, values between 0.5cm during dry winter days to 4cm during hot humid summer days may be more frequently encountered[15].

Fig. 13 shows a family of curves for AM1.2 for water vapor contents from 1 to 5cm (summer range); Fig. 14 shows such a family for AM2.3 for water vapor contents from 0.2 to 1.6cm (winter range).

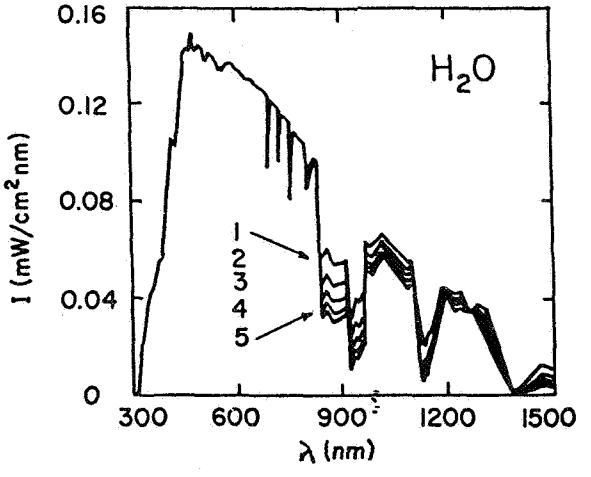


Fig. 13. Spectral distribution of the direct component of sunlight for different amounts of precipitable water (family parameter changes from 1 to 5 in steps of 1 for curves 1-6) for airmass 1.2 other parameters as in Fig. 1.

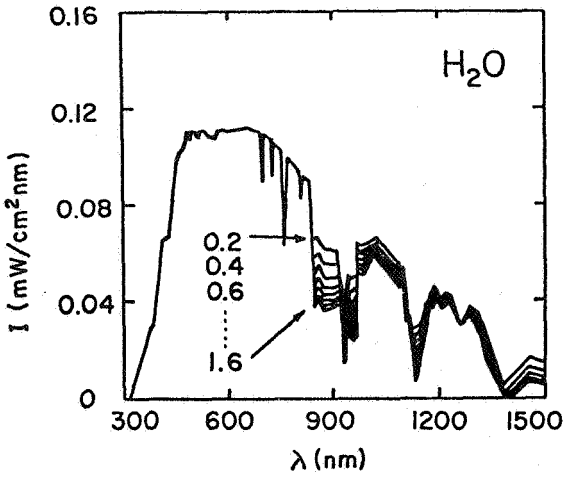


Fig. 14. As Fig. 13, however, for airmass 2.3; the family parameter changes from 0.2 to 1.6 in steps of 0.2 for curves 1-7.

### 2.2.5. Other Molecular Absorption

As indicated above[12] (See Fig. 2), there are 3 other components which contribute to the optical absorption: A strong but rather narrow oxygen line at 762.1nm and several other much weaker $O_2$ lines at 340, 579.6, 628.8, 637.9, 688.4, 689.7, 690.1, 697.0, 762.0, 771 and 1067nm. Other very weak lines are due to electronic transition in $O_4$ at 477.4, 577.0 and 629.0nm.

The first pronounced $CO_2$ absorption is at 1434nm, and more pronounced bands start at 1540nm. The first $CH_4$ absorption starts at 1670nm.

The total absorption of these molecules in the spectral range of interest ($300<\lambda<1500$nm) lies well below 1% and is consequently neglected[10] for the purpose of this paper.

## 2.3. Airmass Consideration

The amount of attenuation by absorption and scattering depends exponentially on the optical path, i.e., on the airmass.

For 40° latitude (Delaware), the noon elevation on June 22 is 73°40' corresponding to airmass 1.04, and at December 22, it is 26°46' corresponding to airmass 2.22. The solar elevation $\phi$ is given by

$$\sin\phi = \sin L \sin\delta + \cos L \cos\delta \cos(\pi h/12) \qquad (7)$$

with L the latitude, h the hours (counted from solar noon), and $\delta$ the solar declination given by

$$\delta = 23^{\circ}27' \sin\{2\pi\ (284+N)/365\} \qquad (8)$$

with N the number of days after January 1.

In Fig. 15, the airmass is shown as a function of the time of day for different months of the year (for latitude 40°). One sees that during the summer month, the airmass stays for more than four hours at around noon between 1.05 and 1.3. As a typical value, we will select $m_S$=1.2. During the November to February period, the airmass varies between 2 and 2.8 during the same four hours. As a typical winter average, we select $m_W$=2.3. A spring/fall average is $m_{Sf}$=1.5 (See Fig. 15).

The spectral distribution of sunlight for different airmasses in the range of interest is given in Fig. 16, indicating (especially in the range of 400 to 1000nm) a more pronounced change in intensity. This is caused by the strong influence of ozone and of light scattering in this range and has major consequences for the conversion efficiency of solar cells, since most of them (especially the $CdS/Cu_2S$ cell) are most sensitive in this range.

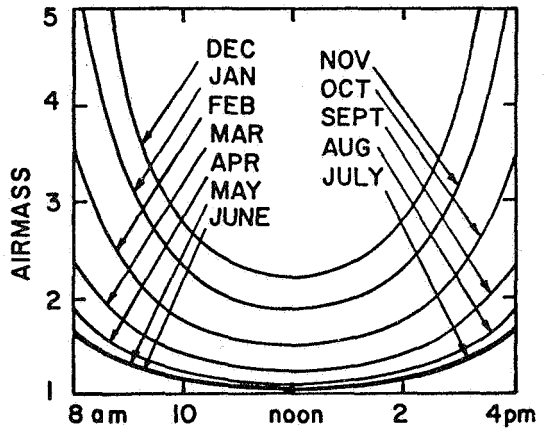


Fig. 15. Airmass as a function of time of day for different days of the year (approximately the 25th day of the month indidated).

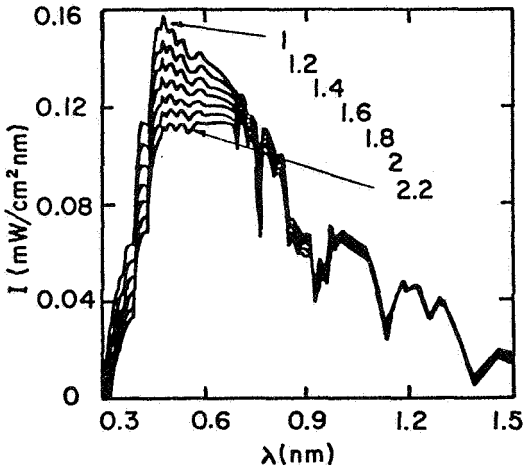


Fig. 16. Spectral distribution of the direct component of sunlight for different airmass (family parame ters); other parameters as in Fig. 1.

## 2.4. Selection of Typical Clear Weather Models

We will provide five model spectral distributions which are reasonably close to the distribution of the direct solar component at certain clear weather days which can easily be identified and, consequently, used for calibration purposes.

In defining such model distributions, we will consider common trends, such as, in general, lower turbidity during winter months and higher ozone during the fall. Using the parameter range as given in sections 2.2, we suggest the values given in Table 3 (See also Ref. 16).

| Code | Typical Days | M | $O_3$ | $H_2O$ | $\alpha$ | $\beta$ | $P_t$ | $P_{\Delta\lambda}$ | $P_{\Delta\lambda}/P_t$ | Fig./ Curve |
|---|---|---|---|---|---|---|---|---|---|---|
| W | Very clear cold (-10°C) Winter day: | 2.3 | .34 | .4 | 1.5 | .03 | 72.6 | 64.2 | 88.4% | 19/1 |
| SP | Clear cool (5°C) Spring day: | 1.5 | .25 | 1.0 | 1.3 | .06 | 83.2 | 73.2 | 88.2 | 19/2 |
| S | Clear cool (15°C) Summer day: | 1.2 | .34 | 1.5 | 1.1 | .09 | 82.9 | 73.4 | 88.5 | 17/1 |
| SH | Hazy hot (35°C) Summer day: | 1.2 | .34 | 4.5 | 0.6 | .25 | 62.5 | 55.4 | 88.6 | 17/2 |
| F | Hazy warm (20°C) Fall day: | 1.5 | .44 | 3 | 0.8 | .15 | 65.8 | 58.0 | 88.1 | 19/3 |

TABLE 3

The respective spectral distributions are given in Figs. 17 and 18 and show a great deal of variation, not only in total intensity,

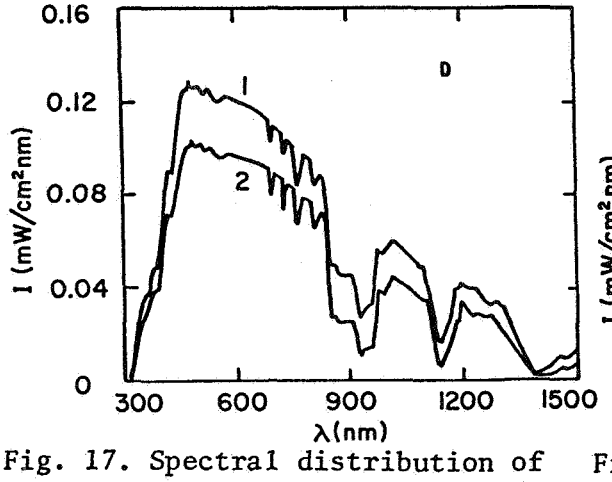


Fig. 17. Spectral distribution of the direct component of sunlight for typical clear weather days curve 1:S, curve 2:SH (code in Table 1)

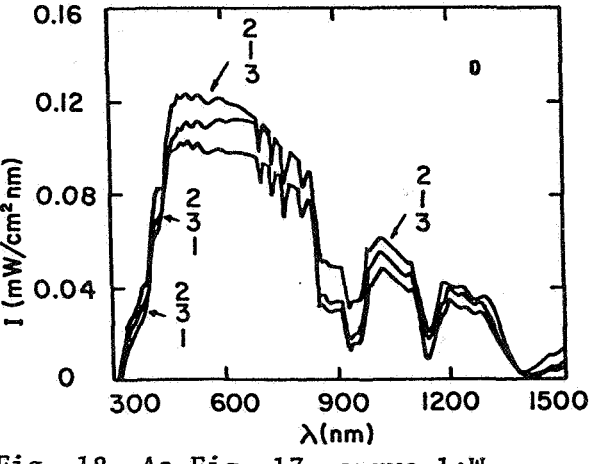


Fig. 18. As Fig. 17, curve 1:W, curve 2:SP, curve 3:F (attention, crossing curves).

but specifically in the ratio short-to-long wavelength content. The total ($P_t$) and partial ($P_{\Delta\lambda}$) radiances* of the direct beam are also given in Table 3.

The total intensity of the direct beam varies between 46 and 61% of the sunlight above the atmosphere. A major fraction of the lost radiation is scattered and can be recovered from the sky radiation. About 88% of the total radiance of the direct beam is in the wavelength range of interest.

## 2.5. Direct Solar Component

For measurement of the direct solar component, an almost perfect collimation is necessary in order to separate this component from the intense forward scattering of the Mie component. Most of the Mie scattering is confined within a cone of $10^o$ aperture (Fig. 5). The solar disk has an aperture of approximately** $1/2^o$.

A collimator tube of an approximately 1/50 diameter-to-length ratio is required to provide an aperture of $1.15^o$ and seems to be sufficient to exclude most of the Mie Scattering.

The inside of the collimator tube should be perfectly black to prevent forward reflection of scattered light. Due to the large length-to-diameter ratio, matte carbon black is sufficient.

The measurement needs proper tracking. The spectral distributions for the direct component and the typical days is given as D in Fig. 19-23.

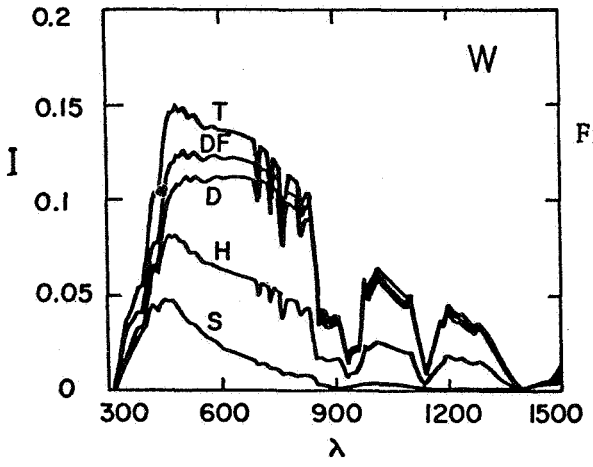


Fig. 19. Spectral distribution of different components of sunlight for clear weather day, W. Code explanation in Tables 3 and 4. I in $mW/cm^2nm$, $\lambda$ in nm.

* In $mW/cm^2$

** 32'36" at the perihel and 31'32" at the aphel.

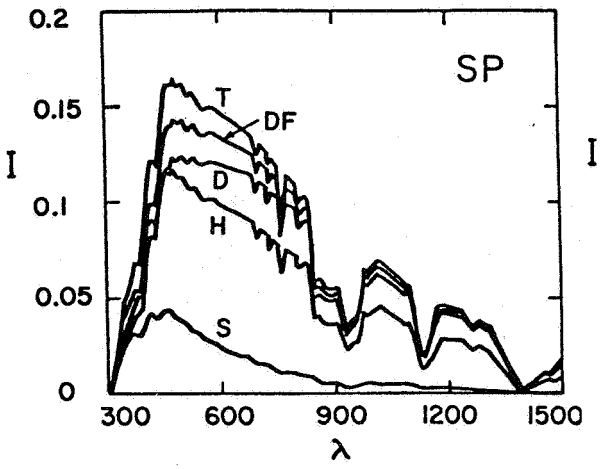


Fig. 20. As Fig. 19, for day SP.

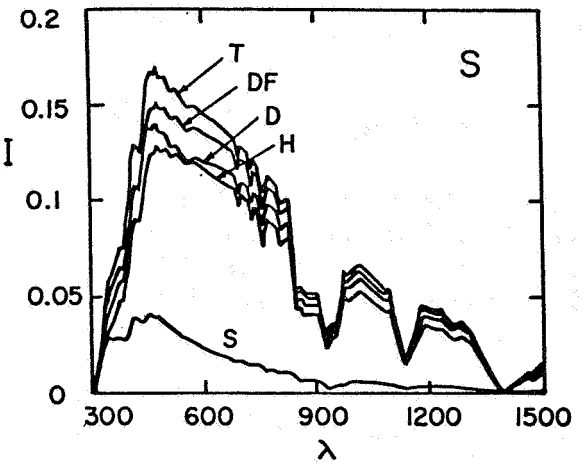


Fig. 21. As Fig. 19, for day S.

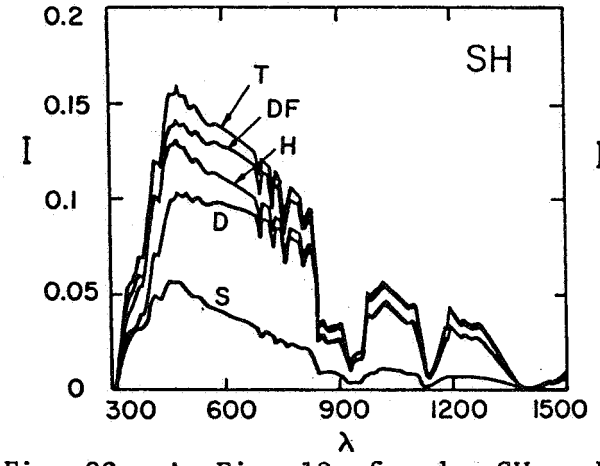


Fig. 22. As Fig. 19, for day SH.

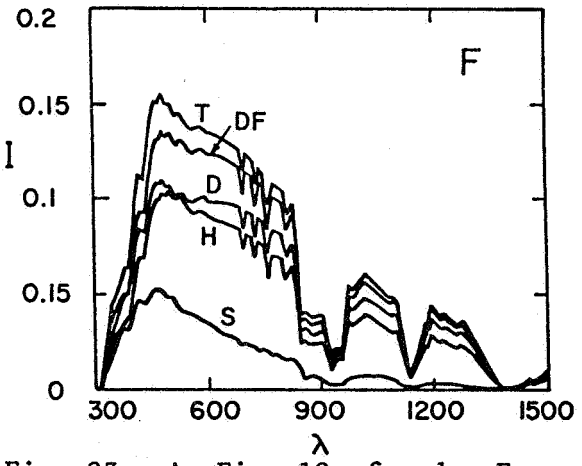


Fig. 23. As Fig. 19, for day F.

## 2.6 Direct Solar Plus Forward Mie Component

Best suited for calibration is the direct solar plus forward Mie component. It is less sensitive to slight tracking errors and to changes in turbidity, since most of the scattered light is added back to the incident beam.

A collimator tube of a diameter-to-length ratio of 1/5 presents an aperture of almost $12^{o}$, sufficient to permit penetration of the forward Mie component and to eliminate most of the skylight and reflected light from adjacent surfaces.

The solar flux of the direct plus forward Mie component is given by ($I_D(\lambda)$ given in equ. 1):

$$I_{DF}(\lambda) = I_D(\lambda)\left\{1+\varepsilon\left[\exp\left(\frac{\beta m}{\lambda\alpha}\right)-1\right]\right\} \qquad (9)$$

with $\varepsilon$ the fraction of the forward scattered Mie component. Approximately 20% of the total Mie component is absorbed an 10% is back scattered adding to the earth's albedo. Of the rest, approximately 90% is assumed to be forward scattered, hence $\varepsilon$=0.63 (For an example, see Fig. 5).

Curves DF in Figs. 19-23 give the spectral distributions for the direct plus forward Mie component for the five typical clear weather conditions.

### 3. Direct Plus Sky Radiation

The radiation given in Section 2.4 is only the direct component of the sunlight, excluding the scattered sky radiation. The latter, however, is a major component contributing to the solar radiation impinging on a flat surface.

However, since scattering of light occurs also from light which is first reflected from terrestrial surfaces, the scattered component is much more complex and depends not only on the turbidity of the earth atmosphere, but also on the spectral distribution of the reflected light. Little is known about the reflected and, then, backscattered fraction. All present skylight measurements include this fraction. It is of substantial influence in regions of high albedo* (light sand and snow) and for higher turbidity (up to 10%)[17].

Since the Rayleigh scattering is essentially isotropic, approximately 50% of it will impinge on terrestrial surfaces, the rest is backscattered, hence adds to the earth's albedo[18].

In respect to the Mie Scattering, the situation is much more complicated. The angular distribution of the scattered light depends on the particulate size, shape, index of refraction, and wavelength of the light. In general, the scattering is substantially a more forward scattering, as shown in Fig. 5.

---

* The average earth's albedo[22] is 29% with major variation of reflectances from earth surface features (Given in Table 4).

A number of studies are done to determine the angular and spectral distribution of the sky radiance for different atmospheric conditions. However, it is presently not possible to give representative spectral distributions for typical clear weather conditions for the integral sky radiation. Until such data are available, we have proposed (See Section 2.6) to assume an angular distribution with the forward scattering component at an amplitude of 70% of the scattered light (20% of the light is absorbed by the aerosol, the remaining 10% is back scattered).

Consequently, we define for the purpose of this paper the total sky radiance as given by*

$$I_S(\lambda) = I_D(\lambda)\{0.5[\exp(\kappa_1 m)-1] + 0.7[\exp(\tfrac{\beta m}{\lambda^{\alpha}})-1]\} \qquad (9)$$

and shown as curves S in Figs. 19-23 for the five model distributions (The change in the atmospheric path length for scattered light is neglected).

## 3.1. Solar Irradiance at Horizontal Surfaces

The direct component and the skylight are observed at horizontal surfaces which are sufficiently elevated to avoid direct radiation from reflecting surfaces.

Since the receiving surface is not normal to the direct component, this part of the irradiance has to be reduced by $\sin\phi$ (with $\phi$ the solar elevation).

Because of the relatively strong component of forward scattering (See Fig. 11), again approximately 90% of the Mie component must be reduced by $\sin\phi$ . The rest of the Mie and all of the Rayleigh component are not subject to such a reduction. The total irradiance on a horizontal surface for the five model distributions is given by

$$I_H(\lambda) = I_D(\lambda)\{\sin\phi[1+0.63(\exp(\tfrac{\beta m}{\lambda^{\alpha}})-1)] + 0.5[\exp(\kappa_1 m)-1] + 0.07[\exp(\tfrac{\beta m}{\lambda^{\alpha}})-1]\} \qquad (10)$$

and is shown as curves H in Figs. 19-23.

* Multiple scattering is neglected. The effect of multiple Rayleigh scattering is investigated by Chandrasekhar[19] and is found to reduce the factor 0.5 to 0.46 for $\lambda$=300nm and to 0.49 at $\lambda$=400nm, while causing little change at larger $\lambda$. The multiple Mie scattering is not yet analyzed. However, since only 10% of the Mie scattering contributes to large angle component, little changes of the overall spectrum are expected.

## 3.2. Total Irradiance on Surface Normal to the Direct Solar Component

On an inclined surface (solar elevation $<90^{o}$) normal to the direct solar radiation, the total irradiance is given by the direct component $I_D(\lambda)$ plus the fraction of the unobstructed skylight plus the reflected light from adjacent surfaces.

The skylight is reduced on inclined surfaces because these surfaces obstruct part of the sky. The ratio of the skylight impinging onto such surface is given by $(90^{o}+\phi)/180^{o}$.

The reflected light is more difficult to estimate. The spectral distribution depends on the color of adjacent objects, on the intensity of the angle of inclination of the collector surface, and on the reflection R from the adjacent surfaces. It depends also on the angle of illumination and is substantially lower for low solar elevation since more shaded surfaces point towards the observer.

The reflection from the ground[17] is approximately 17% from vegetation (grass), 10% from water, 25% from light sand, and 80% from new snow. Only the fraction $(90^{o}-\phi)/180^{o}$ falls onto the inclined collector surface.

Typical values for the ground reflection are difficult to define (See Table 4). However, for the purpose of definiteness, we will assume a value of R=0.2. For the total irradiance, one obtains

$$I_r(\lambda) = I_D(\lambda)\left\{1 + \frac{90-\phi}{180} R + 0.63\left[\exp\left(\frac{\beta m}{\lambda\alpha}\right)-1\right] + \frac{90^{o}+\phi}{180}\left[0.5\{\exp(\kappa_1 m)-1\} + 0.07\left\{\exp\left(\frac{\beta m}{\lambda\alpha}\right)-1\right\}\right]\right\} \tag{11}$$

| Reflecting Surface | Total Reflectance | Remarks |
|---|---|---|
| Soil and Rocks | 5 to 45% | Maximum reflectance for small angles (forward). |
| Vegetation | 5 to 25% | Mainly back scattering. |
| Water | 5 to 20% | Maximum reflectance for small angles. |
| Snow | 25 to 80% | Diffuse and mirror components. |
| Clouds | 10 to 80% | |

Table 4[28]

Figs. 19-23 contain as T the curves for total irradiation on an inclined surface normal to the direct solar radiation and as $I_D$ the direct radiation alone.

In Table 5, the flux densities integrated between 300 and 1500nm of the different components for the five given clear weather days are presented.

| Code | D | S | H | DF | T |
|---|---|---|---|---|---|
| W | 64.2 | 13.8 | 37.8 | 69.4 | 79.1 |
| SP | 73.2 | 14.1 | 60.1 | 80.3 | 88.8 |
| S | 73.4 | 14.2 | 71.4 | 81.4 | 88.6 |
| SH | 55.4 | 21.9 | 63.3 | 71.5 | 77.9 |
| F | 58.1 | 19.4 | 53.5 | 71.0 | 78.4 |

Table 5

Irradiation in $mW/cm^2$

## 4. Summary

From Figs. 19-23 and Table 5, it is evident that the scattered and reflected light adds 18-29% to the direct component. While the direct component varies substantially (between 55 and 73 $mW/cm^2$), the total sunlight impinging on a surface normal to the direct beam varies considerably less (between 78 and 89 $mW/cm^2$) for different clear weather days (Figs. 24 and 25).

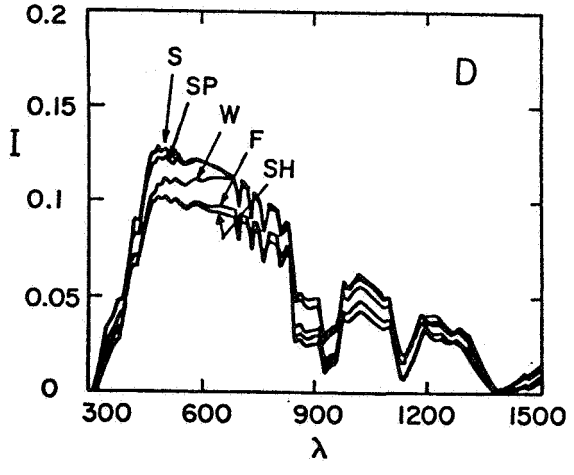


Fig. 24. Spectral distribution of the direct components for all typical days as defined in Table 3. I in $mW/cm^2nm$, $\lambda$ in nm.

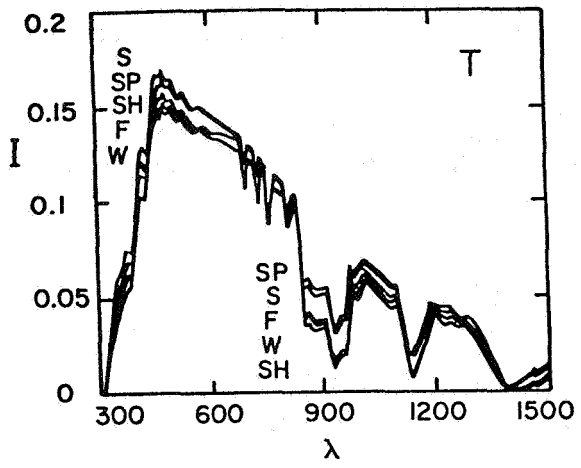


Fig. 25. As Fig. 24, for the total radiation normal to the direct solar beam.

From spring through fall, for days of low turbidity ($\beta \lesssim 0.1$), the total sunlight impinging on the surface normal to the direct beam in the entire spectral range is indeed close to 100mW/cm$^2$ (with ~ 88% of the sunlight in the range $300<\lambda<1500$). However, for higher turbidity (SH, F) and during the winter, a reduction of approximately 10% is observed.

The direct and forward Mie components stay about 10% below the total sunlight on a surface normal to the direct beam.

The reflection from adjacent surfaces adds between 4 and 7% (summer to winter) to the total sunlight on such surfaces normal to the direct beam (for 20% assumed surface reflectance).

The most pronounced seasonal changes are a lower content of short wave radiation during the winter (larger airmass in conjunction with ozone absorption) and more light in the water absorption bands (with exception of very cold, low humidity summer days).

Much error can be made by using only the direct component of sunlight for calibration. It is difficult to separate from the forward scattered Mie component measured with a black collimator tube of 1:5 diameter/length ratio (For general information in respect to measurements, see Ref. 20).

The interim solar cell testing procedures for terrestrial applications[21] are useful guidelines, however, with the following additional conditions:

1. Calibration of solar cells should preferably be done with 1:5 collimator tubes.
2. The measurement should be done on clear weather days with atmospheric conditions, avoiding extremes in turbidity and water content. The airmass should be below 1.5 with tur-

bidity between $\beta$=0.05 and 0.1 and precipitable water between 0.7 and 1.5cm (For these values, the spectral distributions for DF are within $\pm$ 3% of each other).

3. Only if collimator tubes are impractical may the standard solar cell method be applied, however, only if the solar intensity measured with a pyranometer is larger than 90 mW/cm$^2$.

For calibration of standard cells, the following changes are suggested:

1. Increase of collimator angle (field of view) from 5°42' to 10°.
2. DF intensity (all wavelength) 80 to 90mW/cm$^2$.
3. Turbidity should be $0.05<\beta<0.1$.
4. Airmass should be $1<m<1.5$.
5. No clouds within 50°, in order to obtain similar spectral distribution for the selected clear weather days and to minimize calibration errors. It is, moreover, advisable to register the pertinent weather data ($H_2O$, $O_3$, $\alpha$, $\beta$ and m) and make these part of the record of the standard cell.

## 5. Acknowledgements

Helpful discussions with M. P. Thekaekara, W. E. Shenk, T. T. Wilheit, R. A. McClatchey, and R. W. Fenn are gratefully acknowledged.

The work was stimulated by discussions with H. Hadley[23]. The assistance in setting up the basic computer program by D. Lamb is gratefully acknowledged. Thanks are due to Dr. Cockayne for sending a copy of the original card deck for the direct components.

## 6. Literature

1. Terrestrial Photovoltaic Measurements, Workshop Prodeedings NASA TM X 71802 (1975).
2. H. Windawi, Internat. Workshop on CdS Solar Cells and Other Abrupt Heterojunctions, Del., May (1975), NSF, AER-75-15858, 528.
3. F. S. Johnson, Journal of Meterology 11, 431 (1954).
4. M. P. Thekaekara, et. al., NASA Rep. x-322-68-304 (1968).
5. F. S. Johnson, Handb. Geophys. 16, 17 (1960).
6. M. P. Thekaekara, Suppl. Proc. 20th Ann. Meeting Inst. Environm. Sci., Mount Prospect, Ill. (1974), NASA.
7. R. Penndorf, T. Opt. Soc. Am. 47, 176, 603, and 1010 (1957).

8. R. A. McClatchey, R. W. Fenn, T. E. A. Selby, F. E. Volz, and T. S. Garig, Airforce Environm. Res. Paper No. 411, Aug. (1972), AFCRL-R-0497.

9. A. Ångstrom, Geogr. Am. 11, 156 (1929), 12, 130 (1930).

10. T. Bilton, E. C. Flowers, R. A. McCormick and K. R. Kurfis, Solar Energy Data Workshop NSF/RANN 74-062, Nov. (1973), Silver Springs, Md., 61.

11. F. Linke, Handb. Geophys. 8, 239 (1342).

12. Ye. A. Makarova and A. V. Kharitonov, NASA Techn. Transl., NASA TT F-803.

13. R. M. Goody, The Physics of the Stratosphere, (Cambridge Univ. Press), N.Y. (1958).

14. D. M. Gates and W. J. Harrop, Appl. Optics 2, 887 (1963).

15. W. E. Shenk and T. T. Wilheit, personal communication.

16. M. P. Thekaekara, Proc. Conf. Comples, Darhan, Saudi Arabia (1975).

17. R. Schulze, Das Strahlenklima der Erde, D. Steinkopf Verl. Darmstadt (1970).

18. H. P. Berlage, Meteor. Z. 45, 174 (1928).

19. S. Chandrasekhar, Radiat. Transfer, Oxford (1950).

20. Solar Energy Data Workshop NASA/RANN 74-062, Silver Springs, Md. (1973).

21. H. Brandhorst, T. Hickey, H. Curtis, and E. Ralph, Interims Solar Cell Testing Procedures for Terrestrial Applications, NASA-TMX 71771 (1975).

22. NASA, SP 8067, July (1971).

23. H. Hadley, Technical Report NSF/RANN/SE/G1-34872/TR74/3.

24. M. P. Thekaekara, Solar Energy 14, 109 (1973), Appl. Optics 13, 518 (1974).

25. NASA Space Veh. Design Criteria, NASA, Wash. D.C., May (1971), SP8005 and Ann. Book of ASTM Standards, ASTM, Phil. (1974), E4773a, part 41, 609-615.

26. M. P. Thekaekara, R. Kruger, and C. H. Duncan, Appl. Optics 8, 1713 (1969).

27. L. Elterman and R. B. Toolin, "Atmospheric Optics" in Handbook of Geophysics and Space Environments, ed. by S. L. Balley, 7-12, 27-35 (McGraw-Hill Book Co.), N.Y. (1965).

28. F. L. Bartman, Techn. Rep. NASA DR-83954 (1967).

## APPENDIX

This Appendix contains the computer printout of the spectral energy distribution of the four insolation modes D, H, DF, and T for the five typical clear weather days W, SP, S, SH, and F as defined in the main text of the paper.

| λ (nm) | I(D/W) mW/cm$^2$nm |
|---|---|
| 300 | 7.921E-07 |
| 307 | 2.291E-05 |
| 313 | 3.112E-04 |
| 320 | 3.392E-03 |
| 327 | 6.128E-03 |
| 334 | 9.609E-03 |
| 340 | 1.392E-02 |
| 347 | 1.618E-02 |
| 354 | 1.879E-02 |
| 360 | 2.136E-02 |
| 367 | 2.531E-02 |
| 374 | 2.812E-02 |
| 380 | 2.973E-02 |
| 387 | 3.145E-02 |
| 394 | 3.603E-02 |
| 401 | 4.812E-02 |
| 407 | 5.892E-02 |
| 414 | 6.469E-02 |
| 421 | 6.681E-02 |
| 427 | 6.725E-02 |
| 434 | 7.027E-02 |
| 441 | 8.130E-02 |
| 447 | 9.171E-02 |
| 454 | 9.897E-02 |
| 461 | 1.022E-01 |
| 468 | 1.037E-01 |
| 474 | 1.065E-01 |
| 481 | 1.098E-01 |
| 488 | 1.075E-01 |
| 494 | 1.100E-01 |
| 501 | 1.113E-01 |
| 508 | 1.104E-01 |
| 515 | 1.082E-01 |
| 521 | 1.096E-01 |
| 528 | 1.114E-01 |
| 535 | 1.111E-01 |
| 541 | 1.097E-01 |
| 548 | 1.086E-01 |
| 555 | 1.086E-01 |
| 561 | 1.080E-01 |
| 568 | 1.095E-01 |
| 575 | 1.109E-01 |
| 582 | 1.114E-01 |
| 588 | 1.116E-01 |
| 595 | 1.110E-01 |
| 602 | 1.105E-01 |
| 608 | 1.108E-01 |
| 615 | 1.112E-01 |
| 622 | 1.114E-01 |
| 628 | 1.116E-01 |
| 635 | 1.120E-01 |
| 642 | 1.124E-01 |
| 649 | 1.125E-01 |
| 655 | 1.124E-01 |
| 662 | 1.122E-01 |
| 669 | 1.118E-01 |
| 675 | 1.114E-01 |
| 682 | 1.110E-01 |
| 689 | 1.108E-01 |
| 696 | 9.490E-02 |
| 702 | 1.094E-01 |
| 709 | 1.086E-01 |
| 716 | 1.076E-01 |
| 722 | 1.015E-01 |
| 729 | 9.894E-02 |
| 736 | 1.047E-01 |
| 742 | 1.036E-01 |
| 749 | 1.027E-01 |
| 756 | 8.345E-02 |
| 763 | 6.530E-02 |
| 769 | 9.642E-02 |
| 776 | 9.888E-02 |
| 783 | 9.787E-02 |
| 789 | 9.689E-02 |
| 796 | 9.588E-02 |
| 803 | 8.834E-02 |
| 809 | 8.257E-02 |
| 816 | 8.623E-02 |
| 823 | 8.988E-02 |
| 830 | 9.023E-02 |
| 836 | 8.302E-02 |
| 843 | 5.066E-02 |
| 850 | 3.478E-02 |
| 856 | 3.675E-02 |
| 863 | 3.611E-02 |
| 870 | 3.251E-02 |
| 877 | 3.217E-02 |
| 883 | 3.240E-02 |
| 890 | 3.263E-02 |
| 897 | 3.290E-02 |
| 903 | 3.342E-02 |
| 910 | 3.422E-02 |
| 917 | 3.157E-02 |
| 923 | 1.918E-02 |
| 930 | 1.172E-02 |
| 937 | 1.717E-02 |
| 944 | 1.919E-02 |
| 950 | 1.836E-02 |
| 957 | 2.122E-02 |
| 964 | 2.295E-02 |
| 970 | 3.851E-02 |
| 977 | 5.074E-02 |
| 984 | 4.825E-02 |
| 991 | 4.941E-02 |
| 997 | 5.137E-02 |
| 1004 | 5.334E-02 |
| 1011 | 5.530E-02 |
| 1017 | 5.726E-02 |
| 1024 | 5.633E-02 |
| 1031 | 5.506E-02 |
| 1037 | 5.380E-02 |
| 1044 | 5.253E-02 |
| 1051 | 5.127E-02 |
| 1058 | 5.000E-02 |
| 1064 | 4.874E-02 |
| 1071 | 4.747E-02 |
| 1078 | 4.621E-02 |
| 1084 | 4.493E-02 |
| 1091 | 4.362E-02 |
| 1098 | 4.565E-02 |
| 1104 | 4.377E-02 |
| 1111 | 3.326E-02 |
| 1118 | 2.275E-02 |
| 1125 | 1.223E-02 |
| 1131 | 8.228E-03 |
| 1138 | 8.178E-03 |
| 1145 | 1.150E-02 |
| 1151 | 1.357E-02 |
| 1158 | 1.848E-02 |
| 1165 | 2.339E-02 |
| 1172 | 2.831E-02 |
| 1178 | 3.309E-02 |
| 1185 | 3.401E-02 |
| 1192 | 3.917E-02 |
| 1198 | 4.046E-02 |
| 1205 | 3.904E-02 |
| 1212 | 3.761E-02 |
| 1218 | 3.618E-02 |
| 1225 | 3.568E-02 |
| 1232 | 3.622E-02 |
| 1239 | 3.597E-02 |
| 1245 | 3.443E-02 |
| 1252 | 3.289E-02 |
| 1259 | 3.135E-02 |
| 1265 | 3.041E-02 |
| 1272 | 3.184E-02 |
| 1279 | 3.248E-02 |
| 1285 | 3.200E-02 |
| 1292 | 3.057E-02 |
| 1299 | 2.855E-02 |
| 1306 | 2.653E-02 |
| 1312 | 2.451E-02 |
| 1319 | 2.170E-02 |
| 1326 | 1.863E-02 |
| 1332 | 1.556E-02 |
| 1339 | 1.317E-02 |
| 1346 | 1.122E-02 |
| 1353 | 9.261E-03 |
| 1359 | 7.305E-03 |
| 1366 | 5.349E-03 |
| 1373 | 3.392E-03 |
| 1379 | 1.436E-03 |
| 1386 | 1.425E-04 |
| 1393 | 3.708E-04 |
| 1399 | 5.991E-04 |
| 1406 | 8.274E-04 |
| 1413 | 1.056E-03 |
| 1420 | 1.284E-03 |
| 1426 | 1.512E-03 |
| 1433 | 1.822E-03 |
| 1440 | 2.617E-03 |
| 1446 | 3.412E-03 |
| 1453 | 4.207E-03 |
| 1460 | 4.561E-03 |
| 1466 | 4.291E-03 |
| 1473 | 4.386E-03 |
| 1480 | 6.181E-03 |
| 1487 | 7.976E-03 |
| 1493 | 9.771E-03 |
| 1500 | 1.157E-02 |

| λ (nm) | I(D/SP) mW/cm$^2$nm |
|---|---|
| 300 | 1.239E-04 |
| 307 | 6.542E-04 |
| 313 | 2.726E-03 |
| 320 | 1.004E-02 |
| 327 | 1.518E-02 |
| 334 | 2.015E-02 |
| 340 | 2.488E-02 |
| 347 | 2.746E-02 |
| 354 | 3.034E-02 |
| 360 | 3.284E-02 |
| 367 | 3.770E-02 |
| 374 | 4.060E-02 |
| 380 | 4.162E-02 |
| 387 | 4.299E-02 |
| 394 | 4.810E-02 |
| 401 | 6.280E-02 |
| 407 | 7.572E-02 |
| 414 | 8.189E-02 |
| 421 | 8.330E-02 |
| 427 | 8.257E-02 |
| 434 | 8.497E-02 |
| 441 | 9.683E-02 |
| 447 | 1.076E-01 |
| 454 | 1.150E-01 |
| 461 | 1.179E-01 |
| 468 | 1.188E-01 |
| 474 | 1.212E-01 |
| 481 | 1.241E-01 |
| 488 | 1.207E-01 |
| 494 | 1.228E-01 |
| 501 | 1.234E-01 |
| 508 | 1.223E-01 |
| 515 | 1.196E-01 |
| 521 | 1.208E-01 |
| 528 | 1.226E-01 |
| 535 | 1.220E-01 |
| 541 | 1.202E-01 |
| 548 | 1.188E-01 |
| 555 | 1.186E-01 |
| 561 | 1.178E-01 |
| 568 | 1.194E-01 |
| 575 | 1.209E-01 |
| 582 | 1.213E-01 |
| 588 | 1.214E-01 |
| 595 | 1.206E-01 |
| 602 | 1.199E-01 |
| 608 | 1.195E-01 |
| 615 | 1.192E-01 |
| 622 | 1.187E-01 |
| 628 | 1.183E-01 |
| 635 | 1.180E-01 |
| 642 | 1.177E-01 |
| 649 | 1.171E-01 |
| 655 | 1.166E-01 |
| 662 | 1.160E-01 |
| 669 | 1.151E-01 |
| 675 | 1.143E-01 |
| 682 | 1.136E-01 |
| 689 | 1.130E-01 |
| 696 | 1.027E-01 |
| 702 | 1.109E-01 |
| 709 | 1.100E-01 |
| 716 | 1.088E-01 |
| 722 | 1.046E-01 |
| 729 | 1.026E-01 |
| 736 | 1.055E-01 |
| 742 | 1.043E-01 |
| 749 | 1.032E-01 |
| 756 | 8.737E-02 |
| 763 | 7.237E-02 |
| 769 | 9.727E-02 |
| 776 | 9.895E-02 |
| 783 | 9.783E-02 |
| 789 | 9.673E-02 |
| 796 | 9.562E-02 |
| 803 | 9.067E-02 |
| 809 | 8.677E-02 |
| 816 | 8.839E-02 |
| 823 | 9.001E-02 |
| 830 | 8.970E-02 |
| 836 | 8.441E-02 |
| 843 | 6.208E-02 |
| 850 | 5.111E-02 |
| 856 | 5.243E-02 |
| 863 | 5.161E-02 |
| 870 | 4.834E-02 |
| 877 | 4.778E-02 |
| 883 | 4.771E-02 |
| 890 | 4.766E-02 |
| 897 | 4.764E-02 |
| 903 | 4.789E-02 |
| 910 | 4.839E-02 |
| 917 | 4.572E-02 |
| 923 | 3.416E-02 |
| 930 | 2.597E-02 |
| 937 | 3.201E-02 |
| 944 | 3.423E-02 |
| 950 | 3.330E-02 |
| 957 | 3.594E-02 |
| 964 | 3.738E-02 |
| 970 | 4.905E-02 |
| 977 | 5.815E-02 |
| 984 | 5.615E-02 |
| 991 | 5.687E-02 |
| 997 | 5.818E-02 |
| 1004 | 5.948E-02 |
| 1011 | 6.079E-02 |
| 1017 | 6.209E-02 |
| 1024 | 6.132E-02 |
| 1031 | 6.031E-02 |
| 1037 | 5.929E-02 |
| 1044 | 5.828E-02 |
| 1051 | 5.727E-02 |
| 1058 | 5.626E-02 |
| 1064 | 5.524E-02 |
| 1071 | 5.423E-02 |
| 1078 | 5.322E-02 |
| 1084 | 5.156E-02 |
| 1091 | 4.871E-02 |
| 1098 | 5.117E-02 |
| 1104 | 4.524E-02 |
| 1111 | 3.696E-02 |
| 1118 | 2.868E-02 |
| 1125 | 2.040E-02 |
| 1131 | 1.787E-02 |
| 1138 | 1.764E-02 |
| 1145 | 2.138E-02 |
| 1151 | 2.315E-02 |
| 1158 | 2.782E-02 |
| 1165 | 3.248E-02 |
| 1172 | 3.714E-02 |
| 1178 | 4.166E-02 |
| 1185 | 4.167E-02 |
| 1192 | 4.177E-02 |
| 1198 | 4.153E-02 |
| 1205 | 4.117E-02 |
| 1212 | 4.081E-02 |
| 1218 | 4.045E-02 |
| 1225 | 4.018E-02 |
| 1232 | 4.002E-02 |
| 1239 | 3.916E-02 |
| 1245 | 3.717E-02 |
| 1252 | 3.517E-02 |
| 1259 | 3.318E-02 |
| 1265 | 3.180E-02 |
| 1272 | 3.285E-02 |
| 1279 | 3.397E-02 |
| 1285 | 3.522E-02 |
| 1292 | 3.500E-02 |
| 1299 | 3.391E-02 |
| 1306 | 3.282E-02 |
| 1312 | 3.173E-02 |
| 1319 | 2.891E-02 |
| 1326 | 2.551E-02 |
| 1332 | 2.210E-02 |
| 1339 | 1.912E-02 |
| 1346 | 1.641E-02 |
| 1353 | 1.371E-02 |
| 1359 | 1.100E-02 |
| 1366 | 8.290E-03 |
| 1373 | 5.583E-03 |
| 1379 | 2.876E-03 |
| 1386 | 1.194E-03 |
| 1393 | 1.867E-03 |
| 1399 | 2.541E-03 |
| 1406 | 3.214E-03 |
| 1413 | 3.888E-03 |
| 1420 | 4.561E-03 |
| 1426 | 5.235E-03 |
| 1433 | 5.979E-03 |
| 1440 | 7.145E-03 |
| 1446 | 8.311E-03 |
| 1453 | 9.477E-03 |
| 1460 | 1.000E-02 |
| 1466 | 9.615E-03 |
| 1473 | 9.556E-03 |
| 1480 | 1.102E-02 |
| 1487 | 1.248E-02 |
| 1493 | 1.394E-02 |
| 1500 | 1.540E-02 |

| λ (nm) | I(D/S) mW/cm$^2$nm |
|---|---|
| 300 | 1.315E-04 |
| 307 | 7.549E-04 |
| 313 | 3.356E-03 |
| 320 | 1.310E-02 |
| 327 | 1.952E-02 |
| 334 | 2.556E-02 |
| 340 | 3.114E-02 |
| 347 | 3.381E-02 |
| 354 | 3.676E-02 |
| 360 | 3.916E-02 |
| 367 | 4.437E-02 |
| 374 | 4.719E-02 |
| 380 | 4.777E-02 |
| 387 | 4.886E-02 |
| 394 | 5.414E-02 |
| 401 | 7.002E-02 |
| 407 | 8.386E-02 |
| 414 | 9.011E-02 |
| 421 | 9.106E-02 |
| 427 | 8.969E-02 |
| 434 | 9.169E-02 |
| 441 | 1.038E-01 |
| 447 | 1.146E-01 |
| 454 | 1.219E-01 |
| 461 | 1.246E-01 |
| 468 | 1.250E-01 |
| 474 | 1.270E-01 |
| 481 | 1.296E-01 |
| 488 | 1.256E-01 |
| 494 | 1.272E-01 |
| 501 | 1.275E-01 |
| 508 | 1.259E-01 |
| 515 | 1.228E-01 |
| 521 | 1.238E-01 |
| 528 | 1.253E-01 |
| 535 | 1.244E-01 |
| 541 | 1.223E-01 |
| 548 | 1.205E-01 |
| 555 | 1.201E-01 |
| 561 | 1.191E-01 |
| 568 | 1.205E-01 |
| 575 | 1.218E-01 |
| 582 | 1.221E-01 |
| 588 | 1.220E-01 |
| 595 | 1.210E-01 |
| 602 | 1.200E-01 |
| 608 | 1.196E-01 |
| 615 | 1.192E-01 |
| 622 | 1.187E-01 |
| 628 | 1.181E-01 |
| 635 | 1.178E-01 |
| 642 | 1.174E-01 |
| 649 | 1.168E-01 |
| 655 | 1.162E-01 |
| 662 | 1.155E-01 |
| 669 | 1.146E-01 |
| 675 | 1.138E-01 |
| 682 | 1.130E-01 |
| 689 | 1.123E-01 |
| 696 | 1.012E-01 |
| 702 | 1.102E-01 |
| 709 | 1.092E-01 |
| 716 | 1.080E-01 |
| 722 | 1.036E-01 |
| 729 | 1.014E-01 |
| 736 | 1.046E-01 |
| 742 | 1.034E-01 |
| 749 | 1.023E-01 |
| 756 | 8.810E-02 |
| 763 | 7.467E-02 |
| 769 | 9.657E-02 |
| 776 | 9.791E-02 |
| 783 | 9.677E-02 |
| 789 | 9.565E-02 |
| 796 | 9.452E-02 |
| 803 | 8.926E-02 |
| 809 | 8.514E-02 |
| 816 | 8.698E-02 |
| 823 | 8.882E-02 |
| 830 | 8.858E-02 |
| 836 | 8.306E-02 |
| 843 | 5.954E-02 |
| 850 | 4.799E-02 |
| 856 | 4.940E-02 |
| 863 | 4.861E-02 |
| 870 | 4.529E-02 |
| 877 | 4.477E-02 |
| 883 | 4.474E-02 |
| 890 | 4.473E-02 |
| 897 | 4.475E-02 |
| 903 | 4.503E-02 |
| 910 | 4.557E-02 |
| 917 | 4.290E-02 |
| 923 | 3.121E-02 |
| 930 | 2.310E-02 |
| 937 | 2.908E-02 |
| 944 | 3.129E-02 |
| 950 | 3.038E-02 |
| 957 | 3.306E-02 |
| 964 | 3.455E-02 |
| 970 | 4.669E-02 |
| 977 | 5.619E-02 |
| 984 | 5.415E-02 |
| 991 | 5.494E-02 |
| 997 | 5.634E-02 |
| 1004 | 5.774E-02 |
| 1011 | 5.915E-02 |
| 1017 | 6.055E-02 |
| 1024 | 5.977E-02 |
| 1031 | 5.874E-02 |
| 1037 | 5.771E-02 |
| 1044 | 5.668E-02 |
| 1051 | 5.565E-02 |
| 1058 | 5.462E-02 |
| 1064 | 5.359E-02 |
| 1071 | 5.256E-02 |
| 1078 | 5.153E-02 |
| 1084 | 4.991E-02 |
| 1091 | 4.718E-02 |
| 1098 | 4.966E-02 |
| 1104 | 4.472E-02 |
| 1111 | 3.603E-02 |
| 1118 | 2.735E-02 |
| 1125 | 1.866E-02 |
| 1131 | 1.589E-02 |
| 1138 | 1.569E-02 |
| 1145 | 1.939E-02 |
| 1151 | 2.123E-02 |
| 1158 | 2.596E-02 |
| 1165 | 3.069E-02 |
| 1172 | 3.542E-02 |
| 1178 | 4.000E-02 |
| 1185 | 4.012E-02 |
| 1192 | 4.100E-02 |
| 1198 | 4.107E-02 |
| 1205 | 4.050E-02 |
| 1212 | 3.992E-02 |
| 1218 | 3.935E-02 |
| 1225 | 3.901E-02 |
| 1232 | 3.892E-02 |
| 1239 | 3.824E-02 |
| 1245 | 3.658E-02 |
| 1252 | 3.491E-02 |
| 1259 | 3.325E-02 |
| 1265 | 3.210E-02 |
| 1272 | 3.297E-02 |
| 1279 | 3.375E-02 |
| 1285 | 3.442E-02 |
| 1292 | 3.393E-02 |
| 1299 | 3.276E-02 |
| 1306 | 3.158E-02 |
| 1312 | 3.040E-02 |
| 1319 | 2.757E-02 |
| 1326 | 2.418E-02 |
| 1332 | 2.079E-02 |
| 1339 | 1.790E-02 |
| 1346 | 1.533E-02 |
| 1353 | 1.276E-02 |
| 1359 | 1.019E-02 |
| 1366 | 7.625E-03 |
| 1373 | 5.056E-03 |
| 1379 | 2.488E-03 |
| 1386 | 8.758E-04 |
| 1393 | 1.461E-03 |
| 1399 | 2.046E-03 |
| 1406 | 2.631E-03 |
| 1413 | 3.216E-03 |
| 1420 | 3.801E-03 |
| 1426 | 4.386E-03 |
| 1433 | 5.047E-03 |
| 1440 | 6.162E-03 |
| 1446 | 7.277E-03 |
| 1453 | 8.391E-03 |
| 1460 | 8.893E-03 |
| 1466 | 8.527E-03 |
| 1473 | 8.493E-03 |
| 1480 | 1.000E-02 |
| 1487 | 1.151E-02 |
| 1493 | 1.302E-02 |
| 1500 | 1.453E-02 |

| λ (nm) | I(D/SH) mW/cm$^2$nm |
|---|---|
| 300 | 1.064E-04 |
| 307 | 6.096E-04 |
| 313 | 2.706E-03 |
| 320 | 1.056E-02 |
| 327 | 1.571E-02 |
| 334 | 2.054E-02 |
| 340 | 2.501E-02 |
| 347 | 2.713E-02 |
| 354 | 2.947E-02 |
| 360 | 3.137E-02 |
| 367 | 3.553E-02 |
| 374 | 3.777E-02 |
| 380 | 3.822E-02 |
| 387 | 3.908E-02 |
| 394 | 4.329E-02 |
| 401 | 5.597E-02 |
| 407 | 6.702E-02 |
| 414 | 7.200E-02 |
| 421 | 7.276E-02 |
| 427 | 7.165E-02 |
| 434 | 7.325E-02 |
| 441 | 8.294E-02 |
| 447 | 9.156E-02 |
| 454 | 9.738E-02 |
| 461 | 9.953E-02 |
| 468 | 9.992E-02 |
| 474 | 1.015E-01 |
| 481 | 1.036E-01 |
| 488 | 1.004E-01 |
| 494 | 1.017E-01 |
| 501 | 1.020E-01 |
| 508 | 1.007E-01 |
| 515 | 9.830E-02 |
| 521 | 9.909E-02 |
| 528 | 1.003E-01 |
| 535 | 9.968E-02 |
| 541 | 9.799E-02 |
| 548 | 9.659E-02 |
| 555 | 9.629E-02 |
| 561 | 9.556E-02 |
| 568 | 9.673E-02 |
| 575 | 9.778E-02 |
| 582 | 9.803E-02 |
| 588 | 9.798E-02 |
| 595 | 9.722E-02 |
| 602 | 9.652E-02 |
| 608 | 9.624E-02 |
| 615 | 9.593E-02 |
| 622 | 9.554E-02 |
| 628 | 9.515E-02 |
| 635 | 9.494E-02 |
| 642 | 9.468E-02 |
| 649 | 9.419E-02 |
| 655 | 9.375E-02 |
| 662 | 9.324E-02 |
| 669 | 9.258E-02 |
| 675 | 9.193E-02 |
| 682 | 9.133E-02 |
| 689 | 9.083E-02 |
| 696 | 7.665E-02 |
| 702 | 8.919E-02 |
| 709 | 8.843E-02 |
| 716 | 8.748E-02 |
| 722 | 8.217E-02 |
| 729 | 7.986E-02 |
| 736 | 8.483E-02 |
| 742 | 8.388E-02 |
| 749 | 8.306E-02 |
| 756 | 7.155E-02 |
| 763 | 6.068E-02 |
| 769 | 7.852E-02 |
| 776 | 7.964E-02 |
| 783 | 7.875E-02 |
| 789 | 7.787E-02 |
| 796 | 7.698E-02 |
| 803 | 7.048E-02 |
| 809 | 6.554E-02 |
| 816 | 6.875E-02 |
| 823 | 7.195E-02 |
| 830 | 7.231E-02 |
| 836 | 6.627E-02 |
| 843 | 3.913E-02 |
| 850 | 2.580E-02 |
| 856 | 2.741E-02 |
| 863 | 2.692E-02 |
| 870 | 2.403E-02 |
| 877 | 2.378E-02 |
| 883 | 2.397E-02 |
| 890 | 2.418E-02 |
| 897 | 2.440E-02 |
| 903 | 2.484E-02 |
| 910 | 2.550E-02 |
| 917 | 2.344E-02 |
| 923 | 1.370E-02 |
| 930 | 8.006E-03 |
| 937 | 1.215E-02 |
| 944 | 1.368E-02 |
| 950 | 1.307E-02 |
| 957 | 1.528E-02 |
| 964 | 1.665E-02 |
| 970 | 2.941E-02 |
| 977 | 3.945E-02 |
| 984 | 3.740E-02 |
| 991 | 3.835E-02 |
| 997 | 3.996E-02 |
| 1004 | 4.156E-02 |
| 1011 | 4.317E-02 |
| 1017 | 4.477E-02 |
| 1024 | 4.399E-02 |
| 1031 | 4.293E-02 |
| 1037 | 4.187E-02 |
| 1044 | 4.082E-02 |
| 1051 | 3.976E-02 |
| 1058 | 3.871E-02 |
| 1064 | 3.765E-02 |
| 1071 | 3.660E-02 |
| 1078 | 3.554E-02 |
| 1084 | 3.464E-02 |
| 1091 | 3.402E-02 |
| 1098 | 3.541E-02 |
| 1104 | 3.621E-02 |
| 1111 | 2.722E-02 |
| 1118 | 1.823E-02 |
| 1125 | 9.245E-03 |
| 1131 | 5.670E-03 |
| 1138 | 5.649E-03 |
| 1145 | 8.173E-03 |
| 1151 | 9.807E-03 |
| 1158 | 1.364E-02 |
| 1165 | 1.747E-02 |
| 1172 | 2.130E-02 |
| 1178 | 2.504E-02 |
| 1185 | 2.593E-02 |
| 1192 | 3.183E-02 |
| 1198 | 3.336E-02 |
| 1205 | 3.173E-02 |
| 1212 | 3.010E-02 |
| 1218 | 2.847E-02 |
| 1225 | 2.787E-02 |
| 1232 | 2.845E-02 |
| 1239 | 2.862E-02 |
| 1245 | 2.813E-02 |
| 1252 | 2.763E-02 |
| 1259 | 2.714E-02 |
| 1265 | 2.689E-02 |
| 1272 | 2.763E-02 |
| 1279 | 2.735E-02 |
| 1285 | 2.564E-02 |
| 1292 | 2.389E-02 |
| 1299 | 2.212E-02 |
| 1306 | 2.035E-02 |
| 1312 | 1.858E-02 |
| 1319 | 1.640E-02 |
| 1326 | 1.408E-02 |
| 1332 | 1.176E-02 |
| 1339 | 9.956E-03 |
| 1346 | 8.474E-03 |
| 1353 | 6.993E-03 |
| 1359 | 5.512E-03 |
| 1366 | 4.031E-03 |
| 1373 | 2.549E-03 |
| 1379 | 1.068E-03 |
| 1386 | 8.099E-05 |
| 1393 | 2.295E-04 |
| 1399 | 3.779E-04 |
| 1406 | 5.264E-04 |
| 1413 | 6.749E-04 |
| 1420 | 8.233E-04 |
| 1426 | 9.718E-04 |
| 1433 | 1.183E-03 |
| 1440 | 1.769E-03 |
| 1446 | 2.355E-03 |
| 1453 | 2.942E-03 |
| 1460 | 3.202E-03 |
| 1466 | 3.001E-03 |
| 1473 | 3.099E-03 |
| 1480 | 4.587E-03 |
| 1487 | 6.074E-03 |
| 1493 | 7.562E-03 |
| 1500 | 9.050E-03 |

| λ (nm) | I(D/F) mW/cm$^2$nm |
|---|---|
| 300 | 6.048E-06 |
| 307 | 9.542E-05 |
| 313 | 8.752E-04 |
| 320 | 6.624E-03 |
| 327 | 1.086E-02 |
| 334 | 1.555E-02 |
| 340 | 2.066E-02 |
| 347 | 2.292E-02 |
| 354 | 2.546E-02 |
| 360 | 2.769E-02 |
| 367 | 3.178E-02 |
| 374 | 3.422E-02 |
| 380 | 3.506E-02 |
| 387 | 3.621E-02 |
| 394 | 4.051E-02 |
| 401 | 5.287E-02 |
| 407 | 6.373E-02 |
| 414 | 6.890E-02 |
| 421 | 7.008E-02 |
| 427 | 6.947E-02 |
| 434 | 7.148E-02 |
| 441 | 8.145E-02 |
| 447 | 9.049E-02 |
| 454 | 9.664E-02 |
| 461 | 9.904E-02 |
| 468 | 9.969E-02 |
| 474 | 1.016E-01 |
| 481 | 1.039E-01 |
| 488 | 1.010E-01 |
| 494 | 1.026E-01 |
| 501 | 1.031E-01 |
| 508 | 1.019E-01 |
| 515 | 9.946E-02 |
| 521 | 1.003E-01 |
| 528 | 1.016E-01 |
| 535 | 1.010E-01 |
| 541 | 9.933E-02 |
| 548 | 9.795E-02 |
| 555 | 9.766E-02 |
| 561 | 9.694E-02 |
| 568 | 9.814E-02 |
| 575 | 9.922E-02 |
| 582 | 9.949E-02 |
| 588 | 9.944E-02 |
| 595 | 9.868E-02 |
| 602 | 9.806E-02 |
| 608 | 9.811E-02 |
| 615 | 9.813E-02 |
| 622 | 9.806E-02 |
| 628 | 9.800E-02 |
| 635 | 9.811E-02 |
| 642 | 9.817E-02 |
| 649 | 9.800E-02 |
| 655 | 9.776E-02 |
| 662 | 9.743E-02 |
| 669 | 9.693E-02 |
| 675 | 9.644E-02 |
| 682 | 9.601E-02 |
| 689 | 9.567E-02 |
| 696 | 8.198E-02 |
| 702 | 9.429E-02 |
| 709 | 9.355E-02 |
| 716 | 9.260E-02 |
| 722 | 8.742E-02 |
| 729 | 8.517E-02 |
| 736 | 8.999E-02 |
| 742 | 8.904E-02 |
| 749 | 8.823E-02 |
| 756 | 7.471E-02 |
| 763 | 6.194E-02 |
| 769 | 8.332E-02 |
| 776 | 8.483E-02 |
| 783 | 8.393E-02 |
| 789 | 8.305E-02 |
| 796 | 8.216E-02 |
| 803 | 7.574E-02 |
| 809 | 7.084E-02 |
| 816 | 7.394E-02 |
| 823 | 7.704E-02 |
| 830 | 7.733E-02 |
| 836 | 7.119E-02 |
| 843 | 4.363E-02 |
| 850 | 3.012E-02 |
| 856 | 3.180E-02 |
| 863 | 3.125E-02 |
| 870 | 2.816E-02 |
| 877 | 2.787E-02 |
| 883 | 2.806E-02 |
| 890 | 2.826E-02 |
| 897 | 2.849E-02 |
| 903 | 2.894E-02 |
| 910 | 2.963E-02 |
| 917 | 2.735E-02 |
| 923 | 1.671E-02 |
| 930 | 1.027E-02 |
| 937 | 1.499E-02 |
| 944 | 1.674E-02 |
| 950 | 1.605E-02 |
| 957 | 1.850E-02 |
| 964 | 1.999E-02 |
| 970 | 3.333E-02 |
| 977 | 4.383E-02 |
| 984 | 4.170E-02 |
| 991 | 4.271E-02 |
| 997 | 4.441E-02 |
| 1004 | 4.611E-02 |
| 1011 | 4.780E-02 |
| 1017 | 4.950E-02 |
| 1024 | 4.870E-02 |
| 1031 | 4.762E-02 |
| 1037 | 4.654E-02 |
| 1044 | 4.546E-02 |
| 1051 | 4.439E-02 |
| 1058 | 4.331E-02 |
| 1064 | 4.223E-02 |
| 1071 | 4.115E-02 |
| 1078 | 4.007E-02 |
| 1084 | 3.896E-02 |
| 1091 | 3.779E-02 |
| 1098 | 3.960E-02 |
| 1104 | 3.873E-02 |
| 1111 | 2.943E-02 |
| 1118 | 2.013E-02 |
| 1125 | 1.083E-02 |
| 1131 | 7.268E-03 |
| 1138 | 7.225E-03 |
| 1145 | 1.012E-02 |
| 1151 | 1.193E-02 |
| 1158 | 1.622E-02 |
| 1165 | 2.050E-02 |
| 1172 | 2.479E-02 |
| 1178 | 2.896E-02 |
| 1185 | 2.975E-02 |
| 1192 | 3.463E-02 |
| 1198 | 3.585E-02 |
| 1205 | 3.447E-02 |
| 1212 | 3.309E-02 |
| 1218 | 3.171E-02 |
| 1225 | 3.120E-02 |
| 1232 | 3.167E-02 |
| 1239 | 3.160E-02 |
| 1245 | 3.066E-02 |
| 1252 | 2.971E-02 |
| 1259 | 2.877E-02 |
| 1265 | 2.820E-02 |
| 1272 | 2.914E-02 |
| 1279 | 2.928E-02 |
| 1285 | 2.830E-02 |
| 1292 | 2.685E-02 |
| 1299 | 2.511E-02 |
| 1306 | 2.337E-02 |
| 1312 | 2.163E-02 |
| 1319 | 1.918E-02 |
| 1326 | 1.647E-02 |
| 1332 | 1.377E-02 |
| 1339 | 1.166E-02 |
| 1346 | 9.927E-03 |
| 1353 | 8.196E-03 |
| 1359 | 6.466E-03 |
| 1366 | 4.735E-03 |
| 1373 | 3.005E-03 |
| 1379 | 1.274E-03 |
| 1386 | 1.316E-04 |
| 1393 | 3.388E-04 |
| 1399 | 5.460E-04 |
| 1406 | 7.532E-04 |
| 1413 | 9.604E-04 |
| 1420 | 1.168E-03 |
| 1426 | 1.375E-03 |
| 1433 | 1.654E-03 |
| 1440 | 2.365E-03 |
| 1446 | 3.076E-03 |
| 1453 | 3.787E-03 |
| 1460 | 4.104E-03 |
| 1466 | 3.865E-03 |
| 1473 | 3.949E-03 |
| 1480 | 5.537E-03 |
| 1487 | 7.125E-03 |
| 1493 | 8.713E-03 |
| 1500 | 1.030E-02 |

| λ (nm) | I(H/W) mW/cm$^2$nm |
|---|---|
| 300 | 3.043E-06 |
| 307 | 1.181E-04 |
| 313 | 1.328E-03 |
| 320 | 1.221E-02 |
| 327 | 1.894E-02 |
| 334 | 2.587E-02 |
| 340 | 3.308E-02 |
| 347 | 3.432E-02 |
| 354 | 3.595E-02 |
| 360 | 3.720E-02 |
| 367 | 4.046E-02 |
| 374 | 4.156E-02 |
| 380 | 4.088E-02 |
| 387 | 4.046E-02 |
| 394 | 4.362E-02 |
| 401 | 5.505E-02 |
| 407 | 6.398E-02 |
| 414 | 6.693E-02 |
| 421 | 6.610E-02 |
| 427 | 6.382E-02 |
| 434 | 6.415E-02 |
| 441 | 7.159E-02 |
| 447 | 7.809E-02 |
| 454 | 8.165E-02 |
| 461 | 8.189E-02 |
| 468 | 8.082E-02 |
| 474 | 8.085E-02 |
| 481 | 8.137E-02 |
| 488 | 7.788E-02 |
| 494 | 7.802E-02 |
| 501 | 7.734E-02 |
| 508 | 7.530E-02 |
| 515 | 7.248E-02 |
| 521 | 7.214E-02 |
| 528 | 7.219E-02 |
| 535 | 7.093E-02 |
| 541 | 6.903E-02 |
| 548 | 6.739E-02 |
| 555 | 6.650E-02 |
| 561 | 6.533E-02 |
| 568 | 6.550E-02 |
| 575 | 6.562E-02 |
| 582 | 6.524E-02 |
| 588 | 6.468E-02 |
| 595 | 6.370E-02 |
| 602 | 6.286E-02 |
| 608 | 6.251E-02 |
| 615 | 6.217E-02 |
| 622 | 6.180E-02 |
| 628 | 6.146E-02 |
| 635 | 6.125E-02 |
| 642 | 6.103E-02 |
| 649 | 6.068E-02 |
| 655 | 6.025E-02 |
| 662 | 5.977E-02 |
| 669 | 5.920E-02 |
| 675 | 5.866E-02 |
| 682 | 5.817E-02 |
| 689 | 5.775E-02 |
| 696 | 4.923E-02 |
| 702 | 5.651E-02 |
| 709 | 5.584E-02 |
| 716 | 5.505E-02 |
| 722 | 5.174E-02 |
| 729 | 5.022E-02 |
| 736 | 5.291E-02 |
| 742 | 5.218E-02 |
| 749 | 5.154E-02 |
| 756 | 4.173E-02 |
| 763 | 3.255E-02 |
| 769 | 4.790E-02 |
| 776 | 4.897E-02 |
| 783 | 4.833E-02 |
| 789 | 4.770E-02 |
| 796 | 4.707E-02 |
| 803 | 4.325E-02 |
| 809 | 4.032E-02 |
| 816 | 4.200E-02 |
| 823 | 4.367E-02 |
| 830 | 4.373E-02 |
| 836 | 4.014E-02 |
| 843 | 2.444E-02 |
| 850 | 1.675E-02 |
| 856 | 1.765E-02 |
| 863 | 1.731E-02 |
| 870 | 1.555E-02 |
| 877 | 1.536E-02 |
| 883 | 1.544E-02 |
| 890 | 1.553E-02 |
| 897 | 1.562E-02 |
| 903 | 1.585E-02 |
| 910 | 1.620E-02 |
| 917 | 1.492E-02 |
| 923 | 9.050E-03 |
| 930 | 5.521E-03 |
| 937 | 8.078E-03 |
| 944 | 9.015E-03 |
| 950 | 8.624E-03 |
| 957 | 9.940E-03 |
| 964 | 1.073E-02 |
| 970 | 1.799E-02 |
| 977 | 2.368E-02 |
| 984 | 2.248E-02 |
| 991 | 2.300E-02 |
| 997 | 2.388E-02 |
| 1004 | 2.477E-02 |
| 1011 | 2.565E-02 |
| 1017 | 2.653E-02 |
| 1024 | 2.607E-02 |
| 1031 | 2.546E-02 |
| 1037 | 2.485E-02 |
| 1044 | 2.424E-02 |
| 1051 | 2.364E-02 |
| 1058 | 2.303E-02 |
| 1064 | 2.243E-02 |
| 1071 | 2.183E-02 |
| 1078 | 2.123E-02 |
| 1084 | 2.062E-02 |
| 1091 | 2.000E-02 |
| 1098 | 2.092E-02 |
| 1104 | 2.004E-02 |
| 1111 | 1.521E-02 |
| 1118 | 1.040E-02 |
| 1125 | 5.588E-03 |
| 1131 | 3.755E-03 |
| 1138 | 3.730E-03 |
| 1145 | 5.240E-03 |
| 1151 | 6.180E-03 |
| 1158 | 8.411E-03 |
| 1165 | 1.064E-02 |
| 1172 | 1.287E-02 |
| 1178 | 1.503E-02 |
| 1185 | 1.544E-02 |
| 1192 | 1.777E-02 |
| 1198 | 1.835E-02 |
| 1205 | 1.769E-02 |
| 1212 | 1.703E-02 |
| 1218 | 1.638E-02 |
| 1225 | 1.614E-02 |
| 1232 | 1.638E-02 |
| 1239 | 1.625E-02 |
| 1245 | 1.555E-02 |
| 1252 | 1.485E-02 |
| 1259 | 1.414E-02 |
| 1265 | 1.371E-02 |
| 1272 | 1.435E-02 |
| 1279 | 1.463E-02 |
| 1285 | 1.441E-02 |
| 1292 | 1.376E-02 |
| 1299 | 1.284E-02 |
| 1306 | 1.193E-02 |
| 1312 | 1.101E-02 |
| 1319 | 9.751E-03 |
| 1326 | 8.367E-03 |
| 1332 | 6.986E-03 |
| 1339 | 5.911E-03 |
| 1346 | 5.031E-03 |
| 1353 | 4.152E-03 |
| 1359 | 3.274E-03 |
| 1366 | 2.396E-03 |
| 1373 | 1.519E-03 |
| 1379 | 6.429E-04 |
| 1386 | 6.377E-05 |
| 1393 | 1.659E-04 |
| 1399 | 2.679E-04 |
| 1406 | 3.699E-04 |
| 1413 | 4.717E-04 |
| 1420 | 5.736E-04 |
| 1426 | 6.753E-04 |
| 1433 | 8.133E-04 |
| 1440 | 1.168E-03 |
| 1446 | 1.522E-03 |
| 1453 | 1.876E-03 |
| 1460 | 2.033E-03 |
| 1466 | 1.913E-03 |
| 1473 | 1.955E-03 |
| 1480 | 2.754E-03 |
| 1487 | 3.552E-03 |
| 1493 | 4.350E-03 |
| 1500 | 5.148E-03 |

| λ (nm) | I(H/SP) mW/cm$^2$nm |
|---|---|
| 300 | 3.759E-04 |
| 307 | 1.757E-03 |
| 313 | 6.575E-03 |
| 320 | 2.201E-02 |
| 327 | 3.056E-02 |
| 334 | 3.757E-02 |
| 340 | 4.332E-02 |
| 347 | 4.496E-02 |
| 354 | 4.699E-02 |
| 360 | 4.836E-02 |
| 367 | 5.303E-02 |
| 374 | 5.478E-02 |
| 380 | 5.404E-02 |
| 387 | 5.391E-02 |
| 394 | 5.842E-02 |
| 401 | 7.405E-02 |
| 407 | 8.688E-02 |
| 414 | 9.162E-02 |
| 421 | 9.105E-02 |
| 427 | 8.833E-02 |
| 434 | 8.908E-02 |
| 441 | 9.963E-02 |
| 447 | 1.088E-01 |
| 454 | 1.144E-01 |
| 461 | 1.155E-01 |
| 468 | 1.148E-01 |
| 474 | 1.155E-01 |
| 481 | 1.168E-01 |
| 488 | 1.122E-01 |
| 494 | 1.128E-01 |
| 501 | 1.123E-01 |
| 508 | 1.101E-01 |
| 515 | 1.066E-01 |
| 521 | 1.068E-01 |
| 528 | 1.074E-01 |
| 535 | 1.061E-01 |
| 541 | 1.038E-01 |
| 548 | 1.017E-01 |
| 555 | 1.009E-01 |
| 561 | 9.959E-02 |
| 568 | 1.003E-01 |
| 575 | 1.009E-01 |
| 582 | 1.007E-01 |
| 588 | 1.002E-01 |
| 595 | 9.906E-02 |
| 602 | 9.795E-02 |
| 608 | 9.722E-02 |
| 615 | 9.649E-02 |
| 622 | 9.569E-02 |
| 628 | 9.493E-02 |
| 635 | 9.435E-02 |
| 642 | 9.374E-02 |
| 649 | 9.293E-02 |
| 655 | 9.217E-02 |
| 662 | 9.136E-02 |
| 669 | 9.041E-02 |
| 675 | 8.949E-02 |
| 682 | 8.863E-02 |
| 689 | 8.789E-02 |
| 696 | 7.965E-02 |
| 702 | 8.582E-02 |
| 709 | 8.485E-02 |
| 716 | 8.371E-02 |
| 722 | 8.032E-02 |
| 729 | 7.859E-02 |
| 736 | 8.057E-02 |
| 742 | 7.948E-02 |
| 749 | 7.852E-02 |
| 756 | 6.630E-02 |
| 763 | 5.481E-02 |
| 769 | 7.352E-02 |
| 776 | 7.464E-02 |
| 783 | 7.366E-02 |
| 789 | 7.270E-02 |
| 796 | 7.173E-02 |
| 803 | 6.791E-02 |
| 809 | 6.487E-02 |
| 816 | 6.598E-02 |
| 823 | 6.708E-02 |
| 830 | 6.674E-02 |
| 836 | 6.271E-02 |
| 843 | 4.606E-02 |
| 850 | 3.787E-02 |
| 856 | 3.879E-02 |
| 863 | 3.813E-02 |
| 870 | 3.567E-02 |
| 877 | 3.521E-02 |
| 883 | 3.511E-02 |
| 890 | 3.503E-02 |
| 897 | 3.498E-02 |
| 903 | 3.512E-02 |
| 910 | 3.545E-02 |
| 917 | 3.346E-02 |
| 923 | 2.497E-02 |
| 930 | 1.897E-02 |
| 937 | 2.335E-02 |
| 944 | 2.495E-02 |
| 950 | 2.424E-02 |
| 957 | 2.614E-02 |
| 964 | 2.716E-02 |
| 970 | 3.560E-02 |
| 977 | 4.217E-02 |
| 984 | 4.069E-02 |
| 991 | 4.117E-02 |
| 997 | 4.208E-02 |
| 1004 | 4.299E-02 |
| 1011 | 4.390E-02 |
| 1017 | 4.480E-02 |
| 1024 | 4.421E-02 |
| 1031 | 4.345E-02 |
| 1037 | 4.268E-02 |
| 1044 | 4.192E-02 |
| 1051 | 4.117E-02 |
| 1058 | 4.041E-02 |
| 1064 | 3.966E-02 |
| 1071 | 3.890E-02 |
| 1078 | 3.815E-02 |
| 1084 | 3.694E-02 |
| 1091 | 3.487E-02 |
| 1098 | 3.661E-02 |
| 1104 | 3.235E-02 |
| 1111 | 2.641E-02 |
| 1118 | 2.048E-02 |
| 1125 | 1.456E-02 |
| 1131 | 1.275E-02 |
| 1138 | 1.258E-02 |
| 1145 | 1.523E-02 |
| 1151 | 1.649E-02 |
| 1158 | 1.980E-02 |
| 1165 | 2.310E-02 |
| 1172 | 2.641E-02 |
| 1178 | 2.960E-02 |
| 1185 | 2.959E-02 |
| 1192 | 2.965E-02 |
| 1198 | 2.947E-02 |
| 1205 | 2.920E-02 |
| 1212 | 2.893E-02 |
| 1218 | 2.866E-02 |
| 1225 | 2.845E-02 |
| 1232 | 2.833E-02 |
| 1239 | 2.771E-02 |
| 1245 | 2.629E-02 |
| 1252 | 2.487E-02 |
| 1259 | 2.345E-02 |
| 1265 | 2.246E-02 |
| 1272 | 2.319E-02 |
| 1279 | 2.398E-02 |
| 1285 | 2.484E-02 |
| 1292 | 2.468E-02 |
| 1299 | 2.391E-02 |
| 1306 | 2.313E-02 |
| 1312 | 2.235E-02 |
| 1319 | 2.036E-02 |
| 1326 | 1.795E-02 |
| 1332 | 1.555E-02 |
| 1339 | 1.345E-02 |
| 1346 | 1.154E-02 |
| 1353 | 9.632E-03 |
| 1359 | 7.727E-03 |
| 1366 | 5.823E-03 |
| 1373 | 3.920E-03 |
| 1379 | 2.018E-03 |
| 1386 | 8.378E-04 |
| 1393 | 1.310E-03 |
| 1399 | 1.782E-03 |
| 1406 | 2.253E-03 |
| 1413 | 2.724E-03 |
| 1420 | 3.195E-03 |
| 1426 | 3.666E-03 |
| 1433 | 4.186E-03 |
| 1440 | 5.001E-03 |
| 1446 | 5.815E-03 |
| 1453 | 6.629E-03 |
| 1460 | 6.993E-03 |
| 1466 | 6.722E-03 |
| 1473 | 6.679E-03 |
| 1480 | 7.699E-03 |
| 1487 | 8.718E-03 |
| 1493 | 9.736E-03 |
| 1500 | 1.075E-02 |

| λ (nm) | I(H/S) mW/$cm^2$nm |
|---|---|
| 300 | 3.249E-04 |
| 307 | 1.709E-03 |
| 313 | 7.036E-03 |
| 320 | 2.567E-02 |
| 327 | 3.601E-02 |
| 334 | 4.467E-02 |
| 340 | 5.186E-02 |
| 347 | 5.392E-02 |
| 354 | 5.638E-02 |
| 360 | 5.797E-02 |
| 367 | 6.361E-02 |
| 374 | 6.570E-02 |
| 380 | 6.475E-02 |
| 387 | 6.462E-02 |
| 394 | 7.001E-02 |
| 401 | 8.868E-02 |
| 407 | 1.042E-01 |
| 414 | 1.100E-01 |
| 421 | 1.093E-01 |
| 427 | 1.061E-01 |
| 434 | 1.069E-01 |
| 441 | 1.194E-01 |
| 447 | 1.302E-01 |
| 454 | 1.369E-01 |
| 461 | 1.383E-01 |
| 468 | 1.375E-01 |
| 474 | 1.383E-01 |
| 481 | 1.398E-01 |
| 488 | 1.343E-01 |
| 494 | 1.350E-01 |
| 501 | 1.342E-01 |
| 508 | 1.316E-01 |
| 515 | 1.275E-01 |
| 521 | 1.277E-01 |
| 528 | 1.284E-01 |
| 535 | 1.268E-01 |
| 541 | 1.239E-01 |
| 548 | 1.214E-01 |
| 555 | 1.204E-01 |
| 561 | 1.189E-01 |
| 568 | 1.197E-01 |
| 575 | 1.204E-01 |
| 582 | 1.202E-01 |
| 588 | 1.196E-01 |
| 595 | 1.181E-01 |
| 602 | 1.168E-01 |
| 608 | 1.160E-01 |
| 615 | 1.152E-01 |
| 622 | 1.143E-01 |
| 628 | 1.134E-01 |
| 635 | 1.127E-01 |
| 642 | 1.120E-01 |
| 649 | 1.111E-01 |
| 655 | 1.102E-01 |
| 662 | 1.093E-01 |
| 669 | 1.082E-01 |
| 675 | 1.071E-01 |
| 682 | 1.061E-01 |
| 689 | 1.052E-01 |
| 696 | 9.462E-02 |
| 702 | 1.028E-01 |
| 709 | 1.016E-01 |
| 716 | 1.003E-01 |
| 722 | 9.600E-02 |
| 729 | 9.385E-02 |
| 736 | 9.657E-02 |
| 742 | 9.527E-02 |
| 749 | 9.413E-02 |
| 756 | 8.091E-02 |
| 763 | 6.847E-02 |
| 769 | 8.841E-02 |
| 776 | 8.949E-02 |
| 783 | 8.831E-02 |
| 789 | 8.716E-02 |
| 796 | 8.600E-02 |
| 803 | 8.110E-02 |
| 809 | 7.725E-02 |
| 816 | 7.881E-02 |
| 823 | 8.037E-02 |
| 830 | 8.005E-02 |
| 836 | 7.496E-02 |
| 843 | 5.367E-02 |
| 850 | 4.321E-02 |
| 856 | 4.443E-02 |
| 863 | 4.366E-02 |
| 870 | 4.064E-02 |
| 877 | 4.012E-02 |
| 883 | 4.006E-02 |
| 890 | 4.001E-02 |
| 897 | 3.998E-02 |
| 903 | 4.019E-02 |
| 910 | 4.064E-02 |
| 917 | 3.822E-02 |
| 923 | 2.777E-02 |
| 930 | 2.054E-02 |
| 937 | 2.583E-02 |
| 944 | 2.777E-02 |
| 950 | 2.694E-02 |
| 957 | 2.929E-02 |
| 964 | 3.059E-02 |
| 970 | 4.131E-02 |
| 977 | 4.966E-02 |
| 984 | 4.782E-02 |
| 991 | 4.848E-02 |
| 997 | 4.968E-02 |
| 1004 | 5.088E-02 |
| 1011 | 5.208E-02 |
| 1017 | 5.328E-02 |
| 1024 | 5.256E-02 |
| 1031 | 5.161E-02 |
| 1037 | 5.067E-02 |
| 1044 | 4.974E-02 |
| 1051 | 4.880E-02 |
| 1058 | 4.787E-02 |
| 1064 | 4.693E-02 |
| 1071 | 4.600E-02 |
| 1078 | 4.507E-02 |
| 1084 | 4.363E-02 |
| 1091 | 4.122E-02 |
| 1098 | 4.336E-02 |
| 1104 | 3.902E-02 |
| 1111 | 3.142E-02 |
| 1118 | 2.384E-02 |
| 1125 | 1.626E-02 |
| 1131 | 1.383E-02 |
| 1138 | 1.366E-02 |
| 1145 | 1.686E-02 |
| 1151 | 1.845E-02 |
| 1158 | 2.255E-02 |
| 1165 | 2.665E-02 |
| 1172 | 3.074E-02 |
| 1178 | 3.470E-02 |
| 1185 | 3.479E-02 |
| 1192 | 3.559E-02 |
| 1198 | 3.558E-02 |
| 1205 | 3.507E-02 |
| 1212 | 3.455E-02 |
| 1218 | 3.404E-02 |
| 1225 | 3.373E-02 |
| 1232 | 3.364E-02 |
| 1239 | 3.304E-02 |
| 1245 | 3.159E-02 |
| 1252 | 3.014E-02 |
| 1259 | 2.869E-02 |
| 1265 | 2.769E-02 |
| 1272 | 2.843E-02 |
| 1279 | 2.909E-02 |
| 1285 | 2.965E-02 |
| 1292 | 2.922E-02 |
| 1299 | 2.820E-02 |
| 1306 | 2.717E-02 |
| 1312 | 2.615E-02 |
| 1319 | 2.371E-02 |
| 1326 | 2.078E-02 |
| 1332 | 1.786E-02 |
| 1339 | 1.537E-02 |
| 1346 | 1.316E-02 |
| 1353 | 1.095E-02 |
| 1359 | 8.746E-03 |
| 1366 | 6.540E-03 |
| 1373 | 4.336E-03 |
| 1379 | 2.132E-03 |
| 1386 | 7.505E-04 |
| 1393 | 1.251E-03 |
| 1399 | 1.752E-03 |
| 1406 | 2.252E-03 |
| 1413 | 2.752E-03 |
| 1420 | 3.252E-03 |
| 1426 | 3.751E-03 |
| 1433 | 4.315E-03 |
| 1440 | 5.267E-03 |
| 1446 | 6.218E-03 |
| 1453 | 7.169E-03 |
| 1460 | 7.595E-03 |
| 1466 | 7.280E-03 |
| 1473 | 7.249E-03 |
| 1480 | 8.534E-03 |
| 1487 | 9.819E-03 |
| 1493 | 1.110E-02 |
| 1500 | 1.239E-02 |

| λ (nm) | I(H/SH) mW/cm$^2$nm |
|---|---|
| 300 | 2.847E-04 |
| 307 | 1.505E-03 |
| 313 | 6.229E-03 |
| 320 | 2.284E-02 |
| 327 | 3.218E-02 |
| 334 | 4.008E-02 |
| 340 | 4.672E-02 |
| 347 | 4.875E-02 |
| 354 | 5.114E-02 |
| 360 | 5.274E-02 |
| 367 | 5.804E-02 |
| 374 | 6.011E-02 |
| 380 | 5.938E-02 |
| 387 | 5.940E-02 |
| 394 | 6.449E-02 |
| 401 | 8.184E-02 |
| 407 | 9.634E-02 |
| 414 | 1.019E-01 |
| 421 | 1.014E-01 |
| 427 | 9.851E-02 |
| 434 | 9.941E-02 |
| 441 | 1.112E-01 |
| 447 | 1.214E-01 |
| 454 | 1.277E-01 |
| 461 | 1.293E-01 |
| 468 | 1.285E-01 |
| 474 | 1.294E-01 |
| 481 | 1.310E-01 |
| 488 | 1.260E-01 |
| 494 | 1.266E-01 |
| 501 | 1.260E-01 |
| 508 | 1.236E-01 |
| 515 | 1.199E-01 |
| 521 | 1.201E-01 |
| 528 | 1.209E-01 |
| 535 | 1.194E-01 |
| 541 | 1.167E-01 |
| 548 | 1.145E-01 |
| 555 | 1.135E-01 |
| 561 | 1.121E-01 |
| 568 | 1.130E-01 |
| 575 | 1.137E-01 |
| 582 | 1.135E-01 |
| 588 | 1.130E-01 |
| 595 | 1.116E-01 |
| 602 | 1.104E-01 |
| 608 | 1.097E-01 |
| 615 | 1.089E-01 |
| 622 | 1.081E-01 |
| 628 | 1.073E-01 |
| 635 | 1.067E-01 |
| 642 | 1.061E-01 |
| 649 | 1.052E-01 |
| 655 | 1.044E-01 |
| 662 | 1.035E-01 |
| 669 | 1.025E-01 |
| 675 | 1.015E-01 |
| 682 | 1.006E-01 |
| 689 | 9.977E-02 |
| 696 | 8.398E-02 |
| 702 | 9.749E-02 |
| 709 | 9.643E-02 |
| 716 | 9.516E-02 |
| 722 | 8.918E-02 |
| 729 | 8.649E-02 |
| 736 | 9.167E-02 |
| 742 | 9.044E-02 |
| 749 | 8.937E-02 |
| 756 | 7.683E-02 |
| 763 | 6.503E-02 |
| 769 | 8.398E-02 |
| 776 | 8.502E-02 |
| 783 | 8.391E-02 |
| 789 | 8.283E-02 |
| 796 | 8.174E-02 |
| 803 | 7.470E-02 |
| 809 | 6.934E-02 |
| 816 | 7.261E-02 |
| 823 | 7.588E-02 |
| 830 | 7.613E-02 |
| 836 | 6.966E-02 |
| 843 | 4.107E-02 |
| 850 | 2.704E-02 |
| 856 | 2.868E-02 |
| 863 | 2.812E-02 |
| 870 | 2.507E-02 |
| 877 | 2.477E-02 |
| 883 | 2.494E-02 |
| 890 | 2.512E-02 |
| 897 | 2.532E-02 |
| 903 | 2.574E-02 |
| 910 | 2.639E-02 |
| 917 | 2.422E-02 |
| 923 | 1.414E-02 |
| 930 | 8.252E-03 |
| 937 | 1.251E-02 |
| 944 | 1.407E-02 |
| 950 | 1.342E-02 |
| 957 | 1.568E-02 |
| 964 | 1.706E-02 |
| 970 | 3.010E-02 |
| 977 | 4.033E-02 |
| 984 | 3.819E-02 |
| 991 | 3.912E-02 |
| 997 | 4.071E-02 |
| 1004 | 4.230E-02 |
| 1011 | 4.389E-02 |
| 1017 | 4.547E-02 |
| 1024 | 4.463E-02 |
| 1031 | 4.351E-02 |
| 1037 | 4.240E-02 |
| 1044 | 4.129E-02 |
| 1051 | 4.018E-02 |
| 1058 | 3.908E-02 |
| 1064 | 3.798E-02 |
| 1071 | 3.688E-02 |
| 1078 | 3.578E-02 |
| 1084 | 3.484E-02 |
| 1091 | 3.419E-02 |
| 1098 | 3.555E-02 |
| 1104 | 3.632E-02 |
| 1111 | 2.728E-02 |
| 1118 | 1.826E-02 |
| 1125 | 9.250E-03 |
| 1131 | 5.668E-03 |
| 1138 | 5.643E-03 |
| 1145 | 8.158E-03 |
| 1151 | 9.780E-03 |
| 1158 | 1.359E-02 |
| 1165 | 1.739E-02 |
| 1172 | 2.119E-02 |
| 1178 | 2.489E-02 |
| 1185 | 2.576E-02 |
| 1192 | 3.160E-02 |
| 1198 | 3.309E-02 |
| 1205 | 3.145E-02 |
| 1212 | 2.981E-02 |
| 1218 | 2.817E-02 |
| 1225 | 2.756E-02 |
| 1232 | 2.812E-02 |
| 1239 | 2.826E-02 |
| 1245 | 2.775E-02 |
| 1252 | 2.725E-02 |
| 1259 | 2.674E-02 |
| 1265 | 2.648E-02 |
| 1272 | 2.719E-02 |
| 1279 | 2.690E-02 |
| 1285 | 2.520E-02 |
| 1292 | 2.346E-02 |
| 1299 | 2.171E-02 |
| 1306 | 1.996E-02 |
| 1312 | 1.821E-02 |
| 1319 | 1.606E-02 |
| 1326 | 1.378E-02 |
| 1332 | 1.151E-02 |
| 1339 | 9.735E-03 |
| 1346 | 8.281E-03 |
| 1353 | 6.830E-03 |
| 1359 | 5.380E-03 |
| 1366 | 3.932E-03 |
| 1373 | 2.485E-03 |
| 1379 | 1.041E-03 |
| 1386 | 7.886E-05 |
| 1393 | 2.233E-04 |
| 1399 | 3.676E-04 |
| 1406 | 5.117E-04 |
| 1413 | 6.557E-04 |
| 1420 | 7.995E-04 |
| 1426 | 9.431E-04 |
| 1433 | 1.148E-03 |
| 1440 | 1.715E-03 |
| 1446 | 2.282E-03 |
| 1453 | 2.849E-03 |
| 1460 | 3.099E-03 |
| 1466 | 2.903E-03 |
| 1473 | 2.996E-03 |
| 1480 | 4.433E-03 |
| 1487 | 5.867E-03 |
| 1493 | 7.301E-03 |
| 1500 | 8.733E-03 |

| λ (nm) | I(H/F) mW/cm$^2$nm |
|---|---|
| 300 | 1.913E-05 |
| 307 | 2.688E-04 |
| 313 | 2.225E-03 |
| 320 | 1.538E-02 |
| 327 | 2.326E-02 |
| 334 | 3.102E-02 |
| 340 | 3.865E-02 |
| 347 | 4.049E-02 |
| 354 | 4.269E-02 |
| 360 | 4.432E-02 |
| 367 | 4.874E-02 |
| 374 | 5.050E-02 |
| 380 | 4.996E-02 |
| 387 | 4.995E-02 |
| 394 | 5.425E-02 |
| 401 | 6.890E-02 |
| 407 | 8.100E-02 |
| 414 | 8.557E-02 |
| 421 | 8.517E-02 |
| 427 | 8.275E-02 |
| 434 | 8.357E-02 |
| 441 | 9.359E-02 |
| 447 | 1.023E-01 |
| 454 | 1.076E-01 |
| 461 | 1.087E-01 |
| 468 | 1.080E-01 |
| 474 | 1.086E-01 |
| 481 | 1.098E-01 |
| 488 | 1.055E-01 |
| 494 | 1.061E-01 |
| 501 | 1.055E-01 |
| 508 | 1.033E-01 |
| 515 | 9.990E-02 |
| 521 | 9.989E-02 |
| 528 | 1.004E-01 |
| 535 | 9.897E-02 |
| 541 | 9.662E-02 |
| 548 | 9.460E-02 |
| 555 | 9.369E-02 |
| 561 | 9.239E-02 |
| 568 | 9.295E-02 |
| 575 | 9.342E-02 |
| 582 | 9.313E-02 |
| 588 | 9.258E-02 |
| 595 | 9.138E-02 |
| 602 | 9.035E-02 |
| 608 | 8.995E-02 |
| 615 | 8.955E-02 |
| 622 | 8.909E-02 |
| 628 | 8.864E-02 |
| 635 | 8.836E-02 |
| 642 | 8.806E-02 |
| 649 | 8.756E-02 |
| 655 | 8.702E-02 |
| 662 | 8.641E-02 |
| 669 | 8.566E-02 |
| 675 | 8.493E-02 |
| 682 | 8.426E-02 |
| 689 | 8.370E-02 |
| 696 | 7.149E-02 |
| 702 | 8.197E-02 |
| 709 | 8.109E-02 |
| 716 | 8.004E-02 |
| 722 | 7.535E-02 |
| 729 | 7.321E-02 |
| 736 | 7.715E-02 |
| 742 | 7.614E-02 |
| 749 | 7.526E-02 |
| 756 | 6.357E-02 |
| 763 | 5.258E-02 |
| 769 | 7.056E-02 |
| 776 | 7.167E-02 |
| 783 | 7.076E-02 |
| 789 | 6.987E-02 |
| 796 | 6.897E-02 |
| 803 | 6.345E-02 |
| 809 | 5.923E-02 |
| 816 | 6.169E-02 |
| 823 | 6.415E-02 |
| 830 | 6.428E-02 |
| 836 | 5.906E-02 |
| 843 | 3.613E-02 |
| 850 | 2.490E-02 |
| 856 | 2.624E-02 |
| 863 | 2.575E-02 |
| 870 | 2.316E-02 |
| 877 | 2.289E-02 |
| 883 | 2.301E-02 |
| 890 | 2.314E-02 |
| 897 | 2.329E-02 |
| 903 | 2.362E-02 |
| 910 | 2.415E-02 |
| 917 | 2.226E-02 |
| 923 | 1.358E-02 |
| 930 | 8.336E-03 |
| 937 | 1.215E-02 |
| 944 | 1.355E-02 |
| 950 | 1.297E-02 |
| 957 | 1.493E-02 |
| 964 | 1.611E-02 |
| 970 | 2.684E-02 |
| 977 | 3.524E-02 |
| 984 | 3.349E-02 |
| 991 | 3.426E-02 |
| 997 | 3.558E-02 |
| 1004 | 3.690E-02 |
| 1011 | 3.821E-02 |
| 1017 | 3.953E-02 |
| 1024 | 3.885E-02 |
| 1031 | 3.795E-02 |
| 1037 | 3.705E-02 |
| 1044 | 3.615E-02 |
| 1051 | 3.526E-02 |
| 1058 | 3.436E-02 |
| 1064 | 3.347E-02 |
| 1071 | 3.259E-02 |
| 1078 | 3.170E-02 |
| 1084 | 3.079E-02 |
| 1091 | 2.984E-02 |
| 1098 | 3.124E-02 |
| 1104 | 3.052E-02 |
| 1111 | 2.317E-02 |
| 1118 | 1.583E-02 |
| 1125 | 8.509E-03 |
| 1131 | 5.708E-03 |
| 1138 | 5.669E-03 |
| 1145 | 7.938E-03 |
| 1151 | 9.348E-03 |
| 1158 | 1.269E-02 |
| 1165 | 1.603E-02 |
| 1172 | 1.937E-02 |
| 1178 | 2.261E-02 |
| 1185 | 2.321E-02 |
| 1192 | 2.700E-02 |
| 1198 | 2.793E-02 |
| 1205 | 2.684E-02 |
| 1212 | 2.574E-02 |
| 1218 | 2.465E-02 |
| 1225 | 2.423E-02 |
| 1232 | 2.458E-02 |
| 1239 | 2.451E-02 |
| 1245 | 2.376E-02 |
| 1252 | 2.301E-02 |
| 1259 | 2.226E-02 |
| 1265 | 2.181E-02 |
| 1272 | 2.252E-02 |
| 1279 | 2.262E-02 |
| 1285 | 2.184E-02 |
| 1292 | 2.071E-02 |
| 1299 | 1.936E-02 |
| 1306 | 1.801E-02 |
| 1312 | 1.666E-02 |
| 1319 | 1.475E-02 |
| 1326 | 1.267E-02 |
| 1332 | 1.058E-02 |
| 1339 | 8.953E-03 |
| 1346 | 7.619E-03 |
| 1353 | 6.287E-03 |
| 1359 | 4.957E-03 |
| 1366 | 3.628E-03 |
| 1373 | 2.301E-03 |
| 1379 | 9.753E-04 |
| 1386 | 1.007E-04 |
| 1393 | 2.590E-04 |
| 1399 | 4.172E-04 |
| 1406 | 5.752E-04 |
| 1413 | 7.330E-04 |
| 1420 | 8.906E-04 |
| 1426 | 1.048E-03 |
| 1433 | 1.260E-03 |
| 1440 | 1.801E-03 |
| 1446 | 2.342E-03 |
| 1453 | 2.881E-03 |
| 1460 | 3.121E-03 |
| 1466 | 2.936E-03 |
| 1473 | 3.000E-03 |
| 1480 | 4.204E-03 |
| 1487 | 5.407E-03 |
| 1493 | 6.609E-03 |
| 1500 | 7.810E-03 |

| λ (nm) | I(DF/W) mW/cm$^2$nm |
|---|---|
| 300 | 1.053E-06 |
| 307 | 3.015E-05 |
| 313 | 4.057E-04 |
| 320 | 4.383E-03 |
| 327 | 7.853E-03 |
| 334 | 1.222E-02 |
| 340 | 1.757E-02 |
| 347 | 2.027E-02 |
| 354 | 2.339E-02 |
| 360 | 2.641E-02 |
| 367 | 3.111E-02 |
| 374 | 3.437E-02 |
| 380 | 3.613E-02 |
| 387 | 3.802E-02 |
| 394 | 4.334E-02 |
| 401 | 5.760E-02 |
| 407 | 7.020E-02 |
| 414 | 7.674E-02 |
| 421 | 7.892E-02 |
| 427 | 7.912E-02 |
| 434 | 8.235E-02 |
| 441 | 9.492E-02 |
| 447 | 1.067E-01 |
| 454 | 1.147E-01 |
| 461 | 1.181E-01 |
| 468 | 1.194E-01 |
| 474 | 1.222E-01 |
| 481 | 1.257E-01 |
| 488 | 1.227E-01 |
| 494 | 1.252E-01 |
| 501 | 1.263E-01 |
| 508 | 1.251E-01 |
| 515 | 1.223E-01 |
| 521 | 1.235E-01 |
| 528 | 1.252E-01 |
| 535 | 1.247E-01 |
| 541 | 1.228E-01 |
| 548 | 1.213E-01 |
| 555 | 1.210E-01 |
| 561 | 1.201E-01 |
| 568 | 1.216E-01 |
| 575 | 1.229E-01 |
| 582 | 1.233E-01 |
| 588 | 1.232E-01 |
| 595 | 1.223E-01 |
| 602 | 1.216E-01 |
| 608 | 1.218E-01 |
| 615 | 1.219E-01 |
| 622 | 1.220E-01 |
| 628 | 1.220E-01 |
| 635 | 1.223E-01 |
| 642 | 1.226E-01 |
| 649 | 1.225E-01 |
| 655 | 1.222E-01 |
| 662 | 1.218E-01 |
| 669 | 1.212E-01 |
| 675 | 1.206E-01 |
| 682 | 1.201E-01 |
| 689 | 1.197E-01 |
| 696 | 1.025E-01 |
| 702 | 1.180E-01 |
| 709 | 1.170E-01 |
| 716 | 1.158E-01 |
| 722 | 1.091E-01 |
| 729 | 1.063E-01 |
| 736 | 1.123E-01 |
| 742 | 1.110E-01 |
| 749 | 1.100E-01 |
| 756 | 8.927E-02 |
| 763 | 6.979E-02 |
| 769 | 1.030E-01 |
| 776 | 1.055E-01 |
| 783 | 1.043E-01 |
| 789 | 1.032E-01 |
| 796 | 1.020E-01 |
| 803 | 9.395E-02 |
| 809 | 8.774E-02 |
| 816 | 9.155E-02 |
| 823 | 9.536E-02 |
| 830 | 9.567E-02 |
| 836 | 8.795E-02 |
| 843 | 5.363E-02 |
| 850 | 3.680E-02 |
| 856 | 3.886E-02 |
| 863 | 3.810E-02 |
| 870 | 3.433E-02 |
| 877 | 3.395E-02 |
| 883 | 3.416E-02 |
| 890 | 3.439E-02 |
| 897 | 3.465E-02 |
| 903 | 3.519E-02 |
| 910 | 3.600E-02 |
| 917 | 3.319E-02 |
| 923 | 2.016E-02 |
| 930 | 1.231E-02 |
| 937 | 1.803E-02 |
| 944 | 2.014E-02 |
| 950 | 1.928E-02 |
| 957 | 2.224E-02 |
| 964 | 2.404E-02 |
| 970 | 4.032E-02 |
| 977 | 5.311E-02 |
| 984 | 5.047E-02 |
| 991 | 5.167E-02 |
| 997 | 5.370E-02 |
| 1004 | 5.572E-02 |
| 1011 | 5.775E-02 |
| 1017 | 5.977E-02 |
| 1024 | 5.877E-02 |
| 1031 | 5.743E-02 |
| 1037 | 5.608E-02 |
| 1044 | 5.474E-02 |
| 1051 | 5.340E-02 |
| 1058 | 5.207E-02 |
| 1064 | 5.073E-02 |
| 1071 | 4.940E-02 |
| 1078 | 4.806E-02 |
| 1084 | 4.671E-02 |
| 1091 | 4.533E-02 |
| 1098 | 4.743E-02 |
| 1104 | 4.546E-02 |
| 1111 | 3.453E-02 |
| 1118 | 2.361E-02 |
| 1125 | 1.269E-02 |
| 1131 | 8.534E-03 |
| 1138 | 8.479E-03 |
| 1145 | 1.192E-02 |
| 1151 | 1.406E-02 |
| 1158 | 1.914E-02 |
| 1165 | 2.423E-02 |
| 1172 | 2.930E-02 |
| 1178 | 3.425E-02 |
| 1185 | 3.519E-02 |
| 1192 | 4.052E-02 |
| 1198 | 4.184E-02 |
| 1205 | 4.035E-02 |
| 1212 | 3.887E-02 |
| 1218 | 3.738E-02 |
| 1225 | 3.685E-02 |
| 1232 | 3.740E-02 |
| 1239 | 3.714E-02 |
| 1245 | 3.553E-02 |
| 1252 | 3.393E-02 |
| 1259 | 3.233E-02 |
| 1265 | 3.136E-02 |
| 1272 | 3.283E-02 |
| 1279 | 3.340E-02 |
| 1285 | 3.298E-02 |
| 1292 | 3.149E-02 |
| 1299 | 2.940E-02 |
| 1306 | 2.732E-02 |
| 1312 | 2.523E-02 |
| 1319 | 2.234E-02 |
| 1326 | 1.917E-02 |
| 1332 | 1.601E-02 |
| 1339 | 1.355E-02 |
| 1346 | 1.154E-02 |
| 1353 | 9.523E-03 |
| 1359 | 7.510E-03 |
| 1366 | 5.498E-03 |
| 1373 | 3.486E-03 |
| 1379 | 1.476E-03 |
| 1386 | 1.464E-04 |
| 1393 | 3.808E-04 |
| 1399 | 6.151E-04 |
| 1406 | 8.494E-04 |
| 1413 | 1.084E-03 |
| 1420 | 1.318E-03 |
| 1426 | 1.552E-03 |
| 1433 | 1.869E-03 |
| 1440 | 2.684E-03 |
| 1446 | 3.499E-03 |
| 1453 | 4.313E-03 |
| 1460 | 4.675E-03 |
| 1466 | 4.398E-03 |
| 1473 | 4.495E-03 |
| 1480 | 6.333E-03 |
| 1487 | 8.171E-03 |
| 1493 | 1.001E-02 |
| 1500 | 1.184E-02 |

| λ (nm) | I(DF/SP) mW/cm$^2$nm |
|---|---|
| 300 | 1.659E-04 |
| 307 | 8.682E-04 |
| 313 | 3.588E-03 |
| 320 | 1.311E-02 |
| 327 | 1.968E-02 |
| 334 | 2.592E-02 |
| 340 | 3.179E-02 |
| 347 | 3.487E-02 |
| 354 | 3.829E-02 |
| 360 | 4.120E-02 |
| 367 | 4.703E-02 |
| 374 | 5.037E-02 |
| 380 | 5.136E-02 |
| 387 | 5.279E-02 |
| 394 | 5.880E-02 |
| 401 | 7.641E-02 |
| 407 | 9.172E-02 |
| 414 | 9.878E-02 |
| 421 | 1.001E-01 |
| 427 | 9.882E-02 |
| 434 | 1.013E-01 |
| 441 | 1.150E-01 |
| 447 | 1.273E-01 |
| 454 | 1.356E-01 |
| 461 | 1.387E-01 |
| 468 | 1.393E-01 |
| 474 | 1.416E-01 |
| 481 | 1.447E-01 |
| 488 | 1.403E-01 |
| 494 | 1.423E-01 |
| 501 | 1.427E-01 |
| 508 | 1.409E-01 |
| 515 | 1.375E-01 |
| 521 | 1.386E-01 |
| 528 | 1.403E-01 |
| 535 | 1.394E-01 |
| 541 | 1.370E-01 |
| 548 | 1.350E-01 |
| 555 | 1.345E-01 |
| 561 | 1.334E-01 |
| 568 | 1.350E-01 |
| 575 | 1.363E-01 |
| 582 | 1.366E-01 |
| 588 | 1.364E-01 |
| 595 | 1.353E-01 |
| 602 | 1.342E-01 |
| 608 | 1.336E-01 |
| 615 | 1.330E-01 |
| 622 | 1.323E-01 |
| 628 | 1.316E-01 |
| 635 | 1.311E-01 |
| 642 | 1.306E-01 |
| 649 | 1.298E-01 |
| 655 | 1.290E-01 |
| 662 | 1.281E-01 |
| 669 | 1.270E-01 |
| 675 | 1.260E-01 |
| 682 | 1.250E-01 |
| 689 | 1.242E-01 |
| 696 | 1.127E-01 |
| 702 | 1.216E-01 |
| 709 | 1.205E-01 |
| 716 | 1.190E-01 |
| 722 | 1.143E-01 |
| 729 | 1.120E-01 |
| 736 | 1.150E-01 |
| 742 | 1.136E-01 |
| 749 | 1.124E-01 |
| 756 | 9.498E-02 |
| 763 | 7.859E-02 |
| 769 | 1.055E-01 |
| 776 | 1.073E-01 |
| 783 | 1.059E-01 |
| 789 | 1.047E-01 |
| 796 | 1.034E-01 |
| 803 | 9.794E-02 |
| 809 | 9.364E-02 |
| 816 | 9.531E-02 |
| 823 | 9.698E-02 |
| 830 | 9.657E-02 |
| 836 | 9.080E-02 |
| 843 | 6.673E-02 |
| 850 | 5.490E-02 |
| 856 | 5.627E-02 |
| 863 | 5.535E-02 |
| 870 | 5.181E-02 |
| 877 | 5.117E-02 |
| 883 | 5.106E-02 |
| 890 | 5.098E-02 |
| 897 | 5.092E-02 |
| 903 | 5.115E-02 |
| 910 | 5.165E-02 |
| 917 | 4.878E-02 |
| 923 | 3.642E-02 |
| 930 | 2.768E-02 |
| 937 | 3.408E-02 |
| 944 | 3.643E-02 |
| 950 | 3.542E-02 |
| 957 | 3.821E-02 |
| 964 | 3.972E-02 |
| 970 | 5.208E-02 |
| 977 | 6.171E-02 |
| 984 | 5.956E-02 |
| 991 | 6.029E-02 |
| 997 | 6.164E-02 |
| 1004 | 6.299E-02 |
| 1011 | 6.434E-02 |
| 1017 | 6.569E-02 |
| 1024 | 6.404E-02 |
| 1031 | 6.374E-02 |
| 1037 | 6.264E-02 |
| 1044 | 6.154E-02 |
| 1051 | 6.045E-02 |
| 1058 | 5.935E-02 |
| 1064 | 5.826E-02 |
| 1071 | 5.716E-02 |
| 1078 | 5.607E-02 |
| 1084 | 5.430E-02 |
| 1091 | 5.128E-02 |
| 1098 | 5.384E-02 |
| 1104 | 4.759E-02 |
| 1111 | 3.886E-02 |
| 1118 | 3.014E-02 |
| 1125 | 2.143E-02 |
| 1131 | 1.877E-02 |
| 1138 | 1.852E-02 |
| 1145 | 2.244E-02 |
| 1151 | 2.429E-02 |
| 1158 | 2.917E-02 |
| 1165 | 3.405E-02 |
| 1172 | 3.892E-02 |
| 1178 | 4.363E-02 |
| 1185 | 4.363E-02 |
| 1192 | 4.372E-02 |
| 1198 | 4.346E-02 |
| 1205 | 4.307E-02 |
| 1212 | 4.268E-02 |
| 1218 | 4.228E-02 |
| 1225 | 4.199E-02 |
| 1232 | 4.181E-02 |
| 1239 | 4.090E-02 |
| 1245 | 3.881E-02 |
| 1252 | 3.671E-02 |
| 1259 | 3.462E-02 |
| 1265 | 3.318E-02 |
| 1272 | 3.426E-02 |
| 1279 | 3.542E-02 |
| 1285 | 3.670E-02 |
| 1292 | 3.647E-02 |
| 1299 | 3.533E-02 |
| 1306 | 3.418E-02 |
| 1312 | 3.304E-02 |
| 1319 | 3.009E-02 |
| 1326 | 2.654E-02 |
| 1332 | 2.299E-02 |
| 1339 | 1.988E-02 |
| 1346 | 1.706E-02 |
| 1353 | 1.425E-02 |
| 1359 | 1.143E-02 |
| 1366 | 8.613E-03 |
| 1373 | 5.799E-03 |
| 1379 | 2.986E-03 |
| 1386 | 1.240E-03 |
| 1393 | 1.938E-03 |
| 1399 | 2.637E-03 |
| 1406 | 3.335E-03 |
| 1413 | 4.033E-03 |
| 1420 | 4.730E-03 |
| 1426 | 5.427E-03 |
| 1433 | 6.197E-03 |
| 1440 | 7.404E-03 |
| 1446 | 8.611E-03 |
| 1453 | 9.817E-03 |
| 1460 | 1.036E-02 |
| 1466 | 9.956E-03 |
| 1473 | 9.893E-03 |
| 1480 | 1.140E-02 |
| 1487 | 1.291E-02 |
| 1493 | 1.442E-02 |
| 1500 | 1.593E-02 |

| λ (nm) | I(DF/S) mW/cm$^2$nm |
|---|---|
| 300 | 1.730E-04 |
| 307 | 9.861E-04 |
| 313 | 4.355E-03 |
| 320 | 1.690E-02 |
| 327 | 2.502E-02 |
| 334 | 3.257E-02 |
| 340 | 3.946E-02 |
| 347 | 4.261E-02 |
| 354 | 4.610E-02 |
| 360 | 4.887E-02 |
| 367 | 5.511E-02 |
| 374 | 5.835E-02 |
| 380 | 5.881E-02 |
| 387 | 5.991E-02 |
| 394 | 6.612E-02 |
| 401 | 8.518E-02 |
| 407 | 1.016E-01 |
| 414 | 1.088E-01 |
| 421 | 1.096E-01 |
| 427 | 1.076E-01 |
| 434 | 1.096E-01 |
| 441 | 1.237E-01 |
| 447 | 1.362E-01 |
| 454 | 1.444E-01 |
| 461 | 1.472E-01 |
| 468 | 1.473E-01 |
| 474 | 1.493E-01 |
| 481 | 1.519E-01 |
| 488 | 1.466E-01 |
| 494 | 1.484E-01 |
| 501 | 1.483E-01 |
| 508 | 1.462E-01 |
| 515 | 1.423E-01 |
| 521 | 1.431E-01 |
| 528 | 1.445E-01 |
| 535 | 1.432E-01 |
| 541 | 1.405E-01 |
| 548 | 1.382E-01 |
| 555 | 1.374E-01 |
| 561 | 1.361E-01 |
| 568 | 1.375E-01 |
| 575 | 1.387E-01 |
| 582 | 1.387E-01 |
| 588 | 1.384E-01 |
| 595 | 1.370E-01 |
| 602 | 1.358E-01 |
| 608 | 1.351E-01 |
| 615 | 1.344E-01 |
| 622 | 1.336E-01 |
| 628 | 1.328E-01 |
| 635 | 1.323E-01 |
| 642 | 1.317E-01 |
| 649 | 1.308E-01 |
| 655 | 1.299E-01 |
| 662 | 1.290E-01 |
| 669 | 1.279E-01 |
| 675 | 1.268E-01 |
| 682 | 1.257E-01 |
| 689 | 1.248E-01 |
| 696 | 1.124E-01 |
| 702 | 1.222E-01 |
| 709 | 1.210E-01 |
| 716 | 1.195E-01 |
| 722 | 1.145E-01 |
| 729 | 1.120E-01 |
| 736 | 1.153E-01 |
| 742 | 1.139E-01 |
| 749 | 1.126E-01 |
| 756 | 9.688E-02 |
| 763 | 8.204E-02 |
| 769 | 1.060E-01 |
| 776 | 1.074E-01 |
| 783 | 1.060E-01 |
| 789 | 1.047E-01 |
| 796 | 1.034E-01 |
| 803 | 9.755E-02 |
| 809 | 9.297E-02 |
| 816 | 9.491E-02 |
| 823 | 9.684E-02 |
| 830 | 9.650E-02 |
| 836 | 9.041E-02 |
| 843 | 6.476E-02 |
| 850 | 5.216E-02 |
| 856 | 5.366E-02 |
| 863 | 5.276E-02 |
| 870 | 4.912E-02 |
| 877 | 4.852E-02 |
| 883 | 4.845E-02 |
| 890 | 4.841E-02 |
| 897 | 4.840E-02 |
| 903 | 4.867E-02 |
| 910 | 4.923E-02 |
| 917 | 4.632E-02 |
| 923 | 3.306E-02 |
| 930 | 2.490E-02 |
| 937 | 3.133E-02 |
| 944 | 3.369E-02 |
| 950 | 3.209E-02 |
| 957 | 3.556E-02 |
| 964 | 3.714E-02 |
| 970 | 5.017E-02 |
| 977 | 6.034E-02 |
| 984 | 5.811E-02 |
| 991 | 5.893E-02 |
| 997 | 6.040E-02 |
| 1004 | 6.187E-02 |
| 1011 | 6.335E-02 |
| 1017 | 6.482E-02 |
| 1024 | 6.395E-02 |
| 1031 | 6.282E-02 |
| 1037 | 6.169E-02 |
| 1044 | 6.056E-02 |
| 1051 | 5.943E-02 |
| 1058 | 5.830E-02 |
| 1064 | 5.718E-02 |
| 1071 | 5.605E-02 |
| 1078 | 5.493E-02 |
| 1084 | 5.317E-02 |
| 1091 | 5.025E-02 |
| 1098 | 5.287E-02 |
| 1104 | 4.758E-02 |
| 1111 | 3.832E-02 |
| 1118 | 2.907E-02 |
| 1125 | 1.983E-02 |
| 1131 | 1.688E-02 |
| 1138 | 1.667E-02 |
| 1145 | 2.058E-02 |
| 1151 | 2.252E-02 |
| 1158 | 2.753E-02 |
| 1165 | 3.253E-02 |
| 1172 | 3.754E-02 |
| 1178 | 4.238E-02 |
| 1185 | 4.249E-02 |
| 1192 | 4.347E-02 |
| 1198 | 4.347E-02 |
| 1205 | 4.284E-02 |
| 1212 | 4.222E-02 |
| 1218 | 4.160E-02 |
| 1225 | 4.122E-02 |
| 1232 | 4.112E-02 |
| 1239 | 4.039E-02 |
| 1245 | 3.862E-02 |
| 1252 | 3.685E-02 |
| 1259 | 3.508E-02 |
| 1265 | 3.386E-02 |
| 1272 | 3.477E-02 |
| 1279 | 3.558E-02 |
| 1285 | 3.627E-02 |
| 1292 | 3.575E-02 |
| 1299 | 3.450E-02 |
| 1306 | 3.325E-02 |
| 1312 | 3.200E-02 |
| 1319 | 2.901E-02 |
| 1326 | 2.544E-02 |
| 1332 | 2.186E-02 |
| 1339 | 1.882E-02 |
| 1346 | 1.611E-02 |
| 1353 | 1.341E-02 |
| 1359 | 1.071E-02 |
| 1366 | 8.007E-03 |
| 1373 | 5.309E-03 |
| 1379 | 2.611E-03 |
| 1386 | 9.190E-04 |
| 1393 | 1.533E-03 |
| 1399 | 2.146E-03 |
| 1406 | 2.759E-03 |
| 1413 | 3.371E-03 |
| 1420 | 3.983E-03 |
| 1426 | 4.595E-03 |
| 1433 | 5.287E-03 |
| 1440 | 6.453E-03 |
| 1446 | 7.619E-03 |
| 1453 | 8.784E-03 |
| 1460 | 9.307E-03 |
| 1466 | 8.922E-03 |
| 1473 | 8.884E-03 |
| 1480 | 1.046E-02 |
| 1487 | 1.203E-02 |
| 1493 | 1.361E-02 |
| 1500 | 1.518E-02 |

| λ (nm) | I(DF/SH) mW/cm$^2$nm |
|---|---|
| 300 | 1.638E-04 |
| 307 | 9.322E-04 |
| 313 | 4.114E-03 |
| 320 | 1.595E-02 |
| 327 | 2.361E-02 |
| 334 | 3.071E-02 |
| 340 | 3.719E-02 |
| 347 | 4.014E-02 |
| 354 | 4.340E-02 |
| 360 | 4.599E-02 |
| 367 | 5.184E-02 |
| 374 | 5.487E-02 |
| 380 | 5.528E-02 |
| 387 | 5.629E-02 |
| 394 | 6.210E-02 |
| 401 | 7.998E-02 |
| 407 | 9.541E-02 |
| 414 | 1.021E-01 |
| 421 | 1.028E-01 |
| 427 | 1.009E-01 |
| 434 | 1.028E-01 |
| 441 | 1.160E-01 |
| 447 | 1.277E-01 |
| 454 | 1.354E-01 |
| 461 | 1.379E-01 |
| 468 | 1.380E-01 |
| 474 | 1.398E-01 |
| 481 | 1.423E-01 |
| 488 | 1.375E-01 |
| 494 | 1.389E-01 |
| 501 | 1.389E-01 |
| 508 | 1.369E-01 |
| 515 | 1.332E-01 |
| 521 | 1.339E-01 |
| 528 | 1.353E-01 |
| 535 | 1.341E-01 |
| 541 | 1.315E-01 |
| 548 | 1.293E-01 |
| 555 | 1.286E-01 |
| 561 | 1.274E-01 |
| 568 | 1.286E-01 |
| 575 | 1.298E-01 |
| 582 | 1.298E-01 |
| 588 | 1.295E-01 |
| 595 | 1.282E-01 |
| 602 | 1.271E-01 |
| 608 | 1.264E-01 |
| 615 | 1.258E-01 |
| 622 | 1.250E-01 |
| 628 | 1.243E-01 |
| 635 | 1.238E-01 |
| 642 | 1.233E-01 |
| 649 | 1.224E-01 |
| 655 | 1.216E-01 |
| 662 | 1.208E-01 |
| 669 | 1.197E-01 |
| 675 | 1.187E-01 |
| 682 | 1.177E-01 |
| 689 | 1.169E-01 |
| 696 | 9.848E-02 |
| 702 | 1.144E-01 |
| 709 | 1.133E-01 |
| 716 | 1.119E-01 |
| 722 | 1.049E-01 |
| 729 | 1.019E-01 |
| 736 | 1.080E-01 |
| 742 | 1.067E-01 |
| 749 | 1.055E-01 |
| 756 | 9.075E-02 |
| 763 | 7.686E-02 |
| 769 | 9.933E-02 |
| 776 | 1.006E-01 |
| 783 | 9.936E-02 |
| 789 | 9.813E-02 |
| 796 | 9.690E-02 |
| 803 | 8.860E-02 |
| 809 | 8.229E-02 |
| 816 | 8.622E-02 |
| 823 | 9.013E-02 |
| 830 | 9.048E-02 |
| 836 | 8.283E-02 |
| 843 | 4.885E-02 |
| 850 | 3.218E-02 |
| 856 | 3.414E-02 |
| 863 | 3.349E-02 |
| 870 | 2.987E-02 |
| 877 | 2.952E-02 |
| 883 | 2.970E-02 |
| 890 | 2.996E-02 |
| 897 | 3.021E-02 |
| 903 | 3.072E-02 |
| 910 | 3.151E-02 |
| 917 | 2.893E-02 |
| 923 | 1.689E-02 |
| 930 | 9.862E-03 |
| 937 | 1.495E-02 |
| 944 | 1.682E-02 |
| 950 | 1.605E-02 |
| 957 | 1.876E-02 |
| 964 | 2.042E-02 |
| 970 | 3.603E-02 |
| 977 | 4.829E-02 |
| 984 | 4.574E-02 |
| 991 | 4.686E-02 |
| 997 | 4.878E-02 |
| 1004 | 5.070E-02 |
| 1011 | 5.261E-02 |
| 1017 | 5.452E-02 |
| 1024 | 5.352E-02 |
| 1031 | 5.220E-02 |
| 1037 | 5.087E-02 |
| 1044 | 4.955E-02 |
| 1051 | 4.823E-02 |
| 1058 | 4.692E-02 |
| 1064 | 4.560E-02 |
| 1071 | 4.429E-02 |
| 1078 | 4.298E-02 |
| 1084 | 4.186E-02 |
| 1091 | 4.108E-02 |
| 1098 | 4.273E-02 |
| 1104 | 4.366E-02 |
| 1111 | 3.280E-02 |
| 1118 | 2.195E-02 |
| 1125 | 1.112E-02 |
| 1131 | 6.817E-03 |
| 1138 | 6.788E-03 |
| 1145 | 9.814E-03 |
| 1151 | 1.177E-02 |
| 1158 | 1.636E-02 |
| 1165 | 2.094E-02 |
| 1172 | 2.551E-02 |
| 1178 | 2.997E-02 |
| 1185 | 3.102E-02 |
| 1192 | 3.805E-02 |
| 1198 | 3.985E-02 |
| 1205 | 3.788E-02 |
| 1212 | 3.591E-02 |
| 1218 | 3.395E-02 |
| 1225 | 3.322E-02 |
| 1232 | 3.388E-02 |
| 1239 | 3.407E-02 |
| 1245 | 3.346E-02 |
| 1252 | 3.285E-02 |
| 1259 | 3.224E-02 |
| 1265 | 3.193E-02 |
| 1272 | 3.279E-02 |
| 1279 | 3.244E-02 |
| 1285 | 3.039E-02 |
| 1292 | 2.830E-02 |
| 1299 | 2.619E-02 |
| 1306 | 2.408E-02 |
| 1312 | 2.197E-02 |
| 1319 | 1.939E-02 |
| 1326 | 1.664E-02 |
| 1332 | 1.389E-02 |
| 1339 | 1.175E-02 |
| 1346 | 9.998E-03 |
| 1353 | 8.246E-03 |
| 1359 | 6.496E-03 |
| 1366 | 4.748E-03 |
| 1373 | 3.001E-03 |
| 1379 | 1.257E-03 |
| 1386 | 9.526E-05 |
| 1393 | 2.698E-04 |
| 1399 | 4.441E-04 |
| 1406 | 6.183E-04 |
| 1413 | 7.923E-04 |
| 1420 | 9.661E-04 |
| 1426 | 1.140E-03 |
| 1433 | 1.387E-03 |
| 1440 | 2.073E-03 |
| 1446 | 2.759E-03 |
| 1453 | 3.444E-03 |
| 1460 | 3.747E-03 |
| 1466 | 3.510E-03 |
| 1473 | 3.623E-03 |
| 1480 | 5.360E-03 |
| 1487 | 7.095E-03 |
| 1493 | 8.829E-03 |
| 1500 | 1.056E-02 |

| λ (nm) | I(DF/F) mW/cm$^2$nm |
|---|---|
| 300 | 9.107E-06 |
| 307 | 1.426E-04 |
| 313 | 1.298E-03 |
| 320 | 9.754E-03 |
| 327 | 1.588E-02 |
| 334 | 2.260E-02 |
| 340 | 2.982E-02 |
| 347 | 3.289E-02 |
| 354 | 3.631E-02 |
| 360 | 3.927E-02 |
| 367 | 4.482E-02 |
| 374 | 4.800E-02 |
| 380 | 4.894E-02 |
| 387 | 5.028E-02 |
| 394 | 5.599E-02 |
| 401 | 7.273E-02 |
| 407 | 8.728E-02 |
| 414 | 9.396E-02 |
| 421 | 9.516E-02 |
| 427 | 9.394E-02 |
| 434 | 9.627E-02 |
| 441 | 1.093E-01 |
| 447 | 1.210E-01 |
| 454 | 1.287E-01 |
| 461 | 1.314E-01 |
| 468 | 1.318E-01 |
| 474 | 1.339E-01 |
| 481 | 1.365E-01 |
| 488 | 1.323E-01 |
| 494 | 1.339E-01 |
| 501 | 1.341E-01 |
| 508 | 1.322E-01 |
| 515 | 1.287E-01 |
| 521 | 1.294E-01 |
| 528 | 1.308E-01 |
| 535 | 1.296E-01 |
| 541 | 1.271E-01 |
| 548 | 1.250E-01 |
| 555 | 1.244E-01 |
| 561 | 1.231E-01 |
| 568 | 1.244E-01 |
| 575 | 1.255E-01 |
| 582 | 1.255E-01 |
| 588 | 1.252E-01 |
| 595 | 1.239E-01 |
| 602 | 1.229E-01 |
| 608 | 1.227E-01 |
| 615 | 1.225E-01 |
| 622 | 1.221E-01 |
| 628 | 1.218E-01 |
| 635 | 1.217E-01 |
| 642 | 1.216E-01 |
| 649 | 1.211E-01 |
| 655 | 1.206E-01 |
| 662 | 1.200E-01 |
| 669 | 1.192E-01 |
| 675 | 1.184E-01 |
| 682 | 1.176E-01 |
| 689 | 1.170E-01 |
| 696 | 1.001E-01 |
| 702 | 1.149E-01 |
| 709 | 1.139E-01 |
| 716 | 1.125E-01 |
| 722 | 1.061E-01 |
| 729 | 1.032E-01 |
| 736 | 1.089E-01 |
| 742 | 1.076E-01 |
| 749 | 1.065E-01 |
| 756 | 9.001E-02 |
| 763 | 7.453E-02 |
| 769 | 1.001E-01 |
| 776 | 1.018E-01 |
| 783 | 1.006E-01 |
| 789 | 9.940E-02 |
| 796 | 9.821E-02 |
| 803 | 9.042E-02 |
| 809 | 8.447E-02 |
| 816 | 8.806E-02 |
| 823 | 9.163E-02 |
| 830 | 9.188E-02 |
| 836 | 8.448E-02 |
| 843 | 5.172E-02 |
| 850 | 3.566E-02 |
| 856 | 3.761E-02 |
| 863 | 3.692E-02 |
| 870 | 3.324E-02 |
| 877 | 3.286E-02 |
| 883 | 3.305E-02 |
| 890 | 3.325E-02 |
| 897 | 3.348E-02 |
| 903 | 3.398E-02 |
| 910 | 3.476E-02 |
| 917 | 3.205E-02 |
| 923 | 1.956E-02 |
| 930 | 1.201E-02 |
| 937 | 1.752E-02 |
| 944 | 1.954E-02 |
| 950 | 1.872E-02 |
| 957 | 2.155E-02 |
| 964 | 2.327E-02 |
| 970 | 3.878E-02 |
| 977 | 5.094E-02 |
| 984 | 4.843E-02 |
| 991 | 4.956E-02 |
| 997 | 5.149E-02 |
| 1004 | 5.341E-02 |
| 1011 | 5.533E-02 |
| 1017 | 5.725E-02 |
| 1024 | 5.628E-02 |
| 1031 | 5.499E-02 |
| 1037 | 5.370E-02 |
| 1044 | 5.242E-02 |
| 1051 | 5.114E-02 |
| 1058 | 4.986E-02 |
| 1064 | 4.858E-02 |
| 1071 | 4.730E-02 |
| 1078 | 4.603E-02 |
| 1084 | 4.472E-02 |
| 1091 | 4.335E-02 |
| 1098 | 4.539E-02 |
| 1104 | 4.436E-02 |
| 1111 | 3.369E-02 |
| 1118 | 2.302E-02 |
| 1125 | 1.238E-02 |
| 1131 | 8.303E-03 |
| 1138 | 8.249E-03 |
| 1145 | 1.155E-02 |
| 1151 | 1.361E-02 |
| 1158 | 1.848E-02 |
| 1165 | 2.335E-02 |
| 1172 | 2.821E-02 |
| 1178 | 3.294E-02 |
| 1185 | 3.382E-02 |
| 1192 | 3.935E-02 |
| 1198 | 4.071E-02 |
| 1205 | 3.912E-02 |
| 1212 | 3.753E-02 |
| 1218 | 3.595E-02 |
| 1225 | 3.534E-02 |
| 1232 | 3.585E-02 |
| 1239 | 3.576E-02 |
| 1245 | 3.467E-02 |
| 1252 | 3.358E-02 |
| 1259 | 3.250E-02 |
| 1265 | 3.184E-02 |
| 1272 | 3.288E-02 |
| 1279 | 3.303E-02 |
| 1285 | 3.190E-02 |
| 1292 | 3.025E-02 |
| 1299 | 2.828E-02 |
| 1306 | 2.631E-02 |
| 1312 | 2.434E-02 |
| 1319 | 2.156E-02 |
| 1326 | 1.851E-02 |
| 1332 | 1.546E-02 |
| 1339 | 1.309E-02 |
| 1346 | 1.114E-02 |
| 1353 | 9.194E-03 |
| 1359 | 7.250E-03 |
| 1366 | 5.307E-03 |
| 1373 | 3.366E-03 |
| 1379 | 1.427E-03 |
| 1386 | 1.473E-04 |
| 1393 | 3.790E-04 |
| 1399 | 6.105E-04 |
| 1406 | 8.418E-04 |
| 1413 | 1.073E-03 |
| 1420 | 1.304E-03 |
| 1426 | 1.535E-03 |
| 1433 | 1.846E-03 |
| 1440 | 2.638E-03 |
| 1446 | 3.429E-03 |
| 1453 | 4.220E-03 |
| 1460 | 4.572E-03 |
| 1466 | 4.304E-03 |
| 1473 | 4.395E-03 |
| 1480 | 6.160E-03 |
| 1487 | 7.924E-03 |
| 1493 | 9.686E-03 |
| 1500 | 1.145E-02 |

| λ (nm) | I(T/W) mW/cm$^2$nm |
|---|---|
| 300 | 4.048E-06 |
| 307 | 9.910E-05 |
| 313 | 1.166E-03 |
| 320 | 1.124E-02 |
| 327 | 1.825E-02 |
| 334 | 2.610E-02 |
| 340 | 3.491E-02 |
| 347 | 3.782E-02 |
| 354 | 4.131E-02 |
| 360 | 4.449E-02 |
| 367 | 5.027E-02 |
| 374 | 5.354E-02 |
| 380 | 5.449E-02 |
| 387 | 5.571E-02 |
| 394 | 6.192E-02 |
| 401 | 8.044E-02 |
| 407 | 9.607E-02 |
| 414 | 1.031E-01 |
| 421 | 1.043E-01 |
| 427 | 1.030E-01 |
| 434 | 1.058E-01 |
| 441 | 1.205E-01 |
| 447 | 1.339E-01 |
| 454 | 1.425E-01 |
| 461 | 1.454E-01 |
| 468 | 1.458E-01 |
| 474 | 1.480E-01 |
| 481 | 1.511E-01 |
| 488 | 1.465E-01 |
| 494 | 1.486E-01 |
| 501 | 1.491E-01 |
| 508 | 1.468E-01 |
| 515 | 1.428E-01 |
| 521 | 1.435E-01 |
| 528 | 1.450E-01 |
| 535 | 1.438E-01 |
| 541 | 1.411E-01 |
| 548 | 1.389E-01 |
| 555 | 1.381E-01 |
| 561 | 1.366E-01 |
| 568 | 1.379E-01 |
| 575 | 1.391E-01 |
| 582 | 1.391E-01 |
| 588 | 1.388E-01 |
| 595 | 1.374E-01 |
| 602 | 1.363E-01 |
| 608 | 1.362E-01 |
| 615 | 1.362E-01 |
| 622 | 1.360E-01 |
| 628 | 1.358E-01 |
| 635 | 1.359E-01 |
| 642 | 1.360E-01 |
| 649 | 1.357E-01 |
| 655 | 1.353E-01 |
| 662 | 1.346E-01 |
| 669 | 1.338E-01 |
| 675 | 1.330E-01 |
| 682 | 1.323E-01 |
| 689 | 1.317E-01 |
| 696 | 1.126E-01 |
| 702 | 1.296E-01 |
| 709 | 1.284E-01 |
| 716 | 1.269E-01 |
| 722 | 1.195E-01 |
| 729 | 1.163E-01 |
| 736 | 1.228E-01 |
| 742 | 1.213E-01 |
| 749 | 1.201E-01 |
| 756 | 9.742E-02 |
| 763 | 7.612E-02 |
| 769 | 1.122E-01 |
| 776 | 1.149E-01 |
| 783 | 1.136E-01 |
| 789 | 1.123E-01 |
| 796 | 1.110E-01 |
| 803 | 1.021E-01 |
| 809 | 9.534E-02 |
| 816 | 9.944E-02 |
| 823 | 1.035E-01 |
| 830 | 1.038E-01 |
| 836 | 9.542E-02 |
| 843 | 5.816E-02 |
| 850 | 3.990E-02 |
| 856 | 4.211E-02 |
| 863 | 4.134E-02 |
| 870 | 3.717E-02 |
| 877 | 3.676E-02 |
| 883 | 3.698E-02 |
| 890 | 3.722E-02 |
| 897 | 3.748E-02 |
| 903 | 3.805E-02 |
| 910 | 3.893E-02 |
| 917 | 3.588E-02 |
| 923 | 2.178E-02 |
| 930 | 1.330E-02 |
| 937 | 1.947E-02 |
| 944 | 2.175E-02 |
| 950 | 2.082E-02 |
| 957 | 2.401E-02 |
| 964 | 2.594E-02 |
| 970 | 4.351E-02 |
| 977 | 5.730E-02 |
| 984 | 5.445E-02 |
| 991 | 5.573E-02 |
| 997 | 5.790E-02 |
| 1004 | 6.008E-02 |
| 1011 | 6.225E-02 |
| 1017 | 6.443E-02 |
| 1024 | 6.334E-02 |
| 1031 | 6.188E-02 |
| 1037 | 6.043E-02 |
| 1044 | 5.897E-02 |
| 1051 | 5.752E-02 |
| 1058 | 5.608E-02 |
| 1064 | 5.463E-02 |
| 1071 | 5.319E-02 |
| 1078 | 5.175E-02 |
| 1084 | 5.029E-02 |
| 1091 | 4.880E-02 |
| 1098 | 5.105E-02 |
| 1104 | 4.893E-02 |
| 1111 | 3.716E-02 |
| 1118 | 2.540E-02 |
| 1125 | 1.366E-02 |
| 1131 | 9.182E-03 |
| 1138 | 9.122E-03 |
| 1145 | 1.282E-02 |
| 1151 | 1.512E-02 |
| 1158 | 2.059E-02 |
| 1165 | 2.605E-02 |
| 1172 | 3.151E-02 |
| 1178 | 3.683E-02 |
| 1185 | 3.784E-02 |
| 1192 | 4.356E-02 |
| 1198 | 4.498E-02 |
| 1205 | 4.338E-02 |
| 1212 | 4.178E-02 |
| 1218 | 4.018E-02 |
| 1225 | 3.961E-02 |
| 1232 | 4.020E-02 |
| 1239 | 3.991E-02 |
| 1245 | 3.819E-02 |
| 1252 | 3.646E-02 |
| 1259 | 3.474E-02 |
| 1265 | 3.369E-02 |
| 1272 | 3.527E-02 |
| 1279 | 3.597E-02 |
| 1285 | 3.543E-02 |
| 1292 | 3.383E-02 |
| 1299 | 3.159E-02 |
| 1306 | 2.934E-02 |
| 1312 | 2.710E-02 |
| 1319 | 2.399E-02 |
| 1326 | 2.059E-02 |
| 1332 | 1.720E-02 |
| 1339 | 1.455E-02 |
| 1346 | 1.239E-02 |
| 1353 | 1.023E-02 |
| 1359 | 8.064E-03 |
| 1366 | 5.903E-03 |
| 1373 | 3.743E-03 |
| 1379 | 1.584E-03 |
| 1386 | 1.572E-04 |
| 1393 | 4.089E-04 |
| 1399 | 6.605E-04 |
| 1406 | 9.119E-04 |
| 1413 | 1.163E-03 |
| 1420 | 1.415E-03 |
| 1426 | 1.666E-03 |
| 1433 | 2.006E-03 |
| 1440 | 2.881E-03 |
| 1446 | 3.756E-03 |
| 1453 | 4.630E-03 |
| 1460 | 5.018E-03 |
| 1466 | 4.721E-03 |
| 1473 | 4.825E-03 |
| 1480 | 6.798E-03 |
| 1487 | 8.770E-03 |
| 1493 | 1.074E-02 |
| 1500 | 1.271E-02 |

| λ (nm) | I(T/SP) mW/cm$^2$nm |
|---|---|
| 300 | 3.658E-04 |
| 307 | 1.762E-03 |
| 313 | 6.781E-03 |
| 320 | 2.331E-02 |
| 327 | 3.318E-02 |
| 334 | 4.176E-02 |
| 340 | 4.921E-02 |
| 347 | 5.212E-02 |
| 354 | 5.550E-02 |
| 360 | 5.813E-02 |
| 367 | 6.477E-02 |
| 374 | 6.792E-02 |
| 380 | 6.794E-02 |
| 387 | 6.865E-02 |
| 394 | 7.528E-02 |
| 401 | 9.648E-02 |
| 407 | 1.144E-01 |
| 414 | 1.218E-01 |
| 421 | 1.221E-01 |
| 427 | 1.194E-01 |
| 434 | 1.214E-01 |
| 441 | 1.367E-01 |
| 447 | 1.503E-01 |
| 454 | 1.590E-01 |
| 461 | 1.616E-01 |
| 468 | 1.614E-01 |
| 474 | 1.632E-01 |
| 481 | 1.659E-01 |
| 488 | 1.601E-01 |
| 494 | 1.617E-01 |
| 501 | 1.615E-01 |
| 508 | 1.590E-01 |
| 515 | 1.545E-01 |
| 521 | 1.553E-01 |
| 528 | 1.567E-01 |
| 535 | 1.553E-01 |
| 541 | 1.522E-01 |
| 548 | 1.497E-01 |
| 555 | 1.488E-01 |
| 561 | 1.472E-01 |
| 568 | 1.486E-01 |
| 575 | 1.498E-01 |
| 582 | 1.499E-01 |
| 588 | 1.494E-01 |
| 595 | 1.479E-01 |
| 602 | 1.466E-01 |
| 608 | 1.457E-01 |
| 615 | 1.448E-01 |
| 622 | 1.439E-01 |
| 628 | 1.429E-01 |
| 635 | 1.422E-01 |
| 642 | 1.415E-01 |
| 649 | 1.405E-01 |
| 655 | 1.395E-01 |
| 662 | 1.384E-01 |
| 669 | 1.371E-01 |
| 675 | 1.359E-01 |
| 682 | 1.347E-01 |
| 689 | 1.337E-01 |
| 696 | 1.213E-01 |
| 702 | 1.308E-01 |
| 709 | 1.294E-01 |
| 716 | 1.278E-01 |
| 722 | 1.227E-01 |
| 729 | 1.201E-01 |
| 736 | 1.233E-01 |
| 742 | 1.217E-01 |
| 749 | 1.203E-01 |
| 756 | 1.016E-01 |
| 763 | 8.407E-02 |
| 769 | 1.128E-01 |
| 776 | 1.146E-01 |
| 783 | 1.132E-01 |
| 789 | 1.118E-01 |
| 796 | 1.103E-01 |
| 803 | 1.045E-01 |
| 809 | 9.988E-02 |
| 816 | 1.016E-01 |
| 823 | 1.034E-01 |
| 830 | 1.029E-01 |
| 836 | 9.673E-02 |
| 843 | 7.107E-02 |
| 850 | 5.845E-02 |
| 856 | 5.990E-02 |
| 863 | 5.890E-02 |
| 870 | 5.512E-02 |
| 877 | 5.443E-02 |
| 883 | 5.430E-02 |
| 890 | 5.419E-02 |
| 897 | 5.413E-02 |
| 903 | 5.435E-02 |
| 910 | 5.488E-02 |
| 917 | 5.181E-02 |
| 923 | 3.868E-02 |
| 930 | 2.939E-02 |
| 937 | 3.619E-02 |
| 944 | 3.867E-02 |
| 950 | 3.759E-02 |
| 957 | 4.054E-02 |
| 964 | 4.214E-02 |
| 970 | 5.524E-02 |
| 977 | 6.545E-02 |
| 984 | 6.316E-02 |
| 991 | 6.393E-02 |
| 997 | 6.535E-02 |
| 1004 | 6.678E-02 |
| 1011 | 6.820E-02 |
| 1017 | 6.962E-02 |
| 1024 | 6.871E-02 |
| 1031 | 6.754E-02 |
| 1037 | 6.636E-02 |
| 1044 | 6.519E-02 |
| 1051 | 6.403E-02 |
| 1058 | 6.286E-02 |
| 1064 | 6.169E-02 |
| 1071 | 6.053E-02 |
| 1078 | 5.937E-02 |
| 1084 | 5.749E-02 |
| 1091 | 5.428E-02 |
| 1098 | 5.699E-02 |
| 1104 | 5.037E-02 |
| 1111 | 4.113E-02 |
| 1118 | 3.190E-02 |
| 1125 | 2.268E-02 |
| 1131 | 1.986E-02 |
| 1138 | 1.960E-02 |
| 1145 | 2.374E-02 |
| 1151 | 2.570E-02 |
| 1158 | 3.086E-02 |
| 1165 | 3.601E-02 |
| 1172 | 4.117E-02 |
| 1178 | 4.615E-02 |
| 1185 | 4.614E-02 |
| 1192 | 4.624E-02 |
| 1198 | 4.596E-02 |
| 1205 | 4.554E-02 |
| 1212 | 4.512E-02 |
| 1218 | 4.471E-02 |
| 1225 | 4.439E-02 |
| 1232 | 4.420E-02 |
| 1239 | 4.324E-02 |
| 1245 | 4.102E-02 |
| 1252 | 3.881E-02 |
| 1259 | 3.659E-02 |
| 1265 | 3.506E-02 |
| 1272 | 3.620E-02 |
| 1279 | 3.743E-02 |
| 1285 | 3.879E-02 |
| 1292 | 3.854E-02 |
| 1299 | 3.733E-02 |
| 1306 | 3.612E-02 |
| 1312 | 3.491E-02 |
| 1319 | 3.180E-02 |
| 1326 | 2.804E-02 |
| 1332 | 2.429E-02 |
| 1339 | 2.101E-02 |
| 1346 | 1.803E-02 |
| 1353 | 1.505E-02 |
| 1359 | 1.207E-02 |
| 1366 | 9.099E-03 |
| 1373 | 6.126E-03 |
| 1379 | 3.155E-03 |
| 1386 | 1.309E-03 |
| 1393 | 2.047E-03 |
| 1399 | 2.785E-03 |
| 1406 | 3.522E-03 |
| 1413 | 4.259E-03 |
| 1420 | 4.995E-03 |
| 1426 | 5.732E-03 |
| 1433 | 6.545E-03 |
| 1440 | 7.819E-03 |
| 1446 | 9.093E-03 |
| 1453 | 1.037E-02 |
| 1460 | 1.094E-02 |
| 1466 | 1.051E-02 |
| 1473 | 1.045E-02 |
| 1480 | 1.204E-02 |
| 1487 | 1.364E-02 |
| 1493 | 1.523E-02 |
| 1500 | 1.682E-02 |

| λ (nm) | I(T/S) mW/cm$^2$nm |
|---|---|
| 300 | 3.275E-04 |
| 307 | 1.751E-03 |
| 313 | 7.321E-03 |
| 320 | 2.709E-02 |
| 327 | 3.850E-02 |
| 334 | 4.833E-02 |
| 340 | 5.673E-02 |
| 347 | 5.958E-02 |
| 354 | 6.288E-02 |
| 360 | 6.521E-02 |
| 367 | 7.212E-02 |
| 374 | 7.503E-02 |
| 380 | 7.444E-02 |
| 387 | 7.475E-02 |
| 394 | 8.145E-02 |
| 401 | 1.037E-01 |
| 407 | 1.225E-01 |
| 414 | 1.298E-01 |
| 421 | 1.296E-01 |
| 427 | 1.262E-01 |
| 434 | 1.277E-01 |
| 441 | 1.431E-01 |
| 447 | 1.565E-01 |
| 454 | 1.650E-01 |
| 461 | 1.673E-01 |
| 468 | 1.666E-01 |
| 474 | 1.680E-01 |
| 481 | 1.703E-01 |
| 488 | 1.640E-01 |
| 494 | 1.651E-01 |
| 501 | 1.644E-01 |
| 508 | 1.615E-01 |
| 515 | 1.568E-01 |
| 521 | 1.572E-01 |
| 528 | 1.584E-01 |
| 535 | 1.566E-01 |
| 541 | 1.532E-01 |
| 548 | 1.503E-01 |
| 555 | 1.492E-01 |
| 561 | 1.475E-01 |
| 568 | 1.487E-01 |
| 575 | 1.498E-01 |
| 582 | 1.496E-01 |
| 588 | 1.490E-01 |
| 595 | 1.473E-01 |
| 602 | 1.457E-01 |
| 608 | 1.448E-01 |
| 615 | 1.439E-01 |
| 622 | 1.429E-01 |
| 628 | 1.419E-01 |
| 635 | 1.412E-01 |
| 642 | 1.404E-01 |
| 649 | 1.393E-01 |
| 655 | 1.383E-01 |
| 662 | 1.372E-01 |
| 669 | 1.359E-01 |
| 675 | 1.346E-01 |
| 682 | 1.334E-01 |
| 689 | 1.323E-01 |
| 696 | 1.190E-01 |
| 702 | 1.294E-01 |
| 709 | 1.280E-01 |
| 716 | 1.263E-01 |
| 722 | 1.210E-01 |
| 729 | 1.183E-01 |
| 736 | 1.218E-01 |
| 742 | 1.202E-01 |
| 749 | 1.188E-01 |
| 756 | 1.021E-01 |
| 763 | 8.644E-02 |
| 769 | 1.116E-01 |
| 776 | 1.130E-01 |
| 783 | 1.116E-01 |
| 789 | 1.101E-01 |
| 796 | 1.087E-01 |
| 803 | 1.025E-01 |
| 809 | 9.770E-02 |
| 816 | 9.969E-02 |
| 823 | 1.017E-01 |
| 830 | 1.013E-01 |
| 836 | 9.489E-02 |
| 843 | 6.795E-02 |
| 850 | 5.472E-02 |
| 856 | 5.627E-02 |
| 863 | 5.531E-02 |
| 870 | 5.149E-02 |
| 877 | 5.084E-02 |
| 883 | 5.076E-02 |
| 890 | 5.071E-02 |
| 897 | 5.069E-02 |
| 903 | 5.096E-02 |
| 910 | 5.153E-02 |
| 917 | 4.847E-02 |
| 923 | 3.523E-02 |
| 930 | 2.605E-02 |
| 937 | 3.278E-02 |
| 944 | 3.524E-02 |
| 950 | 3.419E-02 |
| 957 | 3.718E-02 |
| 964 | 3.883E-02 |
| 970 | 5.244E-02 |
| 977 | 6.306E-02 |
| 984 | 6.072E-02 |
| 991 | 6.157E-02 |
| 997 | 6.310E-02 |
| 1004 | 6.463E-02 |
| 1011 | 6.616E-02 |
| 1017 | 6.769E-02 |
| 1024 | 6.677E-02 |
| 1031 | 6.558E-02 |
| 1037 | 6.440E-02 |
| 1044 | 6.321E-02 |
| 1051 | 6.203E-02 |
| 1058 | 6.084E-02 |
| 1064 | 5.966E-02 |
| 1071 | 5.848E-02 |
| 1078 | 5.731E-02 |
| 1084 | 5.547E-02 |
| 1091 | 5.241E-02 |
| 1098 | 5.514E-02 |
| 1104 | 4.962E-02 |
| 1111 | 3.997E-02 |
| 1118 | 3.032E-02 |
| 1125 | 2.068E-02 |
| 1131 | 1.760E-02 |
| 1138 | 1.737E-02 |
| 1145 | 2.145E-02 |
| 1151 | 2.348E-02 |
| 1158 | 2.869E-02 |
| 1165 | 3.391E-02 |
| 1172 | 3.912E-02 |
| 1178 | 4.416E-02 |
| 1185 | 4.427E-02 |
| 1192 | 4.530E-02 |
| 1198 | 4.529E-02 |
| 1205 | 4.464E-02 |
| 1212 | 4.399E-02 |
| 1218 | 4.334E-02 |
| 1225 | 4.294E-02 |
| 1232 | 4.283E-02 |
| 1239 | 4.207E-02 |
| 1245 | 4.022E-02 |
| 1252 | 3.838E-02 |
| 1259 | 3.654E-02 |
| 1265 | 3.526E-02 |
| 1272 | 3.620E-02 |
| 1279 | 3.705E-02 |
| 1285 | 3.776E-02 |
| 1292 | 3.722E-02 |
| 1299 | 3.592E-02 |
| 1306 | 3.461E-02 |
| 1312 | 3.331E-02 |
| 1319 | 3.020E-02 |
| 1326 | 2.648E-02 |
| 1332 | 2.275E-02 |
| 1339 | 1.959E-02 |
| 1346 | 1.677E-02 |
| 1353 | 1.396E-02 |
| 1359 | 1.114E-02 |
| 1366 | 8.333E-03 |
| 1373 | 5.525E-03 |
| 1379 | 2.717E-03 |
| 1386 | 9.564E-04 |
| 1393 | 1.595E-03 |
| 1399 | 2.233E-03 |
| 1406 | 2.870E-03 |
| 1413 | 3.508E-03 |
| 1420 | 4.145E-03 |
| 1426 | 4.781E-03 |
| 1433 | 5.500E-03 |
| 1440 | 6.713E-03 |
| 1446 | 7.926E-03 |
| 1453 | 9.138E-03 |
| 1460 | 9.682E-03 |
| 1466 | 9.281E-03 |
| 1473 | 9.241E-03 |
| 1480 | 1.088E-02 |
| 1487 | 1.252E-02 |
| 1493 | 1.416E-02 |
| 1500 | 1.579E-02 |

| λ (nm) | I(T/SH) mW/cm$^2$nm |
|---|---|
| 300 | 2.909E-04 |
| 307 | 1.562E-03 |
| 313 | 6.560E-03 |
| 320 | 2.438E-02 |
| 327 | 3.477E-02 |
| 334 | 4.379E-02 |
| 340 | 5.156E-02 |
| 347 | 5.429E-02 |
| 354 | 5.744E-02 |
| 360 | 5.970E-02 |
| 367 | 6.616E-02 |
| 374 | 6.895E-02 |
| 380 | 6.852E-02 |
| 387 | 6.892E-02 |
| 394 | 7.519E-02 |
| 401 | 9.587E-02 |
| 407 | 1.133E-01 |
| 414 | 1.203E-01 |
| 421 | 1.202E-01 |
| 427 | 1.171E-01 |
| 434 | 1.186E-01 |
| 441 | 1.330E-01 |
| 447 | 1.456E-01 |
| 454 | 1.536E-01 |
| 461 | 1.558E-01 |
| 468 | 1.553E-01 |
| 474 | 1.567E-01 |
| 481 | 1.589E-01 |
| 488 | 1.530E-01 |
| 494 | 1.541E-01 |
| 501 | 1.536E-01 |
| 508 | 1.510E-01 |
| 515 | 1.465E-01 |
| 521 | 1.470E-01 |
| 528 | 1.481E-01 |
| 535 | 1.465E-01 |
| 541 | 1.434E-01 |
| 548 | 1.407E-01 |
| 555 | 1.397E-01 |
| 561 | 1.382E-01 |
| 568 | 1.393E-01 |
| 575 | 1.403E-01 |
| 582 | 1.402E-01 |
| 588 | 1.397E-01 |
| 595 | 1.381E-01 |
| 602 | 1.367E-01 |
| 608 | 1.359E-01 |
| 615 | 1.350E-01 |
| 622 | 1.341E-01 |
| 628 | 1.332E-01 |
| 635 | 1.325E-01 |
| 642 | 1.318E-01 |
| 649 | 1.308E-01 |
| 655 | 1.299E-01 |
| 662 | 1.289E-01 |
| 669 | 1.276E-01 |
| 675 | 1.264E-01 |
| 682 | 1.253E-01 |
| 689 | 1.244E-01 |
| 696 | 1.047E-01 |
| 702 | 1.216E-01 |
| 709 | 1.203E-01 |
| 716 | 1.188E-01 |
| 722 | 1.114E-01 |
| 729 | 1.080E-01 |
| 736 | 1.145E-01 |
| 742 | 1.130E-01 |
| 749 | 1.117E-01 |
| 756 | 9.609E-02 |
| 763 | 8.136E-02 |
| 769 | 1.051E-01 |
| 776 | 1.064E-01 |
| 783 | 1.051E-01 |
| 789 | 1.037E-01 |
| 796 | 1.024E-01 |
| 803 | 9.358E-02 |
| 809 | 8.689E-02 |
| 816 | 9.101E-02 |
| 823 | 9.512E-02 |
| 830 | 9.545E-02 |
| 836 | 8.736E-02 |
| 843 | 5.152E-02 |
| 850 | 3.392E-02 |
| 856 | 3.598E-02 |
| 863 | 3.529E-02 |
| 870 | 3.146E-02 |
| 877 | 3.110E-02 |
| 883 | 3.131E-02 |
| 890 | 3.154E-02 |
| 897 | 3.180E-02 |
| 903 | 3.233E-02 |
| 910 | 3.315E-02 |
| 917 | 3.044E-02 |
| 923 | 1.777E-02 |
| 930 | 1.037E-02 |
| 937 | 1.572E-02 |
| 944 | 1.768E-02 |
| 950 | 1.687E-02 |
| 957 | 1.972E-02 |
| 964 | 2.146E-02 |
| 970 | 3.786E-02 |
| 977 | 5.073E-02 |
| 984 | 4.805E-02 |
| 991 | 4.922E-02 |
| 997 | 5.123E-02 |
| 1004 | 5.324E-02 |
| 1011 | 5.524E-02 |
| 1017 | 5.724E-02 |
| 1024 | 5.618E-02 |
| 1031 | 5.478E-02 |
| 1037 | 5.339E-02 |
| 1044 | 5.200E-02 |
| 1051 | 5.061E-02 |
| 1058 | 4.922E-02 |
| 1064 | 4.784E-02 |
| 1071 | 4.646E-02 |
| 1078 | 4.508E-02 |
| 1084 | 4.390E-02 |
| 1091 | 4.308E-02 |
| 1098 | 4.480E-02 |
| 1104 | 4.577E-02 |
| 1111 | 3.438E-02 |
| 1118 | 2.301E-02 |
| 1125 | 1.166E-02 |
| 1131 | 7.145E-03 |
| 1138 | 7.114E-03 |
| 1145 | 1.029E-02 |
| 1151 | 1.233E-02 |
| 1158 | 1.714E-02 |
| 1165 | 2.194E-02 |
| 1172 | 2.673E-02 |
| 1178 | 3.140E-02 |
| 1185 | 3.249E-02 |
| 1192 | 3.986E-02 |
| 1198 | 4.174E-02 |
| 1205 | 3.967E-02 |
| 1212 | 3.761E-02 |
| 1218 | 3.555E-02 |
| 1225 | 3.478E-02 |
| 1232 | 3.548E-02 |
| 1239 | 3.567E-02 |
| 1245 | 3.503E-02 |
| 1252 | 3.439E-02 |
| 1259 | 3.375E-02 |
| 1265 | 3.343E-02 |
| 1272 | 3.432E-02 |
| 1279 | 3.396E-02 |
| 1285 | 3.181E-02 |
| 1292 | 2.962E-02 |
| 1299 | 2.741E-02 |
| 1306 | 2.520E-02 |
| 1312 | 2.299E-02 |
| 1319 | 2.028E-02 |
| 1326 | 1.741E-02 |
| 1332 | 1.453E-02 |
| 1339 | 1.229E-02 |
| 1346 | 1.046E-02 |
| 1353 | 8.627E-03 |
| 1359 | 6.796E-03 |
| 1366 | 4.967E-03 |
| 1373 | 3.140E-03 |
| 1379 | 1.315E-03 |
| 1386 | 9.964E-05 |
| 1393 | 2.821E-04 |
| 1399 | 4.645E-04 |
| 1406 | 6.466E-04 |
| 1413 | 8.285E-04 |
| 1420 | 1.010E-03 |
| 1426 | 1.192E-03 |
| 1433 | 1.450E-03 |
| 1440 | 2.168E-03 |
| 1446 | 2.885E-03 |
| 1453 | 3.601E-03 |
| 1460 | 3.917E-03 |
| 1466 | 3.670E-03 |
| 1473 | 3.788E-03 |
| 1480 | 5.603E-03 |
| 1487 | 7.417E-03 |
| 1493 | 9.230E-03 |
| 1500 | 1.104E-02 |

| λ (nm) | I(T/F) $mW/cm^2nm$ |
|---|---|
| 300 | 1.895E-05 |
| 307 | 2.742E-04 |
| 313 | 2.335E-03 |
| 320 | 1.657E-02 |
| 327 | 2.568E-02 |
| 334 | 3.503E-02 |
| 340 | 4.457E-02 |
| 347 | 4.760E-02 |
| 354 | 5.109E-02 |
| 360 | 5.391E-02 |
| 367 | 6.019E-02 |
| 374 | 6.323E-02 |
| 380 | 6.337E-02 |
| 387 | 6.411E-02 |
| 394 | 7.039E-02 |
| 401 | 9.031E-02 |
| 407 | 1.072E-01 |
| 414 | 1.142E-01 |
| 421 | 1.146E-01 |
| 427 | 1.122E-01 |
| 434 | 1.141E-01 |
| 441 | 1.285E-01 |
| 447 | 1.414E-01 |
| 454 | 1.495E-01 |
| 461 | 1.518E-01 |
| 468 | 1.516E-01 |
| 474 | 1.532E-01 |
| 481 | 1.555E-01 |
| 488 | 1.501E-01 |
| 494 | 1.514E-01 |
| 501 | 1.511E-01 |
| 508 | 1.484E-01 |
| 515 | 1.440E-01 |
| 521 | 1.445E-01 |
| 528 | 1.456E-01 |
| 535 | 1.439E-01 |
| 541 | 1.409E-01 |
| 548 | 1.382E-01 |
| 555 | 1.372E-01 |
| 561 | 1.356E-01 |
| 568 | 1.367E-01 |
| 575 | 1.376E-01 |
| 582 | 1.375E-01 |
| 588 | 1.369E-01 |
| 595 | 1.354E-01 |
| 602 | 1.340E-01 |
| 608 | 1.336E-01 |
| 615 | 1.332E-01 |
| 622 | 1.327E-01 |
| 628 | 1.322E-01 |
| 635 | 1.320E-01 |
| 642 | 1.317E-01 |
| 649 | 1.311E-01 |
| 655 | 1.304E-01 |
| 662 | 1.296E-01 |
| 669 | 1.286E-01 |
| 675 | 1.277E-01 |
| 682 | 1.268E-01 |
| 689 | 1.261E-01 |
| 696 | 1.078E-01 |
| 702 | 1.237E-01 |
| 709 | 1.224E-01 |
| 716 | 1.209E-01 |
| 722 | 1.139E-01 |
| 729 | 1.108E-01 |
| 736 | 1.168E-01 |
| 742 | 1.154E-01 |
| 749 | 1.141E-01 |
| 756 | 9.642E-02 |
| 763 | 7.980E-02 |
| 769 | 1.072E-01 |
| 776 | 1.089E-01 |
| 783 | 1.076E-01 |
| 789 | 1.063E-01 |
| 796 | 1.050E-01 |
| 803 | 9.661E-02 |
| 809 | 9.022E-02 |
| 816 | 9.402E-02 |
| 823 | 9.781E-02 |
| 830 | 9.804E-02 |
| 836 | 9.012E-02 |
| 843 | 5.516E-02 |
| 850 | 3.802E-02 |
| 856 | 4.009E-02 |
| 863 | 3.935E-02 |
| 870 | 3.541E-02 |
| 877 | 3.500E-02 |
| 883 | 3.520E-02 |
| 890 | 3.541E-02 |
| 897 | 3.564E-02 |
| 903 | 3.617E-02 |
| 910 | 3.699E-02 |
| 917 | 3.410E-02 |
| 923 | 2.081E-02 |
| 930 | 1.278E-02 |
| 937 | 1.863E-02 |
| 944 | 2.078E-02 |
| 950 | 1.990E-02 |
| 957 | 2.291E-02 |
| 964 | 2.473E-02 |
| 970 | 4.120E-02 |
| 977 | 5.412E-02 |
| 984 | 5.144E-02 |
| 991 | 5.264E-02 |
| 997 | 5.468E-02 |
| 1004 | 5.671E-02 |
| 1011 | 5.875E-02 |
| 1017 | 6.078E-02 |
| 1024 | 5.974E-02 |
| 1031 | 5.837E-02 |
| 1037 | 5.699E-02 |
| 1044 | 5.562E-02 |
| 1051 | 5.426E-02 |
| 1058 | 5.289E-02 |
| 1064 | 5.153E-02 |
| 1071 | 5.018E-02 |
| 1078 | 4.882E-02 |
| 1084 | 4.743E-02 |
| 1091 | 4.597E-02 |
| 1098 | 4.813E-02 |
| 1104 | 4.704E-02 |
| 1111 | 3.571E-02 |
| 1118 | 2.441E-02 |
| 1125 | 1.312E-02 |
| 1131 | 8.801E-03 |
| 1138 | 8.743E-03 |
| 1145 | 1.224E-02 |
| 1151 | 1.442E-02 |
| 1158 | 1.958E-02 |
| 1165 | 2.474E-02 |
| 1172 | 2.989E-02 |
| 1178 | 3.490E-02 |
| 1185 | 3.583E-02 |
| 1192 | 4.168E-02 |
| 1198 | 4.312E-02 |
| 1205 | 4.144E-02 |
| 1212 | 3.975E-02 |
| 1218 | 3.807E-02 |
| 1225 | 3.743E-02 |
| 1232 | 3.797E-02 |
| 1239 | 3.787E-02 |
| 1245 | 3.671E-02 |
| 1252 | 3.556E-02 |
| 1259 | 3.441E-02 |
| 1265 | 3.372E-02 |
| 1272 | 3.482E-02 |
| 1279 | 3.497E-02 |
| 1285 | 3.377E-02 |
| 1292 | 3.202E-02 |
| 1299 | 2.993E-02 |
| 1306 | 2.785E-02 |
| 1312 | 2.576E-02 |
| 1319 | 2.282E-02 |
| 1326 | 1.959E-02 |
| 1332 | 1.637E-02 |
| 1339 | 1.385E-02 |
| 1346 | 1.179E-02 |
| 1353 | 9.730E-03 |
| 1359 | 7.672E-03 |
| 1366 | 5.616E-03 |
| 1373 | 3.562E-03 |
| 1379 | 1.510E-03 |
| 1386 | 1.559E-04 |
| 1393 | 4.010E-04 |
| 1399 | 6.460E-04 |
| 1406 | 8.906E-04 |
| 1413 | 1.135E-03 |
| 1420 | 1.379E-03 |
| 1426 | 1.623E-03 |
| 1433 | 1.952E-03 |
| 1440 | 2.790E-03 |
| 1446 | 3.628E-03 |
| 1453 | 4.464E-03 |
| 1460 | 4.836E-03 |
| 1466 | 4.552E-03 |
| 1473 | 4.649E-03 |
| 1480 | 6.515E-03 |
| 1487 | 8.380E-03 |
| 1493 | 1.024E-02 |
| 1500 | 1.211E-02 |

# INSOLATION MEASUREMENTS WITH A PORTABLE $Cu_2S$-CdS RADIOMETER†

by

H. M. Windawi*

Institute of Energy Conversion
University of Delaware
Newark, Delaware 19711
USA

## ABSTRACT

Solar radiation measurements were carried out with a portable $Cu_2S$-CdS radiometer. The measurements were found to be accurate to better than 5% (better than 3% when sophisticated metering is employed). Calibration to an Eppley Precision Pyranometer is discussed.

---

†Supported in part by National Science Foundation under Grant No. NSF/RANN/ AER72-03478.

*Present address: Department of Chemical Engineering
University of Delaware
Newark, Delaware 19711, USA

## Introduction

The development of high efficiency and stable copper sulfide-cadmium sulfide solar cells have suggested their usability for large scale terrestrial applications (1). The development has, likewise, suggested their use in solar radiation intensity measurements. Their spectral response is flat over the wavelength range 0.3-1.0 μm. Their temperature stability and capability to be produced with large active area make them advantageous for use as off-the-shelf or field work radiometers.

Solar intensity measurements were performed with a $Cu_2S$-CdS radiometer whose characteristics are discussed. The measurements were compared with those performed by an Eppley Precision Pyranometer.

## Principle of Operation

The device utilizes the photovoltaic characteristics of a $Cu_2S$-CdS solar cell and its response to light intensity variations. The principle of operation is based on the experimental observation that over many orders of magnitude the light generated current is proportional to the intensity of radiation. Solar to electrical conversion of a solar cell is characterized by a current-voltage curve. The squareness of the curve is denoted by the "fill factor" and is given by the ratio of the maximum power output, $P_m$, to the product of the short circuit current, $I_{sc}$, (where V = 0) and the open circuit voltage, $V_{oc}$, (where I = 0). For a fill factor of $\sim$ 0.75 a flat region in the I-V curve is observed around the $I_{sc}$ value and extends to a few tenths of a volt on both the forward and reverse bias regions. The short circuit current approximates that of the light generated value,

$I_L$, which is a measure of the cell response to light intensity variations;

$$I = I_0 [\exp (\alpha V) - 1] - I_L$$

where $\alpha$ is a temperature dependent diode constant and $I_0$ is the saturation current (2).

For a small load resistance, R, a voltage drop, IR, can be measured across R and gives a measure of the current I. If R is such that I is in the flat region at the proximity of $I_{sc}$, the voltage signal across R represents the cell response to light intensity. A meter with high internal resistance $R_m >> R$ will show a current reading, $I_m$, proportional to the intensity of solar insolation, $I_T$;

$$I_m = csI_T$$

where c is a constant and s is a spectral response parameter ($\sim 1$) (3).

A radiometer based on the principles of operation outlined above was built and is shown in Fig. 1. The device consisted of a $Cu_2S$-CdS solar cell with 55 $cm^2$ active area. The cell was sandwiched between a glass window and a pc-board and potted with transparent Hysol epoxy for total seal. The cell was shunted by a tenth ohm resistor (i.e., R = 0.1 $\Omega$) and the output was connected to a 2.5K$\Omega$, 0-50 $\mu$A ammeter. The meter was attached to the back of the frame assembly (Fig. 1) to avoid reflection of light from the user. The device is self-contained, no external connections or power sources are used.

## Calibration and Spectral Response Parameter

The radiometer was calibrated against an Eppley model PSP pyranometer. Both pyranometer and cell surfaces were tilted at 45° with respect to the horizontal surface and facing South. Figure 2 shows the current, $I_m$ (μA), as a function of intensity, $I_T$ (mW/cm$^2$), measured by the pyranometer for a day with variable cloudiness for about an hour around solar noon. For such conditions, a linear relation was observed.

The spectral response parameter was investigated by performing calibration measurements over extended periods of time and correlating these measurements with those for the spectral distribution of solar radiation. Figure 3 summarizes the results obtained for the various conditions indicated. From the figure, it can be seen that the response of the $Cu_2S$-CdS radiometer is lower for clear day measurements around solar noon (± one hour) than for early hours and variable cloudiness conditions by about 6%. If one takes s as unity for the clear day solar noon measurement, then one obtains a value of s = 1.06 for the early hour and variable cloudiness conditions. This is consistent with the spectral content measurements. For the conditions of high s value, it was found that the spectral content was higher in visible rich light by about 3% of total insolation (Table I). This corresponded to ∿ 6% of the visible content. This component may be associated with the increased diffuse component of the solar insolation (5).

If a median calibration line is drawn and used for insolation measurements, a maximum error of ± 3% is encountered from variations in the spectral response. This error may be corrected for by either adding

(for early hours and variable cloudiness conditions) or subtracting (for clear day solar noon ± one hour) 3% of the reading to determine the intensity value in $mW/cm^2$. The accuracy of the measurements is determined to a large degree by the error in meter reading. An overall accuracy better than 5% can be obtained with the present device. This accuracy is fairly acceptable for field work or off-the-shelf radiometer.

## Conclusions

A $Cu_2S$-CdS radiometer was described. The radiometer possessed the following features:

1. It employed a large area cell which makes it compatible with readily available and inexpensive measuring meters. No amplification of signal is required.

2. It is a self-contained device, no external circuitry or power sources are required. This makes it ideal for field work measurements. The device is, however, compatible with sophisticated instrumentation.

3. The spectral effect may be accounted for in the calibration. An overall accuracy of 3-5% can be obtained.

4. Temperature effects can be eliminated by proper choice of cells.

5. The $Cu_2S$-CdS solar cell has an inherently higher blue response than the silicon cell. The red response is somewhat comparable for the two cells.

## References


1. H. M. Windawi, Proceedings, 11th Photovoltaic Specialists Conference (IEEE, New York 1975), p. 464.

2. A. Rothwarf and K. W. Böer, Prog. Solid State Chem. 10, 71 (1975).

3. M. G. Bonner and C. M. Sapsford, Solar Energy 10, 195 (1966).

4. M. P. Thekaekara, Solar Energy 9, 7 (1965).

5. D. M. Gates, Science 151, 523 (1966).


TABLE I - Spectral contents of solar radiation intensity, $I_T$, measured by an Eppley Precision Pyranometer and the spectral Response Parameter measured by the radiometer for two different times of a day.

| | $I_T$ (%) | | |
|---|---|---|---|
| Wavelength (μm) | AMO[4] | Solar Noon (AM1.2) | 10 a.m. |
| to - .50 | 23.5 | 20.0 | 20.5 |
| .50 - .53 | 4.1 | 4.3 | 4.7 |
| .53 - .63 | 13.3 | 14.3 | 15.7 |
| .63 - .70 | 7.9 | 9.3 | 9.8 |
| > .70 | 51.2 | 52.1 | 49.2 |
| S | | 1.00 | 1.06 |

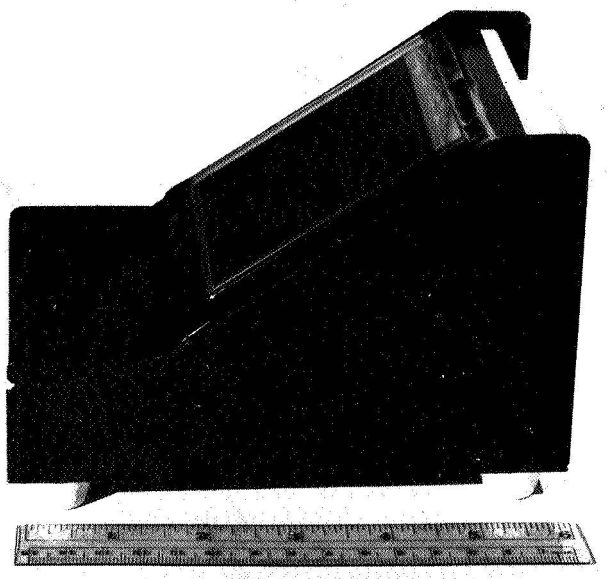

Figure 1. A view of the radiometer showing the $Cu_2S$-CdS solar cell tilted from the horizontal. The meter is on the right side of the instrument.

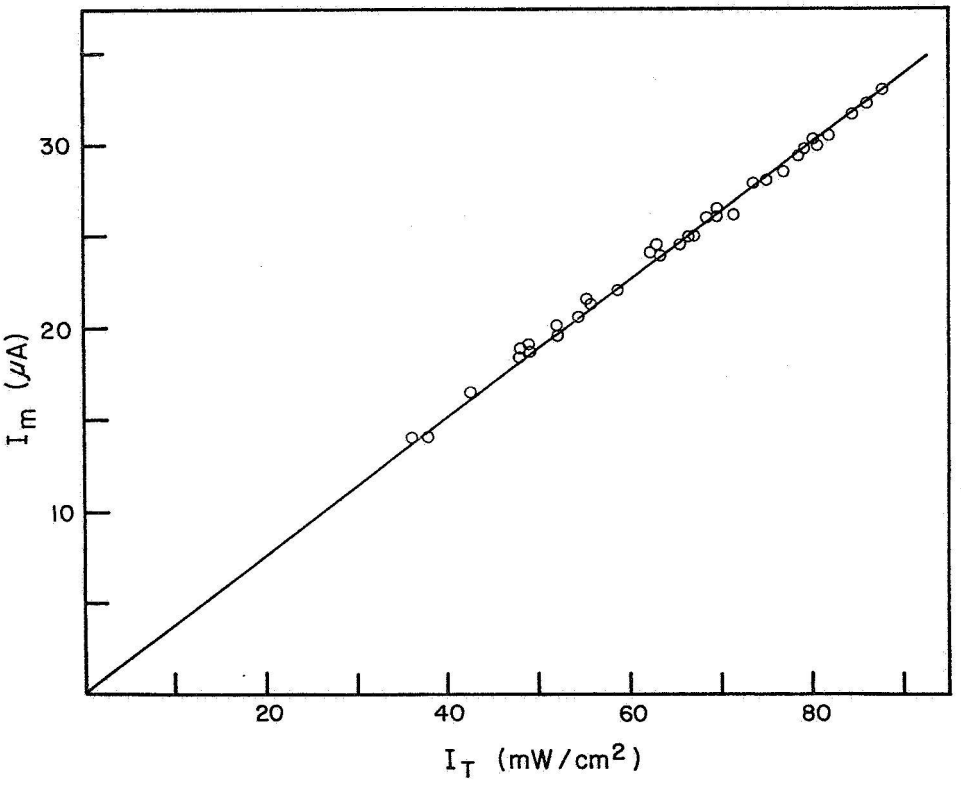


Figure 2. The response of the radiometer (in μA) to light intensity (mW/cm$^2$) measured by an Eppley Precision Pyranometer. Measurements were made for about an hour on a day with variable cloudiness.

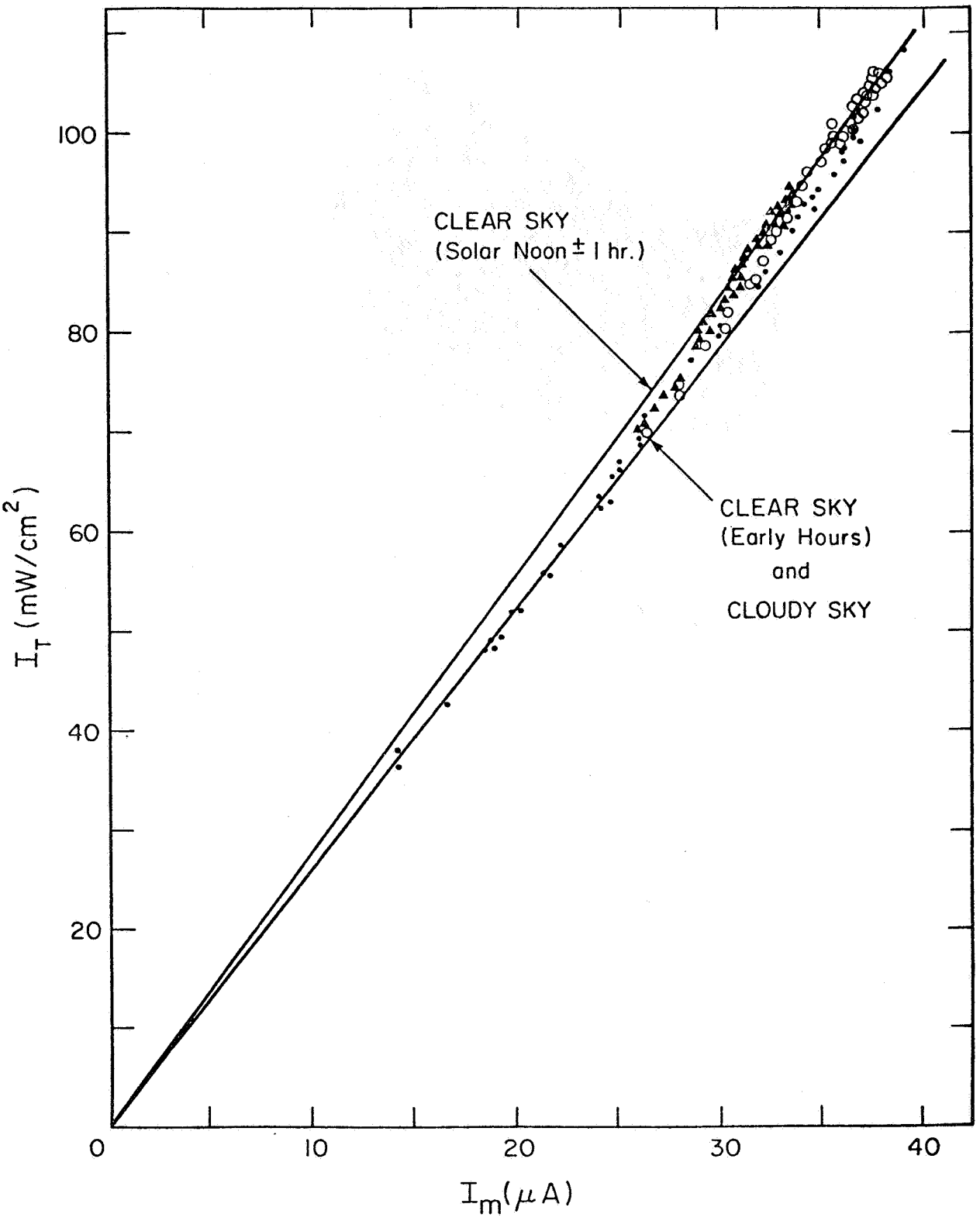


Figure 3. Calibration of the radiometer for various conditions shown.

# TEST FACILITY FOR SOLAR-CELL REFERENCE CONDITIONS

by Thomas M. Klucher

Lewis Research Center
National Aeronautics and Space Administration
Cleveland, Ohio

## ABSTRACT

A test facility, intended primarily for long-term monitoring of the global insolation and its components and the concurrent solar-cell performance under a wide variety of measureable atmospheric and weather conditions, is described. Instruments for the measurement of insolation, cell performance, turbidity, water vapor, and cloud cover are described. Preliminary evaluation of the hourly data base generated over a two-month period for a range of sky conditions from clear to overcast is presented.

## SUMMARY

This report describes the Solar-Cell Reference-Condition Test Facility built for the purpose of long-term monitoring of global insolation (at a given location, the total insolation impinging on a horizontal surface) and concurrent solar-cell performance under a wide variety of atmospheric and weather conditions. Instruments to measure insolation, cell performance, atmospheric turbidity, water vapor and cloud cover are described. Preliminary evaluation of hourly data generated over a two-month period has shown (1) a 9% decrease in cell sensitivity (current output-to-insolation intensity ratio) as sun elevation angle decreases from 56.5° to 19.3° on clear or partly cloudy days and (2) cell sensitivity increases up to 15% with decrease in intensity for overcast skies. Based on these early results, it appears that atmospheric conditions should be clearly established when making cell performance measurements under global insolation.

## INTRODUCTION

At present, there is no long-term data base available which can be used to determine the sensitivity of solar cells to variations in the components of global solar radiation. Furthermore, solar cell performance data are usually obtained only under clear-sky conditions. Such measurements are generally used to establish an index of cell performance for comparisons between cells. While there is a need for these comparative performance indices, there is also a need to determine the sensitivity of cells under the range of atmospheric conditions which may be encountered throughout the year. Such information is valuable not only to those whose main interest is generation of power from solar arrays, but also to the photovoltaic investigator who wishes to relate the performance index of a particular cell with typical insolation conditions.

A reference condition test facility was constructed in June 1976, at the NASA Lewis Research Center (LeRC), Cleveland, Ohio, to meet these needs. The facility, located on the roof of the Energy Conversion Laboratory, is intended primarily for acquisition of averaged hourly data on global insolation and its components and the concurrent silicon solar-cell performance under a wide variety of measured atmospheric and weather conditions. This report describes the capability of the system and instruments for acquisition of insolation, cell performance, turbidity, water vapor and cloud cover data. Typical results of hourly data generated over a two-month period for sky condition from clear to overcast are presented.

## SYSTEM DESCRIPTION

As shown in Figure 1, the data source portion of the system consists of a number of data generation channels, each channel containing

a sensor, a voltage controlled oscillator, and a counter which integrates the data continuously. The data processing subsystem, located in the computing center at the LeRC, consists of a minicomputer which controls the sampling rate of the integrated data, a data collector which receives the data, and the TSS/360 computer used for data base storage and analysis.

The sensor subsystem (Figure 2), is divided into two assemblies, a tracking assembly and a nontracking assembly. The tracking assembly, which is being fabricated, will continuously track the sun and record the direct normal insolation and concurrent solar-cell short-circuit current, and the atmospheric turbidity and water vapor content. The nontracking assembly, which is operational, records the global insolation for surfaces pointed due south at tilt angles of 0°, 37° and 60°. The diffuse sky radiation is also measured. Finally, a camera to record sky conditions will be included in the facility in the near future.

Sensor Subsystem Description

The nontracking insolation and solar cell assembly is shown in Figure 3. Three precision pyranometers measure global insolation received at 0°, 37° and 60° tilt angles. The diffuse component is measured by a fourth pyranometer horizontally mounted and equipped with a shadow band. Solar cell performance is determined with four sensor packages oriented identical to the pyranometers. The solar cell sensors are 1 $cm^2$ in area, soldered on Kovar blocks, and mounted in housings nearly identical to the pyranometer, as shown in Figure 4. Solar cell temperature is measured with a thermocouple attached to the Kovar block and is used to correct cell output for temperature variations. The tilted sensors are equipped with artificial horizons to eliminate surface reflection effects.

## RESULTS AND DISCUSSION

Solar cell sensitivity is defined as the ratio of cell short circuit current, $I_{sc}$, to insolation intensity $I_n$. The sensitivity of horizontally mounted (0°) sensors under differing sky conditions is shown in Figures 5-8. These sensitivities are average values for hourly intervals. The differing symbols stand for different days. Figure 5 shows cell sensitivity as a function of air mass for clear sky days. Clear sky days include those days with light cirrus clouds. It can be seen that cell sensitivity drops from about 0.272 amps/watt at air mass 1.2 (solar elevation of 56.5°) to about 0.247 amp/watt at air mass 3 (solar elevation of 19.3°). The variation at a fixed air mass is caused by changes in the atmospheric turbidity and water vapor. These effects are described in references 1 and 2.

Figure 6 shows the solar cell sensitivity as a function of air mass under partly cloudy skies ($\sim$ 30% cloud cover). For this case sensitivity drops from about 0.269 amps/watt at air mass 1.2 to about 0.245 amps/watt at air mass 3. The sensitivity at air mass 1.2 is about 1% lower than for clear skies. For both clear and partly cloudy skies the percentage decrease in sensitivity is about 9% from air mass 1.2 to air mass 3. This loss in sensitivity is probably due to departures from a cosine response for solar cells with nonnormal incident light. Such departures from cosine behavior have been previously reported (references 3, 4, and 5). The magnitude of the loss and its behavior with air mass are consistent with results in those references.

Figures 7 and 8 demonstrate the sensitivity of the solar cell for several different days under overcast skies. The intensities measured with the pyranometers ranged from 20 to 320 $W/m^2$. The global readings and diffuse readings were practically identical, indicating

that essentially no direct solar radiation was incident on the solar cell and pyranometer. Both figures show considerable scatter in the data; this is probably due to the relatively large errors in the low intensity readings. In figure 7, a plot of the sensitivity versus intensity level appears to display a gradual increase in sensitivity from around 0.27 to about 0.31 as the intensity decreases from 200 to 20 $W/m^2$. In figure 8, the change in sensitivity with air mass may be obscured by the considerable data scatter. The cell current to intensity ratio under global radiation is seen in Figures 5, 6, 7 and 8 to be dependent upon sky condition and sun-cell orientation. Based on these preliminary results, it appears that the atmospheric conditions should be defined when measuring cell performance or performance index by calibration relative to a pyranometer under global insolation.

## APPENDIX - DEFINITIONS

Insolation - Incoming solar radiation flux received by unit area.

Global Insolation - The sum of the solar radiation fluxes received direct from the solid angle of the sun's disk (direct component) and from the solar radiation which has been scattered over the hemispherical sky in traversing the atmosphere (diffuse, or sky, component).

Air Mass - A measure of the length of path through the atmosphere to sea level traversed by light rays from a celestial body, expressed as a multiple of the path length for a light source at the zenith.

Turbidity - Any condition of the atmosphere which reduces its transparency to radiation due to scattering by atmospheric gases, dust and aerosols.

Tilt Angle - The angle which the plane of a sensor makes relative to the horizon.

Sun Photometer - An instrument used to measure the turbidity in the atmosphere.

Pyrheliometer - An instrument for measuring the intensity of direct solar radiation at normal incidence.

Pyranometer - An instrument for measurement of the solar radiation received from the whole hemisphere.

## REFERENCES


1. Klucher, T. M.: Sensitivity of Solar Cell Performance to Atmospheric Variations. I Single Cell
2. Klucher, T. M. and Hart, R. E., Jr.: Sensitivity of Solar Cell Performance to Atmospheric Variations. II Dissimilar Cells at Several Locations
3. Kevern, G. M.: Solar Cell Module Angular Response Technical Memorandum APIP-TM-68-23, Nov. 1968.
4. Tallent, R. J.: Optical Electrical Design Considerations for Concentrating Solar Cell Panels. Paper 62-123, AIEE Summer General Meeting, Denver, Colo., June 17-22, 1962.
5. Selcuk, K. and Yellott, J. I.: Measurement of Direct, Diffuse and Total Radiation with Silicon Photovoltaic Cells, Solar Energy 6, 155-163 (1962).

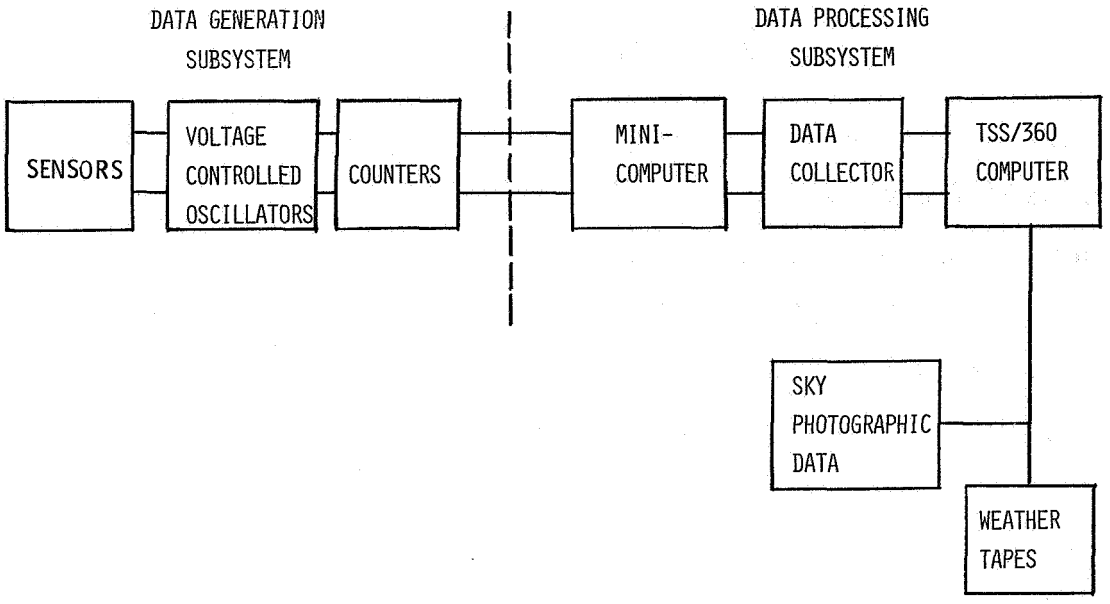


Figure 1. - Reference conditions test facility

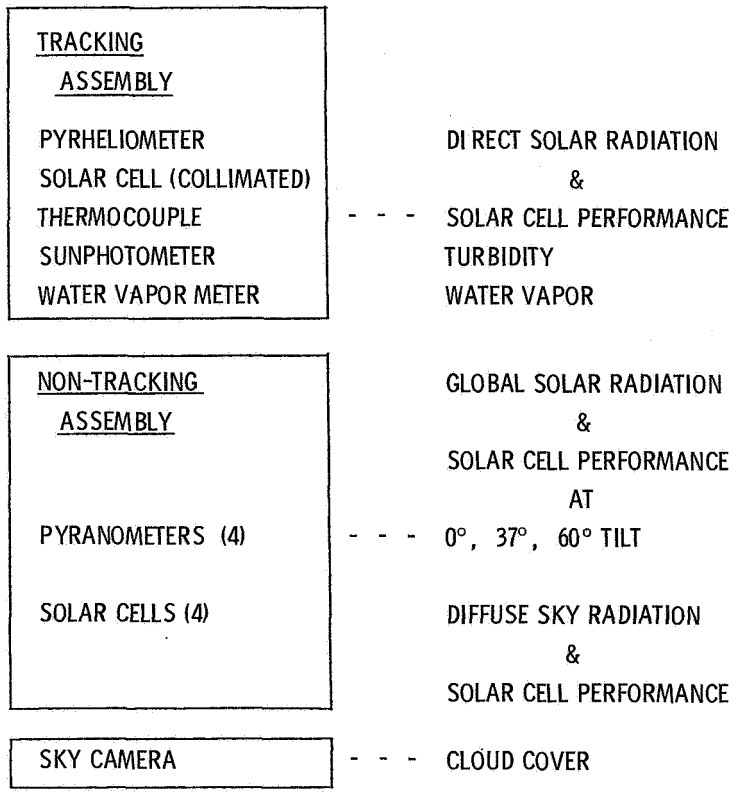


Figure 2. - Sensor Subsystem


Figure 3. - Non-tracking sensor subsystem (pyranometers & solar cells)

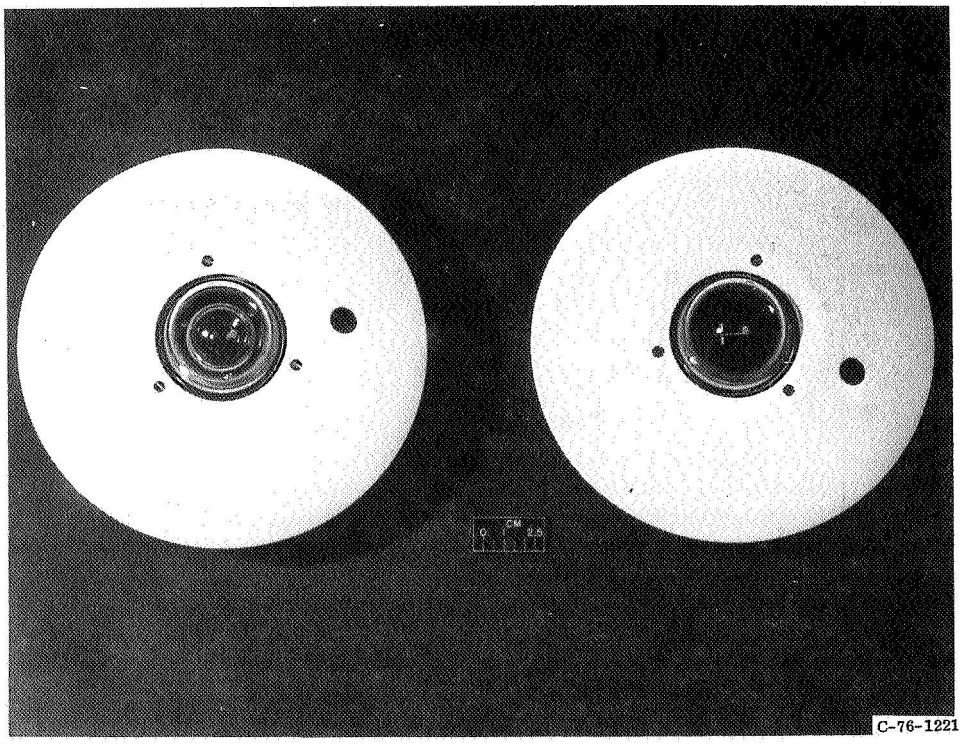


Figure 4. - Pyranometer and solar cells used in solar cell reference conditions test facility

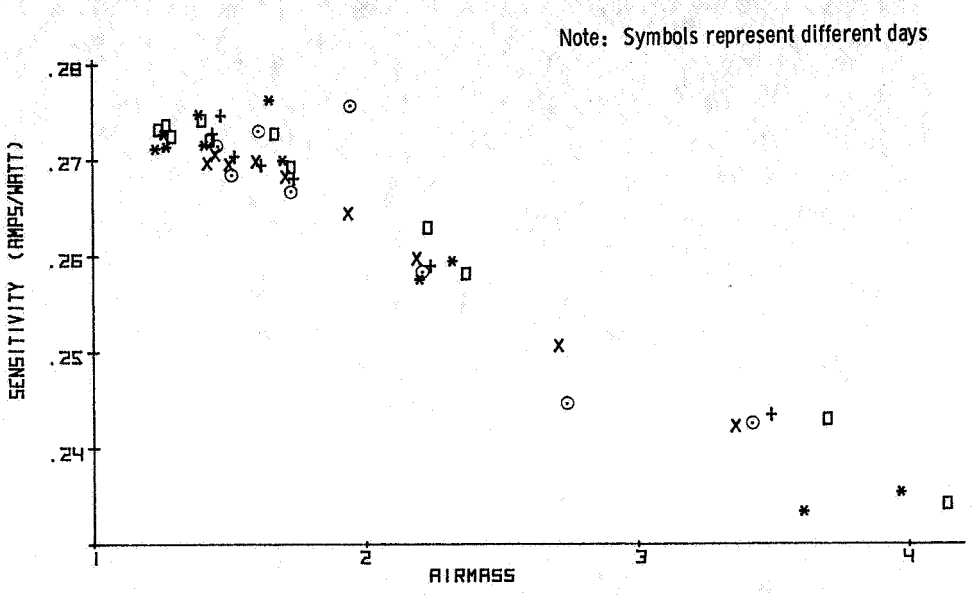


Figure 5. - Sensitivity versus air mass under clear sky (global - 0 tilt)

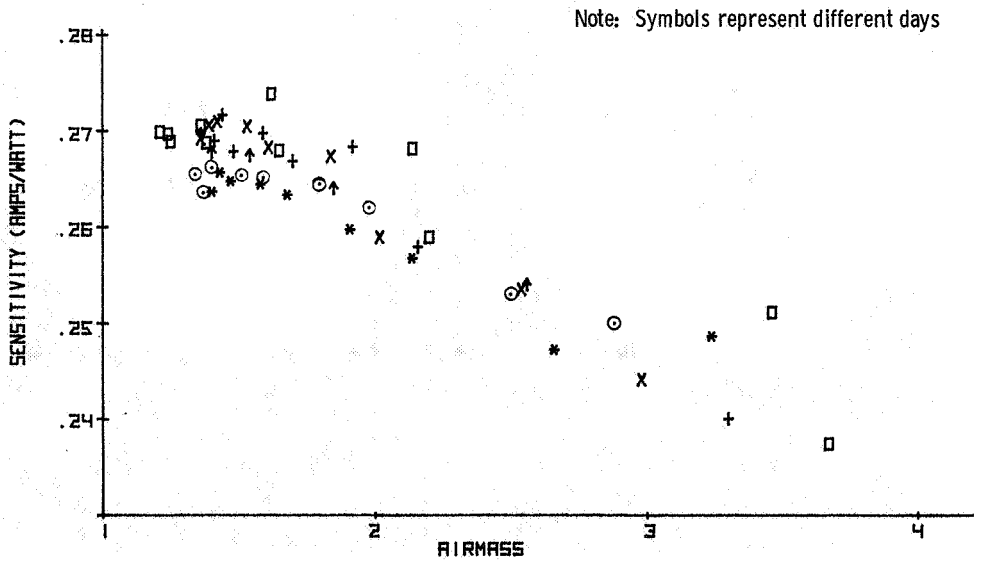


Figure 6. - Sensitivity versus air mass under variable clouds (global - 0 tilt)

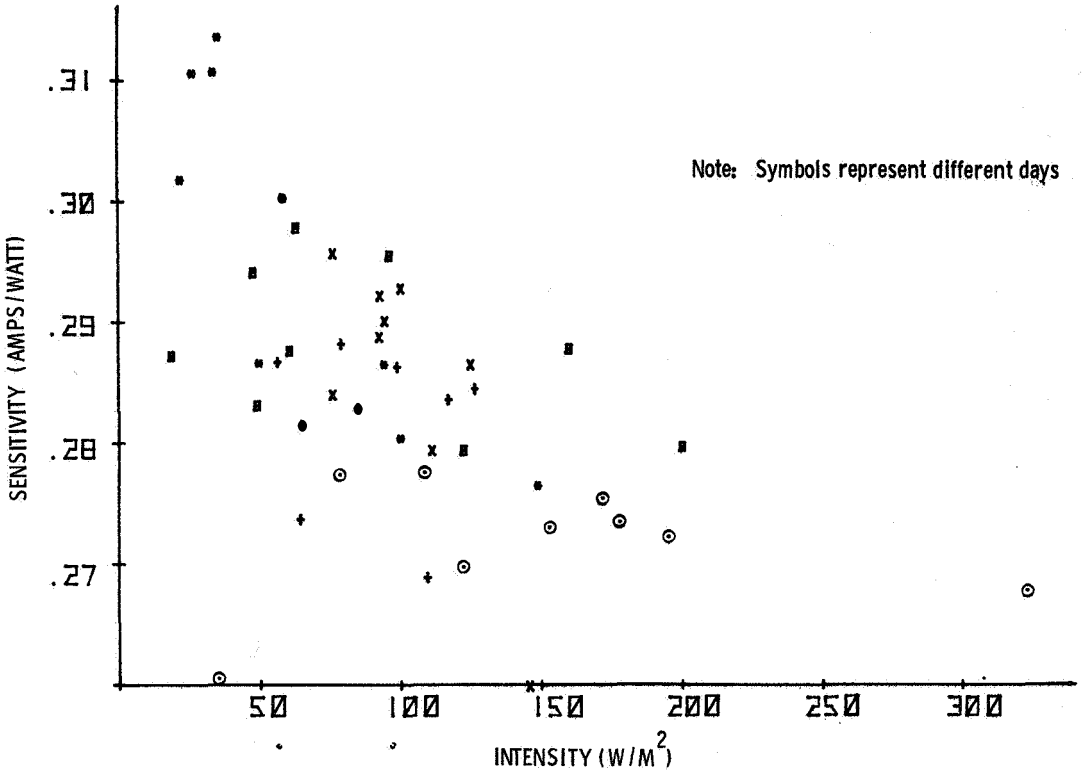


Figure 7. - Sensitivity versus intensity under overcast sky (global - 0 tilt)

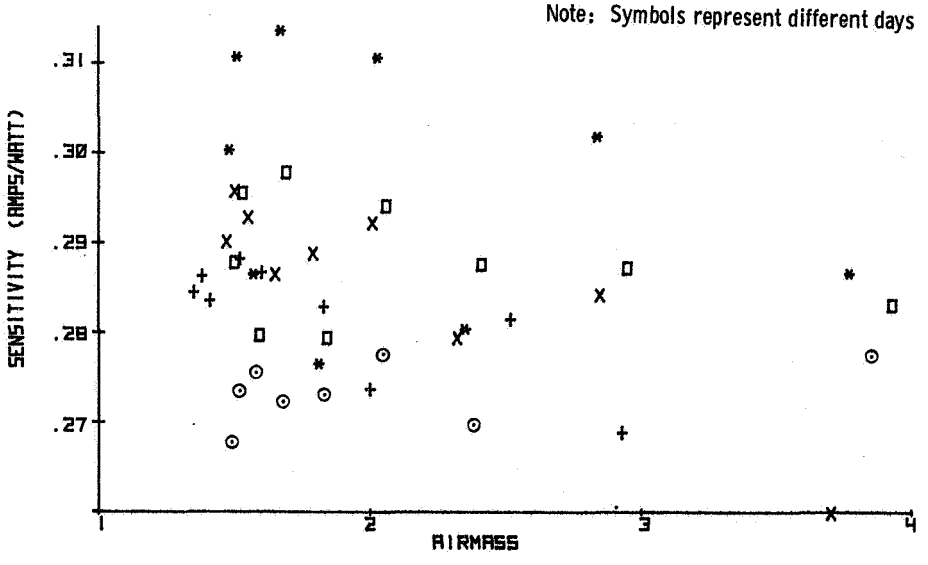


Figure 8. - Sensitivity versus air mass under overcast sky (global - 0 tilt)

# The Effects of Spectral Variations on Silicon Cell Output*

E. C. Boes
I. J. Hall
Sandia Laboratories
Albuquerque, New Mexico 87115

ABSTRACT

The performance of a silicon solar cell at a specific location is usually predicted by multiplying the solar radiation incident at the site by the solar cell's "efficiency." This efficiency is specified as the ratio of the cell's output to the radiant energy input to the cell under specified conditions.

It would be better to use a procedure which takes into account the fact that the performance of a silicon solar cells depends upon the spectral distribution of the incoming energy. This is generally not possible because there are very few records of the spectral distribution of terrestrial solar radiation.

One existing data source consists of spectral measurements of daily, total-horizontal radiation recorded by the Smithsonian Radiation Biology Laboratory at Rockville, Maryland. These data have been analyzed to determine the magnitude and character of the effects in silicon cell output resulting from real variations in the terrestrial solar spectrum. Results are reported.

---

* This work was supported by the United States Energy Research and Development Administration.

# I. INTRODUCTION

The performance of a silicon solar cell at a specific location is usually predicted by multiplying the solar radiation incident at the site by the solar cell's "efficiency." This efficiency is specified as the ratio of the cell's output to the radiant energy input to the cell under specified conditions. This prediction process is inevitably inaccurate because it does not take into account the fact that the solar cell's output depends on the spectral distribution of the incident solar radiation as well as on the total energy flux.

At the present time, there is really no alternative to making performance predictions which neglect the spectral distribution variations because spectral data are generally unavailable. Most people feel that the errors resulting from ignoring spectral variations are generally only a few percent and consequently spectral measurements are not needed on a widespread basis. Nonetheless, the issue has not been definitively resolved. Particularly lacking are results of any study which uses a large body of data to address this question in terms of real differences over a long period of time. The purpose of this paper is to describe the techniques and results of such a study. The differences in solar cell performance predictions based upon (a) spectral measurements and a silicon cell spectral response curve, and (b) a single efficiency for the same cell were analyzed in this study. The Smithsonian Radiation Biology

Laboratory has been making spectral measurements for several years. Although these data are not ideal for this type of study, it is one of the very few existing bodies of spectral data and it includes measurements at accessible locations such as Rockville, MD, whereas some of the other existing spectral data bases were recorded on remote mountains.

The most important feature of this study is the fact that it is based upon a reasonably large body of real data recorded over several years time. It includes data for different seasons and different weather conditions. Hence, the differences in solar cell performance predictions should be representative of the real terrestrial differences due to spectral variations which will be encountered with real photovoltaic installations.

## II. DATA SOURCES AND COMPUTATIONAL PROCEDURE

The data used for this study were the records of daily totals of solar radiation in various wavelength intervals published in Solar Radiation Measurements/1968-1973, by W. H. Klein and B. Goldberg (Smithsonian Radiation Biology Laboratory of Rockville, MD). The Klein-Goldberg report consists of spectral measurements of solar radiation recorded by the Smithsonian Radiation Biology Laboratory. The data was recorded at Rockville, MD between June of 1970 and December of 1973. The measurements were made with Eppley precision pyranometers with various bandpass filters. The instruments were mounted horizontally and each had a 180° field of view. Further details regarding data recording procedures, instruments, calibrations, and accuracy can be found in this publication.

Although this publication contains similar data records for Washington, DC and somewhat shorter data records for Barrow, AK and Panama Canal Zone, it was felt that analyzing the data for Rockville would be a reasonable first step in studying this general problem. Moreover, it was decided that studying the data for all 12 months is probably unnecessary. Data were analyzed for the months of January, April, July, and October.

The basic question addressed is the difference in actual solar cell output and the output as predicted by using a single efficiency

rating for the cell. In this study, actual cell output, AO, was computed each day as follows: The Klein-Goldberg report gives the total daily energy (in Langleys) in each of six wavelength cells. For each wavelength cell we multiplied the energy values by 11.63 and then divided by a length of day value to obtain an average energy intensity value in watt/$m^2$. The intensity values were weighted by values obtained from the response curve given in Figure 2.1 for the silicon solar cell No. Z-33 and then summed to obtain a mean short circuit current, ISC, (in amps/$m^2$) for each day.

Next the open circuit voltage was computed using the formula,

$$VOC = \frac{kT}{q} \ln (ISC/Io)$$

where k is Boltzmann's constant, T is temperature in degrees K, q is electron charge, and $I_o$ is reverse saturation current. The temperature was fixed at 301$^oK$, and the reverse saturation current was calculated for the standard silicon solar cell, identified as Z-33. The calculation of $I_o$ was based upon calibration data for this cell provided by the NASA Lewis Research Center, Cleveland, OH. Finally, the energy output was calculated using the formula,

$$AO = FF \cdot ISC \cdot VOC$$

where the fill factor, FF, was given by NASA-LeRC as .783.

Since the spectral data used as input for this study is not high resolution data in the sense that wavelength intervals are

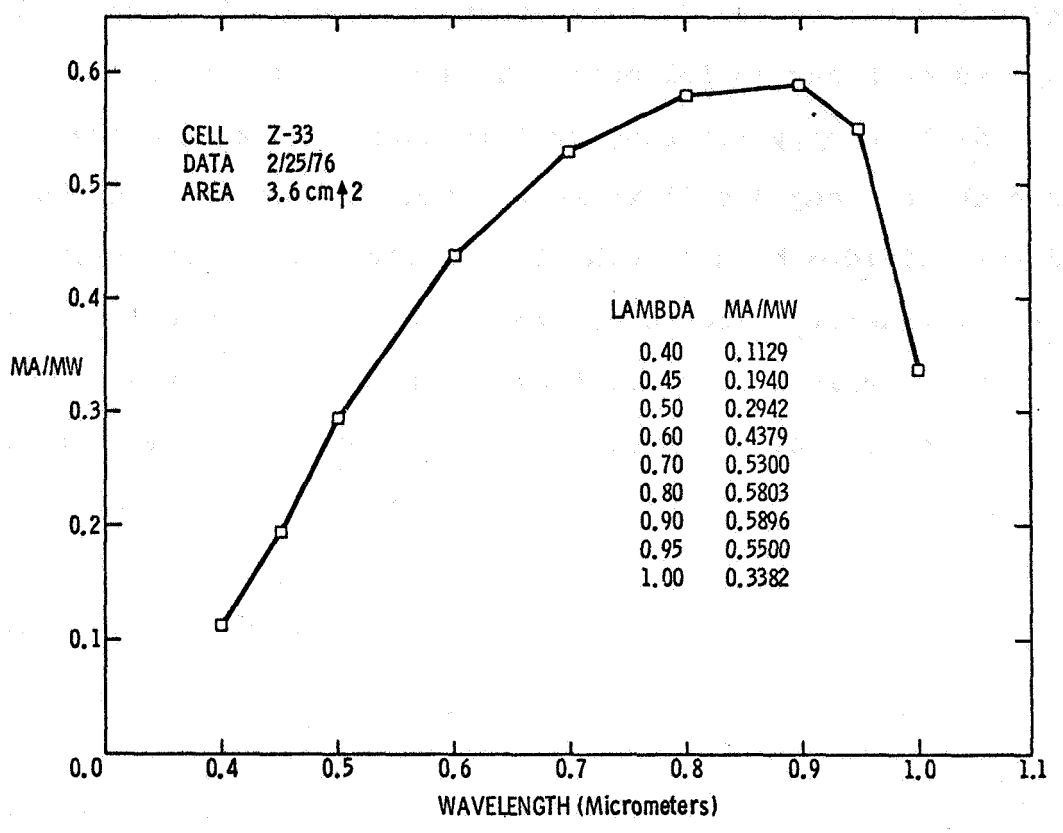


Figure 2.1

quite large, it was necessary to "distribute" the energy recorded in each interval into smaller intervals. Between .4 and .8 microns the energy was simply redistributed from the given .1 micron intervals into intervals of .05 micron width. However, the recorded energy in the rather large .8 - 2.8 micron interval was also redistributed into wavelength intervals of .05 micron width, and this redistribution is important because both the peak response region and the cut-off for the silicon cell occur in this interval. In all cases, the redistribution was based upon the proportions in the air mass 2 solar spectrum.

It should be pointed out that in the calculation of open circuit voltage VOC, the value for short circuit current ISC was treated as an average short circuit current for the day. Calculation of this average short circuit current requires that the recorded energy distribution for each day be converted to an intensity distribution by division of day length. A single day length was used in each month for simplicity; these are given in Table 2.2, which also lists the total number of days in the data sample for each of the four months.

In order to duplicate the usual procedure for predicting solar cell output, an "efficiency" was determined for the cell for each month. This efficiency in each month was defined as the ratio of actual energy output from the cell, AO, divided by total energy input to the cell for the two "best" days. These

TABLE 2.2

Sample Sizes, Day Lengths, and Efficiencies Used in the Study

| | Jan | Apr | Jul | Oct |
|---|---|---|---|---|
| Sample Size (days) | 83 | 72 | 111 | 115 |
| Day Length (hours) | 9.67 | 13.03 | 18.13 | 11.05 |
| Efficiencies (%) | 13.9 | 14.0 | 14.2 | 14.5 |

two "best" days for each month were simply selected as the two days having the highest recorded solar radiation values for that month over the years of the data base. It was felt that this method of specifying efficiencies would offer a reasonable compromise between the wish to calibrate under sunny conditions and the desire to measure an efficiency under conditions resembling the hypothetical operating conditions of this cell, oriented horizontally and operating throughout the day. The efficiencies computed for the cell as described and used in the study are given in Table 2.2. The predicted output, PO, of the cell for each day was calculated very simply as the product of the total energy available for the day and the cell efficiency.

Another possible way to assign an efficiency to the cell would have been to simply use the efficiency rating assigned to this cell by NASA-LeRC. This efficiency is 12.94%. The effect of using 12.94% instead of the efficiencies given in Table 2.2 would be that all of the values for predicted output, PO, would be lowered by about 7%. The resulting effects on the results of this study are discussed briefly in Section 4.

# III. RESULTS

For the month of January, the mean percent error was 3.5%. In other words, 3.5% is the mean of the numbers (PO(I)-AO(I))/AO(I) where I ranges over the 83 days for January in the sample. The standard deviation of these errors is 4.4%. Thus, if the errors are normally distributed, approximately 95% of the errors should lie between -5.3% and +12.3%. The same calculations of percent errors were made for the data samples for April, July, and October. Table 3.1 gives the means and standard deviations of these percent errors for all four months. As stated above, these percent errors are the difference PO-AO expressed as a percent of AO for each day. Note also that the entries in the last column were calculated by simply taking weighted means of the entries in the first four columns, where the weights are proportional to the numbers of days.

These data suggests that reasonably large percent errors are not uncommon. However, large percent errors are not too important in conditions of low solar irradiance when solar cell outputs are quite low anyway. For this reason, the differences between AO and PO were also studied as a percent of cell output for sunny days. This study was also performed on a monthly basis. For each month, AOMAX was calculated as the average of the two highest values of cell output, AO. Then the daily differences PO-AO were computed and analyzed as a percent of AOMAX. The means and standard deviations of these "percent of sunny day output" errors are given in Table 3.2. This table indicates that the difference in PO and AO is generally only about 1% of the cell output for sunny days.

The differences in actual cell output and predicted cell output were studied in yet another way. For each month, the data was ranked according to the daily values of output AO, and then sorted into quartiles with respect to this ranking. In each quartile, the ratio of the mean error to the mean output was computed; the precise formula for this ratio is $(\sum(PO-AO))/(\sum AO)$. These ratios are given for all four quartiles for each of the four months in Table 3.3.

TABLE 3.1

Summary of Percent Errors

| | Jan | Apr | Jul | Oct | Means |
|---|---|---|---|---|---|
| Number of days | 83 | 72 | 111 | 115 | |
| Mean errors | 3.5% | 1.3% | 2.0% | 5.5% | 3.25% |
| Std. dev. of errors | 4.5% | 3.5% | 2.2% | 4.3% | 3.58% |

TABLE 3.2

Statistics of the Differences in Actual and Predicted Outputs Expressed as a Percent of the Output for a Sunny Day

| | Jan | Apr | Jul | Oct | Means |
|---|---|---|---|---|---|
| Number of days | 83 | 72 | 111 | 115 | |
| Mean of nos $\left(100\frac{PO-AO}{AOMAX}\right)\%$ | 0.9% | -0.1% | 1.0% | 2.0% | 1.07% |
| Std. dev. of nos $\left(100\frac{PO-AO}{AOMAX}\right)\%$ | 1.1% | 1.5% | 1.0% | 1.2% | 1.16% |

Inspection of Table 3.3 indicates that generally for those days with relatively high cell outputs the percent errors are quite small. Thus, both Tables 3.2 and 3.3 support the conclusion that the error made in predicting silicon solar cell output by multiplying the total radiation available by a single efficiency is generally very small. Only during rather cloudy conditions does the error represent a significant fraction of the cell's output.

This study has several limitations. The first is that it was performed using only one type of silicon cell. Although the conclusions probably apply to other silicon cells, it is not known whether similar results are valid for other cells, such as gallium arsenide cells or cadmium sulfide cells. Another limitation is the fact that the solar data used consisted of daily totals of radiation. Larger errors might occur for data recorded over shorter time intervals. Also, the input data refer only to a horizontal surface. However, it does not seem likely that errors would be greater for non-horizontal surfaces. A third limitation of this study is the fact that the resolution of the spectral data used was fairly course. The most serious deficiency in resolution was in the last wavelength interval, .8 - 2.8 microns. The problem here, as mentioned in Section II, is that both the peak response and the cut-off for a silicon cell lie in this interval. A final limitation is the fact that this study was performed for only one location.

In spite of these shortcomings, the results of this study are worthwhile because they are based upon a large body of real data. No

previous study of the errors which result from predicting solar cell performance by using a single efficiency used such a large data source recorded over a long period. Hence, this is the first study which can be expected to indicate the types of errors which will occur over long-time intervals in real applications.

TABLE 3.3

Mean Errors as Fractions
of Mean Output for Data Quartiles

| | 1st Quartile | 2nd Quartile | 3rd Quartile | 4th Quartile |
|---|---|---|---|---|
| January | | | | |
| Number of days | 20 | 20 | 20 | 23 |
| Mean output ($W \cdot hr/m^2$ day) | 395 | 330 | 227 | 86 |
| Mean error | -1.185 | 3.300 | 5.902 | 6.880 |
| Ratio: $\frac{\text{Mean error}}{\text{Mean output}}$ | -0.003 | 0.01 | 0.026 | 0.080 |
| April | | | | |
| Number of days | 18 | 18 | 18 | 18 |
| Mean output ($W \cdot hr/m^2$ day) | 975 | 827 | 611 | 224 |
| Mean error | -13.650 | -7.443 | 4.888 | 11.648 |
| Ratio: $\frac{\text{Mean error}}{\text{Mean output}}$ | -0.014 | -0.009 | 0.008 | 0.052 |
| July | | | | |
| Number of days | 27 | 27 | 27 | 30 |
| Mean output ($W \cdot hr/m^2$ day) | 1039 | 901 | 763 | 479 |
| Mean error | 4.156 | 9.010 | 14.497 | 17.723 |
| Ratio: $\frac{\text{Mean error}}{\text{Mean Output}}$ | 0.004 | 0.010 | 0.019 | 0.037 |
| October | | | | |
| Number of days | 28 | 28 | 28 | 31 |
| Mean output ($W \cdot hr/m^2$ day) | 641 | 518 | 315 | 141 |
| Mean error | 12.820 | 12.950 | 17.640 | 13.818 |
| Ratio: $\frac{\text{Mean error}}{\text{Mean Output}}$ | 0.020 | 0.025 | 0.056 | 0.098 |

# IV. CONCLUSIONS

The results presented in the preceding section indicate that the errors in silicon solar cell performance predictions which result from neglecting the variations in the terrestrial solar spectrum are generally less than 5% (Table 3.1). Moreover, these errors are generally less than 2% of the output of the cell on sunny days (Table 3.2). Thus, there does not appear to be a need for spectral data measurements on a widespread basis. It should be kept in mind that even though these results were derived for a single site, the study used a rather large body of real data recorded over several years. Consequently, the results should be indicative of real differences which will be experienced with photovoltaic devices.

Several limitations to this study were pointed out in Section 3. Because of these limitations, similar studies should be performed as time and data permit. These future studies, as well as other future research efforts, will require spectral data. Consequently, spectral data measurements should be recorded at a few sites around the country.

The fact that efficiencies were computed for this cell, as described in Section 2, has little influence on the main results of this study. Using a slightly different efficiency has the effect of translating the differences, PO-AO, but it does not appreciably change the range of errors, and for this study, it is the range of errors that is of primary interest.

# THE EFFECT OF ATMOSPHERIC PARAMETERS ON SILICON CELL PERFORMANCE

Henry B. Curtis
National Aeronautics and Space Administration
Lewis Research Center
Cleveland, Ohio

## ABSTRACT

The effects of changing atmospheric parameters on the performance of a typical silicon solar cell have been calculated. The precipitable water vapor content, airmass and turbidity were varied over wide ranges and the normal terrestrial distribution of spectral irradiance was calculated. The cell short-circuit current was then computed for each spectral irradiance distribution using the cell spectral response. Data are presented in the form of calibration number (cell current/incident irradiance) vs. water vapor content or turbidity.

## INTRODUCTION

The spectral distribution of terrestrial solar irradiance varies widely with changing atmospheric parameters. Variables such as amount of precipitable water vapor, airmass, turbidity and ozone content all affect the spectral distribution. For example, increasing water vapor content increases absorption in the infra-red, but has little effect on visible irradiance. Similarly, turbidity generally affects only the visible portion of the spectrum. Solar cells, in general, respond to a limited portion of the terrestrial solar irradiance, below about 1.2 μm.

Hence, any change in the solar irradiance caused by changes in atmospheric composition will have a variable effect on the solar cell output. For example, changes in water vapor content will affect total irradiance but have a lesser effect on solar cell current because most of the water vapor absorption occurs beyond 1.2 μm. The net result is a significant change in the ratio of cell current to irradiance which is defined as the calibration number.

The purpose of this paper is to calculate the effects of changing atmospheric composition on the output of a typical silicon solar cell. The approach is to calculate the direct spectral solar irradiance as a function of the atmospheric parameters and then calculate cell performance using the spectral response curve of the cell.

## SPECTRAL IRRADIANCE MODEL

The mathematical model and data used for the calculation of direct solar irradiance is from M. Thekaekara of NASA/Goddard (Ref. 1). The terrestrial spectral irradiance is derived from the following equation using the outer space spectral irradiance distribution (AMO) as the source spectrum.

$$E_\lambda = E_\lambda^o \left[ e^{-\left(c_1 + c_2 + \frac{\beta}{\lambda\alpha}\right)m} \right] T_{\lambda i}$$

Where $T_{\lambda i}$ is a transmission factor for various molecular absorptions and has one of the following three different forms at any given wavelength.

$$T_{\lambda 1} = e^{-c_4\sqrt{wm}} \quad ; \quad T_{\lambda 2} = e^{-c_5 wm} \qquad T_{\lambda 3} = 1 - c_6\sqrt{m}$$

Where:

| | |
|---|---|
| $E_\lambda^o$ | AMO Spectral Irradiance (Ref. 2) |
| $c_1$ | optical depth due to ozone |
| $c_2$ | optical depth due to Rayleigh scattering |
| $\lambda$ | wavelength |
| $\beta$, $\alpha$ | turbidity factors |
| w | precipitable water vapor content |
| m | air mass |
| $c_4$, $c_5$, $c_6$ | I.R. absorption constants |

The ozone and Rayleigh constants are from Elterman (Ref. 3) and the IR constants from Gates (Refs. 4, 5).

This model was used by Thekaekara to derive the AM2 distribution presented in the document Interim Solar Cell Testing Procedures for Terrestrial Applications (Ref. 6). This model computes the direct component only and does not include any forward scattering from the turbidity. For the purposes of these calculations, the lack of forward scattering should have no great effect.

One change was made in the values of the infrared (IR) region constants used by Thekaekara. Figure 1 shows the calculated transmission of the atmosphere containing 20 mm of water vapor at an air mass of 2 in the near IR. The solid curve is calculated with Thekaekara's constants. A broad absorption band from about 0.83 $\mu$m to about 1.0 $\mu$m is shown. This absorption band does not appear in any available water vapor absorption data on atmospheric transmission

data, hence it appears erroneous. Therefore the IR constants in the wavelength range of 0.835 μm to 0.925 μm were changed to obtain the transmission curve shown by the dotted line. No further changes were made in Thekaekara's model.

The spectral irradiance was calculated for the following range of atmospheric parameters:

water vapor content - 0 to 30 mm

airmass - 1 to 4

turbidity factor, $\beta$ - 0 to 0.2

turbidity factor, $\alpha$ 1.3

The range of values for airmass, $\beta$ , and water vapor content should cover almost all possible terrestrial situations. There were 4 airmass values, 6 $\beta$ values, and 17 water vapor values. Hence 408 (4x6x17) different spectral irradiance distributions were calculated. For each spectral distribution, a calibration number for a single silicon solar cell was calculated as described in the following section.

## Cell Performance Calculations

The effect of change in atmospheric parameters on silicon solar cell performance was determined by calculation of the cell calibration number. Cell calibration number is defined as follows:

$$\text{Cal \#} = \frac{\int R_\lambda \, E_\lambda \, d\lambda}{\int E_\lambda \, d_\lambda} \times \text{cell active area}$$

where $R_\lambda$ = spectral response (mA/mW) of the silicon solar cell.

$E_\lambda$ solar spectral irradiance ($mW/cm^2 \cdot \mu m$)

The calibration number of the cell is simply the cell short circuit current divided by the irradiance incident upon the cell. A calibration number was calculated for each of the spectral distribution described previously.

The spectral response of the silicon solar cell (#Z-01) used in these calculations is shown in figure 2. The cell is a 2x2 cm cell with SiO antireflection coating. The response of this cell is generally typical of terrestrial silicon solar cells. The response is based on cell active area (3.53 $cm^2$) and was obtained using a series of narrow band pass monochromatic interference filters. Absolute accuracy of the data are probably no better than $\pm$5%.

## THEORETICAL RESULTS AND DISCUSSION

The calculated data are summarized in figures 3-6. Figure 3 shows calibration number plotted against water vapor content at airmass 1 for three different $\beta$ values. Figure 4 is the same except the airmass is 2. In both of these curves, the calibration number increases sharply with water vapor for awhile then the rate of increase tends to level off. In the airmass 1 curve, the break is at a water vapor content of about 5 mm, while in the airmass 2 curve, it occurs at about 3 mm. In both cases, the water vapor-airmass product is 5 to 6 mm. This suggests that the total water vapor content through which the sunlight passes is the important factor. The increase in calibration number with water vapor content results from the increased absorption primarily in the IR region beyond the response of the cell. This leads to a lowering of the incident irradiance. Because the reduction occurs primarily in the infrared, the cell current is not lowered as much. Since calibration number is current/irradiance, the calibration number increases. This increase can be substantial. For airmass 1 and a beta value of 0.12, the calibration number increases 3.6%, for a change of 5 mm to 20 mm of water vapor. The increase jumps to 5.3% for

the airmass 2 case. For water vapor values below 5 mm, the effect is even more dramatic, however, such low water vapor contents are not normally seen in the terrestrial environment.

Figure 5 shows calibration number as function of beta for three water vapor values and an airmass of 1. Figure 6 is the same plot at airmass 2. In opposition to the water vapor case, the calibration number decreases with increasing beta. Note also that the magnitude of the decrease is much larger for the airmass 2 case than in the airmass 1 case. For example, the calibration number drops 2.8% as beta increases from 0.04 to 0.12 at 20 mm of water and airmass 2. The decrease is only 1.0% at airmass 1. This decrease in calibration number with increasing beta occurs because increases in beta affects the irradiance more heavily in the wavelength region where the cell responds. Cell current is lowered by a larger percentage than the irradiance, hence the calibration number decreases.

Similar curves for higher airmass values can be generated, however, at a combination of airmass 3 or 4 and a high value of either beta or water vapor content, the calculated irradiance becomes quite low. At airmass 3, most of the irradiance levels for beta and water vapor values in figures 3-6 are below 55 $mW/cm^2$.

## EXPERIMENTAL VERIFICATION

The changes in calibration number discussed above are the results of calculations. To verify these results, cell Z-01 was measured outdoors under a range of atmospheric conditions. The cell was placed in a collimating tube and aligned perpendicular to the

sun. The cell short circuit current and the output of a normal incidence pyrheliometer (NIP) were measured simultaneously. Both the NIP and the collimating tube had the same field of view (5.3°). At the same time, airmass, water vapor content, and the Schuepp's turbidity coefficient ( $\beta$ at $\alpha$ = 1.3) were measured. Data were only taken when there was a cloud-free direct solar beam. Thirty-seven different data points were obtained over the following range of parameters:

| | |
|---|---|
| airmass | 1.6 - 4.2 |
| beta | .029 - .119 |
| water vapor | 4.6 - 14.1 mm |
| cal. number | 1.058 - 1.149 mA/mW/cm$^2$ |

Beta and water vapor content were measured using a Volz sun photometer. Airmass was calculated from the sun angle and atmospheric pressure. The calibration number was calculated directly from the short circuit current of cell Z-01 and the NIP reading. In order to readily compare the measured calibration numbers to the model, spectral irradiances were calculated for each of the 37 data points. Comparison between calculated and measured irradiance is shown in figure 7. A similar comparison for short circuit currents is shown in figure 8. In both figures, the straight line is the locus of points where calculated and measured values are equal.

In the irradiance figure (fig. 7), the measured values are larger than the calculated values with two exceptions. One is at a very low irradiance level ($\sim$ 34 mW/cm$^2$) and the second near 62 mW/cm$^2$ No explanation for these anomalies is offered. The difference between the curves is about 6%. In the current figure (fig. 8), the data look similar to the irradiance case except the measured value is now about 9% higher than the calculated value. In both cases, the

consistent differences indicate some non-random error. Possible explanations are the incompleteness of the irradiance model, or an error in the measurement of the atmospheric parameters.

Figure 9 shows the comparison between the measured and calculated calibration numbers. In all cases, the measured value is greater than the calculated value. The average difference is 3.1% with a range of 1.4 to 4.9%. Again, the difference is fairly consistent, considering the data scatter between measured and calculated values for irradiance and cell current.

As noted earlier, one change was made in the infrared absorption constants in Thekaekara's irradiance model. Before the change, the difference between measured and calculated values of calibration number was about 7% with a range of 4% to 10%. However, the basic trends of calibration number with increasing water vapor, turbidity or airmass were the same. This suggests that some small additional modification in the irradiance model could bring agreement between the measured and calculated calibration numbers while having no effect on the variation of calibration numbers with increasing atmospheric parameters.

## SUMMARY OF RESULTS

It has been shown that the calibration number (cell current/incident irradiance) of a typical silicon solar cell varies significantly with changing atmospheric parameters. Increases of 5% or more in the calibration number for reasonable changes in atmospheric water vapor content are seen. The effect of changes in turbidity are significant but not quite as large as in the water vapor case. Increasing turbidity reduces the calibration number. Airmass is also an important parameter, especially in the turbidity case, where

changes in calibration number for a given turbidity change are twice as large at airmass 2 than airmass 1. Direct comparison of calculated and experimental data for a silicon solar cell were made under differing atmospheric compositions. Measured values of irradiance, short circuit current, and calibration number were greater than the calculated values by 6%, 9% and 3% respectively. Small changes in the theoretical model may reduce this spread.

## REFERENCES


1. M. P. Thekaekara, Survey of Quantitative Data on the Solar Energy and its Spectral Distribution, Conference of COMPLES, (Cooperation Mediterraneenne sour l'Energie Solaire), Dahran Saudi Arabia, Nov. 1975.
2. Anon, Solar Electromagnetic Radiation, NASA SP-8005 (1971).
3. L. Elterman, UV.Visible and IR Attenuation for Altitudes to 50 km, 1968 AFCRL-68-0153, Office of Aerospace Research, U.S. Air Force, (1968).
4. D. M. Gates and W. J. Harrop, Infrared Transmission of the Atmosphere to Solar Radiation, App. Optics. Vol. 2, p. 887 (1963).
5. D. M. Gates, Near Infrared Atmospheric Transmission to Solar Radiation, J. Opt. Soc. Am. Vol. 50, p. 1299, (1960).
6. H. Brandhorst, et al, Interim Solar Cell Testing Procedures for Terrestrial Applications, NASA TM X-71771 (1975).

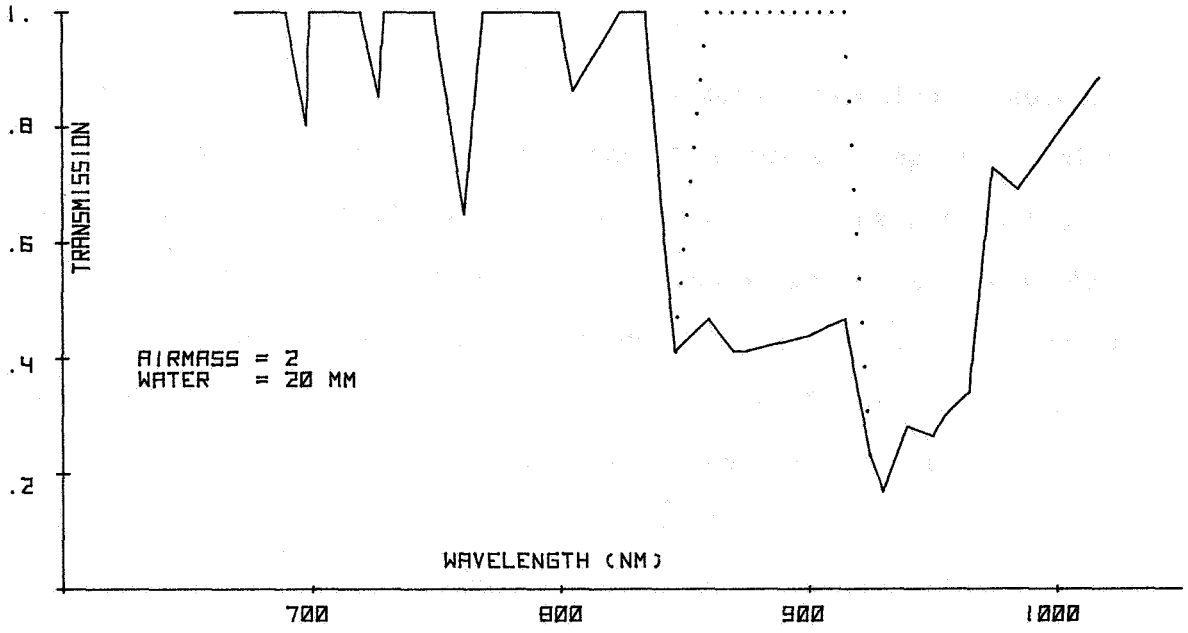


Figure 1. - Transmission of the atmosphere due to water vapor content in the near IR

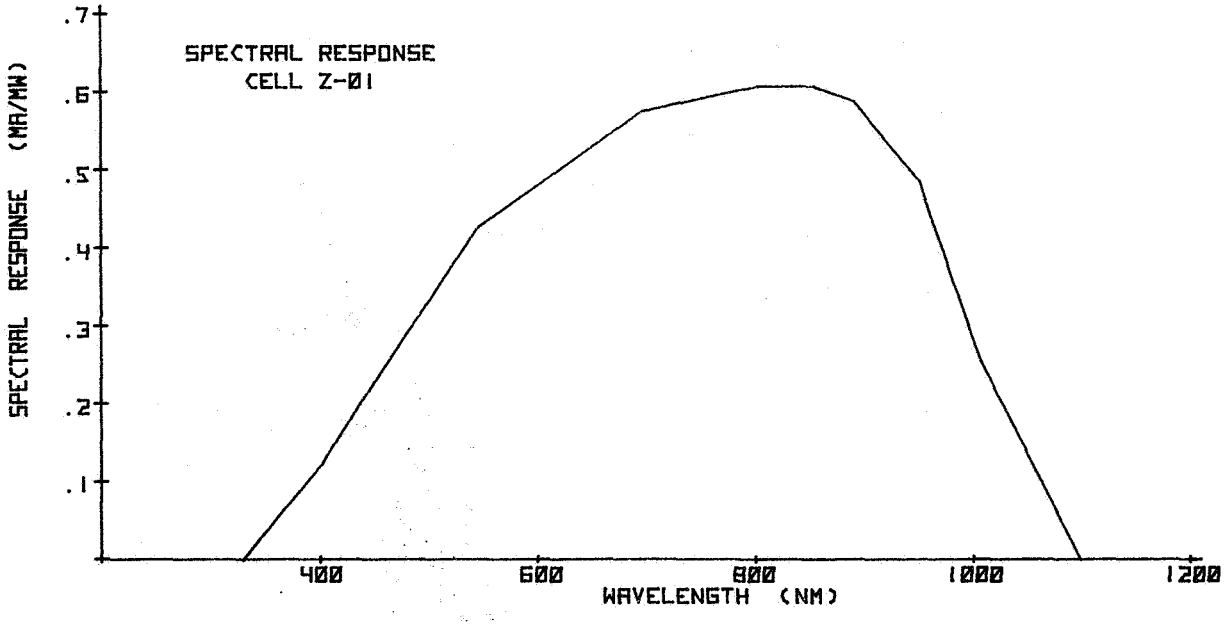


Figure 2. - Spectral response of cell Z-01

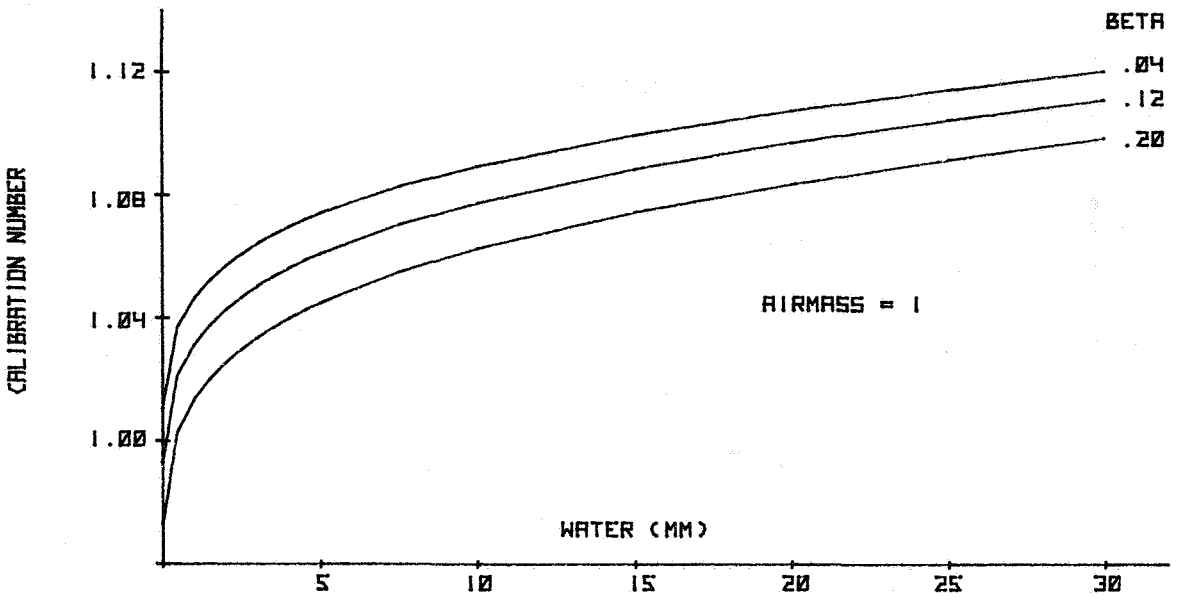


Figure 3. - Effect of water vapor on cell calibration number for Air Mass 1 sunlight

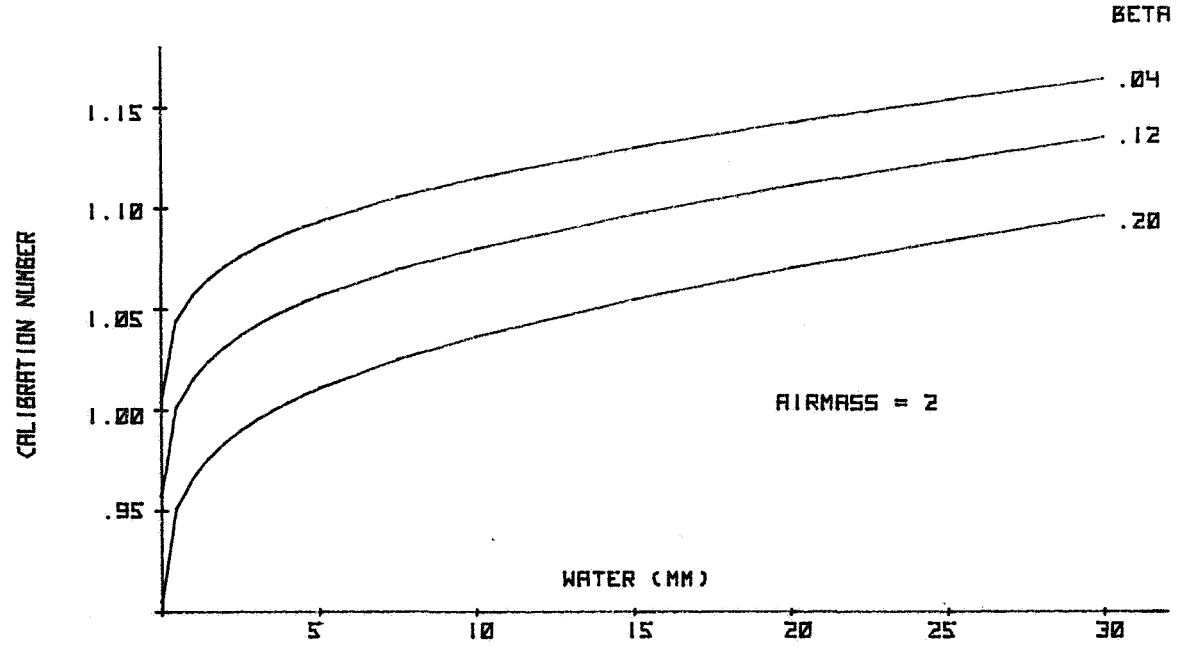


Figure 4. - Effect of water vapor on cell calibration number for Air Mass 2 sunlight

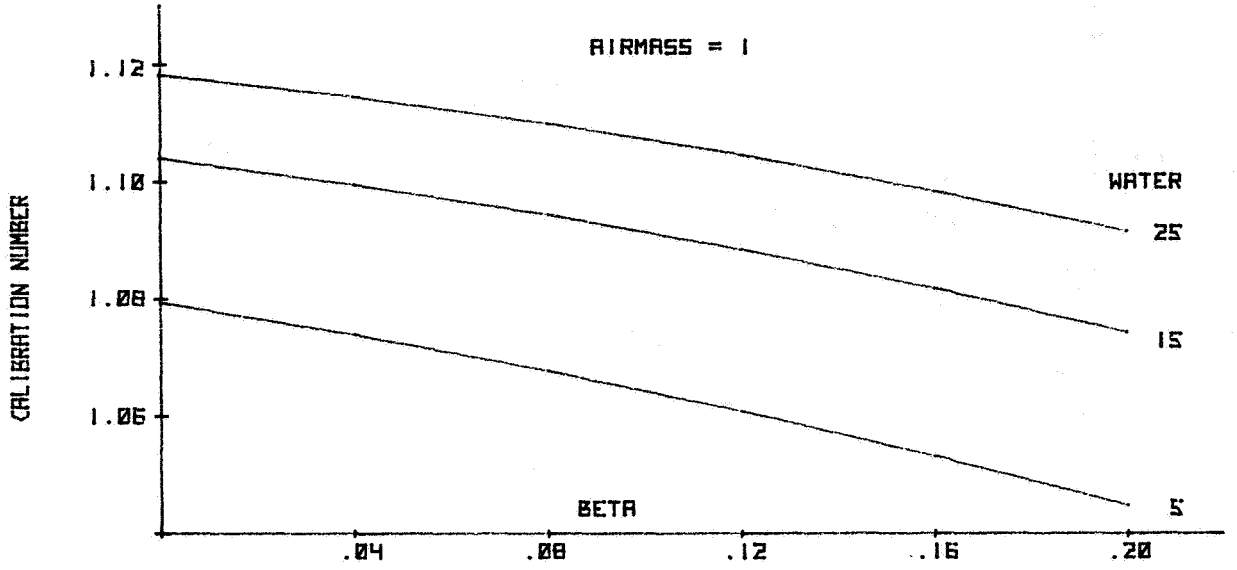


Figure 5. - Effect of turbidity coefficient, beta, on cell calibration number for Air Mass 1 sunlight

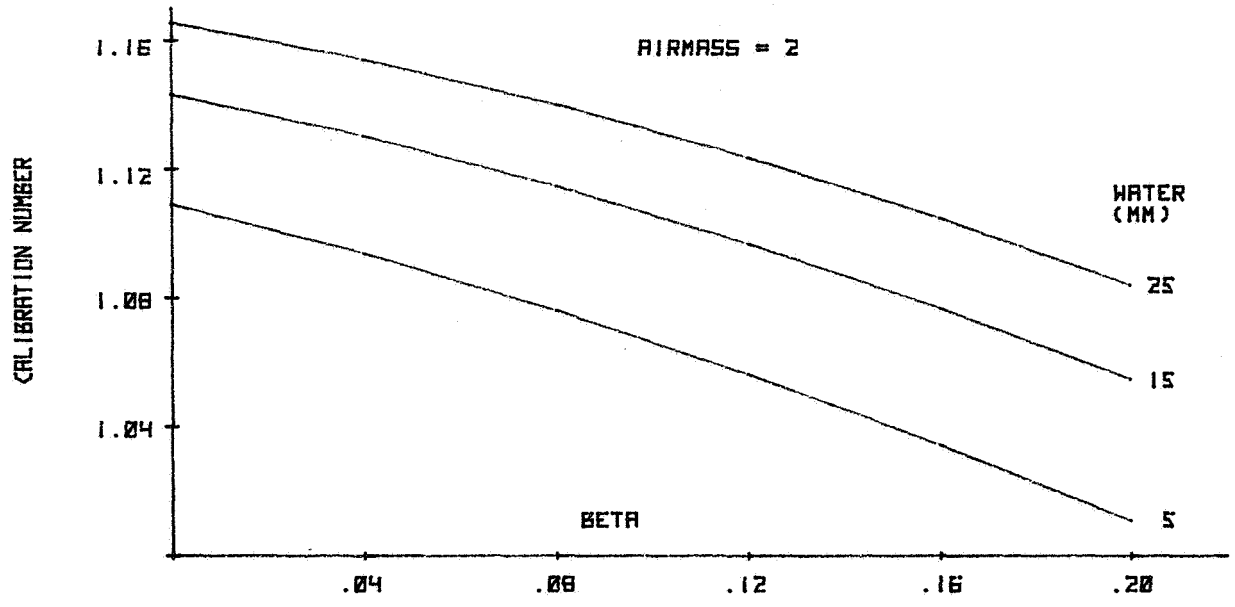


Figure 6. - Effect of turbidity coefficient, beta, on cell calibration number for Air Mass 2 sunlight

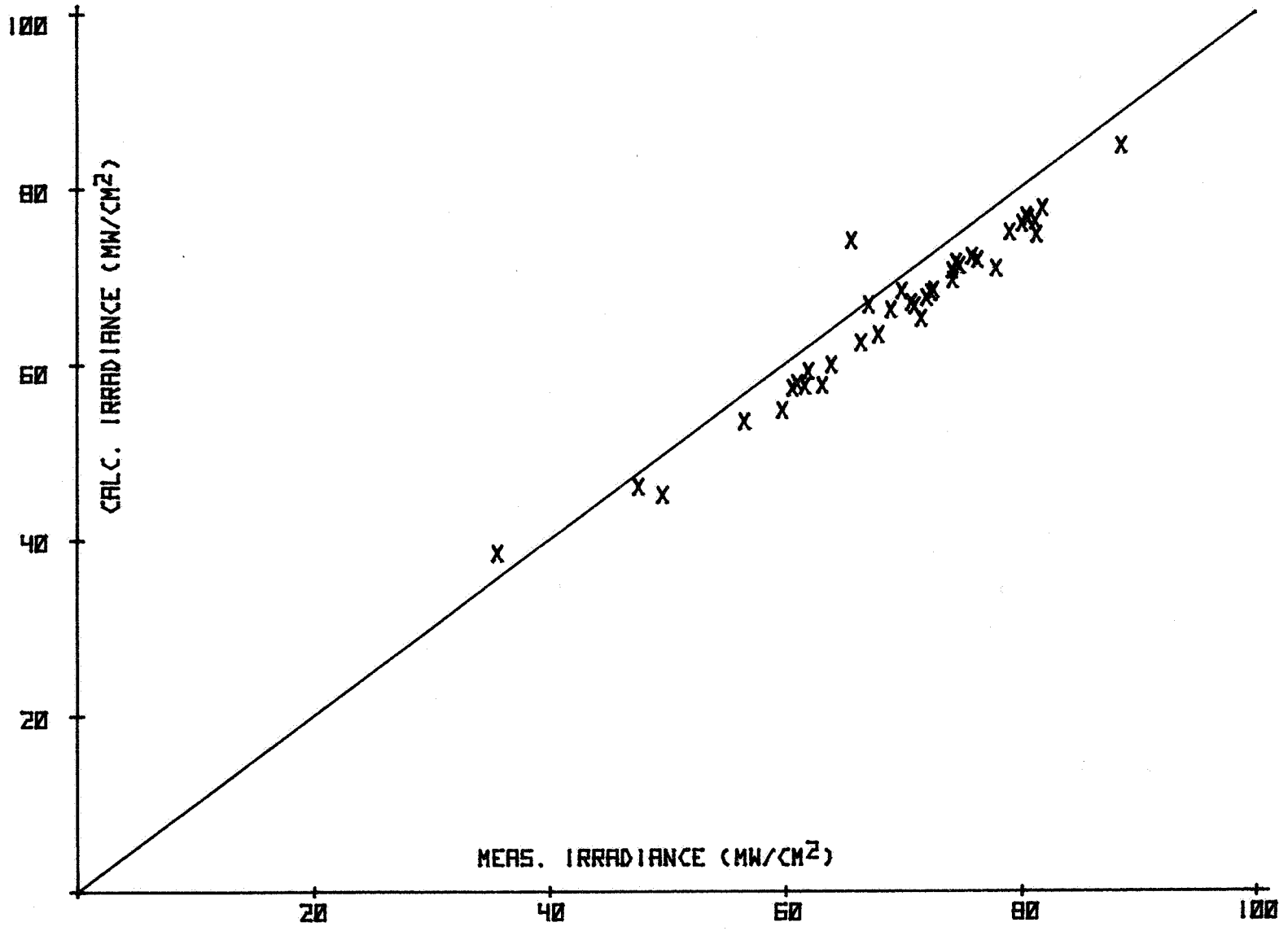


Figure 7. - Comparison of calculated and measured irradiance

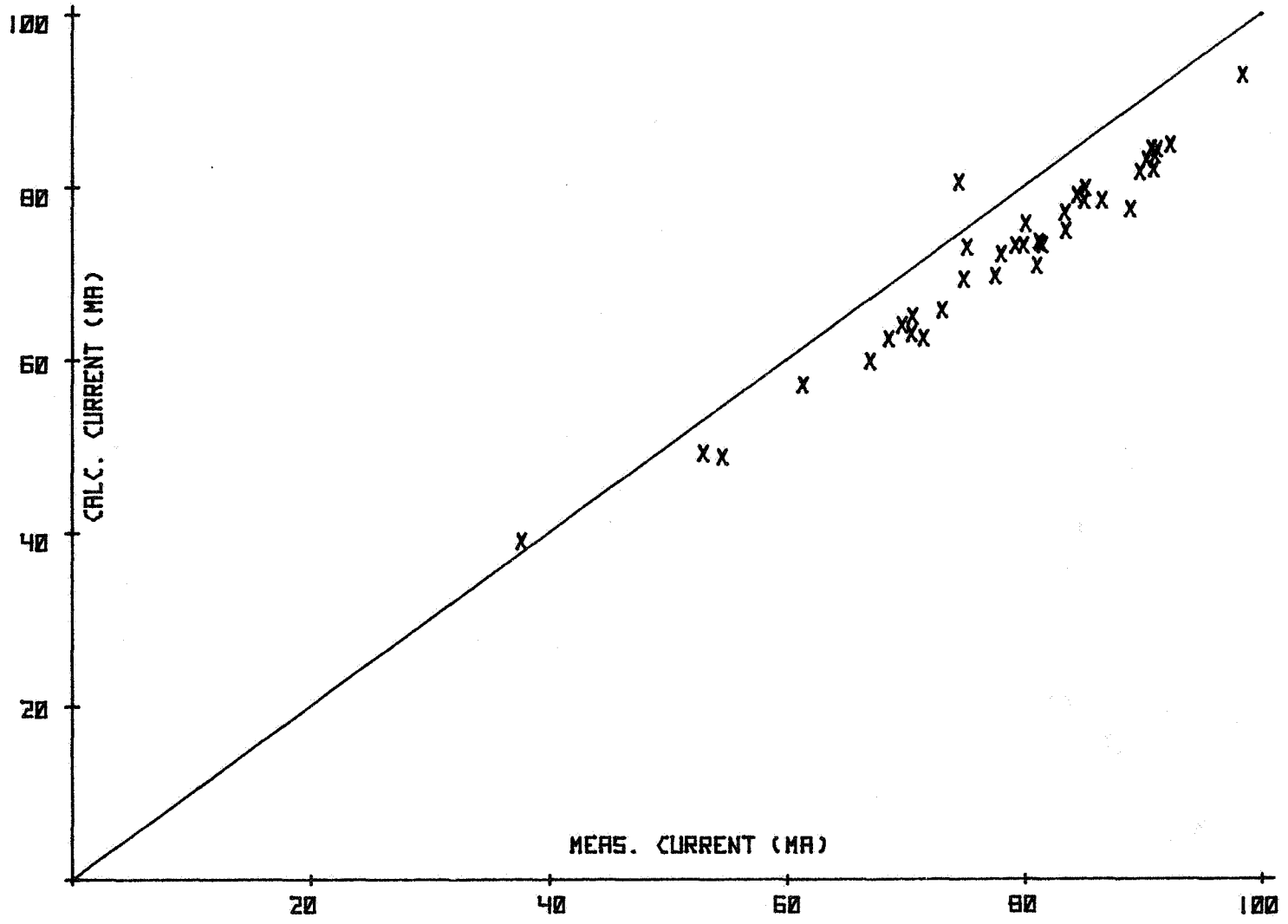


Figure 8. - Comparison of calculated and measured short circuit currents

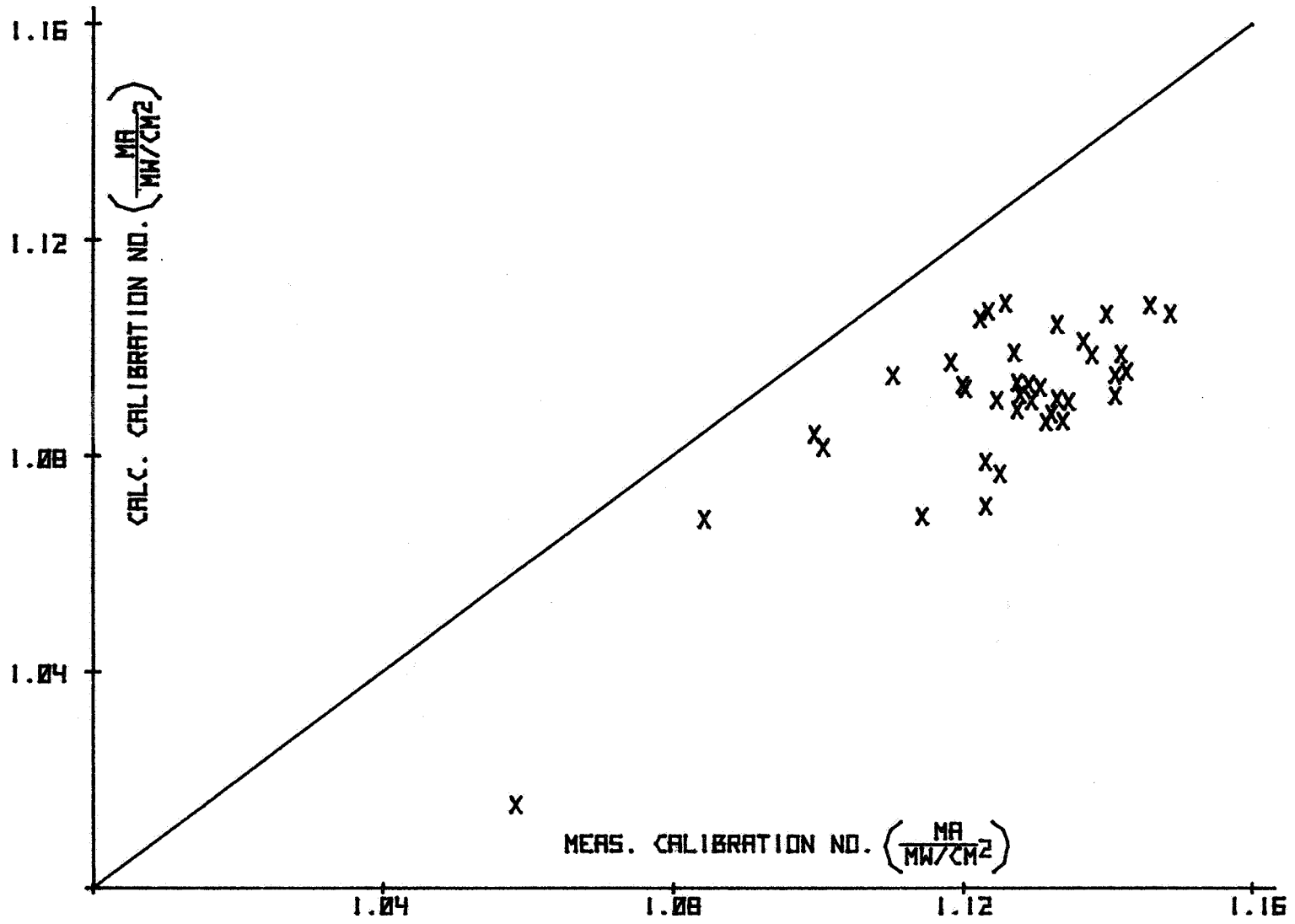


Figure 9. - Comparison of calculated and measured calibration numbers

# SOLAR EXCITATION OF $CdS/Cu_2S$ PHOTOVOLTAIC CELLS+*

K. W. Böer
Institute of Energy Conversion
University of Delaware

And

SES, Incorporated
Newark, Delaware 19711

Solar radiation of five typical clear weather days and under a variety of conditions is used to determine the spectral distribution of the photonflux at different planes of a $CdS/Cu_2S$ solar cell. The fractions of reflected and absorbed flux are determined at each of the relevant interfaces and active volume elements of the solar cell. The density of absorbed photons is given in respect to spectral and spatial distribution. The variance of the obtained distribution, with changes in insolation and absorption spectra of the active solar cell layers, is indicated. A catalogue of typical examples is given in the appendix.

## 1. Introduction

The photovoltaic conversion efficiency is sensitive to the spectral distribution of solar radiation, since only a fraction of the spectrum is used for photocarrier generation. The spectral distribution for a number of typical clear weather days is given in a previous paper.[1]

This light is partially reflected (and absorbed) as it passes through a number of transparent layers before it enters the active $Cu_2S/CdS$ layers of the solar cell.

The transmission into the $Cu_2S/CdS$ also depends on the topography of the surface. The reflection losses are markedly reduced at rough surfaces.[2]

+Sponsored by SES, Inc.

*An Appendix to this paper contains the curves referenced in the text and computer printouts.

Light, which can penetrate through the $Cu_2S$/CdS sandwich, is partially reflected from the back electrode and adds to the carrier generation on its second path.

The rough surface topography contributes to light trapping (multiple reflection) in the $Cu_2S$/CdS sandwich, hence to some further increase of carrier generation.

The total carrier generation rate is sensitive to changes in the extrinsic absorption spectrum of $Cu_2S$ and CdS. Since the photovoltaic mechanisms are different for light absorption in $Cu_2S$ and CdS, and for the latter in different spectral ranges (carrier generation and quenching), separate accounting is required.

For an estimate of the carrier collection efficiency (often referred to as quantum efficiency), integration over the active spectral range and the $Cu_2S$ and CdS layer, as well as the total $Cu_2S$/CdS sandwich, is carried out.

## 2. Photon Flux

The total energy influx from solar radiation is an important parameter to calculate the conversion efficiency of a device. However, for all other purposes related to the photovoltaic cell, it is of advantage to use the spectral distribution of the photon flux $\phi(\lambda)$.

The conversion of light into electric energy proceeds by absorbing photons and by producing essentially one photocarrier for each properly absorbed photon. Excess energy of the photon is converted into phonons and is not beneficial for the photovoltaic conversion.

It is therefore appropriate to convert the solar flux densities given in Ref. 1 into photon flux densities, according to

$$\phi(\lambda) = I(\lambda)\cdot\lambda/hc = 5.03\cdot10^{12}\lambda(nm)I(\lambda)(mW/cm^2nm) \qquad (1)$$

The photon flux densities for the five typical clear weather spectra are given in Fig. 1 for the total (T) and in Fig. 2 for the forward scattered plus direct (DF) component of the sunlight*. The integral photon flux for these distributions in the given range ($300<\lambda<1500$nm) is given in Table 1. The deviation from the SP distribution is shown in Figs. 1a-5a and 6a-10a for T and DF respectively in the appendix.

---

* Curves plotted separately in appendix.

| | W | SP | S | SH | F |
|---|---|---|---|---|---|
| T | 2.87 | 3.26 | 3.21 | 2.74 | 2.80 |
| DF | 2.56 | 2.99 | 2.99 | 2.54 | 2.57 |

Table 1*
(In $10^{17}$ photons/$cm^2$)

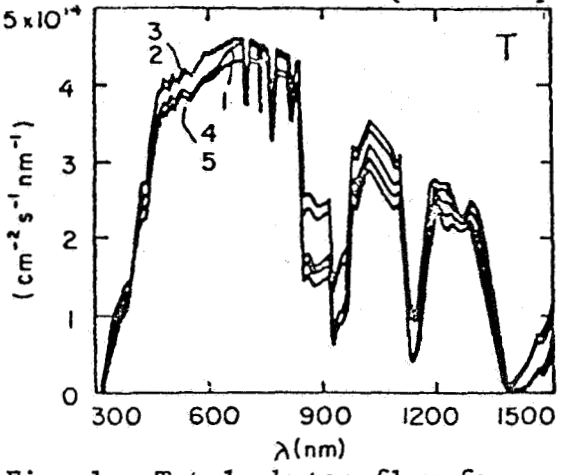


Fig. 1. Total photon flux for 5 typical clear weather days.

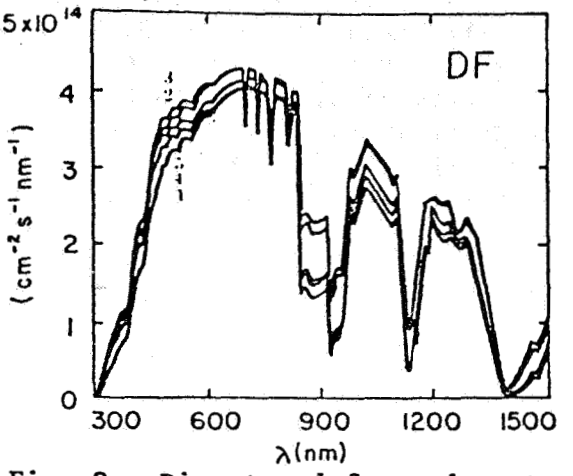


Fig. 2. Direct and forward scattered photon flux for 5 typical clear weather days.

The integral photon flux (See equ. 8 in Section 4.1) contained in the distribution DF/SP up to variable wavelength is given in Fig. 3 as curve 1. The DF/SP flux for $0<\lambda<\infty$ is indicated by the arrow in Fig. 3.

One sees that most of the photonflux impinges between 350 and 1300nm. The wavelength range in which most of these photons are absorbed in $Cu_2S$ lies between 350 and 950nm

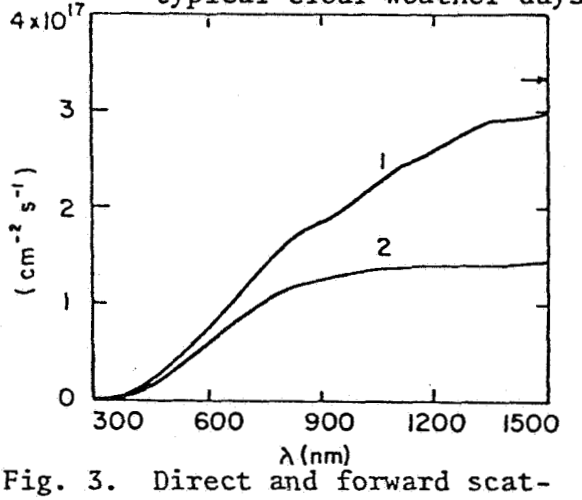


Fig. 3. Direct and forward scattered photon flux integrated from 300nm to the given wavelength for SP day 1:impinging on outer glazing, 2:absorbed in $Cu_2S$.

* The letters W, SP, S, SH, nad F refer to winter, spring, summer, humid summer, and fall respectively, and the insolation conditions are explained in Ref. 1.

and is shown in curve 2 of Fig. 3 (See Section 4.1). In this wavelength range, the DF component depends least on on the chosen clear weather day (compared to other components of the sunlight, D, H, S, T as given in Ref. 1). In Fig. 4, the photonflux close to the highest insolation expected at $40^0$ latitude is given for Total/Summer (T/S) insolation.

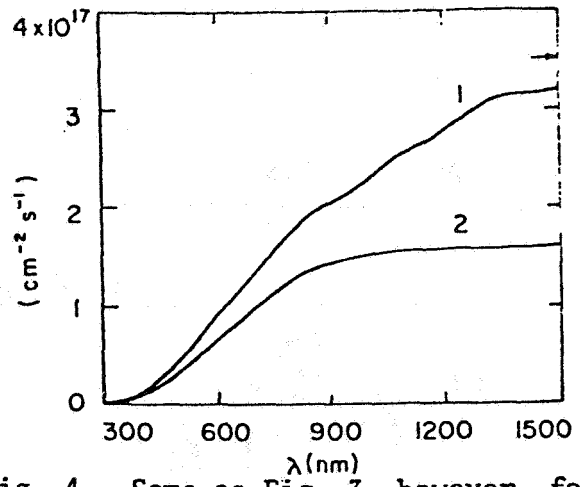


Fig. 4. Same as Fig. 3, however, for total flux and S.

## 3. Transmission Through the Transparent Cover

The $CdS/Cu_2S$ solar cell has a number of transparent cover layers to protect the cell against oxygen and water vapor and to provide means of applying a grid electrode.

Usually, a hermetic seal is established by a glass cover (layer 1). A liquid layer (2) follows to reduce reflection. A macropolymer (often Mylar or Aclar) is the third layer. These three layers are flat, plan-parallel sheets with negligible optical absorption in the spectral range of interest.

A fourth (Epoxy) layer is flat at the outer surface and follows the $Cu_2S$-topography at the inner surface (Fig. 5).

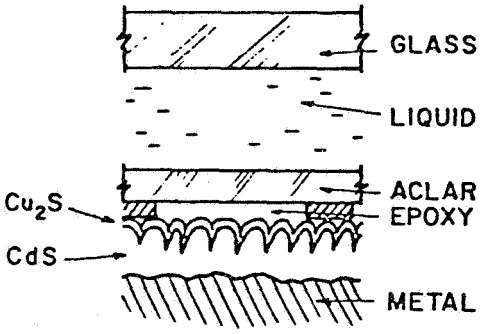


Fig. 5. Cross-section through Cds/$Cu_2S$ solar cell (not to scale).

The index of refraction of these four layers lies between 1.4 and 1.56, hence interface reflection between these layers is less than 0.3% and can be neglected: The total transmission of the transparent sandwich for normal incidence light is given by

$$t_{1-4} = 256 \frac{n_o n_1^2 n_2^2 n_3^2 n_4}{[(n_o+n_1)(n_1+n_2)(n_2+n_3)(n_3+n_4)]^2} \qquad (2)$$

with $n_o$ the index of refraction of air and $n_i$ the index of refraction of the $i^{th}$ layer.

In Fig. 7, curve 1, the transmission spectrum $t_{1-4}$ is given as computed for a given PPG glass sample with $n_1(\lambda)$ and $\kappa_1(\lambda)$ shown in Fig. 6, and $n_2$=1.5, $n_3$=1.416, and $n_4$=1.498 (in the $\lambda$-range of interest $n_2$, $n_3$, and $n_4$ are constant).

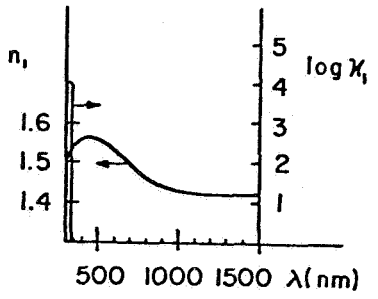


Fig. 6. $n(\lambda)$ and $\kappa_i(\lambda)$ for glass.

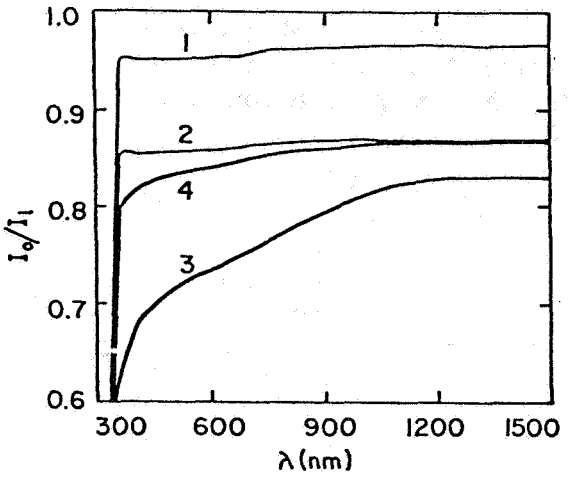


Fig. 7. Transmission of the transparent cell cover: 1:$t_{1-4}$; 2:$t_{1-4}(1-\gamma)$; 3:$t_{1-4}(1-\gamma)(1-R_5)$ (single reflection at $Cu_2S$ surface); 4:$t_{1-4}(1-\gamma)(1-R_5^2)$ (double reflection).

Imbedded in the epoxy layer, a contact grid which has a light transmittance* of $1-\gamma=0.9$ ($\gamma$ is the fraction of grid lines to open space). The composed transmission, $T_{1-4}\cdot(1-\gamma)$ is given as curve 2 in Fig. 7. The single reflection at the epoxy/$Cu_2S$ interface is given by

$$R_5 = \frac{(n_4-n_5)^2 + k_5^2}{(n_4+n_5) + k_5^2} \qquad (3)$$

with $n_5$ and $k_5$ the indices of refraction of $Cu_2S$ ($k_5=\kappa_5\lambda/4\pi$) with $\kappa_5$ the absorption coefficient of $Cu_2S$). $n_5(\lambda)$, $k_5(\lambda)$, and $\kappa_5(\lambda)$ are

* In the following, we will assume that covering a fraction $\gamma$ of the surface with gridlines is equivalent to reducing the homogeneous illumination by $\gamma$.

shown in Fig. 8. (for origin discussion, see Section 4). The composed transmission $T_{1-4}(1-\gamma)\cdot(1-R_5)$ is given as curve 3 in Fig. 7.

For a rough surface, the transmission from the epoxy to the $Cu_2S$ may be approximated as (See Ref. 2):

$$t_5 = 1-R_5^2 \qquad (3a)$$

(The impinging light experiences an average of two reflections at the surface before it leaves). The composed transmission into the upper $Cu_2S$ layer, $t_{1-4}\cdot(1-\gamma)t_5$ is given as curve 4 in Fig. 7.

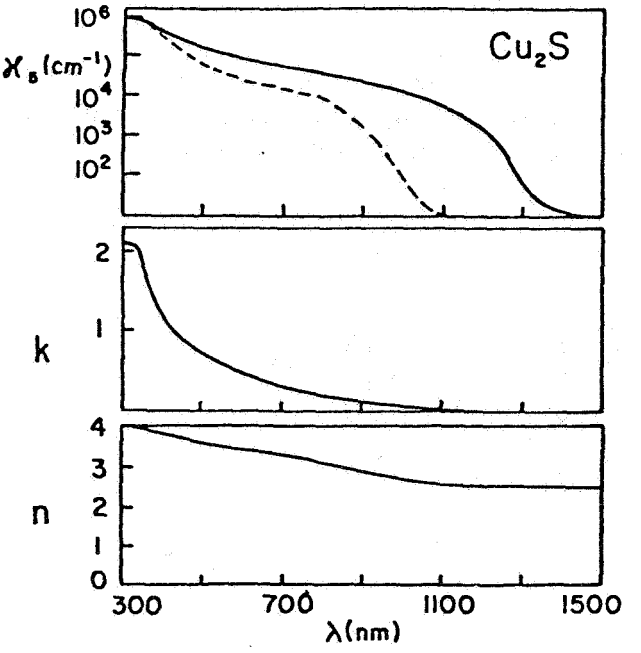


Fig. 8. $\eta(\lambda)$, $k_5(\lambda)$, and $\kappa_5(\lambda)$ for $Cu_2S$ (upper and lower average of observed absorption values as solid and dashed curves respectively).

In the given configuration, an average of approximately 85% of the normal incident light is transmitted into the $Cu_2S$. The major fraction is absorbed by the grid. The average of the total reflected light is less than 5%. However, one should recognize that in the wavelength range between 400 and 800nm, where most of the photoexcitation takes place (see below), the reflection is somewhat higher and, near 400nm, amounts to almost 8%.

For the given example of a rough $Cu_2S$ surface with its average reflection determined by $1-R_5^2$, the use of anti-reflecting coating on this surface would have little effect (compare curves 2 and 4 of Fig. 7). The reduction of the outer surface reflection of glass (e.g., by proper etching or coating) may increase the transmission by a few percent.

## 4. Optical Absorption in the $Cu_2S$ and CdS Layer

The absorption of photons in the two active layers of the $CdS/Cu_2S$ solar cell is key to its performance. The fraction of the photon flux transmitted through the upper $Cu_2S$ surface which is absorbed depends on a number of factors:

a) Absorption coefficient $\kappa_5(\lambda)$ of the $Cu_2S$.
b) Absorption coefficient $\kappa_6(\lambda)$ of the CdS.
c) Thickness $d_5$ and $d_6$ of the $Cu_2S$ and CdS layers respectively.

d) Topography of each surface.
e) Reflectivity of the back electrode.
f) Crystallite boundaries causing light scattering.

In the range of interest, the absorption coefficients of $Cu_2S$ and CdS are not sufficiently known. Different authors give widely differing results from $Cu_2S$, probably because of variations in stoichiometry. In the extrinsic range of CdS, the situation is similar.

In the absence of reliable data obtained from CdS/$Cu_2S$ solar cells of properties similar to the type of cell investigated here, we have chosen an averaging estimate*, more heavily weighing data from better characterized material[3-10]. However, one should recognize that dependent on the deposition technique the defect structure may vary substantially and, hence, the optical absorption. Consequently, the results presented here should not be valued more than as a first indication.

In Figs. 8 and 9, the relevant absorption and refraction data used for this computation are plotted for $Cu_2S$ and CdS.

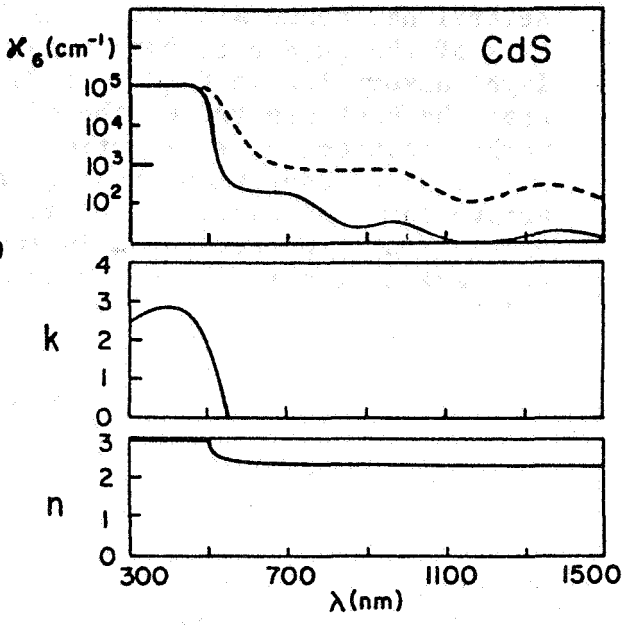


Fig. 9. Same as Fig. 8 for CdS (upper and lower average of observed absorption as dashed and solid curves respectively).

The thickness of CdS is easily determined by weight or direct optical measurement and is usually 20μm for the more common devices (recent attempts to produce thinner layers show promise). The thickness of the $Cu_2S$ layer is much more difficult to determine. Presently, a layer of 0.3μm thickness on most of the pyramide surfaces of the CdS, with some areas (possibly at the top of the pyramides) substantially thinner, seems to be a reasonable estimate.

The topography, as it relates to reflection and light trapping, is discussed elsewhere (Ref. 2).

---

* The two curves (dashed and solid) in Figs. 8 and 9 are upper and lower averages.

Little is known about the reflectivity of the back electrode (usually Zn or a Zn-rich brass phase). In the absence of better data, we will assume that the effective reflectance is 70% (see below).

Numerous crystallite boundaries are contained in the CdS and in the $Cu_2S$ layer. However, since the $Cu_2S$ is topotaxially grown, it is expected that such boundaries are replicas of the original CdS boundaries, which are spaced at the surface typically between one and several μm, hence are substantially more widely spaced than the thickness of the $Cu_2S$ and, consequently, are of little influence for the light absorption in $Cu_2S$. In CdS, this is not the case. Especially near the back electrode, the crystallite size becomes smaller, and marked scattering is expected. Its effect could be a substantial increase in absorption, however far away from the junction, hence inactive for photocarrier generation. The lack of data again necessitates assumptions. We have here included the scattering contribution into the back reflection, justifying a somewhat low effective reflectance (70%).

### 4.1. Computation of the Photon Density Within $Cu_2S$ and CdS, No Reflection From the Back Electrode

With the assumption and data given in the previous section, the photon density of every wavelength interval can be followed as the radiation proceeds from the upper surface into the $Cu_2S$, then through the $Cu_2S$-CdS interface into the CdS.

The spectral and spacial distribution of the photon flux in $Cu_2S$ is given by

$$\phi_5(x,\lambda) = \phi_o(\lambda)t_{1-4}(1-\gamma)(1-R_5^2)\exp(-\kappa_5 x) \tag{4}$$

In CdS, the photon flux is

$$\phi_6(x,\lambda) = \phi_o(\lambda)t_{1-4}(1-\gamma)(1-R_5^2)(1-R_6)\exp(-\kappa_5 d_5-\kappa_6 x) \tag{5}$$

with

$$R_6 = \frac{(n_5-n_6)^2 + (k_5-k_6)^2}{(n_5+n_6)^2 + (k_5+k_6)^2} \tag{6}$$

and $1-R_6$ shown in Fig. 10. $\phi_o(\lambda)$ is the solar flux impinging on the glass surfaces at normal incidence.

In Fig. 11, the spectral and spacial distribution of the photon flux for the insolation DF/SP is shown as it proceeds from the outer glass surface (curve 1) through the transparent layers (curve 2) into the $Cu_2S$ (curves 3-9) and CdS (curves 9-13). The area between any two curves of this family is a measure of the amount of photons absorbed in the denoted sublayer. The widest spread, hence the highest density of absorbed photons, is observed in the uppermost $Cu_2S$ layer between 400 and 700nm. Only a relatively small fraction of photons is added from wavelengths over 900nm. The absorption in the CdS is substantially smaller due to the filtering of the $Cu_2S$ and depends strongly on the spectral distribution of the extrinsic absorption of CdS, which is known to change substantially with different doping and/or heat treatments (For Fig. 11, the absorption spectrum shown as solid curves in Figs. 8 and 9 are used).

Figs. 12a and b give a set of curves which was obtained for a different $Cu_2S$ and CdS absorption spectrum respectively, as shown by dashed curves in Figs. 8 and 9. This difference will also have a marked influence on the amplitude of the reflected light from the back electrode (See Section 4.2.3).

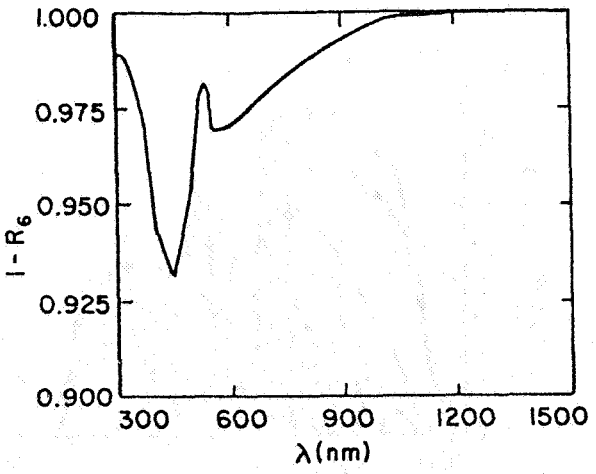


Fig. 10. Transmission through the $Cu_2S$/CdS interface (for solid curves of Figs. 8 and 9).

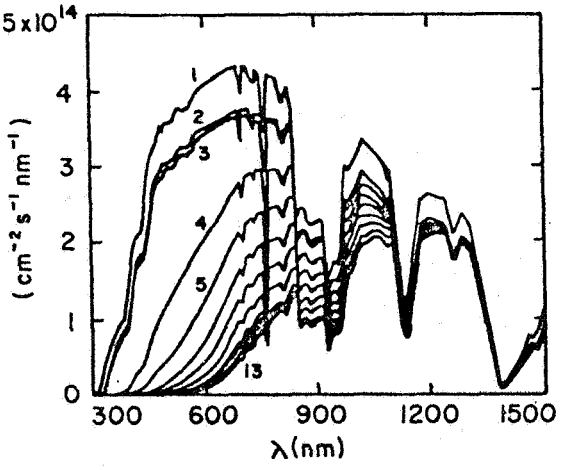


Fig. 11. Spectral and spacial distribution of photon flux in $Cu_2S$ and CdS, shown for DF/SP. Light impinging on 1:outer glass surface; 2:on $Cu_2S$ surface; 3:penetrating through $Cu_2S$ surface; 4-9: penetrating through a plane 0.05, 0.1, 0.15, 0.2, 0.25, and 0.3μm from outer surface in $Cu_2S$; 10-13:penetrating through a plane 5, 10, 15, and 20μm from $Cu_2S$/CdS interface in CdS (absorption given by solid curves in Figs. 8 and 9).

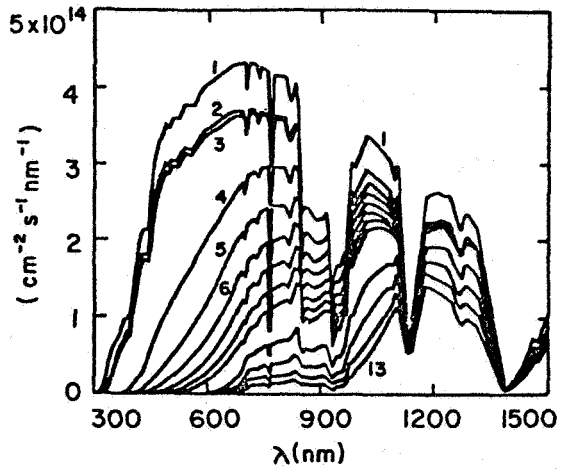


Fig. 12a. As Fig. 11, however, for a CdS layer with higher extrinsic absorption (dashed curve in Fig. 9).

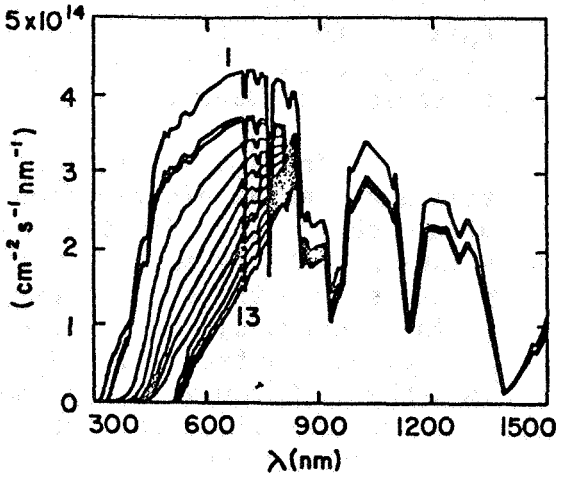


Fig. 12b. As Fig. 11, however, for a $Cu_2S$ layer with lower absorption (dashed curve in Fig. 8).

Fig. 13 shows the spectral distribution of the impinging light (DF/SP), curves 1 (onto glass) and 2 (into the $Cu_2S$) and the fraction absorbed in the $Cu_2S$ layer* (curve 3) for conditions of Fig. 11:

$$\Delta\phi_5(\lambda) = \phi_5(\lambda,-d_5)-\phi_5(\lambda,0) \quad (7)$$

Fig. 14 shows the integrated values for the same curves:

$$N_{ph}(\lambda) = \int_{300}^{\lambda} N(\ell)d\ell \quad (8)$$

again indicating that light beyond 900nm has little effect in $Cu_2S$.

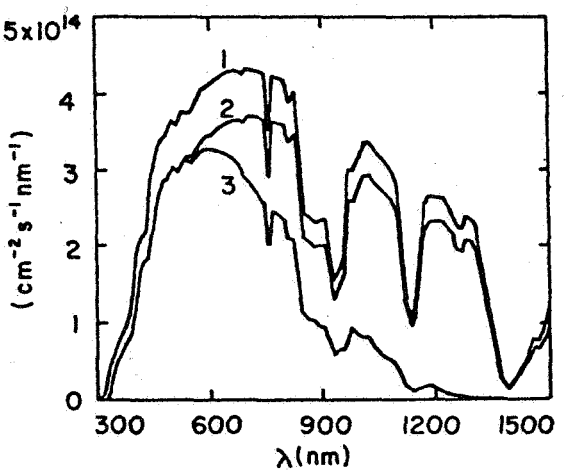


Fig. 13. Photon flux of impinging light on glass (1) and penetrating through top $Cu_2S$ surface (2), and fraction of the photon flux absorbed in the $Cu_2S$ layer (3) - See equ. 7; SP/DF.

* The x-coordinate is assumed to be normal to the junction with x=0 at the junction for equs. 7, 10, and 11.

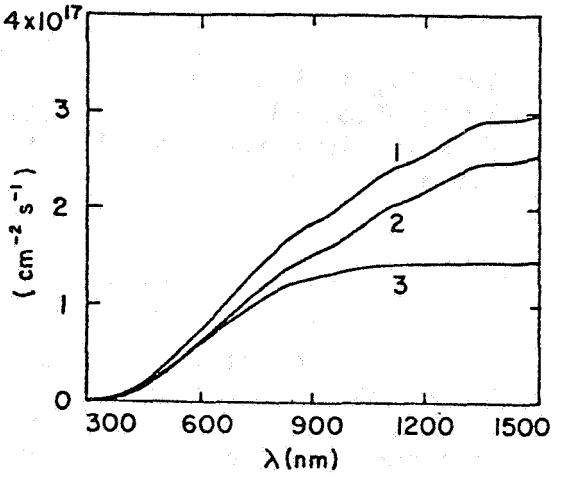


Fig. 14. Integrated photon flux (See equ. 8) for curves, as in Fig. 13.

### 4.1.1. Photon Flux in $Cu_2S$ Protrusions

The part of the $Cu_2S$ layer which protrudes into the CdS grain boundaries and grooves is virtually shielded from direct optical irradiation due to shadowing effects (See Ref. 2). Hence, it will mainly receive back scattered light through the CdS. The photon flux is consequently given by

$$\phi_{5p}(\lambda,x) = \phi_o(\lambda)t_{1-4}(1-\gamma)(1-R_5^2)(1-R_6)^2R_7\exp(-\kappa_5 d_5 - 2\kappa_6 d_6 - \kappa_5 x) \qquad (9)$$

as shown in Figs. 15a and b for CdS of the two absorption spectra given in Fig. 9.

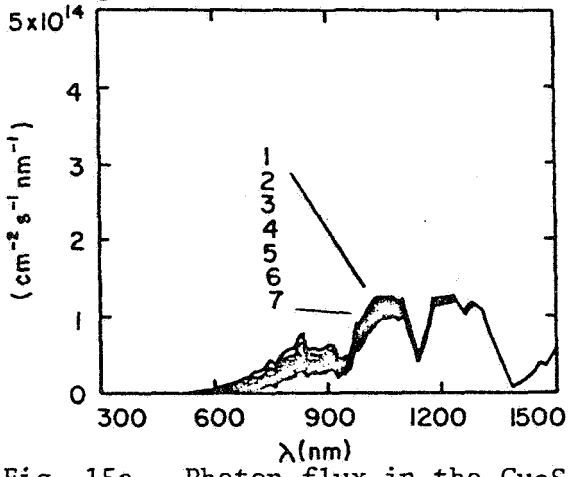


Fig. 15a. Photon flux in the $Cu_2S$ protrusions receiving only back scattered light at faces 0, 0.05, 0.1, 0.15, 0.2, 0.25, and 0.3μm from the junction (curves 1-7).

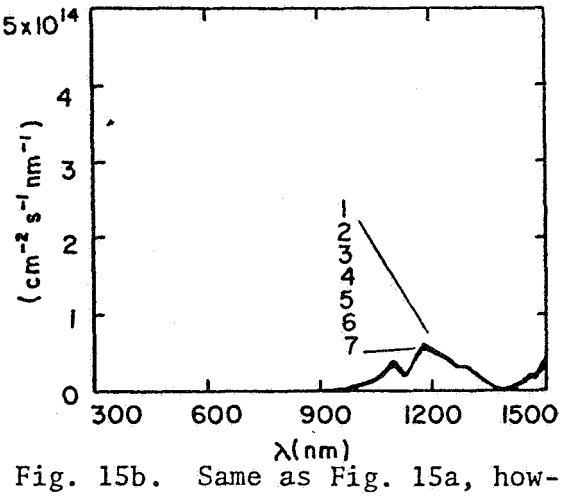


Fig. 15b. Same as Fig. 15a, however, for CdS with higher optical absorption (dashed curve in Fig. 9).

It is evident that the protrusions receive considerably less light than the surface layers of the $Cu_2S$, with slightly more light absorbed near the junction than in the sublayers further away from the junction, and that the photon flux is very sensitive to the CdS absorption.

### 4.2.1. Generation Rate in $Cu_2S$

The carrier generation rate can easily be calculated if one assumes that every photon absorbed creates one minority carrier (quantum - efficiency 1). This is not necessarily the case since high energy photons, with more than twice the band gap energy, may produce a carrier of sufficient energy to create, in turn, another carrier via Auger impact. Photons with energy substantially below the band gap may excite electrons from the valence band into levels in the gap which, in turn, recombine with holes without ever creating a minority carrier (i.e., a conduction electron in $Cu_2S$).

Little is known presently about the rates at which the different processes proceed, hence presently we will assume a quantum efficiency of one in the entire absorption range, however, being alerted that in the short wavelength range (below 500nm) the quantum efficiency is probably somewhat larger than one, and at longer wavelengths (beyond 1000nm), the quantum efficiency may be smaller than one.

The total photonflux as a function of the spacial coordinate (x) is given by

$$\phi(x) = \int_{300}^{1500} \phi(\lambda,x)dx \qquad (10)$$

and is shown for a typical insolation condition (DF/SP) in Fig. 16. The total density of photons absorbed in $Cu_2S$ can be obtained from $\phi_5(x=-3.10^{-5}cm) - \phi_5(x=0)$ and is, for the given example, 57% of the photon flux which penetrates through the upper $Cu_2S$ surface. This, in turn, is 48% of the photon flux impinging onto the outer glass surface in the range $300<\lambda<1500nm$.

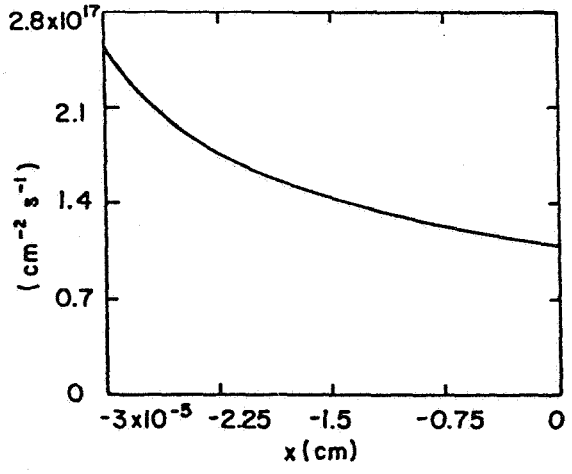


Fig. 16. Total photon flux in $Cu_2S$ (equ. 10) for DF/SP.

Table 2 gives a list of photon flux densities at the outer and junction surface of $Cu_2S$ and the density of photons absorbed in $Cu_2S$, hence the maximum expected current density for an assumed collection efficiency of one, without light reflection from the back electrode and hole contribution from CdS.

| | Photon Density (in $10^{17} cm^{-2} s^{-1}$) | | | | | |
|---|---|---|---|---|---|---|
| Insolation | Impinging on glass | Entering $Cu_2S$ | Leaving $Cu_2S$ | % Absorbed in $Cu_2S$ | Photons absorbed in $Cu_2S$ | $mA/cm^2$ Max. Current |
| DF/W | 2.56 | 2.19 | 0.909 | 50% | 1.28 | 20.4 |
| SP | 2.99 | 2.75 | 1.31 | 48% | 1.44 | 22.9 |
| S | 2.99 | 2.54 | 1.07 | 49% | 1.47 | 23.4 |
| SH | 2.54 | 2.16 | 0.83 | 52% | 1.33 | 21.1 |
| F | 2.57 | 2.19 | 0.88 | 51% | 1.31 | 20.8 |
| T/W | 2.87 | 2.44 | 0.98 | 51% | 1.46 | 23.2 |
| SP | 3.25 | 2.77 | 1.17 | 49% | 1.60 | 25.4 |
| S | 3.21 | 2.72 | 1.12 | 50% | 1.60 | 25.4 |
| SH | 2.74 | 2.32 | 0.87 | 53% | 1.45 | 23.1 |
| F | 2.80 | 2.38 | 0.93 | 52% | 1.45 | 23.1 |

Table 2

One sees that approximately 50% of the impinging light is presently absorbed in the $Cu_2S$. Considerable improvement can be expected by an increase in the thickness of $Cu_2S$ and possible changes in stoichiometry and doping to increase its absorption spectrum. However, these changes must be carefully taylored to avoid counteracting current deterioration because of increased development of protrusions, decrease in $L_n/d_5$ ratio, or insufficient illumination of the CdS barrier region. We will return to these important questions in a following publication[11].

The generation rate g(x) is key input parameter for all microscopic theories of the solar cell operation and can easily be obtained from equ. 10:

$$g(x) = \frac{d}{dx} \phi(x) \tag{11}$$

It is given for $Cu_2S$ and for DF and T insolation in Figs. 17 and 18 respectively for the five typical clear weather conditions (W, SP, S, SH, and F). The variance of g(x) for the given conditions is approximately $\pm$ 10% for the average generation rate.

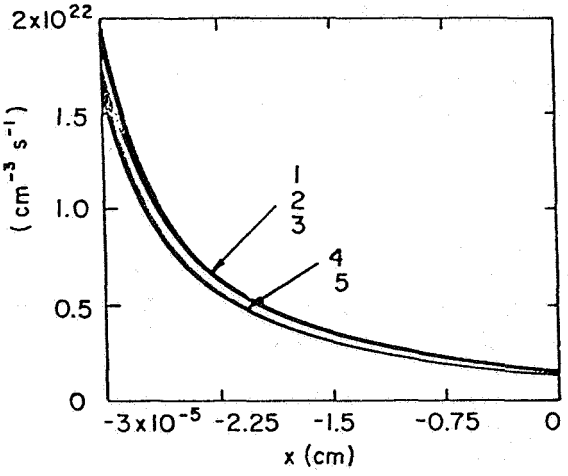


Fig. 17. Rate of minority carrier generation (equ. 11) in $Cu_2S$ for DF and the five typical clear weather days W(3), SP(1), S(2), SH(5), and F(4).

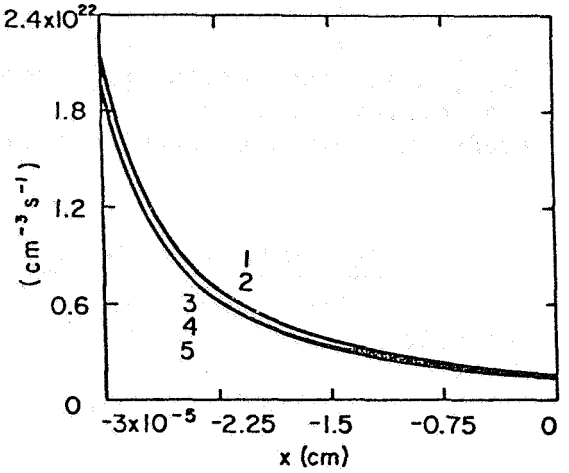


Fig. 18. Same as Fig. 17, however, for T.

It should be noted that the total generation rate decreases less than an exponential fitted to the first part of the curve ($g_f=4.5\cdot10^{19}\cdot\exp(-200000x)$- See Fig. 19) with increasing distance from the upper $Cu_2S$ surface, even though each wavelength component decreases exponentially with x. This is caused by the strong absorption of the short wavelength components in a small fraction of the layer thickness, while the longer wavelength components of the light encounter little absorption.

As a result, the total number of absorbed photons per unit area decreases steeply during the first 1000Å and approaches more slowly lower

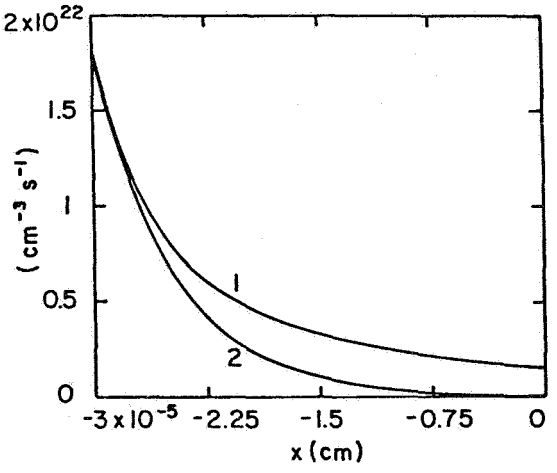


Fig. 19. Rate of carrier generation for DF/SP (1) and exponential (2) fitted to the first part of the carrier generation curve.

values closer to the junction than one expects for a simple exponential law. The integrated photon flux (Fig. 20) shows that more than half of the photons absorbed in the 0.3μm thick slab are already absorbed in the first 750Å and approximately 75% in the first 1500Å.

Consequently, the overall carrier generation does not increase substantially with increasing thickness beyond a few thousand Ångstroms, while the carrier extraction is limited by the diffusion length, hence an increase in thickness of the $Cu_2S$ could result in a net penalty for a given diffusion length. We will return to this question in a following paper[11] and present the relevant quantitative relations.

However, as seen by comparison of Figs. 12a and b, the generation rate is sensitive to the absorption spectrum of $Cu_2S$. But the total generation rate, as shown in Fig. 21 for a 0.3μm thick $Cu_2S$ slab, varies less than one may expect from the substantial difference in the absorption spectra (solid and dashed curves in Fig. 8). The average generation rate has decreased by approximately 50% for the dashed absorption spectrum.

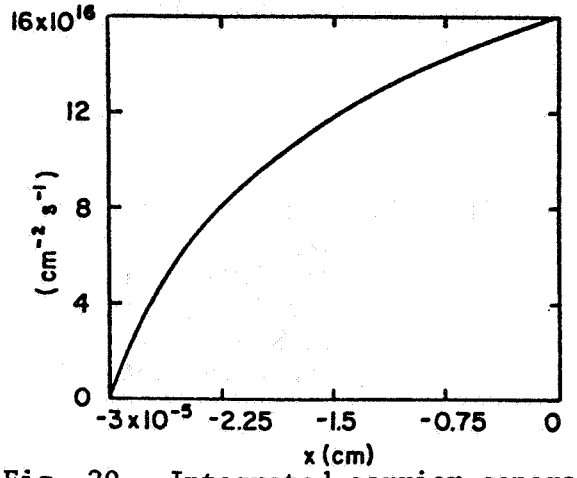


Fig. 20. Integrated carrier generation ($\int_{300}^{1500}\phi(\lambda,x)d\lambda$) in a 0.3μm thick $Cu_2S$ slab with absorption as given in solid curve of Fig. 8.

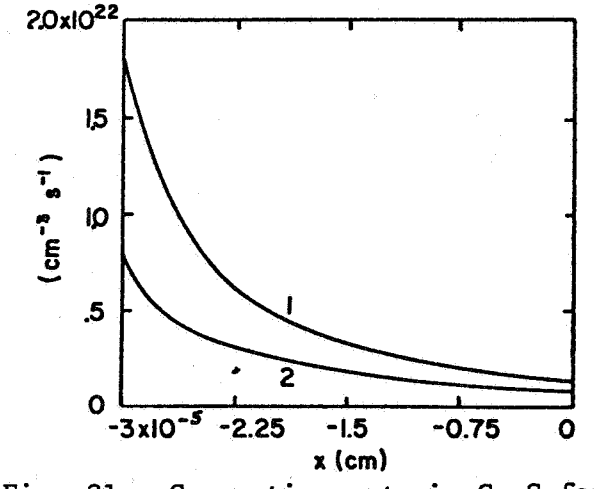


Fig. 21. Generation rate in $Cu_2S$ for DF/SP. Curves 1 and 2 are obtained for solid or dashed curve absorption of Fig. 8 respectively.

The generation rate in the $Cu_2S$ protrusions is approximately two to three orders of magnitude smaller than in the main $Cu_2S$ layer,

as shown in Fig. 22, and varies substantially for the two CdS absorption spectra shown in Fig. 9.

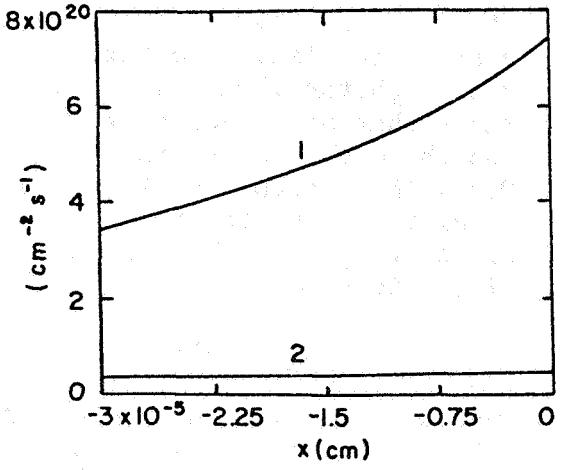


Fig. 22. Generation rate of carriers in $Cu_2S$ protrusions; curves 1 and 2 for photon flux of Figs. 15a and b respectively.

4.2.2. Generation Rate in CdS

The generation rate in CdS, however, depends sensitively on the thickness of the $Cu_2S$ layer.

The $Cu_2S$ acts as a filter which is especially active in the spectral range of high optical absorption of CdS. For a cover of the CdS with a homogeneous layer of $Cu_2S$, essentially all the light is filtered out in the intrinsic range of the CdS-absorption.

However, such a homogeneous cover is often not obtained, as is indicated by the observed light transmission near the band edge of CdS through the entire $Cu_2S$/CdS sandwich[12]. Other indications for a non-homogeneous cover are the appearance of a photocurrent structure near the band gap of CdS in certain cells (preferably in cells with a somewhat thinner $Cu_2S$ layer-probably in the 0.2μm range)[13].

In the absence of reliable data, and for reasons of simplicity, we will assume that a homogeneous layer of $Cu_2S$ covers the CdS. In Fig. 23, the photon flux penetrating through

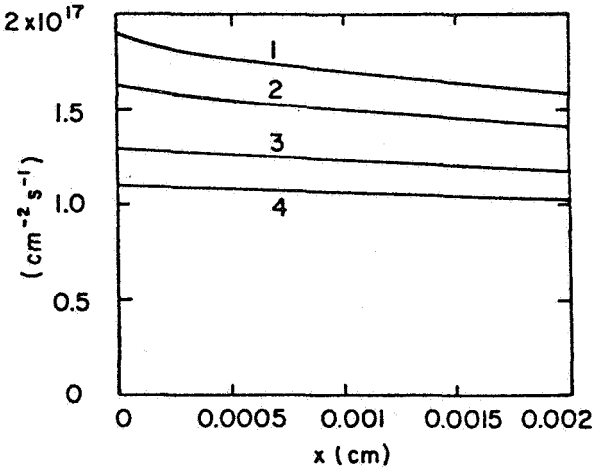


Fig. 23. Total photon flux in CdS for DF/SP with the thickness of the covering $Cu_2S$ layer as family parameter (0.15, 0.2, 0.25, and 0.3 μm for curves 1-4 respectively.

the junction into the CdS is shown for a variety of $Cu_2S$ layers of different thicknesses.

Fig. 24 shows the generation rate in CdS as a function of distance from the junction for different $Cu_2S$ layer thickness as family parameter, using the absorption spectrum given as solid curve in Fig. 9. In Fig. 25 a similar set of generation rates in CdS is shown, however, for the absorption spectrum given as dashed curve in Fig. 9. The high sensitivity of the CdS generation rate to the absorption spectrum in the extrinsic range, hence to the defect structure and to doping, is obvious from a comparison of Figs. 24 and 25.

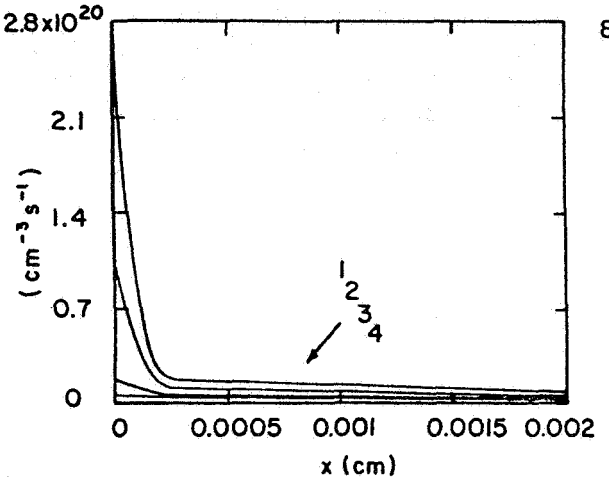


Fig. 24. Rate of carrier generation on CdS for conditions as given in Fig. 23.

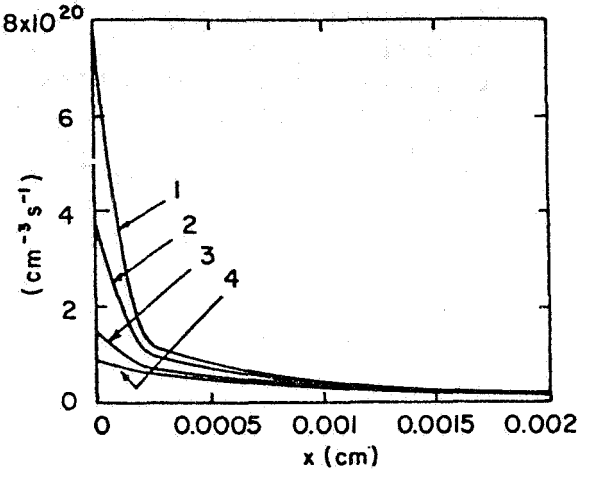


Fig. 25. Same as Fig. 24, however, for CdS absorption as shown in the dashed curve of Fig. 9.

The relatively large changes in the solar spectrum in the extrinsic wavelength range due to the changing water vapor absorption adds to the variance in the generation rate of carriers in CdS. An example is shown in Fig. 26 for DF/SP and DF/F insolation and otherwise same condition (as Fig. 24, for $d_5=3.10^{-5}$cm). It should be noted that the most pronounced changes of influence to the generation rate in CdS occur in the solar spectrum in the water band around 900nm, a spectral range which is

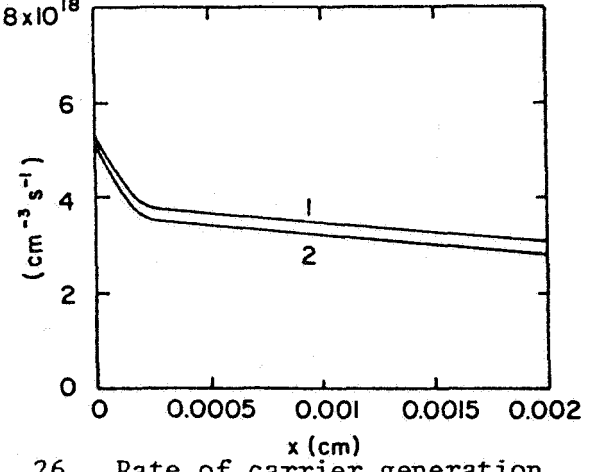


Fig. 26. Rate of carrier generation in CdS for $3.10^{-5}$cm $Cu_2S$ cover and DF/SP (curve 1) and DF/F (curve 2).

known to cause photoquenching in CdS. We will return to this important influence in a following paper[17].

A more detailed study of the generation rates of carriers in CdS must await the availability of absorption data of CdS and $Cu_2S$ in actual cells.

### 4.2.3. Reflection from the Back Electrode

From Table 2, it is seen that approximately 40% of the photon flux entering the top surface of $Cu_2S$ leaves on its first path through the back surface of $Cu_2S$. It was shown that reflection to permit a second path can cause a marked increase of the short circuit current[14]. As indicated earlier, reflected light from the back electrode may indeed be submitted to multiple internal reflection, hence may undergo multiple path traversing of the $Cu_2S$/CdS sandwich.

The roughness of the film and its reflecting back surface with diffuse scattering there, because of a network of crystallites with dimensions less than the wavelength of the light, makes the application of classical thin-film optics questionable.

An estimate about the magnitude of the increase in excitation rate may be obtained by using diffuse (incoherent) backscattering, yielding for the density of additionally absorbed photons

$$\phi_\alpha(\lambda) = \phi_o(\lambda) t_{1-4} (1-\gamma)(1-R_5^2)(1-R_6)^2 R_7 \exp(-\kappa_5 d_5 - 2\kappa_6 d_6) \cdot \{1-\exp(-2\kappa_5 d_5)\} \qquad (12)$$

In Fig. 27, curves 1-3 of Fig. 13 are replotted. Curve 3 is the total flux of absorbed photons without reflection. Curve 4 shows the flux of photons absorbed on the second and third path through $Cu_2S$ after reflecting from the back electrode and front $Cu_2S$ surface, and curve 5 gives the sum of curves 3 and 4 (for solid curve, Fig. 9 - absorption in CdS).

A complete set of such curves containing the reflected fraction is given in the appendix for all DF distributions. The increased amount of absorbed photons in $Cu_2S$ is best seen in Fig. 28 for the DF/SP distribution (See appendix for complete list). It shows an increase of the absorbed photon flux from 1.44 to $1.68 \cdot 10^{17}$ photons/$cm^2$s when reflection is included, i.e., by approximately 14%. In Fig. 29, the spacial distribution of the generation rate for the primary beam (1), the reflected light (2), and the sum of both (3) are shown.

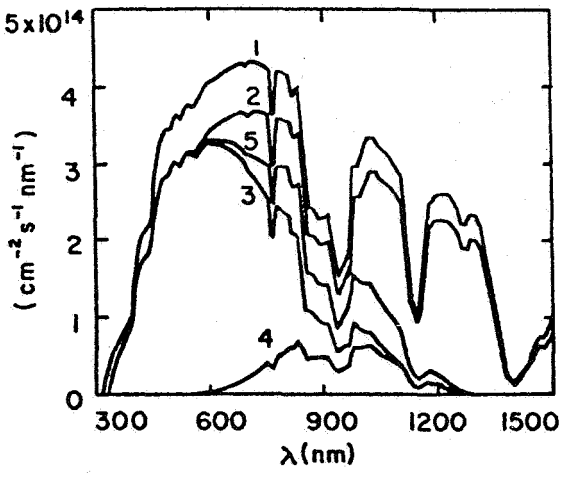


Fig. 27. Curves 1-3 same as in Fig. 13, curve 4 photon flux absorbed in $Cu_2S$ after reflection from back electrode ($R_7$=0.7) and then from front surface of $Cu_2S$ (second and third paths). Curve 5 is sum of curves 3 and 4 (DF/SP insolation).

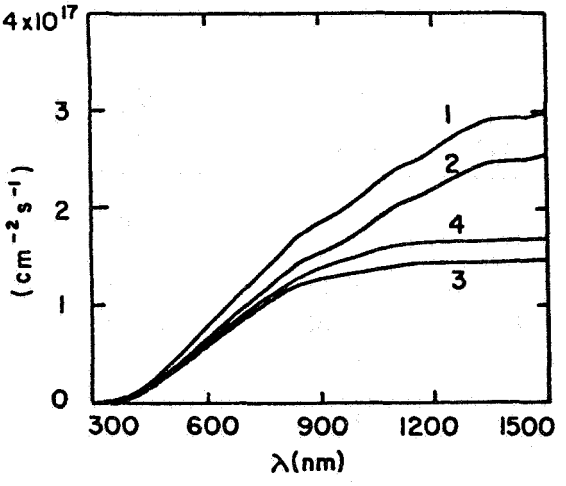


Fig. 28. Curves 1-3 are same as in Fig. 14, curve 4 is integrated curve 5 of Fig. 27.

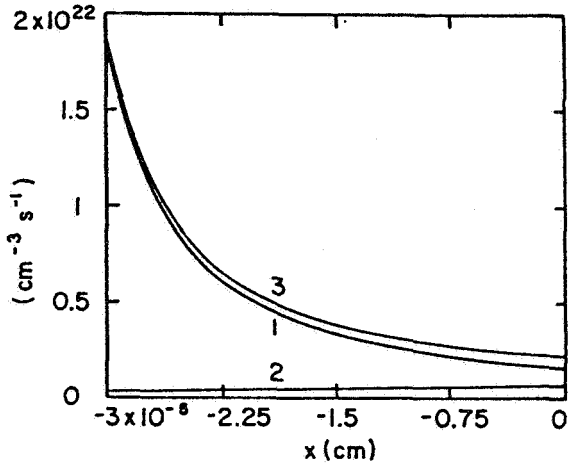


Fig. 29. Generation rate for DF/SP for first path (1), reflected light from back electrode (2), and sum of (1) and (2):(3).

These results are obviously sensitive to the absorption in CdS, and the contribution of the reflected light is substantially less for more absorbing CdS layers. Table 3 summarizes the results for different insolation.

| Insolation | Photons Absorbed in $Cu_2S$ | | Maximum Short-Circuit Current | | Inc. |
|---|---|---|---|---|---|
| | No Reflection | With Reflection | No Reflection | With Reflection | |
| DF/W | 1.28 | 1.48 | 20.4 | 23.5 | 13 |
| SP | 1.44 | 1.68 | 22.9 | 26.7 | 14 |
| S | 1.47 | 1.70 | 23.4 | 27.0 | 13 |
| SH | 1.33 | 1.51 | 21.1 | 24.0 | 12 |
| F | 1.31 | 1.51 | 20.8 | 24.0 | 13 |
| T/W | 1.46 | 1.68 | 23.2 | 26.7 | 13 |
| SP | 1.60 | 1.83 | 25.4 | 29.1 | 13 |
| S | 1.60 | 1.83 | 25.4 | 29.1 | 13 |
| SH | 1.45 | 1.63 | 23.1 | 25.9 | 11 |
| F | 1.45 | 1.64 | 23.1 | 26.0 | 12 |
| | In photons/$cm^2$s | | In $mA/cm^2$ | | % |

Table 3

## 3. Summary

Sunlight impinging onto the glass surface of an encapsulated $CdS/Cu_2S$ solar cell penetrates to about 85% into the $Cu_2S$ layer, assuming that a grid electrode with 90% transparency is used and that the $Cu_2S$ layer has a sufficiently rough surface to permit double reflection for most of the incident light at the $Cu_2S$ surface.

Roughly 50% of the impinging light, or approximately 60% of the light entering through the top surface of the $Cu_2S$, is absorbed in a layer of 0.3µm thickness. Most of this absorption takes place in a wavelength range from 330 to 900nm.

Dependent on the extrinsic absorption of CdS and on the reflectivity of the back electrode, a fraction of the transmitted light is reflected from the back electrode and gives an additional - typically 10% - contribution to the carrier generation in $Cu_2S$.

The maximum current density which could be expected from such a cell lies between 20 and 29$mA/cm^2$, dependent on the specific insolation condition (Table 2) and on reflection (Table 3).

It is concluded that the carrier generation rate depends on the specific insolation condition and sensitively on the extrinsic absorption spectra of CdS and $Cu_2S$.

Table 4 shows a comparison of performance parameters for different insolation conditions. The current densities are calculated by assuming carrier generation in $Cu_2S$ only* and a collection efficiency of 1. The solar cell power density is calculated from the calculated current density in Table 4 and an assumed open circuit voltage of 0.53 volt and fill factor of 75%. The latter two values are already achieved[15]. Hence, power density and efficiency do not represent maximum theoretical values for the $CdS/Cu_2S$ solar cell.

| | SUN | | SOLAR CELL | | | | | |
|---|---|---|---|---|---|---|---|---|
| | Impinging Light $mW/cm^2$ | | Current Density $mA/cm^2$ | | Power Density $mW/cm^2$ | | Calculated "$Cu_2S$ effect" % | |
| Insolation | Total $0<\lambda<\infty$ | Onto Glass $300<\lambda<1500$ | No Ref. | With Ref. | No Ref. | With Ref. | No Ref. | With Ref. |
| DF/W | 77.5 | 69.4 | 20.4 | 23.5 | 8.1 | 9.3 | 10.5 | 12.1 |
| SP | 89.8 | 80.3 | 22.9 | 26.7 | 9.1 | 10.6 | 10.1 | 11.8 |
| S | 90.8 | 81.4 | 23.4 | 27.0 | 9.3 | 10.7 | 10.2 | 11.8 |
| SH | 79.7 | 71.5 | 21.1 | 24.0 | 8.4 | 9.5 | 10.5 | 12.0 |
| F | 79.5 | 71.0 | 20.8 | 24.0 | 8.3 | 9.5 | 10.4 | 12.0 |
| T/W | 89.1 | 79.1 | 23.2 | 26.7 | 9.2 | 10.6 | 10.3 | 11.9 |
| SP | 100.2 | 88.8 | 25.4 | 29.1 | 10.1 | 11.6 | 10.1 | 11.5 |
| S | 99.7 | 88.6 | 25.4 | 29.1 | 10.1 | 11.6 | 10.1 | 11.6 |
| SH | 87.6 | 77.9 | 23.1 | 25.9 | 9.2 | 10.3 | 10.5 | 11.8 |
| F | 88.5 | 78.4 | 23.1 | 26.0 | 9.2 | 10.3 | 10.4 | 11.7 |

Table 4

The calculated efficiency relates only to the generation and carrier collection in $Cu_2S$ - using assumed and constant values for open circuit voltage and fill factor. This "$Cu_2S$-efficiency" shows little sensitivity to the specific insolation.

However, it is known that the measured conversion efficiency of $CdS/Cu_2S$ solar cells and, even more pronounced, of solar cell arrays

* Some additional current contributions can be expected from holes generated in CdS and penetrating through the junction interface.

changes drastically[16] with varying insolation. Some indications are given here that such changes may be caused by the CdS part of the cell, specifically caused by variation of the photonflux in the water vapor bands near 900nm and possibly near 1400nm, causing changes in the quenching of CdS. This will be discussed in a following paper[17] (See also Ref. 18 for a theoretical analysis).

## 4. Acknowledgement

Assistance in setting up the basis for the used computer program by Dr. D. Lamb is gratefully acknowledged.

## 5. Literature

1. K. W. Böer, Proc. Sol. Energy Conf. Winnipeg (1976).
2. K. W. Böer, Rough Surfaces, SES Report (1976), unpublished.
3. D. C. Reynolds, J. Opt. Soc. Am. 45, 136 (1959).
4. W. M. Baker, Tech. Rep. ONR, Nonr-151101 ASTIA AD-111 854.
5. R. Pappalardo and R. E. Dietz, Phys. Rev. 123, 1188 (1961).
6. A. B. Francis and A. I. Carlson, J. Opt. Soc. Am. 50, 118 (1960).
7. B. J. Moulder, Phys. Stat. Sol. (a) 18, 633 (1973).
8. J. Dielemann, Proc. Internat. Workshop on CdS/$Cu_2S$ and Other Heterojunctions, Delaware (1975), 91.
9. B. J. Moulder, Phys. Stat. Sol. (a) 13, 569 (1972), 15, 409, (1973).
10. T. S. TeVelde and J. Dieleman, Philips Res. Rep. 28, 573 (1973).
11. K. W. Böer, Carrier Transport in $Cu_2S$, SES Report (1976), unpublished.
12. E. Fagen, personal communication.
13. G. Storti in Semi-Annual Progress Report NSF/RANN/AER 72-03478-AD4-PR75/4.
14. L. Burton in Final Report NSF/RANN/AER72-03478-AD3-FR75.
15. K. W. Böer, Proc. Internat. Workshop on CdS/$Cu_2S$ and Other Heterojunctions, Delaware (1975), 584.
16. H. M. Windawi, Proc. Internat. Workshop on CdS/$Cu_2S$ and Other Heterojunctions, Delaware (1975), 528.
17. K. W. Böer, Space Charge Region, SES Report (1976), unpublished.
18. K. W. Böer, Phys. Rev. B. 13, 5373 (1976).

## APPENDIX

This Appendix contains the figures and the computer printout of the photonflux of two insolation modes, T (total) and DF (direct plus forward scattered) for the five typical clear weather days. It also contains the deviation of the photonflux of these modes relative to a clear spring day (SP). The spectral distribution of the fraction of the photonflux absorbed in $Cu_2S$ and the integrated photonflux are also shown for all insolation conditions given above.

---

* Supported by SES, Incorporated.

1. Spectral distribution of the photonflux, $\phi(\lambda)$, for the total solar radiation (T) as defined in Section 3.2 of the main text of Ref. 1 for the five typical clear weather days as defined in Section 2.4 of Ref. 1, and indicated by the letters W, SP, S, SH, and F in the figure margins.

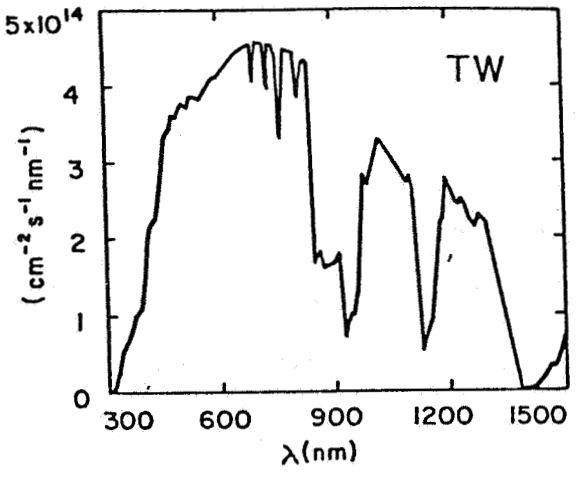


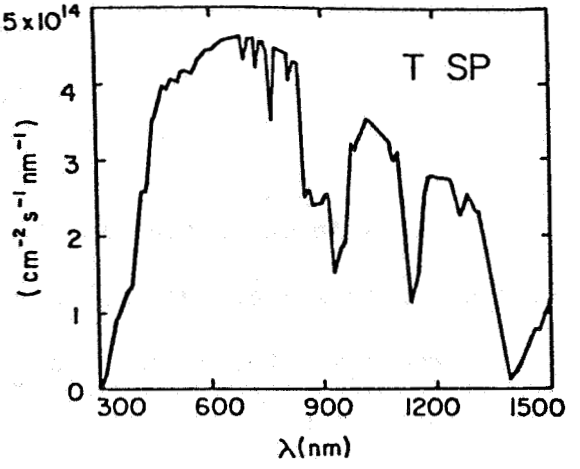


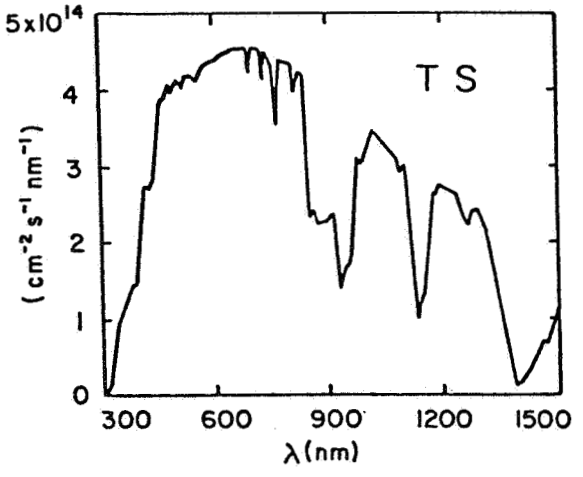


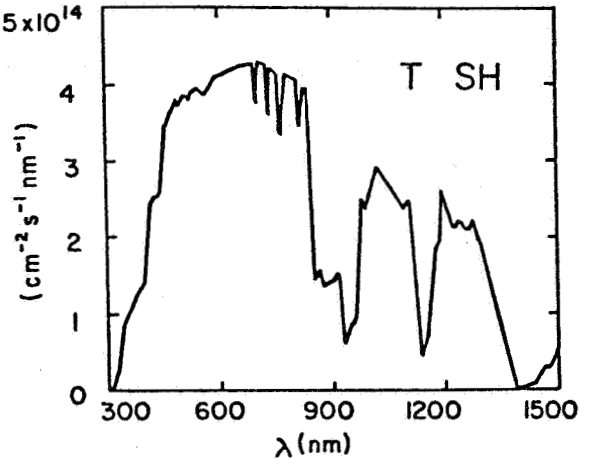


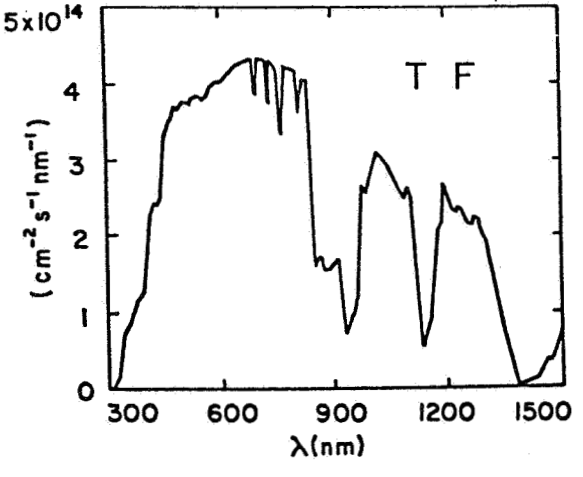

2. Deviation $\phi_i(\lambda)-\phi_{SP}(\lambda)$ from the distribution of photons for a typical spring day (T/SP).

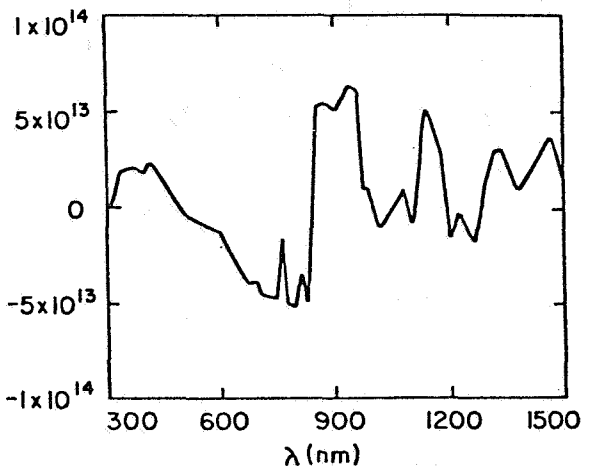


Winter (W)

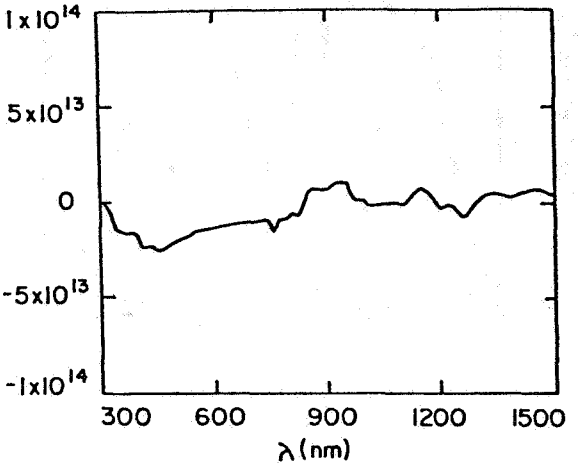


Summer (S)

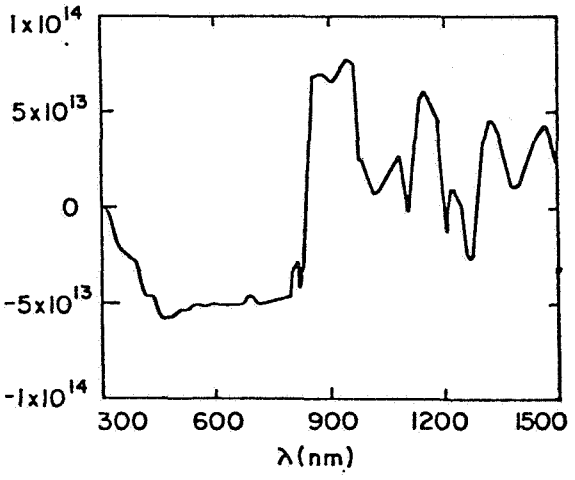


Summer, Humid (SH)

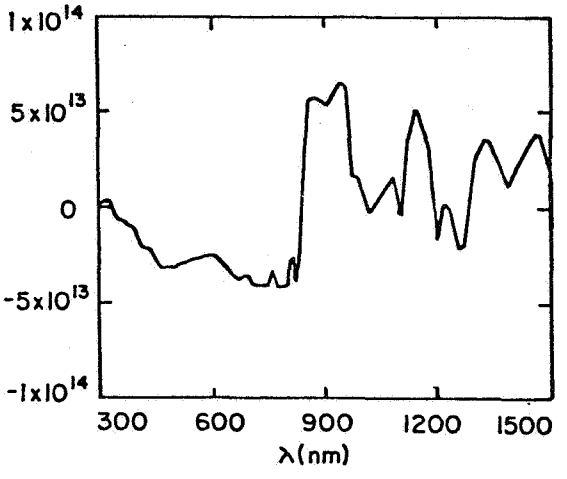


Fall (F)

3. Spectral distribution of the photonflux for the direct plus forward scattered solar radiation (DF) as defined in Section 2.6 of the main text of Ref. 1 for the five typical clear weather days as defined in Section 2.4 of Ref. 1, and indicated by the letters W, SP, S, SH, and F in the figure margins.

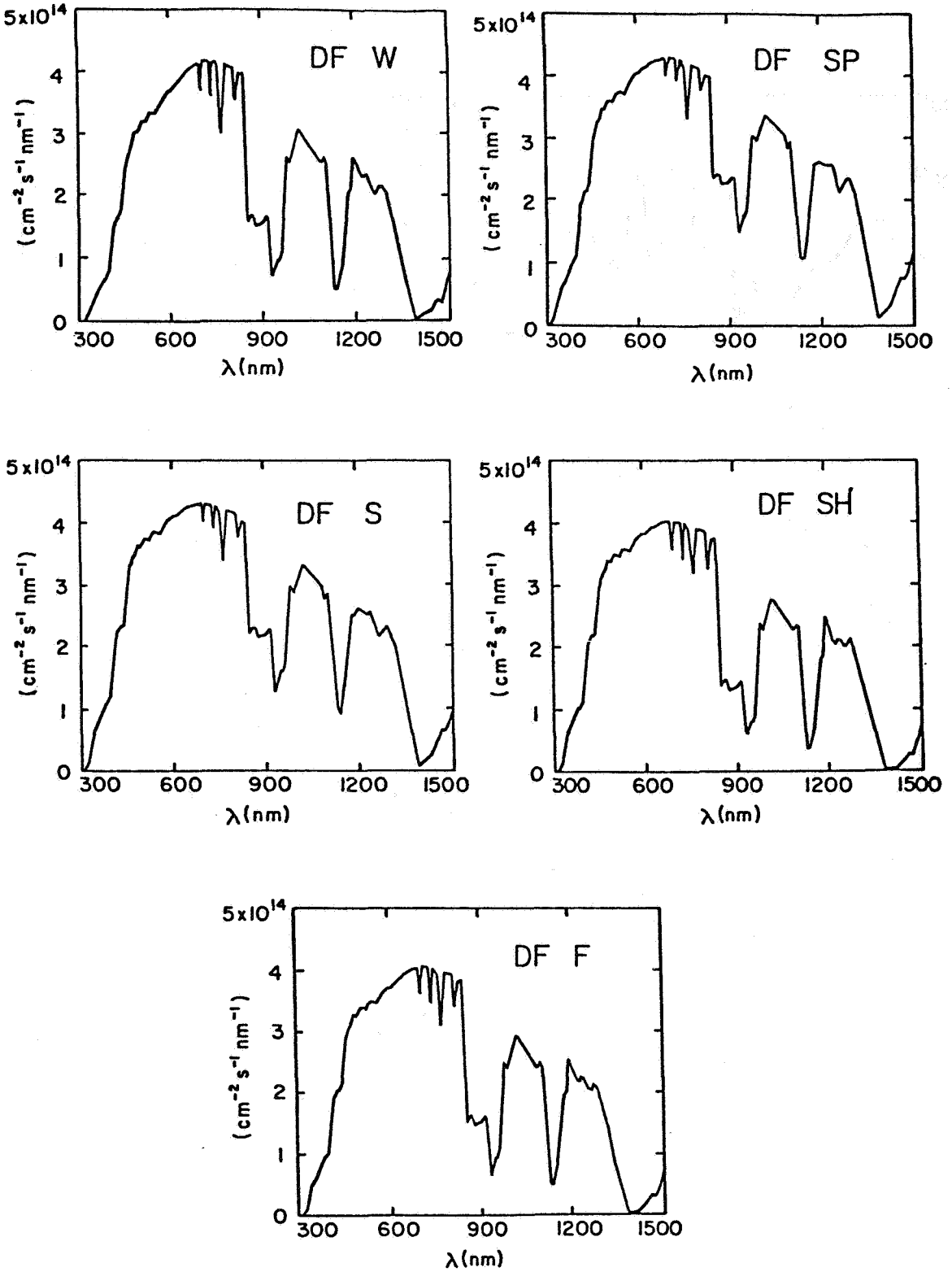

4. Deviation $\phi_i(\lambda)-\phi_{SP}(\lambda)$ from the distribution of photons for a typical spring day (DF/SP).

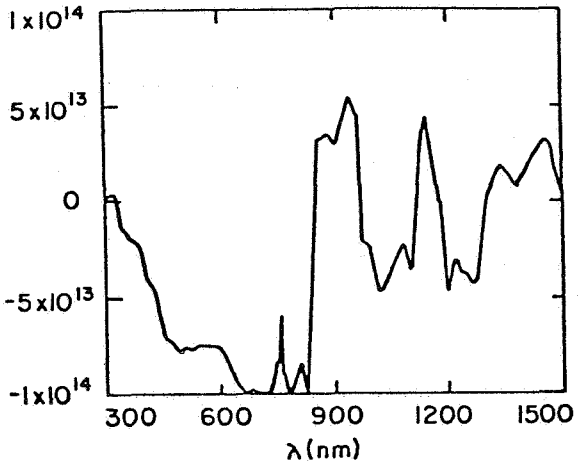


Winter (W)

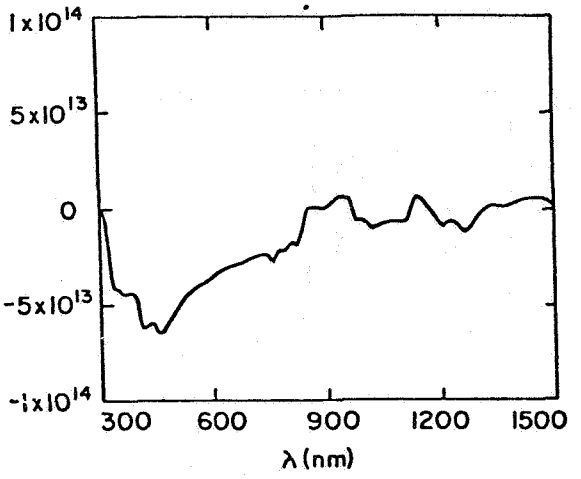


Summer (S)

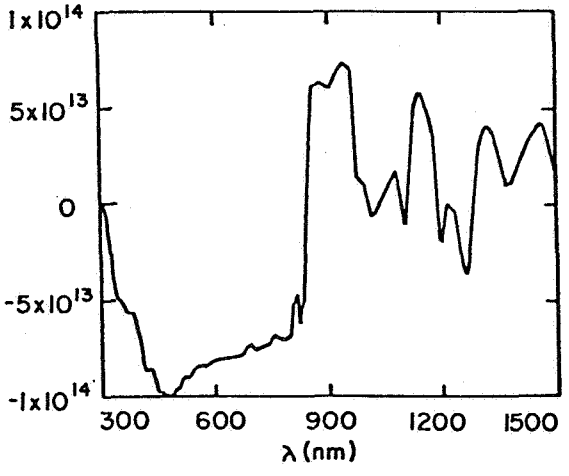


Summer, Humid (SH)

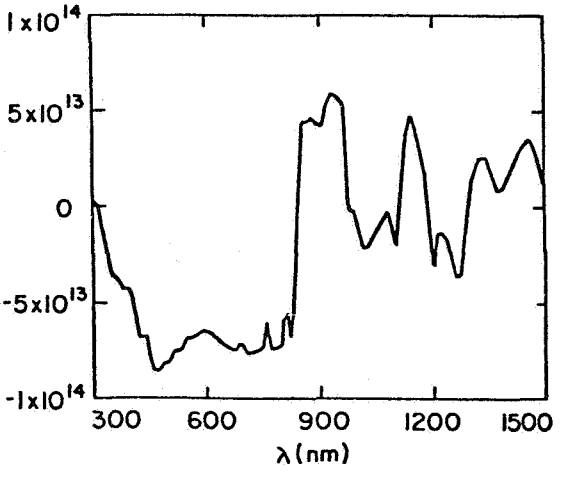


Fall (F)

5. Photonflux impinging on the outer glass surface (curve 1), penetrating through the top $Cu_2S$ surface (curve 2), fraction of the photonflux absorbed in a 0.3μm thick $Cu_2S$ layer with absorption spectrum given as solid curve in Fig. 8 of main text during first path (curve 3), and including reflection from the back electrode ($R_7$=0.7) (curve 4) for the insolation given below each figure (as in Figs. 13 and 27 of the main text).

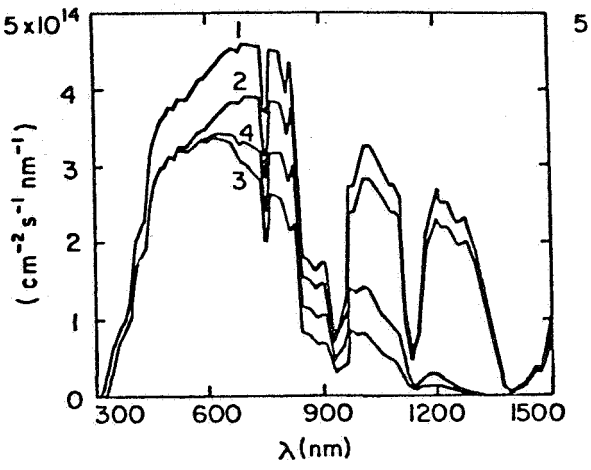


T/W

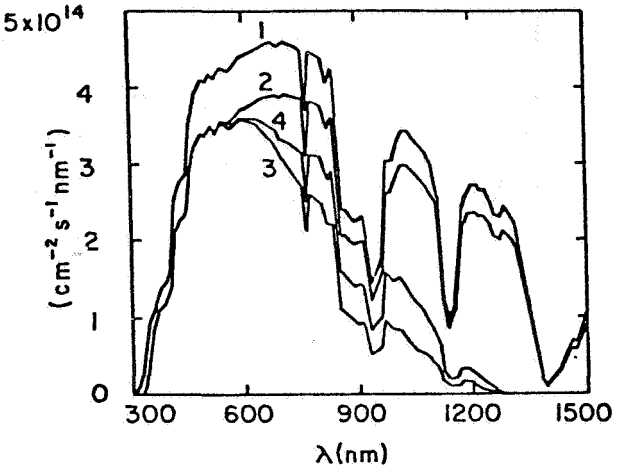


T/SP

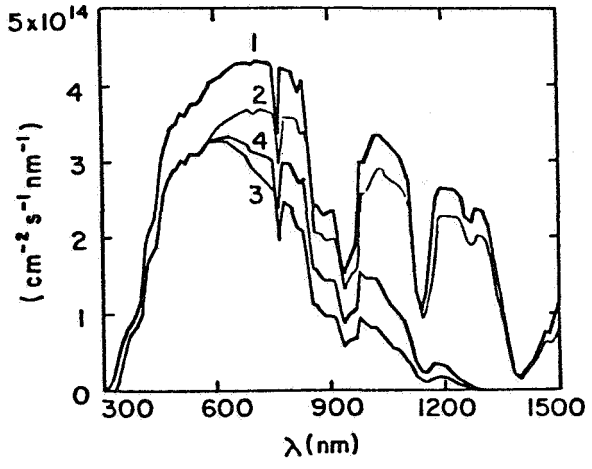


T/S

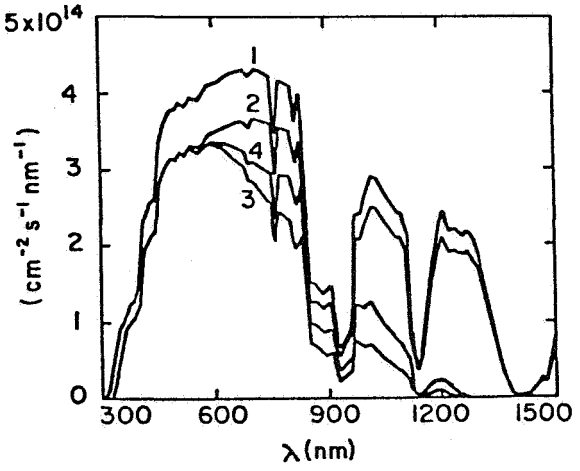


T/SH

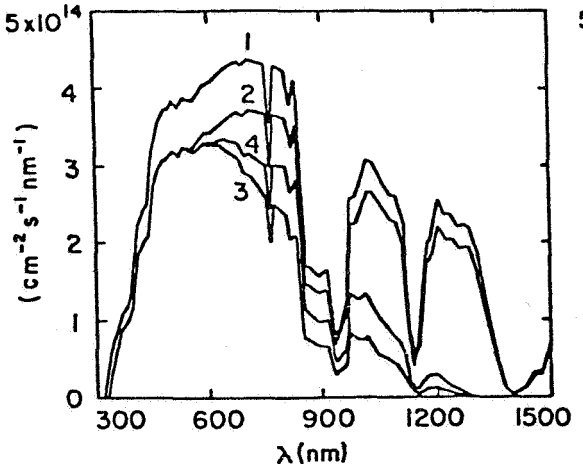


T/F

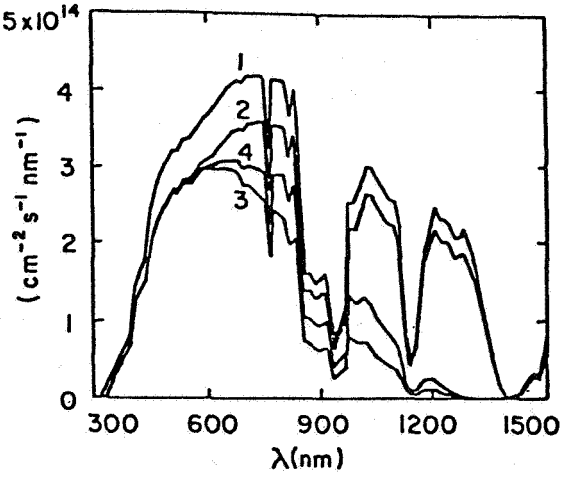


DF/W

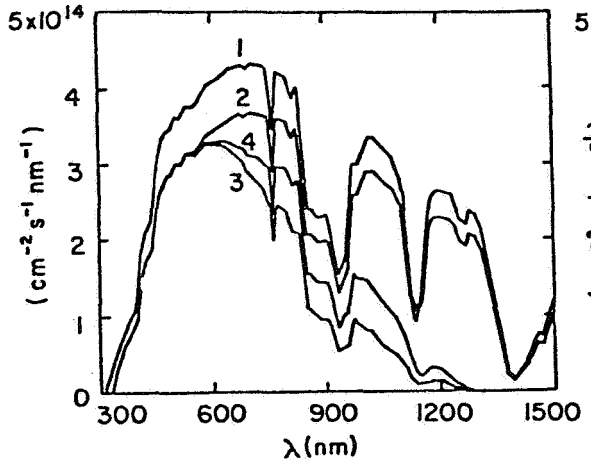


DF/SP

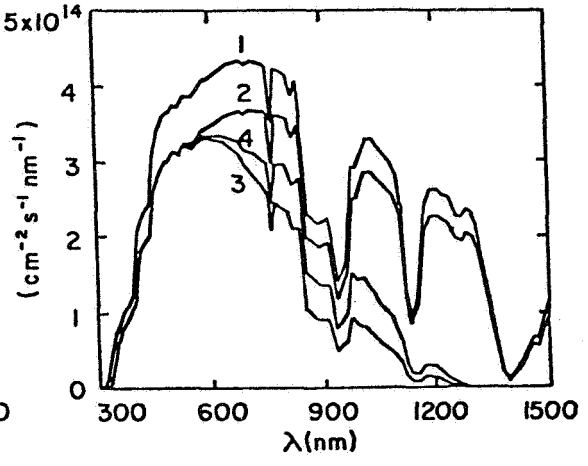


DF/S

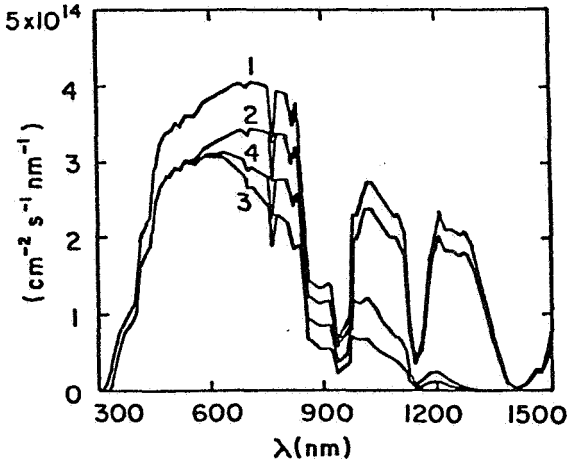


DF/SH

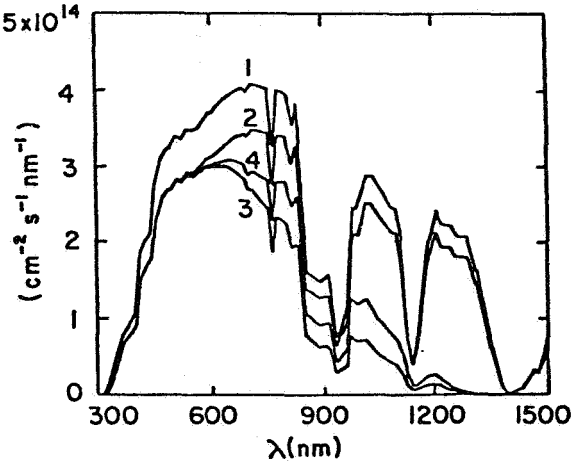


DF/F

6. Photonflux integrated from λ=300μm to the given wavelength for curves 1-4 in Section 5 of this appendix (see also Figs. 4, 14, and 28 of the main text).

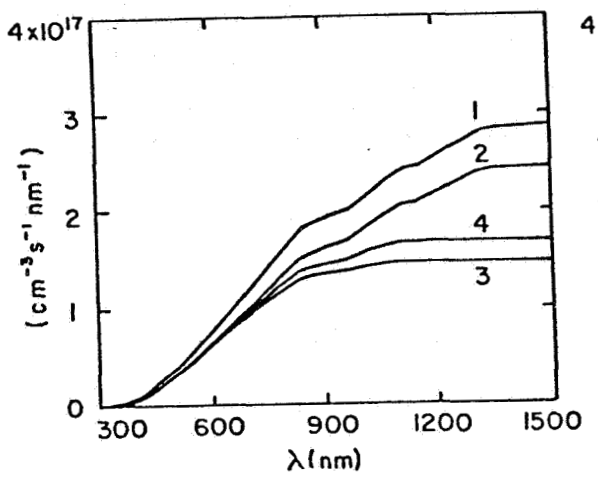


T/W

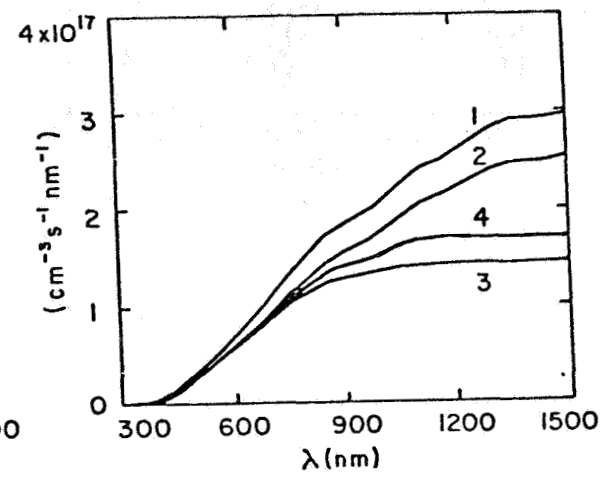


T/SP

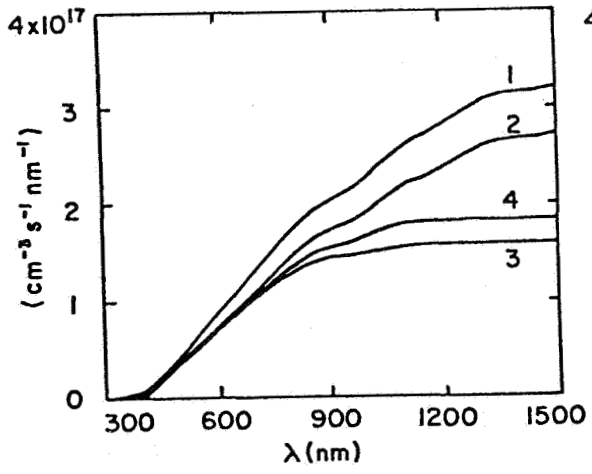


T/S

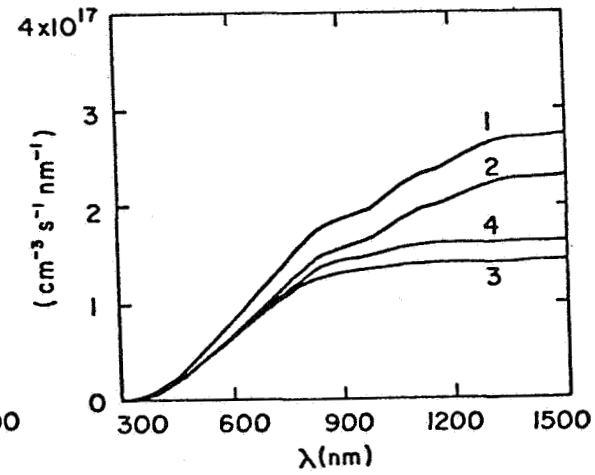


T/SH

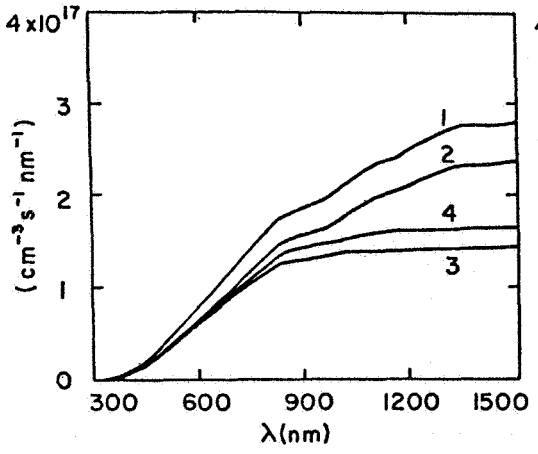


T/F

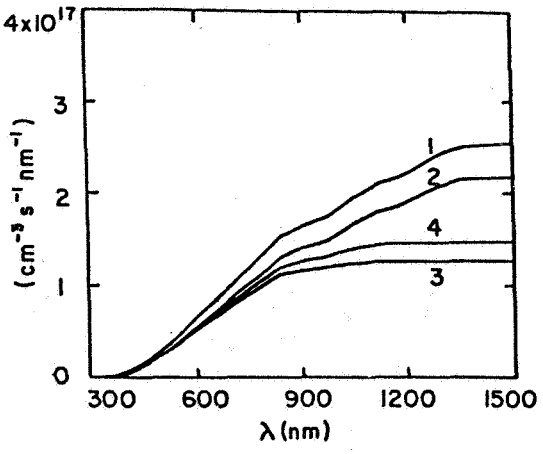


DF/W

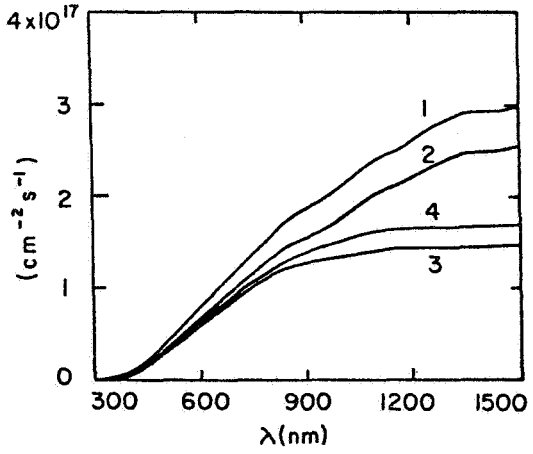


DF/SP

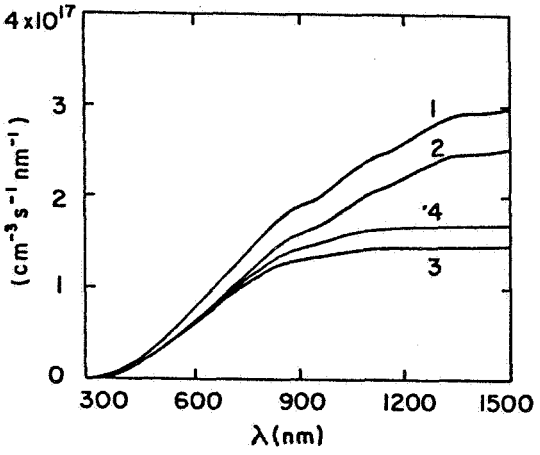


DF/S

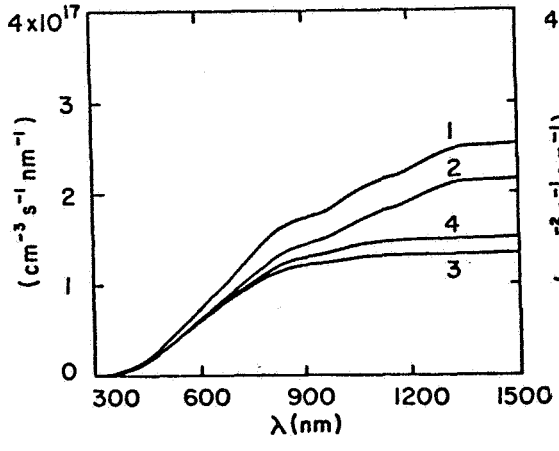


DF/SH

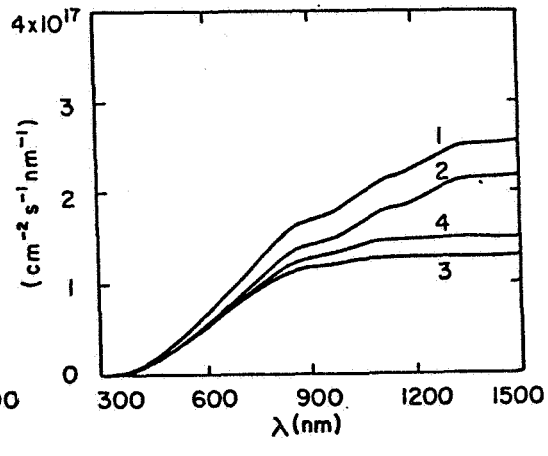


DF/F

7. Computer printout of the photonflux for the T and DF components of the five typical clear weather days in photons per $cm^2 \cdot s \cdot nm$.

| λ (nm) | ϕ(T/W) ph/cm²s nm |
|---|---|
| 300 | 6.108E+09 |
| 307 | 1.529E+11 |
| 313 | 1.839E+12 |
| 320 | 1.809E+13 |
| 327 | 3.001E+13 |
| 334 | 4.379E+13 |
| 340 | 5.974E+13 |
| 347 | 6.600E+13 |
| 354 | 7.349E+13 |
| 360 | 8.064E+13 |
| 367 | 9.281E+13 |
| 374 | 1.006E+14 |
| 380 | 1.043E+14 |
| 387 | 1.085E+14 |
| 394 | 1.227E+14 |
| 401 | 1.621E+14 |
| 407 | 1.968E+14 |
| 414 | 2.147E+14 |
| 421 | 2.207E+14 |
| 427 | 2.215E+14 |
| 434 | 2.310E+14 |
| 441 | 2.671E+14 |
| 447 | 3.014E+14 |
| 454 | 3.256E+14 |
| 461 | 3.370E+14 |
| 468 | 3.428E+14 |
| 474 | 3.531E+14 |
| 481 | 3.655E+14 |
| 488 | 3.594E+14 |
| 494 | 3.696E+14 |
| 501 | 3.758E+14 |
| 508 | 3.750E+14 |
| 515 | 3.696E+14 |
| 521 | 3.764E+14 |
| 528 | 3.851E+14 |
| 535 | 3.866E+14 |
| 541 | 3.842E+14 |
| 548 | 3.828E+14 |
| 555 | 3.853E+14 |
| 561 | 3.858E+14 |
| 568 | 3.942E+14 |
| 575 | 4.021E+14 |
| 582 | 4.070E+14 |
| 588 | 4.106E+14 |
| 595 | 4.112E+14 |
| 602 | 4.125E+14 |
| 608 | 4.169E+14 |
| 615 | 4.213E+14 |
| 622 | 4.253E+14 |
| 628 | 4.294E+14 |
| 635 | 4.343E+14 |
| 642 | 4.390E+14 |
| 649 | 4.428E+14 |
| 655 | 4.458E+14 |
| 662 | 4.484E+14 |
| 669 | 4.501E+14 |
| 675 | 4.519E+14 |
| 682 | 4.539E+14 |
| 689 | 4.564E+14 |
| 696 | 3.939E+14 |
| 702 | 4.578E+14 |
| 709 | 4.578E+14 |
| 716 | 4.567E+14 |
| 722 | 4.343E+14 |
| 729 | 4.264E+14 |
| 736 | 4.544E+14 |
| 742 | 4.531E+14 |
| 749 | 4.525E+14 |
| 756 | 3.704E+14 |
| 763 | 2.920E+14 |
| 769 | 4.343E+14 |
| 776 | 4.486E+14 |
| 783 | 4.472E+14 |
| 789 | 4.459E+14 |
| 796 | 4.445E+14 |
| 803 | 4.124E+14 |
| 809 | 3.882E+14 |
| 816 | 4.083E+14 |
| 823 | 4.286E+14 |
| 830 | 4.333E+14 |
| 836 | 4.014E+14 |
| 843 | 2.466E+14 |
| 850 | 1.705E+14 |
| 856 | 1.814E+14 |
| 863 | 1.795E+14 |
| 870 | 1.626E+14 |
| 877 | 1.621E+14 |
| 883 | 1.643E+14 |
| 890 | 1.666E+14 |
| 897 | 1.691E+14 |
| 903 | 1.729E+14 |
| 910 | 1.782E+14 |
| 917 | 1.654E+14 |
| 923 | 1.012E+14 |
| 930 | 6.222E+13 |
| 937 | 9.176E+13 |
| 944 | 1.032E+14 |
| 950 | 9.950E+13 |
| 957 | 1.156E+14 |
| 964 | 1.258E+14 |
| 970 | 2.124E+14 |
| 977 | 2.816E+14 |
| 984 | 2.694E+14 |
| 991 | 2.776E+14 |
| 997 | 2.904E+14 |
| 1004 | 3.034E+14 |
| 1011 | 3.165E+14 |
| 1017 | 3.297E+14 |
| 1024 | 3.262E+14 |
| 1031 | 3.208E+14 |
| 1037 | 3.153E+14 |
| 1044 | 3.097E+14 |
| 1051 | 3.041E+14 |
| 1058 | 2.983E+14 |
| 1064 | 2.925E+14 |
| 1071 | 2.865E+14 |
| 1078 | 2.805E+14 |
| 1084 | 2.743E+14 |
| 1091 | 2.678E+14 |
| 1098 | 2.819E+14 |
| 1104 | 2.718E+14 |
| 1111 | 2.077E+14 |
| 1118 | 1.4_8E+14 |
| 1125 | 7.726E+13 |
| 1131 | 5.225E+13 |
| 1138 | 5.221E+13 |
| 1145 | 7.381E+13 |
| 1151 | 8.758E+13 |
| 1158 | 1.199E+14 |
| 1165 | 1.526E+14 |
| 1172 | 1.857E+14 |
| 1178 | 2.182E+14 |
| 1185 | 2.255E+14 |
| 1192 | 2.611E+14 |
| 1198 | 2.711E+14 |
| 1205 | 2.629E+14 |
| 1212 | 2,546E+14 |
| 1218 | 2.462E+14 |
| 1225 | 2.441E+14 |
| 1232 | 2.491E+14 |
| 1239 | 2.486E+14 |
| 1245 | 2.392E+14 |
| 1252 | 2.296E+14 |
| 1259 | 2.200E+14 |
| 1265 | 2.145E+14 |
| 1272 | 2,257E+14 |
| 1279 | 2.314E+14 |
| 1285 | 2,291E+14 |
| 1292 | 2.199E+14 |
| 1299 | 2,064E+14 |
| 1306 | 1.927E+14 |
| 1312 | 1.789E+14 |
| 1319 | 1.592E+14 |
| 1326 | 1,373E+14 |
| 1332 | 1.153E+14 |
| 1339 | 9.803E+13 |
| 1346 | 8,387E+13 |
| 1353 | 6.957E+13 |
| 1359 | 5.513E+13 |
| 1366 | 4.056E+13 |
| 1373 | 2.584E+13 |
| 1379 | 1.099E+13 |
| 1386 | 1.096E+12 |
| 1393 | 2.864E+12 |
| 1399 | 4.649E+12 |
| 1406 | 6.450E+12 |
| 1413 | 8.267E+12 |
| 1420 | 1.010E+13 |
| 1426 | 1.195E+13 |
| 1433 | 1.446E+13 |
| 1440 | 2.086E+13 |
| 1446 | 2.732E+13 |
| 1453 | 3.384E+13 |
| 1460 | 3.685E+13 |
| 1466 | 3.482E+13 |
| 1473 | 3.575E+13 |
| 1480 | 5.060E+13 |
| 1487 | 6.558E+13 |
| 1493 | 8.068E+13 |
| 1500 | 9.592E+13 |

| λ (nm) | φ(T/SP) ph/cm$^2$s nm |
|---|---|
| 300 | 5.521E+11 |
| 307 | 2.718E+12 |
| 313 | 1.069E+13 |
| 320 | 3.753E+13 |
| 327 | 5.454E+13 |
| 334 | 7.005E+13 |
| 340 | 8.422E+13 |
| 347 | 9.095E+13 |
| 354 | 9.873E+13 |
| 360 | 1.054E+14 |
| 367 | 1.196E+14 |
| 374 | 1.277E+14 |
| 380 | 1.300E+14 |
| 387 | 1.337E+14 |
| 394 | 1.491E+14 |
| 401 | 1.944E+14 |
| 407 | 2.343E+14 |
| 414 | 2.536E+14 |
| 421 | 2.584E+14 |
| 427 | 2.567E+14 |
| 434 | 2.650E+14 |
| 441 | 3.031E+14 |
| 447 | 3.382E+14 |
| 454 | 3.632E+14 |
| 461 | 3.745E+14 |
| 468 | 3.795E+14 |
| 474 | 3.893E+14 |
| 481 | 4.013E+14 |
| 488 | 3.929E+14 |
| 494 | 4.021E+14 |
| 501 | 4.071E+14 |
| 508 | 4.061E+14 |
| 515 | 4.000E+14 |
| 521 | 4.071E+14 |
| 528 | 4.162E+14 |
| 535 | 4.175E+14 |
| 541 | 4.145E+14 |
| 548 | 4.126E+14 |
| 555 | 4.151E+14 |
| 561 | 4.158E+14 |
| 568 | 4.247E+14 |
| 575 | 4.333E+14 |
| 582 | 4.384E+14 |
| 588 | 4.422E+14 |
| 595 | 4.428E+14 |
| 602 | 4.435E+14 |
| 608 | 4.459E+14 |
| 615 | 4.481E+14 |
| 622 | 4.499E+14 |
| 628 | 4.518E+14 |
| 635 | 4.544E+14 |
| 642 | 4.569E+14 |
| 649 | 4.582E+14 |
| 655 | 4.597E+14 |
| 662 | 4.609E+14 |
| 669 | 4.612E+14 |
| 675 | 4.610E+14 |
| 682 | 4.621E+14 |
| 689 | 4.632E+14 |
| 696 | 4.243E+14 |
| 702 | 4.620E+14 |
| 709 | 4.615E+14 |
| 716 | 4.600E+14 |
| 722 | 4.458E+14 |
| 729 | 4.406E+14 |
| 736 | 4.562E+14 |
| 742 | 4.544E+14 |
| 749 | 4.533E+14 |
| 756 | 3.864E+14 |
| 763 | 3.225E+14 |
| 769 | 4.366E+14 |
| 776 | 4.474E+14 |
| 783 | 4.456E+14 |
| 789 | 4.438E+14 |
| 796 | 4.418E+14 |
| 803 | 4.220E+14 |
| 809 | 4.067E+14 |
| 816 | 4.172E+14 |
| 823 | 4.279E+14 |
| 830 | 4.294E+14 |
| 836 | 4.069E+14 |
| 843 | 3.013E+14 |
| 850 | 2.498E+14 |
| 856 | 2.580E+14 |
| 863 | 2.557E+14 |
| 870 | 2.411E+14 |
| 877 | 2.400E+14 |
| 883 | 2.412E+14 |
| 890 | 2.426E+14 |
| 897 | 2.441E+14 |
| 903 | 2.470E+14 |
| 910 | 2.512E+14 |
| 917 | 2.389E+14 |
| 923 | 1.797E+14 |
| 930 | 1.375E+14 |
| 937 | 1.705E+14 |
| 944 | 1.835E+14 |
| 950 | 1.797E+14 |
| 957 | 1.952E+14 |
| 964 | 2.043E+14 |
| 970 | 2.696E+14 |
| 977 | 3.217E+14 |
| 984 | 3.126E+14 |
| 991 | 3.185E+14 |
| 997 | 3.278E+14 |
| 1004 | 3.372E+14 |
| 1011 | 3.467E+14 |
| 1017 | 3.563E+14 |
| 1024 | 3.539E+14 |
| 1031 | 3.501E+14 |
| 1037 | 3.463E+14 |
| 1044 | 3.424E+14 |
| 1051 | 3.384E+14 |
| 1058 | 3.344E+14 |
| 1064 | 3.303E+14 |
| 1071 | 3.261E+14 |
| 1078 | 3.218E+14 |
| 1084 | 3.136E+14 |
| 1091 | 2.979E+14 |
| 1098 | 3.147E+14 |
| 1104 | 2.798E+14 |
| 1111 | 2.299E+14 |
| 1118 | 1.794E+14 |
| 1125 | 1.283E+14 |
| 1131 | 1.130E+14 |
| 1138 | 1.122E+14 |
| 1145 | 1.367E+14 |
| 1151 | 1.488E+14 |
| 1158 | 1.797E+14 |
| 1165 | 2.110E+14 |
| 1172 | 2.426E+14 |
| 1178 | 2.735E+14 |
| 1185 | 2.750E+14 |
| 1192 | 2.772E+14 |
| 1198 | 2.770E+14 |
| 1205 | 2.760E+14 |
| 1212 | 2.750E+14 |
| 1218 | 2.740E+14 |
| 1225 | 2.736E+14 |
| 1232 | 2.739E+14 |
| 1239 | 2.694E+14 |
| 1245 | 2.570E+14 |
| 1252 | 2.444E+14 |
| 1259 | 2.317E+14 |
| 1265 | 2.232E+14 |
| 1272 | 2.317E+14 |
| 1279 | 2.408E+14 |
| 1285 | 2.508E+14 |
| 1292 | 2.505E+14 |
| 1299 | 2.439E+14 |
| 1306 | 2.372E+14 |
| 1312 | 2.304E+14 |
| 1319 | 2.110E+14 |
| 1326 | 1.870E+14 |
| 1332 | 1.628E+14 |
| 1339 | 1.415E+14 |
| 1346 | 1.220E+14 |
| 1353 | 1.024E+14 |
| 1359 | 8.255E+13 |
| 1366 | 6.252E+13 |
| 1373 | 4.230E+13 |
| 1379 | 2.189E+13 |
| 1386 | 9.129E+12 |
| 1393 | 1.434E+13 |
| 1399 | 1.960E+13 |
| 1406 | 2.491E+13 |
| 1413 | 3.027E+13 |
| 1420 | 3.567E+13 |
| 1426 | 4.112E+13 |
| 1433 | 4.717E+13 |
| 1440 | 5.662E+13 |
| 1446 | 6.615E+13 |
| 1453 | 7.577E+13 |
| 1460 | 8.030E+13 |
| 1466 | 7.755E+13 |
| 1473 | 7.740E+13 |
| 1480 | 8.963E+13 |
| 1487 | 1.020E+14 |
| 1493 | 1.144E+14 |
| 1500 | 1.269E+14 |

| λ (nm) | ϕ(T/S) ph/cm$^2$s nm |
|---|---|
| 300 | 4.942E+11 |
| 307 | 2.702E+12 |
| 313 | 1.154E+13 |
| 320 | 4.362E+13 |
| 327 | 6.329E+13 |
| 334 | 8.108E+13 |
| 340 | 9.708E+13 |
| 347 | 1.040E+14 |
| 354 | 1.118E+14 |
| 360 | 1.182E+14 |
| 367 | 1.331E+14 |
| 374 | 1.411E+14 |
| 380 | 1.425E+14 |
| 387 | 1.456E+14 |
| 394 | 1.614E+14 |
| 401 | 2.090E+14 |
| 407 | 2.509E+14 |
| 414 | 2.704E+14 |
| 421 | 2.743E+14 |
| 427 | 2.713E+14 |
| 434 | 2.788E+14 |
| 441 | 3.173E+14 |
| 447 | 3.523E+14 |
| 454 | 3.770E+14 |
| 461 | 3.878E+14 |
| 468 | 3.919E+14 |
| 474 | 4.009E+14 |
| 481 | 4.121E+14 |
| 488 | 4.022E+14 |
| 494 | 4.105E+14 |
| 501 | 4.145E+14 |
| 508 | 4.126E+14 |
| 515 | 4.057E+14 |
| 521 | 4.121E+14 |
| 528 | 4.205E+14 |
| 535 | 4.210E+14 |
| 541 | 4.172E+14 |
| 548 | 4.144E+14 |
| 555 | 4.164E+14 |
| 561 | 4.165E+14 |
| 568 | 4.250E+14 |
| 575 | 4.330E+14 |
| 582 | 4.375E+14 |
| 588 | 4.408E+14 |
| 595 | 4.408E+14 |
| 602 | 4.411E+14 |
| 608 | 4.432E+14 |
| 615 | 4.453E+14 |
| 622 | 4.469E+14 |
| 628 | 4.486E+14 |
| 635 | 4.510E+14 |
| 642 | 4.533E+14 |
| 649 | 4.544E+14 |
| 655 | 4.557E+14 |
| 662 | 4.568E+14 |
| 669 | 4.570E+14 |
| 675 | 4.571E+14 |
| 682 | 4.576E+14 |
| 689 | 4.585E+14 |
| 696 | 4.165E+14 |
| 702 | 4.569E+14 |
| 709 | 4.564E+14 |
| 716 | 4.547E+14 |
| 722 | 4.395E+14 |
| 729 | 4.338E+14 |
| 736 | 4.506E+14 |
| 742 | 4.487E+14 |
| 749 | 4.475E+14 |
| 756 | 3.882E+14 |
| 763 | 3.315E+14 |
| 769 | 4.320E+14 |
| 776 | 4.412E+14 |
| 783 | 4.393E+14 |
| 789 | 4.374E+14 |
| 796 | 4.353E+14 |
| 803 | 4.141E+14 |
| 809 | 3.978E+14 |
| 816 | 4.093E+14 |
| 823 | 4.209E+14 |
| 830 | 4.227E+14 |
| 836 | 3.992E+14 |
| 843 | 2.881E+14 |
| 850 | 2.339E+14 |
| 856 | 2.424E+14 |
| 863 | 2.401E+14 |
| 870 | 2.253E+14 |
| 877 | 2.242E+14 |
| 883 | 2.255E+14 |
| 890 | 2.270E+14 |
| 897 | 2.286E+14 |
| 903 | 2.316E+14 |
| 910 | 2.359E+14 |
| 917 | 2.235E+14 |
| 923 | 1.636E+14 |
| 930 | 1.219E+14 |
| 937 | 1.545E+14 |
| 944 | 1.673E+14 |
| 950 | 1.634E+14 |
| 957 | 1.790E+14 |
| 964 | 1.882E+14 |
| 970 | 2.560E+14 |
| 977 | 3.099E+14 |
| 984 | 3.005E+14 |
| 991 | 3.067E+14 |
| 997 | 3.165E+14 |
| 1004 | 3.204E+14 |
| 1011 | 3.363E+14 |
| 1017 | 3.464E+14 |
| 1024 | 3.439E+14 |
| 1031 | 3.400E+14 |
| 1037 | 3.360E+14 |
| 1044 | 3.320E+14 |
| 1051 | 3.278E+14 |
| 1058 | 3.237E+14 |
| 1064 | 3.194E+14 |
| 1071 | 3.150E+14 |
| 1078 | 3.106E+14 |
| 1084 | 3.025E+14 |
| 1091 | 2.876E+14 |
| 1098 | 3.045E+14 |
| 1104 | 2.757E+14 |
| 1111 | 2.234E+14 |
| 1118 | 1.705E+14 |
| 1125 | 1.170E+14 |
| 1131 | 1.001E+14 |
| 1138 | 9.945E+13 |
| 1145 | 1.235E+14 |
| 1151 | 1.360E+14 |
| 1158 | 1.672E+14 |
| 1165 | 1.987E+14 |
| 1172 | 2.305E+14 |
| 1178 | 2.617E+14 |
| 1185 | 2.699E+14 |
| 1192 | 2.715E+14 |
| 1198 | 2.730E+14 |
| 1205 | 2.706E+14 |
| 1212 | 2.681E+14 |
| 1218 | 2.656E+14 |
| 1225 | 2.646E+14 |
| 1232 | 2.654E+14 |
| 1239 | 2.621E+14 |
| 1245 | 2.519E+14 |
| 1252 | 2.417E+14 |
| 1259 | 2.313E+14 |
| 1265 | 2.244E+14 |
| 1272 | 2.316E+14 |
| 1279 | 2.383E+14 |
| 1285 | 2.442E+14 |
| 1292 | 2.419E+14 |
| 1299 | 2.346E+14 |
| 1306 | 2.273E+14 |
| 1312 | 2.199E+14 |
| 1319 | 2.004E+14 |
| 1326 | 1.766E+14 |
| 1332 | 1.525E+14 |
| 1339 | 1.319E+14 |
| 1346 | 1.135E+14 |
| 1353 | 9.495E+13 |
| 1359 | 7.619E+13 |
| 1366 | 5.726E+13 |
| 1373 | 3.814E+13 |
| 1379 | 1.885E+13 |
| 1386 | 6.668E+12 |
| 1393 | 1.117E+13 |
| 1399 | 1.572E+13 |
| 1406 | 2.030E+13 |
| 1413 | 2.493E+13 |
| 1420 | 2.959E+13 |
| 1426 | 3.430E+13 |
| 1433 | 3.964E+13 |
| 1440 | 4.861E+13 |
| 1446 | 5.766E+13 |
| 1453 | 6.679E+13 |
| 1460 | 7.109E+13 |
| 1466 | 6.846E+13 |
| 1473 | 6.847E+13 |
| 1480 | 8.099E+13 |
| 1487 | 9.360E+13 |
| 1493 | 1.063E+14 |
| 1500 | 1.192E+14 |

| λ (nm) | ϕ(T/SH) ph/cm$^2$s nm |
|---|---|
| 300 | 4.389E+11 |
| 307 | 2.410E+12 |
| 313 | 1.034E+13 |
| 320 | 3.925E+13 |
| 327 | 5.715E+13 |
| 334 | 7.346E+13 |
| 340 | 8.823E+13 |
| 347 | 9.474E+13 |
| 354 | 1.022E+14 |
| 360 | 1.082E+14 |
| 367 | 1.221E+14 |
| 374 | 1.296E+14 |
| 380 | 1.311E+14 |
| 387 | 1.342E+14 |
| 394 | 1.490E+14 |
| 401 | 1.932E+14 |
| 407 | 2.322E+14 |
| 414 | 2.505E+14 |
| 421 | 2.543E+14 |
| 427 | 2.518E+14 |
| 434 | 2.589E+14 |
| 441 | 2.950E+14 |
| 447 | 3.278E+14 |
| 454 | 3.510E+14 |
| 461 | 3.612E+14 |
| 468 | 3.652E+14 |
| 474 | 3.738E+14 |
| 481 | 3.844E+14 |
| 488 | 3.754E+14 |
| 494 | 3.833E+14 |
| 501 | 3.872E+14 |
| 508 | 3.856E+14 |
| 515 | 3.792E+14 |
| 521 | 3.854E+14 |
| 528 | 3.934E+14 |
| 535 | 3.940E+14 |
| 541 | 3.905E+14 |
| 548 | 3.880E+14 |
| 555 | 3.899E+14 |
| 561 | 3.902E+14 |
| 568 | 3.982E+14 |
| 575 | 4.058E+14 |
| 582 | 4.101E+14 |
| 588 | 4.132E+14 |
| 595 | 4.133E+14 |
| 602 | 4.137E+14 |
| 608 | 4.158E+14 |
| 615 | 4.178E+14 |
| 622 | 4.194E+14 |
| 628 | 4.211E+14 |
| 635 | 4.234E+14 |
| 642 | 4.256E+14 |
| 649 | 4.267E+14 |
| 655 | 4.281E+14 |
| 662 | 4.291E+14 |
| 669 | 4.293E+14 |
| 675 | 4.295E+14 |
| 682 | 4.300E+14 |
| 689 | 4.309E+14 |
| 696 | 3.664E+14 |
| 702 | 4.296E+14 |
| 709 | 4.291E+14 |
| 716 | 4.276E+14 |
| 722 | 4.047E+14 |
| 729 | 3.962E+14 |
| 736 | 4.239E+14 |
| 742 | 4.222E+14 |
| 749 | 4.211E+14 |
| 756 | 3.654E+14 |
| 763 | 3.121E+14 |
| 769 | 4.066E+14 |
| 776 | 4.154E+14 |
| 783 | 4.136E+14 |
| 789 | 4.118E+14 |
| 796 | 4.100E+14 |
| 803 | 3.779E+14 |
| 809 | 3.538E+14 |
| 816 | 3.736E+14 |
| 823 | 3.937E+14 |
| 830 | 3.983E+14 |
| 836 | 3.675E+14 |
| 843 | 2.184E+14 |
| 850 | 1.450E+14 |
| 856 | 1.550E+14 |
| 863 | 1.532E+14 |
| 870 | 1.377E+14 |
| 877 | 1.371E+14 |
| 883 | 1.391E+14 |
| 890 | 1.412E+14 |
| 897 | 1.434E+14 |
| 903 | 1.469E+14 |
| 910 | 1.518E+14 |
| 917 | 1.404E+14 |
| 923 | 8.255E+13 |
| 930 | 4.853E+13 |
| 937 | 7.408E+13 |
| 944 | 8.393E+13 |
| 950 | 8.066E+13 |
| 957 | 9.490E+13 |
| 964 | 1.040E+14 |
| 970 | 1.848E+14 |
| 977 | 2.493E+14 |
| 984 | 2.378E+14 |
| 991 | 2.452E+14 |
| 997 | 2.570E+14 |
| 1004 | 2.688E+14 |
| 1011 | 2.808E+14 |
| 1017 | 2.929E+14 |
| 1024 | 2.894E+14 |
| 1031 | 2.840E+14 |
| 1037 | 2.786E+14 |
| 1044 | 2.731E+14 |
| 1051 | 2.675E+14 |
| 1058 | 2.618E+14 |
| 1064 | 2.561E+14 |
| 1071 | 2.503E+14 |
| 1078 | 2.444E+14 |
| 1084 | 2.394E+14 |
| 1091 | 2.364E+14 |
| 1098 | 2.474E+14 |
| 1104 | 2.543E+14 |
| 1111 | 1.922E+14 |
| 1118 | 1.294E+14 |
| 1125 | 6.596E+13 |
| 1131 | 4.066E+13 |
| 1138 | 4.072E+13 |
| 1145 | 5.922E+13 |
| 1151 | 7.142E+13 |
| 1158 | 9.983E+13 |
| 1165 | 1.285E+14 |
| 1172 | 1.575E+14 |
| 1178 | 1.861E+14 |
| 1185 | 1.937E+14 |
| 1192 | 2.389E+14 |
| 1198 | 2.516E+14 |
| 1205 | 2.405E+14 |
| 1212 | 2.292E+14 |
| 1218 | 2.179E+14 |
| 1225 | 2.143E+14 |
| 1232 | 2.198E+14 |
| 1239 | 2.222E+14 |
| 1245 | 2.194E+14 |
| 1252 | 2.166E+14 |
| 1259 | 2.137E+14 |
| 1265 | 2.128E+14 |
| 1272 | 2.196E+14 |
| 1279 | 2.184E+14 |
| 1285 | 2.057E+14 |
| 1292 | 1.925E+14 |
| 1299 | 1.791E+14 |
| 1306 | 1.655E+14 |
| 1312 | 1.518E+14 |
| 1319 | 1.346E+14 |
| 1326 | 1.161E+14 |
| 1332 | 9.740E+13 |
| 1339 | 8.282E+13 |
| 1346 | 7.081E+13 |
| 1353 | 5.869E+13 |
| 1359 | 4.646E+13 |
| 1366 | 3.412E+13 |
| 1373 | 2.168E+13 |
| 1379 | 9.120E+12 |
| 1386 | 6.946E+11 |
| 1393 | 1.977E+12 |
| 1399 | 3.269E+12 |
| 1406 | 4.573E+12 |
| 1413 | 5.888E+12 |
| 1420 | 7.214E+12 |
| 1426 | 8.551E+12 |
| 1433 | 1.045E+13 |
| 1440 | 1.570E+13 |
| 1446 | 2.099E+13 |
| 1453 | 2.632E+13 |
| 1460 | 2.876E+13 |
| 1466 | 2.707E+13 |
| 1473 | 2.807E+13 |
| 1480 | 4.171E+13 |
| 1487 | 5.546E+13 |
| 1493 | 6.933E+13 |
| 1500 | 8.330E+13 |

| λ (nm) | ϕ(T/F) ph/cm$^2$s nm |
|---|---|
| 300 | 2.859E+10 |
| 307 | 4.230E+11 |
| 313 | 3.680E+12 |
| 320 | 2.668E+13 |
| 327 | 4.222E+13 |
| 334 | 5.876E+13 |
| 340 | 7.627E+13 |
| 347 | 8.306E+13 |
| 354 | 9.088E+13 |
| 360 | 9.771E+13 |
| 367 | 1.111E+14 |
| 374 | 1.189E+14 |
| 380 | 1.213E+14 |
| 387 | 1.248E+14 |
| 394 | 1.395E+14 |
| 401 | 1.820E+14 |
| 407 | 2.195E+14 |
| 414 | 2.378E+14 |
| 421 | 2.424E+14 |
| 427 | 2.411E+14 |
| 434 | 2.490E+14 |
| 441 | 2.850E+14 |
| 447 | 3.182E+14 |
| 454 | 3.416E+14 |
| 461 | 3.520E+14 |
| 468 | 3.565E+14 |
| 474 | 3.654E+14 |
| 481 | 3.763E+14 |
| 488 | 3.681E+14 |
| 494 | 3.765E+14 |
| 501 | 3.808E+14 |
| 508 | 3.791E+14 |
| 515 | 3.728E+14 |
| 521 | 3.787E+14 |
| 528 | 3.865E+14 |
| 535 | 3.870E+14 |
| 541 | 3.835E+14 |
| 548 | 3.811E+14 |
| 555 | 3.829E+14 |
| 561 | 3.829E+14 |
| 568 | 3.907E+14 |
| 575 | 3.980E+14 |
| 582 | 4.022E+14 |
| 588 | 4.051E+14 |
| 595 | 4.051E+14 |
| 602 | 4.057E+14 |
| 608 | 4.090E+14 |
| 615 | 4.122E+14 |
| 622 | 4.151E+14 |
| 628 | 4.180E+14 |
| 635 | 4.217E+14 |
| 642 | 4.252E+14 |
| 649 | 4.277E+14 |
| 655 | 4.299E+14 |
| 662 | 4.317E+14 |
| 669 | 4.327E+14 |
| 675 | 4.338E+14 |
| 682 | 4.350E+14 |
| 689 | 4.367E+14 |
| 696 | 3.770E+14 |
| 702 | 4.368E+14 |
| 709 | 4.366E+14 |
| 716 | 4.353E+14 |
| 722 | 4.139E+14 |
| 729 | 4.062E+14 |
| 736 | 4.323E+14 |
| 742 | 4.308E+14 |
| 749 | 4.299E+14 |
| 756 | 3.666E+14 |
| 763 | 3.061E+14 |
| 769 | 4.146E+14 |
| 776 | 4.251E+14 |
| 783 | 4.235E+14 |
| 789 | 4.220E+14 |
| 796 | 4.203E+14 |
| 803 | 3.901E+14 |
| 809 | 3.673E+14 |
| 816 | 3.860E+14 |
| 823 | 4.048E+14 |
| 830 | 4.091E+14 |
| 836 | 3.791E+14 |
| 843 | 2.339E+14 |
| 850 | 1.625E+14 |
| 856 | 1.727E+14 |
| 863 | 1.708E+14 |
| 870 | 1.549E+14 |
| 877 | 1.543E+14 |
| 883 | 1.564E+14 |
| 890 | 1.585E+14 |
| 897 | 1.608E+14 |
| 903 | 1.643E+14 |
| 910 | 1.693E+14 |
| 917 | 1.573E+14 |
| 923 | 9.667E+13 |
| 930 | 5.978E+13 |
| 937 | 8.777E+13 |
| 944 | 9.862E+13 |
| 950 | 9.511E+13 |
| 957 | 1.103E+14 |
| 964 | 1.199E+14 |
| 970 | 2.011E+14 |
| 977 | 2.660E+14 |
| 984 | 2.546E+14 |
| 991 | 2.623E+14 |
| 997 | 2.743E+14 |
| 1004 | 2.864E+14 |
| 1011 | 2.986E+14 |
| 1017 | 3.110E+14 |
| 1024 | 3.077E+14 |
| 1031 | 3.026E+14 |
| 1037 | 2.974E+14 |
| 1044 | 2.921E+14 |
| 1051 | 2.868E+14 |
| 1058 | 2.814E+14 |
| 1064 | 2.759E+14 |
| 1071 | 2.703E+14 |
| 1078 | 2.646E+14 |
| 1084 | 2.587E+14 |
| 1091 | 2.523E+14 |
| 1098 | 2.658E+14 |
| 1104 | 2.613E+14 |
| 1111 | 1.996E+14 |
| 1118 | 1.372E+14 |
| 1125 | 7.421E+13 |
| 1131 | 5.008E+13 |
| 1138 | 5.005E+13 |
| 1145 | 7.049E+13 |
| 1151 | 8.351E+13 |
| 1158 | 1.141E+14 |
| 1165 | 1.450E+14 |
| 1172 | 1.761E+14 |
| 1178 | 2.068E+14 |
| 1185 | 2.136E+14 |
| 1192 | 2.498E+14 |
| 1198 | 2.599E+14 |
| 1205 | 2.512E+14 |
| 1212 | 2.423E+14 |
| 1218 | 2.333E+14 |
| 1225 | 2.307E+14 |
| 1232 | 2.353E+14 |
| 1239 | 2.359E+14 |
| 1245 | 2.300E+14 |
| 1252 | 2.239E+14 |
| 1259 | 2.178E+14 |
| 1265 | 2.146E+14 |
| 1272 | 2.228E+14 |
| 1279 | 2.249E+14 |
| 1285 | 2.184E+14 |
| 1292 | 2.081E+14 |
| 1299 | 1.956E+14 |
| 1306 | 1.829E+14 |
| 1312 | 1.701E+14 |
| 1319 | 1.514E+14 |
| 1326 | 1.306E+14 |
| 1332 | 1.097E+14 |
| 1339 | 9.331E+13 |
| 1346 | 7.981E+13 |
| 1353 | 6.619E+13 |
| 1359 | 5.245E+13 |
| 1366 | 3.858E+13 |
| 1373 | 2.459E+13 |
| 1379 | 1.048E+13 |
| 1386 | 1.087E+12 |
| 1393 | 2.809E+12 |
| 1399 | 4.547E+12 |
| 1406 | 6.299E+12 |
| 1413 | 8.067E+12 |
| 1420 | 9.849E+12 |
| 1426 | 1.165E+13 |
| 1433 | 1.407E+13 |
| 1440 | 2.021E+13 |
| 1446 | 2.639E+13 |
| 1453 | 3.263E+13 |
| 1460 | 3.551E+13 |
| 1466 | 3.358E+13 |
| 1473 | 3.445E+13 |
| 1480 | 4.850E+13 |
| 1487 | 6.266E+13 |
| 1493 | 7.695E+13 |
| 1500 | 9.134E+13 |

| λ (nm) | φ(DF/W) ph/cm$^2$s nm |
|---|---|
| 300 | 1.588E+09 |
| 307 | 4.651E+10 |
| 313 | 6.395E+11 |
| 320 | 7.057E+12 |
| 327 | 1.291E+13 |
| 334 | 2.050E+13 |
| 340 | 3.007E+13 |
| 347 | 3.538E+13 |
| 354 | 4.160E+13 |
| 360 | 4.787E+13 |
| 367 | 5.744E+13 |
| 374 | 6.462E+13 |
| 380 | 6.914E+13 |
| 387 | 7.403E+13 |
| 394 | 8.587E+13 |
| 401 | 1.161E+14 |
| 407 | 1.438E+14 |
| 414 | 1.598E+14 |
| 421 | 1.670E+14 |
| 427 | 1.701E+14 |
| 434 | 1.798E+14 |
| 441 | 2.105E+14 |
| 447 | 2.401E+14 |
| 454 | 2.621E+14 |
| 461 | 2.738E+14 |
| 468 | 2.809E+14 |
| 474 | 2.916E+14 |
| 481 | 3.041E+14 |
| 488 | 3.010E+14 |
| 494 | 3.115E+14 |
| 501 | 3.185E+14 |
| 508 | 3.194E+14 |
| 515 | 3.164E+14 |
| 521 | 3.237E+14 |
| 528 | 3.326E+14 |
| 535 | 3.352E+14 |
| 541 | 3.344E+14 |
| 548 | 3.343E+14 |
| 555 | 3.376E+14 |
| 561 | 3.391E+14 |
| 568 | 3.474E+14 |
| 575 | 3.554E+14 |
| 582 | 3.606E+14 |
| 588 | 3.646E+14 |
| 595 | 3.660E+14 |
| 602 | 3.680E+14 |
| 608 | 3.726E+14 |
| 615 | 3.772E+14 |
| 622 | 3.815E+14 |
| 628 | 3.858E+14 |
| 635 | 3.908E+14 |
| 642 | 3.957E+14 |
| 649 | 3.996E+14 |
| 655 | 4.029E+14 |
| 662 | 4.057E+14 |
| 669 | 4.078E+14 |
| 675 | 4.099E+14 |
| 682 | 4.121E+14 |
| 689 | 4.148E+14 |
| 696 | 3.584E+14 |
| 702 | 4.169E+14 |
| 709 | 4.173E+14 |
| 716 | 4.167E+14 |
| 722 | 3.966E+14 |
| 729 | 3.896E+14 |
| 736 | 4.155E+14 |
| 742 | 4.147E+14 |
| 749 | 4.143E+14 |
| 756 | 3.394E+14 |
| 763 | 2.677E+14 |
| 769 | 3.984E+14 |
| 776 | 4.118E+14 |
| 783 | 4.106E+14 |
| 789 | 4.098E+14 |
| 796 | 4.086E+14 |
| 803 | 3.794E+14 |
| 809 | 3.573E+14 |
| 816 | 3.759E+14 |
| 823 | 3.947E+14 |
| 830 | 3.992E+14 |
| 836 | 3.700E+14 |
| 843 | 2.274E+14 |
| 850 | 1.573E+14 |
| 856 | 1.674E+14 |
| 863 | 1.657E+14 |
| 870 | 1.502E+14 |
| 877 | 1.497E+14 |
| 883 | 1.518E+14 |
| 890 | 1.540E+14 |
| 897 | 1.563E+14 |
| 903 | 1.599E+14 |
| 910 | 1.648E+14 |
| 917 | 1.531E+14 |
| 923 | 9.363E+13 |
| 930 | 5.759E+13 |
| 937 | 8.495E+13 |
| 944 | 9.557E+13 |
| 950 | 9.216E+13 |
| 957 | 1.071E+14 |
| 964 | 1.165E+14 |
| 970 | 1.968E+14 |
| 977 | 2.610E+14 |
| 984 | 2.498E+14 |
| 991 | 2.574E+14 |
| 997 | 2.693E+14 |
| 1004 | 2.814E+14 |
| 1011 | 2.936E+14 |
| 1017 | 3.059E+14 |
| 1024 | 3.027E+14 |
| 1031 | 2.977E+14 |
| 1037 | 2.927E+14 |
| 1044 | 2.875E+14 |
| 1051 | 2.823E+14 |
| 1058 | 2.770E+14 |
| 1064 | 2.716E+14 |
| 1071 | 2.661E+14 |
| 1078 | 2.605E+14 |
| 1084 | 2.548E+14 |
| 1091 | 2.488E+14 |
| 1098 | 2.619E+14 |
| 1104 | 2.526E+14 |
| 1111 | 1.930E+14 |
| 1118 | 1.328E+14 |
| 1125 | 7.180E+13 |
| 1131 | 4.856E+13 |
| 1138 | 4.854E+13 |
| 1145 | 6.862E+13 |
| 1151 | 8.143E+13 |
| 1158 | 1.115E+14 |
| 1165 | 1.419E+14 |
| 1172 | 1.727E+14 |
| 1178 | 2.030E+14 |
| 1185 | 2.097E+14 |
| 1192 | 2.429E+14 |
| 1198 | 2.522E+14 |
| 1205 | 2.446E+14 |
| 1212 | 2.369E+14 |
| 1218 | 2.291E+14 |
| 1225 | 2.271E+14 |
| 1232 | 2.317E+14 |
| 1239 | 2.313E+14 |
| 1245 | 2.226E+14 |
| 1252 | 2.137E+14 |
| 1259 | 2.047E+14 |
| 1265 | 1.996E+14 |
| 1272 | 2.101E+14 |
| 1279 | 2.154E+14 |
| 1285 | 2.133E+14 |
| 1292 | 2.047E+14 |
| 1299 | 1.921E+14 |
| 1306 | 1.794E+14 |
| 1312 | 1.665E+14 |
| 1319 | 1.482E+14 |
| 1326 | 1.279E+14 |
| 1332 | 1.073E+14 |
| 1339 | 9.128E+13 |
| 1346 | 7.810E+13 |
| 1353 | 6.479E+13 |
| 1359 | 5.134E+13 |
| 1366 | 3.777E+13 |
| 1373 | 2.407E+13 |
| 1379 | 1.024E+13 |
| 1386 | 1.021E+12 |
| 1393 | 2.668E+12 |
| 1399 | 4.330E+12 |
| 1406 | 6.008E+12 |
| 1413 | 7.700E+12 |
| 1420 | 9.408E+12 |
| 1426 | 1.113E+13 |
| 1433 | 1.347E+13 |
| 1440 | 1.944E+13 |
| 1446 | 2.545E+13 |
| 1453 | 3.152E+13 |
| 1460 | 3.433E+13 |
| 1466 | 3.244E+13 |
| 1473 | 3.331E+13 |
| 1480 | 4.715E+13 |
| 1487 | 6.110E+13 |
| 1493 | 7.518E+13 |
| 1500 | 8.937E+13 |

| λ (nm) | φ(DF/SP) ph/cm$^2$s nm |
|---|---|
| 300 | 2.504E+11 |
| 307 | 1.339E+12 |
| 313 | 5.657E+12 |
| 320 | 2.112E+13 |
| 327 | 3.235E+13 |
| 334 | 4.349E+13 |
| 340 | 5.441E+13 |
| 347 | 6.085E+13 |
| 354 | 6.811E+13 |
| 360 | 7.468E+13 |
| 367 | 8.682E+13 |
| 374 | 9.470E+13 |
| 380 | 9.829E+13 |
| 387 | 1.028E+14 |
| 394 | 1.165E+14 |
| 401 | 1.539E+14 |
| 407 | 1.879E+14 |
| 414 | 2.057E+14 |
| 421 | 2.118E+14 |
| 427 | 2.124E+14 |
| 434 | 2.212E+14 |
| 441 | 2.550E+14 |
| 447 | 2.866E+14 |
| 454 | 3.099E+14 |
| 461 | 3.215E+14 |
| 468 | 3.277E+14 |
| 474 | 3.379E+14 |
| 481 | 3.500E+14 |
| 488 | 3.442E+14 |
| 494 | 3.538E+14 |
| 501 | 3.596E+14 |
| 508 | 3.600E+14 |
| 515 | 3.558E+14 |
| 521 | 3.633E+14 |
| 528 | 3.725E+14 |
| 535 | 3.748E+14 |
| 541 | 3.730E+14 |
| 548 | 3.722E+14 |
| 555 | 3.754E+14 |
| 561 | 3.768E+14 |
| 568 | 3.857E+14 |
| 575 | 3.942E+14 |
| 582 | 3.996E+14 |
| 588 | 4.037E+14 |
| 595 | 4.049E+14 |
| 602 | 4.062E+14 |
| 608 | 4.089E+14 |
| 615 | 4.116E+14 |
| 622 | 4.138E+14 |
| 628 | 4.160E+14 |
| 635 | 4.189E+14 |
| 642 | 4.216E+14 |
| 649 | 4.233E+14 |
| 655 | 4.251E+14 |
| 662 | 4.266E+14 |
| 669 | 4.273E+14 |
| 675 | 4.280E+14 |
| 682 | 4.289E+14 |
| 689 | 4.302E+14 |
| 696 | 3.944E+14 |
| 702 | 4.297E+14 |
| 709 | 4.295E+14 |
| 716 | 4.284E+14 |
| 722 | 4.155E+14 |
| 729 | 4.108E+14 |
| 736 | 4.256E+14 |
| 742 | 4.242E+14 |
| 749 | 4.234E+14 |
| 756 | 3.611E+14 |
| 763 | 3.015E+14 |
| 769 | 4.084E+14 |
| 776 | 4.187E+14 |
| 783 | 4.171E+14 |
| 789 | 4.156E+14 |
| 796 | 4.139E+14 |
| 803 | 3.955E+14 |
| 809 | 3.813E+14 |
| 816 | 3.913E+14 |
| 823 | 4.014E+14 |
| 830 | 4.030E+14 |
| 836 | 3.820E+14 |
| 843 | 2.830E+14 |
| 850 | 2.346E+14 |
| 856 | 2.424E+14 |
| 863 | 2.403E+14 |
| 870 | 2.267E+14 |
| 877 | 2.256E+14 |
| 883 | 2.269E+14 |
| 890 | 2.282E+14 |
| 897 | 2.297E+14 |
| 903 | 2.324E+14 |
| 910 | 2.364E+14 |
| 917 | 2.249E+14 |
| 923 | 1.692E+14 |
| 930 | 1.295E+14 |
| 937 | 1.606E+14 |
| 944 | 1.729E+14 |
| 950 | 1.693E+14 |
| 957 | 1.839E+14 |
| 964 | 1.925E+14 |
| 970 | 2.542E+14 |
| 977 | 3.033E+14 |
| 984 | 2.947E+14 |
| 991 | 3.004E+14 |
| 997 | 3.092E+14 |
| 1004 | 3.181E+14 |
| 1011 | 3.271E+14 |
| 1017 | 3.362E+14 |
| 1024 | 3.340E+14 |
| 1031 | 3.305E+14 |
| 1037 | 3.269E+14 |
| 1044 | 3.232E+14 |
| 1051 | 3.195E+14 |
| 1058 | 3.157E+14 |
| 1064 | 3.119E+14 |
| 1071 | 3.079E+14 |
| 1078 | 3.039E+14 |
| 1084 | 2.962E+14 |
| 1091 | 2.814E+14 |
| 1098 | 2.973E+14 |
| 1104 | 2.644E+14 |
| 1111 | 2.172E+14 |
| 1118 | 1.695E+14 |
| 1125 | 1.212E+14 |
| 1131 | 1.068E+14 |
| 1138 | 1.060E+14 |
| 1145 | 1.292E+14 |
| 1151 | 1.407E+14 |
| 1158 | 1.699E+14 |
| 1165 | 1.995E+14 |
| 1172 | 2.293E+14 |
| 1178 | 2.586E+14 |
| 1185 | 2.600E+14 |
| 1192 | 2.621E+14 |
| 1198 | 2.620E+14 |
| 1205 | 2.611E+14 |
| 1212 | 2.601E+14 |
| 1218 | 2.591E+14 |
| 1225 | 2.588E+14 |
| 1232 | 2.591E+14 |
| 1239 | 2.548E+14 |
| 1245 | 2.431E+14 |
| 1252 | 2.312E+14 |
| 1259 | 2.192E+14 |
| 1265 | 2.112E+14 |
| 1272 | 2.192E+14 |
| 1279 | 2.278E+14 |
| 1285 | 2.373E+14 |
| 1292 | 2.371E+14 |
| 1299 | 2.308E+14 |
| 1306 | 2.245E+14 |
| 1312 | 2.181E+14 |
| 1319 | 1.997E+14 |
| 1326 | 1.770E+14 |
| 1332 | 1.541E+14 |
| 1339 | 1.339E+14 |
| 1346 | 1.155E+14 |
| 1353 | 9.692E+13 |
| 1359 | 7.814E+13 |
| 1366 | 5.918E+13 |
| 1373 | 4.004E+13 |
| 1379 | 2.072E+13 |
| 1386 | 8.642E+12 |
| 1393 | 1.358E+13 |
| 1399 | 1.856E+13 |
| 1406 | 2.359E+13 |
| 1413 | 2.866E+13 |
| 1420 | 3.377E+13 |
| 1426 | 3.893E+13 |
| 1433 | 4.467E+13 |
| 1440 | 5.362E+13 |
| 1446 | 6.265E+13 |
| 1453 | 7.175E+13 |
| 1460 | 7.605E+13 |
| 1466 | 7.344E+13 |
| 1473 | 7.331E+13 |
| 1480 | 8.489E+13 |
| 1487 | 9.656E+13 |
| 1493 | 1.083E+14 |
| 1500 | 1.202E+14 |

| λ (nm) | ϕ(DF/S) ph/cm$^2$s nm |
|---|---|
| 300 | 2.611E+11 |
| 307 | 1.521E+12 |
| 313 | 6.865E+12 |
| 320 | 2.721E+13 |
| 327 | 4.114E+13 |
| 334 | 5.463E+13 |
| 340 | 6.752E+13 |
| 347 | 7.436E+13 |
| 354 | 8.199E+13 |
| 360 | 8.857E+13 |
| 367 | 1.018E+14 |
| 374 | 1.097E+14 |
| 380 | 1.126E+14 |
| 387 | 1.167E+14 |
| 394 | 1.310E+14 |
| 401 | 1.716E+14 |
| 407 | 2.082E+14 |
| 414 | 2.266E+14 |
| 421 | 2.319E+14 |
| 427 | 2.313E+14 |
| 434 | 2.394E+14 |
| 441 | 2.744E+14 |
| 447 | 3.065E+14 |
| 454 | 3.299E+14 |
| 461 | 3.412E+14 |
| 468 | 3.465E+14 |
| 474 | 3.561E+14 |
| 481 | 3.676E+14 |
| 488 | 3.602E+14 |
| 494 | 3.690E+14 |
| 501 | 3.736E+14 |
| 508 | 3.734E+14 |
| 515 | 3.682E+14 |
| 521 | 3.751E+14 |
| 528 | 3.837E+14 |
| 535 | 3.852E+14 |
| 541 | 3.825E+14 |
| 548 | 3.809E+14 |
| 555 | 3.834E+14 |
| 561 | 3.843E+14 |
| 568 | 3.928E+14 |
| 575 | 4.009E+14 |
| 582 | 4.058E+14 |
| 588 | 4.094E+14 |
| 595 | 4.100E+14 |
| 602 | 4.109E+14 |
| 608 | 4.134E+14 |
| 615 | 4.158E+14 |
| 622 | 4.179E+14 |
| 628 | 4.199E+14 |
| 635 | 4.226E+14 |
| 642 | 4.251E+14 |
| 649 | 4.266E+14 |
| 655 | 4.283E+14 |
| 662 | 4.296E+14 |
| 669 | 4.301E+14 |
| 675 | 4.306E+14 |
| 682 | 4.313E+14 |
| 689 | 4.325E+14 |
| 696 | 3.931E+14 |
| 702 | 4.316E+14 |
| 709 | 4.314E+14 |
| 716 | 4.301E+14 |
| 722 | 4.159E+14 |
| 729 | 4.107E+14 |
| 736 | 4.269E+14 |
| 742 | 4.253E+14 |
| 749 | 4.244E+14 |
| 756 | 3.683E+14 |
| 763 | 3.147E+14 |
| 769 | 4.102E+14 |
| 776 | 4.191E+14 |
| 783 | 4.174E+14 |
| 789 | 4.158E+14 |
| 796 | 4.140E+14 |
| 803 | 3.939E+14 |
| 809 | 3.786E+14 |
| 816 | 3.896E+14 |
| 823 | 4.008E+14 |
| 830 | 4.027E+14 |
| 836 | 3.803E+14 |
| 843 | 2.746E+14 |
| 850 | 2.230E+14 |
| 856 | 2.311E+14 |
| 863 | 2.290E+14 |
| 870 | 2.149E+14 |
| 877 | 2.139E+14 |
| 883 | 2.153E+14 |
| 890 | 2.167E+14 |
| 897 | 2.183E+14 |
| 903 | 2.212E+14 |
| 910 | 2.253E+14 |
| 917 | 2.136E+14 |
| 923 | 1.564E+14 |
| 930 | 1.165E+14 |
| 937 | 1.477E+14 |
| 944 | 1.599E+14 |
| 950 | 1.563E+14 |
| 957 | 1.712E+14 |
| 964 | 1.800E+14 |
| 970 | 2.449E+14 |
| 977 | 2.965E+14 |
| 984 | 2.876E+14 |
| 991 | 2.936E+14 |
| 997 | 3.030E+14 |
| 1004 | 3.124E+14 |
| 1011 | 3.220E+14 |
| 1017 | 3.317E+14 |
| 1024 | 3.294E+14 |
| 1031 | 3.257E+14 |
| 1037 | 3.219E+14 |
| 1044 | 3.180E+14 |
| 1051 | 3.141E+14 |
| 1058 | 3.101E+14 |
| 1064 | 3.061E+14 |
| 1071 | 3.019E+14 |
| 1078 | 2.977E+14 |
| 1084 | 2.900E+14 |
| 1091 | 2.758E+14 |
| 1098 | 2.919E+14 |
| 1104 | 2.643E+14 |
| 1111 | 2.142E+14 |
| 1118 | 1.635E+14 |
| 1125 | 1.122E+14 |
| 1131 | 9.605E+13 |
| 1138 | 9.540E+13 |
| 1145 | 1.185E+14 |
| 1151 | 1.304E+14 |
| 1158 | 1.604E+14 |
| 1165 | 1.906E+14 |
| 1172 | 2.212E+14 |
| 1178 | 2.511E+14 |
| 1185 | 2.532E+14 |
| 1192 | 2.606E+14 |
| 1198 | 2.620E+14 |
| 1205 | 2.597E+14 |
| 1212 | 2.573E+14 |
| 1218 | 2.550E+14 |
| 1225 | 2.540E+14 |
| 1232 | 2.548E+14 |
| 1239 | 2.516E+14 |
| 1245 | 2.419E+14 |
| 1252 | 2.321E+14 |
| 1259 | 2.221E+14 |
| 1265 | 2.155E+14 |
| 1272 | 2.225E+14 |
| 1279 | 2.289E+14 |
| 1285 | 2.345E+14 |
| 1292 | 2.323E+14 |
| 1299 | 2.254E+14 |
| 1306 | 2.183E+14 |
| 1312 | 2.112E+14 |
| 1319 | 1.925E+14 |
| 1326 | 1.696E+14 |
| 1332 | 1.465E+14 |
| 1339 | 1.267E+14 |
| 1346 | 1.091E+14 |
| 1353 | 9.123E+13 |
| 1359 | 7.321E+13 |
| 1366 | 5.502E+13 |
| 1373 | 3.665E+13 |
| 1379 | 1.812E+13 |
| 1386 | 6.407E+12 |
| 1393 | 1.074E+13 |
| 1399 | 1.510E+13 |
| 1406 | 1.951E+13 |
| 1413 | 2.396E+13 |
| 1420 | 2.844E+13 |
| 1426 | 3.297E+13 |
| 1433 | 3.811E+13 |
| 1440 | 4.673E+13 |
| 1446 | 5.543E+13 |
| 1453 | 6.420E+13 |
| 1460 | 6.834E+13 |
| 1466 | 6.581E+13 |
| 1473 | 6.583E+13 |
| 1480 | 7.786E+13 |
| 1487 | 8.999E+13 |
| 1493 | 1.022E+14 |
| 1500 | 1.146E+14 |

| λ (nm) | ϕ(DF/SH) ph/cm$^2$s nm |
|---|---|
| 300 | 2.471E+11 |
| 307 | 1.438E+12 |
| 313 | 6.485E+12 |
| 320 | 2.509E+13 |
| 327 | 3.082E+13 |
| 334 | 5.152E+13 |
| 340 | 6.364E+13 |
| 347 | 7.005E+13 |
| 354 | 7.720E+13 |
| 360 | 8.335E+13 |
| 367 | 9.571E+13 |
| 374 | 1.031E+14 |
| 380 | 1.058E+14 |
| 387 | 1.096E+14 |
| 394 | 1.230E+14 |
| 401 | 1.612E+14 |
| 407 | 1.955E+14 |
| 414 | 2.126E+14 |
| 421 | 2.176E+14 |
| 427 | 2.169E+14 |
| 434 | 2.245E+14 |
| 441 | 2.572E+14 |
| 447 | 2.874E+14 |
| 454 | 3.092E+14 |
| 461 | 3.197E+14 |
| 468 | 3.246E+14 |
| 474 | 3.336E+14 |
| 481 | 3.443E+14 |
| 488 | 3.374E+14 |
| 494 | 3.455E+14 |
| 501 | 3.501E+14 |
| 508 | 3.496E+14 |
| 515 | 3.447E+14 |
| 521 | 3.512E+14 |
| 528 | 3.592E+14 |
| 535 | 3.606E+14 |
| 541 | 3.581E+14 |
| 548 | 3.565E+14 |
| 555 | 3.589E+14 |
| 561 | 3.597E+14 |
| 568 | 3.676E+14 |
| 575 | 3.752E+14 |
| 582 | 3.798E+14 |
| 588 | 3.832E+14 |
| 595 | 3.837E+14 |
| 602 | 3.845E+14 |
| 608 | 3.869E+14 |
| 615 | 3.892E+14 |
| 622 | 3.911E+14 |
| 628 | 3.930E+14 |
| 635 | 3.956E+14 |
| 642 | 3.979E+14 |
| 649 | 3.994E+14 |
| 655 | 4.009E+14 |
| 662 | 4.021E+14 |
| 669 | 4.026E+14 |
| 675 | 4.032E+14 |
| 682 | 4.039E+14 |
| 689 | 4.050E+14 |
| 696 | 3.445E+14 |
| 702 | 4.042E+14 |
| 709 | 4.040E+14 |
| 716 | 4.028E+14 |
| 722 | 3.813E+14 |
| 729 | 3.735E+14 |
| 736 | 3.998E+14 |
| 742 | 3.984E+14 |
| 749 | 3.975E+14 |
| 756 | 3.450E+14 |
| 763 | 2.948E+14 |
| 769 | 3.843E+14 |
| 776 | 3.927E+14 |
| 783 | 3.912E+14 |
| 789 | 3.897E+14 |
| 796 | 3.880E+14 |
| 803 | 3.578E+14 |
| 809 | 3.351E+14 |
| 816 | 3.540E+14 |
| 823 | 3.731E+14 |
| 830 | 3.776E+14 |
| 836 | 3.484E+14 |
| 843 | 2.072E+14 |
| 850 | 1.375E+14 |
| 856 | 1.471E+14 |
| 863 | 1.454E+14 |
| 870 | 1.307E+14 |
| 877 | 1.302E+14 |
| 883 | 1.321E+14 |
| 890 | 1.341E+14 |
| 897 | 1.362E+14 |
| 903 | 1.396E+14 |
| 910 | 1.442E+14 |
| 917 | 1.334E+14 |
| 923 | 7.848E+13 |
| 930 | 4.614E+13 |
| 937 | 7.045E+13 |
| 944 | 7.983E+13 |
| 950 | 7.673E+13 |
| 957 | 9.029E+13 |
| 964 | 9.899E+13 |
| 970 | 1.759E+14 |
| 977 | 2.373E+14 |
| 984 | 2.264E+14 |
| 991 | 2.335E+14 |
| 997 | 2.447E+14 |
| 1004 | 2.560E+14 |
| 1011 | 2.674E+14 |
| 1017 | 2.790E+14 |
| 1024 | 2.757E+14 |
| 1031 | 2.706E+14 |
| 1037 | 2.655E+14 |
| 1044 | 2.602E+14 |
| 1051 | 2.549E+14 |
| 1058 | 2.496E+14 |
| 1064 | 2.441E+14 |
| 1071 | 2.386E+14 |
| 1078 | 2.330E+14 |
| 1084 | 2.283E+14 |
| 1091 | 2.255E+14 |
| 1098 | 2.359E+14 |
| 1104 | 2.425E+14 |
| 1111 | 1.833E+14 |
| 1118 | 1.234E+14 |
| 1125 | 6.292E+13 |
| 1131 | 3.879E+13 |
| 1138 | 3.885E+13 |
| 1145 | 5.651E+13 |
| 1151 | 6.816E+13 |
| 1158 | 9.527E+13 |
| 1165 | 1.227E+14 |
| 1172 | 1.503E+14 |
| 1178 | 1.776E+14 |
| 1185 | 1.849E+14 |
| 1192 | 2.281E+14 |
| 1198 | 2.402E+14 |
| 1205 | 2.296E+14 |
| 1212 | 2.189E+14 |
| 1218 | 2.080E+14 |
| 1225 | 2.047E+14 |
| 1232 | 2.099E+14 |
| 1239 | 2.122E+14 |
| 1245 | 2.096E+14 |
| 1252 | 2.069E+14 |
| 1259 | 2.041E+14 |
| 1265 | 2.032E+14 |
| 1272 | 2.090E+14 |
| 1279 | 2.087E+14 |
| 1285 | 1.965E+14 |
| 1292 | 1.840E+14 |
| 1299 | 1.711E+14 |
| 1306 | 1.581E+14 |
| 1312 | 1.450E+14 |
| 1319 | 1.286E+14 |
| 1326 | 1.109E+14 |
| 1332 | 9.309E+13 |
| 1339 | 7.915E+13 |
| 1346 | 6.768E+13 |
| 1353 | 5.610E+13 |
| 1359 | 4.441E+13 |
| 1366 | 3.262E+13 |
| 1373 | 2.072E+13 |
| 1379 | 8.719E+12 |
| 1386 | 6.641E+11 |
| 1393 | 1.890E+12 |
| 1399 | 3.126E+12 |
| 1406 | 4.373E+12 |
| 1413 | 5.630E+12 |
| 1420 | 6.898E+12 |
| 1426 | 8.177E+12 |
| 1433 | 9.996E+12 |
| 1440 | 1.501E+13 |
| 1446 | 2.007E+13 |
| 1453 | 2.517E+13 |
| 1460 | 2.751E+13 |
| 1466 | 2.589E+13 |
| 1473 | 2.685E+13 |
| 1480 | 3.990E+13 |
| 1487 | 5.306E+13 |
| 1493 | 6.632E+13 |
| 1500 | 7.969E+13 |

| λ (nm) | φ(DF/F) ph/cm$^2$s nm |
|---|---|
| 300 | 1.874E+10 |
| 307 | 2.200E+11 |
| 313 | 2.046E+12 |
| 320 | 1.571E+13 |
| 327 | 2.610E+13 |
| 334 | 3.791E+13 |
| 340 | 5.104E+13 |
| 347 | 5.739E+13 |
| 354 | 6.459E+13 |
| 360 | 7.118E+13 |
| 367 | 8.274E+13 |
| 374 | 9.024E+13 |
| 380 | 9.365E+13 |
| 387 | 9.792E+13 |
| 394 | 1.109E+14 |
| 401 | 1.465E+14 |
| 407 | 1.788E+14 |
| 414 | 1.956E+14 |
| 421 | 2.014E+14 |
| 427 | 2.019E+14 |
| 434 | 2.102E+14 |
| 441 | 2.423E+14 |
| 447 | 2.723E+14 |
| 454 | 2.940E+14 |
| 461 | 3.047E+14 |
| 468 | 3.101E+14 |
| 474 | 3.194E+14 |
| 481 | 3.304E+14 |
| 488 | 3.245E+14 |
| 494 | 3.331E+14 |
| 501 | 3.381E+14 |
| 508 | 3.377E+14 |
| 515 | 3.331E+14 |
| 521 | 3.393E+14 |
| 528 | 3.472E+14 |
| 535 | 3.485E+14 |
| 541 | 3.462E+14 |
| 548 | 3.447E+14 |
| 555 | 3.470E+14 |
| 561 | 3.478E+14 |
| 568 | 3.554E+14 |
| 575 | 3.627E+14 |
| 582 | 3.671E+14 |
| 588 | 3.704E+14 |
| 595 | 3.709E+14 |
| 602 | 3.719E+14 |
| 608 | 3.754E+14 |
| 615 | 3.789E+14 |
| 622 | 3.820E+14 |
| 628 | 3.851E+14 |
| 635 | 3.889E+14 |
| 642 | 3.925E+14 |
| 649 | 3.952E+14 |
| 655 | 3.976E+14 |
| 662 | 3.996E+14 |
| 669 | 4.008E+14 |
| 675 | 4.021E+14 |
| 682 | 4.036E+14 |
| 689 | 4.054E+14 |
| 696 | 3.502E+14 |
| 702 | 4.060E+14 |
| 709 | 4.061E+14 |
| 716 | 4.051E+14 |
| 722 | 3.854E+14 |
| 729 | 3.784E+14 |
| 736 | 4.030E+14 |
| 742 | 4.018E+14 |
| 749 | 4.011E+14 |
| 756 | 3.422E+14 |
| 763 | 2.859E+14 |
| 769 | 3.874E+14 |
| 776 | 3.973E+14 |
| 783 | 3.960E+14 |
| 789 | 3.947E+14 |
| 796 | 3.933E+14 |
| 803 | 3.651E+14 |
| 809 | 3.439E+14 |
| 816 | 3.615E+14 |
| 823 | 3.793E+14 |
| 830 | 3.834E+14 |
| 836 | 3.554E+14 |
| 843 | 2.193E+14 |
| 850 | 1.524E+14 |
| 856 | 1.620E+14 |
| 863 | 1.603E+14 |
| 870 | 1.454E+14 |
| 877 | 1.449E+14 |
| 883 | 1.468E+14 |
| 890 | 1.489E+14 |
| 897 | 1.510E+14 |
| 903 | 1.544E+14 |
| 910 | 1.591E+14 |
| 917 | 1.478E+14 |
| 923 | 9.087E+13 |
| 930 | 5.621E+13 |
| 937 | 8.254E+13 |
| 944 | 9.275E+13 |
| 950 | 8.947E+13 |
| 957 | 1.038E+14 |
| 964 | 1.128E+14 |
| 970 | 1.893E+14 |
| 977 | 2.504E+14 |
| 984 | 2.396E+14 |
| 991 | 2.469E+14 |
| 997 | 2.582E+14 |
| 1004 | 2.697E+14 |
| 1011 | 2.813E+14 |
| 1017 | 2.929E+14 |
| 1024 | 2.899E+14 |
| 1031 | 2.851E+14 |
| 1037 | 2.802E+14 |
| 1044 | 2.753E+14 |
| 1051 | 2.703E+14 |
| 1058 | 2.652E+14 |
| 1064 | 2.600E+14 |
| 1071 | 2.548E+14 |
| 1078 | 2.495E+14 |
| 1084 | 2.439E+14 |
| 1091 | 2.379E+14 |
| 1098 | 2.506E+14 |
| 1104 | 2.465E+14 |
| 1111 | 1.883E+14 |
| 1118 | 1.295E+14 |
| 1125 | 7.000E+13 |
| 1131 | 4.725E+13 |
| 1138 | 4.722E+13 |
| 1145 | 6.651E+13 |
| 1151 | 7.880E+13 |
| 1158 | 1.077E+14 |
| 1165 | 1.368E+14 |
| 1172 | 1.662E+14 |
| 1178 | 1.952E+14 |
| 1185 | 2.016E+14 |
| 1192 | 2.358E+14 |
| 1198 | 2.454E+14 |
| 1205 | 2.371E+14 |
| 1212 | 2.288E+14 |
| 1219 | 2.203E+14 |
| 1225 | 2.178E+14 |
| 1232 | 2.222E+14 |
| 1239 | 2.228E+14 |
| 1245 | 2.172E+14 |
| 1252 | 2.115E+14 |
| 1259 | 2.057E+14 |
| 1265 | 2.027E+14 |
| 1272 | 2.104E+14 |
| 1279 | 2.124E+14 |
| 1285 | 2.063E+14 |
| 1292 | 1.966E+14 |
| 1299 | 1.847E+14 |
| 1306 | 1.728E+14 |
| 1312 | 1.607E+14 |
| 1319 | 1.431E+14 |
| 1326 | 1.234E+14 |
| 1332 | 1.036E+14 |
| 1339 | 8.816E+13 |
| 1346 | 7.542E+13 |
| 1353 | 6.255E+13 |
| 1359 | 4.957E+13 |
| 1366 | 3.646E+13 |
| 1373 | 2.324E+13 |
| 1379 | 9.900E+12 |
| 1386 | 1.027E+12 |
| 1393 | 2.655E+12 |
| 1399 | 4.298E+12 |
| 1406 | 5.954E+12 |
| 1413 | 7.625E+12 |
| 1420 | 9.310E+12 |
| 1426 | 1.101E+13 |
| 1433 | 1.330E+13 |
| 1440 | 1.910E+13 |
| 1446 | 2.495E+13 |
| 1453 | 3.085E+13 |
| 1460 | 3.357E+13 |
| 1466 | 3.175E+13 |
| 1473 | 3.257E+13 |
| 1480 | 4.585E+13 |
| 1487 | 5.925E+13 |
| 1493 | 7.275E+13 |
| 1500 | 8.637E+13 |

## References


1. K. W. Böer, The Solar Spectrum at Typical Clear Weather Days, (in preparation).

2. K. W. Böer, Solar Excitation of CdS/$Cu_2S$ Photovoltaic Cells, (in preparation).

# INSOLATION MEASUREMENTS AND ASSOCIATED SPECTRAL EFFECTS AT REMOTE MILITARY INSTALLATIONS

John W. Bond, Jr.

US Army Mobility Equipment Research & Development Command

19 November 1976

The Department of Defense (DOD) is rapidly evolving a substantial market for solar cell power based on cost effectiveness. The immediate applications are for field instrumentation at remote test sites and other military installations. Between August, 1975, and Spring, 1977, at least 50 kWp* will have been procured by DOD, independent of the ERDA/DOD program. Many MWe may be presently cost effective; and many more MWe will become cost effective as the cost of solar cell power decreases in the near future. Several DOD funded studies are under way for remote instrumentation with power requirements up to 10 MWp.

In making sizing estimates it has been customary in the past to assume five "no-sun" days for battery discharge, followed by 5 - 30 "average-sun" days during which the batteries would be charged. This procedure is clearly incorrect; a more correct procedure is being developed. However, the type of insolation information needed to evaluate remote DOD installations is seldom available. In most cases, the only recourse for DOD to obtain the data needed to size solar cell panels is to apply to the Air Weather Service, AWS. Since DOD does not officially report insolation data, the data are obtained from NOAA. However, NOAA stations are generally located at airports near high population centers. Radiation conditions at (nearby) remote sites, if they are mountainous or intense marine sites, can be quite different. As an example, an Air Force radar site at 6300 Ft altitude on Mt. Laguna, about 150 miles southeast of Los Angeles, is being studied for possible application of solar cell power. The NOAA station at San Diego does not record solar insolation; the nearest station is at the Los Angeles airport. Comparison of a few daily measurements made on Mt. Laguna by DOD and by San Diego State University with those made by NOAA at the LA airport show factors of two differences.

---

*kWp is kilowatts of peak power meaning solar cell output under peak sunlight conditions, 100 mW/cm$^2$, at a cell temperature of 28$^{o}$C. kWe is kilowatts of rated or used power, Wp is 2-10 times We, depending on conditions and applications.

In previous sizing estimates, it had been assumed that up to 30% degradation in cell output may result from changes in the spectral distribution of solar radiation caused by intense, thick cloud covers, such as occur at Ft. Lewis, Washington (being considered for solar cell power application). The assumed workshop value is 20%. This is an expensive uncertainty for multi-megawatt systems.

Most of the solar cell power systems in present use by DOD involve panel (array) sizes of 50 - 500 Wp. In sizing these panels, safety factors at 25 to 100% are usually applied. The total DOD procurement of solar cell panels through Spring, 1977, will amount to $1 - 2M, much of which is due to insolation uncertainty.

The cost resulting from uncertainties in solar intensity and spectral data could be reduced significantly by installing pyranometers and solar cells at key military installations. The cost for such installations would be relatively small. Personnel are available at the installations to record and transmit the data. Other types of weather data are already being transmitted from Army test sites to the Atmospheric Science Laboratory (ASL) at the Army's White Sands Missile Range (WSMR). These data are reduced, stored, and disseminated by ASL. The solar insolation and spectral data could be included.

In view of the lack of relevant insolation information, DOD has started in a small way to acquire the needed data. Programs are presently under way at WSMR, at the Navy's Pt. Mugu (PMTC) and Port Hueneme (CEL) complex, at the Air Force Academy,at Tyndall Air Force Base, and at the Army's Fort Hunter-Liggett (FHL). Many of the new solar cell panels being acquired by DOD (60) will be instrumented to obtain I-V curves and cell temperatures. These measurements will be accompanied by (standard) solar cell and pyranometer measurements.

It is recommended that ERDA begin immediately to provide instrumentation at key military installations to obtain the needed solar insolation and spectral data. The cost would be relatively small and the benefits large for both ERDA and DOD. These data would also augment the ERDA/NOAA data base.

# Report of Working Group

# on

# Solar Irradiance Measurements

# for

# Photovoltaic Application

Michael R. Riches/ERDA

Units, Terminology, and Radiation Scales:

The units, terminology, and radiation scales will follow the recommendations of the World Meteorological Organization (WMO). ERDA will be using ASTM, ASHRAE, etc., to make these industry-wide standards. The basic units will be:

integrals - Kilo Joules per square meter

intensities - Watts per square meter

The radiation scale will be the "absolute" radiation scale as defined by the radiometer PACRAD III. ERDA will establish a date and factor for the paper change and widely publish these. Additionally, a date for actual calibration to the scale will be set.

The most difficult problem will be standardization of terminology and symbols. Again, ERDA will use WMO guidance and ASTM, ASHRAE, etc., to standardize terminology.

Data Networks:

Research Network: ERDA plans 4 to 6 research sites. These sites will measure all parameters of interest at state-of-the-art accuracy.

Measurements will include direct, global, diffuse, reflected and spectral radiation; water vapor; turbidity; and many other atmospheric variables. At least two of these will be established in FY 1977 with one year to set up. Additional short term research data sets will include:

- o Mountain Valley radiation differences
- o Urban Rural radiation differences
- o Seacoast Inland radiation differences
- o Solar Radiation on an incline at each Solar Heating and Cooling Demonstration Project (about 100 sites)

Results of the research site data will impact future general network plans. It was agreed that the one year setup, one year of data acquisition, one year to act on results, and thus one more year before general sites would have a year long data set, would not adversely effect photovoltaics. The research sites would also act as regional training centers and master calibration centers. The special data collected will be correlated to the more general network data.

NOAA Network: The 35-station NOAA solar radiation network will measure global solar radiation. Additionally, 10 of these 35 sites will measure diffuse. In about one year all 35 sites will measure direct irradiance. ERDA-NOAA should consider:

- o turbidity and water vapor measurements at each site.
- o adding 10 to 15 more high quality sites either directly or through cooperative efforts.

Adding special measurements such as spectral measurements may be needed, but that decision can wait for input from the research network. Thus NOAA should insure the pyrheliometers added next year can use a standard five-position filter wheel if needed.

General Network: the general network archived or cataloged by ERDA should measure at least daily totals of global radition with on accuracy of $\pm$ 10 percent or so. Additionally, at least 50 sites, well distributed, are required. Data will be rated through adherance to a standard practice guide and type of sensor. Thus, this general network will have an error bound or a confidence interval on the data. The bound will depend on the sensor and recording system.

Instrumentation:

No particular needs were specified. Again, the research site data will help define new instrument requirements.

The Role of Solar Radiation Models:

The group did not have the expertise to discuss this point. ERDA/NOAA experts should evaluate existing techniques and interface with the other groups so a standard solar spectrum for a given set of atmospheric variables can be established.

Site Specific Data:

DOD (Dr. John Bond) brought up the site specific data problem. The question is how best to get an estimate of the solar radiation at the site of application. This can be handled by using mobile units and relating this short term data to other nearby sites. Also, models based on cloudiness, such as being developed by Dr. Machta of NOAA, may help. It was suggested ERDA may want to provide site specific monitoring capabilities and the techniques to relate this data to nearby locations as a service.

The mobile unit for photovoltaics should include at least the following:

- o meteorological data to correlate with near by sites
- o spare channels for special parameters
- o sky camera
- o direct solar radiation with filter wheel
- o global solar radiation

## Report of Working Group on Effects of Spectral Variations on Cell Performance

Karl Böer/IEC, Univ. of Delaware and SES

There were several topics of discussion in this session including the following:

- The important atmospheric parameters which influence cell performance.
- The effect of clouds on cell sensitivity.
- The definition of a standard atmosphere for purposes of cell measurement and calibration.
- What instrumentation is needed for solar spectral measurements?

### MAJOR CONCLUSIONS

1. The atmosphere introduces significant variations in cell calibration coefficients. The "clear" atmosphere parameters such as (water vapor content, ozone, airmass turbidity) can give $\pm$ 5% variations. Their effect, at least for normal incidence irradiation, can be calculated. The effect of clouds on cell sensitivity is much greater (on the order of 20%) and is not readily calculated. Work should continue in atmospheric modeling for all dry conditions.
2. The terrestrial spectral irradiance curve in the Interim Proceedings should be revised. The airmass value should be 1.5, rather than 2, and provisions should be made for including some forward scattering in the direct beam.
3. A simple instrument should be developed for measuring

the spectral distribution of irradiance in the wavelength region of interest for photovoltaics (0.3 - 1.1 μm in 0.1 μm intervals).

# APPLICATION OF XENON LAMPS TO LOW COST AIR MASS TWO SOLAR SIMULATION

James Lovelady/Spectrolab

The Xenon Arc Lamp is well established as the only practical light source capable of simulating Air Mass Zero sunlight accurately enough for spacecraft testing. However, the high cost of spacecraft quality simulation equipment often precludes its use for terrestrial system development. This paper will describe three approaches to adapting spacecraft techniques to terrestrial applications to achieve high-quality simulation (good spectral distribution, spatial uniformity and stability) at reduced cost.

A small, high-performance unit for laboratory testing provides an 8" square beam. A lenticular optical system provides excellent beam uniformity and optical filters give a close spectral match to Air Mass Two sunlight.

For large area testing, particularly of thermal collector systems, long-arc Xenon lamps offer an inexpensive source of high power light with reasonable spectral properties. With the addition of optical filters, a good spectral match is obtained. Modular construction permits a wide variety of target sizes.

Some photovoltaic solar panels have a very fast response time, allowing them to be tested with a short (0.001 second) pulse of light. For this application a very large area simulator with excellent spatial uniformity can be economically constructed, including special high-speed electronic test equipment. With this technique a 16-foot diameter flat panel can be completely evaluated in a few minutes.

# ERRORS IN SHORT CIRCUIT CURRENT MEASUREMENTS DUE TO SPECTRAL MISMATCH BETWEEN SUNLIGHT AND SOLAR SIMULATORS

Henry B. Curtis
National Aeronautics and Space Administration
Lewis Research Center
Cleveland, Ohio

## ABSTRACT

Errors in short-circuit-current measurement were calculated for a variety of spectral mismatch conditions. Parameters included were the differences in spectral irradiance between terrestrial sunlight and three types of solar simulator, as well as the differences in spectral response between three types of reference solar cells and various test cells. The simulators considered are a short-arc xenon-lamp AMO sunlight simulator, an ordinary quartz halogen lamp, and ELH-type quartz-halogen lamp. The three types of solar cell are a silicon cell, a cadmium sulfide cell and a gallium arsenide cell.

## INTRODUCTION

The output of solar cells has been measured using solar simulators for many years. No simulator exactly duplicates the spectral distribution of terrestrial solar irradiance (spectral irradiance); hence there are spectral mismatches between sunlight and solar simulators. The short-circuit current of a solar cell is proportional to total irradiance and is a function of spectral irradiance. Therefore, there may be errors in short-circuit-current measurements due to spectral mismatch when using a solar simulator. In an attempt to reduce this spectral error, a calibrated reference cell, with spectral response similar to the cell being measured, is used to adjust the simulator intensity. The feasibility of this practice can be substantiated with the following analysis.

The short-circuit current of a solar cell may be calculated from

the spectral response of the cell ( $R_\lambda$ ) and the spectral irradiance incident on the cell ( $E_\lambda$ )

$$I = \int E_\lambda \; R_\lambda \; d\lambda \tag{1}$$

For clarity in the subsequent analysis, two subscripts are added to the current symbol indicating cell function (reference or test) and light source (sunlight or simulator). Hence $I_{ref\text{-}sun}$ is short circuit current calculated for the reference cell in sunlight. $I_{cell\text{-}sim}$ is for the test cell in the simulator.

In measuring a solar cell, either in sunlight or with a simulator, the key performance parameter desired is $I_{cell\text{-}sun}$ at a standard irradiance level. However, when using a solar simulator, the value $I_{cell\text{-}sim}$ is actually measured. Also, the irradiance of the simulator has been measured using the calibrated reference cell. The measured value $I_{cell\text{-}sim}$ is multiplied by the ratio $(I_{ref\text{-}sun}/I_{ref\text{-}sim})$ to adjust to the proper intensity. (In practice, the simulator irradiance level is adjusted, which is the mathematical equivalent.) Therefore, the quantity $I_{cell\text{-}sim} \left[\frac{I_{ref\text{-}sun}}{I_{ref\text{-}sim}}\right]$ is actually measured when the parameter $I_{cell\text{-}sun}$ is desired (Fig. 1). This can be shown mathematically as:

$$I_{cell\text{-}sun} = \int E_{sim} \; R_{cell} \; d\lambda \left[ \frac{\int E_{sun} \; R_{ref} d\lambda}{\int E_{sim} \; R_{ref} d\lambda} \right] \tag{2}$$

It can be seen that if the simulator has the same spectral irradiance as the sun ($E_{sun} = E_{sim}$), the quantity in brackets is unity and $I_{cell\text{-}sun}$ equals $I_{cell\text{-}sim}$. Similarly, if the test and reference cells have identical spectral responses ($R_{ref} = R_{cell}$) the terms containing $E_{sim}$ cancel and an exact value of $I_{cell\text{-}sim}$ is measured independent of the spectral distribution of the simulator. In practice, absolute matching of spectral responses is rarely achieved, nor do simulators exactly duplicate

terrestrial sunlight hence errors can be expected. The percent error in the measurement is:

$$\left[\frac{I_{cell\text{-}sun} - I_{cell\text{-}sim}\left[\frac{I_{ref\text{-}sun}}{I_{ref\text{-}sim}}\right]}{I_{cell\text{-}sun}}\right] \times 100\% \qquad (3)$$

The purpose of this paper is to calculate the magnitude of such errors for a variety of simulators and reference-test cell pairs.

## SPECTRAL IRRADIANCE DATA

To calculate the various short circuit currents, several spectral irradiances and spectral responses are needed. The solar irradiance used is the air mass 2 curve by Thekaekara given in the "Interim Solar Cell Testing Procedures for Terrestrial Applications" (Ref. 1). This is shown in figure 2. Figures 3, 4 and 5 show measured spectral irradiance curves for three types of solar simulators:

Figure 3 - a short arc xenon lamp simulator

Figure 4 - a quartz-halogen tungsten lamp

Figure 5 - an ELH lamp

All have been normalized to equal area. The short arc xenon lamp simulator, measured using a high resolution spectrophotometer, is a typical AMO simulator, rich in ultraviolet light. The quartz-halogen tungsten lamp shown is a standard of spectral irradiance supplied by NBS. The lamp is a 1000-watt quartz-halogen bulb and is typical of many "tungsten lamp" simulators. The ELH lamp is a 300-watt quartz halogen lamp within a dichroic-coated reflector. The reflector transmits a significant portion of the infra-red radiation while reflecting the visible. Hence the output beam has much less infrared light than the normal quartz-halogen lamp.

Upon inspection of the four spectral irradiance curves, it can be seen that the xenon arc lamp and the ELH lamp give fairly good matches to the AM2 solar spectrum. However, the plain quartz-halogen lamp

gives a poor match.

## SPECTRAL RESPONSE DATA

To complete the data needed for the analysis, the spectral response of several reference cell-test cell combinations are needed. This was done mathematically by using one reference cell spectral response and generating many test cell spectral responses by perturbations on the reference cell response. Figure 6 shows a spectral response of a typical silicon cell. This is used as the reference cell response. One of the test cell spectral responses is indicated by the X's. The system for generating different test cell responses was as follows. The reference cell response was transformed in the y-direction (response) by an amount equal to 25% of the maximum standard cell response. This transformation was done on only part of the wavelength region as the example in figure 6 shows. There is no transformation beyond 0.9 μm in this example. The transformation could be either positive or negative. Literally hundreds of cell responses were generated by varying the wavelengths at which the perturbation started and stopped. The 25% value was chosen to be representative of a fairly poor match between reference cell and test cell in practice.

With a solar spectral irradiance and three simulator spectral irradiances along with a reference cell response and many test cell responses, all combinations of short-circuit current measurement error may be calculated. This analysis was also done for a cadmium sulfide solar cell and a gallium arsenide solar cell. Again, a set of test cells was generated from the reference cell response. The reference cell responses for cadmium sulfide and gallium arsenide are shown in figures 7 and 8.

## RESULTS AND DISCUSSION

Table I summarizes the results for the silicon cell reference. For each of the three simulators, the average of the absolute value of about 100 different reference cell-test cell combinations is given. Also shown is the largest error found. The xenon lamp produces the smallest errors. The ELH lamp is just slightly higher than the xenon. This is in accord with the closeness of their spectral irradiances to AM2 sunlight. The tungsten-halogen lamp produces much larger errors than either the xenon or ELH lamps. This was expected because the tungsten-halogen lamp gives the worst spectral fit to the sunlight curve. Average errors of 8.4% with a maximum of 11%, when using a reference cell of the same general spectral response are much too large to tolerate. This makes the tungsten-halogen lamp simulator a very poor choice for measuring solar cells unless much closer spectral matching of test and reference cells is ensured. The xenon simulator produces the lowest errors, is the most expensive and probably best represents the current state of the art in solar simulators. Hence it appears to be the best choice for measuring silicon solar cells. However, the ELH lamps have only slightly greater errors than the xenon lamp simulator. Their advantages of simplicity and low cost seem to make them a good second choice for a solar simulator source.

The error calculations were repeated for the cadmium sulfide and gallium arsenide reference cell responses. Tables II and III give the results for these two types of cells. In both cases, the trends are essentially the same as discussed for the silicon cell case. The error magnitudes shift somewhat but the tungsten-halogen lamp is still an acceptable solar simulator. In the gallium arsenide case, the average error was less for the ELH lamp than for the xenon lamp, and the errors are somewhat larger than for the other two types of cells. This appears due to the very narrow spectral response range of the gallium arsenide cell.

It is interesting to note that, in general, the short arc xenon lamp simulator is the best choice for measuring terrestrial photovoltaic devices, even though it is essentially an airmass zero simulator. This can be explained by considering the black body temperature of the various radiation sources. The sun can be considered approximately a 6000°K black body. The effect of the atmosphere on solar irradiance is, of course, quite significant. However, the terrestrial spectral irradiance still has roughly the same overall shape as the AMO curve, and hence about the same black body radiation temperature. A tungsten filament can be considered to be a 3000°K black body, while a xenon arc is much closer to the 6000°K temperature of the sun. Thus, the xenon lamp will have a much better fit to either AMO or terrestrial sunlight than a plain tungsten lamp. The ELH lamp is a special case due to the effect of the dichroic-coated reflector. It is deficient in the ultraviolet region but this has little or no effect on the results presented here.

## EXPERIMENTAL RESULTS

The above data were all computer generated. Therefore, to assess the accuracy of these results, measurements of several silicon cells were made under the different light sources. A terrestrial silicon cell (Z-01) was chosen as the reference cell and six other silicon cells were used as test cells. Figures 9 through 14 show spectral response of Z-01 compared to each of the six other cells. Z-01 and Z-00 (Fig. 9) are both terrestrial cells from one manufacturer. Their responses are almost identical. The other five cells are from other terrestrial solar cell suppliers. A variety of spectral response shapes is represented by this group of cells. The spectral mismatchs between Z-01 and each of the last five cells are about the same magnitude as used in the calculations. Each cell was measured outdoors in a collimating tube. Sunlight

intensity was measured with a normal incidence pyrheliometer (NIP).

The collimating tube had the same field of view as the NIP (5.7°). The short circuit currents for each cell, normalized to 100 $mW/cm^2$ are shown in Table IV under the "SOLAR" heading. Each cell was then measured in a xenon arc simulator, an ELH lamp simulator and a tungsten lamp simulator. Cell Z-01 was used as the reference cell. These results are also shown in Table IV. The current Z-01 was identical in all three cases because it was the reference. Cell Z-00, (the same manufacturer of Z-01) had nearly the same current in all three simulators as it has in terrestrial sunlight. This agreement is due to the excellent spectral match between Z-00 and Z-01. For the other five silicon cells, errors of different magnitude arise. Again, the tungsten lamp gives larger errors in current than either the xenon or ELH lamp simulators. The average errors of 0.92% for xenon, 1.87% for ELH, and 10.9% for tungsten were calculated excluding cell Z-00. These data are in excellent agreement with the calculated results shown in Table I.

These data are indicative of the amount of spectral matching required for accurate measurements. If the spectral responses for the reference cell and test cell are essentially identical (as Z-00 and Z-01 in Fig. 9), almost any light source is adequate. However, in practice, such spectral response matching is probably rare and the cases represented by the calculations (Fig. 6) or the experimental data (Figs. 10-14) are more representative. In this case xenon and ELH-type lamp simulators give acceptably low errors (<2%), while the tungsten lamp simulators give rise to excessively high errors.

## SUMMARY OF RESULTS

It has been shown that solar simulators utilizing either short-arc xenon lamps or ELH-type quartz-halogen lamps as a radiation source give low errors (<2%) when making performance measurements of terrestrial photovoltaic cells. This analysis assumes that a reference cell, matched in spectral response to the test cell, is used to set the simulator irradiance. A simulator using a plain tungsten lamp as a radiation source gives larger errors unless the reference-cell - test-cell spectral match is extremely good.

## REFERENCE

1. H. W. Brandhorst, et al: Interim Solar Cell Testing Procedures for Terrestrial Applications. NASA TMX-71771 (1975).

TABLE I. - CALCULATED ERRORS IN $I_{SC}$ DUE TO SPECTRAL MISMATCH FOR THREE SIMULATORS

SILICON CELL

| SIMULATOR | AVE. ERROR | MAX. ERROR |
|---|---|---|
| XENON | 1.2% | 2.2% |
| TUNGSTEN | 8.4 | 11.0 |
| ELH | 1.4 | 3.5 |

TABLE II. - CALCULATED ERRORS IN $I_{SC}$ DUE TO SPECTRAL MISMATCH FOR THREE SIMULATORS

CADMIUM SULFIDE CELL

| SIMULATOR | AVE. ERROR | MAX. ERROR |
|---|---|---|
| XENON | 1.4% | 2.9% |
| TUNGSTEN | 6.7 | 12.8 |
| ELH | 2.8 | 6.5 |

TABLE III. - CALCULATED ERRORS IN $I_{SC}$ DUE TO SPECTRAL MISMATCH FOR THREE SIMULATORS

GALLIUM ARSENIDE CELL

| SIMULATOR | AVE. ERROR | MAX. ERROR |
|---|---|---|
| XENON | 4.8% | 5.3% |
| TUNGSTEN | 13.5 | 15.7 |
| ELH | 3.4 | 5.8 |

TABLE IV. - MEASURED $I_{SC}$ FOR VARIOUS TERRESTRIAL CELLS USING Z-01 AS A STANDARD UNDER DIFFERENT SOLAR SIMULATORS

| CELL | SUNLIGHT | XENON | | TUNGSTEN | | ELH | |
|---|---|---|---|---|---|---|---|
| | | $I_{SC}$ | % Δ | $I_{SC}$ | % Δ | $I_{SC}$ | % Δ |
| Z-01 | 112.2 | 112.2 | | 112.2 | | 112.2 | |
| Z-00 | 113.6 | 113.1 | | 113.6 | | 112.9 | |
| Z-36 | 116.8 | 117.6 | 0.7 | 126.0 | 7.9 | 116.5 | -0.3 |
| Z-23 | 97.9 | 98.2 | 0.3 | 116.0 | 18.5 | 99.7 | 1.8 |
| Z-70 | 102.3 | 100.7 | -1.6 | 97.2 | - 5.0 | 98.1 | -4.1 |
| Z-27 | 104.7 | 106.7 | 1.9 | 114.4 | 9.3 | 106.9 | 2.1 |
| Z-43 | 95.3 | 95.5 | 0.2 | 108.5 | 13.9 | 96.3 | 1.0 |
| AVE. ERROR | | | 0.9% | | 10.9% | | 1.9% |

Figure 1. - Spectral distribution of terrestrial sunlight

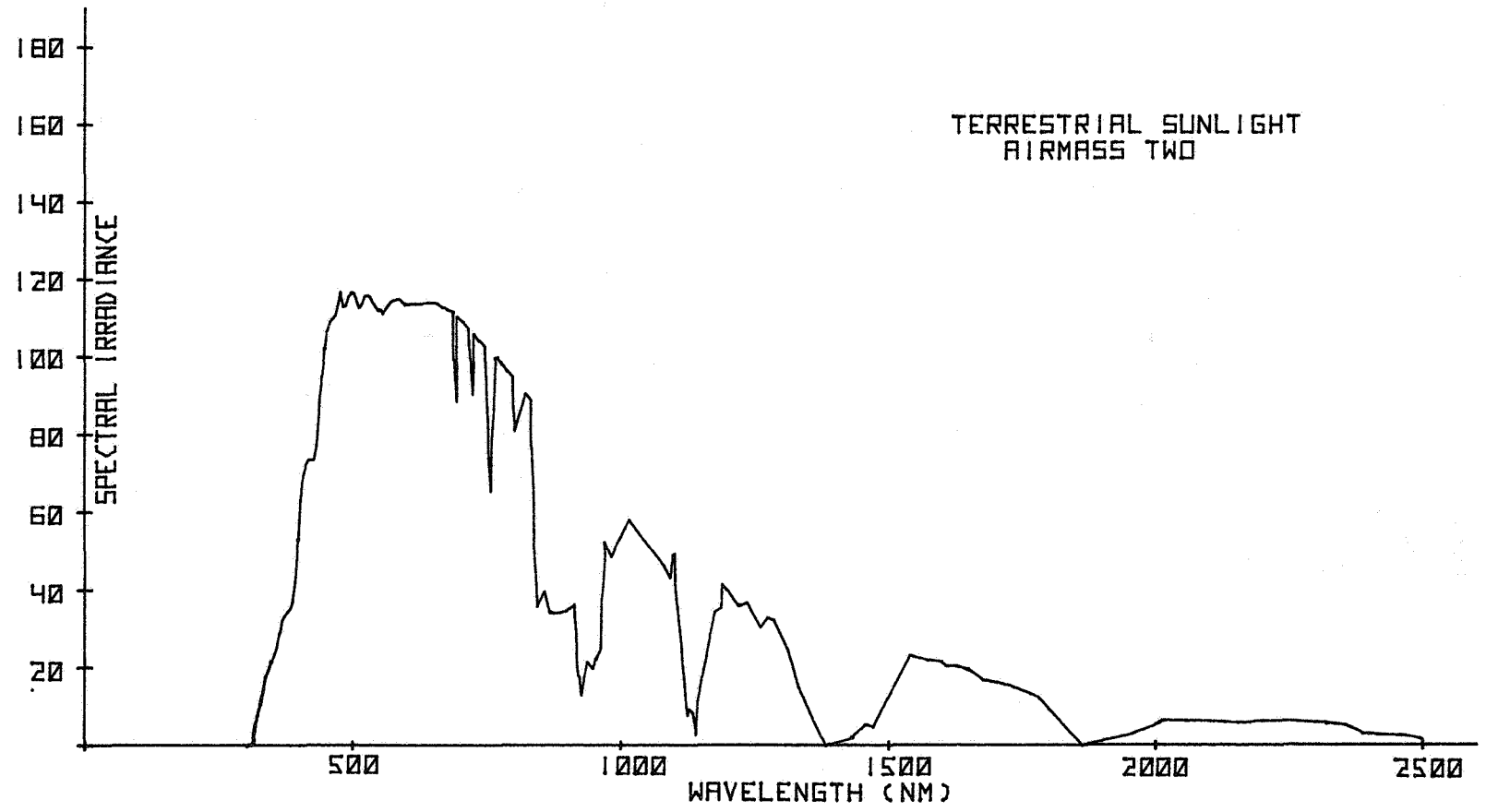

Figure 2. - Spectral distribution of xenon lamp simulator

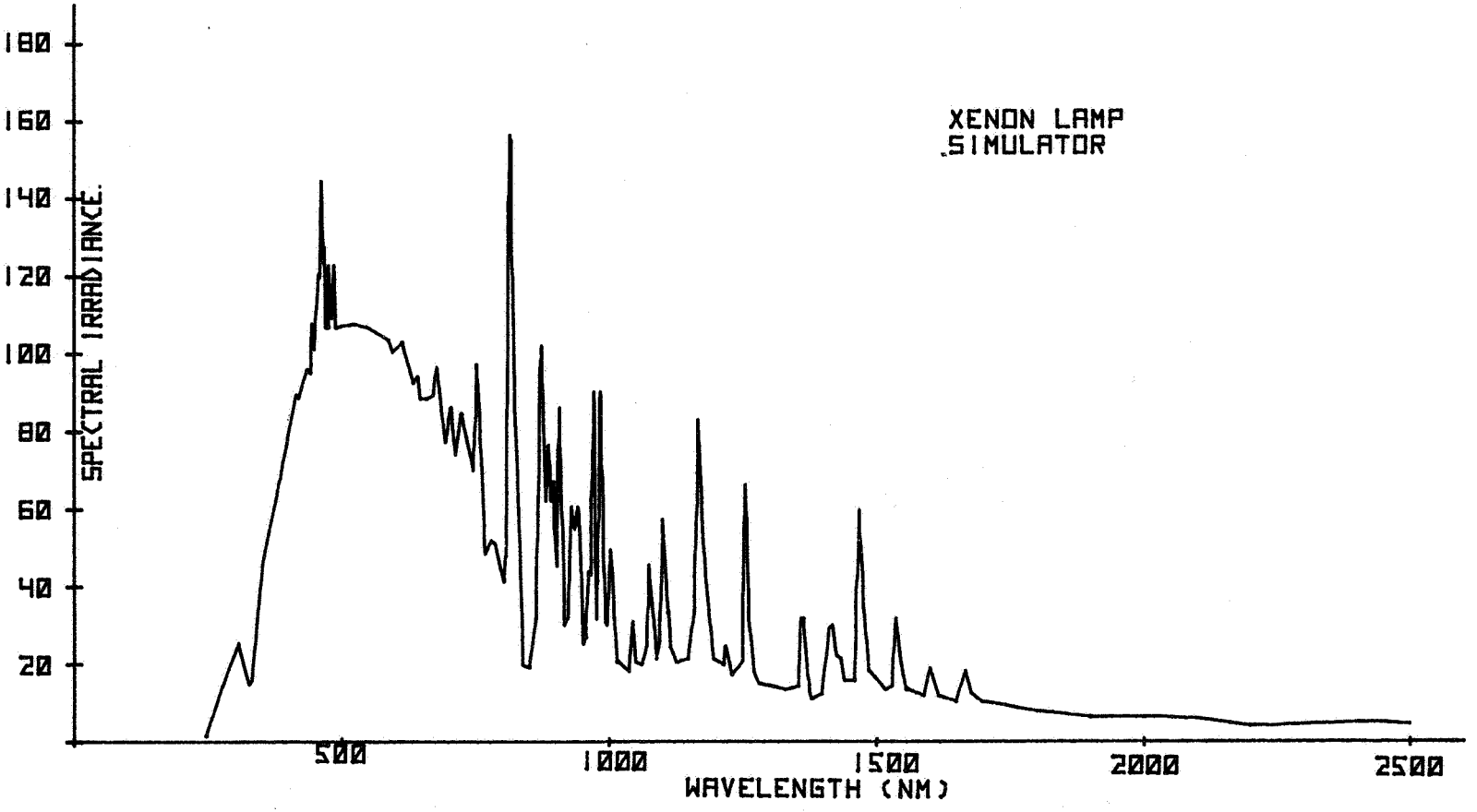

Figure 3. - Spectral distribution of tungsten lamp simulator

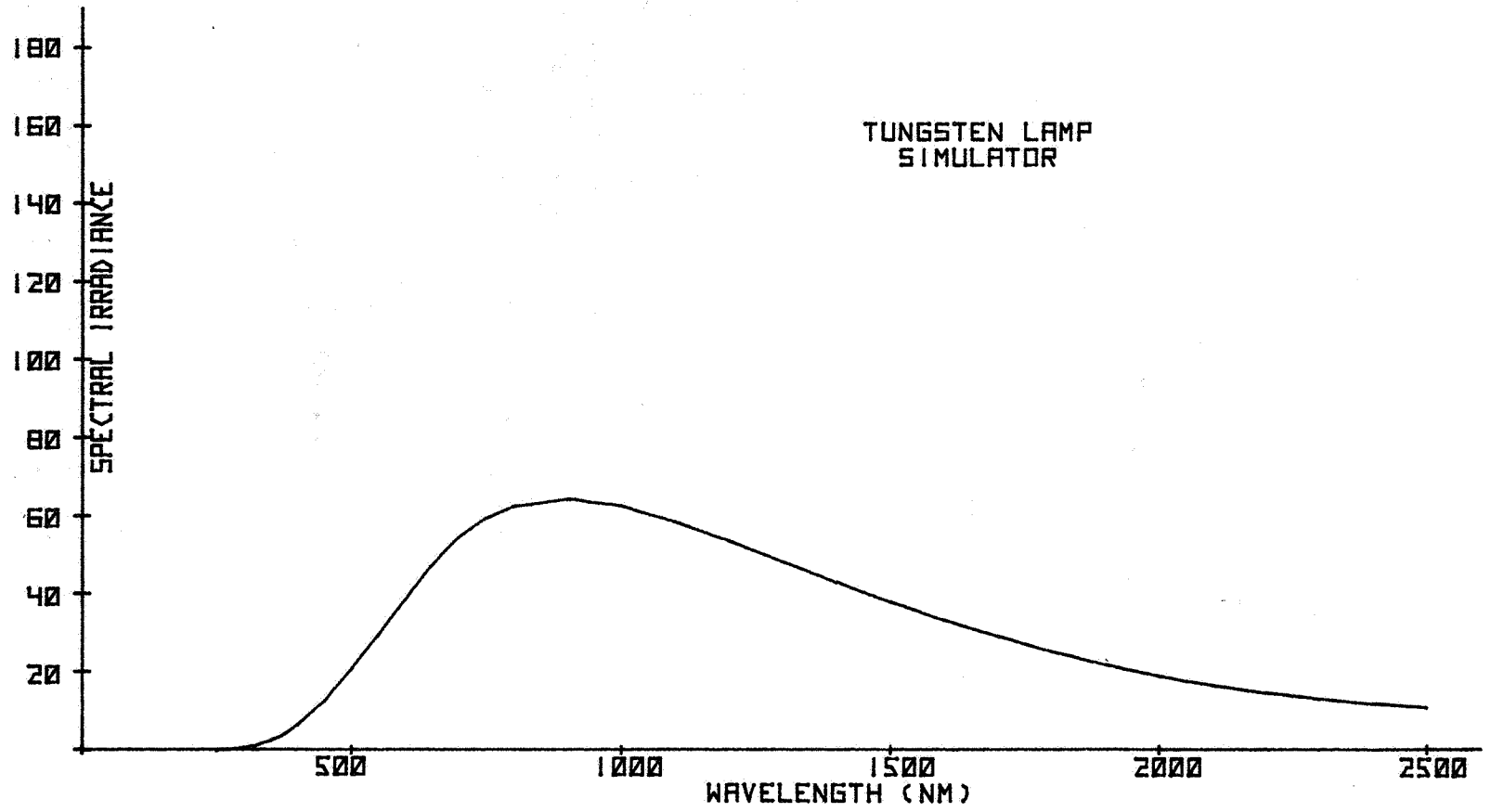

Figure 4. - Spectral distribution of ELH lamp simulator

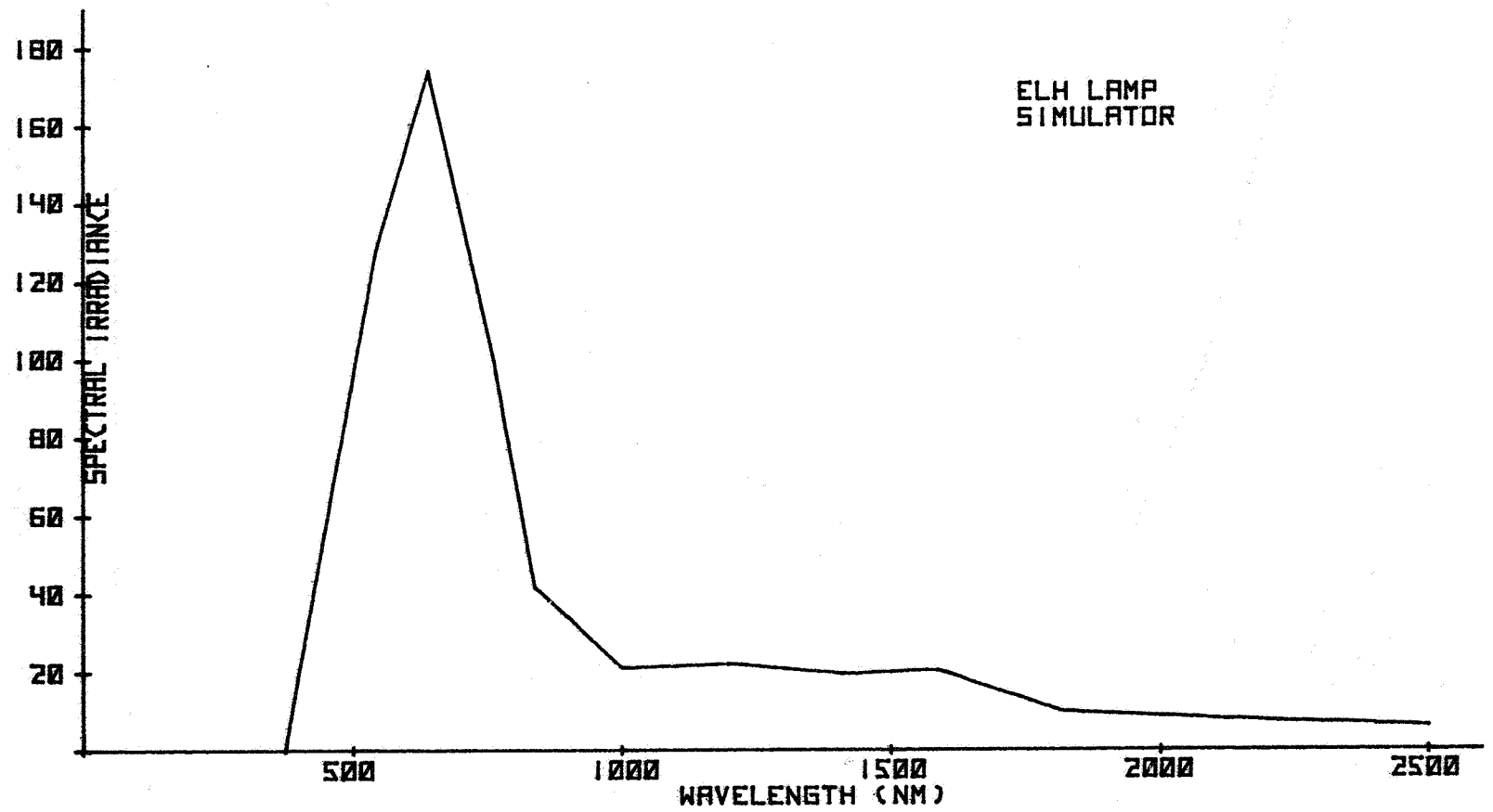

Figure 5. - Example of calculated and standard solar cell relative spectral responses

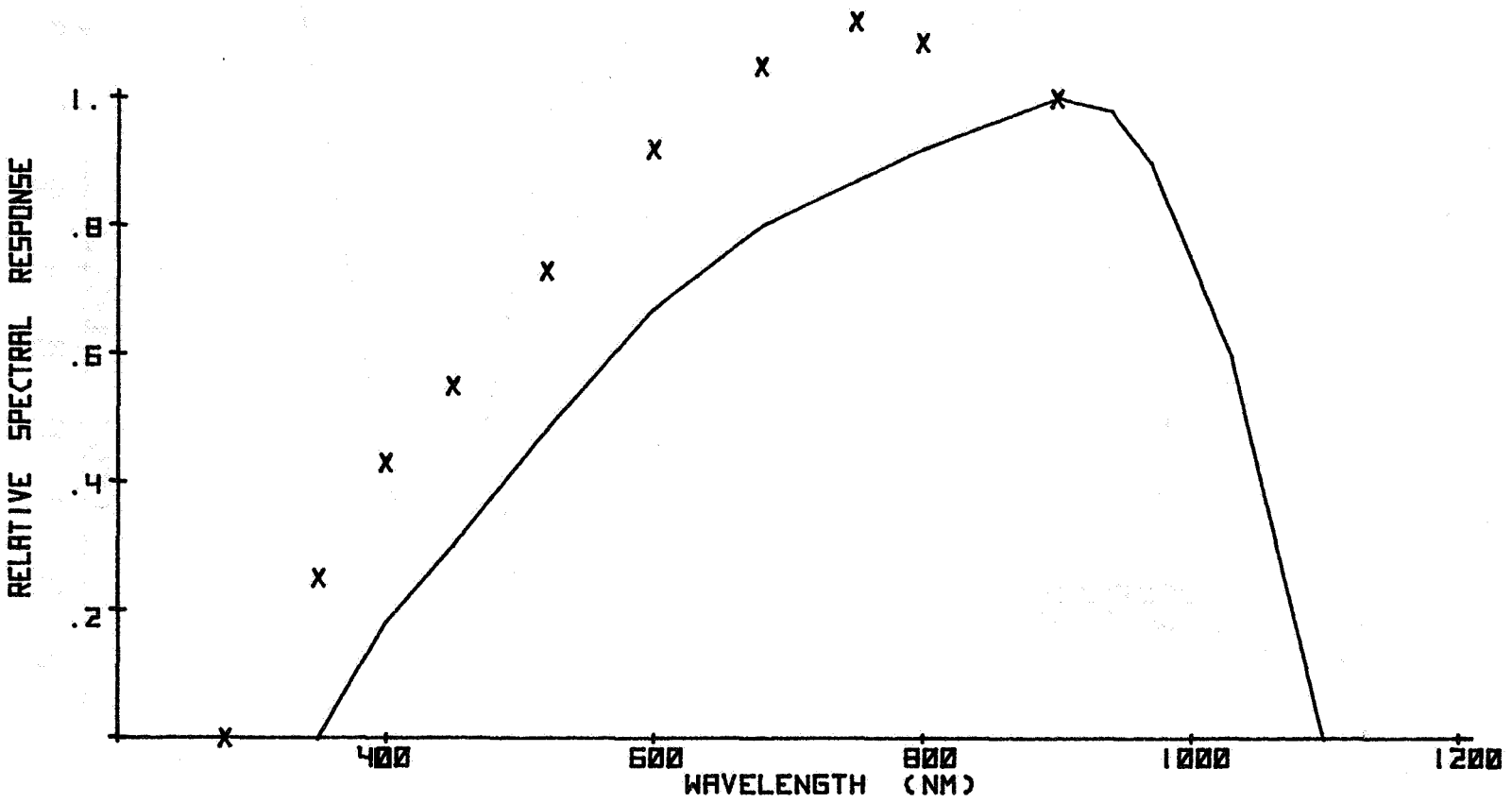

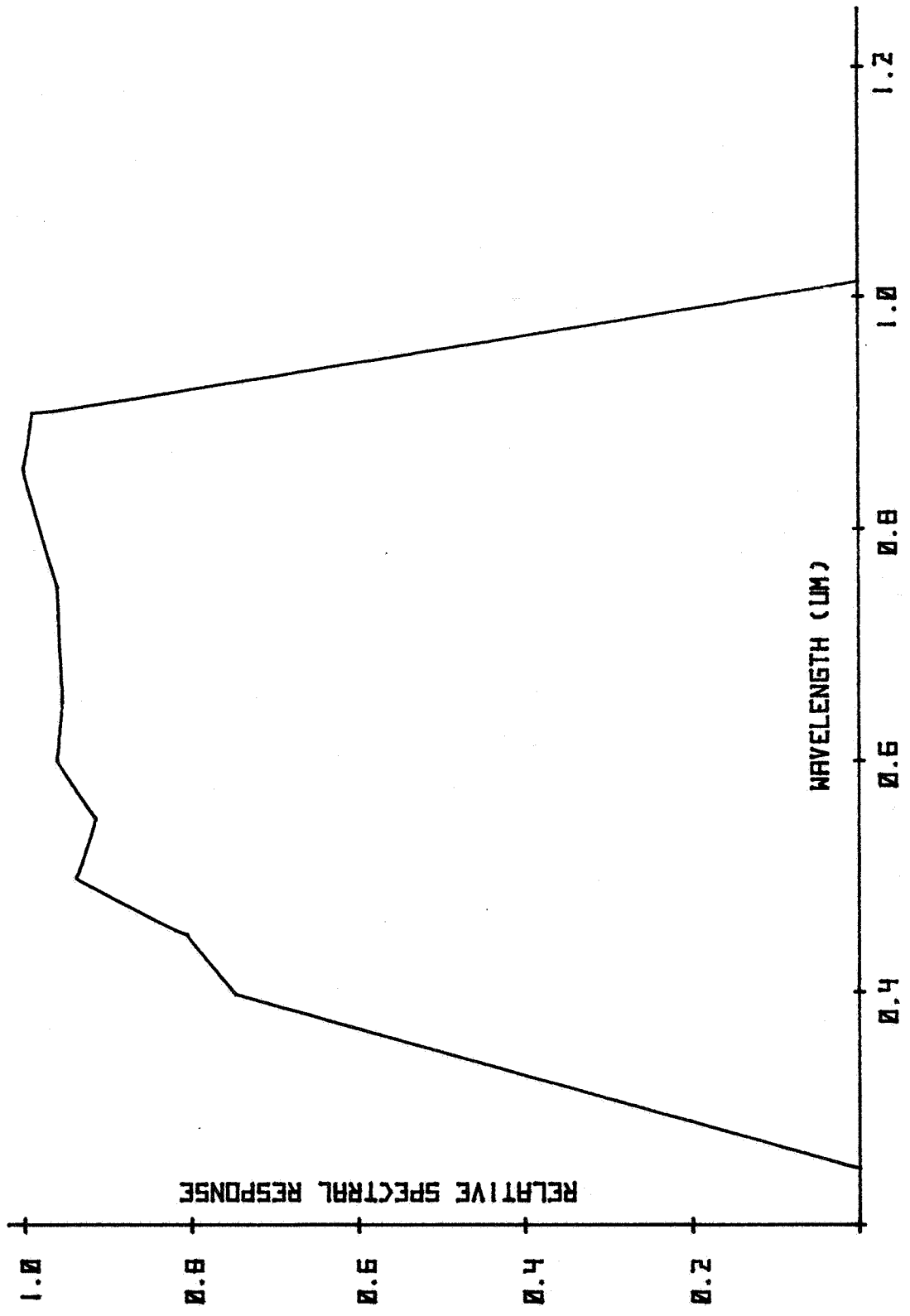


Figure 6. - CdS solar cell spectral response

Figure 7. - GaAs solar cell spectral response

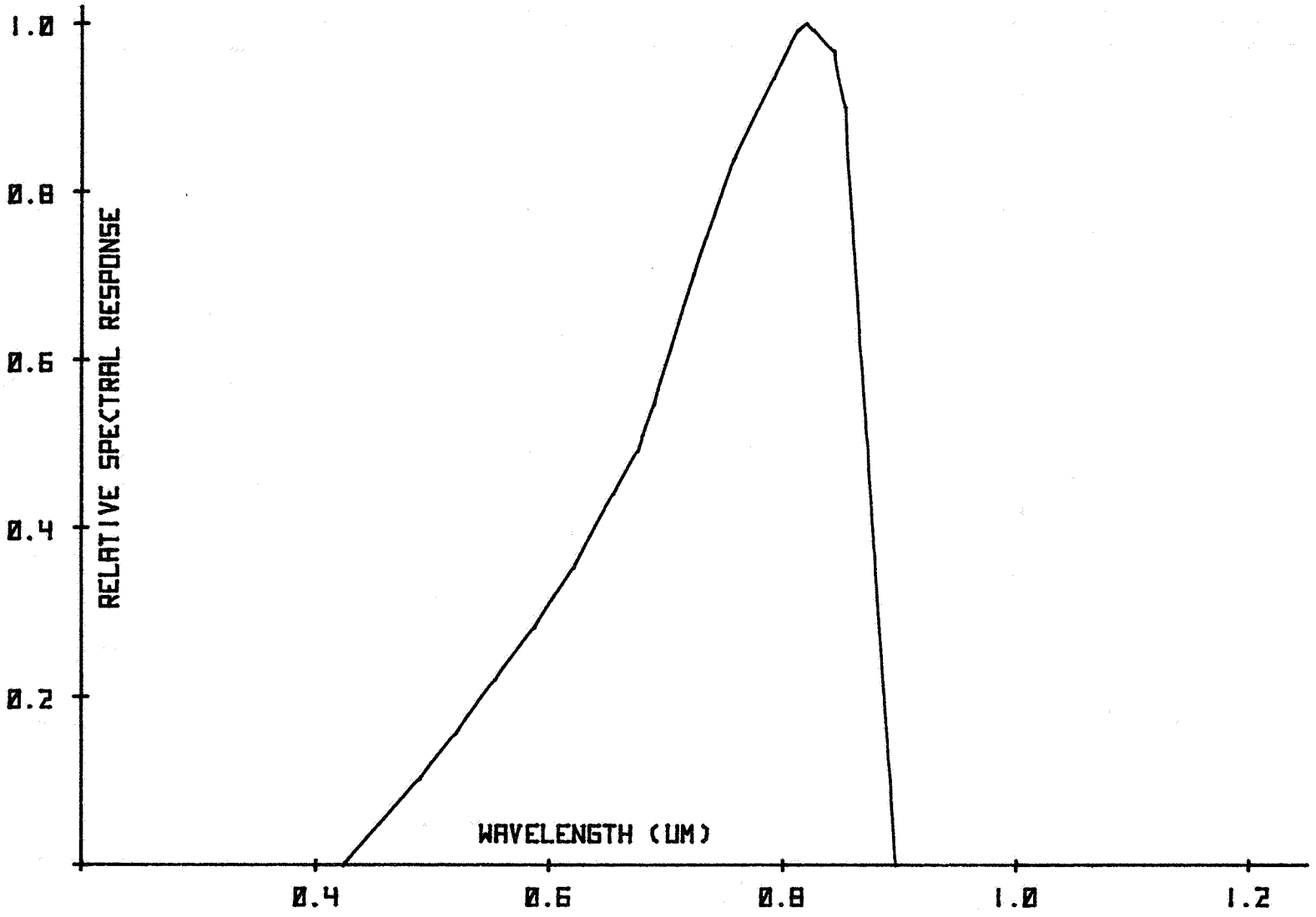

Figure 8. - Comparison of spectral responses of cells Z-00 and Z-01

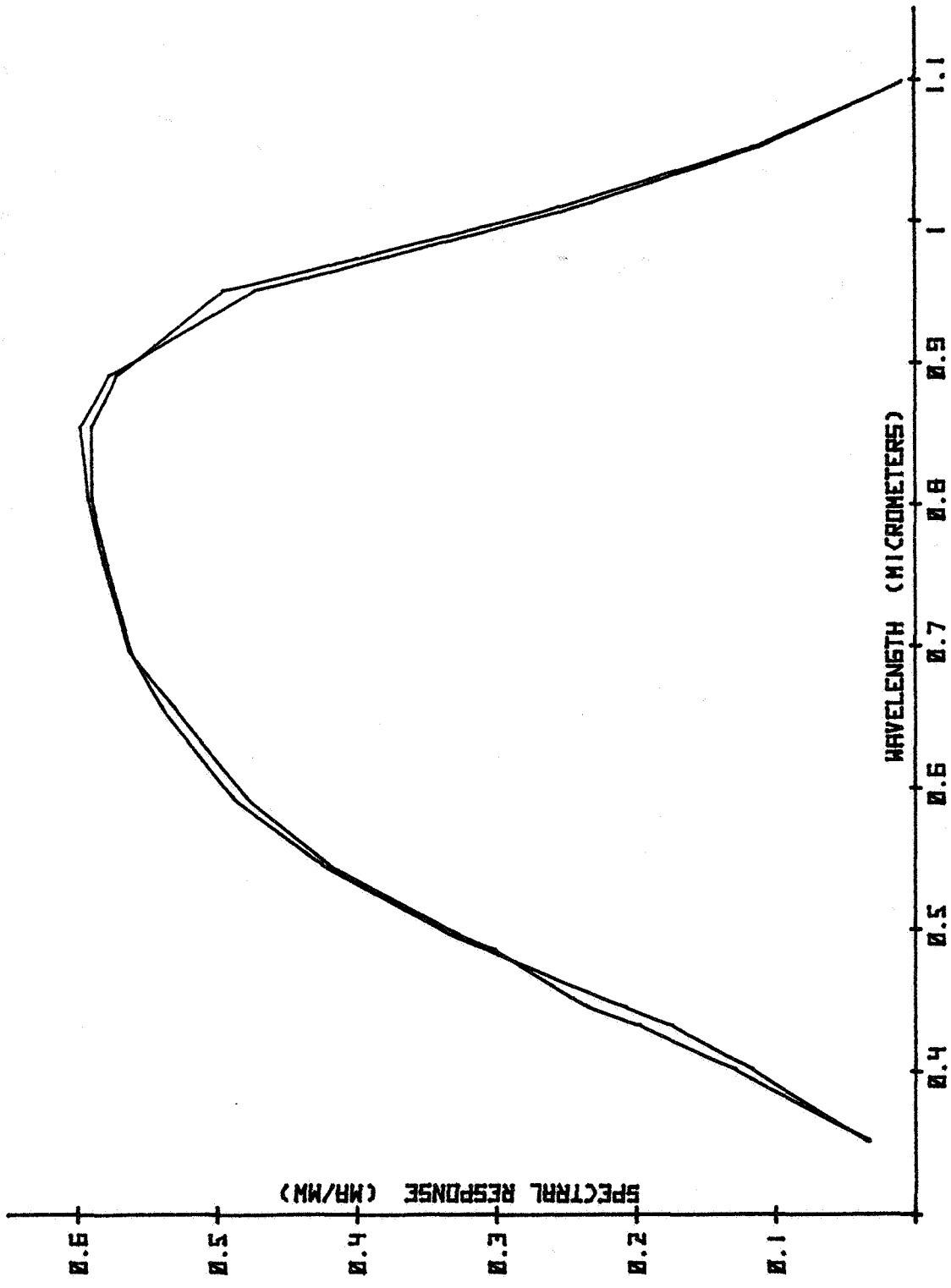

Figure 9. - Comparison of spectral responses of cells Z-23 and Z-01

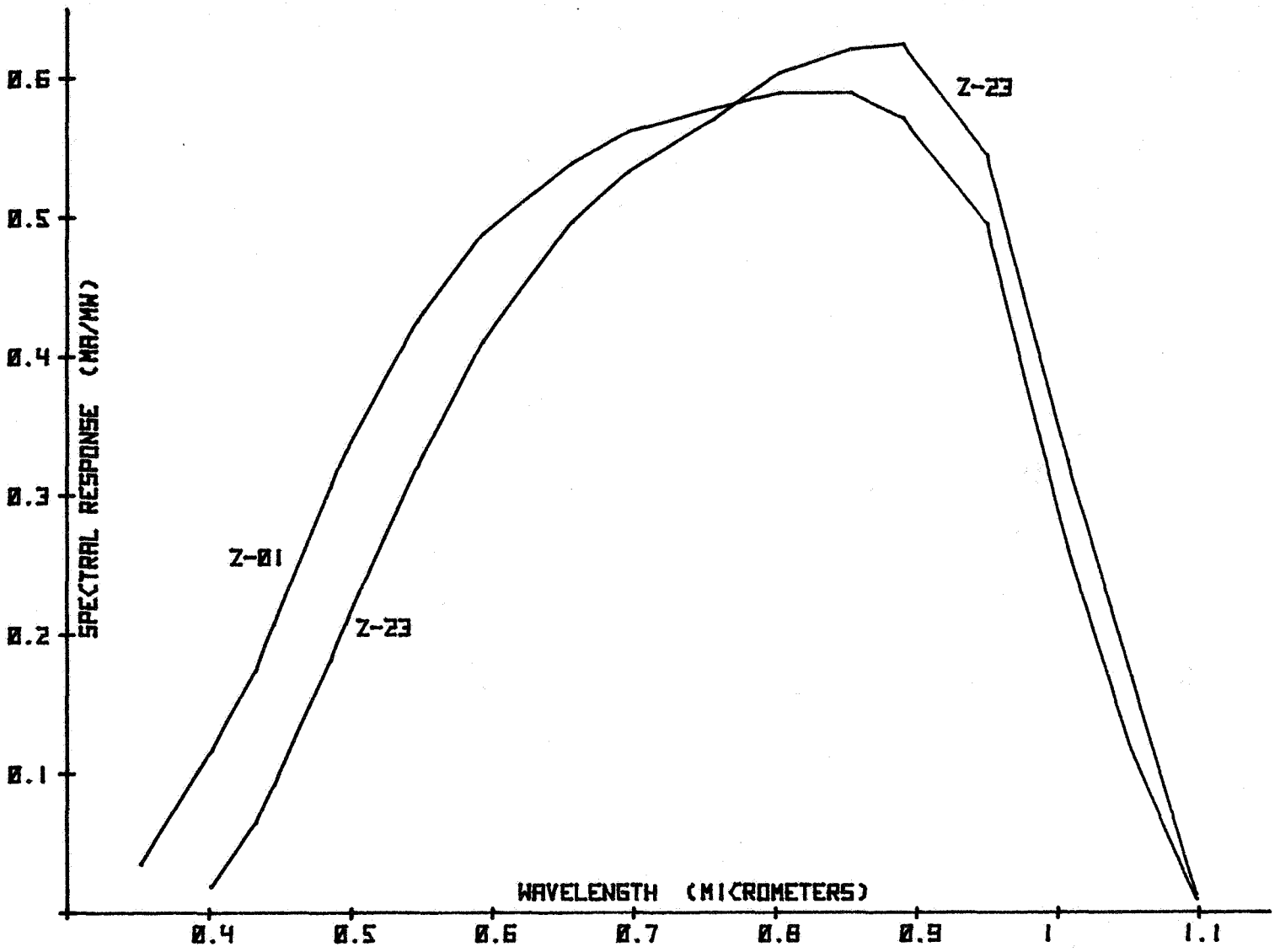

Figure 10. - Comparison of spectral responses of cells Z-27 and Z-01

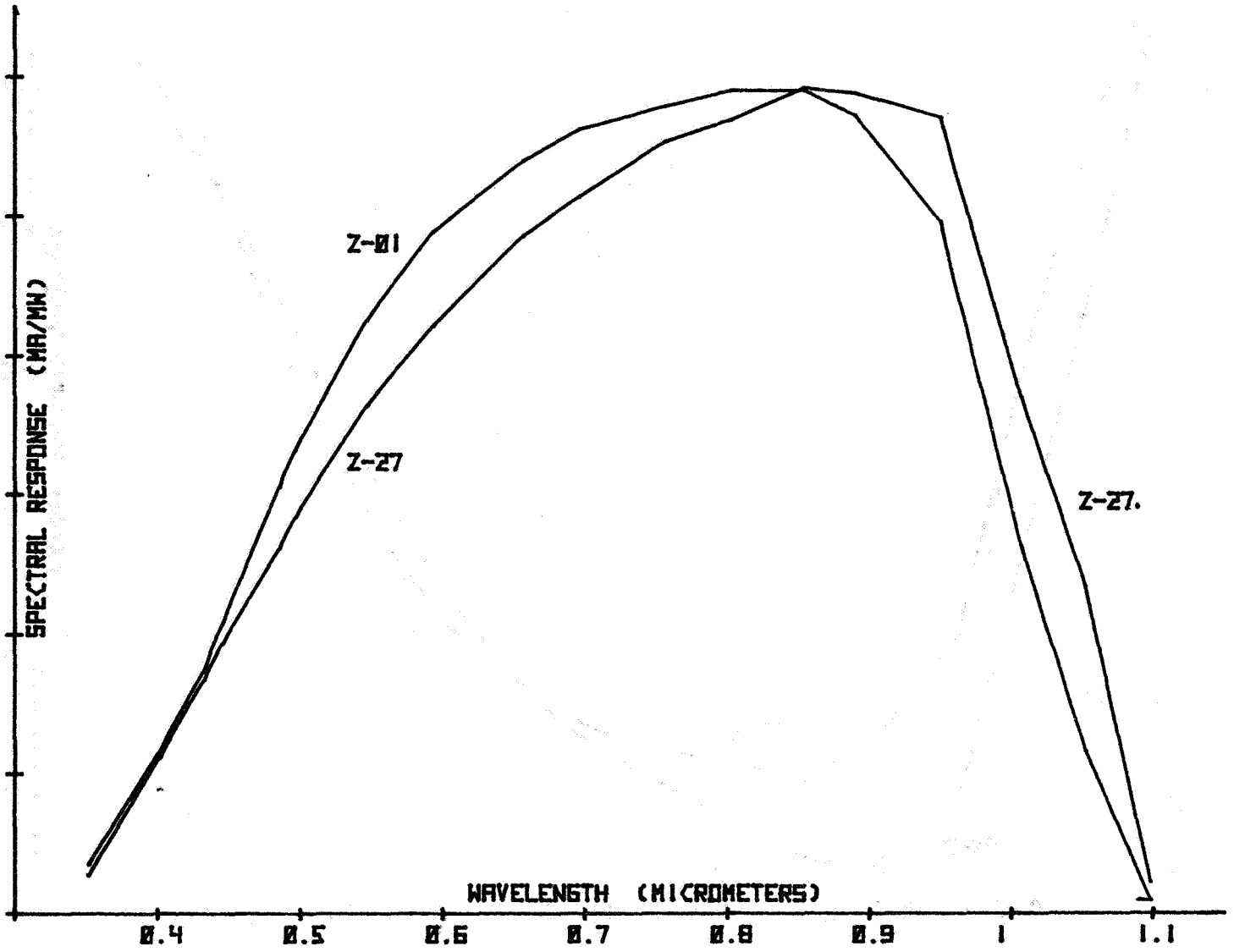

Figure 11. - Comparison of spectral responses of cells Z-36 and Z-01

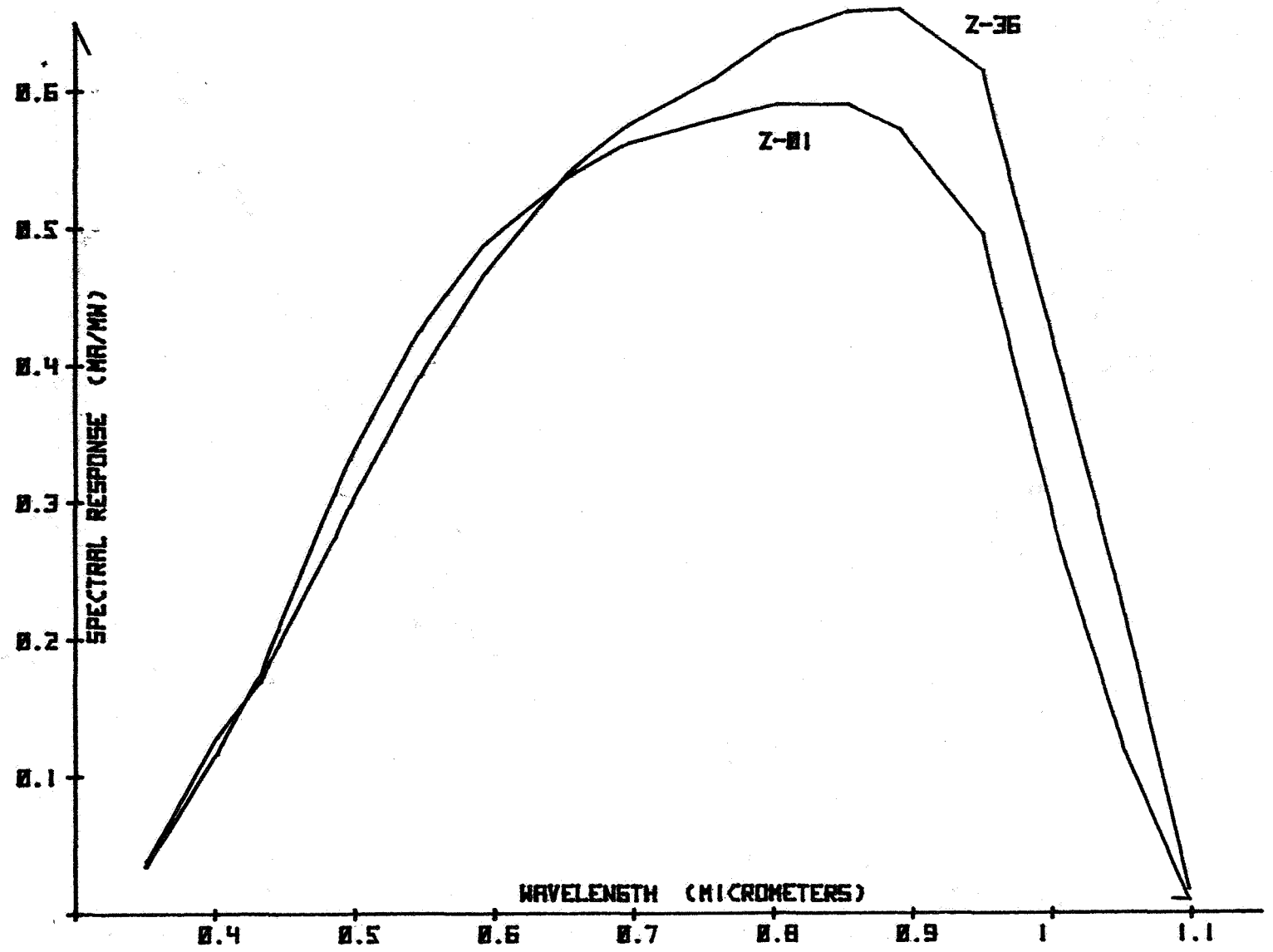

Figure 12. - Comparison of spectral responses of cells Z-43 and Z-01

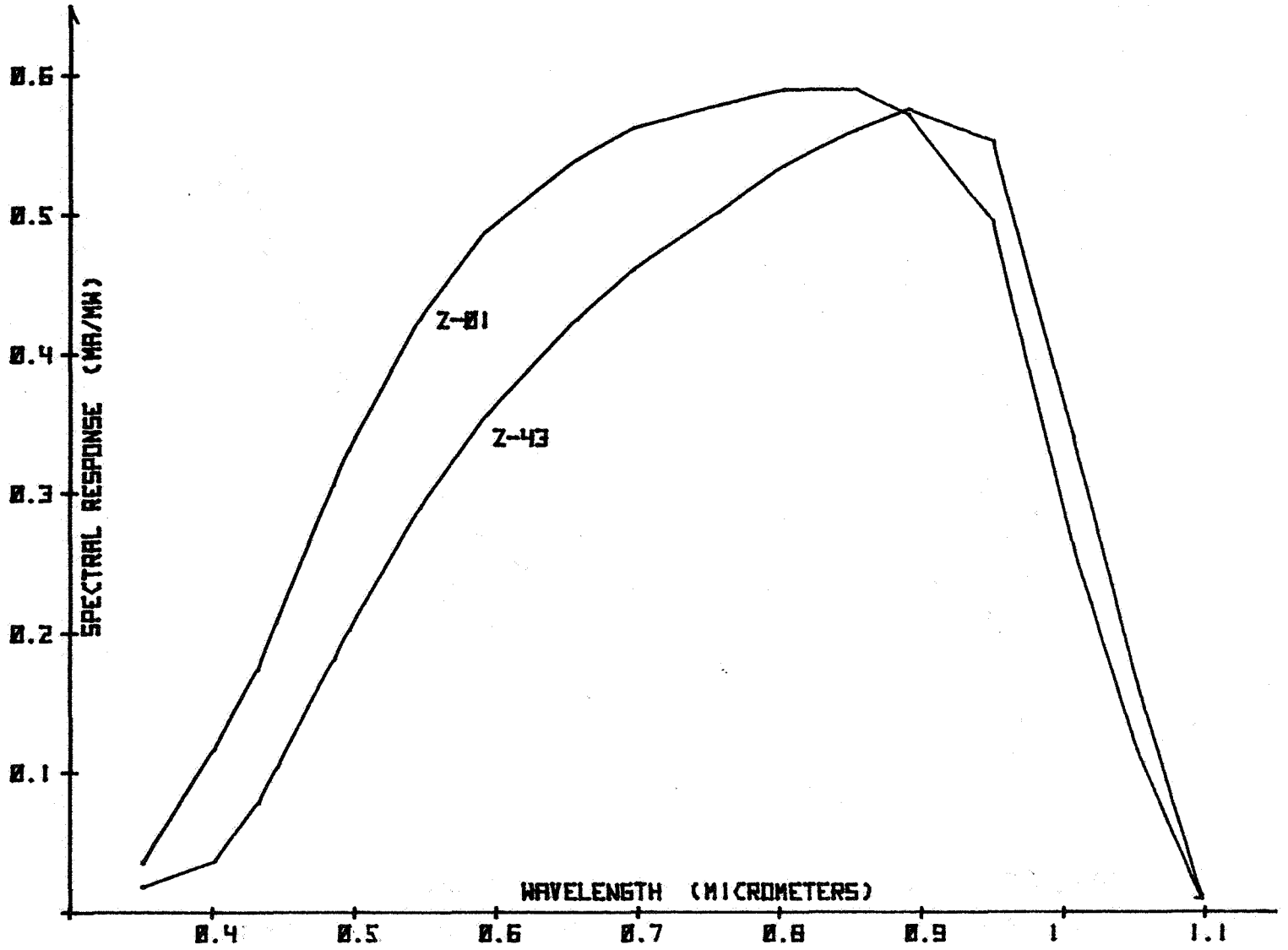

Figure 13. - Comparison of spectral responses of cells Z-70 and Z-01

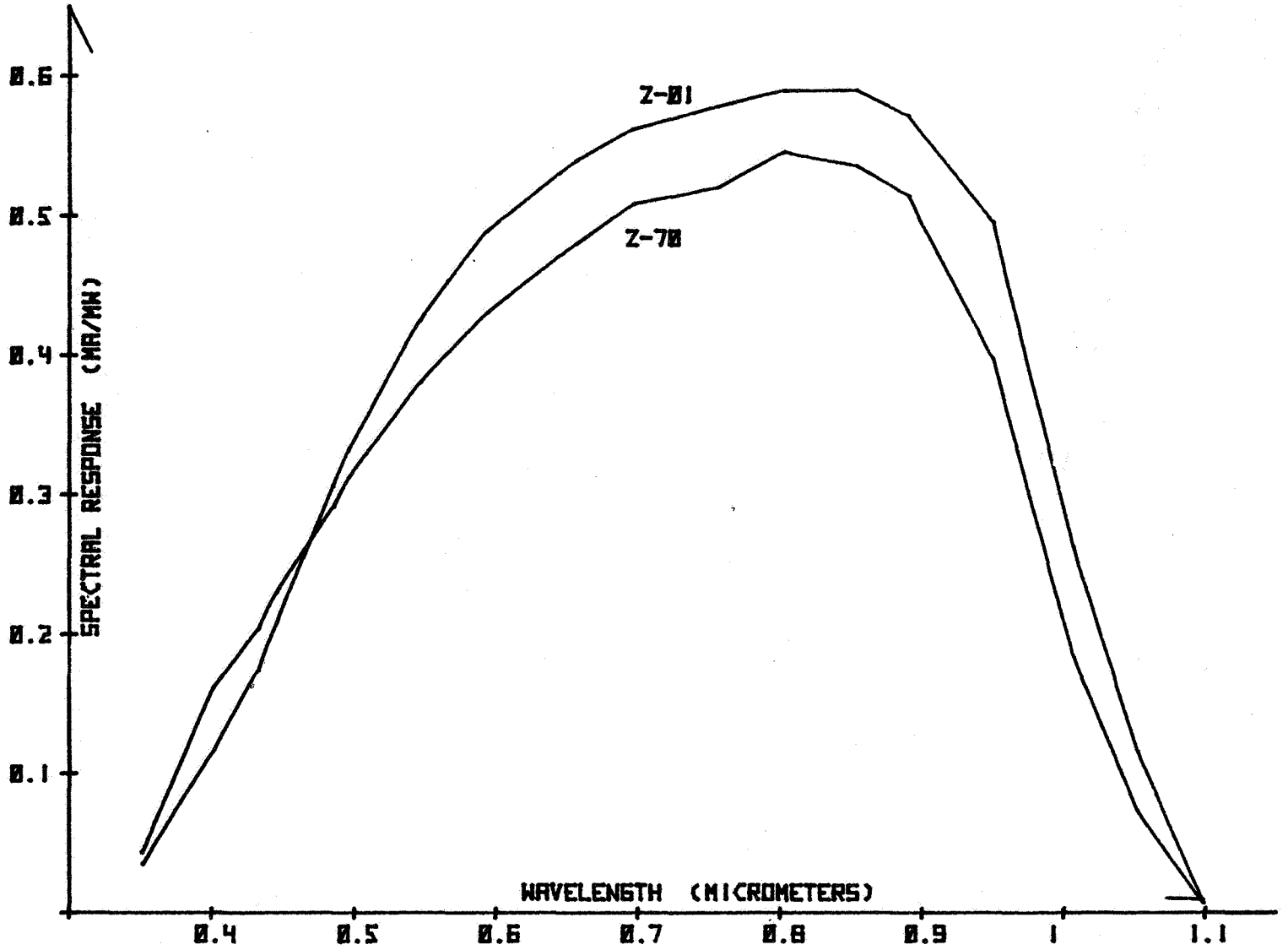

# A NEW RAPID METHOD OF SOLAR SIMULATOR CALIBRATION

by Bernd Ross, Consultant to AF Aero-Propulsion Laboratory

## SUMMARY

A quick method for checking solar simulator spectral content will be presented. The method is based upon a solar cell of extended spectral sensitivity and known absolute response, and a dichroic mirror with the reflection-transmission transition close to the peak wavelength of the Thekaekara AMO distribution.

The method was chosen because it is low cost to buy and use. It compromises the need for spectral discrimination with the ability to integrate wide spectral regions of the distribution which was considered important due to the spiky nature of the high pressure xenon lamp in common use. The results can be expressed in terms of a single number, the blue/red ratio, which, combined with the total (unfiltered) output, provides a simple adequate characterization.

Measurements were conducted at eleven major facilities across the country and a total of eighteen simulators was measured including five pulsed units. Measurements consisted of exposing the violet solar cell to the simulator light by transmission through the dichroic mirror and reflection from its front surface. A backup measurement was done using five bandpass filters furnished by NASA-Goddard Space Flight Center. The filters and mirror were made available at no cost to the Air Force and the several firms and organizations generously provided their time, facilities and cooperation in these measurements.

Data will be presented from the results of the measurements, and compared with the expected values from calculations. The degree of agreement will be discussed and problem areas identified. Extension of the method to AM2 simulation is simple and requires but one further calculation.

This work was done with the support of USAF Systems Command Aero-Propulsion Lab under contract F33615-76C-2050 Task II and was partly carried out at their facility.

## INTRODUCTION

The problem of space sunlight simulation on earth comprises two major requirements: (A) the construction of a light source capable of giving off radiation of proper intensity over the spectral regions involved and (B) a means for maintaining the calibration of this light source.

Recent advances [1,2] in solar cell construction have altered the cell response sufficiently, that "old" methods of simulator set up were found to be wanting. The problem was compounded by the use of "old" standard cells which had been flown in space or on balloons. While these cells were well characterized for output in space sunlight, their spectral response was sufficiently different (usually low at the extreme wavelengths) that simulator calibration with such cells introduced errors considered intolerable in flight hardware predictions.[3] Discrepancies of as much as 15% between simulator prediction and actual space output have been reported. [4]

The present study was undertaken with the objective to find a rapid, simple, low cost method to determine whether a simulator was in calibration and if not, what needed to be done to obtain a satisfactory adjustment.

## METHOD

Figure 1 shows the spectral output of a high pressure xenon arc lampsimulator (Spectrolab X25), which is the most prevalent commercial unit in the USA. The measurement was carried out with a spectral radiometer using an IR 63 detector and includes the spectral characteristics of the folding mirror system which is also subject to the aging process. The curve denoted by circles gives the output of the newly installed lamp and the trace with X's shows a similar trace after 1000 hrs. of use. Particularly significant are the large spikes in the range between 770nm and 1100nm, as well as the changes taking place in that region and in the blue region around 400nm as a function of aging.

Our initial plan was to pick several narrow band or band pass filters, stratigically chosen with regard to wavelength limits, and couple them with a solar cell, to obtain a rough calibration of the spectral nature of the output.

This procedure became doubtful when viewed in the light of Figure 1 due to the discontinuous nature of the spectral output. The use of a sharp cuton filter in the proximity of the enormous positive and negative spikes appeared to be an invitation to allow second order effects, such as temperature changes, to attain first order importance. The most continuous portion of the distribution appeared to be near the AMO peak. We therefore decided to look for a means of integrating the extremes of the curve, particularly the region of the high intensity lines. A dichroic mirror was finally selected, with a transmission-reflection transition bisecting the AMO peak. The filter was furnished gratis by OCLI

and is known in the industry as a 45° ultra violet cold mirror,[5]. It has several advantages. Since the mirror is used in the 45° position it can be used with either a spectrally matched pair of cells simultaneously, or with a single cell sequentially, in order to obtain a blue/red ratio of integrated solar cell short circuit current. It is a stock item, relatively inexpensive, rugged and is made in large sheets providing reasonable assurance of uniformity.

The spectral characteristic of the dichroic mirror is shown in Figure 2 with the dashed trace giving the reflected light and the solid trace the transmitted light.

It can be seen that the dichroic mirror comes close to the ideal: high reflectance near 1.o at wavelengths shorter than 0.5μm (500nm) with low reflectance at wavelengths greater than .6μm (600nm) and a relatively sharp transition in between. Similarly the transmittance below .5μm is near 0 and above .6μm near 0.8 and 0.9.

Figure 3 shows the AM2 spectrum multiplied at 25nm wavelengths intervals by the spectral response of a solar cell. The integrated curve (area under the curve) gives the expected total short circuit current of that solar cell under average terrestrial sunlight illumination. The airmass 2 distribution [6] was adopted as the standard for average terrestrial sunlight at the 1975 Terrestrial Photovoltaic Workshop (Nasa-Lewis Research Center, Cleveland, OH.).

The expected solar cell current under dichroic illumination by transmitted and reflected light from the terrestrial sun [6] is calculated in the usual way according to [1] and [2].

Reflected $$I_B = \int_\lambda H_\lambda R_\lambda Q_\lambda \, d\lambda \qquad (1)$$

and

Transmitted $$I_R = \int_\lambda H_\lambda T_\lambda Q_\lambda \, d\lambda \qquad (2)$$

with $I_B$ = Blue (reflected) short circuit current
$I_R$ = Red (transmitted) short circuit current
$H_\lambda$ = AM2 distribution[6]
$R_\lambda$ = Spectral reflection characteristic of dichroic mirror
$Q_\lambda$ = Absolute spectral response of test cell
$T_\lambda$ = Spectral transmission characteristic of dichroic mirror
$d\lambda$ = Wavelength interval (25nm)

Figure 4 shows the results of this calculation for the airmass 2 distribution. The ordinate gives the spectral current density. The dashed curve on the lefthand side of the figure shows the contribution from the blue light reflected from the dichroic mirror surface, and the

large solid curve on the righthand side pictures the contribution from the red light transmitted by the dichroic mirror. The integrals, or areas under the curve yield the shortcircuit currents under each condition. The blue/red ratio for the terrestrial sun is considerably smaller, 0.320, than that for the space sun, AMO[7], 0.413. This is due to the greater relative absorption of short wavelength light by the terrestrial atmosphere.

An optical jig was built to facilitate the measurement. The jig consists of a diagonal frame holding the dichroic mirror, pivoting on a hinge to allow swinging the mirror out of the way for a total current measurement, and to allow access to the cell when changing its position. The cells were OCLI 2x2cm violet cells mounted on balloon flight modules with two parallel 1-ohm resistors providing a 1/2-ohm load to sense the short circuit condition. The modules could be pushed onto pins to assure indexing in repeatable positions, and to provide stable mounting in the vertical plane for reflected light measurement. For instrument repeatability a digital multimeter (NLS LM 3.5) was carried along to the various locations, as well as a spare solar cell, and spare dichroic mirrors.

Figure 5 shows a diagrammatic sketch of the optical jig. The incoming light is directed downward onto the 45° mirror. It is split into reflected and transmitted components directed to the solar cell. The same cell is placed into vertical and horizontal positions for alternate measurements.

Figures 6 and 7 are photographs illustrating the use of the jig in measurements:

Fig. 6 vertical position of module, reflected light measurement.

Fig. 7 flipped up dichroic mirror for total light measurement.

As a theoretical test case the two curves of Figure 1 were used to obtain blue/red ratios to determine the sensitivity of the method. Using a typical violet cell absolute response the calculation was made according to [1]. In the initial calculation the interval $d\lambda$ was 100nm and $P_{1\lambda}$ and $P_{2\lambda}$ were substituted for $H_\lambda$, constituting the simulator distributions for the new and aged lamps respectively. A significant difference (17%) was found between the two blue/red ratios, attesting to the sensitivity of the method.

It is interesting to note that light flux of the wavelength of the reflecting-transmitting transition of the dichroic mirror is 95% absorbed within 0.15μm of the surface of the solar cell. This means that the

mirror roughly divides the simulator distribution into energies absorbed in the diffused (blue) and the bulk (red) regions, respectively. Since the fluxes involved are of respectable intensities, close to AMO insolation, this method of obtaining a spectral split may find use in diagnostic techniques.

The prediction of the cell output under various conditions implies knowledge of several spectral quantities, including the light spectral distribution, the filter or mirror characteristic and, significantly, the absolute spectral response of the solar cell. The absolute spectral response of the cell used on the measurements is shown in Figure 8. Three curves are shown. The top curve shown was used in the calculations.

Calculations were initially made with the spectral response in Figure 8 indicated by dots. This response was measured with an AMO bias applied. The AMO output prediction obtained was about 6% higher than what was believed to be the correct value. One of the difficulties with the measured response was the lack of data below 400nm which required extrapolation. It was therefore decided to redo the calculations using the response indicated by the solid line. This response was done at a different facility without AMO bias. All response measurements were made with filter wheel spectrometers using a xenon light source. The striking difference between responses caused concern, however, a detailed investigation of this problem was not within the scope of the project.

As an alternate method five bandfilters were supplied by Goddard Space Flight Center. The characteristics of these filters are shown in Figure 9 in terms of the solar cell spectral output and AMO sunlight by plotting the components of

(2) $$I_f = \int_\lambda P_\lambda T_{f\lambda} R_\lambda \, d\lambda$$

where $I_f$ = short circuit current of the filtered cell

$T_{f\lambda}$ = spectral transmission of the filter

$P_\lambda$ = Thekaekara AMO Spectrum

$R_\lambda$ = absolute spectral response as before

As can be seen from the curve due to filter #5 the transmission onset is at a wavelength sufficiently long that when combined with the solar cell spectral response a minimal output results.

## MEASUREMENTS

A total of eleven commercial organizations and government laboratories were visited and measurements were carried out on eighteen simu-

lators including five pulsed units. While measurements were done with two cells, due to the press of time only one set of data is reported. The responses of the two cells were well matched, based both on response measurements and the output under different spectral conditions. Also the data on one simulator is not being reported as it was measured with the other solar cell only.

Measurements proved to be easy to do and no interfacing difficulties were encountered, due to the excellent cooperation of all the participating organizations and personnel, and the simplicity of test instrumentation and method.

The results are shown in Table 1.

Since the theoretical transmitted light value is higher than any measured value, it suggests that the red response of Fig. 8 is higher than the actual response.

The theoretical values were calculated by a point by point multiplication of the spectral parameters at 10nm intervals, and subsequent summing. While this was a somewhat laborious procedure, it was done to eliminate all doubt when dealing with the characteristics exhibiting high shear rates (filter cuton, spectral response near IR cutoff, simulator xenon line spectra). In the case of filters #4 and #5 the match between predicted and actual values is very poor (75% and 2 orders of magnitude respectively). Since both filters are near the cutoff of response (see Fig. 8 and 9) measurements are particularly susceptible to false signals due to extraneous light. This problem was compounded by the expedient use of white BFS modules with cell dimensions almost as large as those of the filters. Also in the facilities calling for vertical testplanes the filters had to be handheld over the cell. However there was no significant difference between filter #5 readings on these simulators. A recheck on the filter transmission characteristics is being undertaken.

The variation in both reflected light outputs (29%) and in blue/red ratios (37%) shows a good deal of slack in spectral distribution among simulators. Not surprisingly, the total intensity envelope is considerably tighter (9%).

Figure 10 gives a graphical presentation suggested by H. Brandhorst of the data in Table I. The blue/red ratio is plotted as the ordinate, against the reflected current as the abscissa. The pulsed simulator ratios appear in a cluster near the middle of the graph, well above the line, showing a quite different spectral mix than the X25 simulators.

The theoretical ratio, based upon the measured spectral response and mirror characteristics multiplied by AMO distribution and summed, is given by the $\overline{\pi}$ symbol in the lower right hand portion of the figure. Its low value is probably due to an excessively high calculated red (transmitted current) from an anomalously high measured red response of the solar cell.

The example of xenon lamp aging mentioned previously was repeated this time making the calculation with a measured spectral response rather than a typical characteristic and using 10nm intervals. The blue/red ratio changed from an initial .354 to .277 after 1000 hrs., a change of 21% compared with the earlier 17%.

## CONCLUSION

A rapid simple, easy to use and low cost method of simulator spectral assessment has been presented along with measurement data obtained in field trials.

While it extends the older methods of blue/red filter measurement to make it independent of different degrees of color blindness of solar cells and is thus applicable to present day and future cell fabrication innovations, it never-the-less requires an accurate measurement of spectral response of the cells specifically under actual use conditions. Evidence suggests that spectral response measurements are as troubled as simulator calibrations.

The author takes pleasure in acknowledging the wholehearted cooperation of personnel and organizations in contributing their time and the use of laboratory and in some cases production facilities:
D. Peterson and D. Briggs, Aeronutronic-Ford; E. Neighbours and A. Lunde, Boeing-Kent; A. Meulenberg and J. Allison, COMSAT Labs.; E. Stofel, G. Goodelle and R. Opjorden, Hughes Aircraft Co., El Segundo; R. Greenwood and G. Downing, JPL; N. Mejia, E. Gaddy and L. Slifer, NASA Goddard Space Flight Center; R. Hart, H. Curtis and H. Brandhorst, NASA Lewis Research Center; L. Rost and P. Iles, Optical Coating Labs, Inc.; H. Chamberlain and E. Ralph, Spectrolab-Hughes; G. Mesch, H. Rauschenbach, W. Luft, TRW, and S. Douple and P. Rahilly, Air Force Aero-Propulsion Laboratory.

Our further thanks are due to Mr. J. Wise, AF Aero-Propulsion Laboratory, USAF Systems Command for suggesting and supporting the study.

## LIST OF REFERENCES


1. J. Lindmayer, J. F. Allison, COMSAT. TECH. REV., 3, 1 (1973)
2. P. A. Iles, D. K. Zemmrich, PROC. 9TH PHOTOVOLT. SPEC. CONF., p200 (1973)
3. K. Bogus, PROC. of the INTL. PHOTOVOLTAIC POWER GENERATION CONF., p291 Hamburg, W. Germany, 25-27 Sept. 1974
4. R. L. Statler, D. H. Walker, PROC. PHOTOVOLT. SPEC. CONF. p130 (May 1975)
5. Stock filter catalog, visual section p17, Publ. by Optical Coating Laboratory, Inc. POB 1599 Santa Rosa, CA 95402
6. Nasa TM X-71771, Interim solar cell testing procedure for terrestrial applications, July 1975
7. M. P. Thekaekara, J. ENV. SCI. 13, 6 (1970)

# TABLE I

## A COMPARISON OF SIMULATOR SPECTRAL CHARACTERISTICS BY DICHROIC MIRROR AND FILTER METHODS

| FACILITY | A | B | C | D | E | F | G | H | I |
|---|---|---|---|---|---|---|---|---|---|
| RED TRANSMITTED (ma) | 98 | 99 | 101 | 100 | 104 | 88 | 100 | 99 | 94.4 |
| BLUE REFLECTED (ma) | 42 | 44 | 42 | 46 | 36 | 42.6 | 47 | 42 | 43.8 |
| TOTAL (ma) | 158 | 159 | 161 | 163 | 160 | 153.6 | 162 | 162 | 159.3 |
| BLUE/RED | .429 | .444 | .416 | .460 | .346 | .484 | .470 | .424 | .464 |
| BLUE FILTER # 1 (ma) | 34 | 42 | 38 | 39 | 30 | 36.2 | 48 | 38.4 | 40.3 |
| 2 (" ") | 70 | 72 | 66 | 68 | 68 | 55.2 | 74 | 58.6 | 56.8 |
| 3 (" ") | 56 | 60 | 60.5 | 61 | 68 | 62.2 | 61 | 58 | 62.6 |
| 4 (" ") | 28 | 26 | 28 | 30 | 29.5 | 27.8 | 23 | 25.1 | 27.3 |
| RED 5 (" ") | 10 | 10 | 10 | 10 | 10 | 10.8 | 8 | 8 | 6.9 |

## TABLE I - CONTINUED

### A COMPARISON OF SIMULATOR SPECTRAL CHARACTERISTICS BY DICHROIC MIRROR AND FILTER METHODS

| FACILITY (ma) | | J | K | L | M | N | O | P | Q |
|---|---|---|---|---|---|---|---|---|---|
| RED TRANSMITTED (ma) | | 93.8 | 102.2 | 97.6 | 97.8 | 101.4 | 101 | 100 | 96.2 |
| BLUE REFLECTED (ma) | | 43.6 | 42.8 | 48.6 | 42.4 | 42.2 | 42.6 | 49.5 | 43.6 |
| TOTAL (ma) | | 157.5 | 166.2 | 166.6 | 161.2 | 163.4 | 164 | 168. | 159.6 |
| BLUE/RED | | .465 | .419 | .498 | .434 | .416 | .422 | .495 | .453 |
| BLUE FILTER | # 1 (ma) | 44.2 | 40.4 | 45.7 | 38.6 | 38.5 | 40 | 47 | 41.1 |
| ↓ | 2 (" ") | 58.5 | 68.8 | 69.8 | 65.7 | 68.8 | 73 | 70 | 63.2 |
| | 3 (" ") | 62.2 | 61.8 | 60.0 | 58.7 | 69.1 | 56 | 54 | 55.8 |
| | 4 (" ") | 28.9 | 28.4 | 28.4 | 29.2 | 24.5 | 24 | 27 | 26.8 |
| RED | 5 (" ") | 12.3 | 8.6 | 13.4 | 8.6 | 14.0 | 8 | 10 | 8.4 |

# A COMPARISON OF SIMULATOR SPECTRAL CHARACTERISTICS BY DICHROIC MIRROR AND FILTER METHODS

| FACILITY (ma) | AVERAGES | MAX. DEV. | THEORETICAL |
|---|---|---|---|
| RED TRANSMITTED (ma) | 98.4 | 16 14% | 111.40 |
| BLUE REFLECTED (ma) | 43.5 | 13.5 29% | 45.96 |
| TOTAL (ma) | 161.4 | 14.4 9% | 164.78 |
| BLUE/RED | .443 | 37% | .413 |
| BLUE FILTER NO. 1 (ma) | 40.1 | 18.0 52% | 34.67 |
| 2 (" ") | 66.8 | 18.8 31% | 60.25 |
| 3 (" ") | 60.4 | 15.1 30% | 51.05 |
| 4 (" ") | 27.2 | 7.0 27% | 15.20 |
| 5 (" ") | 9.8 | 6.0 60% | 0.086 |

RED

Figure 1

AGING OF XENON ARC LAMP

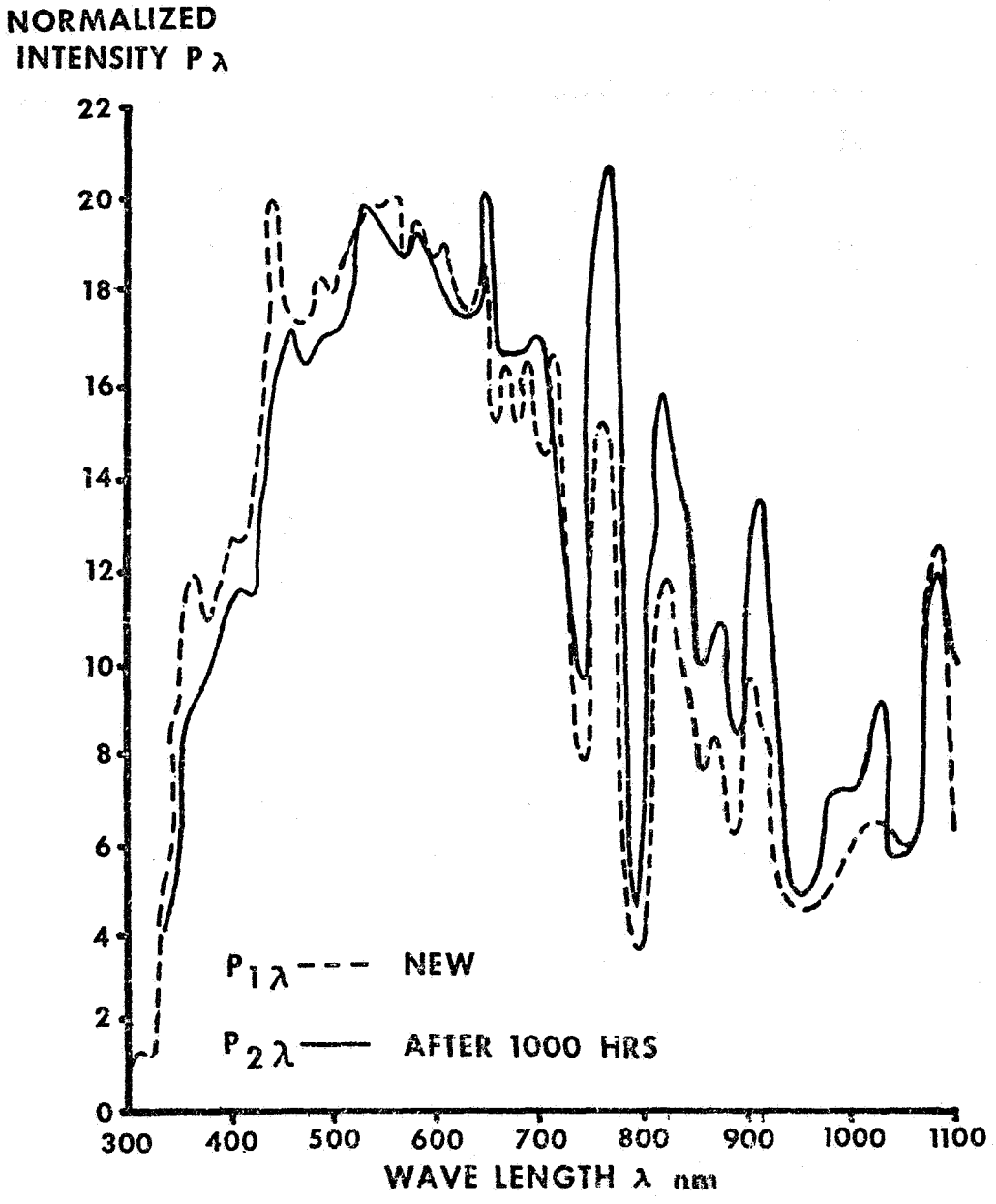

Figure 2

DICHROIC MIRROR CHARACTERISTIC AT 45° ∠

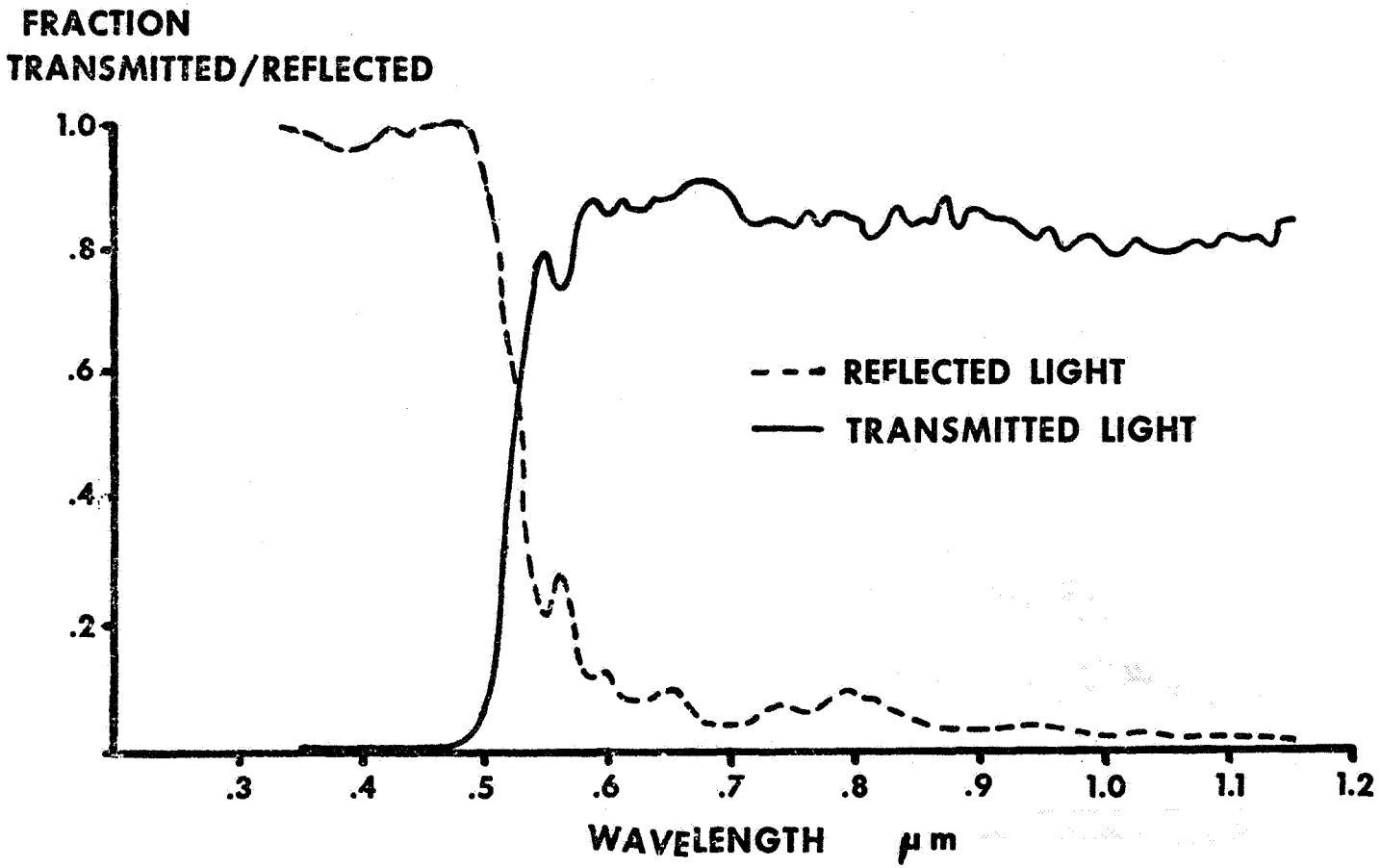

Figure 3

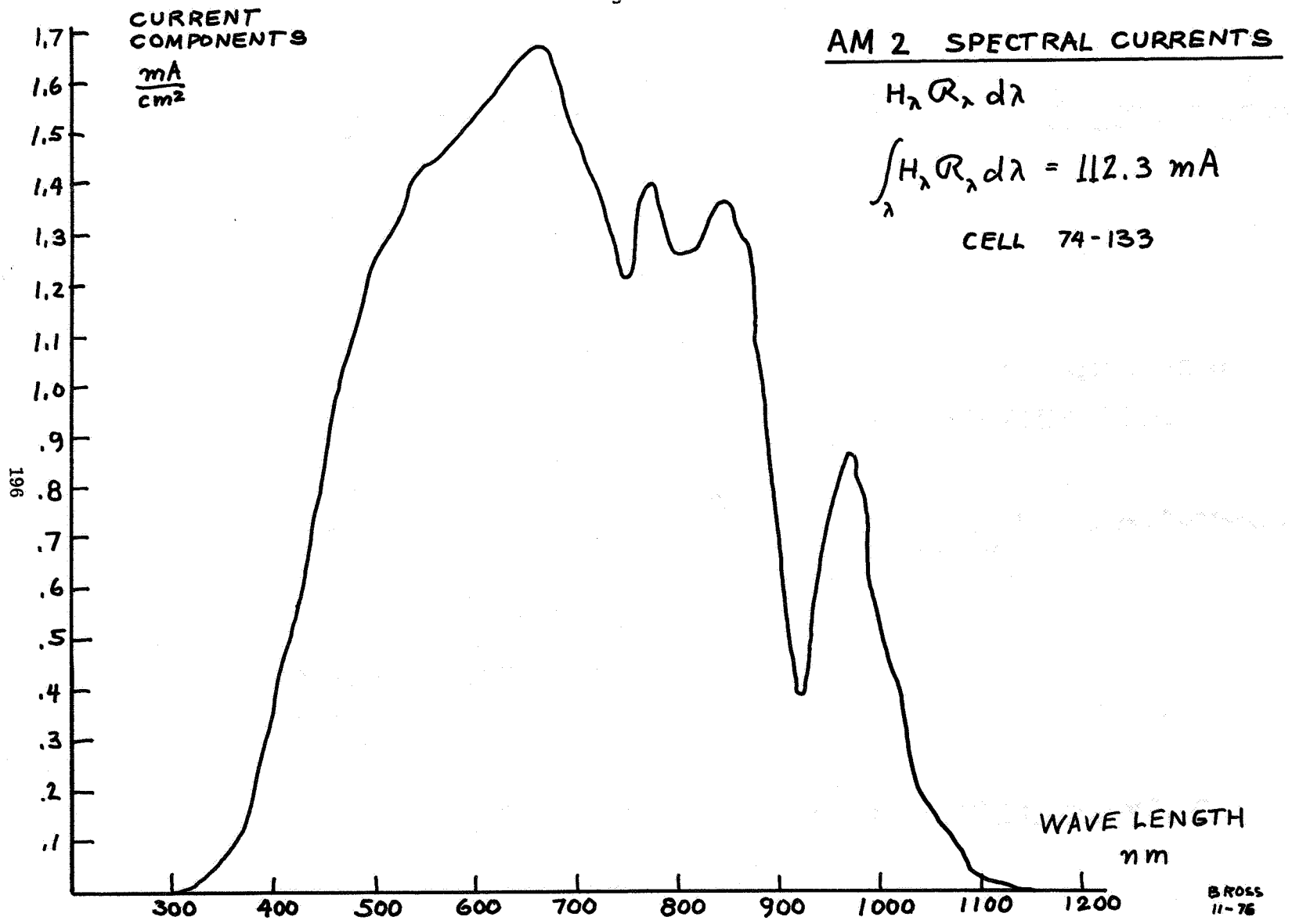
CURRENT COMPONENTS
mA/cm²
AM 2 SPECTRAL CURRENTS
$H_\lambda R_\lambda d\lambda$
$\int_\lambda H_\lambda R_\lambda d\lambda = 112.3$ mA
CELL 74-133
1.7
1.6
1.5
1.4
1.3
1.2
1.1
1.0
.9
.8
.7
.6
.5
.4
.3
.2
.1
300
400
500
600
700
800
900
1000
1100
1200
WAVE LENGTH
nm
B ROSS
11-76

Figure 4

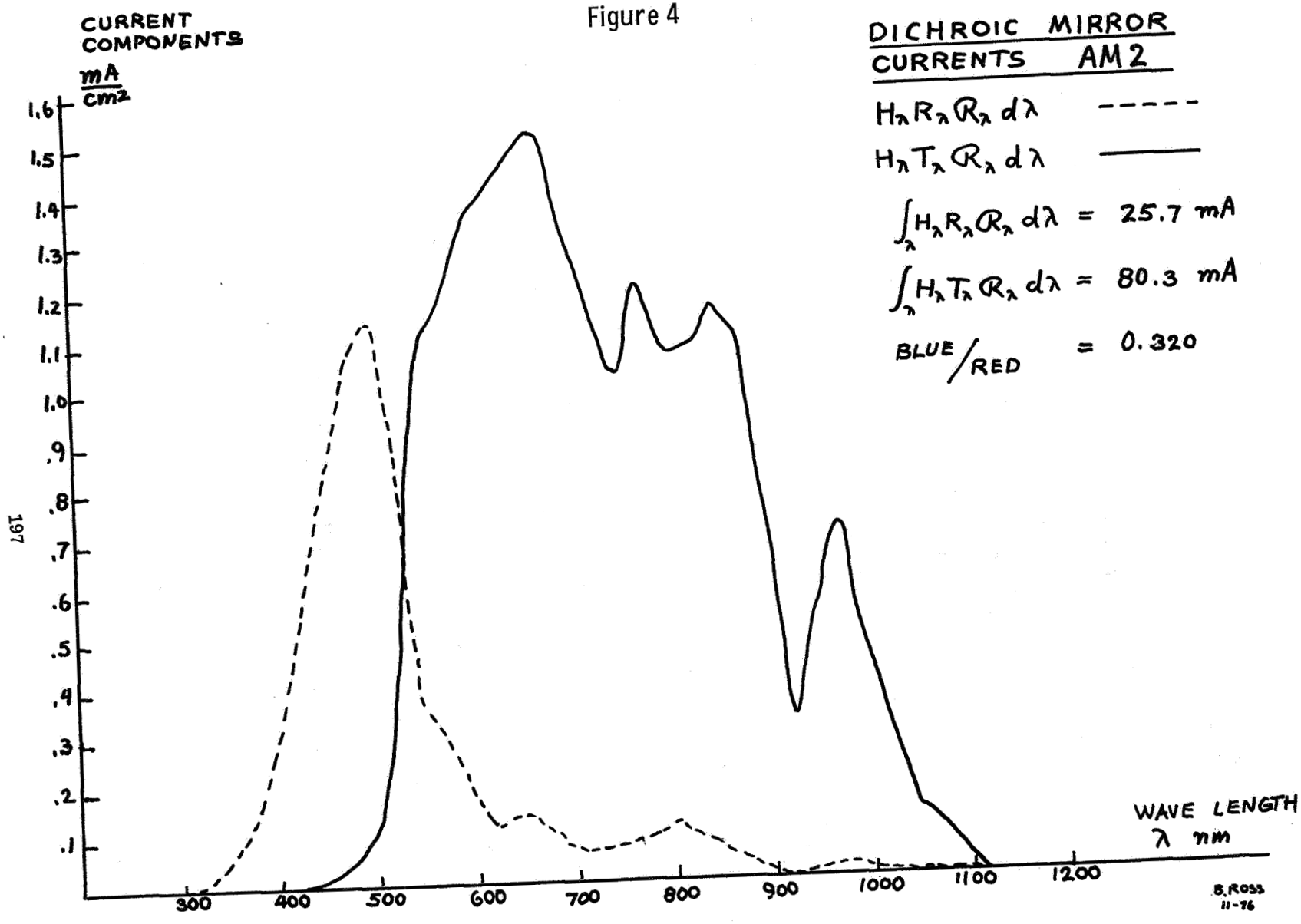
CURRENT COMPONENTS
mA / cm2
1.6
1.5
1.4
1.3
1.2
1.1
1.0
.9
.8
.7
.6
.5
.4
.3
.2
.1
300
400
500
600
700
800
900
1000
1100
1200
WAVE LENGTH
λ nm
B. ROSS
11-76
DICHROIC MIRROR
CURRENTS AM2
$H_\lambda R_\lambda R_\lambda d\lambda$ -----
$H_\lambda T_\lambda R_\lambda d\lambda$ ——
$\int_\lambda H_\lambda R_\lambda R_\lambda d\lambda$ = 25.7 mA
$\int_\lambda H_\lambda T_\lambda R_\lambda d\lambda$ = 80.3 mA
BLUE/RED = 0.320

Figure 5

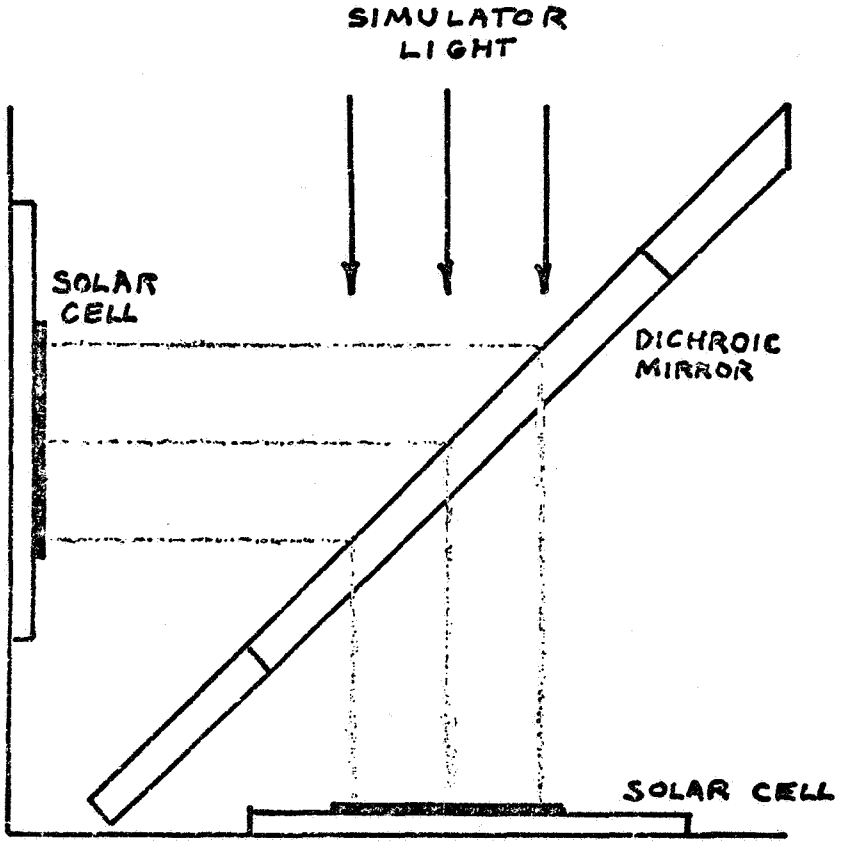


TEST JIG

Figure 6

OPTICAL JIG, VERTICAL POSITION OF BFS MODULE FOR REFLECTED LIGHT MEASUREMENT

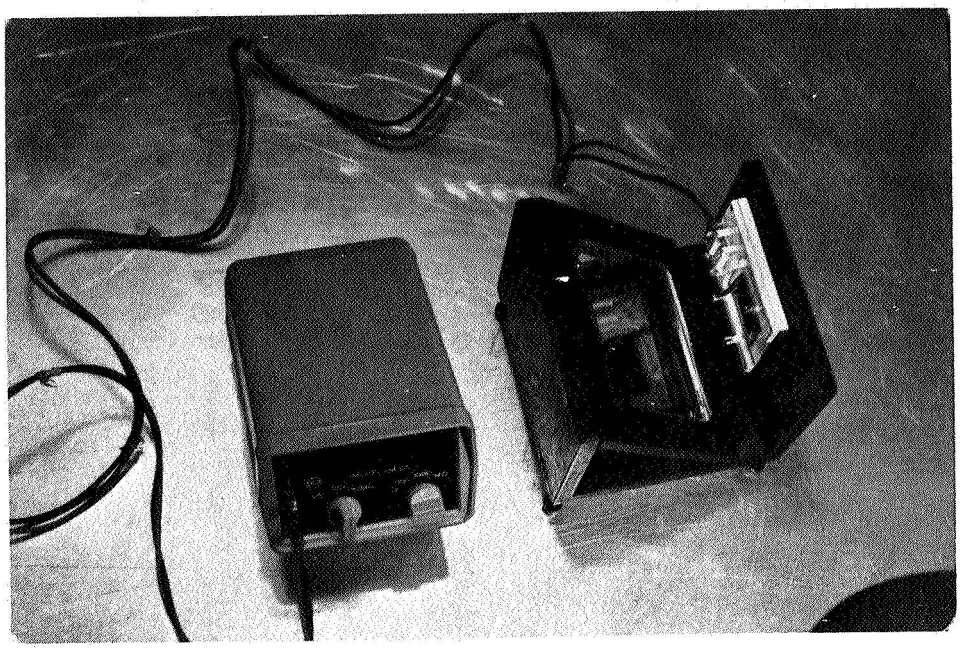

Figure 7

OPTICAL JIG, DICHROIC MIRROR FLIPPED UP FOR TOTAL LIGHT MEASUREMENT

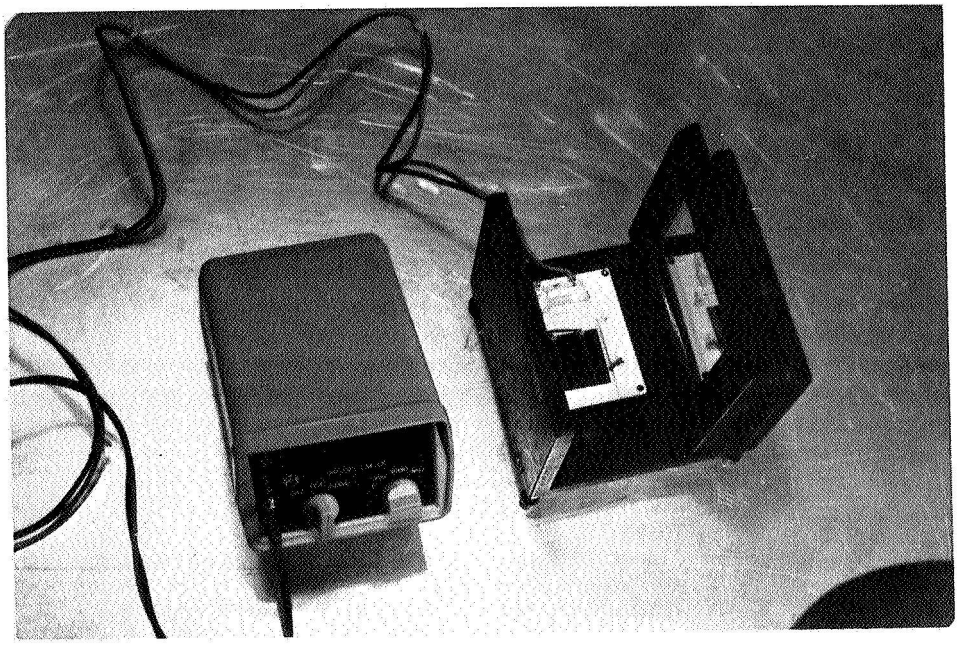

Figure 8

ABSOLUTE RESPONSE OF CELL 74 - 133

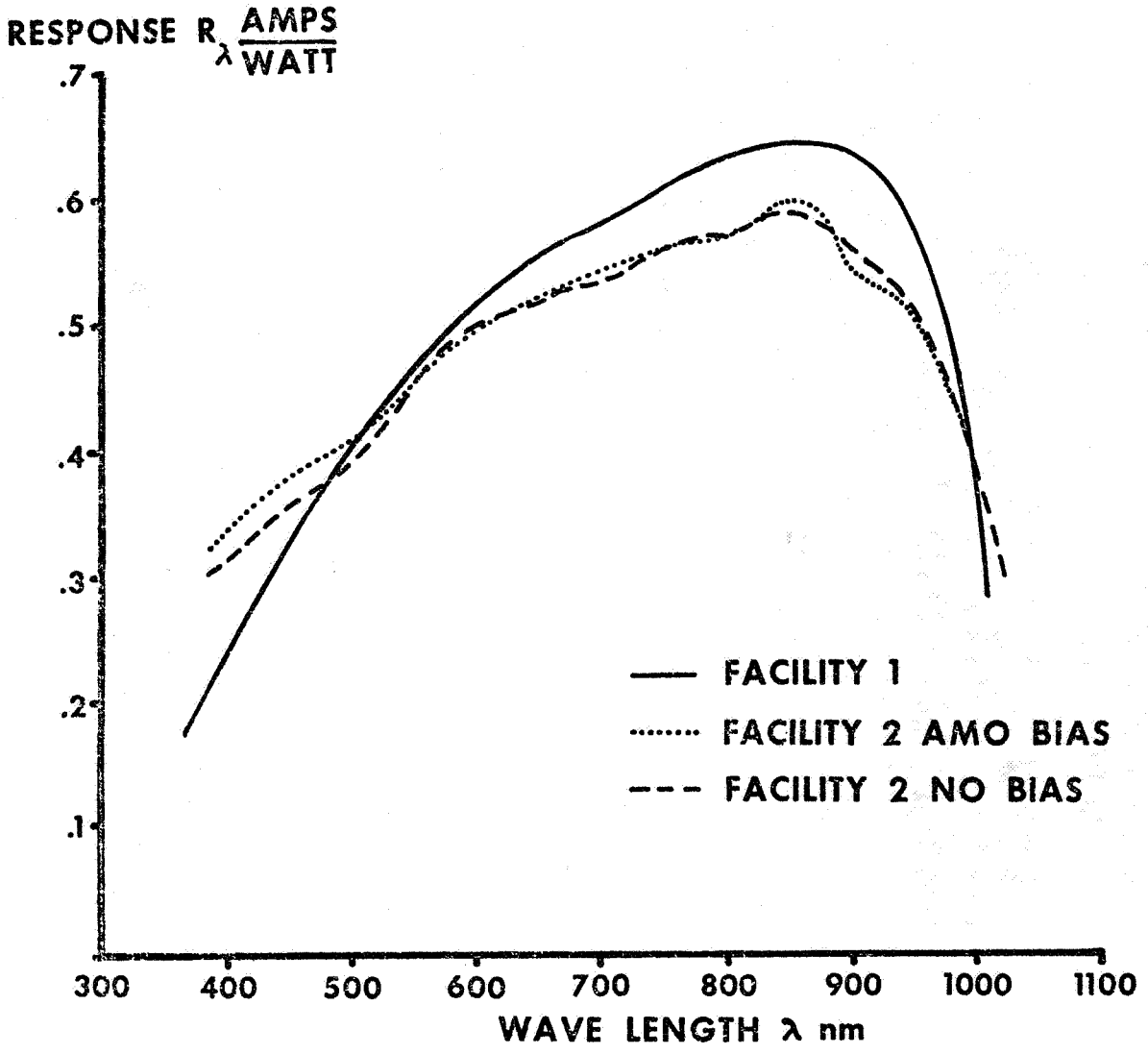

Figure 9

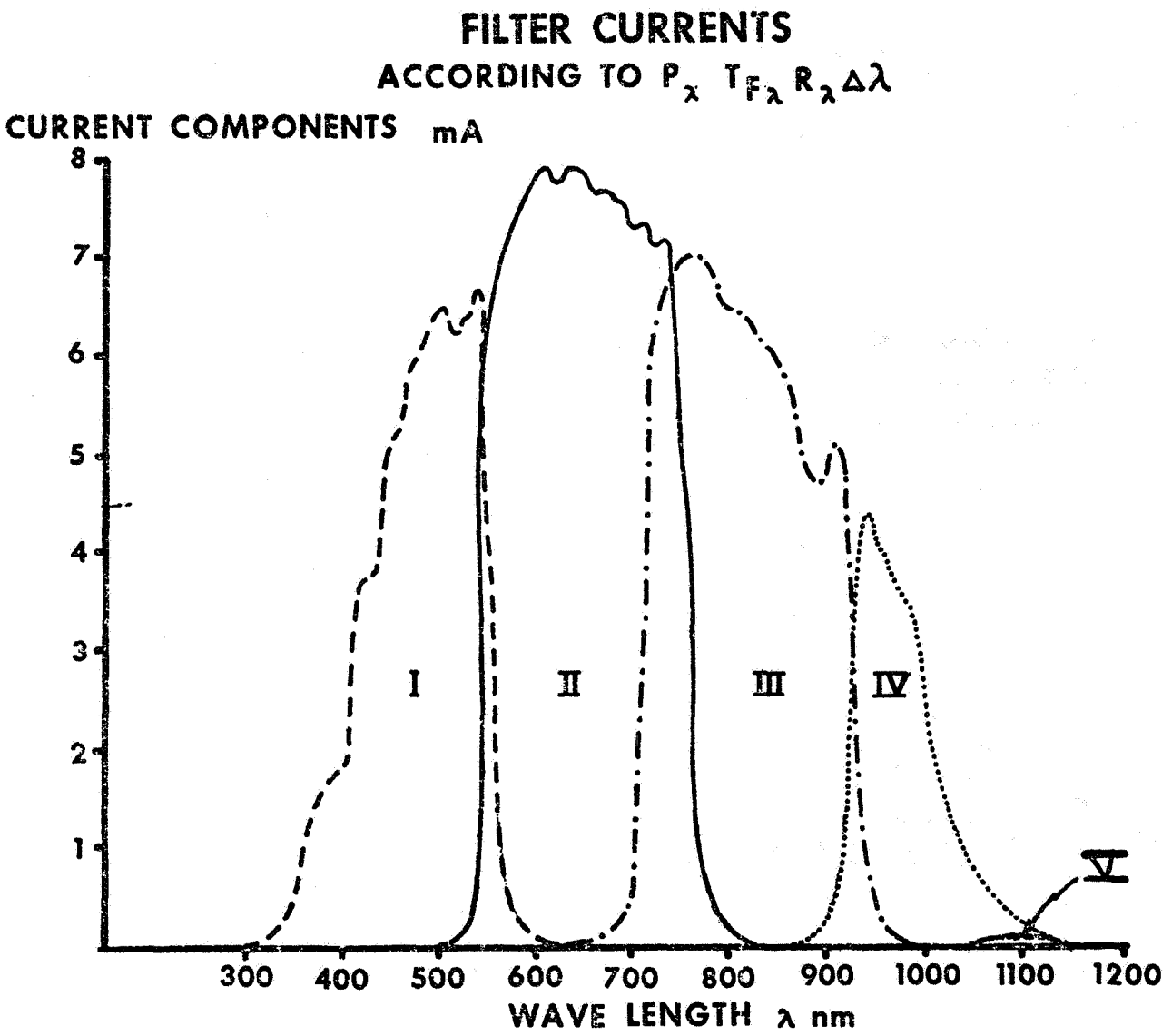
FILTER CURRENTS
ACCORDING TO $P_\lambda T_{F\lambda} R_\lambda \Delta\lambda$
CURRENT COMPONENTS mA
8
7
6
5
4
3
2
1
I
II
III
IV
V
300
400
500
600
700
800
900
1000
1100
1200
WAVE LENGTH λ nm

Figure 10

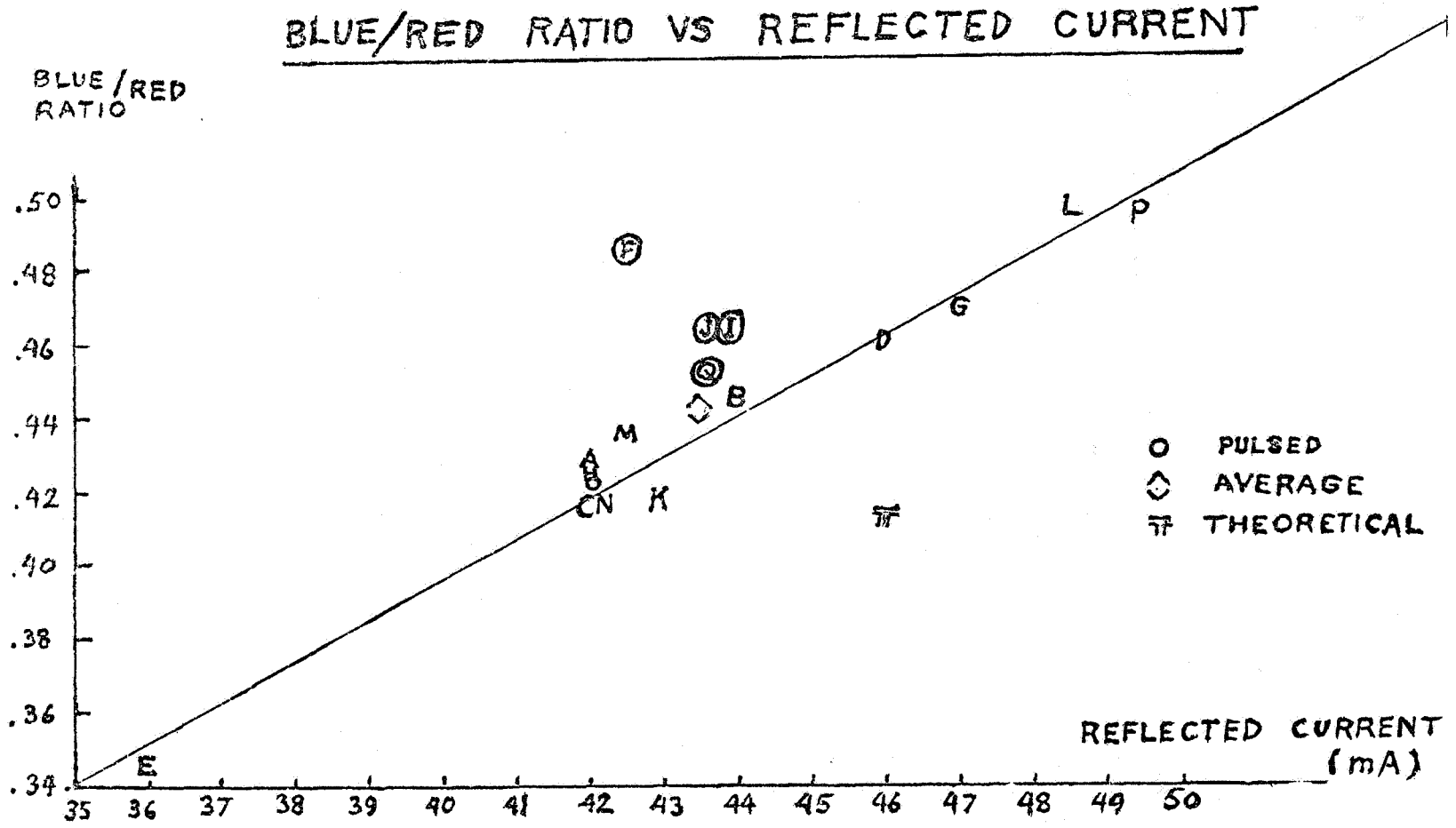
BLUE/RED RATIO VS REFLECTED CURRENT
BLUE/RED RATIO
.50
.48
.46
.44
.42
.40
.38
.36
.34
35 36 37 38 39 40 41 42 43 44 45 46 47 48 49 50
REFLECTED CURRENT (mA)
PULSED
AVERAGE
THEORETICAL

# CONSIDERATION OF DESIGN AND CALIBRATION OF TERRESTRIAL REFERENCE SOLAR CELLS

by V. G. Weizer

Lewis Research Center
National Aeronautics and Space Administration
Cleveland, Ohio

## ABSTRACT

The function of a reference solar cell is the accurate measurement of the power incident on a test plane from either the sun or a solar simulator. The reference cell must be capable of monitoring at least the direct component of the insolation. It is desirable, however, that it also be capable of measuring the total flux. A discussion of the problems encountered in the attempt to design a reference cell that meets these criteria is presented, starting with basic design considerations, and proceeding with the precautions taken to ensure a global monitoring capability. The effects of the variations in atmospheric conditions on the calibration and use of reference cells are presented along with a discussion of the simplifications brought about by the use of spectrally matched test and reference cells. Finally, a method of matching test modules and arrays to reference cells by a red/blue response ratio technique is described.

## INTRODUCTION

It is essential to establish reference conditions and measurement methods which will ensure the reproducibility and comparability of data taken by the many investigators in the field of photovoltaic energy conversion. To this end a system of standardized reference cells which have been calibrated under controlled conditions is being established. Many difficulties arise, however, when one attempts to design a reference solar cell package for use in the terrestrial environment. The purpose of this paper is threefold: (1) to present the design of a reference cell package

which is capable of measuring either the direct or the total insolation, (2) to point out the considerable simplification in calibration and testing procedures that can be effected through the use of references that are spectrally matched to the modules being tested, and (3) to show how the red/blue response ratio can be used to match reference cells and test modules and arrays.

## REFERENCE CELL DESIGN

Interim Reference Cell - In November, 1975, distribution of an interim reference cell was begun. The essential features of the interim cell are shown in figure 1. The package consists of a chrome-plated brass base fitted with a 1/16"-thick optical grade quartz window. The cell is hermetically sealed in an atmosphere of dry inert gas. An iron-constantan thermocouple monitors the temperature of the top surface of the cell. Electrical access consists of a four-point contact system. Mounting holes are provided so that the unit may be bolted to a heat exchanger if desired.

It was clear when the interim reference cell holder was being designed that considerable work would have to be done before a reference cell suitable for global use could be developed. A deep well design was adopted, therefore, to discourage use of the interim reference cell as a global measurement device.

A data package was issued with each of the reference cells which consisted of (1) the calibration factor (sensitivity) obtained under collimated (10:1) conditions in natural sunlight with a solar intensity between 80 and 100 $mW/cm^2$, and a cell temperature of 28 $\pm$2°C, (2) a nine-point spectral response curve, (3) the illuminated current-voltage characteristic at 100 $mW/cm^2$ solar intensity, and (4) the value of the atmospheric water vapor content at the time of calibration.

Global Measurement Capability

It is desirable that a reference cell have the capability of measuring the total insolation as well as the direct component. Two factors

influence the design of a holder with global sensitivity: shadowing and reflectivity.

To determine the influence of shadowing, a variable geometry cell enclosure was mounted on a solar tracker. The cell enclosure was geometrically similar to the interim reference cell holder with the added capability of continuous wall height variation. In this way the view angle, $\theta$, (as defined in figure 2) could be varied and the reduction in cell current due to the loss of low angle illumination could be monitored. Since it was suspected that cell surface texturization would increase cell sensitivity to the diffuse component, both texturized and planar surfaced cells were investigated.

Measurements were made in natural sunshine under conditions ranging from clear (B=0.1) to very turbid (B= 0.35), where B is the Schüepp turbidity coefficient.[1] Some typical results are shown in figure 2 where the percent reduction in cell current due to side wall shadowing is plotted against view angle. As suspected, the texturized cells were more sensitive to the diffuse component than were the planar-surfaced cells. The curves also show the significant effect that turbidity has on cell output.

As a compromise between shadowing and ease of fabrication, a view angle of 7° was selected to be incorporated in an advanced ("intermediate") reference cell holder design. As indicated in the figure, this design introduces a maximum error of only a few tenths of a percent, even under extremely turbid conditions. For the interim cell, on the other hand, with a view angle of 23°, errors of several percent are indicated.

The fact that side wall shadowing is negligible does not, by itself, validate the use of a reference cell as a global measurement device. It must also be shown that the cell does not preferentially reflect a

significant portion of the low angle diffuse component. To do this, the sensitivity (cell current per unit incident power density) was measured under both collimated and uncollimated conditions. As can be seen in figure 3, the ratio of the uncollimated sensitivity to the collimated sensitivity for cell Y-1 in a holder with a view angle of 7° is 0.95. This indicates that the cell is selectively reflecting a significant amount of shallow angle light. In an attempt to improve the optical coupling, a number of cells in identical holders were encapsulated in a silicone resin with an intermediate index of refraction ( $n = 1.43$).

The results of the double calibration of a resin encapsulated cell, Y-65, are shown in figure 3. As seen in the figure, the two sensitivities now agree to within one percent, indicating that the encapsulated cell does not preferentially reflect. Cell Y-65, in fact, now appears to be a preferential absorber of shallow angle light. This, of course, cannot be so, the excess current being due to spectral differences between the direct and the total insolation.

It can be concluded, therefore, that the improvement in optical coupling afforded by silicone resin encapsulation is sufficient to remove restrictions to the use of the flat solar cell as a global radiation monitor.

Intermediate Reference Cell

The above features have been incorporated into the design of an updated "intermediate" reference cell holder (figure 4). As seen in the figure the new design incorporates many of the features of the interim design. There are, however, two basic differences: (1) the view angle is reduced from 23° in the interim holder to 7°, (2) the cell is encapsulated in an optically clear silicone resin. These changes enable the intermediate reference cell to be used to measure both direct and total insolation.

## REFERENCE CELL CALIBRATION

### Effect of Atmospheric Variables

The primary function of a reference cell is the measurement of solar intensity. To perform this measurement accurately, the output of the cell must be proportional to the incident power. Changes in the spectral distribution of the incident illumination, however, can produce changes in cell output that are not proportional to the incident power. To avoid error in solar intensity measurements, therefore, the reference cell should always be used under the same spectral conditions under which it was calibrated.

Changes in the terrestrial solar spectrum are brought about by variations in any one of a number of atmospheric parameters: water vapor, ozone, particulates, air mass, oxygen, carbon dioxide, etc. Of these, water vapor has the most influence on solar cell measurements. The variation in calibration factor or sensitivity with atmospheric water vapor content for a typical silicon reference cell is shown in figure 5. A variation of 5 percent is seen as the water vapor content changes from winter conditions (0.5 cm) to summer conditions (3.0 cm) in the midwest. These large variations make it clear that considerable error may be incurred unless care is taken to ensure that the reference cell employed was calibrated under conditions that correspond to the test conditions at hand. The user, therefore, must continuously monitor atmospheric conditions and make timely changes in the reference cell calibration factor (sensitivity). Although, if used properly, this system would provide highly accurate data, it is clear that a simpler method of measuring array efficiency is desirable. Such a method, requiring the use of spectrally matched test and reference cells, is described next.

### The Need for Spectral Response Matching

Measurement procedures can be simplified considerably by using

reference cells that are spectrally matched to the cells being tested. Two cells are spectrally matched if their spectral response curves are in the same proportion to each other at all wavelengths. If the spectral responses of two cells are proportional, the same proportionality holds for their sensitivities as long as they are both illuminated with the same spectrum. As mentioned previously, the sensitivity of a cell depends upon the spectral distribution of the light with which it is illuminated. A change in this distribution will cause a change in the sensitivity. Two cells that are spectrally matched will experience changes in sensitivity with spectrum change, but their sensitivities will always remain in the same proportion to each other. In other words, the ratio of the sensitivities of two matched cells will remain constant regardless of how the spectrum of the incident illumination changes.

To determine the sensitivity of a test cell by means of a matched reference cell, all that must be known is the constant of proportionality between the sensitivities of the two cells. Since this constant remains unchanged regardless of spectral changes, the appropriate measurements can be made under an arbitrary light source. The required test cell sensitivity can then be computed using this factor and the reference cell sensitivity.

In the special case where the reference and test cells are perfectly matched, i.e., unit proportionality constant, no measurement is needed. In this case, since the two cells are identical, the sensitivity of the test cell is equal to the sensitivity (calibration factor) of the reference cell.

In the more general case where the cells are spectrally matched but not identical, the constant of proportionality between the sensitivities must be found by measurement. The product of this constant with the reference cell sensitivity (calibration factor) will then yield the sensitivity of the test cell.

Let us consider, for example, two spectrally matched cells, one of which has been calibrated against a black body under atmospheric conditions, A. The proportionality constant between the reference and the test cell sensitivities can be found by measuring the short circuit currents of both cells under an arbitrary set of atmospheric conditions, B. If $I_R$ and $I_T$ are the reference and test cell short circuit currents and P is the solar intensity, all under atmospheric conditions, B, then the sensitivities of the test and reference cells are, respectively, $I_T/P$ and $I_R/P$. Taking the ratio of these senstivities we find that the proportionality factor is $I_T/I_R$, the ratio of the short circuit currents. The product of this factor, then, with the reference cell sensitivity yields the test cell sensitivity under atmospheric conditions, A.

Thus, the use of spectrally matched cells permits sensitivity measurements to be made without regard to the solar spectrum or concern about the selection of a calibration factor to match spectral conditions.

Although the measurements described here are simple and straightforward, they are based on the assumption that the reference and test cells are spectrally matched. In reality, however, matching may not be completely achieved. To get a rough indication of the error introduced by the use of a reference cell that is not spectrally matched to the cell being tested, a computer analysis was performed on three cells, the spectral responses of which are shown in figure 6. As seen in the figure there is some mismatch in the spectral responses of these cells. If the sensitivity ratios between these cells were established under one set of atmospheric conditions, say AM1, then any deviation in the solar spectrum from AM1 conditions should cause a deviation in the ratios such that if one of the cells were used as a reference to provide measurements on the other two, errors in the measured sensitivities for the two test cells

would result. To quantize these errors, the sensitivities of the three cells were calculated under both AM1 and AM3 conditions using insolation data computed from the extraterrestrial spectrum.[2] The atmospheric conditions assumed in the calculations were: water vapor, 2 cm; ozone, 0.34 cm; turbidity parameters, $\alpha$ = 1.3, B = 0.04. If the cells were spectrally matched they should respond identically to the spectral changes incurred in going from AM1 to AM3, i.e., the ratio of sensitivities at AM3 should be the same as that at AM1. Because the cells are not matched, however, we should find deviations in the sensitivity ratios. These deviations can be interpreted directly as a measurement error if one of the cells were used as a reference to provide sensitivity measurements on the others.

Before discussing the results of the calculations, it would be appropriate to devise a convenient way of indicating the degree of mismatch in the spectral response curves. One way to do this is to calculate the average fractional difference (AFD) between the curves. This factor can be arrived at as follows. First, each of the two sets of spectral response data to be compared is normalized to an arbitrary data point in the set, such as the 0.7$\mu$m response point. This normalization removes any absolute differences in the curves. Next, the two normalized data sets are compared with each other, point for point, and the fractional difference found for each point. The absolute values of the fractional differences are then averaged over the nine points. The resulting factor (AFD) can then be used to characterize the closeness of the spectral match.

Let us return now to the results of the sensitivity calculations. The results are shown in figure 7 where deviations in the sensitivity ratio, i.e., measurement error , are compared with the corresponding mismatch parameter, the AFD. In comparing cell 1 with cell 2 (AFD = 0.1)

we find that a measurement error of 0.4% is expected. A comparison of cells 1 and 3 with a larger mismatch (AFD = 0.24) indicates a 1% error for the same spectral change. Bearing in mind that these calculations are merely illustrative and reflect the conditions of this particular example, we see that in this case the AFD must be kept below about 0.12 if measurement error is to be less than 0.5% for an AM1 to AM3 spectral change.

## SPECTRAL RESPONSE MATCHING

### The Red/Blue Ratio Technique

The requirement that there be a close spectral response match between the reference cell and the solar panels being tested has been established. Since the spectral response of a module or other large area device cannot be measured by conventional methods, an alternate technique must be used. To this end, a technique making use of a large area pulsed simulator and a pair of optical filters is being used. The filters were chosen to examine cell response to both the red and blue ends of the spectrum. Transmission curves for the filters used at this laboratory are shown in figure 8. The test cell short circuit current is measured under both red and blue filtered conditions. The ratio $I_{sc}$ (red)/$I_{sc}$ (blue) is then used to characterize the cell spectrally.

The details of the technique can be explained with the aid of figure 9. The first step is the calibration of a monitor cell with a standard reference cell (figure 9a). The two cells are placed on the test plane of the pulsed simulator. One of the filters is placed over the monitor cell and the cells are illuminated, the reference cell ensuring an intensity of 100 mW/cm$^2$ incident on the filter. The monitor cell is then used as in figure 9b to ensure 100 mW/cm$^2$ on the face of the filter when both the monitor and the test cell or array are exposed to filtered light. The process is repeated for both filters.

The ratio of test cell short circuit current under red filtered conditions to that under blue filtering, termed the red/blue (R/B) ratio, is then used as the basis for spectral comparison.

The relationship of the R/B ratio of an entire module to the R/B ratios of the cells in that module is presented schematically in figure 10. The R/B ratio of each of the cells in the module was measured along with that of the module itself. As indicated in the figure, the R/B ratio of the entire module is very close to the average cell R/B ratio.

Comparison with Multipoint Spectral Response Data

The question that presents itself at this point is whether or not the two point R/B ratio technique can be used to replace the nine point spectral response method without a significant loss of spectral information.

If such a substitution were possible, we should be able to show that, when two cells or modules are compared and found to be spectrally matched on the basis of their R/B ratios, agreement will be found also in the nine-point spectral response data. Since there are many different spectral response curve shapes that will yield the same R/B ratio,agreement between the two systems is not assured. We must rely, unfortunately, on empirical information gained from measurements on real cells.

To evaluate the degree of correlation that exists between the two methods, both R/B ratio and multipoint spectral response measurements were performed on a group of 100 cells, 25 from each of four manufacturers. For each set a reference cell was chosen and each of the other cells in the set compared to it. Plots of the AFD vs the fractional difference in the R/B ratio are given in figures 11 to 14. While there is some scatter in

the data, there appears to be a reasonable correlation in each case. Extrapolating the data to zero R/B ratio mismatch, it can be seen that a maximum AFD of about 0.04 is expected for the cases considered here. According to figure 7 , an AFD of 0.04 would result in a measurement error of only a few tenths of a percent for an AM1 to AM3 spectrum change.

If we now consider cross-manufacturer comparisons, problems arise. The results of comparing the set of Sensor Technology cells with a Solarex reference cell are shown in figure 15, where the curves from figures 11 to 14 are included for reference. As indicated by the extrapolation to zero R/B ratio mismatch, an AFD of 0.2 is expected. Referring again to figure 7 , we see that in this case, even with perfect R/B ratio matching, a measurement error approaching 1% is to be expected.

The conclusion that can be drawn from these limited data, therefore, is that the R/B ratio technique may be used to match cells and arrays if one is comparing devices from the same manufacturer. Cross-company comparisons, on the other hand, may lead to significant error.

## SUMMARY OF RESULTS

The results of the preceding paragraphs can be summarized as follows:

(1) It was shown that both the geometry of the cell holder and the optical coupling between the cell and its environment are critical in determining the feasibility of using the flat solar cell as a global insolation measurement device. The design of a reference cell holder that can be used to measure total insolation is presented.

(2) Reference cell calibration was shown to be very sensitive to the spectral variations caused by water vapor and other atmospheric constituents. This sensitivity introduces severe complications into solar cell array testing procedures. The procedures can be greatly simplified if the spectral response of the reference cell used is

closely matched to the spectral response of the array being tested.

(3) A technique is described whereby spectral information is obtained from large area arrays enabling them to be spectrally matched to reference solar cells. The technique involves the use of two broad-band optical filters and a large area pulsed simulator. The results of measurements on a large-number of cells and arrays indicate that as long as spectral comparisons are restricted to devices produced by the same manufacturer, the technique provides valid spectral characterization. Intercompany comparisons, however, have been shown to introduce error.

## REFERENCES


1. Schuepp, W.: Arc. Meteor. Geophys. Bioklim. B1 257 (1949).
2. Thekaekara, M. P.: Conference Proceedings, COMPLES, Dahran, Saudi Arabia, Nov. 1975.

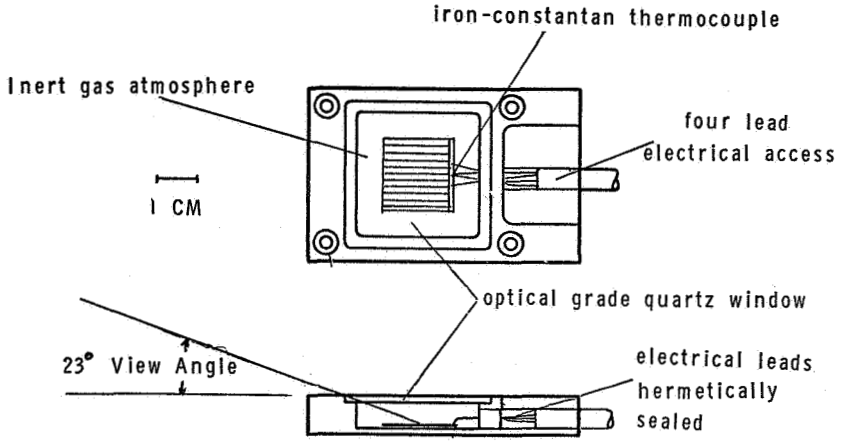


Figure 1. - Interim reference cell

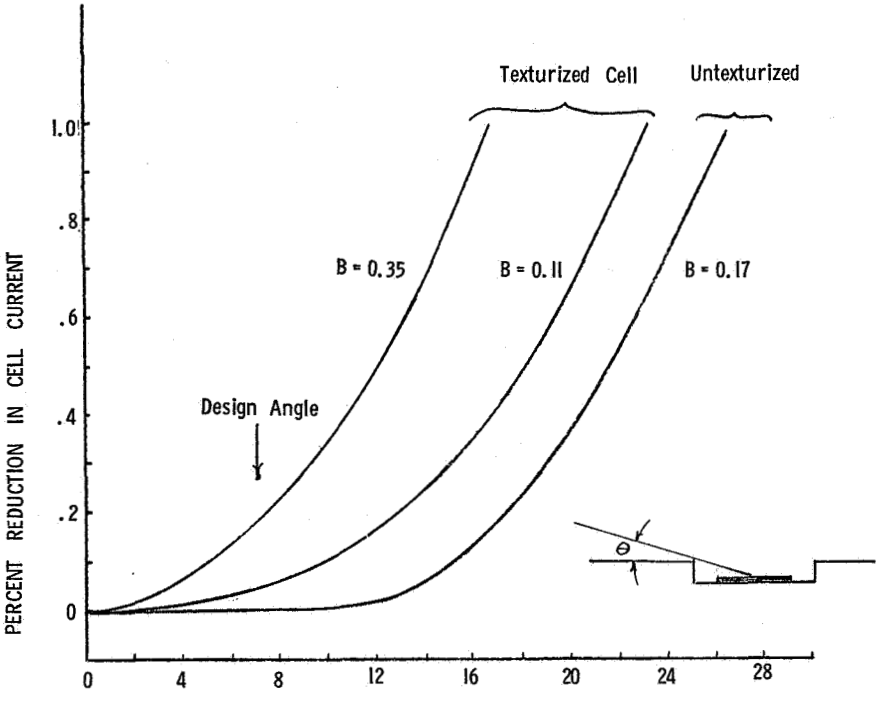


Figure 2. - Reduction in cell current due to side-wall shadowing

| | UNCOLLIMATED CAL. FACTOR* | COLLIMATED CAL. FACTOR* | UNCOLLIMATED C. F. / COLLIMATED C. F. |
|---|---|---|---|
| CELL Y1 INERT GAS | 1.031 | 1.090 | .95 |
| CELL Y-56 SILICONE RESIN | 1.202 | 1.185 | 1.01 |

* $\frac{MA}{MW/CM^2}$

Figure 3. - Comparison of calibration factor measured under collimated and uncollimated conditions

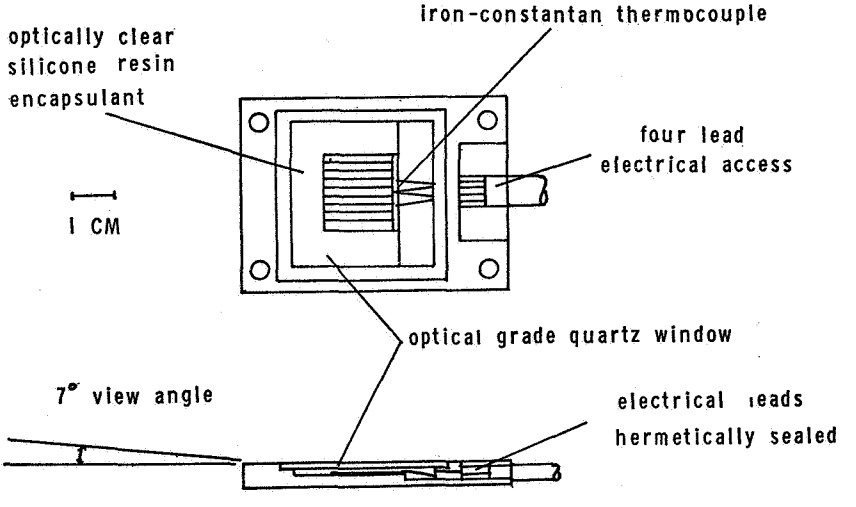


Figure 4. - Intermediate reference cell

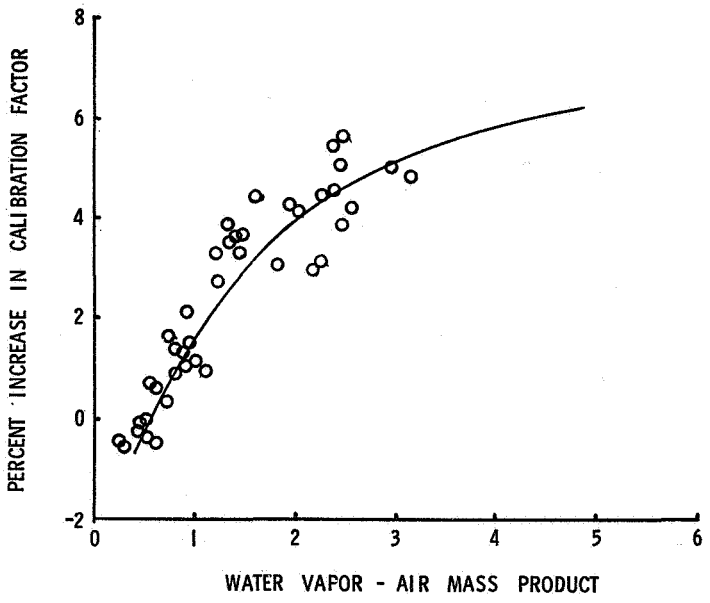


Figure 5. - Effect of water vapor on the calibration factor.

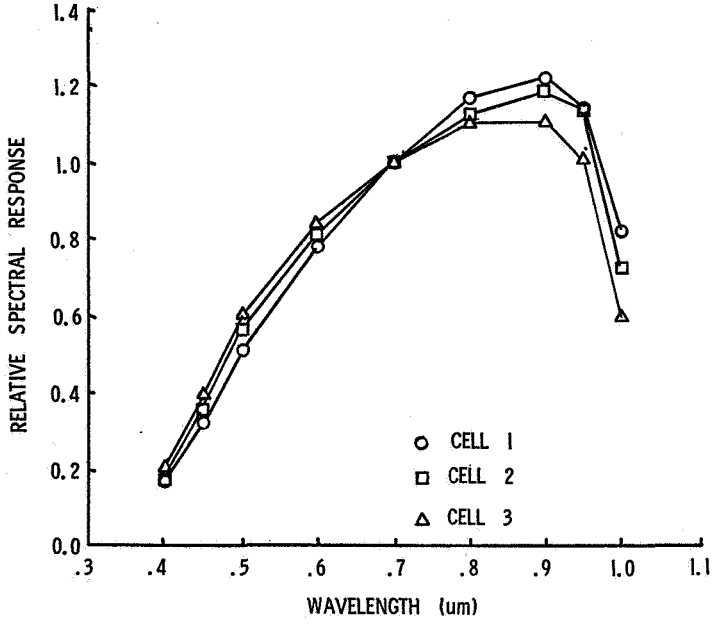


Figure 6. - Relative spectral responses of unmatched cells

| REFERENCE CELL | TEST CELL | AFD | MEASUREMENT ERROR AM1 --> AM3 |
|---|---|---|---|
| 1 | 2 | 0.10 | 0.4% |
| 1 | 3 | 0.24 | 1.0% |

Figure 7. - Measurement errors due to spectral mismatch

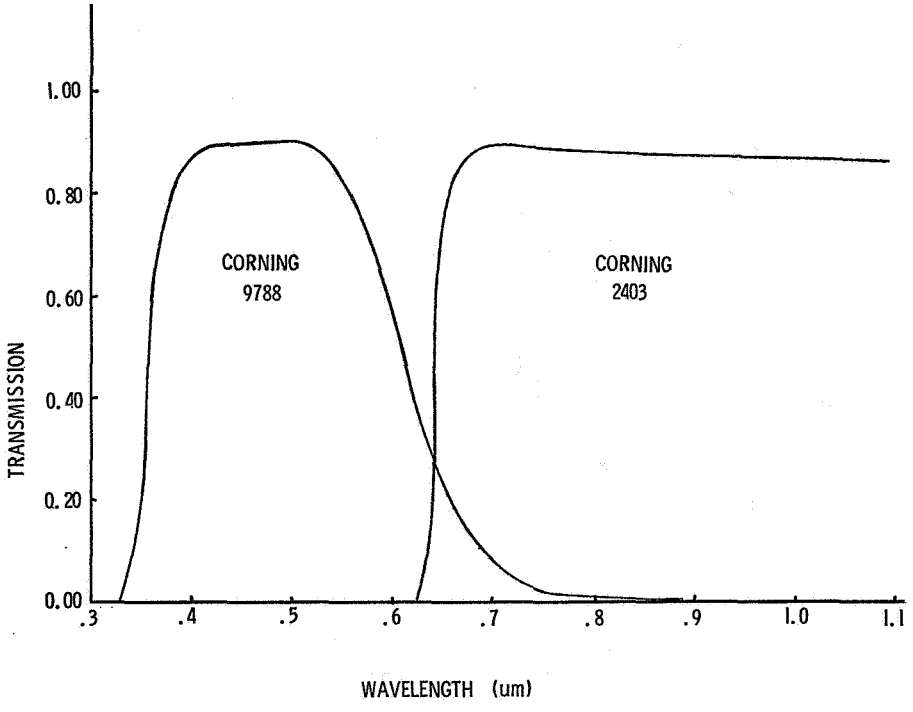


Figure 8. - Transmission curves for broad-band filters

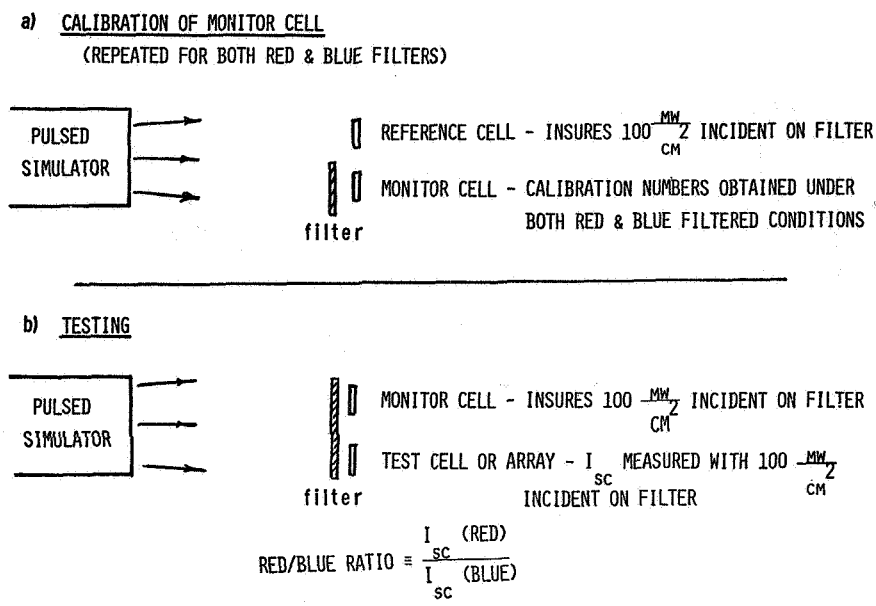


Figure 9. - Schematic diagram illustrating the red/blue ratio measurement technique

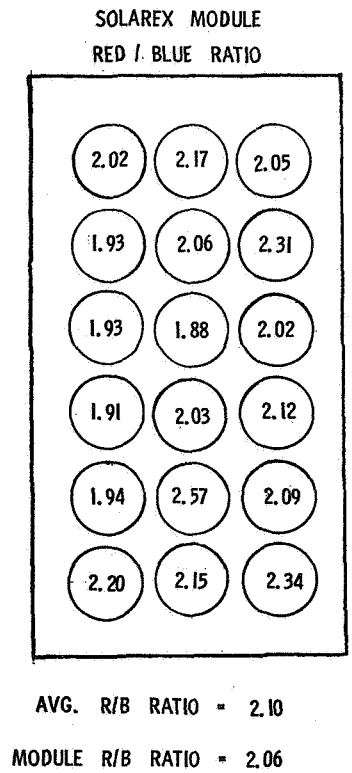


Figure 10. - Red/blue ratios of individual cells in a module

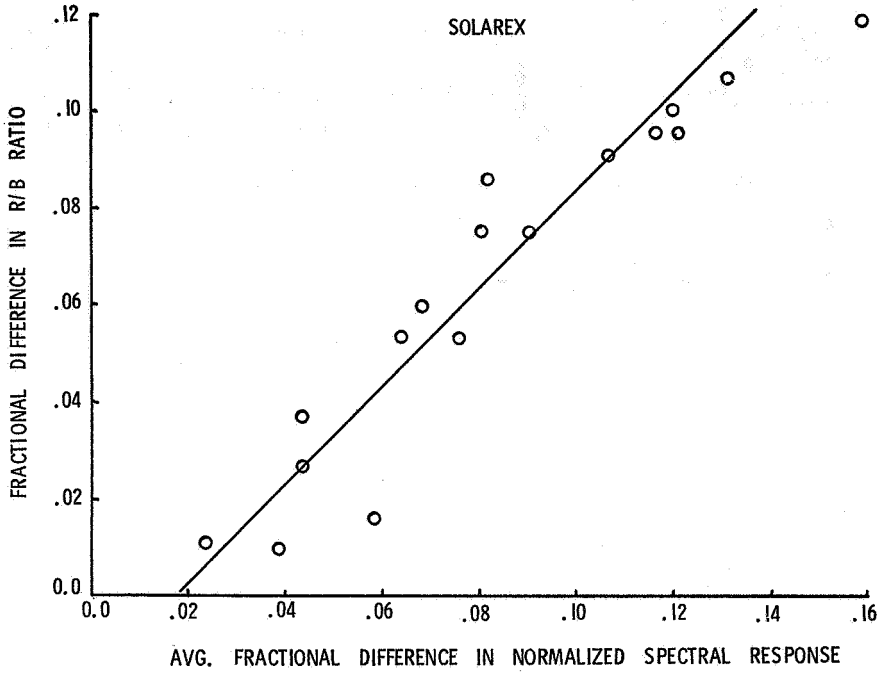


Figure 11. - Red/blue ratio, spectral response correlation for Solarex cells

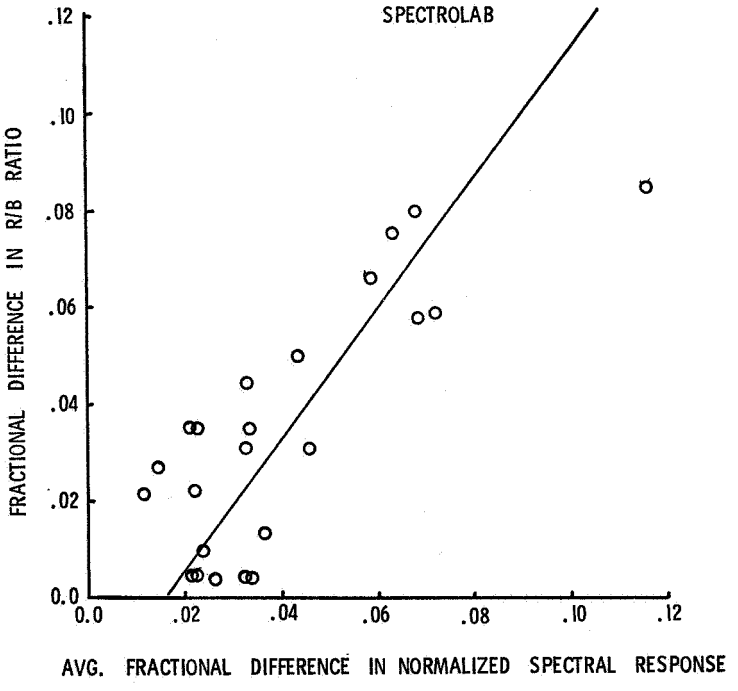


Figure 12. - Red/blue ratio, spectral response correlation for Spectrolab cells

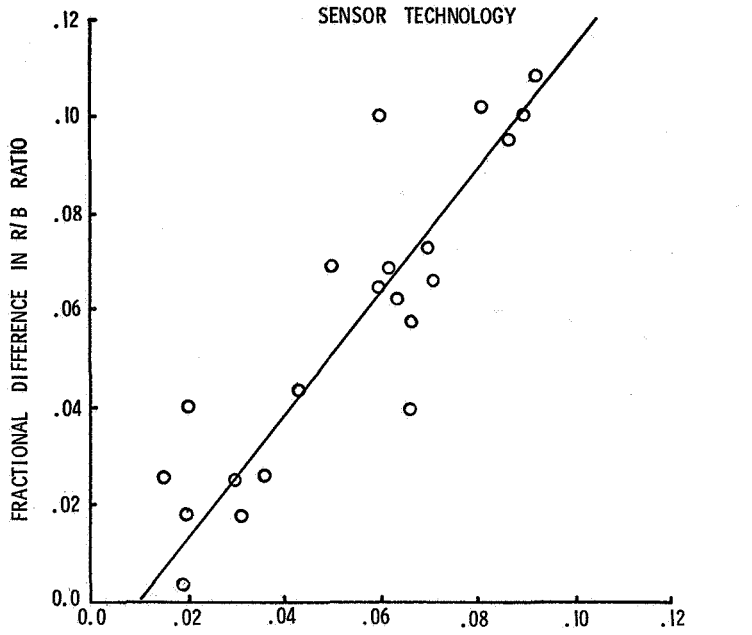


Figure 13. - Red/blue ratio, spectral response correlation for Sensor Technology cells

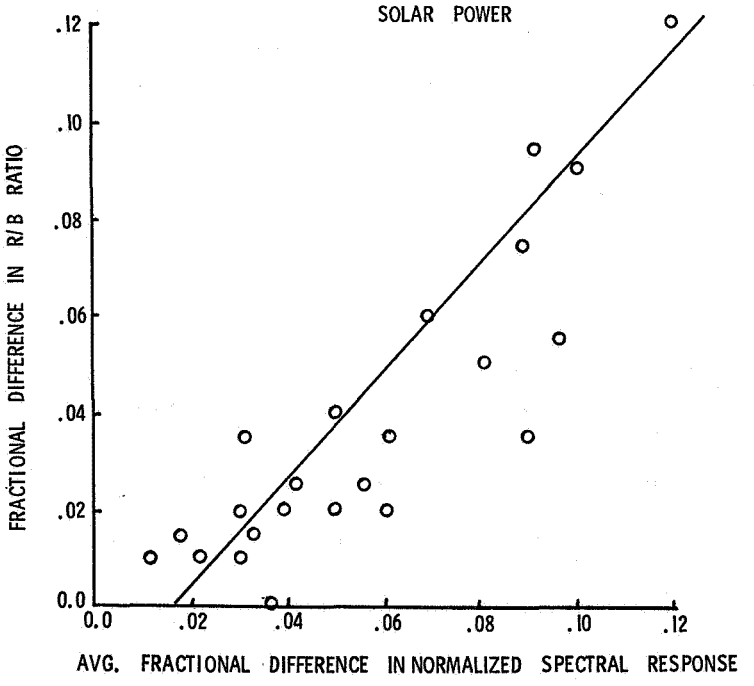


Figure 14. - Red / blue ratio, spectral response correlation for Solar Power cells

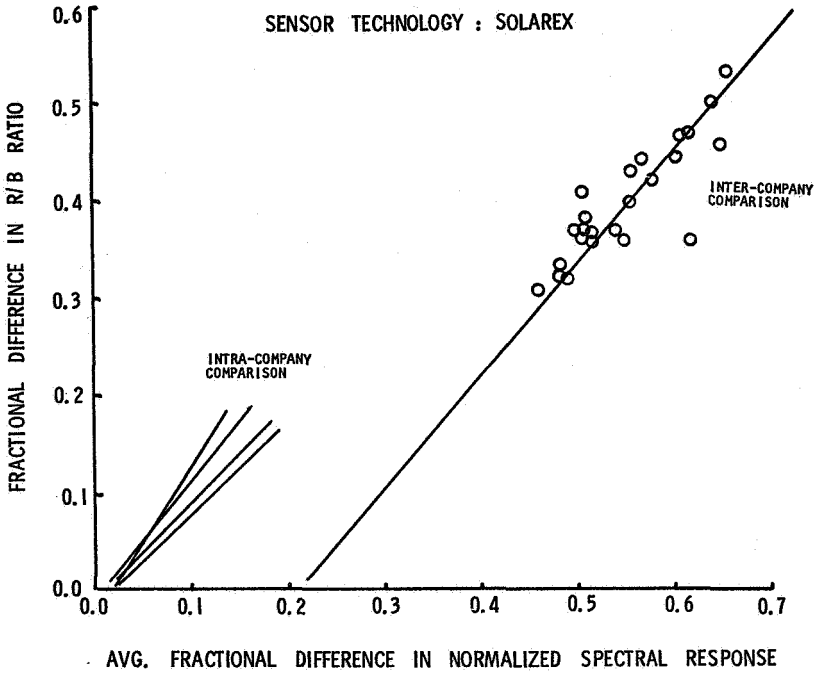


Figure 15. - Red/blue ratio, spectral response correlation for Sensor Technology cells compared with a Solarex reference

# A LASER BASED CHARACTERIZATION FACILITY FOR SILICON PHOTOCELL STUDIES

Jon Geist, Michael A. Lind, A. Russell Schaefer, and Edward F. Zalewski
National Bureau of Standards
Washington, D. C. 20234

Since the last workshop, we have constructed a computer-controlled, laser-based characterization facility. We have been using this facility for detailed studies of silicon photodetectors, and most recently for preliminary spectral response measurements on a few silicon solar cells. Moreover, the facility plays a major role in our study of the new approach to radiometry[1][1]

For most radiometric purposes, cw lasers approximate delta functions in wavelength, position, direction, and polarization. This greatly simplifies precise characterization of optical instruments with respect to variations of these parameters. Computer control assists these characterizations as well as those with respect to time, temperature, power level and power density. The power in the laser beam is measured with respect to electrical standards using an electrically calibrated pyroelectric radiometer.[2] The combination of laser facility and the radiometer is synergistic, since the facility is used to determine the equivalence of the radiometer's response to radiant and electrical power.

Our facility is modular, providing flexibility for growth, as well as for a variety of characterization activities. This flexibility has also proven useful in support of other activities that require accurately known quantities of monochromatic power. Figure 1 is a schematic diagram of the present configuration of the facility. It is set up on a 4' x 18' rigid-honeycomb, optical table made from three 4' x 6' sections. The top of the table is ¼" thick magnetic steel with tapped ¼-20 mounting holes on 1" centers.

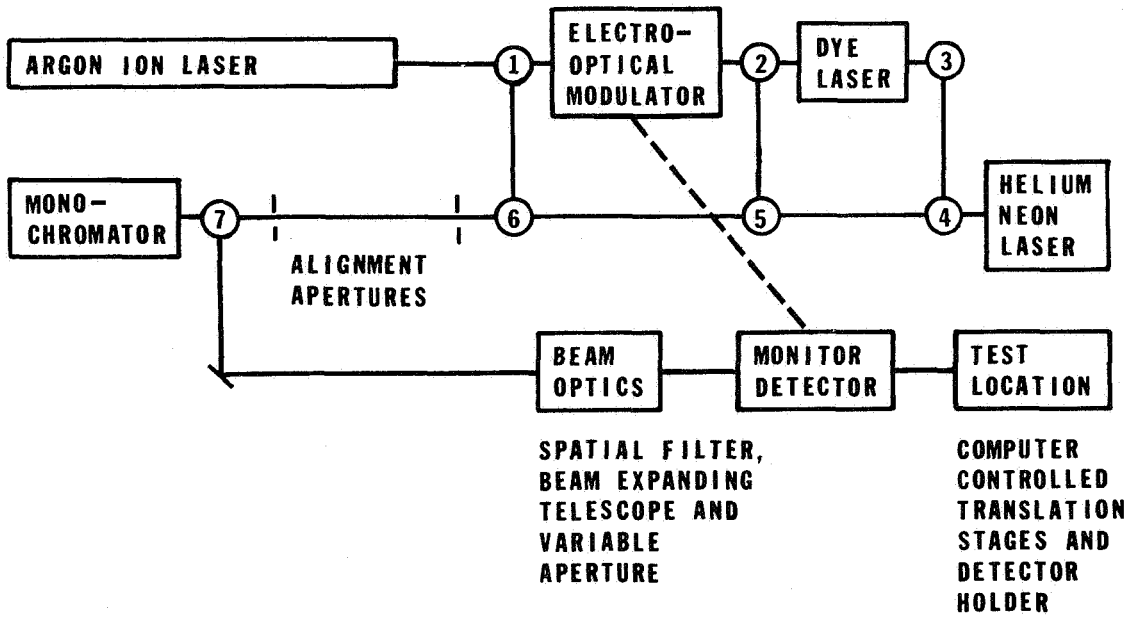


Fig. 1: Block diagram of the laser-based radiometric characterization facility.

[1]Figures in brackets indicate the literature references at the end of this paper.

The numbered circles in Fig. 1 represent kinematically mounted mirrors that permit removal and simple realignment. The alignment apertures have proven useful for preliminary alignment of the test beam from the different radiation sources. By suitable placement of the appropriate mirrors it is possible to direct the argon-ion laser radiation into either the test beam, the spectrometer for wavelength calibration, or the dye laser where it pumps a jet of fluorescent dye which in turn lases. The dye laser beam can be directed into the test beam or into the spectrometer for calibration of the dye laser wavelength scale. Similarly, it is possible to direct the HeNe laser beam into the test beam or into the spectrometer.

The power in the test beam is stabilized using an electro-optic modulator (EOM) in a feedback loop[3]. Part of the radiation in the test beam is split off via a reflection from a wedged quartz beamsplitter. This radiation is directed onto a diffuser covering the active area of a uv-stable silicon photodiode. Both the beamsplitter and the diode are mounted in a temperature controlled housing shown in Fig. 2. The temperature of the housing is maintained at a few degrees above ambient to within ±0.1 C using the simple thermistor controlled DC power amplifier shown schematically in Fig. 3.

The output from the silicon photodiode is amplified in a high gain DC servo amplifier illustrated in Fig. 4. The output of the current to voltage converter on the input stage of this amplifier is fed into an adjustable lag-lead compensation network and also to a buffer amplifier which can be used to monitor the silicon detector. The output of the compensation amplifier feeds one junction of a X100 summing amplifier. The other junctions allow for the injection of both an offset bias which is used to control the DC power level of the test beam and an external auxiliary signal. The auxiliary input is needed for such functions as stable sinusoidal modulation, etc. The X100 amplifier feeds another X1000 amplifier for additional DC gain. This signal is then used to drive a X10 high voltage amplifier which in turn provides the necessary 240 volt P-P half wave voltage for the electro-optical modulator.

The modulator itself is a 45° X cut ADP crystal mounted in an index matching fluid enclosed in an aluminum housing for thermal stability. The modulator is capable of handling optical powers up to 6 watts in the 300 to 800 nm spectral range. In practice we have used the device to stabilize lines from 257 nm to 1.09 μm.

Depending upon the source and wavelength of the laser radiation, beam power stabilities of 0.1% to 0.01% have been obtained within a dc to 5 kHz bandwidth with the system described above. By using faster amplifiers it is possible to extend the bandwidth to several MHz with only a small degradation of performance.

The spatial filter, beam expanding telescope and variable aperture in Fig. 1 are used to "clean up" the laser beam, and to select the uniform central region of gaussian and/or diffraction limited beam patterns (with consequent reduction of beam power) for applications requiring a relatively uniform beam. The computer controlled translation stages are used to investigate the angular and spatial sensitivity of detectors, optical elements and instruments of moderate size. A temperature-controlled detector holder attached to the translation stages allows the investigation of the sensitivity of various parameters to small temperature variations above ambient. The present wavelength coverage of the facility is shown in Fig. 5. Also shown there is the wavelength range to which we hope to expand the facility in the near future.

An example illustrating the application of this facility to linearity measurements may be of interest to the solar photovoltaic community, since it is similar to the AC-DC light bias spectral response technique. Here a well collimated stable beam of light is split into two parts with a low reflectance beamsplitter. The main beam is passed through a variable attenuator. Notice that it is not important that the attenuator be well characterized as it must be in other linearity techniques. The low power beam is chopped to make up the AC component. Both beams are then recombined on the test detector.

In practice the dynamic range and linearity of the current amplifier limit the ratio of $\Delta P/P$ to about 0.01. Thus, the variable attenuator need have only two decades of attenuation. This does not impose any fundamental limitations on the technique, however, since the main beam can also be attenuated and overlapping measurements made one decade at a time.

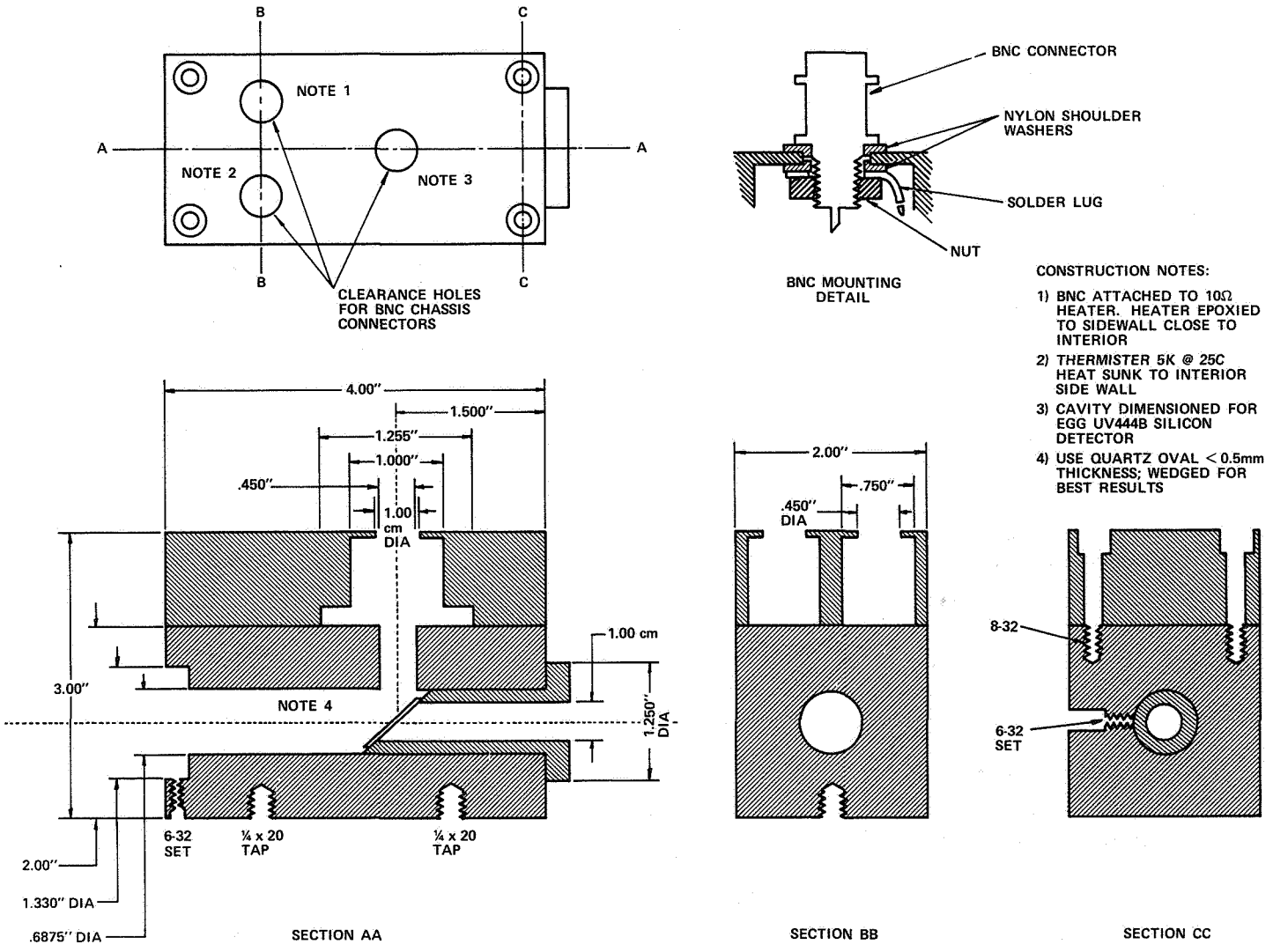


Fig. 2: Beam splitter and temperature controlled detector housing.

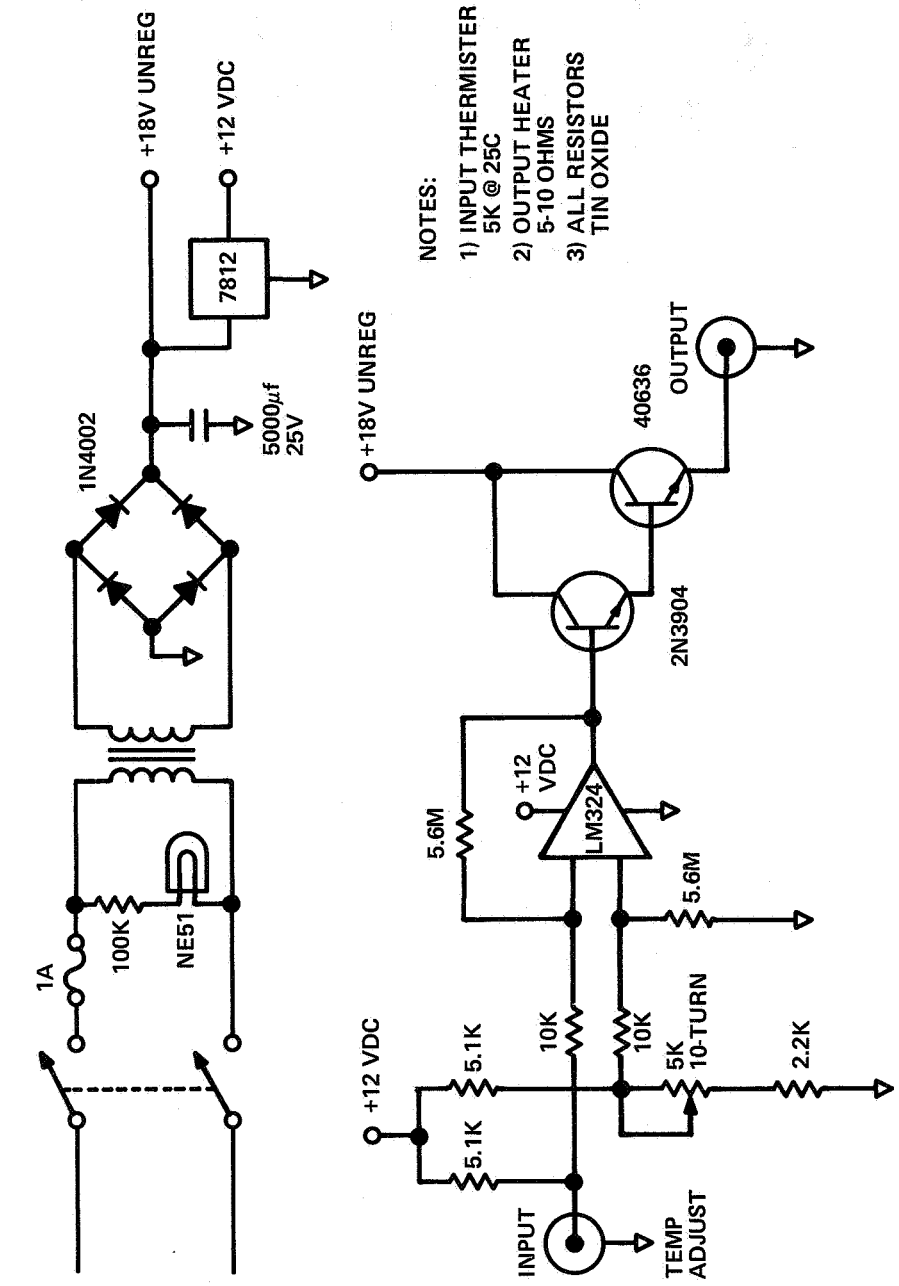


Fig. 3: Temperature controller.

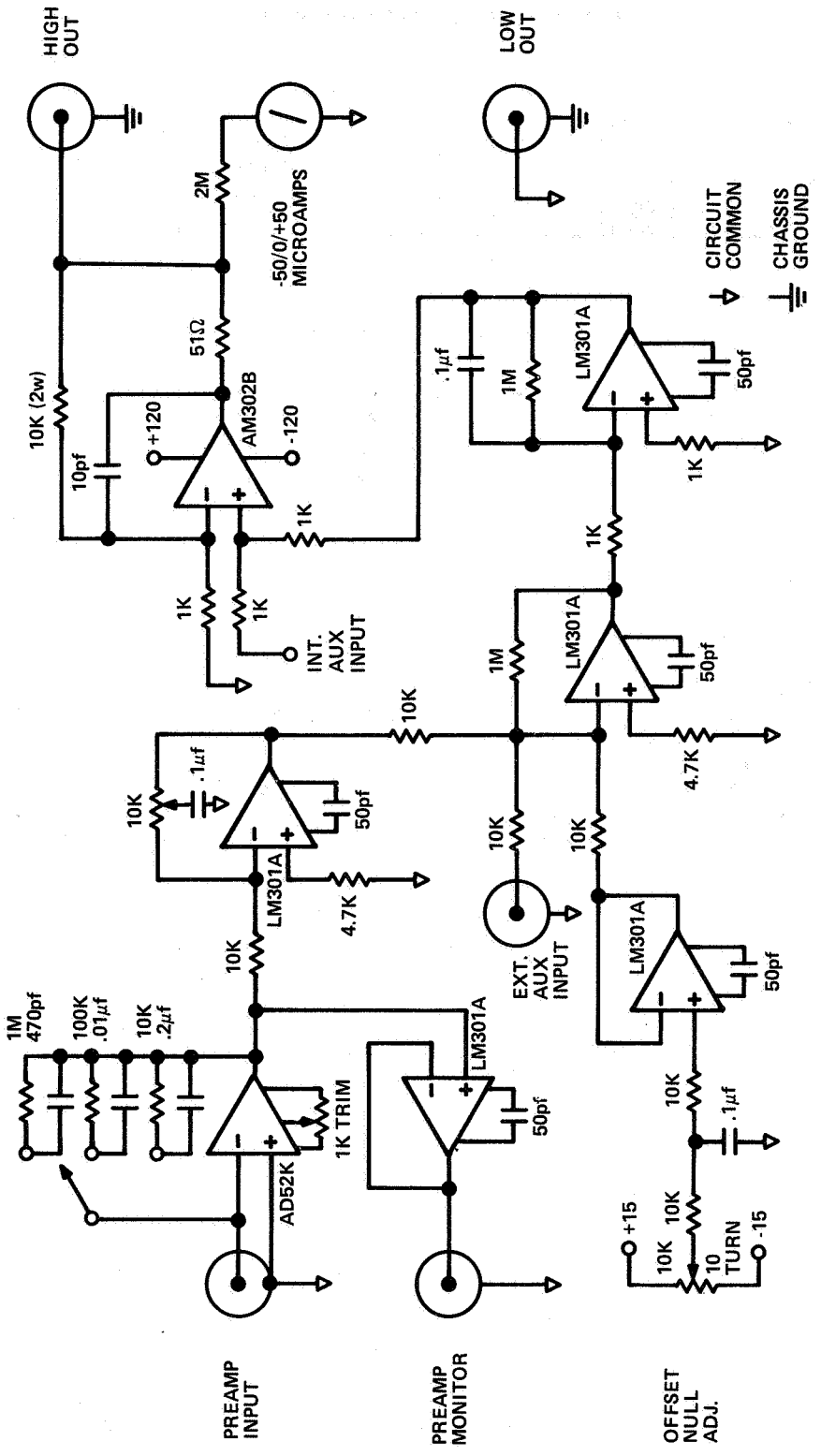


Fig. 4: Laser beam power stabilization servo-amplifier.

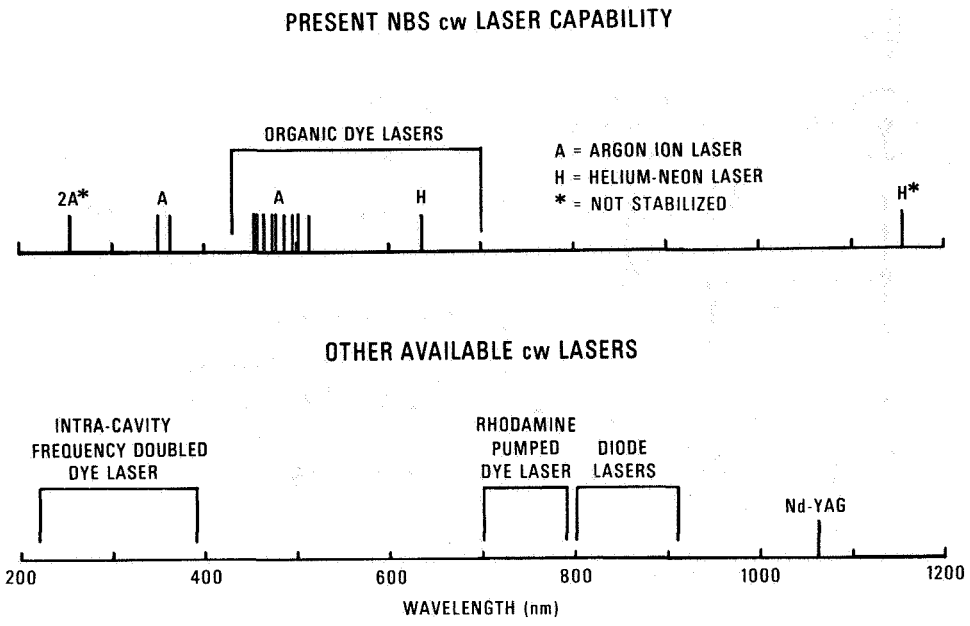


Fig. 5: Present and future wavelength capability of the laser-based characterization facility.

Using this technique we have been able to map the linearity functions of silicon diodes over 7 decades. In addition, because of the simplicity of the technique and its freedom from geometrical constraints we have actually been able to measure the spatial linearity of some silicon detectors. The map of one such detector is shown below. The data were taken at nine points on the detector using a uniform 1 mm diameter beam scanned in a 2 mm grid across the surface of the detector. Here the numbers represent the percent deviation of the differential responsivity between the indicated power densities,

$$\frac{r_H}{r_L} - 1 \times 100 \qquad (1)$$

| | | | |
|---|---|---|---|
| -1.52 | -2.34 | -3.75 | $P_H$ = 20 mW/cm$^2$ |
| -2.11 | -2.85 | -3.88 | $P_L$ = 2.0 mW/cm$^2$ |
| -2.32 | -3.16 | -3.83 | ERROR ± 0.10 |
| -0.29 | -0.28 | -0.28 | $P_H$ = 200 μW/cm$^2$ |
| -0.28 | -0.27 | -0.29 | $P_L$ = 20 μW/cm$^2$ |
| -0.27 | -0.28 | -0.28 | ERROR ± 0.03 |
| -0.03 | -0.12 | -0.11 | $P_H$ = 2.0 μW/cm$^2$ |
| -0.07 | -0.14 | -0.09 | $P_L$ 200 nW/cm$^2$ |
| -0.15 | -0.11 | -0.13 | ERROR ± 0.03 |

The error that is given represents the three standard deviation precision of the measurement. Notice that this particular detector is well into the saturation region at an incident power density of 20 mW/cm$^2$. Notice that certain areas of the cell tend to saturate sooner than others.

Another example is the recently observed[4] enhancement of spectral response of certain types of silicon pn photodiodes by exposure to near ultraviolet radiation. In this study, a 2 mm diameter area of the detector surface was irradiated by a reasonably uniform laser beam at 364 nm with an average incident power density of 4 $mW/cm^2$. The responsivity of this area increased about 25% during the course of one hour, as shown in Fig. 6. When beams of

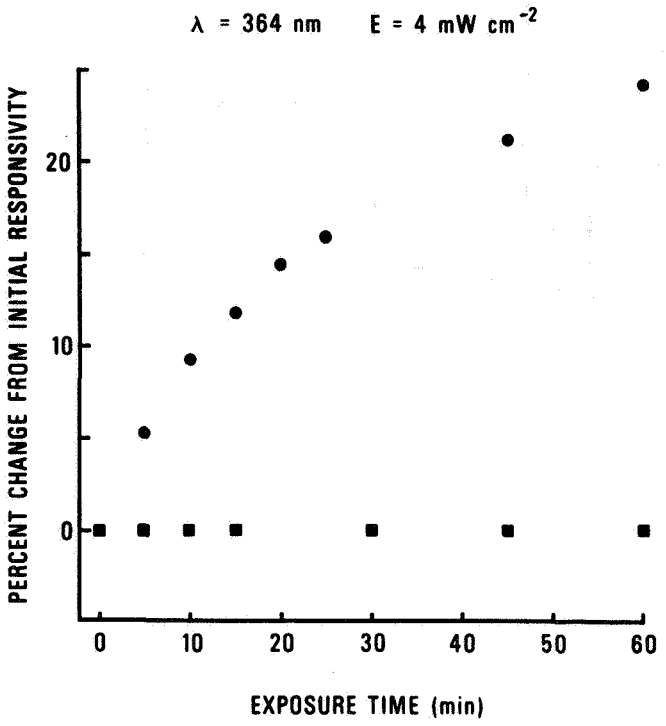


Fig. 6: Response of 2 mm diameter area on the surface of a silicon cell as a function of time of irradiation with a 2 mm diameter beam of 4 $mW/cm^2$ power density and 364 nm wavelength compared to the response of an unirradiated area.

other wavelengths were scanned across the detector surface, the enhancement of the response at the "burned in" spot was very evident, even at 633 nm as shown in Fig. 7. This enhanced responsivity decreased back to normal over a period of several days.

Several possible explanations of the enhancement effect have been investigated experimentally. The results presented in detail elsewhere[5], will be discussed briefly here. A probable explanation of the effect lies in the presence of extra available energy states due to crystalline discontinuities and impurities trapped near the surface of the detector. One simple model that was considered postulates an impurity material near the detector surface which possesses an intermediate metastable state that can only be populated by incident ultraviolet photons. Electrons in this intermediate state could then be further excited into the conduction band by absorption of other ultraviolet or visible photons. These additional carriers would result in an enhanced responsivity until the intermediate levels were depleted.

In a mechanism of this type, one should be able to depopulate the metastable state by irradiating the enhanced area with visible light. Experiments were performed in which the relative response of an enhanced detector was recorded as a function of time. This was done first with the detector in the dark, except for brief responsivity measurements, and then with the detector irradiated with visible light. These measurements were performed at a variety of wavelengths from 405 nm to 633 nm. In no case was the enhancement seen to decrease

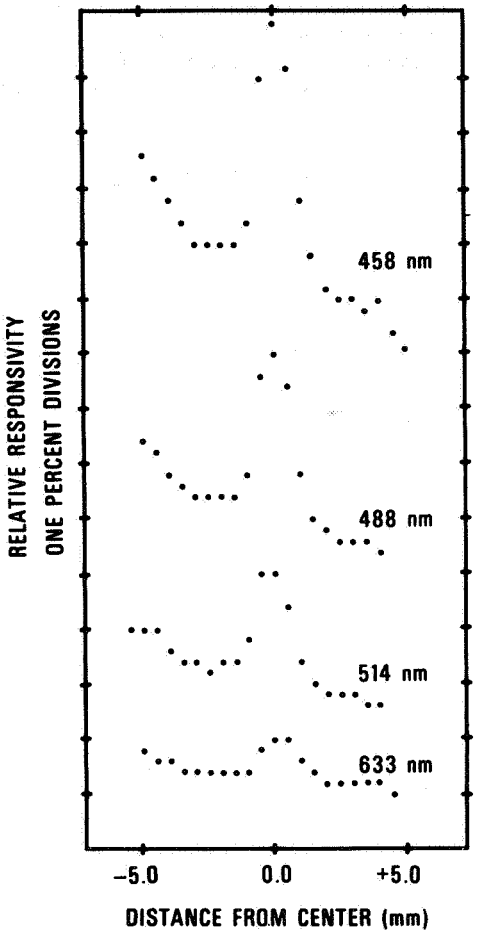


Fig. 7: Relative responses of the cell of figure 6 for different incident wavelengths as a function of position across a diameter passing through the area that was irradiated with 364 nm wavelength radiation.

with a time constant different from the approximate three hour time constant observed in the dark. This result rules out this simple model.

Another possibility considered was that, due to some physical phenomenon in the detector surface, the reflectance of the ultraviolet irradiated area would decrease, resulting in an increased number of photons absorbed and an apparent increased responsivity. To check this hypothesis, one of the new type of ultraviolet stable detectors was employed. This stable detector was irradiated with ultraviolet radiation to ascertain that it did indeed show no enhancement effect. The stable detector was then used to measure the reflectance of the test detector as a function of time while it was being irradiated with 3 $mW/cm^2$ of 334 nm radiation, and again using 0.4 $mW/cm^2$ of 254 nm radiation. Although a response enhancement of 25% was observed, no change in the reflectance of the detector surface was observed.

Other possible models have been proposed to explain this effect. In one such mechanism, surface or impurity states between the conduction and valence bands are affecting the apparent quantum efficiency by trapping photon generated carriers. Electrons trapped in these extra states, together with the positive ions left behind, alter the potential barrier in the surface region, as well as other parameters such as conductivity and recombination rate. The

spectral response of the detector is thus directly related to surface state availablility and population. More detailed experimentation would be required to isolate the specific mechanism involved in the enhancement effect. Perhaps the ultraviolet photons ionize a sufficient number of impurity atoms to result in a significant depopulation of the surface states, causing an increased detector efficiency due to the reduced surface energy barrier. The response could then be observed to slowly decrease again in the dark, as the impurity induced states once again trapped electrons and the detector returns to its former condition.

## REFERENCES


1. Jon Geist, Modern Radiometry for Photovoltaic Solar Conversion, Terrestrial Photovoltaic Measurements Workshop Proceedings, 67, March 19-21, 1975, NASA TMX-71802.

2. R. J. Phelan and A. R. Cook, Appl. Opt. 12, 2494 (1973);
   J. Geist and W. R. Blevin, Appl. Opt. 12, 2532 (1973);
   W. M. Doyle, B. C. McIntosh and Jon Geist, Proceedings Soc. Phot. Opt. Inst. Eng. 62, 166 (1975).

3. R. L. Barger, M. S. Sorem and J. L. Hall, Appl. Phys. Lett. 22, 573 (1973) and R. L. Barger, J. B. West and T. C. English, Appl. Phys. Lett. 27, 31 (1975).

4. M. Lind and E. Zalewski, Appl. Opt. 15, 1377 (1976).

5. A. R. Schaefer, to be published.

# SOME BASIC CONSIDERATIONS OF MEASUREMENTS INVOLVING COLLIMATED DIRECT SUNLIGHT

by An-Ti Chai

Lewis Research Center
National Aeronautics and Space Administration
Cleveland, Ohio

## ABSTRACT

The geometry of collimators for devices or instruments dealing with terrestrial direct sunlight is discussed. Effects of the opening angle and slope angle of a collimator on the measurements are investigated with regard to variations of turbidity and air mass. Based on this investigation, geometric dimensions for collimators and certain realistic terrestrial reference conditions are recommended for the purpose of solar cell calibration in terrestrial applications.

## SUMMARY

The geometry of collimators for devices or instruments dealing with terrestrial direct sunlight is discussed. Effects of the opening angle and slope angle of a collimator on the measurements are investigated with regard to variations of atmospheric turbidity and air mass. It is pointed out that the slope angle should be specified after considering the collimator size and the tracking capability of the instrument. The size of opening angle affects the amount of circumsolar radiation and skylight entering a collimator and the uniformity of illumination at the receiving aperture. Based on this analysis, an opening angle in the range of 2.5-3°, which is equivalent to a 10 to 1 collimation ratio, with a slope angle between 1° and 1.76° should be appropriate for the purpose of solar cell

calibration in terrestrial applications.

The reference conditions, specifically the air mass and atmospheric turbidity for solar cell calibration are also discussed. It is recommended that the product of air mass and turbidity parameter be restricted to no greater than 0.25 to avoid excessive nonuniformity of illumination at the receiving aperture of a collimator.

## INTRODUCTION

Owing to the technical difficulty in obtaining full knowledge of the relationship between the global solar irradiance and general atmospheric conditions, it has been a general consensus that solar cell calibration under natural sunlight should be done under collimated direct sunlight (ref. 1). In doing so, one is rid of the complication of the general sky conditions, most prominently the cloud effects; however, one is confronted with a new problem - how to construct a proper collimator.

The Joint International Radiation Conference at Davos in 1956 adopted recommendations with regard to the construction of collimators used on pyrheliometers (refs. 2 and 3). Unfortunately, these recommendations may not be universally practiced. The solar cell community, for example, has not strictly followed these recommendations. In a report entitled, "Interim Solar Cell Test Procedures for Terrestrial Applications" (ISCTPTA), which was issued in July 1975, (ref. 1) guidelines on the requirement of collimation and reference conditions were presented for calibration of standard cells. These guidelines do not appear to adequately cover the requirements of collimators in certain realistic circumstances. This paper is intended to clarify some of the confusions associated with these requirements and

to develop requirements for collimators for solar cell measurements.

## BASIC CONSIDERATIONS IN COLLIMATOR DESIGN

There are three angles associated with the aperture conditions of a collimator. If the radius of the limiting aperture is $R$, the radius of the receiving aperture $r$, and the distance between them $\ell$, the angles can be specified as (fig. 1)

$$\text{the opening angle:} \quad \theta_o = \tan^{-1} \frac{R}{\ell}$$

$$\text{the slope angle:} \quad \theta_s = \tan^{-1} \frac{R - r}{\ell}$$

$$\text{the limit angle:} \quad \theta_\ell = \tan^{-1} \frac{R + r}{\ell}$$

According to a recommendation adopted at the Joint International Radiation Conference at Davos in September 1956, (refs. 2 and 3), the slope angle $\theta_s$ should be between $1^o$ and $2^o$ while the opening angle $\theta_o$ must be less than $4^o$. Many pyrheliometer manufacturers and instrument designers do not follow the recommendations strictly, and they often specify only one angle - the opening angle, or equivalently the full aperture angle, central angle, acceptance angle, field of view, etc., which are two times the opening angle. Frequently the ratio of a collimating tube length to its diameter (or aperture diameter) is also used.

Specification of two of the three basic angles is necessary and sufficient for complete design of a collimator. Opening angle and slope angle are usually used for this purpose. In the following sections effects of these two angles on measurements will be analyzed with respect to potential tracking and radiation errors.

## Slope Angle

The slope angle of a collimator is determined by several factors: (angular) size of the light source, initial pointing error, and subsequent tracking error of the instrument during measurements. To show the importance of having a proper slope angle, consider an extreme case, say $\theta_s = 0$.

If the collimator is perfectly aimed at the center of the solar disk, a point near the edge of the receiving area at the bottom of the tube views only part of the solar disk (fig. 2). This leads to a nonuniformity of intensity on the receiving area. Pointing error and tracking error make the situation worse; the solar disk can be out of the view completely from certain edge points. The nonuniformity of irradiance at the receiving area could be large under these circumstances.

It is quite obvious that even if the collimator is perfectly aimed, the slope angle has to be at least half the angular span of the solar disk so that all parts at the receiving area can be illuminated by the entire solar disk. Allowing imperfect aiming, it is necessary to have a slope angle not less than the sum of: (a) one-half of the angular span of the solar disk, from center to rim ($0.26^o$); (b) initial pointing error; and (c) subsequent tracking error of the device.

In ISCTPTA the tracking accuracy was allowed to be $\pm 2^o$. If the allowed pointing error were as low as $0.25^o$, the slope angle of the collimator would have to be $2.76^o$. If the full aperture angle ($2\theta_o$) is $5.7^o$ as specified in ISCTPTA, and the radius of receiving area is 1.5 cm for a typical 2 cm x 2 cm size standard cell, then the length of the collimator must be over 837 cm.

Collimators of such length are quite impractical for day-to-day calibration of solar cells.

In view of the fact that there are inexpensive solar trackers commercially available with accuracy better than $1^{o}$, the tracking requirement should be within $\pm(\theta_s - 0.76^{o})$ with $\theta_s$, the slope angle, specified no greater than $1.76^{o}$. With better tracking, smaller slope angles can be used but should be no less than $1^{o}$.

## Opening Angle

The size of the opening angle determines how much radiation passes through the collimator. In addition to the direct solar radiation, circumsolar radiation and skylight also enter the collimator due to Mie scattering by atmospheric aerosols and Rayleigh scattering by atmospheric molecules. Ideally, one would like to use a collimator of very small opening angle to eliminate the circumsolar radiation and skylight; however, it is not practical to decrease the opening angle much below $5.7^{o}/2$, which is equivalent to the 10 to 1 collimation ratio found on many commercial pyreheliometers. For example, consider a collimator of 20 to 1 ratio (opening angle of $1.43^{o}$). If the slope angle is $1.26^{o}$ as discussed in the previous section, a 1.5 cm radius receiving aperture would require a collimator nearly 500 cm in length. Even with a slope angle of $1^{o}$, the length would be close to 200 cm. Thus a 20 to 1 collimator is much too long for practical use. In the following discussion, the comparisons are made only between collimators of 10 to 1 and 5 to 1 ratios in order to estimate the circumsolar radiation and skylight received through the collimator, uniformity, and relative errors in measurement.

Circumsolar radiation received through the collimator. - The circumsolar radiation due to Mie scattering by atmospheric aerosols is higly directional, with its major portion concentrated in the forward direction. In actual measurement, it is difficult to separate the forward scattered light from the direct sunlight. A certain amount of circumsolar radiation must be included in the measurement.

Summarizing the data and analysis from a number of investigators, Angstrom and Rodhe (ref. 4) presented in graphical form the dependence of radiation from the solar aureole on turbidity parameter $m\beta$ and on full aperture angle of a measuring instrument. The graph of this relationship is reproduced here (fig. 3) for reference. The relative air mass is $m$ and $\beta$ is the turbidity coefficient. The amount of circumsolar radiation is measured in percentage of the direct radiation from the solar disk.

According to figure 3, for $m\beta = 0.2$ the circumsolar radiation received through the 10 to 1 ($5.7^{o}$) collimator is 4.7% of the direct radiation and 7.8% through the 5 to 1 ($11.3^{o}$) collimator. The difference in circumsolar radiation received by these two collimators is then 3.1% of direct. For $m\beta = 0.1$ this difference reduces to 1.5%. It has been proposed that use of a collimator with large opening angle which allows all of the circumsolar radiation to be included in the measurements could be advantageous. However, there are other factors such as skylight and illumination errors at the test plane to be considered.

Skylight radiation received through the collimator. - The amount of skylight (diffused Rayleigh scattering) entering the instrument also increases with the increase of the opening angle of its collimator. For a collimator of 10 to 1 ratio, $2\theta_{o} = 5.7^{o}$, the solid angle subtended at the receiving

area is about 0.125% of the entire hemisphere. Excluding variations in brightness across the sky, this opening angle allows approximately 0.25% of the total skylight, which is the total flux of diffuse light received at a horizontal plane with the collimator removed, to enter the instrument. For a collimator of 5 to 1 ratio ($2\theta_o = 11.3^o$), the figure should be four times that much or about 1% of the total skylight.

Because of the strong wavelength scattering dependence ($\sim 1/\lambda^4$), the Rayleigh scattering coefficient varies from 1 in the near IR to about 30 in the UV. Thus, the skylight due to Rayleigh scattering has a spectral composition significantly different from the direct sunlight; the result is a combination of disproportionately enhanced short wavelengths and much suppressed long wavelengths. Consequently, the skylight affects the solar cell performance measurements much more than the comparable amount of circumsolar light, which has a spectral distribution near to that of direct sunlight.

Preliminary observations indicate that the ratio of short circuit current output to irradiance for solar cells under skylight can be as much as 15% lower than that under normal incident direct sunlight, depending upon general sky conditions. On the other hand, no significant difference in solar cell performance has been observed between measurements with collimators of 10 to 1 ratio and those of 5 to 1 ratio. Thus, the apparent advantage of using larger opening angle to include more circumsolar light may be outweighed by the disadvantage of introducing more spectrally different skylight.

Uniformity of illumination. - The opening angle can also affect the

uniformity of illumination at the receiving aperture. With $2\theta_o = 11.3^o$, the center of the receiving area gets additional radiation from the solar aureole, which amounts to approximately 8% of the direct component for $m\beta = 0.2$ (fig. 3). For slope angle of $1\text{-}2^o$, the circumsolar radiation that can reach the edge of the receiving area is approximately half of that received at the center, that is, approximately 4% of the direct. If we extend the turbidity and air mass range to $m\beta = 0.25$ or more, the difference can be over 5%. This difference, which is a direct measure of the nonuniformity at the receiving plane, is significantly reduced for smaller opening angles. In the case of $2\theta_o = 5.7^o$, the difference should be about 2% for $m\beta = 0.2$.

Relative errors in measurement. - Relative errors in measurement due to pointing and tracking inaccuracies are also different for collimators of different opening angle. Referring to figure 4(a), let $\delta\theta$ be the sum of pointing and tracking errors. The resultant error in the radiation flux which gets through the collimator can be expressed as

$$\Delta F \sim \Delta\Omega \cdot \frac{dI}{d\theta} \qquad (1)$$

where $\Delta\Omega$ is the solid angle error due to the $\delta\theta$ pointing error, $dI/d\theta$ is the gradient of the intensity of the circumsolar radiation per unit solid angle with respect to angular distance from the solar disk. The solid angle $\Delta\Omega$ can be estimated from figure 4(b). When the axis of the collimator is shifted by $\delta\theta$, a diameter at the limiting aperture perpendicular to the shift sweeps an area $(\ell\delta\theta)2R$. Therefore, the solid angle

$$\Delta\Omega = \frac{(\ell\delta\theta)2R}{\ell} = \frac{2R}{\ell}\,\delta\theta \qquad (2)$$

hence

$$\Delta F \sim \frac{2R}{\ell} \cdot \frac{dI}{d\theta} \cdot \delta\theta \qquad (3)$$

The quantity $dI/d\theta$, in percent of the direct solar radiation per unit solid angle, can be estimated from figure 3. For a collimator of 10 to 1 ratio $2R/\ell = 1/10$ and $dI/d\theta \sim -5m\beta(\ell^2/\pi r^2)$. Comparable values for a collimator of 5 to 1 ratio are $1/5$ and $-m\beta(\ell^2/\pi r^2)$. Considering a high turbidity parameter case, say, $m\beta = 0.2$, the uncertainties associated with a pointing error of $0.5^o$ would be around 0.2 and 0.02 percent for collimators of 10 to 1 and 5 to 1 ratios, respectively. For a lower turbidity parameter case such as $m\beta = 0.1$, they are approximately 0.1 and 0.01 percent, both small quantities.

## Sizes of Collimators in Different Configurations

For given opening angle and slope angle, the size of a collimator is dictated by the size of its receiving aperture. Typical reference solar cells are 2 cm x 2 cm squares. A collimator with a receiving aperture radius of 1.5 cm is appropriate for the calibration of such cells under terrestrial sunlight. For a quick comparison, dimensions for collimators of 20 to 1, 10 to 1, and 5 to 1 ratios with different slope angles are given in Table 1. Lengths are measured in centimeters with $r$, the radius of the receiving aperture, fixed at 1.5 cm.

Table 1. COMPARISON OF DIMENSIONS FOR COLLIMATORS OF DIFFERENT OPENING ANGLE AND SLOPE ANGLE

| Collimation Ratios | Opening Angle | Slope Angle | Receiving Aperture radius r cm | Limiting Aperture radius R cm | Collimator length $\ell$ cm |
|---|---|---|---|---|---|
| 20/1 | 1.43° | 1° | 1.5 | 4.91 | 198.81 |
| | | 1.26° | | 12.48 | 499.12 |
| | | 1.76° | | — | — |
| 10/1 | 2.85° | 1° | 1.5 | 2.30 | 46.09 |
| | | 1.26° | | 2.68 | 53.56 |
| | | 1.76° | | 3.89 | 77.83 |
| 5/1 | 5.65° | 1° | 1.5 | 1.82 | 18.17 |
| | | 1.26° | | 1.92 | 19.23 |
| | | 1.76° | | 2.17 | 21.65 |

## TERRESTRIAL REFERENCE CONDITIONS

In the ISCTPTA, solar cell calibration in natural sunlight requires the following atmospheric conditions: (1) turbidity coefficient $\beta$ must be less than 0.2, and (2) air mass $m$ must be between 1 and 2.5. Using the worst combination of (1) and (2), the product of $m\beta$ can be as high as 0.5, which according to a linear extrapolation of figure 3 could give circumsolar radiation as much as 20% of the direct. Under this condition, the nonuniformity of irradiance at the receiving area would be unacceptably high even with $2\theta_o = 5.7^o$.

The compelling reason to allow $m$ to be as large as 2.5 and $\beta$ as high as 0.2 is to accommodate the large air mass for winter months in the northern states and the high turbidity for summer months in some populated areas. However, the turbidity parameter which plays the essential role is

the product $m\beta$. According to the survey presented by Flowers, et al. (ref. 5), the turbidity conditions in the United States have values of $m\beta$ less than about 0.25 most of the year. This occurs because in high turbidity summer months the air mass at solar noon is generally small, while in winter months the turbidity is usually lower although the air mass is large. It is recommended, therefore, that the reference conditions concerning turbidity and air mass specified in ISCTPTA be revised by adding: the product of air mass and turbidity coefficient, $m\beta$, must be no greater than 0.25.

It should be noted that the above recommendation is based solely on the consideration of accommodating the typical turbidity conditions with acceptable nonuniformities discussed previously. Other factors may call for even more stringent requirements on turbidity conditions.

## CONCLUSIONS

Using collimators of large opening angle, most of the circumsolar radiation can be included in the measurement. However, for the purpose of solar cell calibration, this advantage can be outweighed by the drawbacks of introducing more skylight and the increasing nonuniformity at the receiving plane. Furthermore, a larger opening angle also makes the measurements more vulnerable to the influence of general sky conditions.

Collimators with a small opening angle such as a 20 to 1 collimation ratio are impractical to use because of their physical sizes. Commercially available pyrheliometers have $2\theta_o$ in the $5\text{-}6^\circ$ range, which is equivalent to a 10 to 1 collimation ratio, and there is no compelling reason to change it. However, it is necessary to have the slope angle of the collimator

specified. Proper slope angle can be easily determined from knowledge of the desired collimator size and tracking accuracy. For collimators of 10 to 1 ratio, a slope angle between $1^{o}$ and $1.76^{o}$ is recommended. Such a collimator should be capable of tracking with an accuracy better than the slope angle minus $0.76^{o}$.

It is also recommended that the terrestrial reference conditions for atmospheric turbidity be restricted to $m\beta \leq 0.25$ to avoid excessive non-uniformity of illumination at the receiving aperture of a collimator.

## REFERENCES


1. Brandhorst, H.; Hickey, T.; Curtis, H.; and Ralph, E.: Interim Solar Cell Testing Procedures for Terrestrial Applications, NASA TM X-71771 (1975).
2. Guide to Meteorological Instrument and Observing Practices.
3. Drummond, A. J.: Current Developments in Phyrheliometric Techniques. Solar Energy 5 19 (1961).
4. Angstrom, A.; and Rodhe, B.: Pyrheliometric Measurements with Special Regard to the Circumsolar Sky Radiation. Tellus 18, 25 (1966).
5. Flowers, E. C.; McCormick, R. A.; and Kurfis, K. R.: Atmospheric Turbidity Over the U.S., 1961-1966, J. Appl. Meteo. 8, No. 6, 955 (1969).

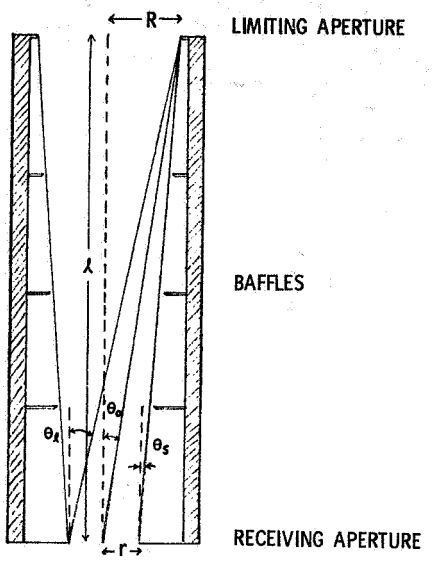


FIG. 1. CROSS-SECTIONAL VIEW OF A COLLIMATOR

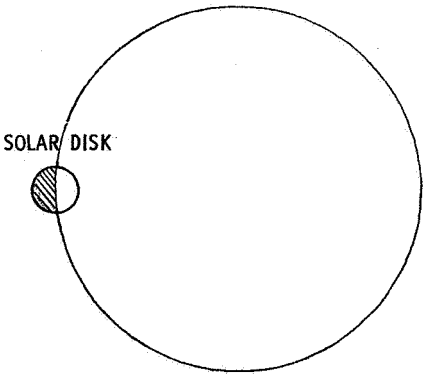


FIG. 2. A VIEW FROM AN EDGE POINT NEAR THE RECEIVING APERTURE OF A COLLIMATOR WITH ZERO SLOPE ANGLE. SHADED PART OF THE SOLAR DISK IS OUT OF SIGHT.

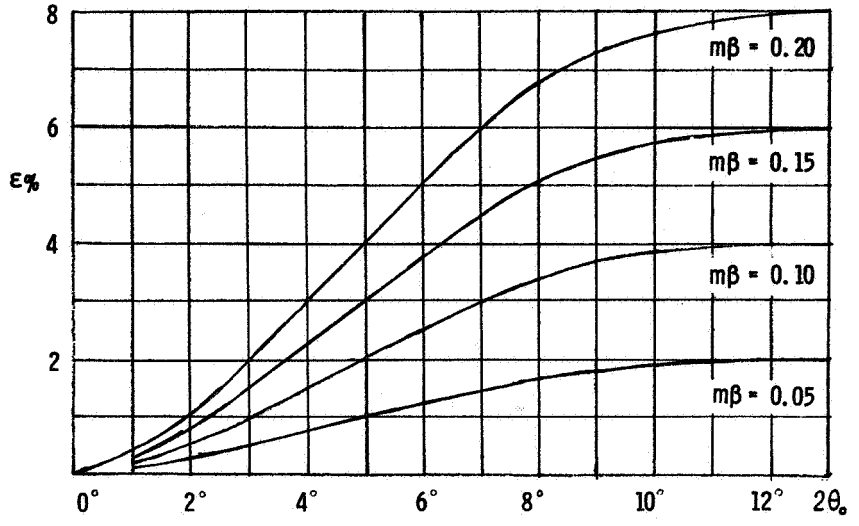


FIG. 3. DEPENDENCE OF THE RADIATION FROM THE AUREOLE ON TURBIDITY PARAMETER AND ON OPENING APERTURE OF THE INSTRUMENT. THE QUANTITY ε IS GIVEN IN PERCENT OF THE DIRECT SOLAR RADIATION. (REPRODUCED FROM REF. 4)

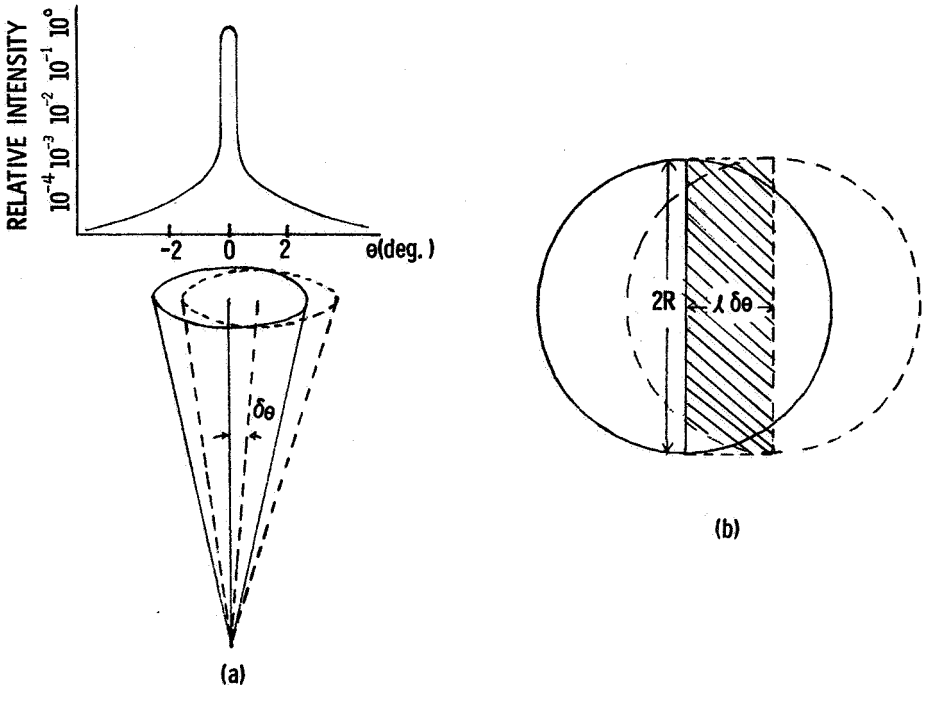


FIG. 4. (a) SIDE VIEW OF A COLLIMATOR HAVING A POINTING & TRACKING ERROR OF $\delta\theta$
(b) TOP VIEW OF SUCH A COLLIMATOR

# SENSITIVITY OF SOLAR CELL PERFORMANCE TO ATMOSPHERIC VARIABLES: I - SINGLE CELL

by Thomas M. Klucher
National Aeronautics and Space Administration
Lewis Research Center
Cleveland, Ohio

## ABSTRACT AND SUMMARY

Measurements of the short-circuit current of a typical silicon solar cell under direct solar radiation were made for a range of turbidity, water vapor content, and air mass to determine the relation of the solar cell calibration value (current-to-intensity ratio) to those atmospheric variables. A modification of a previously developed regression equation was used to describe the relation between calibration value, turbidity, water vapor content, and air mass. Based on the value of the constants obtained by a least-squares fit of the data to the equation, it is found that turbidity lowers the value, while increase in water vapor increases the calibration value. Cell calibration values exhibited a change of about 6% over the range of atmospheric conditions experienced.

## INTRODUCTION

Quantitative information on the amount of solar radiation incident upon solar cells and arrays and the subsequent efficiency of conversion of that radiation into electrical energy is essential to the development of improved cells and arrays and the design of cost-effective systems. Standard reference cells can be calibrated so that the incident solar radiation can be determined by measuring the cell short-circuit current. These reference cells then can be used to establish the intensity during the measurement of the performance of other cells, modules or arrays.

It is well known that the spectral distribution of the incident solar radiation is variable, even under clear skies. This variability is due to the effects of Rayleigh and aerosol scattering, and selective absorption (primarily by atmospheric water vapor) as the sunlight passes through the atmosphere. Because the solar cell is sensitive to a limited range of wavelengths ($\sim$ 0.3 to 1.2 μm), its short-circuit current will vary in a manner different from the intensity of the solar irradiance. Thus, the calibration value--the ratio of short-circuit current to the intensity of solar radiation under normal incidence--will be a function of and sensitive to changes in atmospheric turbidity and water vapor content.

The purpose of this work is to determine the effects of turbidity, water vapor, and air mass on the cell calibration value. To do this, measurements over a one-year period were made on a single cell for widely different measured atmospheric conditions. Measurements of turbidity, water vapor and air mass were taken along with current and intensity. The data accumulated were fitted by the least-squares method to a regression equation developed by Majumdar et. al. (Ref. 1) for solar radiation predictions, but modified herein to solar-cell calibration ratio measurements. The regression coefficients obtained are a measure of the sensitivity of the calibration value to the atmospheric variables.

## APPARATUS AND MEASUREMENTS

Measurements of the direct solar radiation were obtained using a 10:1 collimation ratio Eppley normal incidence pyrheliometer. The unit is temperature compensated within $\pm$ 1% over the temperature range of -20° C to + 40° C and is calibrated with respect to the IPS 1956 standard.

The solar cell, Z01, used in this study was a commercial 2x2 cm cell mounted in a special holder (Figure 1). The spectral response curve is shown in Figure 2. During measurements, the cell was inserted in a 10:1 collimating tube (slope angle $1.76^{o}$) mounted with the pyrheliometer on a sun tracker (Figure 3). The short circuit current of the cell was obtained by measuring the voltage developed across a 0.1 $\Omega \pm .1\%$ resistor located near the cell terminals. The temperature of the cell was controlled to $28^{o}$ C $\pm$ $2^{o}$ C.

Two sunphotometers were used to monitor turbidity, water vapor, and relative air mass during cell measurement (Figure 4). The sunphotometer on the right, on loan from the EPA, was used to measure the Schuepp turbidity coefficient. $B = B_{o}p/p_{o}$, with the relation:

$$I_{\lambda} \times S = I_{o\lambda} \times 10^{-(T_{R\lambda} + T_{3\lambda} + B_{o\lambda})\, M_r \frac{p}{p_o}} \qquad \text{Eq. (1)}$$

where $I_{\lambda}$ is the irradiance at wavelength

$I_{o_{\lambda}}$ is the AM0 irradiance at $\lambda$ and mean sun-earth distance

$S$ is the correction factor for mean sun-earth distance

$T_{R\lambda}$ is scattering coefficient for air molecules at $p_o$

$T_{3\lambda}$ is the absorption coefficient for ozone

$B_{o\lambda}$ is the turbidity coefficient at $p_o$

$M_r$ is the relative air mass

$p$ is the barometric pressure measured at the location

$p_o$ is the standard sea level pressure

Measurements with this instrument are made at a wavelength of 0.5 μm. The sunphotometer provides a current output directly proportional to the irradiance value and is calibrated relative to a standard photometer, routinely calibrated by the Langley Method. The uncertainties in B are believed to be ± 10% (Ref. 2). The second sunphotometer, obtained from Dr. F. Volz, was used to monitor the precipitable water vapor, W, in the atmosphere using the relation (Ref. 3):

$$W = \frac{K}{M_r}\left[\log_{10}\left(\frac{q_o}{q}\right)\right]^2 \qquad \text{Eq. (2)}$$

where K is the calibration constant obtained by comparison with radiosonde measurement of precipitable water.

$M_r$ is the relative air mass

q is the ratio of intensity readings at $\lambda$ = .940 μm and .880 μm at the location.

$q_o$ is the ratio of intensity readings above the atmosphere at .940 μm and .880 μm.

Here again, the current output of the sunphotometers is directly proportional to the intensity readings. The uncertainty in W is believed to be ± 15%.

## BACKGROUND AND METHOD

The sensitivity of the calibration value to variations in atmospheric components can best be demonstrated by theoretical modeling, involving the convolution of spectral irradiance with the cell spectral response curves. However, these methods are fairly elaborate, requiring many computations and accurate data for absorption bands and spectral response. At present, the spectral irradiance curves are generated theoretically and there are few direct comparisons with experimental data to validate the model used.

Also, the measured spectral response curves have errors of about $\pm$ 5%. Thus, calculated calibration values are not reliable at this time.

An alternate way to mathematically describe the sensitivity of solar cell calibration value to the atmospheric variables is through the use of a regression equation. In this method, empirical measurements of the pertinent variables and the solar cell calibration value are made and a curve (or equation) is mathematically fit to the data. This empirical regression equation can then be used to determine calibration values for selected values of the atmospheric variables.

The starting point for this analysis was the regression equation derived by Majumdar et al (Reference 1) to predict the direct solar radiation as a function of air mass and water vapor for clear sky. This equation is:

$$I_n = I_o \times t_1^{M} \times (t_2)^{(WM_r)^{0.25}} \qquad \text{Eq.(3)}$$

where $t_1$ is the scattering transmission coefficient and $t_2$ is the water vapor transmission coefficient, and $M = M_r\, p/p_o$ $I_0$ is the intensity above the troposphere and $I_n$ is the intensity at ground level. Majumdar considered only clear skies with Schuepp turbidity coefficients of around B = 0.045. In this report, this equation has been modified to include above and below B = 0.045 by use of a short-wave radiation turbidity factor T = 10B+1 (Reference 4). This factor is basically the Linke turbidity factor obtained for only the fraction of radiation intensity below the water vapor bands (Reference 5). The turbidity factor was further modified so that at B = 0.045, the modified equation reduces to Equation 3.

Thus, the modified equation is:

$$I_n = I_o \times t_1^{\left[10(B-0.045) + 1\right] M} \times t_2^{(WM_r)^{0.25}} \qquad \text{Eq. (4)}$$

The major assumption made by Majumdar and also in this study is that Beer's law, which is strictly valid only for monochromatic radiation, can be extended to the entire solar radiation spectrum through the use of average transmission coefficients for scattering and absorption. In practice, plots of the logarithm of intensity versus air mass (Langley plot) are observed to be nearly linear up to about air mass 3. In a similar manner, the Langley method has been successfully applied in the past to solar cell measurements using the same assumptions (Ref. 6, 7). Therefore, in this study, the solar cell short circuit current was also assumed to have the form:

$$I_{sc} = I_{sc_o} \times f_1^{\left[10(B-0.045) + 1\right] M} \times f_2^{(WM_r)^{0.25}} \qquad \text{Eq. (5)}$$

Dividing eq. 5 by eq. 4 yields the equation for the calibration value:

$$\frac{I_{sc}}{I_n} = C_0 \times C_1^{\left[10(B-0.045) + 1\right] M} \times C_2^{(WM_r)^{0.25}} \qquad \text{Eq. (6)}$$

Taking the logarithm of both sides of equation 6 yields the linear equation:

$$\log\left(\frac{I_{sc}}{I_n}\right) = \log C_0 + \log C_1 \left[10(B-0.045) + 1\right] M + \log C_2 (WM_r)^{0.25} \qquad \text{Eq. (7)}$$

Measured values for $I_{sc}$, $I_n$, B, W, $M_r$, and M were used to determine the regression constants $C_0$, $C_1$ and $C_2$ by the method of least squares. $C_0$ is the "effective" air mass zero coefficient, $C_1$ is the turbidity coefficient and $C_2$ is the water vapor coefficient.

## RESULTS AND DISCUSSION

During the course of a year, eighty-two (82) concurrent measurements of direct normal incidence solar radiation , $I_n$, solar cell short circuit current , $I_{sc}$, turbidity ,B, water vapor ,W, and air masses ,M and $M_r$, were obtained under clear skies, or through clearings in a partly cloudy sky. The data collected had the following range of values: turbidity, 0.031 to 0.30; water vapor, 0.15 to 1.4 cm; and air masses, 1.05 to 4.2. Turbidity values greater than B = 0.300 and water vapor values greater than 1.4 cm were arbitrarily excluded. The sensitivity coefficients were determined to be:

$$C_0 = 1.017 \text{ mA/mW/cm}^2$$

$$C_1 = .991$$

$$C_2 = 1.114$$

These coefficients are specific for only the single cell studied here. The standard deviation of the difference between measured calibration values and the prediction value is 0.011 $\text{mA/mW/cm}^2$ or about 1%. Figure 5 illustrates the comparison between the measured calibration values and those calculated by the regression equation.

Based on the results of the data set examined here of the regression analysis, the cell calibration value exhibits a change of about 6% over the range of atmospheric conditions experienced. As can be seen from equation 7, regression constants less than 1 indicate a decrease in cell calibration value with increase in the associated atmospheric variable, while constants greater than 1 indicate an increase in calibration value with increase in the atmospheric variable. Thus for cell Z01, the water vapor and turbidity sensitivity factors have opposite effects for concurrent increase or decrease in turbidity, water vapor, and air mass.

## SUMMARY OF RESULTS

The regression analysis performed on data for a single, but typical, solar cell has determined that the ratio of cell short-circuit current to solar intensity exhibits a change of about 6% over a typical range of atmospheric turbidity, water vapor, and air mass conditions. Thus, the measurement of these atmospheric variables is essential to providing an accurate measurement of cell performance even under clear-sky conditions. With the instruments used, the standard deviation of the difference between measured ratio and predicted ratio was found to be about 1%. This simple regression equation may be used as an aid in correcting the calibration value of solar cell standards for a variety of atmospheric conditions.

## References


1. Majumdar, N. C.; Mathur, B. L.; and Kaushik, S. B.: Predictions of Direct Solar Radiation for Low Atmospheric Turbidity. Solar Energy, Vol. 13, 1972 pp 383-394.
2. Flowers, E. C.; McCormick, R. A.; and Kurfis, K. R.: Atmospheric Turbidity Over the United States, 1961-1966. J. of Applied Meteorology, Vol. 8, No. 6, Dec. 1969, pp 955-962.
3. Volz, F. E.: Economical Multispectral Sun Photometer for Measurements of Aerosol Extinction from .44um to 1.6 um and Precipitable Water. Applied Optics, Vol. 13, No. 8, Aug. 1974, pp 1732-1733.
4. Volz, F. E.: Arch. Meteorology. Geophys. Bioklimatol. Series B, Vol. 13, 1964, p 249.
5. Robinson, N. (Editor): Solar Radiation. Elsevier Publishing Co., 1966.
6. Zoutendyk, J. A.: A Method for Predicting the Efficiency of Solar Cell Power System Outside the Earth's Atmosphere. JPL Technical Report 32-359 (1962).
7. Brandhorst, H. W.; and Boyer, E. O.: Calibration of Solar Cells Using High Altitude Aircraft. NASA TN D-2508, February 1965.

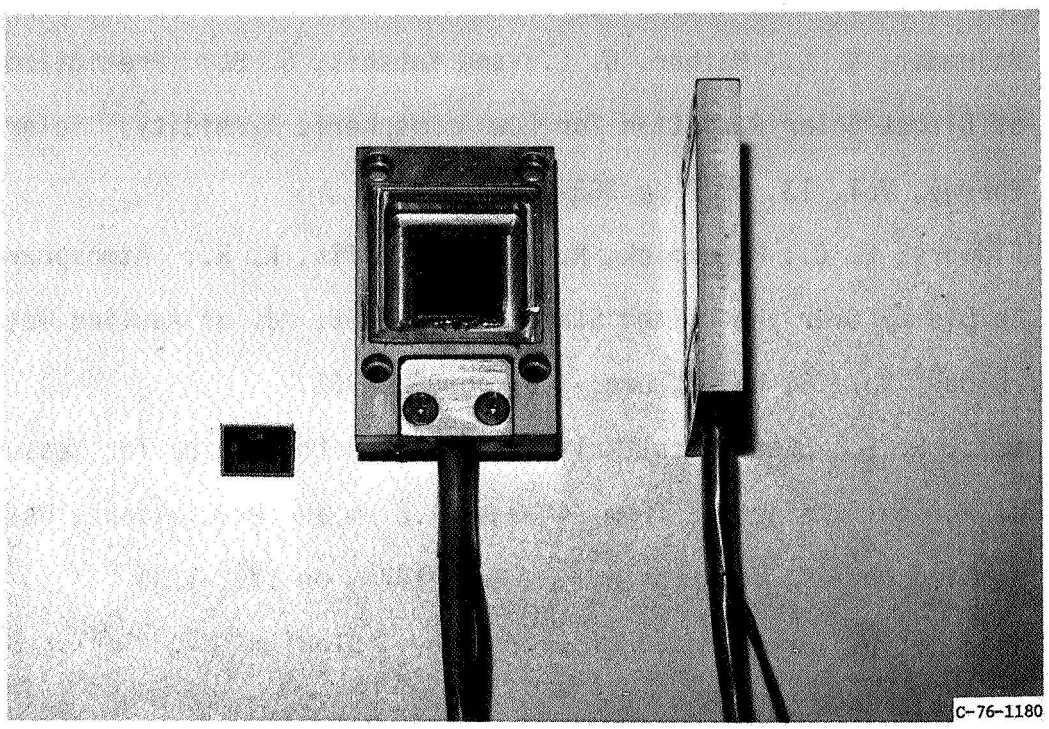


Figure 1. - Solar cell mounted in holder

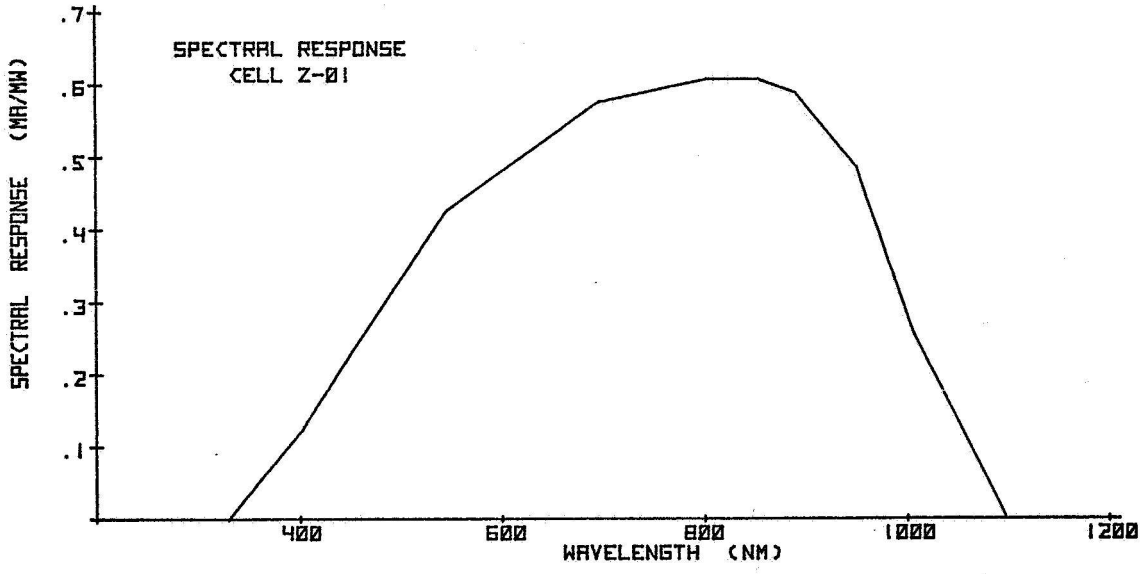


Figure 2. - Spectral response curve of cell Z 01

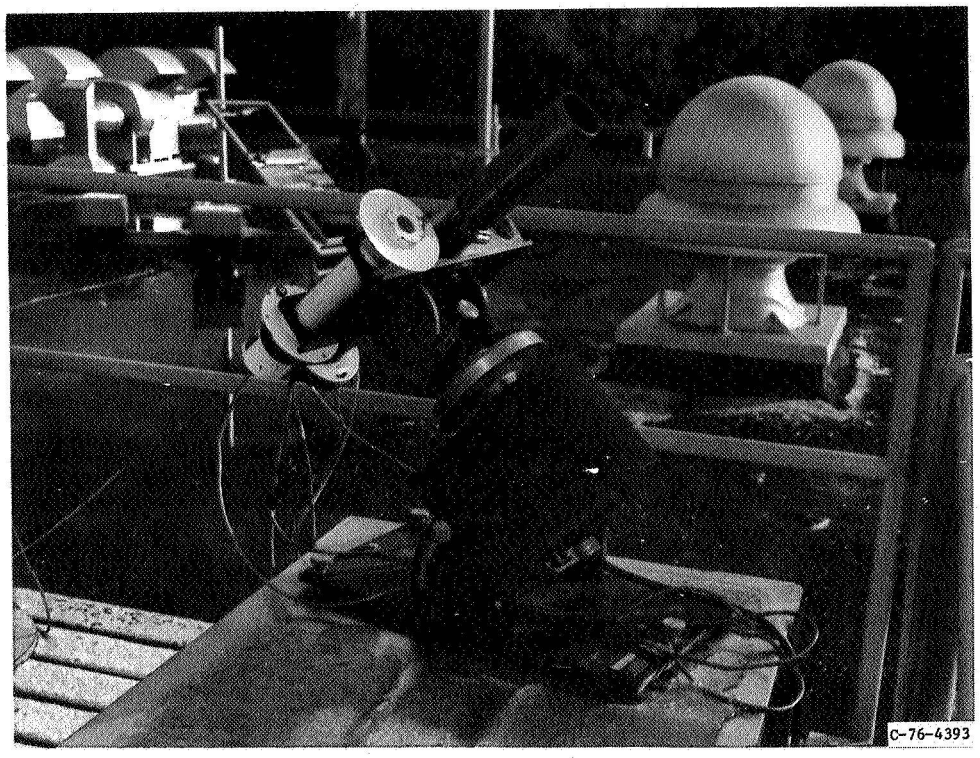


Figure 3. - Solar cell calibration apparatus

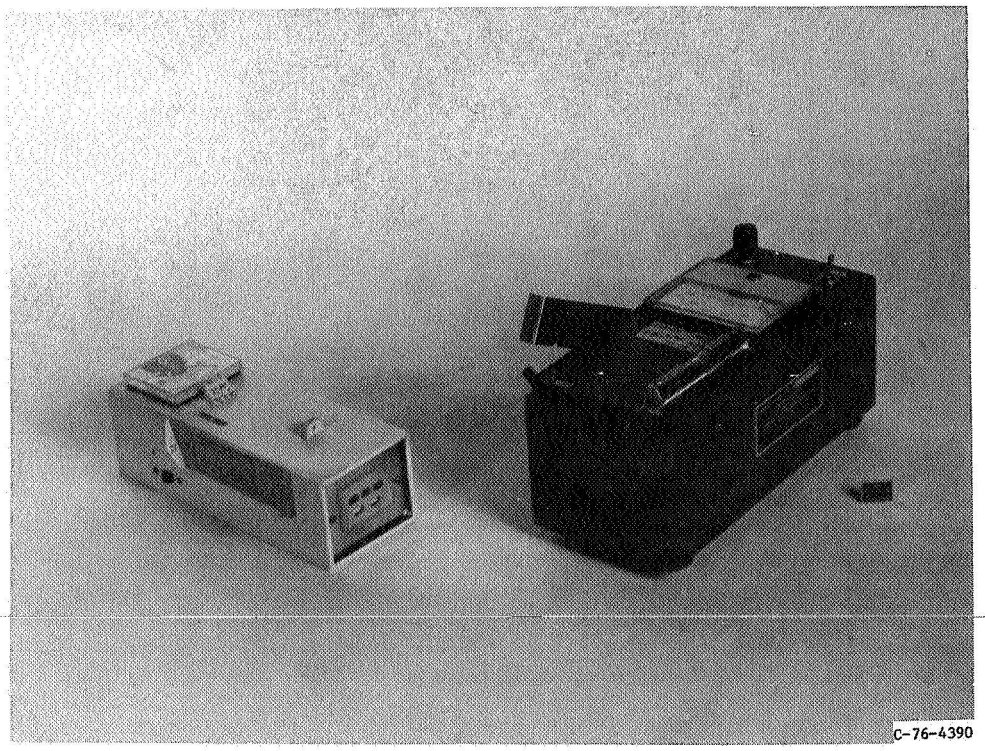


Figure 4. - Sunphotometers used to measure turbidity, water vapor and relative air mass

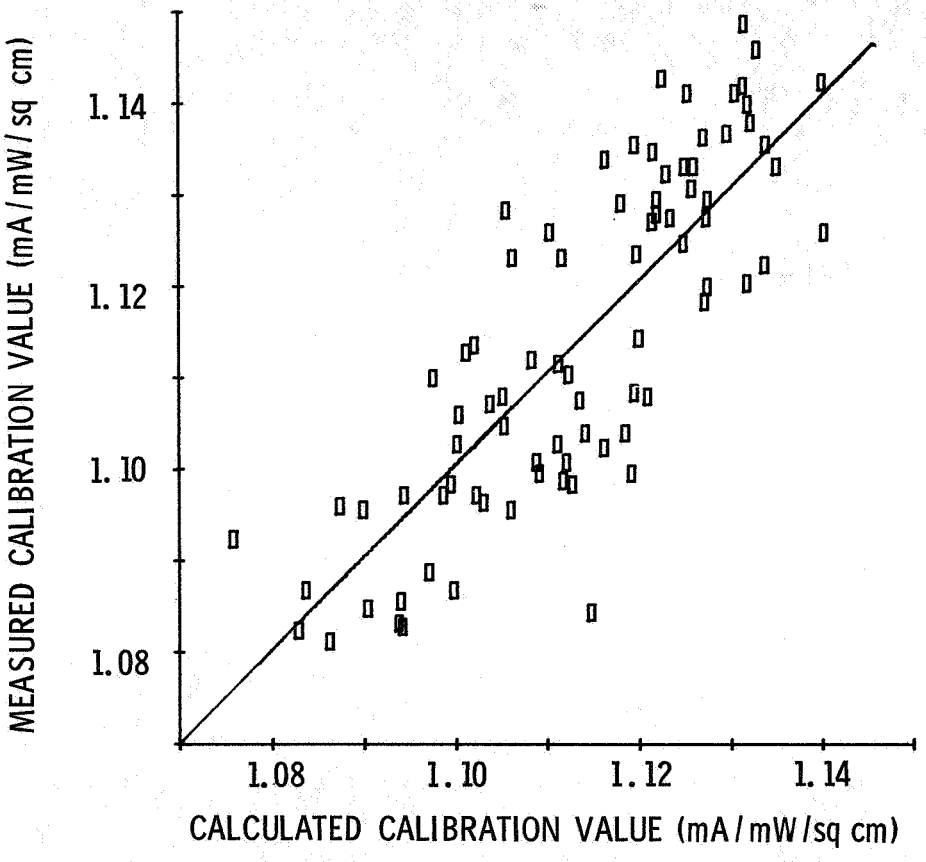


Figure 5. - Measured versus calculated calibration value

# SENSITIVITY OF SOLAR-CELL PERFORMANCE TO ATMOSPHERIC VARIABLES: II - DISSIMILAR CELLS AT SEVERAL LOCATIONS

by Thomas M. Klucher and Russell E. Hart
National Aeronautics and Space Administration
Lewis Research Center
Cleveland, Ohio

## ABSTRACT

Fifteen solar cells, having dissimilar spectral response curves and cell construction, were measured at various locations in the United States to determine sensitivity of cell performance to atmospheric water vapor and turbidity. The locations selected represent a broad range of summer atmospheric conditions, from clear and dry to turbid and humid. Cell short-circuit current under direct normal incidence sunlight, the intensity, water vapor and turbidity were measured. Regression equations were developed from the limited data base in order to provide a single method of prediction of cell current sensitivity to the atmospheric variables.

## SUMMARY

Fifteen solar cells, having dissimilar spectral response curves and cell construction, were measured at various locations in the United States to determine the sensitivity of their performance to atmospheric variables. The locations selected represent a broad range of summer atmospheric conditions, from clear and dry to turbid and humid. Schuepp turbidity values from 0.04 to 0.259, water vapor from 0.70 cm to 2.35 cm and air masses from 0.93 to 2.0 were measured during the trip. The

calibration values--defined as the ratio of measured cell short-circuit current to incident intensity--were compared with the atmospheric variables and inserted in a regression equation developed to predict cell sensitivity. It was found that there was a correlation between the regression constants obtained and the cell spectral response curves. It appears that cell spectral response determines the regression constants and hence the sensitivity of cell calibration value to atmospheric changes.

## INTRODUCTION

Solar cells, which are currently being used for power generation applications on earth by a variety of manufacturers, differ markedly in design and materials used. The cells, eventually combined into large sized arrays and placed in the field, are subjected to environments which may alter their performance. In order to determine their initial performance and subsequent change, if any, the arrays are compared against a reference or standard solar cell. These cells are identical in material and construction to the cells in the array and are periodically calibrated against a total incidence detector. In the case of the cells presently used as standards in the ERDA National Photovoltaic Program, the calibration is performed relative to a normal incidence pyrheliometer under direct normal incidence sunlight (Ref. 1). The standard cells are measured at the short-circuit point of their I-V characteristic and the calibration procedure results in a single calibration value--the ratio of cell short-circuit current generated to the direct solar intensity normally incident on the cell surface.

Both the solar spectral irradiance distribution and the total irradiance vary with changes in the atmospheric constituents. Therefore, the solar cell calibration value can be expected to be sensitive to the atmospheric constituents present during calibration because of the different spectral response characteristics of cell and pyrheliometer. In a previous report (Ref. 2), a simple regression equation was developed for data on a single solar cell. This equation describes the sensitivity of the particular cell's performance to atmospheric turbidity, water vapor, and air mass. This being the case, it is highly desirable to determine the sensitivity of available cells to atmospheric composition and to determine how these changes are related to the basic spectral response of each cell.

Fifteen solar cells, typical of types currently available for terrestrial and space use having dissimilar spectral response curves and/or construction design, were measured within a two-week period at various locations in the United States to determine sensitivity to water vapor, turbidity, and air mass. Silicon, GaAs and $Cu_2S$/CdS solar cells were included. The locations were selected to represent a broad range of summer atmospheric conditions, ranging from clear and dry to turbid and humid. The sensitivity of the calibration value of each cell to water vapor, turbidity, and air mass was evaluated by regression analysis and the results are presented in this report.

## APPARATUS AND MEASUREMENT

The apparatus used to measure the calibration value of each cell consisted of a pyrheliometer and solar cell collimating tube shown in Figure 1. Measurement of the direct solar radiation at normal incidence was obtained using a normal incidence pyrheliometer. The pyrheliometer was mounted on a sun tracker to provide direct intercomparison intensities during the measurement period. The pyrheliometer has a 10:1 collimation ratio and is temperature compensated to within $\pm$ 1% over the temperature range $-20^{o}C$ to $+40^{o}C$. The units were calibrated by Eppley Laboratories with respect to IPS 1956 standard. During measurement, each cell was inserted in the holder at the end of the 10:1 collimating tube and connected to the .1 ohm $\pm$ .1% load resistor. A multichannel voltmeter was used to record cell output voltage, temperature, and pyrheliometer output voltage.

The fifteen solar cells used in this study represented a wide variety of cell constructions and spectral responses. There were 13 silicon solar cells, one GaAs cell and one $Cu_2S/CdS$ cell. Some were developed especially for terrestrial application, while others were space cells which have been applied to terrestrial use or have some unique features. This range of cell types was selected in this study to provide a comprehensive survey of available cells. The cells were all mounted in the special holders described in Ref. 2.

Concurrent with measurements of cell short-circuit current, $I_{SC}$, cell temperature, and the normal incidence irradiance,

$I_n$, the Schuepp turbidity, B, and water vapor, W, and relative air mass $M_r$, were measured by the sunphotometers shown in Figure 2. The procedures used to determine B and W using the sunphotometer are described in Ref. 2. The main differences between the work in this report and that of Ref. 2 are: (1) the altitude of each location visited was used to estimate the pressure needed to determine the atmospheric variables in lieu of actual barometeric measurements, and (2) cell short circuit currents were temperature corrected to a common temperature ($25^{o}$ C) in the absence of a temperature controller.

## REGRESSION EQUATION

The form of the regression equation used to determine the sensitivity of the calibration value of each cell to water vapor, turbidity, and air mass was as previously described in Reference 2, namely

$$\log \frac{I_{sc}}{I_n} = \log C_0 + \log C_1 \left[10(B-0.045)+1\right] M + \log C_2 (WM_r)^{0.25} \qquad \text{eq. (1)}$$

where $C_0$, $C_1$, and $C_2$ are constants determined by a least square fit of the data. $C_0$ is the "extraterrestrial calibration value", $C_1$ is the turbidity regression constant, and $C_2$ is the water vapor regression constant. B is the Schuepp turbidity coefficient, W is the precipitable water vapor, $M_r$ is the relative air mass, and M is the absolute air mass. ($M = M_r p/p_o$, where p is the atmospheric pressure at the location and $p_o$ is the standard atmospheric pressure.)

## RESULTS AND DISCUSSION

Table I indicates the locations visited and the range of atmospheric parameters measured. As can be seen, the measured turbidities and precipitable water vapor represent a broad range of summer atmospheric conditions,

from very clear sky (B = 0.04) to hazy (B = 0.259). Precipitable water ranged from a minimum of 0.70 cm to 2.35 cm. The variation in turbidity does not appear to be strongly correlated with variations in water vapor content. In all, a total of 25 measurements were made on each of 12 cells, 24 on 2 cells, and 23 on one cell.

Figure 3 summarizes the results obtained for the regression constants $C_1$ and $C_2$, where plotted points are indicated by cell number, for all the cell studied. Values for the turbidity regression constant, $C_1$, go from 0.98 to 1.018, while the water vapor regression constants, $C_2$, range from 1.05 to 1.115. As can be seen from Equation 1, regression constants with values less than 1 indicate a decrease in cell calibration value with increase in the associated atmospheric variable while constants greater than 1 indicate an increase in calibration value with increase in the atmospheric variable.

Except for the GaAs cell (#110) there appears to be a correlation between water vapor and turbidity regression constants. The $Cu_2S/CdS$ cell (#67) appears indistinguishable from silicon solar cells. It can be seen that cells with low $C_1$ constants have high $C_2$ constants, and vice versa. To qualitatively gain some understanding of this relationship between constants, relative spectral response curves were plotted in Figure 4 for cells 72, 26, and 43 (located at the extreme and middle portions of the calibration plots); cell 110 was also plotted for comparison. It can be seen from Figure 4 that there is a shift in peak response from blue to red in going from cells 72 to 26 and then to 43.

Since losses in spectral irradiance due to increased turbidity occur mainly in the blue region of the solar spectrum, cells with higher blue relative spectral response should experience increased loss in short circuit

current with increase in atmospheric turbidity. For all except 4 of the cells studied herein, this loss in cell current outweighed the concurrent loss in normal incident irradiance, resulting in turbidity regression constants less than 1. It also follows that those cells with higher blue response have a lower regression constant.

Similarly, cells with higher red response lose current with increased atmospheric water vapor due to the loss of spectral irradiance in the near infrared, primarily in the 0.940 μm region. However, in this case, the normal incident irradiance loss beyond the spectral region of cell response far outweighs the loss of current, resulting in a water vapor regression constant greater than 1 for all cells measured. It also follows that cells with higher red response have a lower water vapor regression constant. As might be expected the spectral response of the cell determines the sensitivity of the calibration value to the atmospheric variables.

Table 2 shows a comparison of results of regression analyses performed on cell 01 using the separate data bases obtained at Cleveland (Ref. 2) and at the other locations visited. As can be seen, the regression constants $C_0$ and $C_1$ obtained at Cleveland are 0.3 to 0.4% higher than the constants obtained from data taken at the several locations visited. This difference is insignificant considering the limited amount of data. The standard deviation of the difference between measured and predicted calibration values was 1% for the data taken at Cleveland and was 0.5% for data taken at the different locations. For the other cells studied, the range of standard deviation was 0.3% to 1%, except for GaAs, which had a standard deviation of 2%. Error analysis of the uncertainties in the measured values of $I_{sc}$, $I_n$, M, $B_3$ and W indicate precision errors of 1 to 1.5% are to be expected.

The anomalous behavior of GaAs in the correlation curve between regression constants, as well as the relatively high standard deviation, possibly may be attributed to its drastically different spectral response, especially the sharp cut off at about 0.88 um.

## SUMMARY OF RESULTS

Measurements of 15 solar cells with dissimilar spectral response and construction were made at five geographically separated locations in the contiguous United States to determine the sensitivity of the cell calibration value to atmospheric water vapor and turbidity. A regresssion equation was used to obtain regression constants associated with each atmospheric variable. The following results were obtained:

1. There is a correlation between regression constants and solar cells, cells with low turbidity regression constants had high water vapor regression constants and conversely.

2. The value of the regression constants and the sensitivity of cell calibration value to the atmospheric variables, water vapor content and turbidity appear to be closely related to spectral response of the silicon and $Cu_2S/CdS$ solar cells.

3. The gallium arsenide solar cell data could not be correlated with the other cells.

NOTE: The data set used in this report is available upon request. Mail request to:

NASA-Lewis Research Center
Attn: Mr. T. M. Klucher, MS 302-1
21000 Brookpark Road
Cleveland, OH 44135

## REFERENCES

1. Brandhorst, H.; Hickey, J.; Curtis, H.; Ralph, E.: Interim Solar Cell Testing Procedures for Terrestrial Applications. NASA TM X-71771, 1975.

2. Klucher, T. M.: Sensitivity of Solar Cell Performance to Atmospheric Variables I. Single Cell To be published.

TABLE I. - LOCATIONS VISITED AND RANGE OF ATMOSPHERIC PARAMETERS

- NEWARK, DELAWARE
- GAINESVILLE, FLORIDA
- PASADENA, CALIFORNIA
- PHOENIX, ARIZONA
- ALBUQUERQUE, NEW MEXICO

RANGE OF ATMOSPHERIC PARAMETERS

| | |
|---|---|
| TURBIDITY | 0.04 - 0.259 |
| WATER VAPOR | 0.70 - 2.35 CM |
| AIR MASS | 0.93 - 2.00 |

TABLE 2 - COMPARISON OF RESULTS OF REGRESSION ANALYSIS CLEVELAND VS. SEVERAL LOCATIONS

| | CELL NO. | $C_0$ - OUTER SPACE | $C_1$ - TURBIDITY | $C_2$ - WATER VAPOR |
|---|---|---|---|---|
| CLEVELAND | 01 | 1.017 MA/MW/CM$^2$ | .991 | 1.114 |
| LOCATIONS | 01 | 1.013 MA/MW/CM$^2$ | .988 | 1.114 |

STANDARD DEVIATIONS IN PERCENT OF DIFFERENCES BETWEEN MEASURED AND CALCULATED CALIBRATION VALUES

| MEASUREMENT SITE | CELL NUMBER | STANDARD DEVIATION |
|---|---|---|
| CLEVELAND | SILICON - 01 | 1% |
| SEVERAL LOCATIONS | SILICON - 01 | 0.5% |
| SEVERAL LOCATIONS | $G_aA_s$ - 110 | 2% |
| SEVERAL LOCATIONS | OTHER CELLS | .3 → 1% |

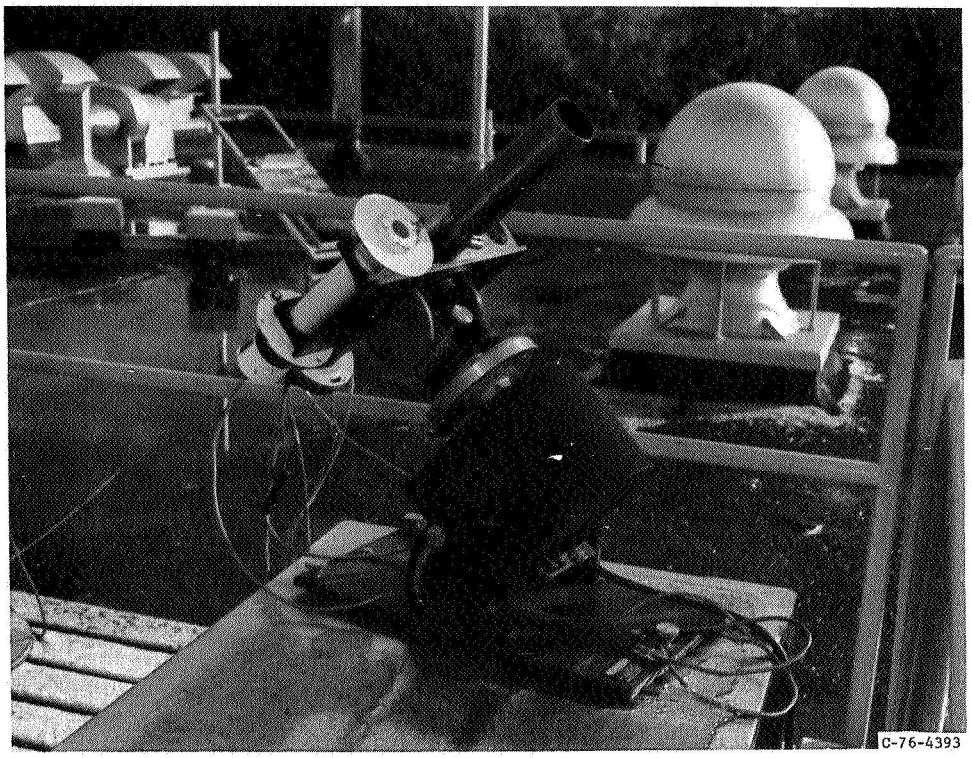


Figure 1. - Solar cell calibration apparatus

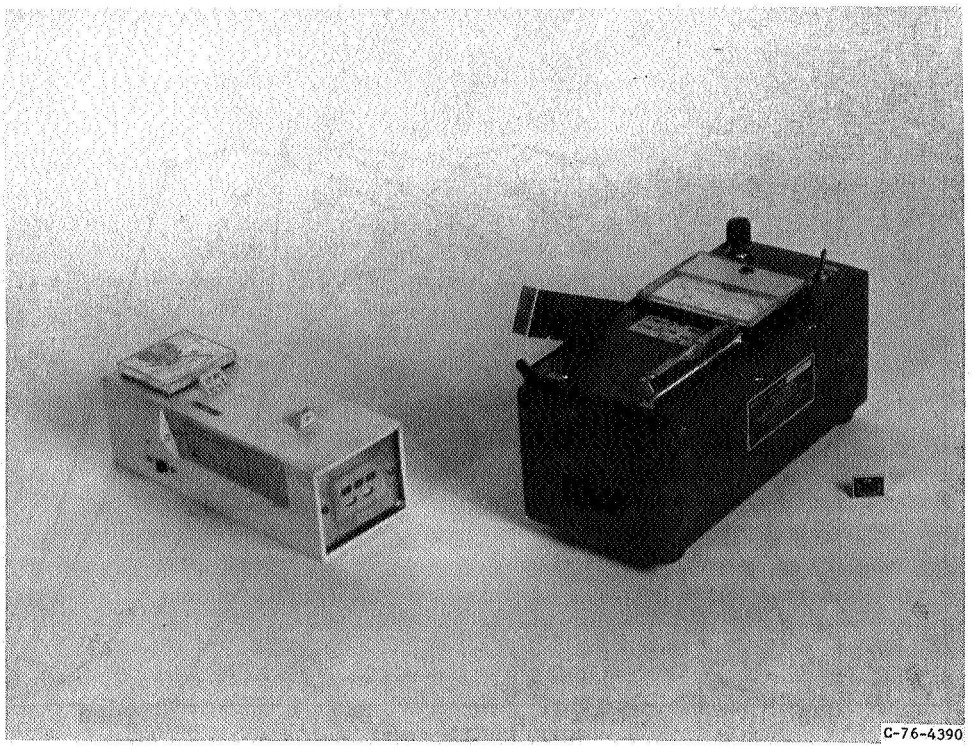


Figure 2. - Sunphotometers used to measure turbidity, water vapor and relative air mass

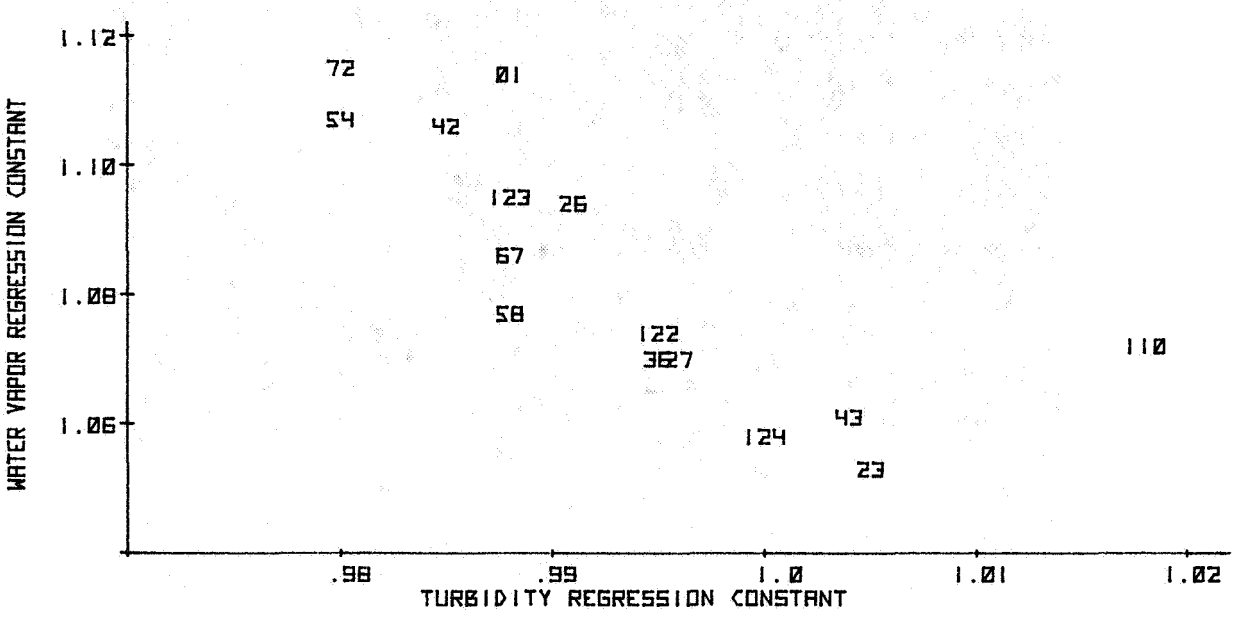


Figure 3. - Correlation between turbidity and water vapor regression constants

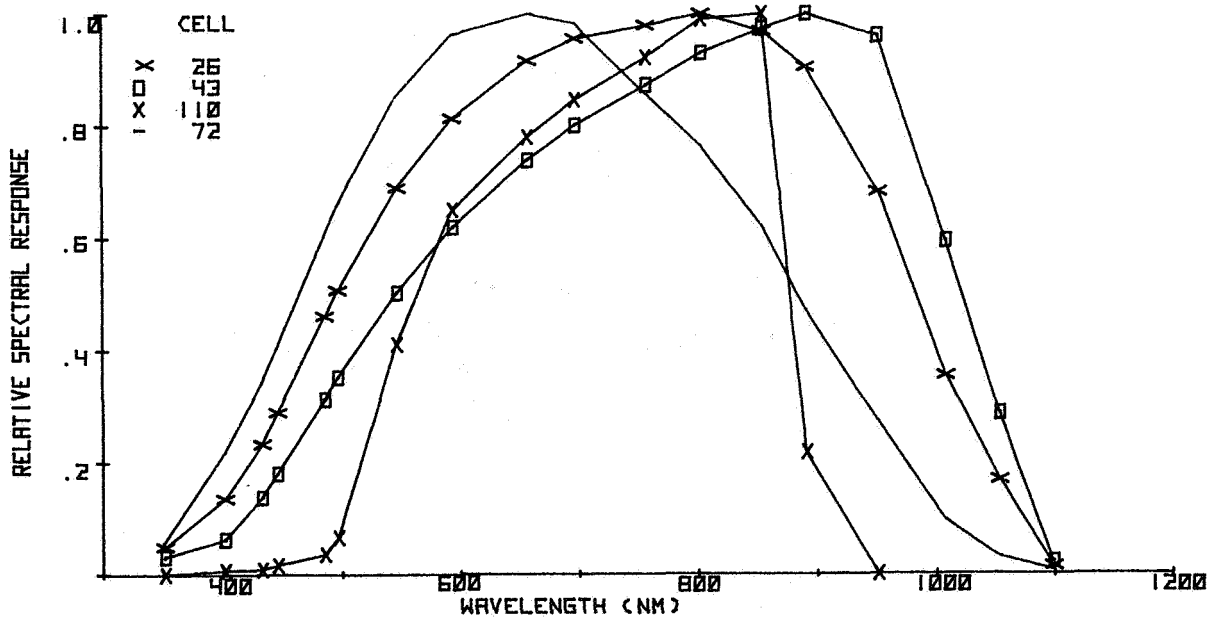


Figure 4. - Comparison of relative spectral response curves of 4 cells

# Report of Working Group on Solar Simulation for Photovoltaic Applications

Gil Downing/JPL

The bulk of the discussions in this session were concerned with types of sources for terrestrial solar simulators and the performance characteristics for simulators. Other topics discussed included the possible need to develop a new type of terrestrial solar simulator, and the possible use of an extensive round-robin to test the feasibility of same easy-to-use spectral irradiance monitor.

In the discussion concerning present-day simulators, the following recommendations were made:

1. There are three types of light sources which are acceptable for terrestrial photovoltaic solar simulators. They are: the xenon short arc lamp with near IR line filtering; the long arc xenon lamp pulsed system, and the dichroic modified 3400$^{o}$K tungsten-halogen lamp. It was felt that each of these sources gives an adequate spectral match to terrestrial sunlight. The short arc xenon lamp is the source used in many AMO simulators with filtering to reduce the near IR line spectrum. The long arc xenon pulsed system (flash simulator) has been developed for measuring large solar cell arrays and is somewhat richer in the ultraviolet than the short arc xenon lamp. The dichroic-modified tungsten halogen lamp (ELH type lamp) is an ordinary tungsten-halogen bulb with a dichroic reflector which reflects the visible and transmits a large portion of the infrared irradiance out of the beam as waste heat. Hence, the irradiance in the reflected beam more closely

duplicates the spectral distribution of terrestrial sunlight.

2. The non-uniformity of irradiance in the test plane shall be less than $\pm$2%. The area of the detector must be less than one-quarter of the test cell area or, (for ribbon cells), the largest dimension of the detector must be less than one-half the cell length and one-half the cell width.

3. The temporal stability of total irradiance must be within $\pm$1% during the test.

4. The simulator must be capable of at least 100 $mW/cm^2$ as measured with a reference solar cell of the same type as the cell being tested.

5. Solar beam subtense angle: The angle subtended by the apparent source of the simulator on a point on the test cell must be less than 30 degrees.

Other conclusions of this workshop were:

1. There was no need at the present time to develop a new type of terrestrial solar simulator. The existing types are adequate.

2. It would be beneficial to the terrestrial photovoltaic community to have a series of round-robin measurements to test the feasibility of utilizing the red filter-blue filter ratio technique as a spectral irradiance distribution monitor.

## Report of Working Group on Design Reference Cell and Calibration

A. F. Forestieri/NASA-Lewis Research Center

Reference Cell

1. How should the interim manual be revised with respect to cell calibration?

a. Specification of atmospheric conditions (air mass, $H_2O$, turbidity, etc.) and their ranges.

- Pick median value for conditions to minimize errors due to correction factors. Derive spectral energy distribution from these conditions to define standard sun.
- Choose standard conditions at one point then correct to that point. Also, give range that will give correct answer within ± some % error.
- Define correlation coefficient as a function of air mass water vapor, turbidity and any other pertinent variable.
- Suggest range for air mass (A) of 1 to 2.5

  turbidity (B) 0.2

  in addition AxB 0.25

  choose a median value for water vapor 2-4cm suggested.
- Suggest change in $\frac{I_{uncoll}}{I_{coll}} < 1.33$ but subject to verification (The above values must be consistent with each other and with standard sun).

b. Type of detectors to be used as references.

NIP - but suggest a study be made for a global technique and then include that technique as an alternate.

c. Size of aperture

- Specify the slope angle at $1.76^{o}$; increase tracking accuracy to $\pm 1.0^{o}$.

d. Reference cell temperature at time of calibration

$28^{o} \pm 2^{o}C$

- Consider higher temperature in future or possibility of temperature coefficient for correction.

2. What intensity scale is to be used and if a change is made, when should it become effective?

- Go along with ERDA (presently IPS) then change to PACRAD III with $\sim$ 1 year to change.
- Change is linear and about 2½%. Change will be made in cooperation with ASTM and WMO.

3. Is the spectral distribution of sunlight at the time of calibration needed?

Allow for the spectral energy distribution of the sun during calibration. However not required so long as other data (atmospheric) is available to allow correction to standard conditions.

4. What improvements can be made in present reference cell package?

- There are reflection problems and water cooling problems. Add specification on thickness and size.
- Suggest that master standard be unpackaged and derive secondary or working standards.

5. What is role of a series of round robin measurements?

- Suggest set up formal round robin $\sim$ yearly.
- Also consider team check out other facilities.

6. At least 2 master cells should be supplied. They can then be checked against each other to determine changes.

# INTRODUCTION TO BASIC SOLAR CELL MEASUREMENTS

by Henry W. Brandhorst, Jr.
National Aeronautics and Space Administration
Lewis Research Center
Cleveland, Ohio

## ABSTRACT

The basic approaches to solar cell performance and diagnostic measurements are described. The light sources, equipment for I-V curve measurement and the test conditions and procedures for performance measurement are detailed. Solar cell diagnostic tools discussed include analysis of I-V curves, series resistance and reverse saturation current determination, spectral response/quantum yield measurement and diffusion length/lifetime determination.

## INTRODUCTION

The accurate, reproducible evaluation of solar cell performance is one of the more difficult and challenging aspects of device development. The short circuit current of a solar cell is strongly dependent on the intensity and spectral distribution of the illuminating source. The problem arises because all available light sources (the sun included) change intensity and spectrum with time. Control of this variable system is possible although filled with many subtleties. Once the experimental challenges of obtaining an accurate device short circuit current have been overcome, the current-voltage (I-V) characteristic and hence the power output and efficiency can be obtained. However, this next step is also subject to errors. Key to eliminating these errors is the understanding

that the solar cell is a power producing device. Thus electrical connection to the solar cell is an important consideration. Finally, the assessment of device performance and understanding of the mechanisms which limit cell performance is the final step that leads to improved device performance.

It is the purpose of this paper to present a general overview of solar cell performance measurement and diagnostic techniques. It is wise for all solar cell investigators to review such basics periodically to guard against the infusion of poor, expeditious techniques that inevitably result in confusion.

## CHARACTERIZATION OF SOLAR CELL PERFORMANCE

First, and by far the most critical parameter to be determined in accurate solar cell performance measurement, is the short circuit current. This parameter is controlled almost exclusively by the light source used and the way its level is adjusted. Considerations on the light sources available and the way to adjust them will be covered subsequently. The next important consideration is the electrical aspects of the circuitry and connections made to the solar cell. Their discussion also follows. The intertwining of these areas is necessary before accurate, reproducible measurements of device performance can be made.

## LIGHT SOURCES

The types of light sources generally used for solar cell measurement are listed in Table I. Natural sunlight is the most desirable; however, it is also the most complex and its availability cannot be assured. If,

however, it is used, details of the appropriate measurement procedures to be used are described in reference 1. These measurements require the use of a reference cell or pyranometer to determine the irradiance. Critical atmospheric components such as water vapor and turbidity must be measured as well. They influence the spectral distribution of sunlight and hence affect the performance of the cell. A variation of about 5% in current can be caused by atmospheric variations. This variation occurs only when a pyranometer is used to monitor the intensity. The black body response of the pyranometer is sensitive to variations in spectrum outside the bandpass of the solar cell. It appears possible to reduce this error through mathematical modelling; however, such approaches have not been thoroughly investigated at this time. More reliable, accurate answers are obtained through use of a reference cell as intensity monitor. As long as spectral response of this cell is the same as the device under test, changes in atmospheric composition will not affect the results.

A second area of difficulty in natural sunlight measurements is translation of the cell performance curve to the recommended (1) standard reference conditions of 100 $mW/cm^2$ and $28^{o}$ C. This translation requires the intensity and temperature of the solar cell or module under test. The intensity is easily obtained from the reference cell. In general, measurements will not be made at 100 $mW/cm^2$; hence correction is necessary. Device temperature can be conveniently controlled for a single cell, but module or array temperature cannot, thus necessitating corrections. Curtis

(2) has discussed the problems and gives a realistic approach for obtaining accurate translated I-V curves from natural sunlight measurements.

Due to the variability of natural sunlight, artificial light sources are more convenient to use. The types of artificial light sources generally used in solar cell measurement are listed in table II. Tungsten sources are the least expensive, pulsed xenon lamps the most. Carbon arc lamps are not included here as they are unstable and contain too much ultraviolet light for good terrestrial simulation. All these light sources are capable of highly accurate, reproducible results. However, their spectral distributions do not exactly match terrestrial sunlight. Hence, all require a reference solar cell to set their intensity so as to minimize errors in short circuit current. A typical tungsten lamp/water filter solar simulator is shown in figure 1, The water filter is used to eliminate the sizable infrared component of the 3400° K tungsten lamp. The ELH lamp simulator looks much the same, except for the elimination of the water filter. The water can be eliminated because the reflector around the bulb is coated with a dichroic filter that allows most of the infrared radiation to escape.

The test plane of a steady-state xenon arc lamp is shown in figure 2. These light sources can uniformly illuminate areas up to 30x30 cm. The pulsed xenon arc lamps can uniformly illuminate areas up to 5½ M diameter. All these light sources can achieve uniformities of ± 2% across the test plane. The spectral distributions have a reasonable match to terrestrial sunlight so that the consequences of not exactly matching spectral response of test and reference cell are not severe (≤ 1%(3)).

Finally, with appropriate electronic controls, their intensity stability is good. The spectral distribution of several of these light sources, referenced to outer space sunlight is shown in figure 3. Curtis (3) has shown that the spectral distributions of these light sources have an adequate match to terrestrial sunlight. The spectral distribution of typical direct beam terrestrial sunlight is shown in figure 4. Failure to adequately match spectral distributions can lead to unexpected results as shown in figure 5. In this extreme example, use of a red wavelength light source completely distorts the performance characteristic of the device. Such an extreme mismatch in spectral distributions is unlikely; however, errors of several percent in magnitude are easily possible with an improperly matched light source especially when the test and reference cell spectral responses are not matched (3).

In summary, the major source of error in solar cell performance measurement is in short circuit current. Accurate measurement of this current requires care and control of a number of variables. When such control takes place, accuracies in current better than $\pm$ 1-2% are possible.

## CURRENT-VOLTAGE CURVE MEASUREMENT

The general types of equipment that can be used to obtain a current voltage (I-V) curve are listed in table II. These are listed in order of increasing cost. Fixed load resistors allow only discrete points along the I-V curve to be obtained. The variable power supply (e.g., ref. 4) allows a continuous power curve to be obtained. Furthermore, this approach

permits biasing of the cell in the forward and reverse direction to obtain additional diagnostic information. The electronic load is basically an automatic power supply tailored for solar cell use. The calculator-controlled system also uses a power supply to obtain the data. This system has the distinct advantage of speed in data reduction. In reality, this system produces answers, not just data.

This instrumentation, when properly maintained in calibration, is capable of faithfully and accurately reproducing device I-V characteristics. However, their output is only as accurate as the input they receive. The electrical connections to the device can distort the shape of the I-V characteristics obtained. This area represents the second most likely source of error. Any wire resistance developed between the test device and the instrumentation will cause losses in power output; hence, an inaccurate I-V curve. These losses can be almost entirely eliminated through use of four-wire connections to the cell (2 voltage, 2 current). With this approach, resistive losses in the wiring and contacts are eliminated because only the voltage at the terminals of the device is measured. However, in using these connections, care must be taken not to separate the voltage and current leads by a great distance or erroneously large fill factors will be obtained. It is also helpful if the current contacts can be as large as possible. This approach will, for the most part, eliminate resistive losses in cell circuitry.

## SOLAR CELL DIAGNOSTICS

Once reliable I-V curves have been obtained, the investigator usually experiences several surprises. Most of these surprises occur because the

shape of the I-V curve is not the clasic square shape as shown by the solid line in figure 6a. The solid curve is the data in the power quadrant while the dashed lines represent the reverse bias (left) and far forward bias (bottom) data. As unusual as they may appear, I-V curves are the first line of solar cell diagnosis. Other diagnostic data that can be obtained include series resistance, dark diode characteristic, reverse saturation current, spectral response and diffusion length. In the following sections, the various diagnostic approaches and the information that can be obtained will be discussed.

## I-V CURVE ANALYSIS

The curves presented in figure 6 represent somewhat idealized cases. Only single failure modes are shown in each curve. In practice, several failure modes can, and usually do, occur together. From inspection of the solid curves alone, it can be seen that different failure mechanisms can have similar shapes in the power (4th) quadrant. Thus the ability to bias the cell in both the forward and reverse direction is essential. Figure 6b represents a junction that has a high excess diode current; this leads to poor fill factors and good currents. The open circuit voltage is not usually affected except in extreme cases. A low shunt resistance (figs. 6c & g) produces a poor fill factor and oftentimes reduced open circuit voltages. High series resistance (fig. 6d and f) reduces fill factor, but generally does not affect voltage. In extreme cases (fig. 6f), short circuit current is reduced. Biasing in the reverse direction will indicate the true light generated current. Also, the

forward diode characteristic becomes more linear with high series resistance. A non-ohmic contact (fig. 6e) is most often seen as a curvature near open circuit voltage but may also occur near short circuit current in some devices.

These few idealized examples serve to indicate the scope and importance of the I-V curve as a diagnostic tool. The other diagnostic tools serve only to further confirm and determine the magnitude of the physical factors affecting device performance.

## SERIES RESISTANCE MEASUREMENT

Cell series resistance is an important factor in improved cell designs. Measurement of its magnitude is necessary to continued device improvement, especially for devices exposed to concentrated sunlight. The following techniques are most commonly used.

Easiest to use is the far forward characteristic (5) in which the voltage drop between 300 and 400 mA (for a 1x2 cm cell) is used to obtain the series resistance. The value obtained generally represents a lower limit and is composed of bulk and contact resistance. The exact values of the forward current are not critical so long as the I-V curve is linear. In practice, the minimum forward current is about 3 to 6 times the cell short circuit current.

The next most common techniques for obtaining series resistance were described by Wolf and Rauschenbach (6). The two light level method requires two I-V curves obtained at different intensities. Cell series

resistance can be computed from the short circuit current difference between the two curves combined with the voltage shift of a point on the I-V curve. It should be noted that series resistance values obtained with this technique generally depend on the point selected on the I-V curve. This can lead to erroneous results.

The next two techniques require the use of the $V_{oc}$-$I_{sc}$ (open circuit voltage-short circuit current) characteristic of the cell. This characteristic is obtained by determining the $V_{oc}$ and $I_{sc}$ of I-V curves generated over a wide range of light intensities. Each $V_{oc}$-$I_{sc}$ combination is plotted as a single point on an I-V or log I vs V characteristic. Use of these two points from the I-V curve eliminates the effect of series resistance, so long as the short circuit current equals the light generated current. In the case of high series resistances, reverse biasing must be used to obtain the light generated current. To obtain the series resistance, the $V_{oc}$-$I_{sc}$ characteristic is subtracted from either the dark forward or the illuminated forward characteristics. (The illuminated forward characteristic is obtained by subtracting light generated current from the I-V curve.) An example of this technique for the dark characteristic is shown in figure 7. It can be seen that there is little difference between the two curves until the voltage reaches about 0.6V. The voltage difference between these curves at a fixed current is due to the device series resistance. Values of series resistance obtained by this technique are accurate. Small differences between series resistance in the dark and light are seen but are to be expected from theory.

## REVERSE SATURATION CURRENT

For many analyses, the reverse saturation current (Io) and the slope of the forward diode characteristic are of importance. Techniques used to obtain these parameters are generally not detailed in technical reports. Some methods used are not accurate and have led to erroneous conclusions. Figure 8 shows a typical forward diode characteristic. Because this curve is composed of the sum of a variety of diode currents (e.g., diffusion, generation-recombination, shunt and surface), the component parts must be resolved in turn. Through this procedure, an accurate assessment of the magnitude and type of current present can be made. For example, the solid curves indicate the resolution of two of these components. No prior knowledge of the slope of the curve is needed for this procedure. Were the raw data to be used, significant errors in the slope of the diffusion component (A=1) and its intercept (Io) would occur. While somewhat more time consuming, subtraction of the component curves (beginning with the lowest current component, ususally the shunt resistance) appears to be the most reliable way of reaching firm conclusions.

## SPECTRAL RESPONSE

Solar cell spectral response provides the most diagnostic information next to the I-V characteristic. In this approach, monochromatic lights illuminate the cell and the current produced is measured. Monochromators and narrow band pass monochromatic interference filters are the most common sources of light. Monochromators can range continuously but are

limited in area coverage, uniformity and intensity. Interference filters do not suffer from these limitations, but their response generally cannot be continuously varied over a wide range. Figure 9 shows a system using interference filters. This system as shown does not employ a white bias light to simultaneously illuminate the cell. Simple modifications to permit use of bias light are shown in figure 10. The bias light enters through a side port and is reflected onto the cell. Neither monochromatic nor bias lights are chopped in this system. In other systems, the monochromatic beam is chopped, while the bias light remains direct current. Either approach can be employed with the bias light system and comparable results are obtained. Bias light must be used in cases where cell performance depends on injection level or wavelength. Impurities or induced defects can lead to injection level effects while light ionized recombination or trapping cneters can lead to wavelength dependence. An example of a wavelength dependent spectral response behavior is the $Cu_2S$-CdS solar cell shown in figure 11. With no bias light, the response of this cell falls sharply above 0.7 μm. Slow current decays are also seen (7). However, the presence of bias light eliminates these effects and a reproducible spectral response is obtained.

The additional advantage of spectral measurements is that the quantum yield of the device can be obtained from the spectral response curve. Quantum yield is defined as electrons generated per photon incident. Such a curve for the $Cu_2S$-CsS cell is shown in figure 12. This information leads to a basic understanding of cell losses that can lead to future device improvements.

In all spectral response measurements, absolute accuracy is a substantial problem. Peak accuracy is no better than ± 5% at the present time. In practice errors of ± 20% are not unusual (8). Thus intercomparison of data from different sources is risky, and conclusions based on such comparison may not be warranted.

## DIFFUSION LENGTH/LIFETIME MEASUREMENT

The measurement of diffusion length or lifetime of minority carriers in a solar cell is needed for modelling, process control and device improvement. A variety of techniques, such as shown in Table III, have been used in the past. This list is not all-inclusive but represents most of the common approaches.

When penetrating radiation is employed, the current collected for a fixed input is proportional to diffusion length. Calibration curves showing this proportionality are obtained both theoretically and experimentally (9, 10), Comparable results are obtained with electrons, x-rays and infrared light. Cells containing a junction or barrier layer are necessary. In general, this technique is the quickest to use.

The photoconductive decay method measures the response of a sample of material to a short pulse of light. After cessation of the light pulse, the light generated carriers decay with a time constant proportional to the lifetime. Sample geometry and carrier trapping are variables in this approach. Interpretation of the data can be time consuming.

Steady state photoconductivity and surface photovoltage measurement are techniques that can be used on bulk material or devices. They are generally more time consuming than the penetrating radiation approaches but also yield comparable results.

Electrical techniques for obtaining lifetime generally employ forward then reverse biasing of a device with an electrical pulse. The decay of the voltage or current (short circuited device) in the device after cessation of the pulse yields the lifetime. An example of an open circuit voltage decay curve is shown in figure 13. The sharp drop after cessation of the pulse (t = 0) yields device series resistance while the slope of the curve after t = 0 yields the lifetime. In general, sample size may be limited due to capacitance effects. Surface effects can also influence results. While these methods all yield comparable results, all require careful attention to obtain consistency.

## CONCLUDING REMARKS

The art of solar cell measurement and diagnosis is more complex than is often recognized and requires a high degree of competence to achieve accurate, reproducible results. Considerable experience has already been built up. It is strongly recommended that those entering this field consult with experienced solar cell investigators to gain the benefit of their experience. In so doing, uniform measurements and accurate data will result which will hopefully lead to rapid progress in device development and improvement.

## REFERENCES


1. Brandhorst, Henry W., Jr., et. al.: "Interim Solar Cell Testing Procedures for Terrestrial Applications", NASA TMX-71771 (1975).

2. Curtis, H. B.: "Outdoor Module and Array Measurements at NASA-Lewis". Proceedings of the Second Terrestrial Solar Cell Measurement Procedures Workshop, Nov. 1976.

3. Curtis, H. B.: "Effect of Simulator Spectral Differences on Short Circuit Current Measurements". Proceedings of the Second Terrestrial Solar Cell Measurement Procedures Workshop, Nov. 1976.

4. Brandhorst, H. W. and Hart, R. E.: "Radiation Damage to CdS Solar Cells", NASA TN D-2932, July 1965.

5. Mandelkorn, J., et. al.: "Fabrication and Characteristics of Phosphorus Diffused Silicon Solar Cells", J. Electrochem. Soc. 109, 313 (1962).

6. Wolf, M. and Rauschenbach, H.: "Series Resistance Effects on Solar Cell Measurements", Adv. Energy Conv. 3, 455-479 (1963).

7. Brandhorst, H. W., Schalla, R. L., Potter, A. E. and Rosenblum, L.: "Effects of Bias Light and Heat Treatment on the Spectral Response of Cadmium Sulfide Thin Film Photovoltaic Cells", NASA TN D-5521, January 1970.

8. Geist, J.: "Standard and Silicon Detectors as Applied to Photovoltaics". Proceedings of the Second Terrestrial Solar Cell Measurement Procedures Workshop, Nov. 1976.

9. Reynolds, J. H. and Meulenberg, A.: "Measurement of Diffusion Length in Solar Cells", J. Appl. Phys. 45, 2582 (1974).

10. Lamneck, J. H., Jr.: "Diffusion Lengths in Silicon Obtained by an X-ray Method", NASA TM X-1894, Oct. 1969.

TABLE I - LIGHT SOURCES USED FOR PERFORMANCE MEASUREMENT

- SUNLIGHT
- TUNGSTEN LAMPS
  - ELH LAMP (~ AM2)
  - $3400^{0}$ K LAMP PLUS WATER FILTER
- XENON ARC LAMPS
- PULSED XENON LAMPS

TABLE II - TYPES OF EQUIPMENT FOR I-V CURVE MEASUREMENTS

- FIXED LOAD RESISTOR BANK
- VARIABLE POWER SUPPLY (BATTERY ETC.)
- ELECTRONIC LOAD
- CALCULATOR-CONTROLLED ELECTRONIC LOAD AND DATA ACQUISITION AND REDUCTION SYSTEM

TABLE III - TECHNIQUES FOR DIFFUSION LENGTH/LIFETIME MEASUREMENT

OPTICAL

- PENETRATING RADIATION
  - X-RAYS
  - 1 MeV ELECTRONS
  - INFRARED LIGHT ( $1.1 > \lambda > 0.9\ \mu m$)
- PHOTOCONDUCTIVE DECAY
- STEADY STATE PHOTOCONDUCTIVITY
- SURFACE PHOTOVOLTAGE

ELECTRICAL

- OPEN CIRCUIT VOLTAGE DECAY
- COLLECTION OF STORED CHARGE (CURRENT DECAY)

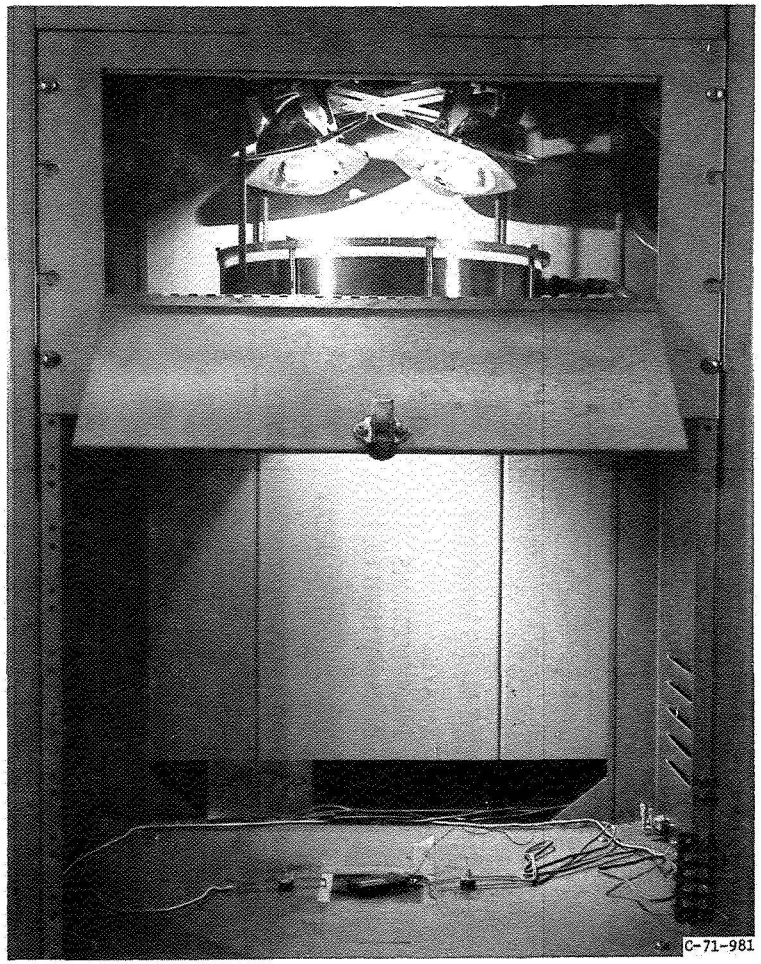


Figure 1. - Tungsten Light Solar Simulator

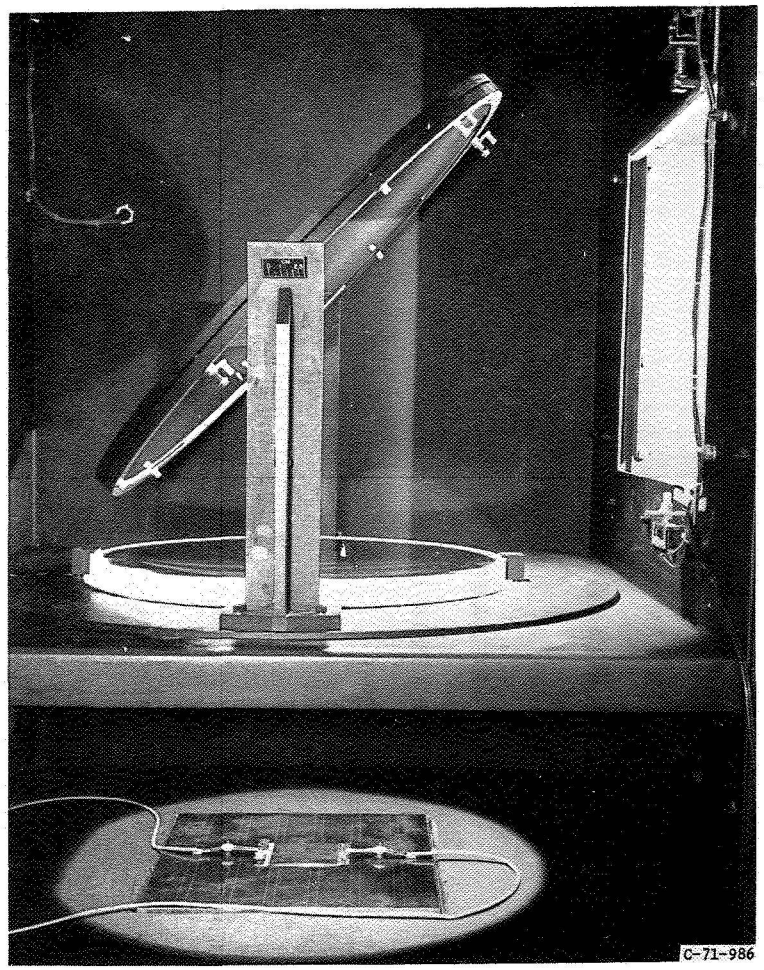


Figure 2. - Test Plane of Steady State Xenon Arc Simulator

## SPECTRAL DISTRIBUTION OF SOLAR SIMULATORS

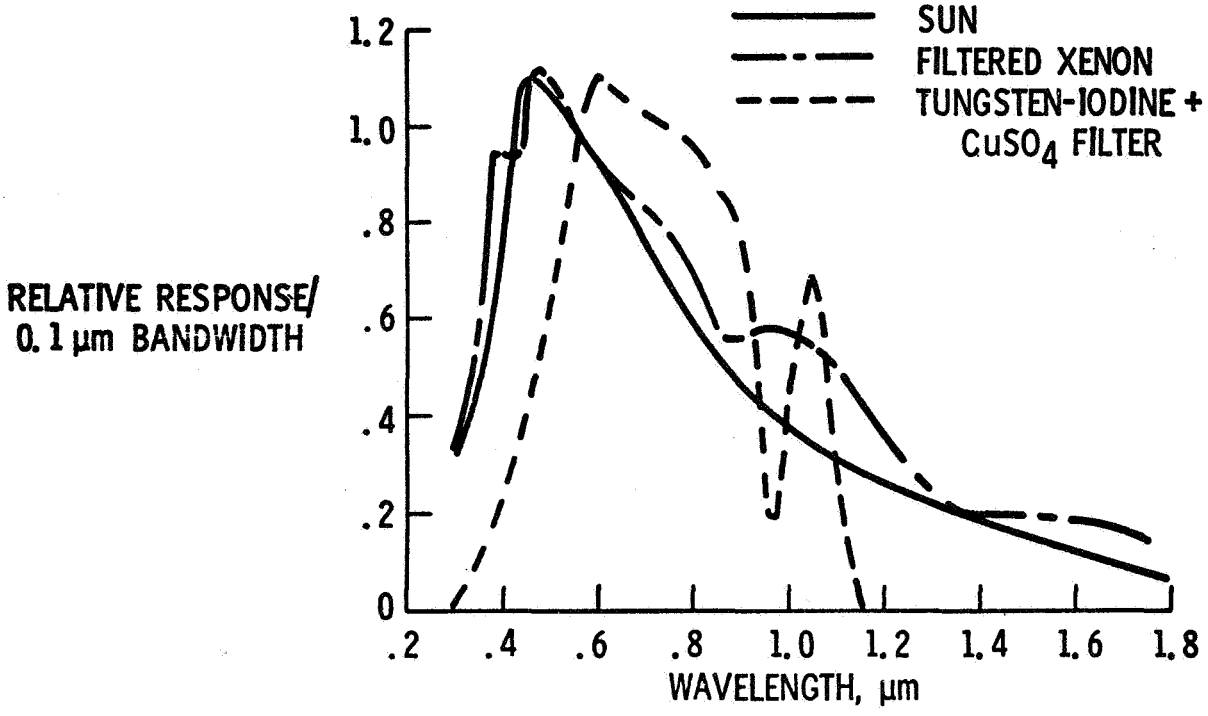


Figure 3.

Figure 4. - Spectral distribution of terrestrial sunlight

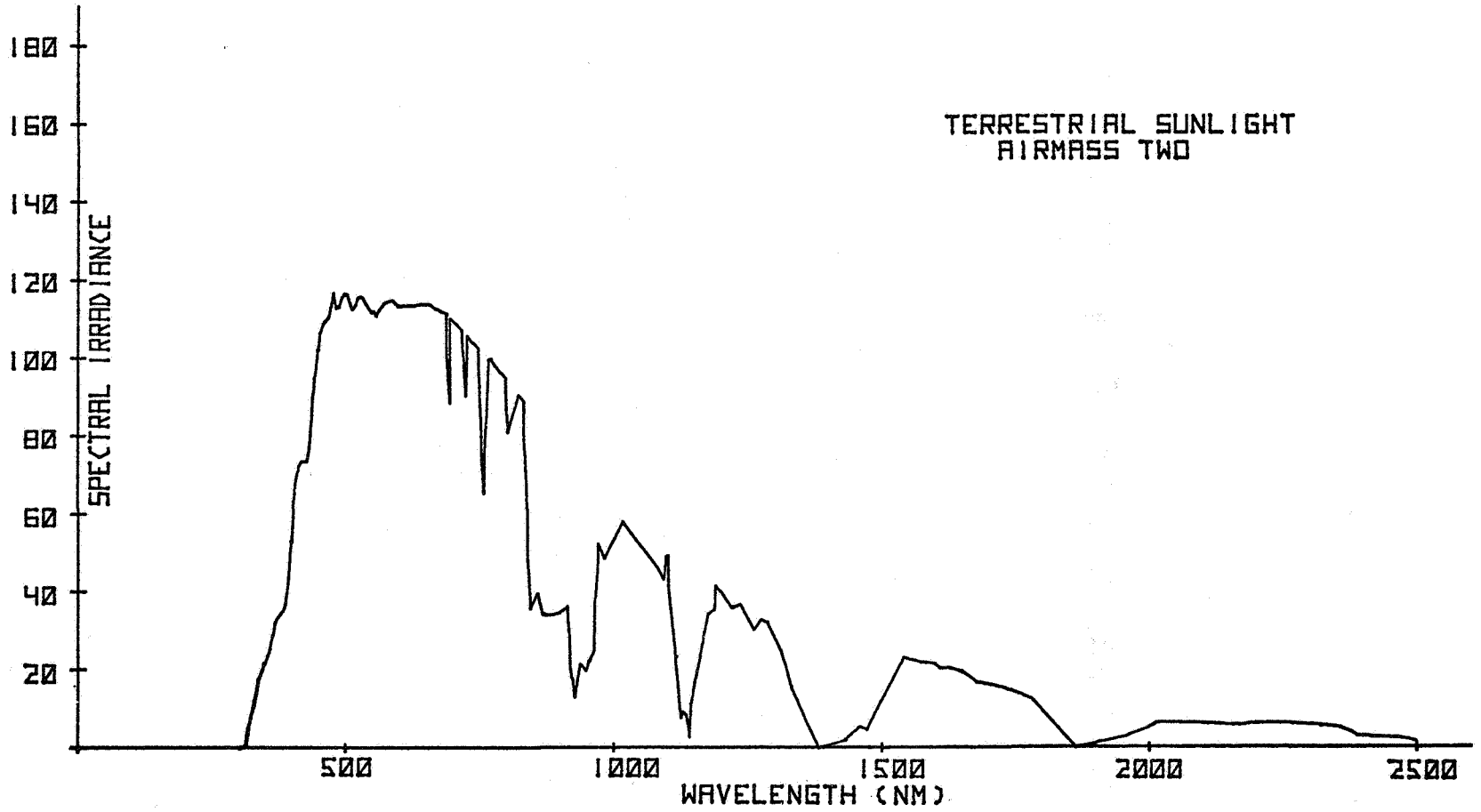

CURRENT–VOLTAGE CURVES OF A $Cu_2S$–CdS CELL ILLUMINATED WITH RED AND WHITE LIGHT

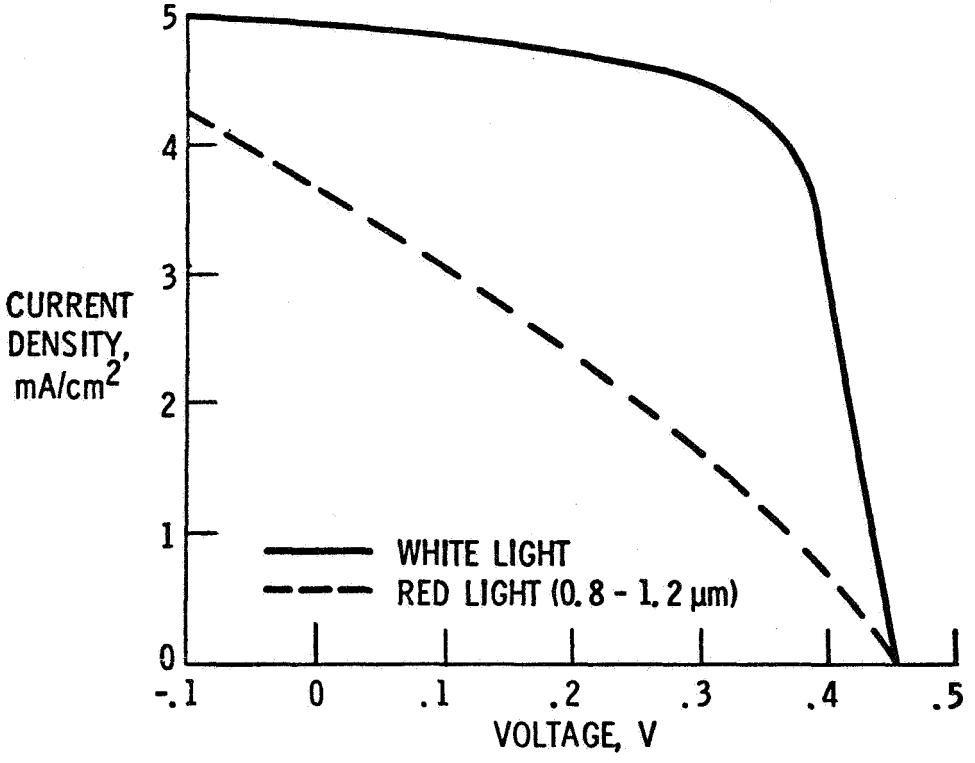


Figure 5.

Figure 6. - Solar cell current-voltage characteristics
(Current axis, vertical, voltage axis horizontal)

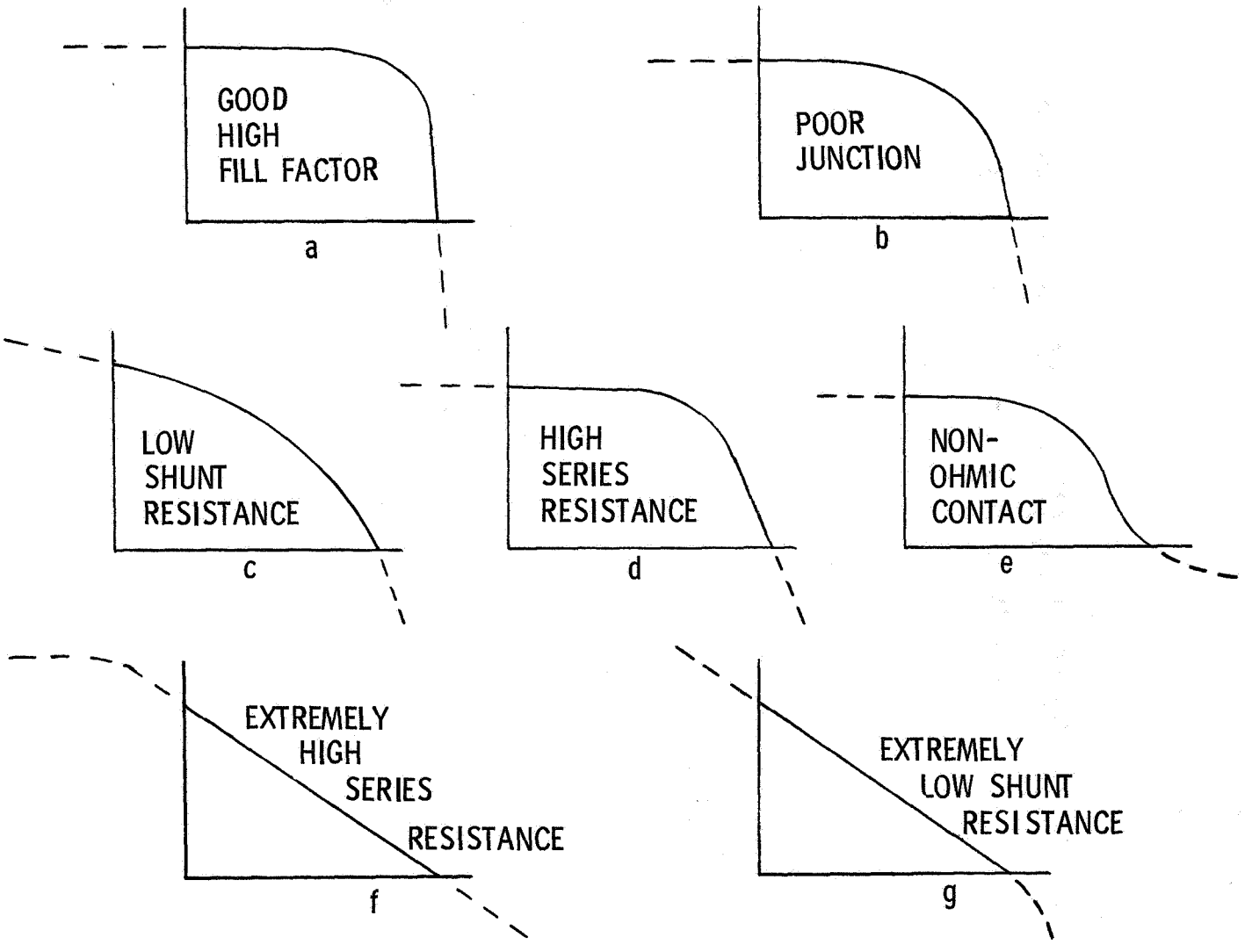

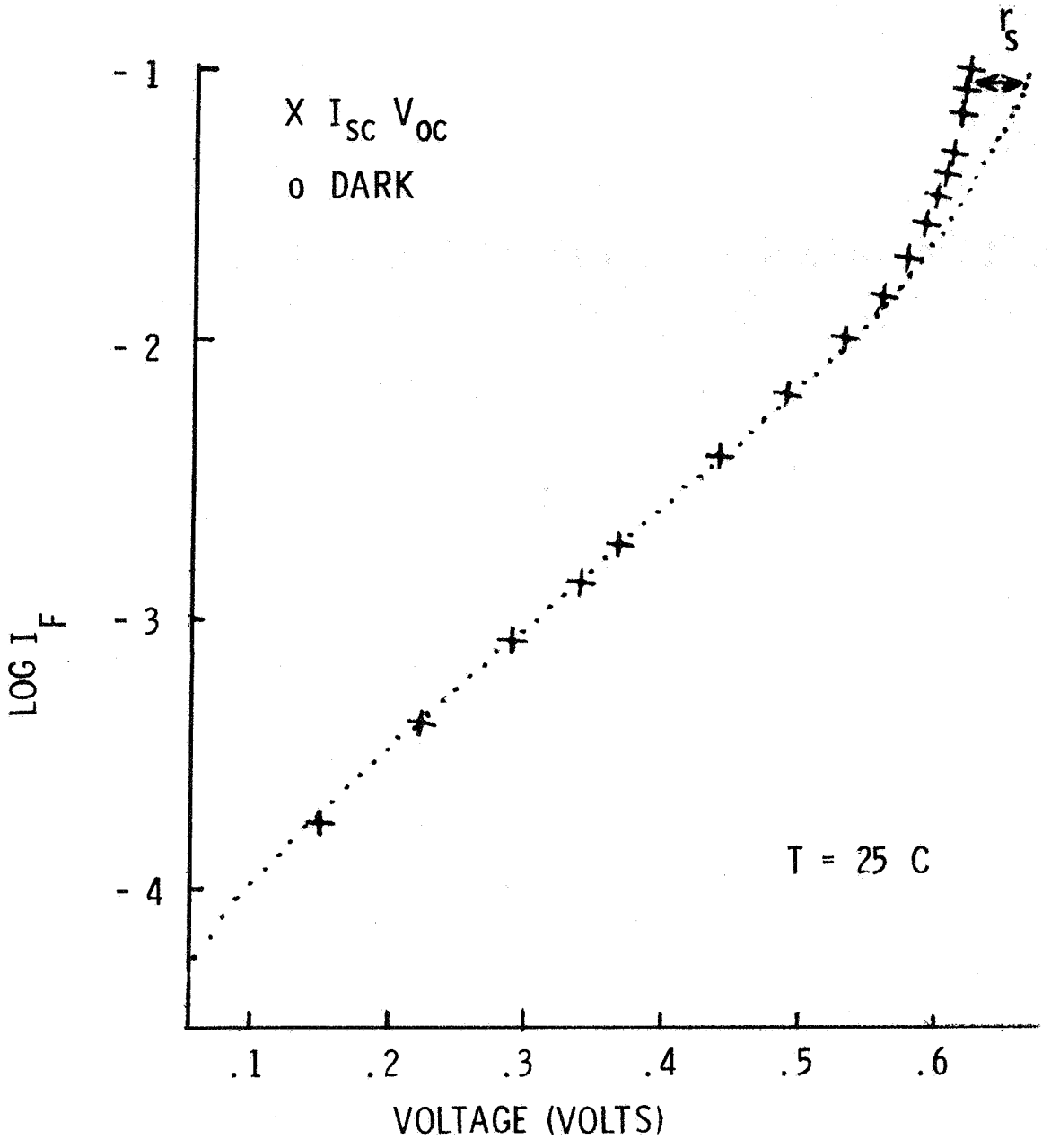


Figure 7. - Solar cell forward I-V characteristics measured by dark and illuminated methods

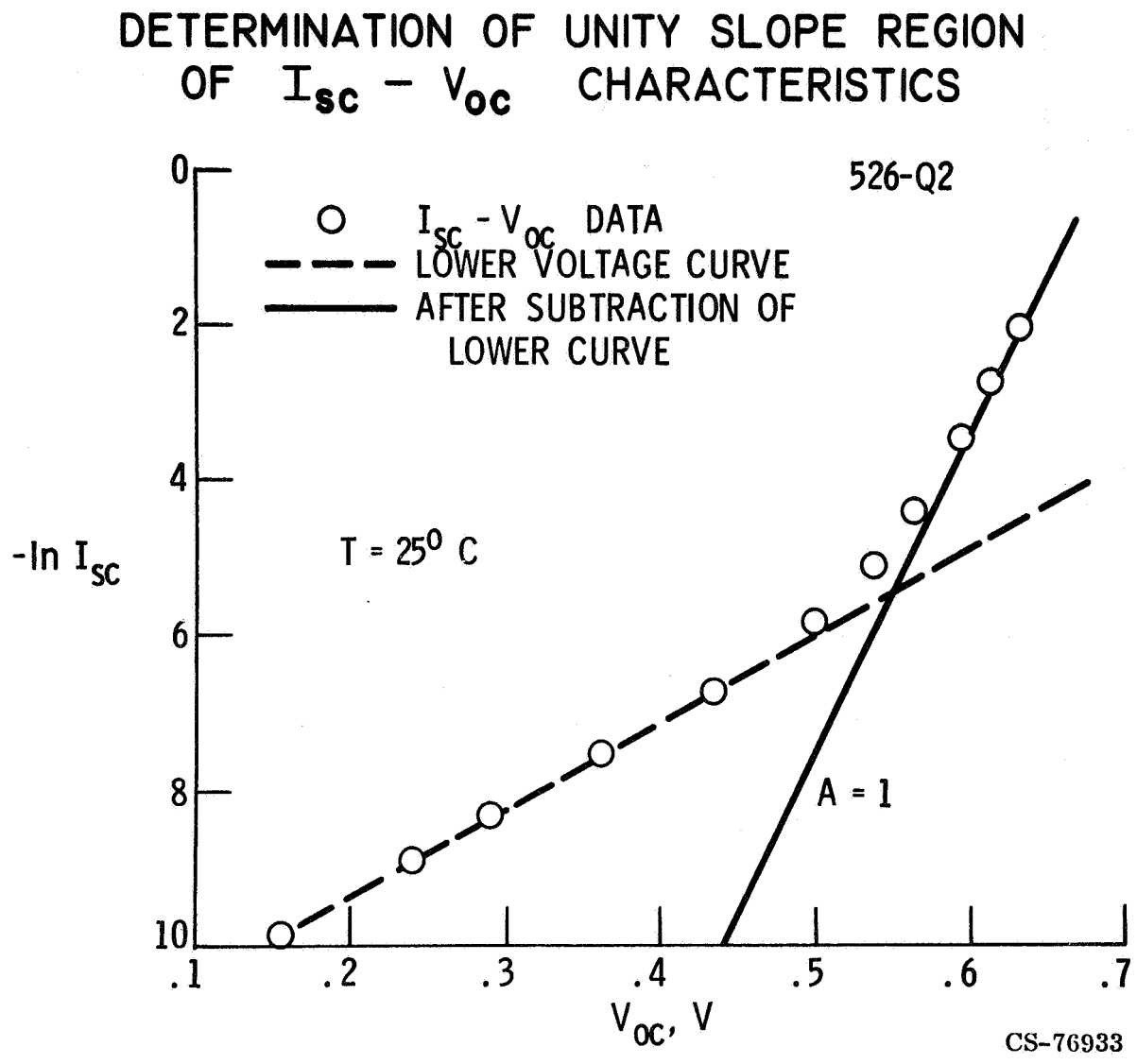
DETERMINATION OF UNITY SLOPE REGION
OF $I_{sc} - V_{oc}$ CHARACTERISTICS
526-Q2
$I_{sc} - V_{oc}$ DATA
LOWER VOLTAGE CURVE
AFTER SUBTRACTION OF LOWER CURVE
T = 25° C
A = 1
-ln $I_{sc}$
$V_{oc}$, V
0
2
4
6
8
10
.1
.2
.3
.4
.5
.6
.7
CS-76933

Figure 8.

## APPARATUS FOR MEASURING SPECTRAL RESPONSE

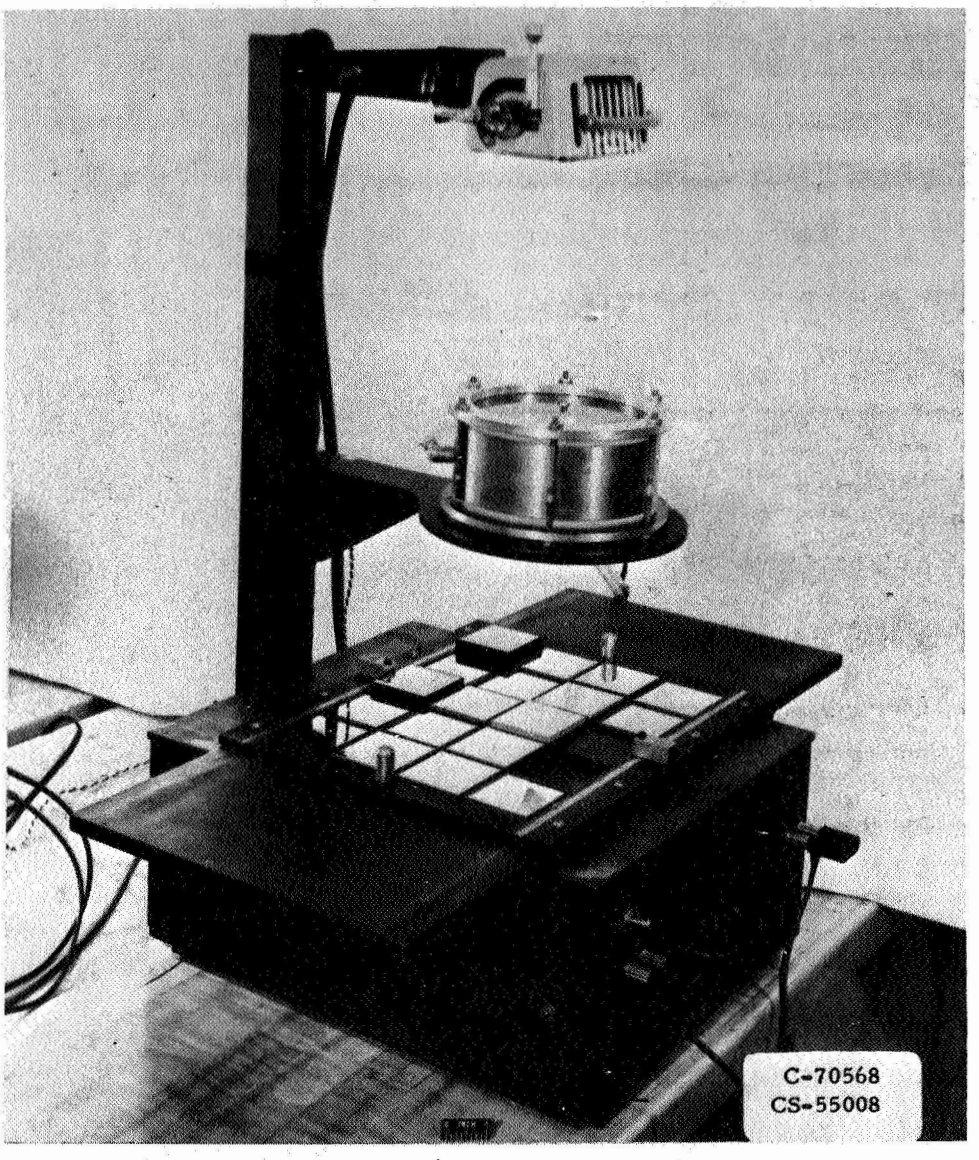


Figure 9.

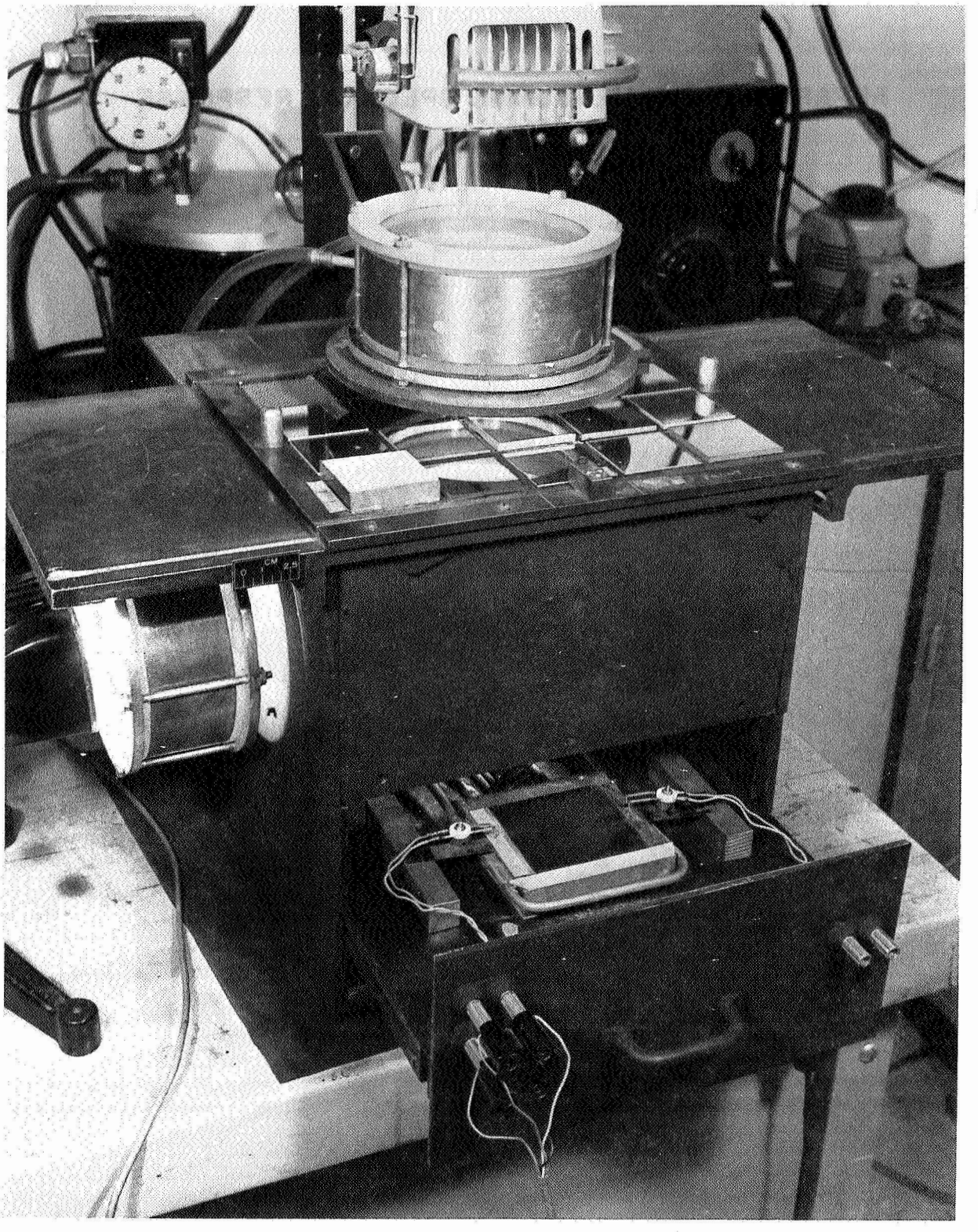

Figure 10. - Spectral response measurement with white light bias

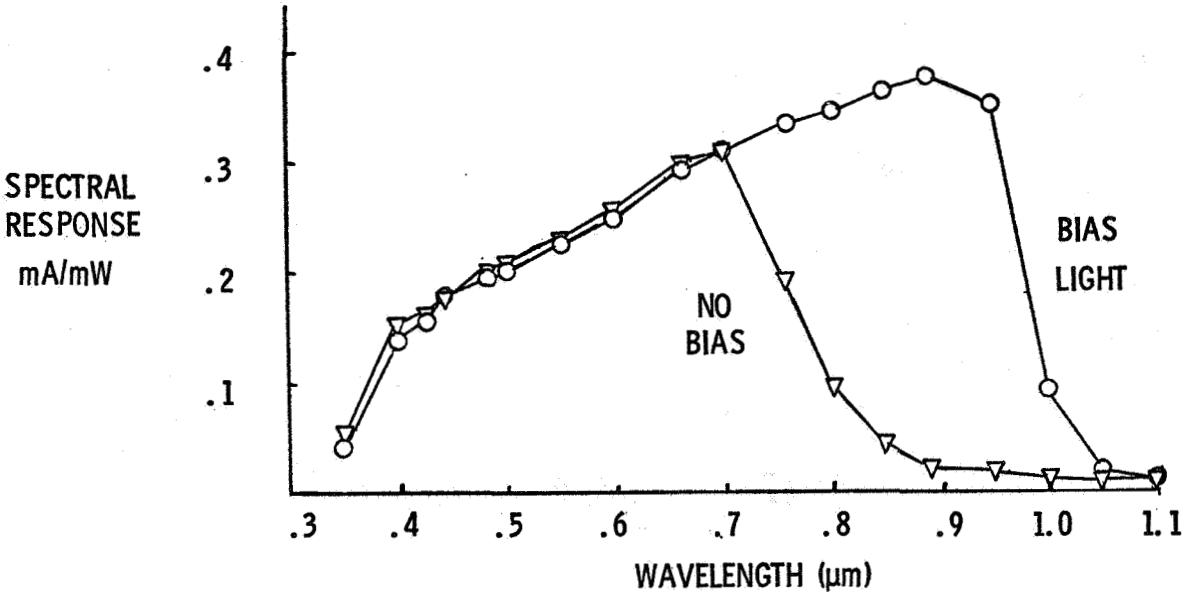


Figure 11. - Spectral response of a CdS solar cell

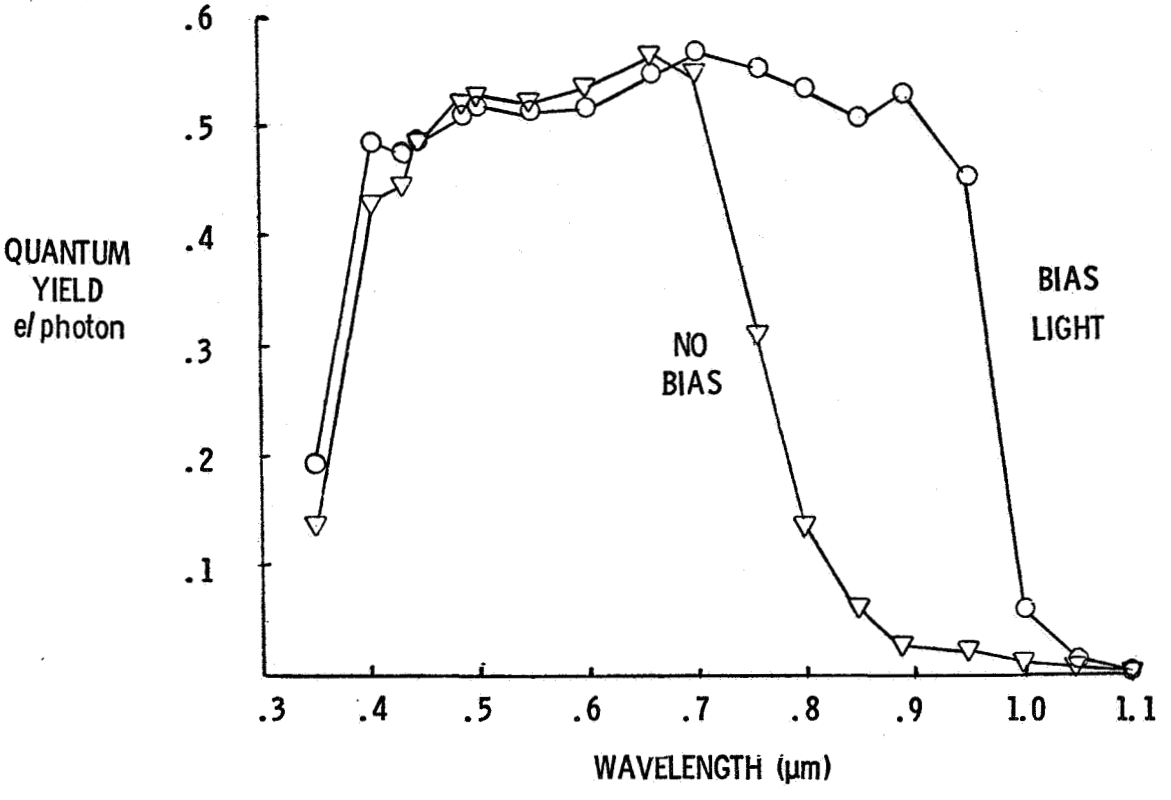


Figure 12. - Quantum yield of a CdS solar cell

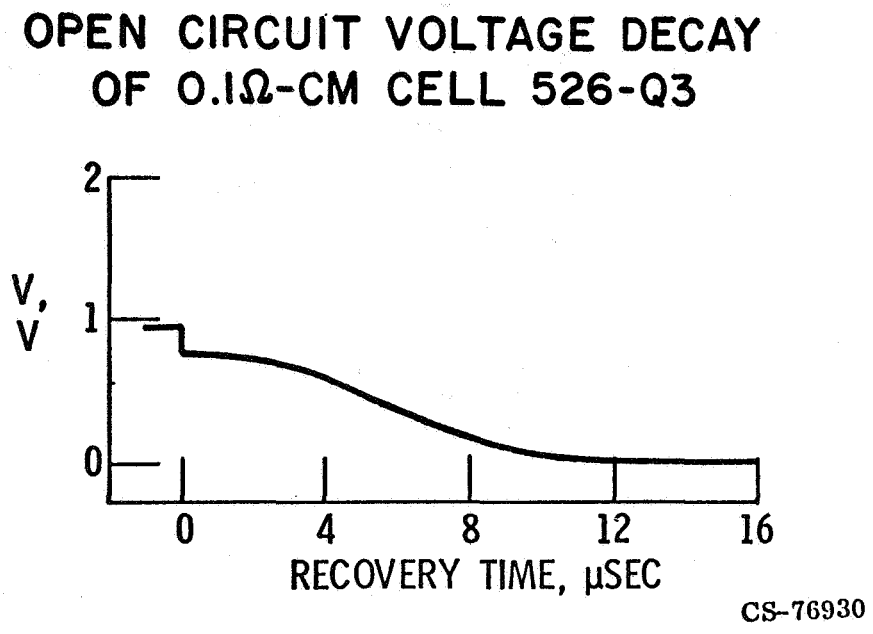
OPEN CIRCUIT VOLTAGE DECAY
OF 0.1Ω-CM CELL 526-Q3
2
V,
V
1
0
0
4
8
12
16
RECOVERY TIME, μSEC
CS-76930

Figure 13.

# CELL AND MODULE TEST PROCEDURES SEEN FROM THE MANUFACTURER AND THE USER POINT OF VIEW

by Dr. Henry DURAND
Laboratoires d'Electronique et de Physique appliquée
B. P. no. 15, Limeil-Brévannes (France)

Summary

This paper summarizes some of the problems which are usually not taken into account by "conventional" test procedures, but which are of the utmost importance to the manufacturers and users of solar modules. Amongst them, a clear definition, - and its related measurement -, of the "rated" power of a module should be of great help to define the actual performance of a module.

A very simple temperature test, acceptable for modules thanks to their higher thermal capacity, is suggested. Various practical considerations dealing with cell and module technologies lead to the conclusion that reference bare cells are not well suited for module test procedures. Finally, some suggestions are made for environmental module and array tests and for some other practical data to be introduced in the future specifications.

## 1. Rated power and rated voltage.

The factor of merit of a bare solar cell is usually given as its maximal efficiency ( AM 1 at 28°C), or as its peak power (28°C) per unit area under a standard 1 kW/m$^2$ illumination. Although this value is of utmost importance for the physicists and the manufacturers, and represents indeed the "quality" of the technology involved, it can seldom be of a practical use for the system engineer. The peak-power, as given on a bundle of curves such as those of Fig. 1 ([1]), is the point where the I-V curve tangents the P = constant hyperbolas. Not only the peak-power but also the impedance of the optimum load depends heavily on the temperature. It is therefore in practice a rather unrealistic notion for the user.

([1]) I-V characteristics for several temperatures for a module BPX47A manufactured by RTC, Paris, France.

Generally, a buffer battery and a blocking diode are inserted in the system (the pumping of water being sometimes an exception to this rule, since electrical storage can in principle be avoided in this case). The battery imposes therefore its voltage $V_b$ to the system (allowing for over 10 % variation rate between the charging and the discharging operations). The example of Fig. 1, meant to illustrate a 12 volt floating battery system, shows the $V_b$ zone comprised between 12 and 13.5 volts, to which 0.8 volt should be added for the blocking diode : the rated voltage $V_r$ should therefore be here 14.3 volts. Actually, this value is not just the addition of various voltages; but for a properly engineered module, it should correspond to an intrinsic property : the rated voltage of a module corresponds to the operation where the influence of temperature on the output power is minimized over the range of field temperature operation. Figure 2 shows that this particular example is well optimized at a rated power of about 10 watts over the 0 - 55°C temperature range. This range depends on the technology of the encapsulation. In the case described here (double glass encapsulation), the heating of the junction above the ambient temperature is about 15° C only under the standard AM1 illumination in a still atmosphere. One can therefore "rate" the power at 10 watts for any ambient temperature from -15 to +40°C. Other encapsulations, such as an epoxy-resin back-panel, may lead to temperature raises up to 25 or even 30° C above ambient temperature.

In consequence, one can suggest a definition by which the "rated power" should be such that, for a given "rated voltage", its relative variations over a $(T_1, T_2)$ temperature range should be less than "p" percent.

2. Temperature measurements of a module.

This implies, as for other test procedures, that the real junction temperature of the cells encapsulated in a module of a given technology is well known. Various methods have been proposed for testing the temperature of the cell (flash method, for instance). In the case of a module, the situation is relatively easier, due to its high thermal capacity. The "flash" can be rather long. In the case cited here (double glass encapsulation, a rather heavy structure), the influence of the 1 $kW/m^2$ illumination, as indicated by the variation of $V_{oc}$ for instance, is negligible for the first 20 or 30 seconds of exposure (less than 1 to 2°C variation). One has therefore all the time required to draw the I-V curve, either under simulation, or even outdoors under real sunshine. With lighter encapsulations, this time might be reduced to a few seconds only, but is long enough to work under very classical conditions.

3. Reference cells.

At the final control of the manufacturing process, each cell is tested under a xenon simulated light, with respect to a "reference cell". Such reference cells are periodically measured and checked by the C.N.E.S. (French Space Agency, in Toulouse). This means in practice that the reference cells are mainly used to get sure that the simulator behaves properly and allows for immediate correction if some drift appears in the illumination provided by the simulator.

In other terms, the reference cell is considered as a secondary standard from the test equipment itself.

In the research laboratory, we usually prefer to "qualify" new technologies by the spectral response : it is an excellent tool, not only for physical measurements (light absorbtion, diffusion length, etc.), but also for a good appreciation of the overall quality of the process involved, and for a better understanding of the cell behaviour.

Indeed, the use of a reference cell alone for the characterization of new technologies can be misleading : a given reference cell can only be used to achieve comparison tests with cells of similar technology (i. e. with similar spectral responses). If the differences are too striking, the corrections that one has to make cannot be considered as first order adjustments, and a new reference cell has to be used. Things are getting worse for modules, because aside from the particular cell technology, further distortions are introduced by the kind of encapsulation, especially by the nature of the front window, the optical coupling between the cell and the window, etc.

Our conclusion here is that different reference cells should be used for the qualification of each particular technology of module and/or cells.

4. The influence of technology on calibration.

In order to illustrate these considerations, let us consider Figure 3 ([2]), which shows clearly the combined influence of some technical parameters on the overall quality of encapsulated cells. One sees the relationship between the efficiency and :

- the cell manufacturing process (texturized or "normal");
- the quality of the A.R. coating (thickness of $TiO_2$ in abcissa);
- the rôle of encapsulation (glass window).

---

([2]) From a paper to be presented by J.Michel at the 12th Photovoltaic Specialists Conference, Baton Rouge, November 15-18, 1976

Particularly striking is the latter, since the behaviour of glass covered cells is totally quite different for the case of texturized and of "normal" cells.

Another good example showing how difficult the straight calibration of a new technology can be, is given in Figure 4 ([3]): it shows the spectral response of a MIS cell without anti-reflecting coating (curve a) and with a $TiO_2$ coating (curve b). In the latter case, the spectral response is quite close to that of a $n^+/p$ diffused cell, and a calibration with a diffused reference cell can be used (and gives a 11.7 % overall efficiency). In the former case, the spectral response is very different (and quite poorer) with a relatively flatter response, in the lower end of the spectrum. Diffused reference cell cannot be used here without knowing the exact emission spectrum of the simulator, and a straight calibration becomes suspicious : mathematical corrections taking into account such an unusual spectrum response have to be performed, or, if possible a special reference cell has to be calibrated.

A last remark deals with non-normal light beam measurements. Experience shows that, for most of bare cells of various technologies, the influence of the light incidence follows rather closely the cosine law up to angles of about 60°. This agreement is not as good for encapsulated modules, where reflections on the window become more important, due to its glazed surface. Although this type of phenomena is damped by the cosine factor (i.e. high incidence light contributes rather little to the total daily energy received), it is not negligible, and a proper integration of the solar energy should take into account this effect, including the related anisotropic response of the module to diffused light.

5. Other important considerations for the system engineer.

Although I deviate here, strictly speaking, from test procedure considerations, and deal more with "standards", one should not forget that some other specifications are important for the user of solar modules :

- Environmental tests. As an example, Table I gives the list of tests performed by our associated manufacturing company, RTC. They are mostly inspired by the electronic component standards, to which sand blowing and wind resistance tests have been added.

---

([3]) From a paper to be presented by E. Fabre, J. Michel and Y. Baudet at the 12th Photovoltaic Specialists Conference, Baton Rouge, Nov. 15-18, 1976

- Dimensional standards and rated voltage. For a given rated voltage, the number of indifidual cells in a module is approximately given (one needs for instance 32 to 35 cells in order to charge at any reasonable temperature a 12 volt battery). With the predictable increasing size of individual cells (100 mm or more), the "economical" size of a module will increase, and a proper compromise between the overall size and the rated voltage will become more crucial to module designers. For instance, in the very hypothetical case of 8" wafers (which is however sometimes considered by "prospective" authors), a module capable of charging a 12 volt battery would contain some 1.1 $m^2$ of silicon area (unless the wafers are cut in smaller pieces) and would then have a total area of some 1.5 $m^2$ ...

  Worse case operating conditions . Large arrays of modules should be properly interconnected and protected. In a serie-connected array, short-circuit conditions can impose on one single cell (if shadowed, for instance) a reverse voltage equal to the total direct voltage of all others : parallel diodes should then protect the modules against such hazards. Similarly, in parallel-connected array, in the case of open-voltage, one module can receive the reverse current provided by all others : serie-diodes should there be used to present breakdown. In serie-parallel systems, a proper matricing of the connection reduces statistically these hazards, since alternative paths exist to by-pass a shadowed module, but diode-protection remains a good safety . Yet, measurements of the maximum reverse voltage (and reverse current) admissible is of utmost importance for the system designer, and should be clearly indicated in the specification sheets.

## 6. Conclusion.

This paper represents more the fruit of years of practical experience in the field of terrestrial solar cells, modules or arrays than a consistent approach to the problem of test procedures . Its aim is to introduce in the Workshop some practical considerations and hopefully some scattered suggestions which may be of interest to the participants .

---

ENVIRONMENTAL TESTS

The modules are subjected to the following IEC tests and some additional tests:

| Test | In accordance with | Conditions | | |
|---|---|---|---|---|
| Cold | IAC68-2-1, test Ab | Temperature: −40 °C, duration: 16 h | | |
| Rapid change of temperature | IEC68-2-14, test Na | Low temperature: | −40 | °C |
| | | High temperature: | +85 | °C |
| | | Number of cycles: | 10 | |
| | | Duration of exposures: | 30 | min |
| Dry heat | IEC68-2-2, test Bb | Temperature: | +85 | °C |
| | | Duration: | 16 | h |
| Composite temperature/ humidity cyclic test | IEC68-2-38, test Z/AD | 10 cycles, +25 °C, +65 °C, −10 °C | | |

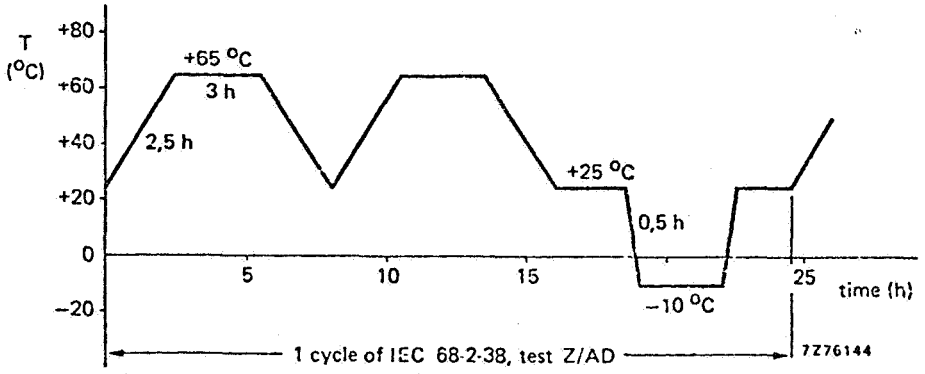


| | | | | |
|---|---|---|---|---|
| Salt mist | IEC68-2-11, test Ka | Temperature: | +35 | °C |
| | | Duration: | 48 | h |
| Wind | – | Pressure equivalent to an air velocity of 280 km/h | | |
| Sand blown | AIR 7.303 | | | |
| Frost with water | – | High temperature: | +25 | °C |
| | | Low temperature: | −40 | °C |
| | | Duration: | 16 | h |

Table I

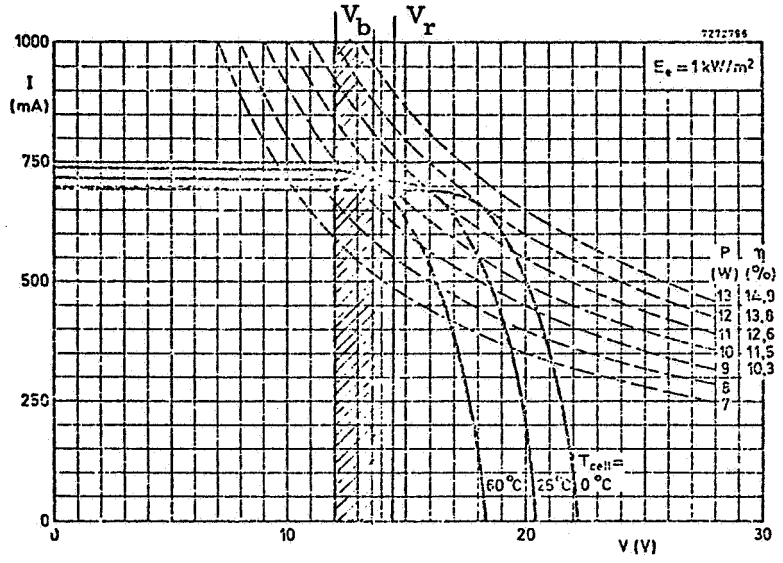


Fig. 1

Bundle of I V curves, against temperature: $V_b$ represents the battery voltage range and $V_r$ the rated voltage of the module

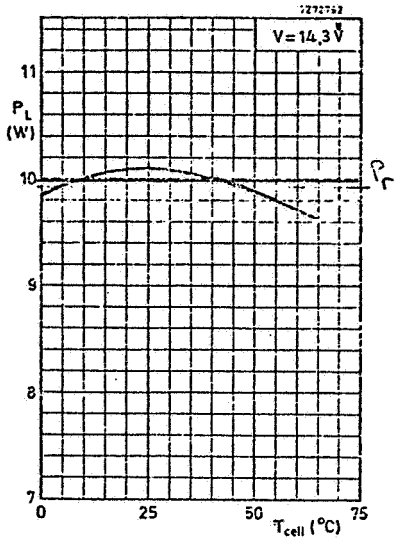


Fig. 2

Power at rated voltage against temperature

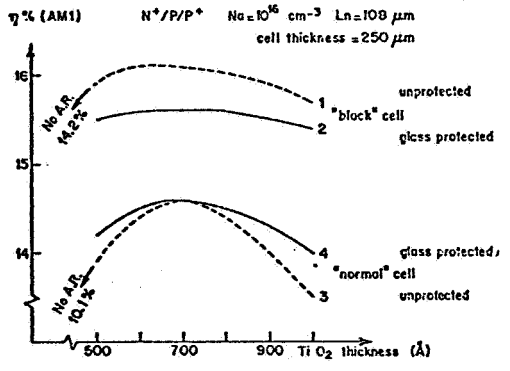


Fig. 3

Influence of various technologies on cell performances

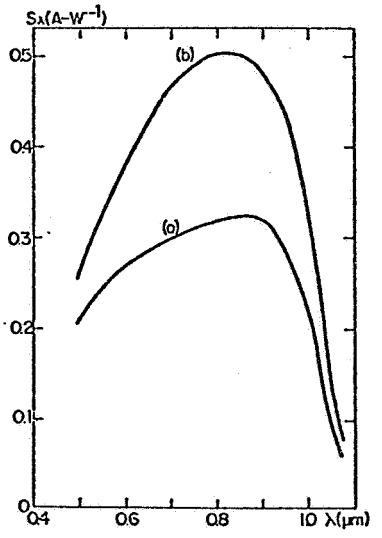


Fig. 4

Influence of technology (anti-reflecting coating): spectral response of a bare MIS cell

# INDOOR AND OUTDOOR MEASUREMENTS OF PERFORMANCE OF PHOTOVOLTAIC ARRAYS

by Henry B. Curtis

Lewis Research Center
National Aeronautics and Space Administration
Cleveland, Ohio

## ABSTRACT

A description of the techniques and methodology for making outdoor I-V measurements of solar cells is given. Temperature and irradiance measurement, experimental arrangement, data acquisition system and I-V data transformations are discussed. Data are presented comparing outdoor measurement to indoor measurements using a pulsed solar simulator.

## INTRODUCTION

Performance measurement of solar cells, modules and arrays is a necessary adjunct to low-cost solar cell array development. Module performance data are needed for sub-array and array sizing. There is a need to match modules in sub-arrays to operating current and voltage. Data on finished arrays are also needed to determine baseline performance for eventual degradation analysis.

Generally, modules and arrays are too large to test using conventional steady-state solar simulators, hence other methods for obtaining performance (I-V) measurements must be used. The approach used by NASA-Lewis is to measure modules indoors using a long-arc xenon-lamp pulsed solar simulator, and outdoors using natural sunlight. The indoor pulsed simulator method has the advantages of easy availability and, because of the short duration of the irradiance pulse (2 msec), there is no heating of the solar cell arrays. Flash intensity is controlled and data are taken at room temperature. Only

minor data corrections are used to reach standard conditions of 28° C and 100 mW/cm$^2$. However, to fully characterize module or array performance, data should also be obtained at actual operating conditions. These data are needed to assess the effects of temperature on the array performance. These effects would most probably appear only under steady-state illumination. To determine these effects, data need to be taken at a variety of irradiance and temperature levels. Current and voltage corrections, used to transform data to the standard 28° C, 100 mW/cm$^2$ conditions, can be large and may be significant sources of error. The purpose of this paper is to describe the techniques for obtaining and correcting module and array outdoor I-V measurements used at NASA-Lewis. The test arrangement and data transformations are discussed; also data comparing outdoor sunlight and indoor flash simulator measurements are presented.

## EXPERIMENTAL APPROACH

### Measurements Methodology

Figure 1 is a schematic drawing of the outdoor I-V measurement arrangement. The measurement procedures used are described in the Interim Solar Cell Testing Procedures for Terrestrial Applications (ref. 1). The module or array is oriented perpendicular to the sun. A reference cell whose spectral response is matched to the array under test is co-planar with the array. The reference cell mount has provisions for temperature control to maintain the temperature near 28° C. A 0.1Ω precision resistor is placed across the reference cell and the resulting voltage drop yields cell short

circuit current which is directly proportional to the irradiance.

Module temperature is obtained from a thermocouple taped to the rear of the test module directly behind a central cell. The thermocouple reference junction is maintained at 25° C and is located close to the module. This eliminates the need for long thermocouple extension leads. The relationship between actual cell temperature and means of thermocouple attachment will be described later.

To minimize voltage drop (IR) losses in the measurement apparatus, a conventional four-wire hookup (2 current leads, 2 voltage leads) is used. For individual modules, the four-wire attachment is made at the module binding posts or at the end of the integral cable. For arrays, the attachment is made at a junction box. Therefore, any small IR drop in these leads and in the inter-array wiring is included in the I-V measurement. An appropriate cable is used to bring the four I-V leads, the two thermocouple leads and the two reference cell leads indoors to a data acquisition system.

A programmable calculator is the central part of the automatic data system. The system includes the necessary voltmeters, a variable programmable power supply, a current measuring shunt and output devices. In about 30 seconds, approximately 50 data points in the power quadrant and several points beyond both open circuit voltage and short circuit current are obtained. Obtaining data outside the power quadrant assures full I-V curves after temperature and irradiance transformations.

## Module Temperature Measurement

Cell temperature in the module or array is measured by a small bead thermocouple taped to the back of the module, directly behind a central

cell. The thermocouple is not directly attached to a cell because such attachment would destroy the integrity of the module. In order to determine the difference between temperatures measured in this way with actual cell temperature, comparisons were made on fully instrumentated modules. Holes were drilled through the module substrate and thermocouples were directly attached to the back surfaces of 10 of the 18 cells. In addition, two thermocouples were taped to the back of the module behind two cells. Figure 2 shows a temperature distribution of the 10 cells with thermocouples. The temperature of the indicated central cell is $50^{o}$ C and the data numbers are temperature differences between each cell and the central cell. Temperatures of cells in the module ranged from $44^{o}$ C to $51^{o}$ C, while the thermocouple taped behind the indicated central cell read $47^{o}$ C. The range of cell temperatures ($7^{o}$ C) was larger than the temperature difference between the indicated central cell and the module back ($3^{o}$ C) behind this same central cell. The second thermocouple taped to the module back was behind a corner cell (lower right in fig. 2). The difference between corner cell and module back was also $3^{o}$ C. However, because this corner cell had a lower-than-average temperature, the taped thermocouple being $3^{o}$ C cooler gave a very poor representation of the average temperature of cells in the module. Hence, the thermocouple taped behind a central cell was used to give indication of the average temperature of the module.

These data were repeated under a variety of ambient temperature conditions and incident irradiance levels. The trend of results remained the same. The taped thermocouple on the middle of the module back consistently gave a representative cell temperature.

It should be noted also that the reproducible spread of cell temperatures within the module represents an additional source of error. Since cell temperature is used in the I-V transformation equations, there is really no single temperature that can be used for all cells in the module or array. This leads to an uncertainty in the corrected I-V curves compared to data obtained under uniform conditions. However, under operating conditions, the modules will also reach this spread of cell temperatures, hence data taken under natural sunlight will be representative of actual module performance.

## I-V Data Analysis

Voltage and current transformations. - During outdoor I-V measurements, data are taken at a wide variety of temperature and irradiance levels. Since the I-V data are generally used for comparison purposes or eventual degradation analysis, it is necessary to convert all data to standard conditions. These conditions have been defined to be $28^{\circ}$ C and 100 $mW/cm^2$ as measured by a reference solar cell (ref. 1). Equations used for I-V curve transformation are found throughout the literature. The following equations are from Sandstrom (ref. 2):

$$\Delta I = I_{SC}\left(\frac{100}{E} - 1\right) + \alpha\left(28 - T\right)A \tag{1}$$

$$I' = I + \Delta I \tag{2}$$

$$V' = V + \beta(28 - T) - \Delta I R_S - K(28 - T)I' \tag{3}$$

where

| | |
|---|---|
| $I, V, I_{SC}$ | measured values of current, voltage and short-circuit current |
| $E\left(\frac{mW}{cm^2}\right)$ | irradiance during measurement |
| $T(^oC)$ | temperature during measurement |
| $A(cm^2)$ | cell area |
| $I'$ $V'$ | current, voltage corrected to $28^o$ C and 100 $mW/cm^2$ |
| $\alpha\left(\frac{amps}{cm^2\ ^oC}\right)$ | current temperature coefficient |
| $\beta\left(\frac{volts}{^oC}\right)$ | voltage temperature coefficient |
| $R_S$ (ohms) | series resistance |
| $K\left(\frac{ohms}{^oC}\right)$ | curve correction coefficient |

All the data and constants are assumed positive except $\beta$, the voltage temperature coefficient, which is negative.

The last two terms in the voltage transformation (Eq. (3)) are the series resistance term and the curve correction term. The series resistance term ($\Delta IR_S$) is proportional to the current transformation ($\Delta I$) and is constant for all voltages. The curve correction term is negligible near open circuit voltage and has a small effect on short circuit current. The main effect of the curve correction term occurs near the maximum power point where it softens the I-V curve as temperature increases.

These last two terms are not normally used or needed for small temperature and irradiance corrections. For example, the pulsed simulator uses a computer program which incorporates only the irradiance and the $\alpha$ and $\beta$ temperature corrections. However, for the range of corrections encountered in outdoor measurements, all correction terms are needed. For example, consider a 40 $cm^2$ terrestrial solar cell with a short circuit current of 1 ampere at 100 $mW/cm^2$. If data are assumed to be taken at 80 $mW/cm^2$ and 38° C, a $\Delta I$ of about 190 mA will be obtained (200 mA for irradiance correction - 10 mA for the temperature correction). For a series resistance of 0.05 Ω/cell a 9.5 mV/cell correction to the voltage transformation is obtained. This value represents about a 2% change in maximum power and clearly should be taken into account.

A value for the K coefficient is not readily available. If a K value of $1.25 \times 10^{-3}$ ohms/°C is assumed (ref. 2), with a current of 0.95A at maximum power, an additional voltage transformation of 11.9 mV/cell is obtained at the maximum power point. This also is about a 2 percent change and should be taken into account. However, the actual value of the K factor must be obtained from measurements of cells or modules at different temperatures. These data are not presently available, hence the K term correction is not presently being used.

Series resistance determination. - The method used at NASA-Lewis to determine the total series resistance of a module or array is based on the slope of the I-V curve near open circuit voltage. In this approach, the I-V data are adjusted for irradiance only. Next, the change in open

circuit voltage due to the irradiance correction transformation is noted ($\Delta V_{OC}$(meas)). From simple theory for a cell with no series resistance we know:

$$I = I_o(e^{\frac{qV}{kT}} - 1) - I_L \tag{4}$$

at open circuit voltage, $V = V_{OC}$, $I = 0$ and $I_L = I_{SC}$. Also $e(qV_{OC}/kT)$ is much larger than unity, hence we obtain:

$$I_{SC} = I_o\, e^{\frac{qV_{OC}}{kT}} \tag{5}$$

The ratio of short circuit currents for two irradiance levels becomes:

$$\frac{I_{SC1}}{I_{SC2}} = \frac{\left(I_o\, e^{\frac{qV_{OC1}}{kT}}\right)}{\left(I_o\, e^{\frac{qV_{OC2}}{kT}}\right)} \tag{6}$$

The $I_o$ term cancels and taking natural logarithms of both sides leads to:

$$\ln\left(\frac{I_{SC1}}{I_{SC2}}\right) = \frac{q}{kT}\left(\Delta V_{OC}\right) \tag{7}$$

Since short-circuit current is proportional to irradiance ($I_{SC}$ = constant x E), we obtain:

$$\Delta V_{OC} = \frac{kT}{q} \ln\left(\frac{E_1}{E_2}\right) \tag{8}$$

where $E_1$ is 100 mW/cm$^2$ and $E_2$ is the irradiance at time of measurement.

The measured $\Delta V_{OC}$ will always be larger than the theoretical $\Delta V_{OC}$ due to series resistance. This increase is represented by

$$\Delta V_{OC(meas)} - \Delta V_{OC(theory)} = \Delta I_{SC} R_S \qquad (9)$$

where $\Delta I_{SC}$ is the change in short-circuit current due to the irradiance transformation. This leads to a value of series resistance that can be used in the I-V transformation equations.

Flash Simulator - Outdoors Measurement Comparison

Several modules and arrays have been measured both outdoors and with the flash simulator indoors. This provides a basis of comparison of the two methods. The data were taken using the same reference cell indoors and outdoors. This greatly reduces possible errors due to spectral mismatch. Table I shows the results of measurements on four typical metal-backed modules. The outdoor measurements were taken at an irradiance of 78 $mW/cm^2$ as measured by the reference cell. Module temperature was $36^o$ C as measured by the taped thermocouple. The flash simulator measurements were performed at room temperature and at an intensity within 2 percent of the 100 $mW/cm^2$ irradiance level. All data are corrected to $28^o$ C and 100 $mW/cm^2$.

An array of six series-connected fiberglass-backed modules was also measured inside and outdoors. These comparisons are presented in Table II. In this case, the outdoor data were measured at 97.7 $mW/cm^2$ at an array temperature of $41^o$ C.

In both cases, there is excellent agreement in short-circuit current (outdoors about 0.5 percent higher); good agreement in open-circuit voltage

(outdoors about 1 percent lower); and only fair agreement in maximum power (outdoors nearly 3 percent lower. The difference in short circuit current is well within the measurement accuracies of the two systems. A difference of 1% in open circuit voltage corresponds to about a $3^{o}$ C error in temperature measurement. This difference may be related to the spread in temperatures within the modules as described earlier. This magnitude of error is not great, however. The maximum power obtained outdoors is almost 3 percent lower than the flash simulator results. This difference is too large to be readily attributed to measurement errors. It is most likely caused by the lack of a K factor correction term. The data were taken at temperatures above $28^{o}$ C and the K term corrects for a softening of the knee of the I-V curve at higher temperatures. Hence the correction would be in the proper direction. Its estimated magnitude of 2-3 percent would account for the difference observed.

## SUMMARY

The techniques and methodology for making outdoor I-V measurements at NASA-Lewis have been described. Temperature measurements indicate a significant spread of individual cell temperatures within the same module when the module is outdoors in sunlight. In order to make proper I-V data transformations to a standard set of temperature and irradiance corrections, several module or array parameters must be known. Not only are the values of the current and voltage temperature coefficients ($\alpha$ and $\beta$) needed, but also values for module or array series resistance and K factor correction coefficient are necessary for most accurate measurements

## REFERENCES


1. Brandhorst, Henry W., Jr., et al.: Interim Solar Cell Testing Procedures for Terrestrial Applications. NASA TM X-71771 (1975).

2. Sandstrom, J. P.: A Method for Predicting Solar Cell Current-Voltage Characteristics as a Function of Incident Solar Intensity and Cell Temperature. 6th Photovoltaic Specialists Conference, Vol. I, p. 199, March 1967.

TABLE I. - COMPARISON OF OUTDOOR TO FLASH I-V MEASUREMENTS
AVERAGE OF 4 SIMILAR MODULES

DATA TAKEN AT 78 MW/CM$^2$ 36° C

| | FLASH | OUTDOORS | % DIFF. |
|---|---|---|---|
| $I_{sc}$ | .526 A | .528 | + 0.4% |
| $V_{oc}$ | 14.0 V | 13.8 | - 1.2 |
| $P_{max}$ | 5.78 W | 5.62 | - 2.8 |

TABLE II. - COMPARISON OF OUTDOOR TO FLASH I-V MEASUREMENTS
ARRAY OF SIX FIBERGLASS BACKED MODULES

| | FLASH | OUTDOORS | % DIFF. |
|---|---|---|---|
| $I_{sc}$ | 1.467 | 1.478 | 0.7 |
| $V_{oc}$ | 76.0 | 75.5 | - 0.7 |
| $P_{max}$ | 84.0 | 81.6 | - 2.9 |

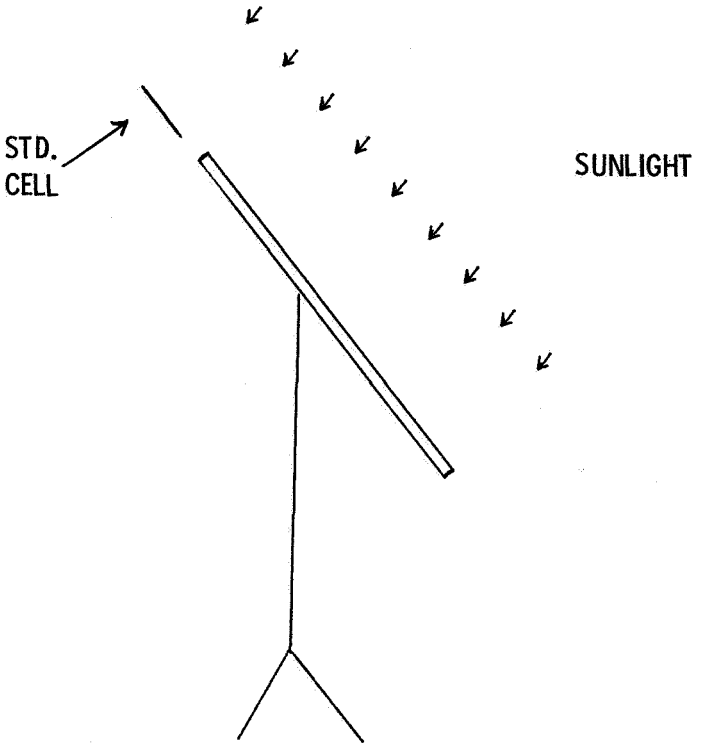


Figure 1. - Outdoor setup for module and array I-V measurements

| | | | | | |
|---|---|---|---|---|---|
| X | X | X | X | X | X |
| -X | | | +X | | -2 |
| X | X | X | X | X | X |
| | 0 | | -1 | | |
| X | X | X | X | X | X |
| -6 | | -4 | | | -5 |

Figure 2. - Cell temperature distribution on 18 cell modules, temp. of indicated cell 50 C, temp. behind indicated cell 47 C

# RECOMMENDATIONS FOR THE PERFORMANCE RATING OF FLAT PLATE TERRESTRIAL PHOTOVOLTAIC SOLAR PANELS

F. C. Treble

Royal Aircraft Establishment, Farnborough, Hants. UK

## 1 Introduction

Earlier this year, (1976) the author made recommendations for standardising the performance rating of flat-plate terrestrial solar panels[1] which were subsequently amended at a meeting of the Solar Photovoltaic Working Group of the Commission of the European Communities (CEC)[2].

In this paper, it is proposed to review the amended recommendations and indicate where they differ from the ERDA/NASA Interim Procedures[3]. While the Working Group recommendations cannot yet be assumed to represent an official CEC viewpoint, it is hoped that this discussion will lead the way to an international standard code of practice for performance rating, which will enable all engaged in the research, design, development, marketing and procurement of solar panels to evaluate different designs on a valid and reliable basis.

Some of the content of the earlier paper is repeated here in order to present a complete argument. For simplicity, the term 'solar panel' is used throughout, but the argument applies equally to single solar cells and sub-modules. Although written with flat-plate silicon panels in mind, the paper has equal relevance to $Cu_2S$-CdS and other types of solar cell.

## 2 Panel Characterisation

To characterise the performance of a solar panel, the following data are required and should ideally be supplied by the manufacturer in his descriptive brochure:-

a. The voltage - current characteristic at a fixed temperature (eg 28°C) in sunlight at an irradiance of 1 $kWm^{-2}$ with a spectral energy distribution conforming to an agreed standard (hereafter referred to as the 'standard sun').

b. The temperature coefficients of voltage and current or the voltage-current characteristics at one or two other temperature of significance (eg 0°C and 60°C).

c. The effect of changes of irradiance on the voltage-current characteristic at a fixed temperature.

d. The possible spectral response spread of the cells composing the panel.

e. The temperature at which the panel will stabilise under standard conditions of irradiance, environment and mounting (yet to be defined).

With this information, it would be possible for the user or array designer to compute within an acceptable tolerance the performance of the panel at any location and under any environmental conditions, provided that he could measure or deduce the spectral energy distribution of the sunlight and estimate the effect of the environment on the panel temperature.

In this paper, we will limit ourselves to discussing the first of the above requirements.

## 3 Basic Measurement Procedure

The photovoltaic performance is measured by exposing the panel to natural or simulated sunlight, monitoring its temperature and tracing its voltage current characteristic while the load is swept from short to open-circuit. Alternatively, output currents at selected voltages may be measured by switching load resistors. The irradiance is monitored while the electrical measurements are made.

## 4 Performance Measurement in Natural Sunlight

For measurements in natural sunlight, the panel, together with a co-planar irradiance-monitoring device, may be mounted horizontally or kept at normal incidence to the direct solar beam. In either case, an irradiance of at least 800 $Wm^{-2}$ is desirable to minimize errors in extrapolating to 1 $kWm^{-2}$ and the irradiance should not vary in the course of a measurement.

With horizontal mounting, a high solar elevation is required to give the necessary irradiance and in some cases unacceptable errors may arise from differences in angle of incidence dependence between panel and monitor. Normal incidence measurement is therefore to be preferred. With this method, collimators can be used to restrict the field of view to a small area of sky around the sun and thus render the measurement insensitive to the presence of clouds and nearby obstructions. But if this is done, it is essential that both collimators are non-reflective, give the same field of view and are accurately aligned and orientated. This is difficult with large panels. Without collimators, the set-up is simpler and the orientation requirement can be relaxed to $\pm 5^{\circ}$. Also, uncollimated testing is more akin to the normal mode of operation of the panel.

It is recommended that the irradiance be monitored by means of a standard solar cell. This is a stable cell having essentially the same relative spectral response as the panel, whose short circuit current Is when irradiated by the standard sun at 1 $kWm^{-2}$ has been pre-determined at a controlled temperature by a calibration technique.

If Im is the measured short-circuit current of the standard cell when the panel performance is measured, the panel short-circuit current may be corrected to an irradiance of 1 $kWm^{-2}$ by multiplying it by the ratio Is/Im. The voltage-current characteristic of the panel under standard sun conditions may then be obtained by moving the measured characteristic bodily upwards to the corrected short-circuit current value and adjusting the open-circuit voltage by applying the following equation:-

$$V_{ocs} = V_{ocm} + \frac{nkT}{q} \log_e \frac{Is}{Im}$$

where $V_{ocs}$ is the open-circuit voltage under the standard sun.
$V_{ocm}$ is the measured open-circuit voltage
$n$ is the number of series-connected cells in the panel.
$k$ is Boltzmann's Constant.
$T$ is the absolute temperature
$q$ is the charge of an electron.

Provided the irradiance during the measurement exceeds 800 $Wm^{-2}$, this simple correction is sufficiently accurate over the working voltage range. Note that the standard cell technique not only enables one to correct for intensity but also automatically corrects to the standard sun spectrum.

The Interim Procedures[3] at present permit the use of pyranometers and pyrheliometers for irradiance monitoring during performance measurements, but it is strongly recommended that these thermopile instruments be disallowed when the intention of the measurement is to establish the performance of the panel under standard sun conditions. Having an essentially flat response, they cannot, like a standard solar cell, take account of local and temporal variations in the spectral content of the sunlight and therefore they do not automatically relate the readings to standard sun conditions. The output power of a panel measured against a thermopile radiometer in the sun and normalised to 1 $kWm^{-2}$ can vary by as much as 15% on different days at the same location. Furthermore, because thermopile radiometers have a much slower response than solar cells (15 to 30 s compared with 20 $\mu$s) any short-term fluctuations in the irradiance, caused by cloud or haze, can result in error. Thermopile instruments are also more temperature-dependent than a solar cell (used in the short-circuit mode) and more difficult for the non-specialist to use and maintain in good condition.

As the power output of silicon cells falls by about 0.5% for every degree Centigrade rise in temperature, it is important to measure the cell temperature accurately during a performance test and ensure that this temperature is uniform throughout the panel. This is a difficult problem in natural sunlight because radiative, convective and conductive cooling effects are likely to be non-uniform and wind velocity has a marked influence. Moreover, thermocouples or other sensors applied to the front or back of the panel may not register the cell temperature to the required accuracy and corrections may therefore be necessary. One way to alleviate these difficulties is to fix thermocouples to the cells of a panel of the same design and mount the instrumented panel beside the test panel in precisely the same fashion. Both panels are protected from sun and wind until everything is ready for the performance measurement, and readings are then taken as quickly as possible after exposure. The temperature should preferably be measured to an accuracy of $\pm 1^{\circ}C$ but $\pm 2^{\circ}C$ is probably a more realistic target in view of the practical difficulties. With large designs, the instrumented panel should have thermocouples in the centre and at the four corners to check the uniformity.

Knowing the temperature of the panel, the performance data may be corrected to the standard temperature (eg $28^{\circ}C$) by applying the appropriate voltage and current temperature coefficients, determined experimentally by tests on individual cells.

The standard solar cell should be maintained at its calibration temperature while in use. In this case, a tolerance of $\pm 2^{\circ}C$ is adequate, as the temperature dependence of short-circuit current is quite small (typically 0.03% per $^{\circ}C$ for silicon).

Voltage and current instrumentation errors can and should be kept under $\pm 0.5\%$ by the use of frequently-calibrated digital voltmeters or potentiometric recorders and separate voltage and current leads. Short-circuit currents of panel and standard cell are preferably measured at zero voltage, using an electronic load but if they are measured by voltage drop across a series resistor, the terminal voltage should not exceed 20 mV per cell.

## 5 Performance Measurement In Simulated Sunlight

When measurements are made in simulated sunlight, the panel is mounted at normal incidence to the centre-line of the beam and the irradiance set to simulate the standard sun with a standard solar cell. (Here the Interim Procedures do not permit pyranometers or pyrheliometers.)

The accuracy of the measurement is primarily dependent on two inter-related factors:-

a. The quality of the simulator, that is, how well its spectral energy distribution matches that of the standard sun.

b. How well the spectral response of the standard cell matches that of the cells in the test panel.

The worse the simulator, the more important does it become to ensure a good spectral response match. Errors of several percent can result from the use of unmatched standard cells with poor simulators such an unfiltered xenon lamp[4]. It is recommended that simulators used for standard performance rating should match the standard sun spectral energy distribution to the extent necessary to limit errors due to spectral response spread in the cells composing the panels to less than $\pm 1\%$. This requirement can be translated into tolerances for various wavebands, if the spectral response spread is known. The smaller the spread, the greater the allowable tolerances.

Uniformity of illumination is important, particularly with cells connected in single series strings, as they usually are in terrestrial panels. If one cell is under-illuminated, the consequent reduction in generated current will affect the whole string. The Interim Procedures specify that non-uniformity shall be less than $\pm 5\%$ over the panel area, but it is recommended that this tolerance be reduced to $\pm 2\%$, as measured by the short-circuit current of a cell of the same size and shape as those in the panel. Also, the Interim Procedures limit of $\pm 2\%$ on temporal instability should be reduced to $\pm 1\%$. The specified $30^{\circ}$ limit on the angle subtended by the apparent source of the simulator on a point of the test panel is agreed.

The Interim Procedures stipulate that the simulator source should be a short-arc xenon lamp modified by optics and filters to meet the spectral requirements. It is recommended that the pulsed simulators which have become available in recent years should also be permitted, indeed they should be recommended as the preferred type. They can illuminate large areas uniformally (one model covers a 3.8 m x 4.6 m target area to a uniformity of $\pm 2\%$) and can match terrestrial sunlight well, without sophisticated optics and filters (Fig 1). Their other big advantage is that there is negligible heat input to the test panel, so the cells remain uniformly at the ambient temperature. This can be easily and accurately measured and it is close enough to the recommended standard temperature of $28^{\circ}C$ to facilitate accurate extrapolation.

## 6 Standard Solar Cells

It will be clear from what has already been said that the key to standardising the performance rating of solar panels lies in the selection and calibration of standard solar cells.

As previously stated, the main requirement in selecting cells for calibration as standards is that they should be stable devices having essentially the same relative spectral response as the panels being tested. The matching should take account of the response spread in production cells and the effects, if any, of the panel window and encapsulent. Ideally, at least two master standards, representing the response spread, should be selected and calibrated. The mean of their short-circuit currents can then be used to monitor or set the irradiance for test purposes, and this will minimise errors due to response mismatch. Moreover, any change in the ratio of the short-circuit currents will indicate that one of the standards has degraded. To save wear and tear on the master standards, it is good practice to use working standards for day-to-day use as irradiance monitors. These should be mounted on robust temperature-controlled blocks and protected by easily cleaned distortion-free windows. They should be calibrated against the appropriate master standards under the appropriate test conditions and checked from time to time. If such working standards are used, it is not necessary to package the master standards, which can be kept locked away for protection except when required for periodic checks.

To calibrate a master standard, it is necessary to determine what the short-circuit current of the cell would be if it were exposed to the standard sun at an intensity of 1 $kWm^{-2}$. Two techniques are in use:-

The 'Normal Incidence' Method (as specified in the Interim Procedures)

A normal incidence pyrheliometer (NIP) and the solar cell, suitably temperature controlled and masked by a collimator from the diffuse sky radiation, are kept pointed at the sun while simultaneous measurements are made of irradiance and short-circuit current. The short-circuit current is normalised to 1 $kWm^{-2}$ or alternatively expressed in $mAmW^{-1}cm^{2}$. The average of at least three measurements on at least two different days is used as the calibration value. The solar spectral energy distribution is not measured, so the correction to standard sun conditions can only be done indirectly from measurements of air mass, turbidity and atmospheric water vapour content. The accuracy of such a technique has not yet been proven.

The 'Global' Method (used by RAE)

The cell, uncollimated, is mounted horizontally on a temperature-controlled block, co-planer with a horizontal pyranometer and simultaneous readings of irradiance and short-circuit current are taken in global sunlight. The spectral energy distribution of the global sunlight is measured within a short time of the calibration. The calibration value is then computed from the short-circuit current

(normalised to 1 $kWm^{-2}$), the spectral response of the cell, the measured solar spectral energy distribution and the agreed 'standard sun' distribution. To minimise errors, the value is averaged over at least three different days.

The global method is simpler and free from collimator alignment and field-of-view errors but it requires the following special conditions for accurate and consistent calibration:-

a. Clear, sunny weather, with the diffuse irradiance not greater than 0.25 of the global. (This sets a limit on the turbidity.)

b. Global irradiance above 800 $Wm^{-2}$.

c. Solar elevation not less than $54^{\circ}$.

d. Radiation sufficiently stable to allow the spectral energy distribution to be measured.

e. No atmospheric pollution.

f. Prevailing good weather, so that measurements can be taken on three suitable days without undue delay.

Malta ($36^{\circ}N$, $14^{\circ}30$ E) has been found to satisfy these requirements during the summer months on sunny days between 10.00 and 13.00 hours. The site at the Radio Sonde station in the SW of the island has been used for solar cell calibration since 1960. Table 1 lists relevant weather statistics from data recorded between 1947 and 1972. Radio Sonde measurements show that the atmospheric water vapour content varies between 2.3 and 3.3 cm.[5] The spectral energy distribution of Malta sunlight has been measured on many occasions[6]. The curve in Fig 1 is the mean of eleven observations taken in good conditions on four days in July 1976 between 10.00 and 12.30 hours. Fig 2 shows the spread of these observations. RAE are using the Fig 1 curve (AM1 approx) as their 'standard sun' pending international agreement on this matter.

It has been established that Malta calibrations are repeatable from year to year within 1%. Table 2 gives details of measurements on ten cells in three successive years. Some of the cells were heavily irradiated with 1 MeV electrons to produce a marked reduction in infrared response and thus test the sensitivity of the technique to wide spectral response variations.

In view of the success of the global technique in Malta, it is recommended that it be allowed as a standard calibration procedure. Concerning the standard sun, it is essential that international agreement on this matter be achieved as quickly as possible. Whether it is AM1, AM2 or something in between is of less importance than that all concerned should accept a common standard and work to it.

The Interim Procedures say that standard cells must be "obtained from the recognised calibration facility, NASA/Lewis, or be traceable to that facility." It is agreed that calibration should be confined to agencies with the necessary facilities and expertise, but, for international acceptance, it will probably be necessary for agencies other than NASA/Lewis to be recognised. There can be no valid objection to more than one agency, provided, of course, that their calibrations are consistent and can be related to the standard sun.

## 7 Definition of 'Peak Power'

The term 'peak power' is often used to describe the power which a panel will deliver at an irradiance of 1 $kWm^{-2}$. As it stands, this terminology is imprecise, because the voltage and temperature at which the power output is measured are sometimes not stated and the solar spectral energy distribution is not defined. In the light of the points made in the foregoing discussion, the following definition is recommended:-

'Peak power' is the power output measured in natural or simulated sunlight at a declared voltage, corrected to a temperature of 28°C and referred to an agreed solar spectral energy distribution (the 'standard sun') at an intensity of 1 $kWm^{-2}$ by means of standard solar cells, of matching spectral response, calibrated by a recognised agency.

## 8 Summary

To summarise, it is recommended that the Interim Procedure be amended as follows:-

1 Specify a standard solar spectral energy distribution ('standard sun') to which all performance ratings of terrestrial solar cells and panels are to be related.

2 Disallow the use of pyranometers or pyrheliometers for sunlight measurements aimed at establishing the voltage-current characteristic under standard sun irradiation. Instead, specify that, whether such measurements are carried out in natural or simulated sunlight, the irradiance must be monitored by means of a standard solar cell of matching spectral response calibrated by a recognised agency.

3 Allow the 'global' method of calibrating standard cells as an alternative to the 'normal incidence' method.

4 Specify that at least two master standards be selected and calibrated for each programme and that, to save wear and tear on these masters, and obviate the need for expensive packaging, robust, well-protected working standards be kept for day-to-day use.

5 Recognise other qualified agencies for the calibration of standard cells.

6 Permit pulsed simulators (indeed recommend them as the preferred type).

7 Reduce the tolerance on the non-uniformity of irradiance from $\pm 5\%$ to $\pm 2\%$ and stability tolerance from $\pm 2\%$ to $\pm 1\%$.

8 Stipulate that the simulator must match the standard sun spectral energy distribution to the extent necessary to limit errors due to the spectral response spread in the cells composing the panels to less than $\pm 1\%$.

9 Include the above definition of 'peak power'.

9 Acknowledgments

The author thanks his collegues Messrs A A Dollery and M W Walkden for their help in preparing this paper.

References


| | | |
|---|---|---|
| 1 | F C Treble | Performance Rating of Photovoltaic Solar Generators for Terrestrial Applications. International Conference on Solar Electricity, Toulouse, 1-5 March 1976 |
| 2 | | Meeting of the Solar Photovoltaic Working Group of the Commission of the European Communities, 17 September 1976 |
| 3 | L M Magid and H W Brandhorst | ERDA/NASA Interim Solar Cell Testing Procedures for Terrestrial Applications, July 1975. |
| 4 | M W Walkden | An Evaluation of Light-Sources for Routine Solar Cell Performance Measurement. RAE Tech Memo Space 99, (1967) |
| 5 | F C Treble | The Calibration of Standard Solar Cells (Malta 1961). RAE Tech Note EL 198 August 1961. |
| 6 | M W Walkden | The Spectral Energy Distribution of Sunlight in Malta. RAE Technical Report 67248, (1967) |

Table 1

MALTA WEATHER STATISTICS*

| Parameter | Jan | Feb | March | April | May | June | July | Aug | Sept | Oct | Nov | Dec |
|---|---|---|---|---|---|---|---|---|---|---|---|---|
| Mean daily maximum temperature °C | 15.0 | 15.2 | 16.5 | 18.9 | 23.0 | 27.5 | 30.2 | 30.6 | 27.8 | 23.8 | 20.1 | 16.5 |
| Mean number of sunshine hours per day | 5.54 | 6.44 | 7.41 | 8.54 | 10.04 | 11.33 | 12.25 | 11.44 | 9.13 | 7.26 | 6.49 | 5.28 |
| Mean monthly rainfall mm | 84.1 | 54.0 | 44.6 | 24.9 | 7.7 | 4.1 | 0.9 | 9.3 | 43.3 | 131.2 | 80.3 | 101.5 |

*Extracted from the General Climatological tables for Luqa, Malta by courtesy of the British Meteorological Office.

Period of observations:- 1 September 1947 to 31 August 1972

Table 2

CONSISTENCY OF STANDARD SOLAR CELL CALIBRATION IN MALTA

(Ferranti 2cm x 2cm x 300$\mu$m 10 ohm cm silicon solar cells)

| Cell No | 1MeV electron fluence | Short circuit current (mA) at 25°C normalised to 100mW cm$^{-2}$ intensity | | | | Maximum deviation (per cent) |
|---|---|---|---|---|---|---|
| | | July 1973 (mean of 4 days) | June 1974 (mean of 4 days) | Sept 1975 (mean of 6 days) | Overall mean | |
| 1/11 | Nil | 116.1 | 115.4 | 116.7 | 116.1 | 0.6 |
| 1/33 | Nil | 113.6 | 113.6 | 114.6 | 113.9 | 0.6 |
| 1/34 | Nil | 115.3 | 115.0 | 116.3 | 115.3 | 0.7 |
| 1/40 | Nil | 116.6 | 115.8 | 117.3 | 116.6 | 0.7 |
| 1/19 | $10^{14}$ | 111.4 | 110.9 | 112.2 | 111.5 | 0.6 |
| 1/18 | $10^{14}$ | 111.5 | 110.9 | 112.1 | 111.5 | 0.5 |
| 1/24 | $3 \times 10^{14}$ | 102.8 | 101.3 | 102.3 | 102.1 | 0.8 |
| 1/26 | $3 \times 10^{14}$ | 103.7 | 102.8 | 103.4 | 103.3 | 0.5 |
| 1/35 | $3 \times 10^{15}$ | 93.8 | 93.5 | 94.1 | 93.8 | 0.3 |
| 1/44 | $3 \times 10^{15}$ | 92.3 | 91.9 | 92.8 | 92.3 | 0.5 |

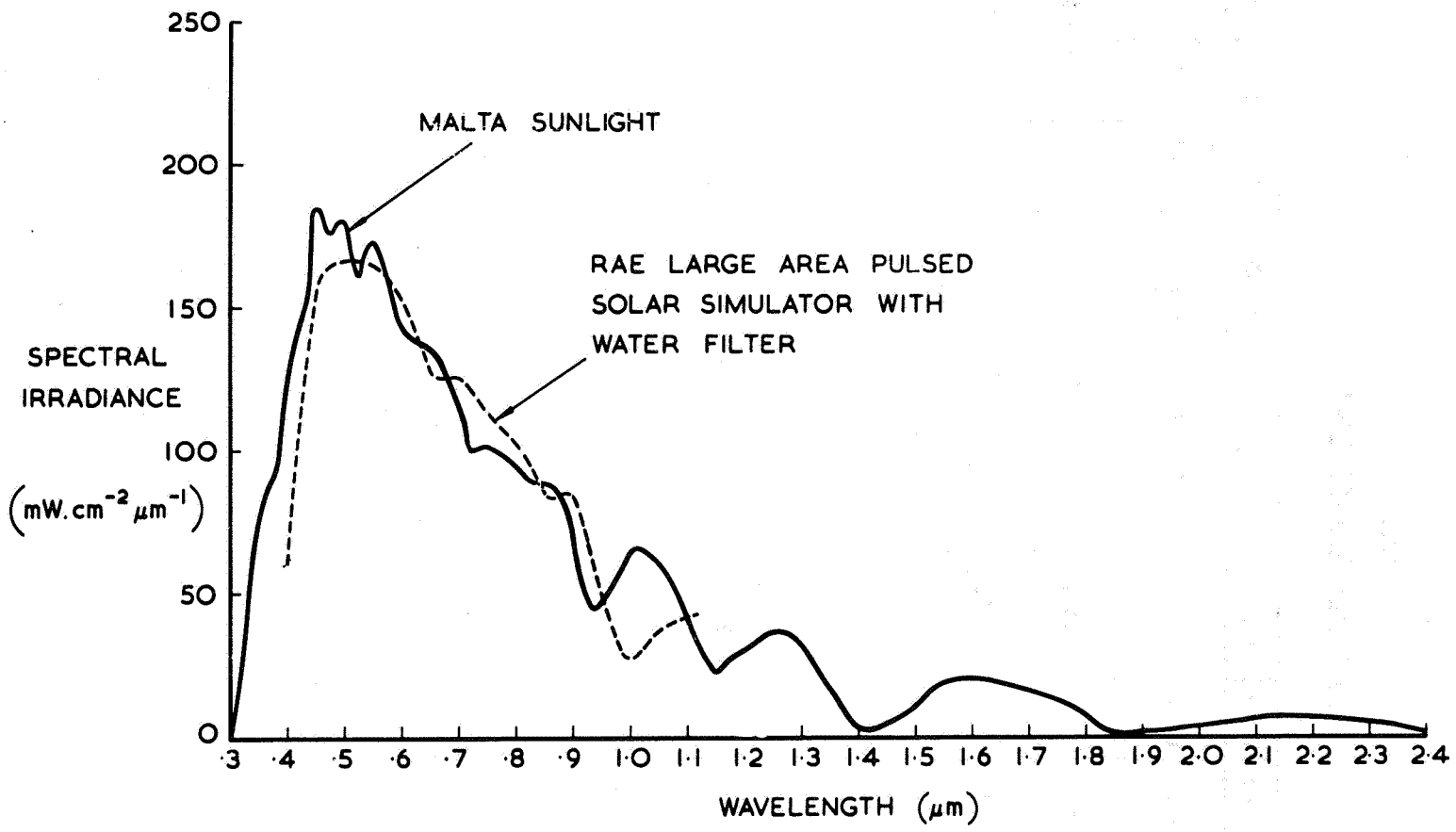


FIG.1 SPECTRAL ENERGY DISTRIBUTION OF LAPSS COMPARED WITH MALTA SUNLIGHT

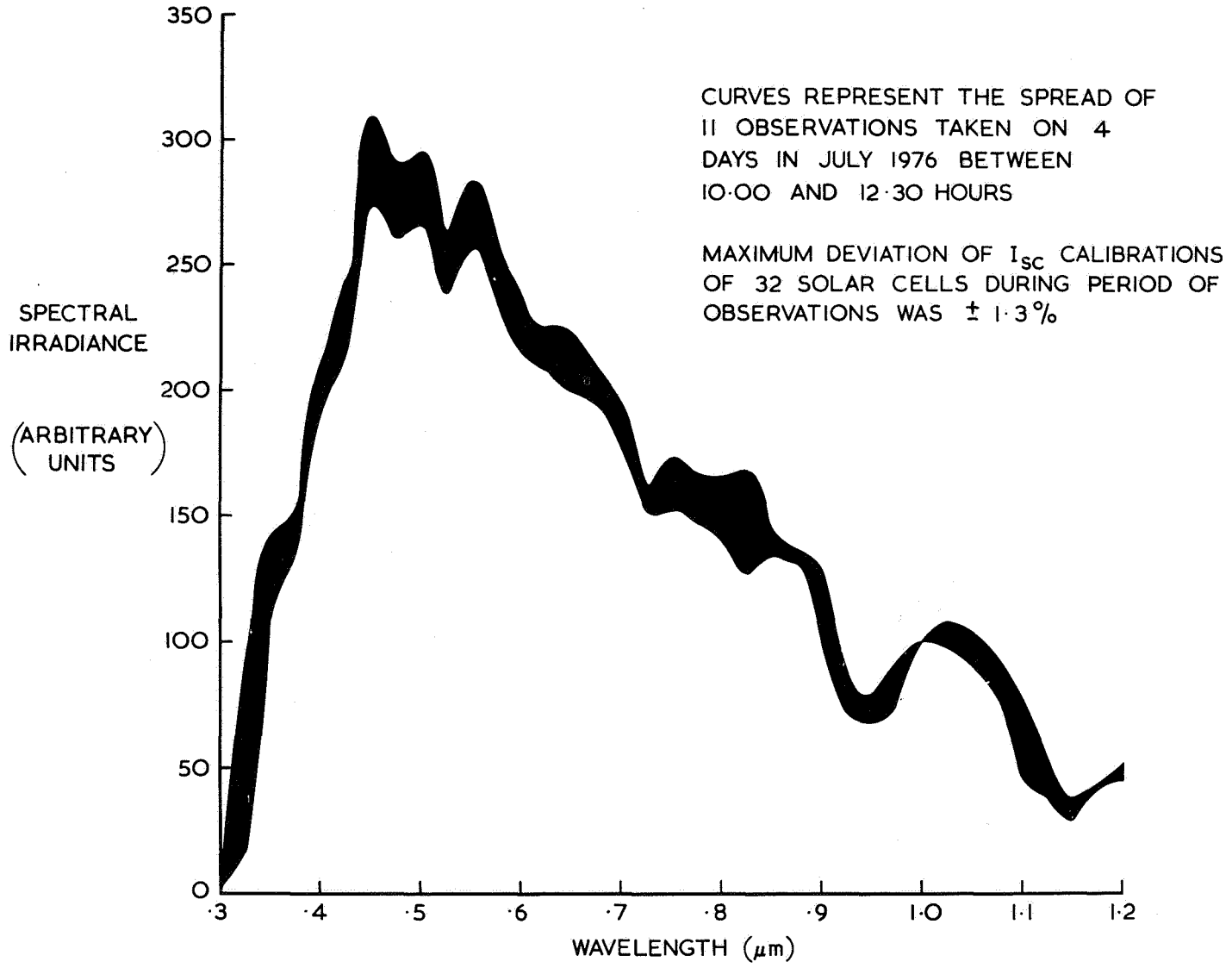


FIG. 2 VARIATION OF SPECTRAL ENERGY DISTRIBUTION OF GLOBAL MALTA SUNLIGHT

# SILICON SOLAR CELL TESTING IN CONCENTRATED SUNLIGHT AND SIMULATED SUNLIGHT*

E. L. Burgess and K. W. Mitchell
Sandia Laboratories, Albuquerque, NM 87115

## ABSTRACT

A method is described for testing silicon solar cells in concentrated sunlight and simulated sunlight. Concentrated sunlight is obtained using an acrylic Fresnel lens; the simulated sunlight source is a short-arc Xenon lamp. Average illumination levels during the tests are inferred from an assumed linear relationship between short circuit current and illumination. This linearity assumption is investigated for 0.3 Ω-cm base resistivity silicon cells and found to be valid. Some typical results are presented to illustrate the type of information obtained during the testing.

## INTRODUCTION

There is a growing interest in the possibility of reducing the cost of electric power from solar cells by concentrating sunlight on the cells and, hence, increasing their output power density. Silicon solar cells are being considered for use in these concentrated sunlight applications. The conventional silicon cell is not directly applicable in a concentrator system because of its relatively high internal series resistance which produces significant degradation in cell performance at high illumination levels. Our laboratory is engaged in a development program to optimize the performance of silicon solar cells when operating at sunlight concentration levels in the range 20-100X.

There exists, at this time, no standard method for testing solar cells at high illumination such as exists for cell testing under one-sun conditions (1). This paper discusses a procedure which has been adopted for testing the silicon cells being developed at this laboratory. The interim solar cell testing procedures outlined by this workshop in March 1975 (1) have been adopted when applicable. In areas where the procedures are not applicable care has been taken to insure that the measurements are meaningful. The test procedures outlined in this paper are offered, for consideration by the workshop, as interim procedures for concentrated sunlight testing.

## TESTING SEQUENCE AND PROCEDURES

The chart in Fig. 1 outlines the testing sequence. Each step in the sequence involves the use of one or more of the following components: 1) the test cell to be evaluated, 2) a normal incident pyr-

*This work was supported by the United States Energy Research and Development Administration (ERDA).

heliometer (NIP), and 3) a standard test cell calibrated by the NASA Lewis Research Center. For the first step in the sequence, the test cell is "calibrated" in unconcentrated sunlight. The procedure is similar to that outlined in Ref. 1. Both the test cell and standard cell are equipped with a 10:1 field-of-view tube. The standard cell is used to determine the solar flux, $\phi_s$, using the calibration factor, $\beta_s$, determined for the cell by the NASA Lewis Research Center, in conjunction with its measured short circuit current, $J_{sc}$, i.e.,

$$\phi_s = J_{sc}/\beta_s \tag{1}$$

The $\phi_s$ is compared to the NIP reading, $\phi_o$, for reference purposes. These two flux values generally are in agreement within 1.5%. A calibration factor, $\beta_o$, is then determined for the test cell from its short circuit current as

$$\beta_o = J_{sc}/\phi_o \simeq J_{sc}/\phi_s \tag{2}$$

This calibration factor is used in subsequent testing to determine the actual illumination on the test cell.

The next step in the sequence is to evaluate the test cell at various illumination levels. An acrylic Fresnel lens is used to concentrate the sunlight on the test cell. In this case the 10:1 field-of-view tube is removed from the test cell since any scattered light is negligible compared to the light focused by the Fresnel lens. The actual illumination on the test cell as a result of the focusing lens is determined assuming a linear relationship between short circuit current and illumination. The $\beta_o$ of Eqn. 2 is the proportionality constant. Thus, the concentrated flux, $\phi_c$, is

$$\phi_c = J_{sc,c}/\beta_o \tag{3}$$

where $J_{sc,c}$ is the test cell short circuit current in concentrated sunlight. For reference purposes the actual concentration ratio, C, of the concentrator may be determined as

$$C = J_{sc,s}/\beta_o\phi_1 \tag{4}$$

where $\phi_1$ is measured at the time of the test with the NIP. The validity of the assumption of a linear relationship between short circuit current and illumination will be addressed later.

The final step is to repeat the first step after the evaluation of the test cell. This is done to insure that $\beta_o$ has not changed due to the changing air mass from morning to noon and noon to afternoon. In general, there is up to 5% variation in $\beta$ from early morning to noon or noon to late afternoon due to this changing air mass. Because of this

fact it is desirable to conduct the tests during a period around solar noon, say 10:00 am to 2:00 pm.

Testing with a solar simulator follows a procedure very similar to the natural sunlight procedure. A $\beta_o$ (Eqn. 2) is determined in natural sunlight and this is used in the solar simulator testing. A short-arc Xenon lamp is used as the light source. Spectral filtering of the lamp is unnecessary since use of Eqn. 3 and $\beta_o$ determined in natural sunlight to determine $\phi_c$ effectively corrects the spectrum to the natural sunlight situation. In fact, if the standard cell $\phi_s$ is used to calculate $\beta_o$, the test is referred all the way back to the conditions of the standard cell calibration.

## DESCRIPTION OF TEST EQUIPMENT

The experimental equipment used in the natural sunlight testing is illustrated in Fig. 2. Two equatorial mounts are used to track the sun during testing. One mount contains the NIP and standard cell. In addition, a global, full hemispherical field-of-view pyranometer is used to yield a qualitative measure of the atmospheric conditions as determined by the ratio of the global-to-NIP readings. On a very clear day in Albuquerque this ratio is as low as 1.10-1.11; hazy days producing more scattered light can yield ratios as high as 1.20. The second mount holds the lens, test-cell holder, and XYZ translator used for centering the cell and changing the illumination level. Higher illuminations are obtained by moving the test-cell holder along the lens axis (Z-axis) closer to the focal point. Lower illuminations are obtained by moving the test-cell holder closer to the lens and away from the focal point.

One difficulty experienced with using a standard commercial Fresnel lens as shown here is the nonuniformity of the illumination on the test cell. In addition to the normal nonuniformity expected from a perfect spherical lens, a large peak usually is observed in the center of the image due to the more efficient transmission of the central portion of the lens. Attempts are made to correct this nonuniformity by masking portions of the lens. The white opaque disk visable on the lens in Fig. 2 is for this purpose. The uniformity is checked by placing a cover with a small aperture over the test cell and mapping the short circuit current as the test-cell holder is moved in the X-Y plane (perpendicular to the lens axis). Of course, the ideal solution to this problem would be to use special Fresnel lenses designed to yield constant illumination over the image. This could be accomplished by making each Fresnel facet with a different focal length. This is somewhat impractical since several different lenses would be required to yield a range of concentration ratios and Fresnel lens masters are expensive. A more practical solution would be to use a multi-scattering device such as a bundle of light pipes.

Fig. 3 shows a close-up of the test-cell holder. The cell is held down with a vacuum. Provision is made for heating or cooling the copper test-cell block. The heater is a resistive wire heater and is visable around the edge of the block. Cooling is accomplished by blowing cool nitrogen gas on the back of the block; this gas is derived from a liquid nitrogen dewer with a heater submerged in it. The temperature of the cell is measured with a chromel-alumel thermocouple welded to the main bus bar on the front of the cell. This thermocouple is visable in Fig. 3 with a "shade" over it to prevent the high illumination from falling directly on the junction and causing erroneous readings. The copper block is the electrical connection to the back of the cell. Three leads are used on the front bus bar; two are for current, located at each end of the bus bar, and the third is the potential lead, attached to the center of the bus bar.

## VALIDITY OF THE LINEAR CURRENT-ILLUMINATION ASSUMPTION

The validity of the assumption of linear short circuit current versus illumination was investigated experimentally. The experiment consisted of concentrating sunlight on solar cells with a concentration ratio of about 100X, altering the concentrated light with neutral density filters of various optical densities, and observing the change in short circuit current. The results from this experiment are illustrated in Fig. 4 for a 0.3 $\Omega$-cm base resistivity silicon cell. The calibration factor, $\beta$, at concentrated sunlight, as calculated by Eqn. 2 and normalized by the $\beta_o$ for unconcentrated sunlight, is plotted against intensity. The solid line corresponding to $\beta/\beta_o = 1$ is equivalent to the linear assumption.

The open circles represent experimentally determined $\beta/\beta_o$ ratios. The highest density filter used produced a short circuit current of about 1.5 times the unconcentrated sunlight short circuit current. The illumination with this filter in place was assigned a value of 1.5 times the unconcentrated value. Subsequent illuminations were determined from the ratios of the filter transmissions to the transmission of the highest optical density filter. These illumination values were then used in Eqn. 2 to calculate the corresponding $\beta$'s. The 5% error bars shown on the data points are an estimate of the error introduced by uncertainties in the filter transmission calibration. These data exhibit the linear relationship within experimental error.

Also shown in Fig. 4 are two values of the ratio, $\beta/\beta_o$, calculated using a numerical device analysis code (DAC) which solves the transport equations describing the solar cell physics (2). These theoretical calculations also support the linear relationship assumption. There is a slight supralinearity predicted by the DAC calculations but it is less than 1% at 100X.

This supralinearity is expected to increase for higher base resis-

tivity cells. A 10 Ω-cm cell exhibited a $\beta/\beta_o$ ratio of about 1.1 at 50 suns. The reason for this nonlinear increase in short circuit current with illumination is high level injection altering the internal electric field which, in turn, improves the collection efficiency. To insure that accurate intensities were measured for higher base resistivity cells, the 0.3 Ω-cm cell was used as a flux detector.

These experiments indicate that it is accurate to infer illumination from the short circuit current for 0.3 Ω-cm base resistivity cells up to a concentration of 100X. Care should be taken when doing this for higher base resistivity cells, particularly 10 Ω-cm cells. In general, if high level injection is not present then the short circuit current and illumination are proportional.

## TYPICAL RESULTS

The instrumentation used in these tests included an electronic load and a minicomputer-controlled data acquisition system. Typical data include those discussed by Brandhorst (3). Fig. 5 illustrates efficiency versus illumination for cells of three different base resistivities. The 0.1 Ω-cm and 0.3 Ω-cm cells exhibited linear short circuit current versus illumination for the full concentration ratio range. This was not the case for the 10 Ω-cm cell and illumination was determined, in that case, with a 0.3 Ω-cm cell. The cell area which was used in these efficiency calculations was the total cell area which was designed to be illuminated. This included the front grid finger area but not the main bus bar area since the optical system could be designed so as not to illuminate that area.

Fig. 6 illustrates some other important data which is possible with the actively cooled or heated test-cell holder. This study involved determining the effect of temperature on efficiency. It was necessary to be able to accurately control temperature during these tests. As is illustrated in Fig. 6, temperature is a very important parameter affecting cell performance. In concentrated sunlight systems cells are likely to experience a considerable temperature rise.

## CONCLUSIONS

The method for testing silicon solar cells in concentrated sunlight which was described here is believed to yield accurate results. Two problems which affect the accuracy of the results are measurement of the illumination and insuring uniformity of illumination over the active cell area. Short circuit current is an accurate measurement of illumination if high level injection is not present. The consequences of nonuniform illumination are unknown and the philosophy should be to make the illumination as uniform as possible until uniformity limits can be established. Since temperature is such an important parameter affecting cell performance and since large temperature rises are ex-

pected in concentrated sunlight measurements, the test-cell holder should provide for both heating and cooling.

## REFERENCES


1. H. Brandhorst, J. Hickey, H. Curtis, and E. Ralph, "Interim Solar Cell Testing Procedures for Terrestrial Applications," NASA TM X-71771, July 1975.

2. J. G. Fossum, Solid State Electronics 19, 269 (1976).

3. H. W. Brandhorst, "Introduction to Basic Solar Cell Measurements," this Workshop.


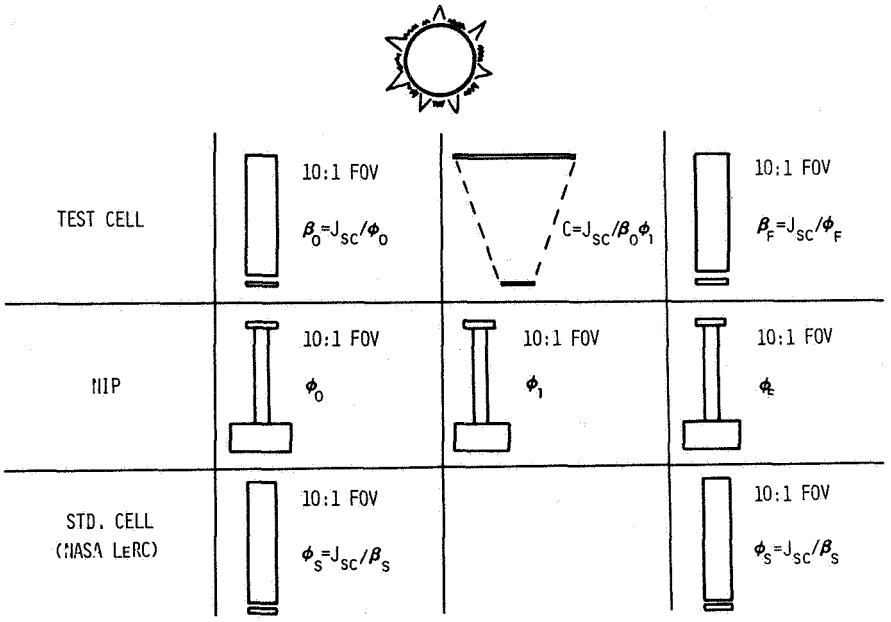


Figure 1 - Test sequence used for testing cells in concentrated sunlight.

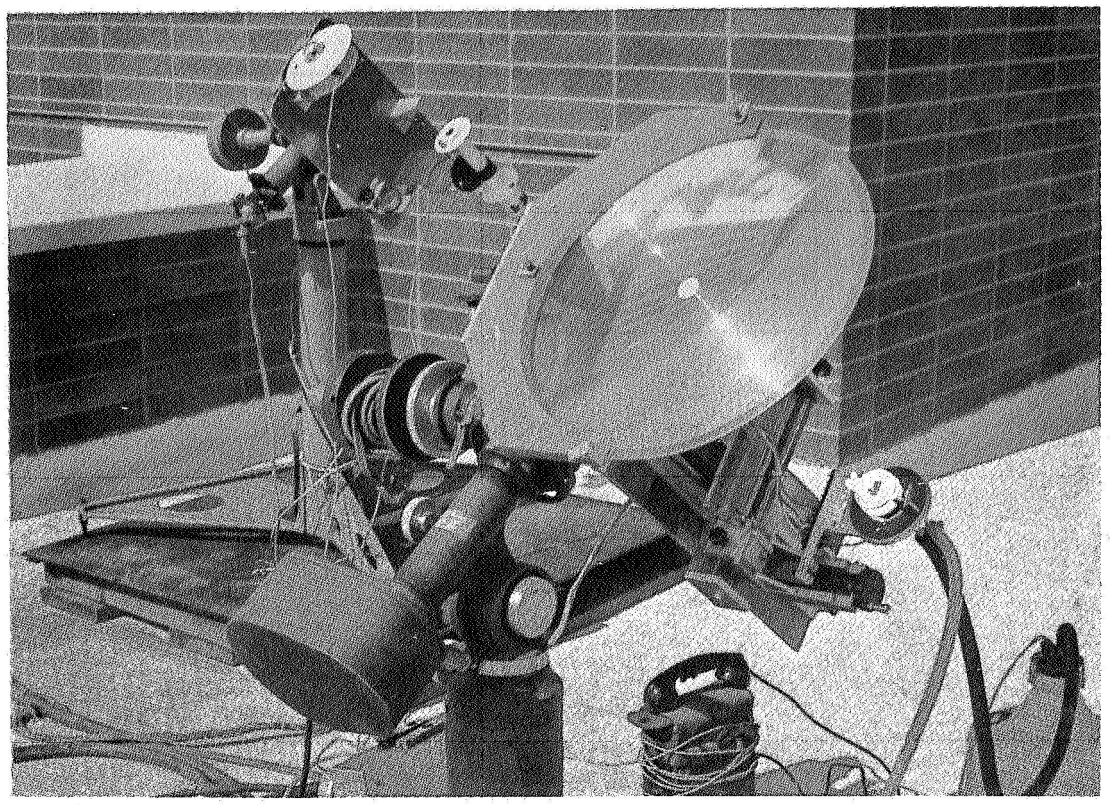

Figure 2 - Photograph of experimental equipment.

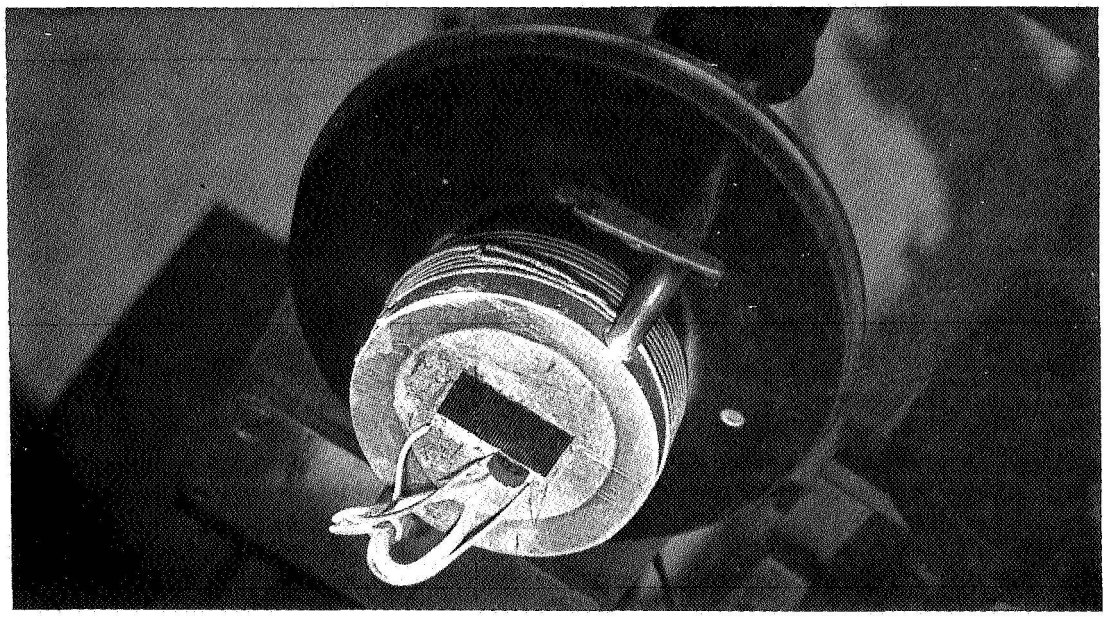

Figure 3 - Close-up photograph of test-cell holder.

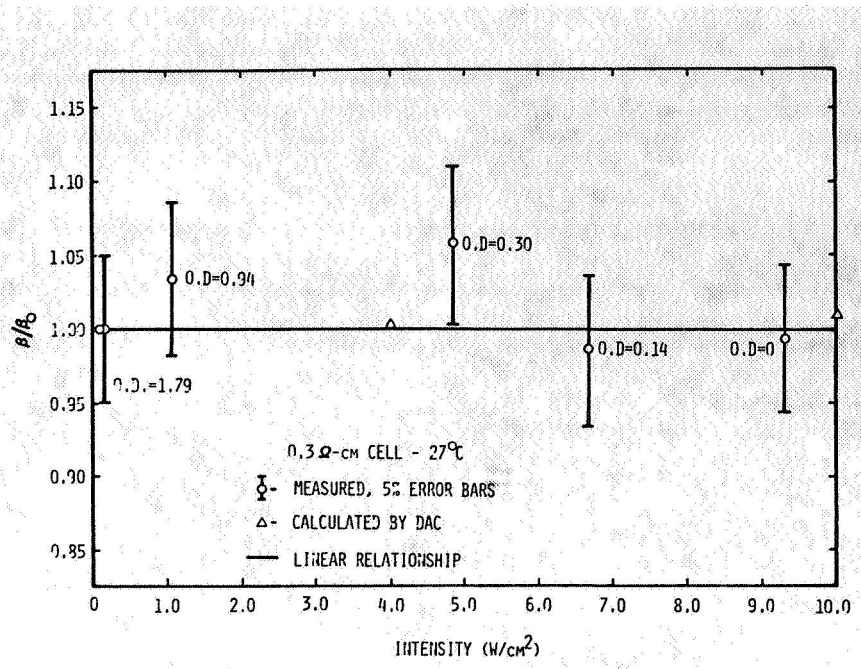


Figure 4 - Normalized calibration factor versus cell illumination.

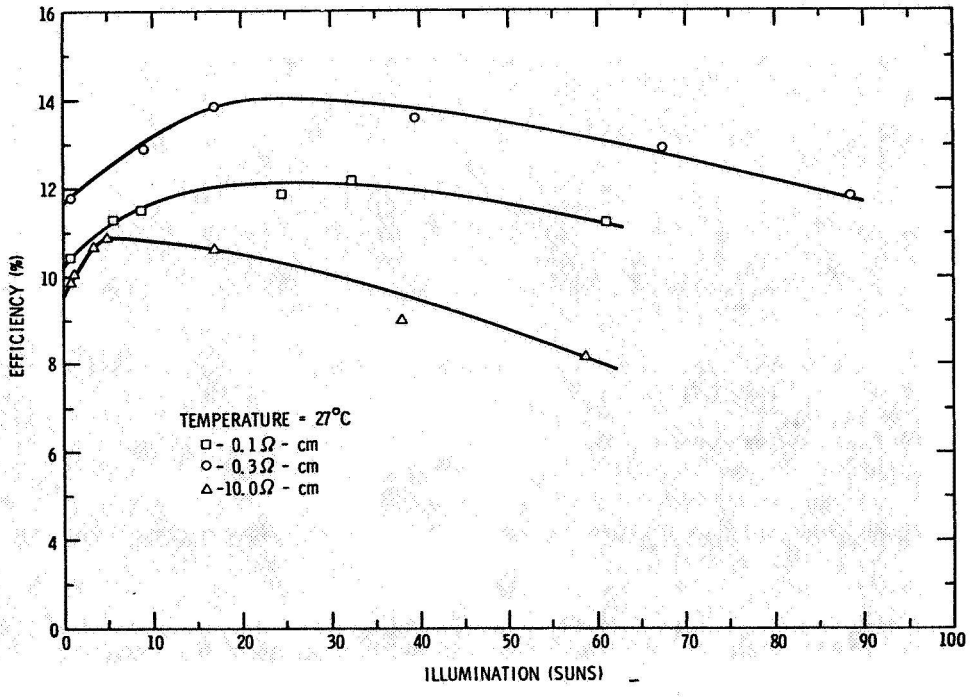


Figure 5 - Cell efficiency versus illumination (1 Sun ≙ 0.1 W/cm$^2$).

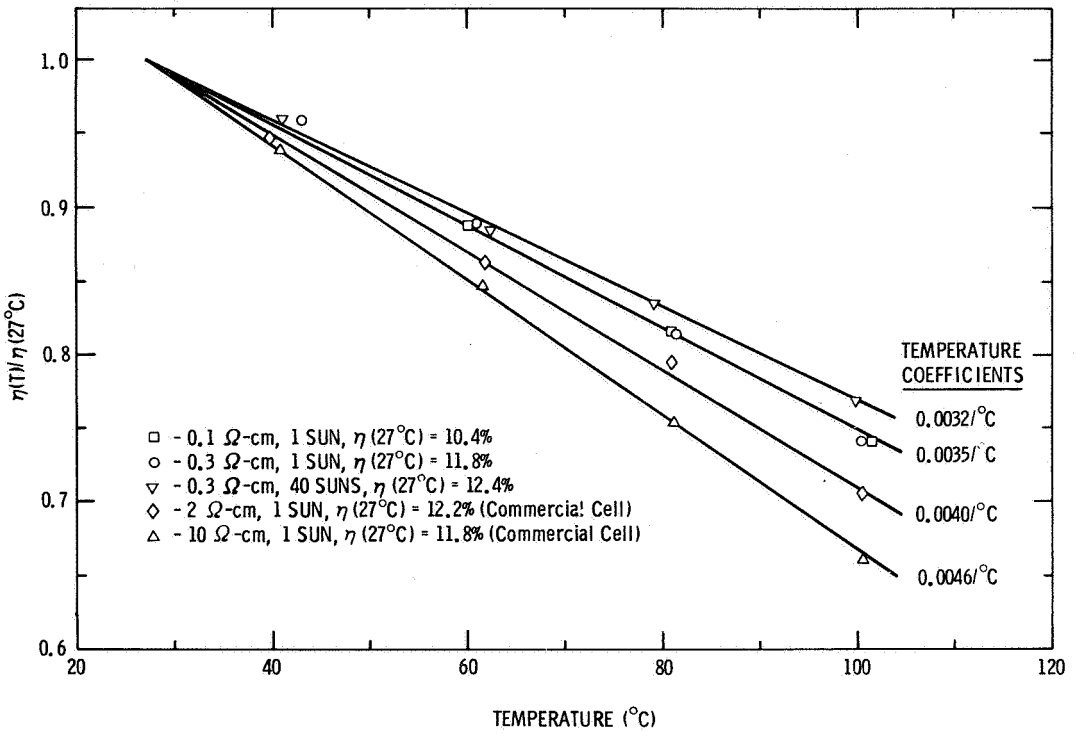


Figure 6 - Normalized cell efficiency versus temperature.

# On the Determination of Series Resistance and Diode Quality Factor of Solar Cells

R.L. Anderson
Physical Electronics Laboratory
Electrical and Computer Engineering Dept.
Syracuse University
Syracuse, N.Y. 13210

## ABSTRACT

The series resistance and diode quality factor are important parameters used for evaluation of solar cell performance. These parameters are normally deduced from the terminal I-V characteristics under forward bias. This method produces a smaller series resistance and a larger value for diode quality factor than appropriate for the device when operating as a solar cell. It is suggested that the diode quality factor be determined from measured saturated photocurrent - open circuit voltage characteristics and the series resistance be measured with an r-f bridge or calculated from a measurement of the surface sheet resistance.

## SERIES RESISTANCE

The series resistance $R_s$ in a solar cell is a distributed quantity because of the lateral current in the surface layer. It is convenient, however, to express $R_s$ as a lumped parameter. This lumped equivalent series resistance can be written

$$R_s = \frac{r_s}{2n} \tag{1}$$

where n is the number of metalization fingers and $r_s$ is the lumped equivalent series resistance of the section of the cell between x = 0 and x = a as shown in Fig. 1. The series resistance depends on the sheet resistance $R_\square$ of the surface layer and the geometry of the cell

$$r_s = \frac{R_\square L}{W} \tag{2}$$

where W, the cell width, is defined in Fig. 1 and L represents the length of the average current path in the surface layer.

At very low currents where the lateral voltage is negligible, the junction current density is uniform and L = a/3 [1]. At higher currents however, the lat-

eral voltage drop can influence the junction bias $V_j(x)$ and thus the current density $J(x)$.

For forward bias, the lateral voltage is of the polarity to cause $V_j(x)$ to decrease with increasing x in Fig. 1 and thus to concentrate the junction current in the region near the electrodes. This current crowding [2] increases with increasing forward current, thus decreasing the average path length L in Eq. 2. As a result the series resistance decreases with increasing forward current.

Under operating conditions the net solar cell current is negative and $V_j(x)$ is positive. The lateral drop tends to increase the dark forward current, and thus decrease the magnitude of the total current, with increasing x. Current crowding exists in this case also, with a reduction of series resistance, but this is at the expense of a reduction in net collection efficiency in the region near x = a. For efficient operation, however, the sheet resistance is small enough so that current crowding is negligible and L = a/3 or the appropriate series resistance for a solar cell is

$$R_s = \frac{R_\square L}{6nW} \tag{3}$$

This effect was investigated experimentally in a commercial n-on-p Si solar cell in shich the buss connection between the metalization fingers was removed. The structure is shown schematically in Fig. 2. A ramp voltage was applied between terminals a and d while the voltage was measured between each set of terminals and plotted against device current on an x-y recorder. The dark I-V characteristics are shown in Fig. 3.

The dark device I-V characteristics of this cell are shown by the curve labelled a-d representing the voltage between terminals a-d as a function of device current.

The curves a-b, a-c, and b-c represent the respective terminal voltages plotted against cell current. At reverse bias the junction current density is uniform and no current crowding occurs as evidenced by linear plots of the I-V characteristics and by the fact that $V_{bc}/V_{ab}$ is less at forward bias than for reverse bias.

Because of the exceptionally long current path in this test cell the series resistance is much larger than for a normal cell, and current crowding is exaggerated. It is clear, however, that the series resistance as determined from the slope of the I-V characteristics is lower than that appropriate for operation as a solar cell. A more accurate value of $R_s$ can be measured with an r-f bridge at zero bias, or calculated from a measurement of sheet resistance (Eq. 3).

## DIODE QUALITY FACTOR

The diode quality factor m from the equation for dark current

$$I = I_o \, (\exp \, qV/mkT/ - 1) \qquad (4)$$

is determined from the measured terminal I-V characteristics of a solar cell. This external diode quality factor is greater than the internal diode quality factor $m_j$ characteristic of the I-$V_j$ relation of the active junction

$$I = I_{oj}(\exp \, qV_j/m_jkT - 1) \qquad (5)$$

where

$$V_j = V - IR_s \qquad (6)$$

and $R_s$ is non-linear as discussed above. Under illumination, Eq. (5) becomes

$$I = I_{oj}(\exp \, qV_j/m_jkT - 1) - I_p(V_j) \qquad (7)$$

where $I_p$ is the photocurrent evaluated at $V_j = V - IR_s$. Under open circuit conditions $I = 0$, $V = V_j$ and

$$I_p(V_{oc}) = I_{oj}(\exp \, qV_{oc}/m_jkT - 1)$$

In Si-based cells, where $I_p$ is essentially independent of voltage, the true junction I - $V_j$ characteristics can be obtained from the experimental $V_{oc}$ - $I_{p\ sat}$ characteristics with illumination intensity as a parameter

$$V_{oc} = \frac{m_jkT}{q} \ln\left(\frac{I_{p\ sat}}{I_{oj}} + 1\right)$$

where $I_{p\ sat}$ is the photocurrent measured in the saturation region - usually at zero or reverse bias.

It is noted that $V_{oc}$ is a function of $m_j$ and $I_{oj}$ rather than m and $I_o$. The value of $m_j$ at the operating voltage can be determined from the slope of the $I_{p\ sat}$ - $V_{oc}$ relation at this voltage while $I_{oj}$ is the extrapolated current to $V_{oc} = 0$.

A comparison of $m_j$ with m is useful to determine the effects of a thin semi-insulating layer in Schottky barrier (MIS) or heterojunction solar cells. In particular it can be determined if this layer forms an integral part of the junction or merely contributes to series resistanc.

The terminal I-V and the $I_{p\ sat}$ - $V_{oc}$ characteristics are shown in Fig. (4) for a small (5 $mm^2$) $SnO_2$/n-Si heterojunction solar cell which contains a semi-

insulating interfacial layer. Although the external diode quality factor m is on the order of 2.7 at the currents characteristic of AM1 operation, $m_j$ is unity indicating that in this case the interfacial layer is not effective in increasing $V_{oc}$ by increasing the diode quality factor, but merely increases the series resistance. $R_s$ can be determined as a function of current by a comparison of the I-V and the $I_{p\ sat} - V_{oc}$ characteristics.

$$R_s = \frac{V - V_{oc}}{I}$$

where V and $V_{oc}$ are evaluated at the same current as indicated in Fig. (4).

References

1) See, for example, A. B. Phillips, Ed., Transistor Engineering, p. 216, McGraw-Hill, New York, (1962).

2) R. M. Burger and R. P. Donovan, Fundamentals of Silicon Integrated Device Technology, Vol. 2, pp. 103-117, Prentice Hall Inc., Englewood Cliffs, (1968).

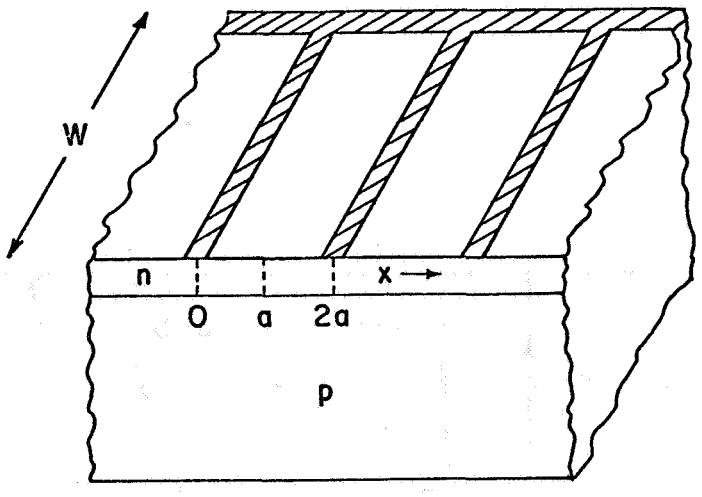


Fig. 1. Section of a solar cell.

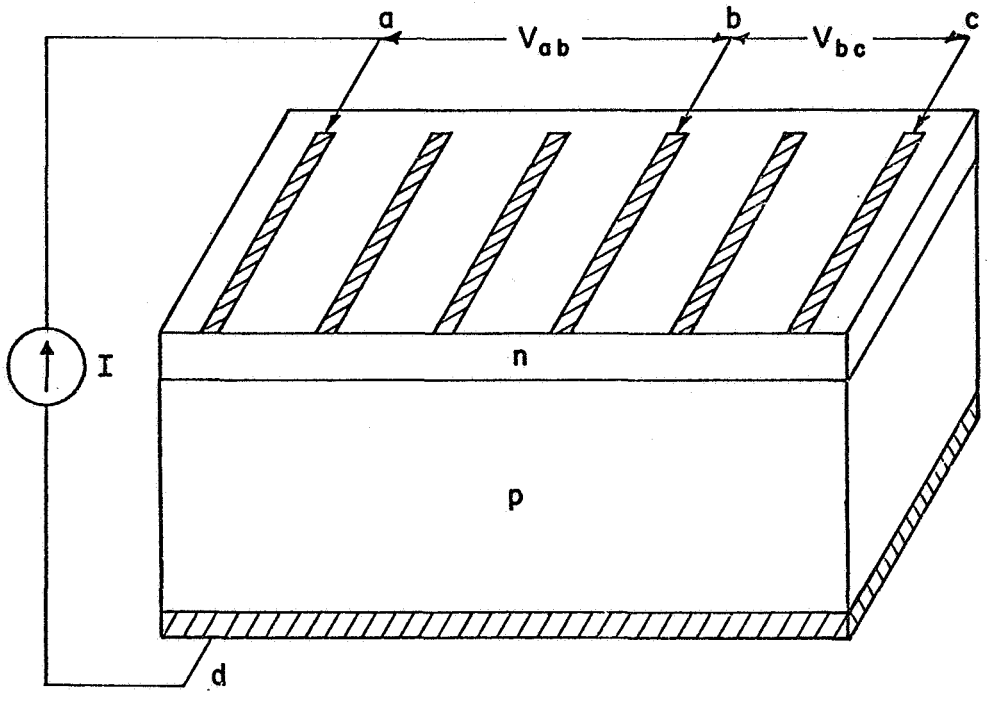


Fig. 2. Schematic diagram of test cell used to investigate current crowding.

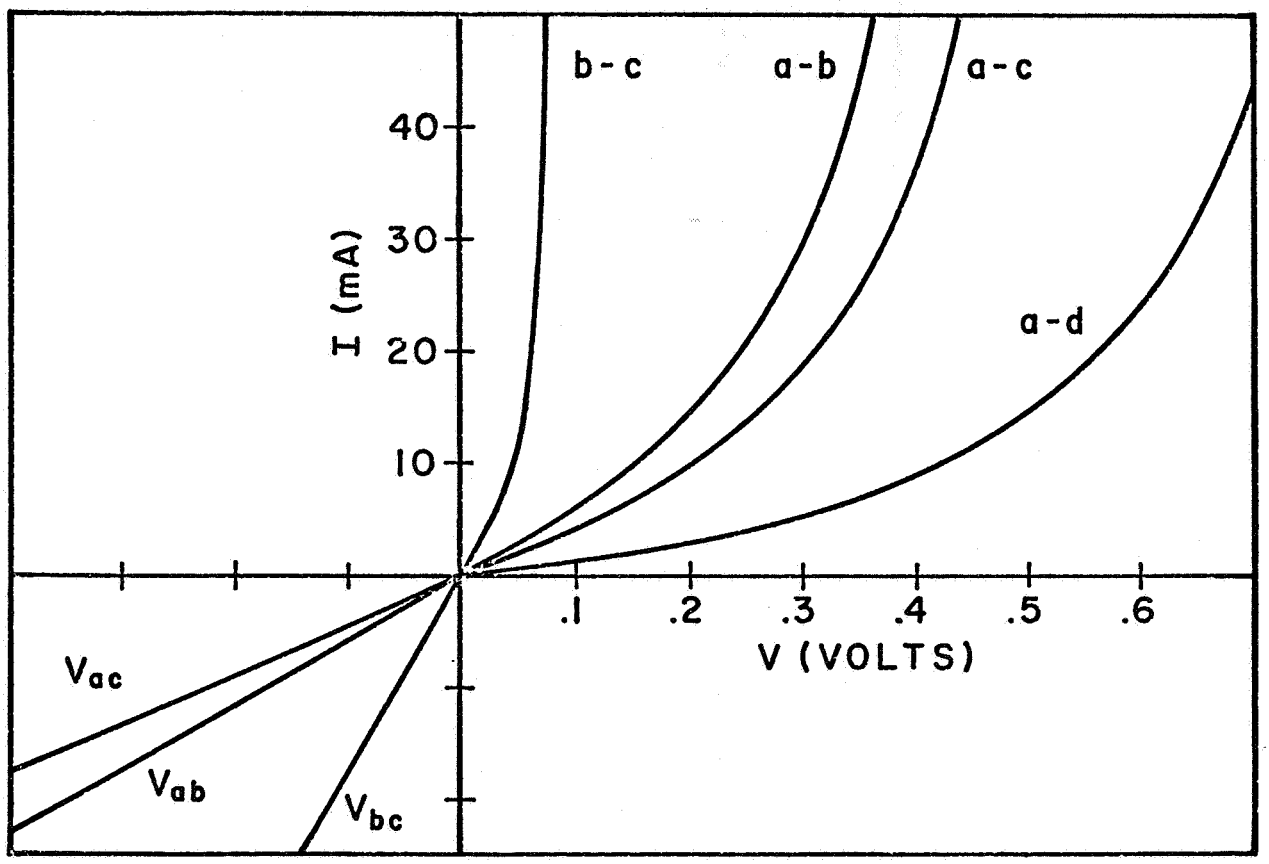


Fig. 3. Dark I-V characteristics of test cell. Bias is applied between terminals a-d while voltage is measured between terminals a-d, a-b, a-c and b-c.

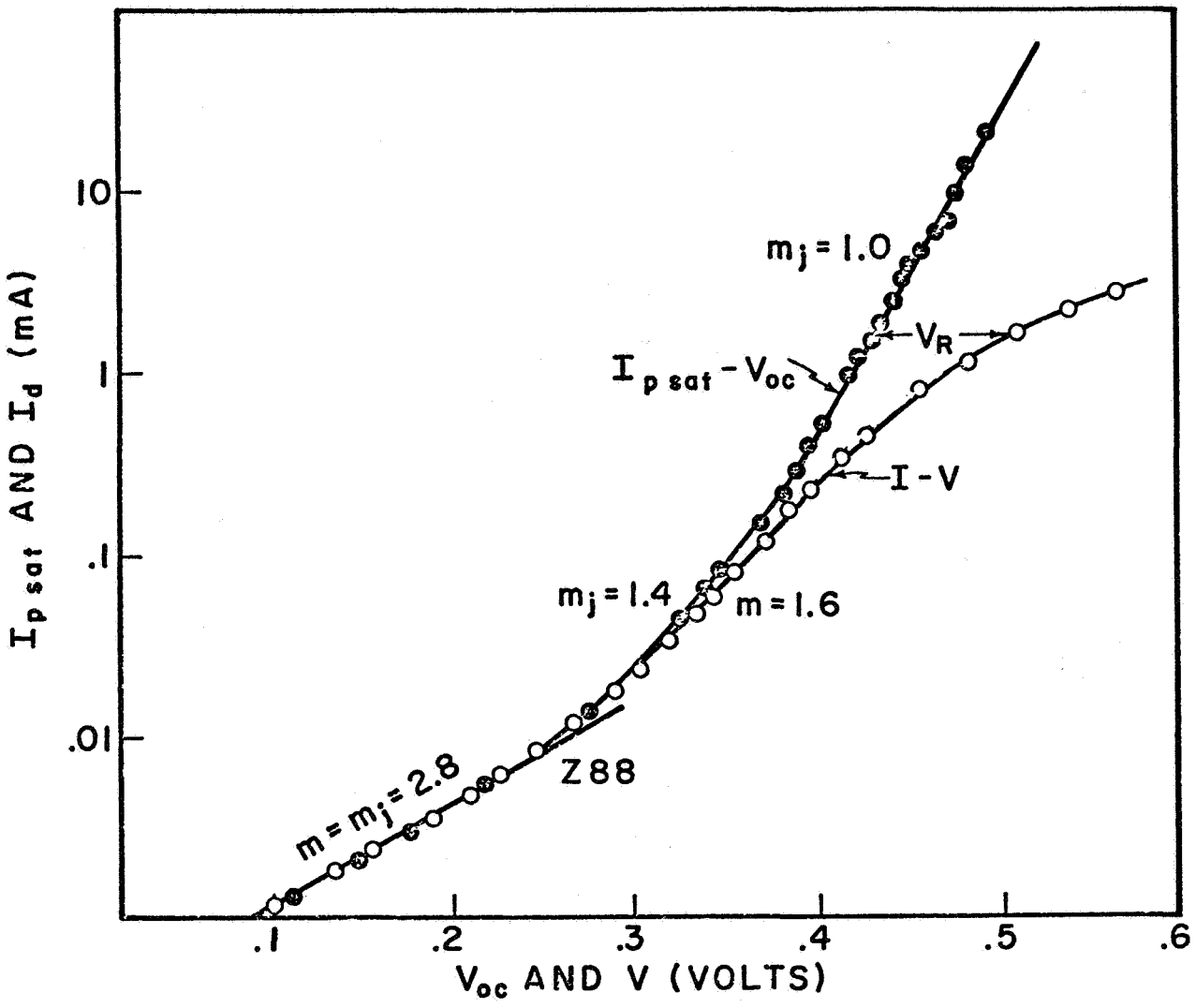


Fig. 4. Semi-log plots of dark I-V characteristics, and $I_{p\,sat} - V_{oc}$ characteristics for a $SnO_2$/n-Si heterojunction solar cell. Values for internal, or junction quality factor $m_j$ and external, or terminal diode quality factor m are indicated.

# PROBLEMS IN PHOTORESPONSE DISTRIBUTION MEASUREMENT

Shigekazu Minagawa and Terunori Warabisako

Central Research Laboratory, Hitachi Ltd.
1-280 Higashi-koigakubo
Kokubunji, Tokyo 185
Japan

Photoresponse distribution measurement by scanning a light spot across a surface of a semiconductor device is often used in a variety of sections of device characterization.[1)2)3)4)]

This technique is very useful for solar cell characterization because the measured quantity is the direct expression of the distribution of the desired performance of the device.

Researchers of the thin-film solar cell must be implemented with this kind of apparatus, because the thin-film cell includes many defects, grain boundaries and precipitates in some cases which cause nonuniform and poor performance. Characterization of these defects and techniques for eliminating these maleffects must be explored before the thin-film solar cells can supply low cost electric energy.

The authors set up an apparatus for measuring the photoresponse distribution and use it in the development of polysilicon thin-film solar cells.

A schematic diagram of the apparatus and an example of measurement are shown in Figs. 1 and 2.

In using this apparatus, however, there exist several conditions to be satisfied if one wants to guarantee that the measured photocurrent expresses correctly the local photovoltaic property of the spot irradiated.

## ELECTRIC PROPERTY OF CELL

Schematic diagrams of a polysilicon thin-film solar cell made on a ceramic substrate irradiated by a spot of light together with an equivalent circuit corresponding to it are shown in Fig. 3.

The equivalent circuit corresponding to the irradiated part i can be expressed by a parallel combination of a current source $I_{Li}$, an ideal diode and a shunt resistance $R_{SHi}$ connected to a series resistance $R_{Si}$. The remaining dark part is similarly expressed with a shunt resistance $R_{SH}$, a series resistance Rs and a leak current $I_D$. The total equivalent circuit is a parallel combination of these two circuit via a series resistance $R_B$ which depends on the mutual positions of the light spot and the electric contacts.

The measured short circuit current $I_L$ for this system is given by

$$I_L = I_{Li} - I_D$$

$$= \frac{R_{SHi}}{R_{SHi} + R_{Si} + R_B} \left(I_o' + \frac{Vi}{R_{SHi}}\right) - I_D \qquad (1)$$

where

$$I_o' = I_{oi} \{\exp \beta(V_i - R_{si}I_{Li}) - 1\} \qquad (2)$$

$$I_D = \frac{R_{SH}}{R_{SH} + R_s} I_o \{\exp \beta(V - R_sI_D) - 1\} + \frac{V}{R_{SH} + R_S} \qquad (3)$$

The sympols $\beta$, Vi and V have usual meanings.

These equations show that the measured current $I_L$ agrees with the photocurrent of the irradiated part i if the leak current $I_D$ and the series resistance $R_B$, which often tend to be large particularly in thin-film cells, are small enough.

Absence of a systematic variation in photocurrent distribution with regards to the positions of the light spot and the electrodes guarantees this condition holds.

## SCANNING SPEED

A limit is imposed on the scanning speed due to a large junction capacitance of a solar cell. When the surface of a solar cell with dimensions of $\ell_1$ by $\ell_2$ is scanned by a light spot of diameter $\phi$ at line frequency $\omega_1$ and frame frequency $\omega_2$, the transit time of the light spot $\tau_\phi$ must be smaller than the charging time constant of the junction capacitance $\tau_c$ = RC, i.e.

$$RC = \tau_c < \tau_\phi = \frac{\phi}{\ell_1\omega_1} . \qquad (4)$$

Where, R is the equivalent series resistance of a solar cell and C is the junction capacitance given by

$$C = \left( \frac{qK_S \varepsilon_o C_B}{2\phi_B} \right)^{1/2} \ell_1 \ell_2 \qquad (5)$$

Ks : permittivity of silicon, $\varepsilon_O$ : permittivity of free space

$C_B$ : free carrier concentration of the lower impurity concentratio side of a step junction, $\phi_B$ : built in potential.

Equations (4) and (5)are combined to give the limiting condition for line frequency,

$$\omega_1 < \phi / \{R\ell_1^2 \ell_2 (qK_S \varepsilon_o C_B / 2\phi_B)^{1/2}\}. \qquad (6)$$

The frame frequence, $\omega_2 = \phi\omega_1/\ell_2$ is also governed by the same condition. Numeric calculation using the values shown in Table I indicates that the upper limit of the line frequency is 90.4 $H_Z$ and the time required for measuring one frame is 138 seconds.

## RESOLUTION AND DENSITY OF SCANNING LINES

There exists a trade-off between the spot size and the density of the scanning lines with regards to the resolution and the frame frequency.

The spot size of light should be determined according to the object of the measurement: whether the whole photoresponse image across a cell or the fine structure of a specific area is required. In the former case, the minimum time necessary for measurement is restricted to $\ell_2 / \phi\omega_1$ as described above. A standard condition for measuring the whole image of a solar cell with dimensions of 10 cm by 10 cm is $\omega_1$ = 1 $kH_Z$, $\omega_2$ = 30 $H_Z$ and $\phi$ = 1.5 mm. In the latter, resolution is limitted to about 0.8 μm even if the best available optics is employed for He - Ne laser light. On the other hand, the spot size need not be focused smaller than the diffusion length of the minority carriers.

## OTHER FACTORS

The absorption coefficient of silicon and the diffusion length of the minority carrier should be taken into consideration when a light for

scanning is selected. Use of light sources with different wavelengths provides us with informations on the photorespose distribution in depth direction.

For example, He - Ne laser light (6328Å) and Ar laser lights (4880Å and 5145Å) in silicon correspond to the penetration depth of 2.7 μm, 0.75 μm and 1.0 μm, respectively, which are comparable to the magnitude of the diffusion length of the minority carrier often encountered in the thin-film solar cell.

Roughness of the surface of a thin-film solar cell may complicate quantitative understanding of the result of the distribution measurement because the condition of normal incidence does not hold and the effect of multireflection on the uneven surface may occur if the spot size becomes comparable to the roughness of surface.

Acknowledgements

This work was partially supported by the Agency of Industrial Science and Technology, Ministry of International Trade and Industry, Japan.

References

1) C.N. Potter and D.E. Sawyer, Rev. Sci. Instr., 39 180 (1968)
2) S.T. Soclof and P.A. Iles, Record of the 11th IEEE Photovoltaic Specialists Conference (1975)
3) D.L. Lile and N.M. Danis, Solid-State Electronics, 18 699 (1975)
4) L.A. Kasprzak, Rev. Sci. Instr., 46 257 (1975)

Table I. Values used for frequency limit calculation

| | |
|---|---|
| diameter of light spot | $\phi = 2\ \mu m$ |
| cell dimensions | $\ell_1 = \ell_2 = 25$ mm |
| equivalent series resistance of cell | $R = 1\Omega$ |
| permittivity of silicon | $K_S = 11.7$ |
| permittivity of free space | $\varepsilon_O = 8.86 \times 10^{-14}$ F cm$^{-1}$ |
| impurity concentration | $C_B = 10^{17}$ cm$^{-3}$ |
| built-in potential | $\phi_B = 0.414$ V |
| electron charge | $q = 1.602 \times 10^{-19}$C |

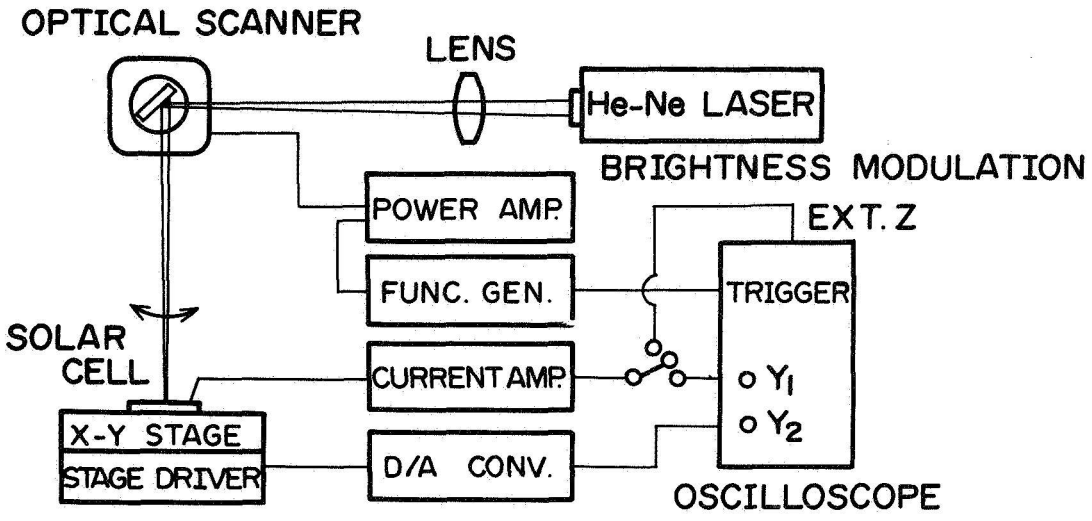


Fig.1 Apparatus for photocurrent distribution measurement.

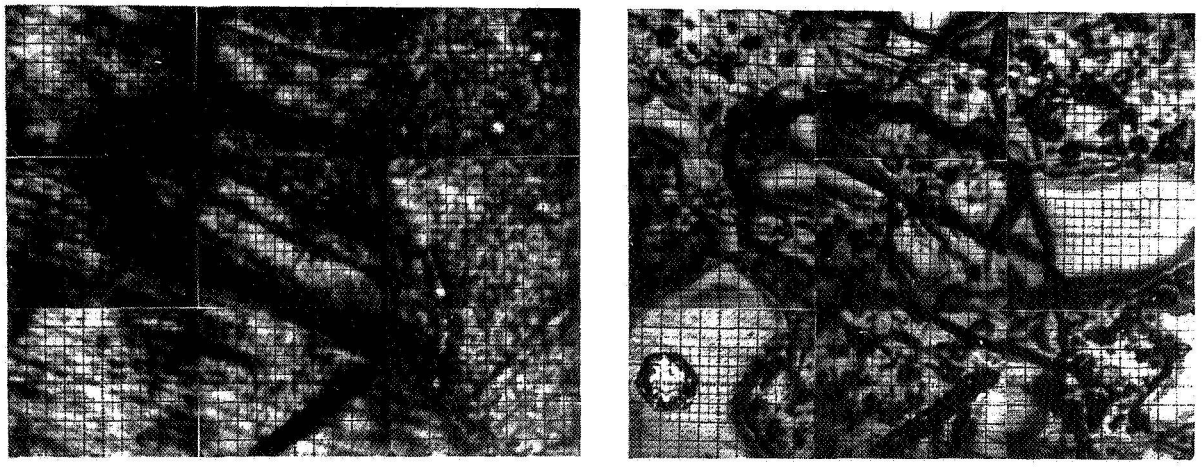


(a) photocurrent map

(b) surface optical micrograph

Fig.2 A photocurrent distribution map of a thin-film silicon solar cell.

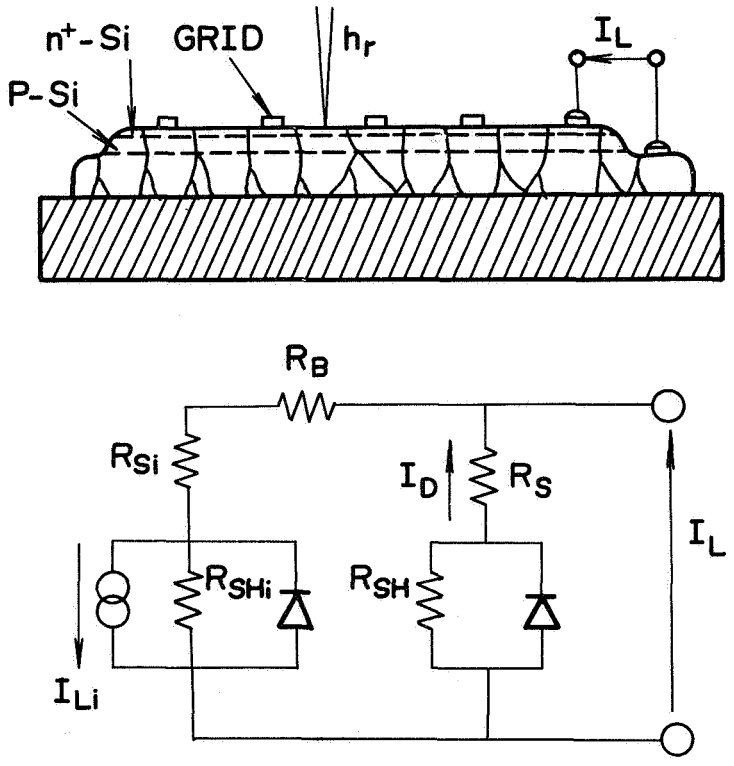


Fig.3 Photocurrent measurement by scanning a laser spot.

# COLLECTION EFFICIENCY MEASUREMENTS FOR SOLAR CELL RESEARCH*

by Harry L. Hampton and Larry C. Olsen

Joint Center for Graduate Study
Richland, Washington 99352

## 1. INTRODUCTION AND SUMMARY

A system has been established for measuring absolute, spectral collection efficiency that is well suited to solar cell research and development. In particular, the required equipment is relatively inexpensive, the measurement procedure is straight forward, and the approach allows for the study of high resistance or "leaky" cells. Determination of spectral collection efficiency, $Q(\lambda)$, involves measurements of the incident photon intensity, the device reflection coefficient $R(\lambda)$, and the cell short-circuit current $I_{sc}(\lambda)$. A monochromatic photon flux is obtained with a high intensity Bausch and Lomb monochromator, and an Epply thermopile detector is used to measure incident intensity. Normal incidence reflectivity measurements are achieved with a prism type beam splitter.

Reflectivity vs $\lambda$ has been measured for evaporated Ag films and agree to within 2% of those previously reported by Haas in the visible region. Measurements of $Q_\lambda$ vs $\lambda$ have been made for 2 $\Omega$-cm, silicon solar cells and for $Cu_2O$ devices. The same silicon cells were sent to NASA-Lewis for quantum-yield measurements. Our results agree extremely well with those of NASA-Lewis.

The experimental approach is discussed in Section 2, measurements of the reflectivity of evaporated silver films are considered in Section 3, collection efficiency measurements of silicon solar cells are presented in Section 4, and collection efficiency studies of $Cu_2O$ solar cells are discussed in Section 5.

*This work has been supported by the National Science Foundation under Grant AER75-20501.

## 2. EXPERIMENTAL APPROACH

The absolute spectral collection efficiency of a solar cell is given by

$$Q(\lambda) = \frac{I_{PH}(\lambda)}{[1 - R(\lambda)]\, I_{max}(\lambda)} \qquad (1)$$

where $I_{PH}(\lambda)$ refers to the photocurrent produced by a cell for an incident beam of photons with wavelength $\lambda$, $R(\lambda)$ is the reflectivity and $I_{max}(\lambda)$ is the maximum possible value obtainable for photocurrent. If the cell series resistance is zero, then $I_{PH} = I_{sc}$, where $I_{sc}$ is current measured under short-circuit conditions. Approaches utilized to measure $I_{PH}$, R and $I_{max}$ are discussed below.

### 2.1 Photocurrent Measurement

Solar cells which are at an early stage of development may produce a photocurrent in the range of $10^{-9}$ A/cm$^2$ to $10^{-6}$ A/cm$^2$, while a well developed cell will produce a current well above $10^{-6}$ A/cm$^2$ when coupled to a high-intensity monochromator. As a result, to carry out solar cell research on new devices, such as copper-oxide cells, a system had to be developed which could readily measure currents in this range to at least three significant figures, with reasonable stability and ease of operation.

The arrangement of apparatus for measuring photocurrent is shown in Figure 1. A nulling technique is used to determine the short-circuit current produced by a cell when coupled to the monochromator. The measuring circuit is shown in Figure 2. When the current generator ($I_g$) is adjusted so that the voltage drop across the 15 megohm resistor is zero, then

$$I_g = I_{sc} \qquad (2)$$

The current produced by a solar cell can be written as

$$I = I_{PH} - I_o\left[\exp\left(\frac{V + R_s I}{nkT}\right) - 1\right] - \frac{V + R_s I}{R_{sh}} \qquad (3)$$

In the case of short-circuit conditions, or when the voltage across the load (V) goes to zero, we have

$$I_{sc} = I_{PH} - I_o\left[\exp\left(\frac{R_s I_{sc}}{nkT}\right) - 1\right] - \frac{R_s I_{sc}}{R_{sh}} \qquad (4)$$

Usually the $I_o$-term can be neglected, and

$$I_{PH} \simeq \left(1 + \frac{R_s}{R_{sh}}\right) I_{sc} \qquad (5)$$

In most cells, $R_s/R_{sh} << 1$, but for devices which are in an early development stage this correction factor can be important.

## 2.2 Normal Incidence Reflection

The measurement of reflectivity under normal incidence conditions is illustrated in Figure 3. The arrangement provides a relatively simple means of acquiring data both rapidly and with reasonable accuracy (2 to 3%). To determine the reflectivity of a sample, $R(\lambda)$, one must measure the incident photon flux and the reflected flux. These two steps are accomplished as shown in Figure 4. The incident beam is characterized by detector No. 2, while a quantity related to the photon flux reflected from the sample is obtained with the incident beam entering the prism as indicated in Figure 4. In order to determine an expression for $R(\lambda)$, it is necessary to consider the transmission properties of the prism.

Referring to Figure 5, let the incoming photon flux be $N_o$, $f_1N_o$ be the flux which emerges from the top face of the prism, $TN_o$ the flux which is transmitted directly through the prism, and $f_2N_o$ the flux which emerges from the bottom face due to reflection at the glass/air interface. Coefficients $f_1$, $f_2$ and T must be determined as a function of wavelength.

Now consider a sample placed at the "top" side as indicated in Figure 4.

The flux incident on the sample is $f_1N_o$. To calculate R, it is necessary to know the flux reflected from the sample which enters the prism. Multiple reflections can be accounted for as shown in Figure 6. The flux $N_1$ corresponds to $f_1N_o$. $N_2$ is $Rf_1N_o$ and $N_3 = RR_1f_1N_o$ where $R_1$ is the reflection coefficient for the air/glass interface. Similarly, $N_4 = R_1R^2f_1N_o$, $N_5 = R_1{}^2R^2f_1N_o$, etc. The flux reflected from the sample which enters the prism is

$$N = f_1N_o(R + R^2R_1 + R^3R_1{}^2 + R^4R_1{}^3 + \ldots .) \qquad (6)$$

$$= \frac{Rf_1I_o}{1-R_1R}$$

The photon flux incident on detector No. 1 is

$$N_1 = TN + f_2N_o$$

$$= N_o\left[\frac{TRf_1}{1 - RR_1} + f_2\right] \qquad (7)$$

This expression can be used to solve for R if $N_1$ and $N_o$ are determined. Silicon solar cells are utilized for both detectors in this measurement. $N_1$ gives rise to a short-circuit current of

$$I_{sc}^{(1)} = eA_1N_1Q_1(1 - r_1) \qquad (8)$$

where $Q_1$, $r_1$ and $A_1$ refer to the collection efficiency, the reflection coefficient and illuminated area of detector No. 1, respectively. Detector No. 2 is used to determine $N_o$. With the slide in the appropriate position, $N_o$ incident on detector No. 2 results in a current

$$I_{sc}^{(2)} = eA_2N_oQ_2(1 - r_2) \qquad (9)$$

Substitution of (8) and (9) into (7) yields

$$R = \frac{I_{sc}^{(1)} - f_2 K I_{sc}^{(2)}}{T f_1 K I_{sc}^{(2)} + R_1 I_{sc}^{(1)} - R_1 f_2 K I_{sc}^{(2)}} \tag{10}$$

where

$$K = \frac{Q_1 A_1 (1 - r_1)}{Q_2 A_2 (1 - r_2)} \tag{11}$$

The quantities T, $f_1$ and $f_2$ are properties of the prism and depend on $\lambda$. They are measured only once. $R_1$ is given by

$$R_1 = \frac{(n_{prism} - 1)^2}{(n_{prism} + 1)^2} \tag{12}$$

where $n_{prism}$ is the index of refraction of the prism material. The present approach uses glass. Thus, $R_1$ is independent of wavelength and is

$$R_1 \simeq .053 \tag{13}$$

The factor K is also a function of $\lambda$, but only needs to be measured one time. Details regarding the measurement of K, T, $f_1$ and $f_2$ are discussed in Reference 1.

Determination of the normal incidence reflection from a sample involves measuring $I_{sc}^{(1)}$ and $I_{sc}^{(2)}$. These quantities and the corresponding wavelengths are utilized in a computer code to calculate R vs $\lambda$. With the slide arrangement, data can be taken rapidly. Furthermore, values of $R(\lambda)$ are for normal incidence.

All of the above calculations were performed assuming an incident beam that was both monochromatic and unpolarized. However, the Bausch and Lomb high intensity monochromator is a diffraction grating type monochromator which produces overlapping orders of light. Overlapping of orders, which is characteristics of all grating systems, is eliminated with the use of filters. Corning Color Filter glasses are used in our experiments. The specific filters utilized will be noted in a later section.

It was also found that the grating system did not produce completely

unpolarized light. There is an output in all directions, each grating showing a preference for a particular direction of polarization. Reflectivity is a function of polarization unless complete normal incidence is achieved. In carrying out reflectivity studies on Ag films, R was determined by averaging the results for two distinct polarizations. Results obtained with and without polarizers agree very well. The present approach does not utilize polarizers.

## 2.3 Maximum Current Measurement

A calibrated Eppley thermopile is used to determine the incident photon flux. The thermopile has a sensitivity of .192 mV/mW/cm$^2$ assuming an open circuit voltage measurement. The thermopile is coupled to the monochromator in an arrangement as indicated by Figure 1. The sample holder and the Eppley thermopile are of the same outer dimensions. As a result, the thermopile and the sample holder are interchangable. This approach insures that the beam incident on the thermopile and sample are identical--including the aperature area. The back plate of the thermopile is connected by thermal grease to a temperature control plate containing a brass coil. Forced air is utilized for cooling. Air feedthroughs are installed in the light restricting box and the thermopile is connected via opaque hoses to an external compressed air source.

The aperature area used in device short-circuit current measurements is A = .725 cm$^2$. The power is given by

$$P = eN_0E(eV) \tag{14}$$

and

$$E = h\nu = \frac{1242}{\lambda(nm)}\ eV \tag{15}$$

Assuming that each photon with $h\nu \geq E_g$ generates a single EHP , the maximum possible current produced by a cell for a given wavelength is

$$I = eN_o A \tag{16}$$

where A is the illuminated area of the cell. Utilizing (14) and (15),

$$I_{max} = \frac{P(W/cm^2)A\ (cm^2)\lambda(nm)}{1242} \quad \text{Amps} \tag{17}$$

It is very tedious to determine P (or $I_{max}$) every time the system is used. Thus, it is convenient to relate a short-circuit reading of detector No. 2 to $I_{max}$. When $P(\lambda)$ is measured, we therefore measure $I_{sc}^{(2)}$ and determine a relationship.

$$K_o = \frac{I_{max}}{I_{sc}^{(2)}} \tag{18}$$

Assuming the collection efficiency of detector No. 2 is constant, $I_{max}$ is obtained by simply measuring $I_{sc}^{(2)}$ in any particular collection efficiency study. This approach accounts for any variation in monochromator beam intensity. Finally, the values of $K_o(\lambda)$ are determined at room temperature ($\sim 23^oC$).

## 3. REFLECTIVITY OF A STANDARD

To confirm the validity of this technique for measuring $R(\lambda)$ of a sample, the measurement was performed on a sample of known reflectance. A "freshly" evaporated film of silver was selected as a standard. In particular, the results of Haas[2] were chosen for comparison. Deposition of silver was done in a period of approximately 15 sec. A film of 1063 Angstroms was obtained. The film thickness was chosen to assure that negligible transmission occurs.

Results of this study are given in Table 1. The gratings and filters (Corning) utilized along with the appropriate wavelength range, are listed. Measured values of $R(\lambda)$ are given for two perpendicular polarizations. Results

for the two polarizations always agree within ∿2%. These results indicate that the experimental approach provides essentially normal incidence. Agreement of the average value for $R(\lambda)$ with those of Haas is very good up to 900 nm. From 900 nm to 1300 nm, our values are consistently 10% to 15% lower than those of Haas. It may be that we have more impurities in our film.

## 4. COLLECTION EFFICIENCY FOR SILICON SOLAR CELLS

Collection efficiency vs wavelength has been determined for two silicon solar cells. These cells were also sent to the NASA-Lewis Research Center for similar measurements. The silicon cells are 2 x 2 cm, 2 Ω-cm n/p devices with AR coatings. They were manufactured in 1971 by Heliotek (now Spectrolab).

The area of illumination for our measurements was .725 $cm^2$ with a centered, circular aperature. The ratio of device contact area (area covered by fingers) to illuminated area was ∿.053. The NASA-Lewis measurements were carried out by using full cell illumination and with an approach which utilizes interference filters.[3] Both experimental procedures are believed to have an accuracy of ±5%, or better.

Results of our measurements and those of NASA-Lewis are shown in Figures 7 and 8. The quantum yield in electrons/incident-photon is plotted for the two silicon cells. The dotted curves refer to our results for quantum yield, or collection efficiency, correcting for reflection. The agreement between the JCGS results and those of NASA-Lewis is very good. In the case of Si71-843, the two sets of data agree to within 1%, while for Si71-822 the agreement is always within 3%. The data at 1000 nm appear to disagree. However, the uncertainty in $\lambda$ for the JCGS data is ±5 nm, which alone accounts for the difference.

It is interesting to note that $Q_\lambda > 1$ for a range of $\lambda$ for both cells. Accounting for reflection, we find that $Q_\lambda$ at $\lambda$ = 670 nm is 1.06 for Si71-843 and 1.05 for Si71-822. We must either condlude that both the JCGS and NASA-Lewis

approaches are in error by about 5%, or $Q_\lambda$ is actually greater than 1.0 for these cells. This effect could be due to avalanche effects. The photon energy corresponding to 670 nm is 1.85 eV. Hot carriers crossing the junction region could produce additional electron-hole pairs. Other reported results for $Q_\lambda$ vs $\lambda$ for silicon n/p cells are given in terms of relative values of quantum yield.

## 5. COLLECTION EFFICIENCY STUDIES WITH $Cu_2O$

One research effort being carried out at JCGS is concerned with low cost solar cells based on $Cu_2O$.[4] This program includes studies with backwall and frontwall cells. Many of the early cells have had relatively large values for $R_S$ and low values for $R_{sh}$. Furthermore, the emphasis thus far has been to understand the barrier physics and collection efficiency properties. No effort has been devoted to AR coatings. This problem can be addressed later, after other aspects of the devices have been shown to be favorable.

Figure 9 gives results for backwall cells made by partially oxidizing copper substrates and applying a front contact. The ZCNS contact refers to a chemically deposited contact. Further details are given in Reference 4.

Figure 10 shows results obtained for frontwall cells to date. These devices are fabricated by evaporating copper layers onto solid, polycrystalline $Cu_2O$ wafers. No finger contact pattern was applied. The difference between the frontwall results are not completely understood.

## ACKNOWLEDGEMENTS

We greatly appreciate the cooperation of NASA-Lewis for carrying out measurements on the silicon solar cells discussed in this article. We particularly thank Drs. Brandhorst and Curtis for their help.

## REFERENCES


1. Harry Hampton, "Collection Efficiency Measurements for Solar Cell Research and Application to $Cu_2O$ Cells," In Preparation for Master's Thesis as Partial Fulfillment of Requirements for M.S. Degree in Electrical Engineering.

2. American Institute of Physics Handbook, pp. 6-108 (1957).

3. Henry W. Brandhorst, "Prediction of Terrestrial Solar Cell Short-Circuit Currents by Spectral Analysis," p. 120, Proceedings of Workshop on Terrestrial Photovoltaic Measurements, March 19-21, 1975, Cleveland, Ohio.

4. Larry C. Olsen, "Investigation of Low Cost Solar Cells Based on $Cu_2O$," Semi-Annual Progress Report for Period October 1, 1975 to March 31, 1976, on NSF Grant NSF/RANN/AER75-20501/PR/76/1.

REFLECTIVITY OF Ag FILMS

| Grating | Filter | λ(nm) | R Polarization A | R Polarization B | Average R | $R_{standard}$ | % Error |
|---|---|---|---|---|---|---|---|
| 33-86-76 | CS 0-54 | 400 | .939 | .941 | .940 | .948 | .84 |
| | | 450 | .988 | .966 | .977 | .966 | 1.14 |
| | | 500 | .981 | .977 | .979 | .977 | .20 |
| | | 550 | .983 | .987 | .985 | .979 | .61 |
| | CS 3-69 | 570 | .976 | .980 | .978 | .980 | .20 |
| | | 590 | .988 | .990 | .989 | .981 | .81 |
| | | 610 | .978 | .967 | .972 | .981 | .92 |
| | | 630 | .972 | .976 | .974 | .982 | .81 |
| | | 650 | .973 | .993 | .983 | .983 | .00 |
| | | 670 | .969 | .971 | .970 | .984 | 1.42 |
| | | 700 | .967 | .973 | .970 | .985 | 1.52 |
| | | 750 | .957 | .979 | .968 | .986 | 1.82 |
| | | 800 | .935 | .967 | .951 | .986 | 3.55 |
| 33-86-77 | CS 2-58 | 700 | .977 | .951 | .964 | .985 | 2.13 |
| | | 750 | .972 | .967 | .970 | .986 | 1.62 |
| | | 800 | .965 | .953 | .959 | .986 | 2.74 |
| | | 900 | .898 | .876 | .887 | .987 | 10.13 |
| | | 1000 | .882 | .882 | .882 | .989 | 10.82 |
| | | 1050 | .890 | .886 | .888 | .989 | 10.21 |
| | | 1100 | .875 | .857 | .866 | .989 | 12.44 |
| | | 1150 | .839 | .837 | .838 | .989 | 15.27 |
| | | 1200 | .802 | .821 | .811 | .989 | 18.00 |
| | CS 7-56 | 1250 | .817 | .825 | .821 | .989 | 16.99 |
| | | 1300 | .871 | .889 | .880 | .989 | 11.02 |
| | | 1350 | .935 | .950 | .943 | .989 | 4.65 |
| | | 1400 | .979 | .977 | .978 | .989 | 1.11 |
| | | 1450 | .989 | .972 | .981 | .989 | .81 |

Table 1. Reflectivity of Freshly Evaporated Silver Film.

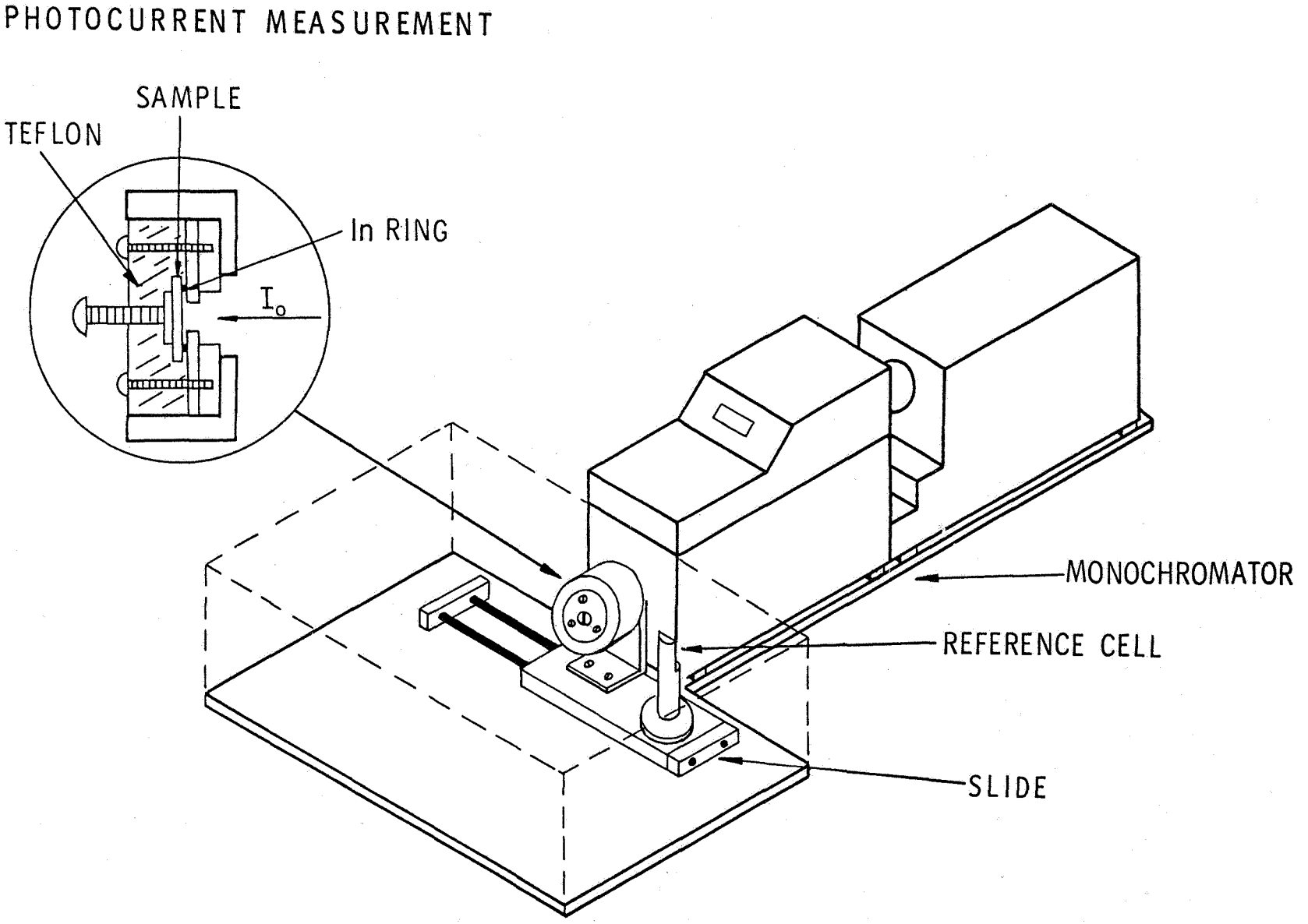


Figure 1. Approach to Photocurrent Measurement.

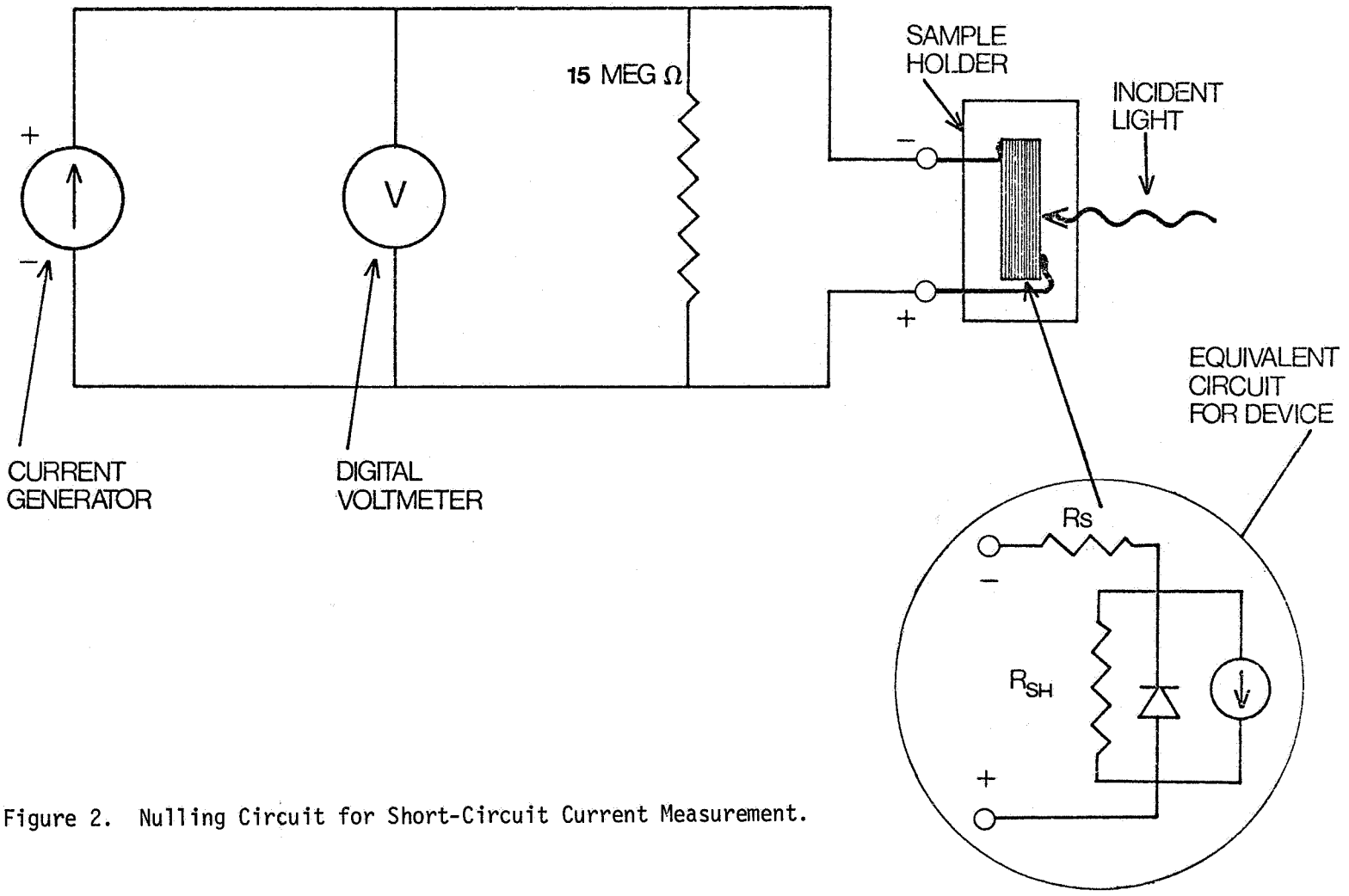


Figure 2. Nulling Circuit for Short-Circuit Current Measurement.

REFLECTIVITY MEASUREMENT

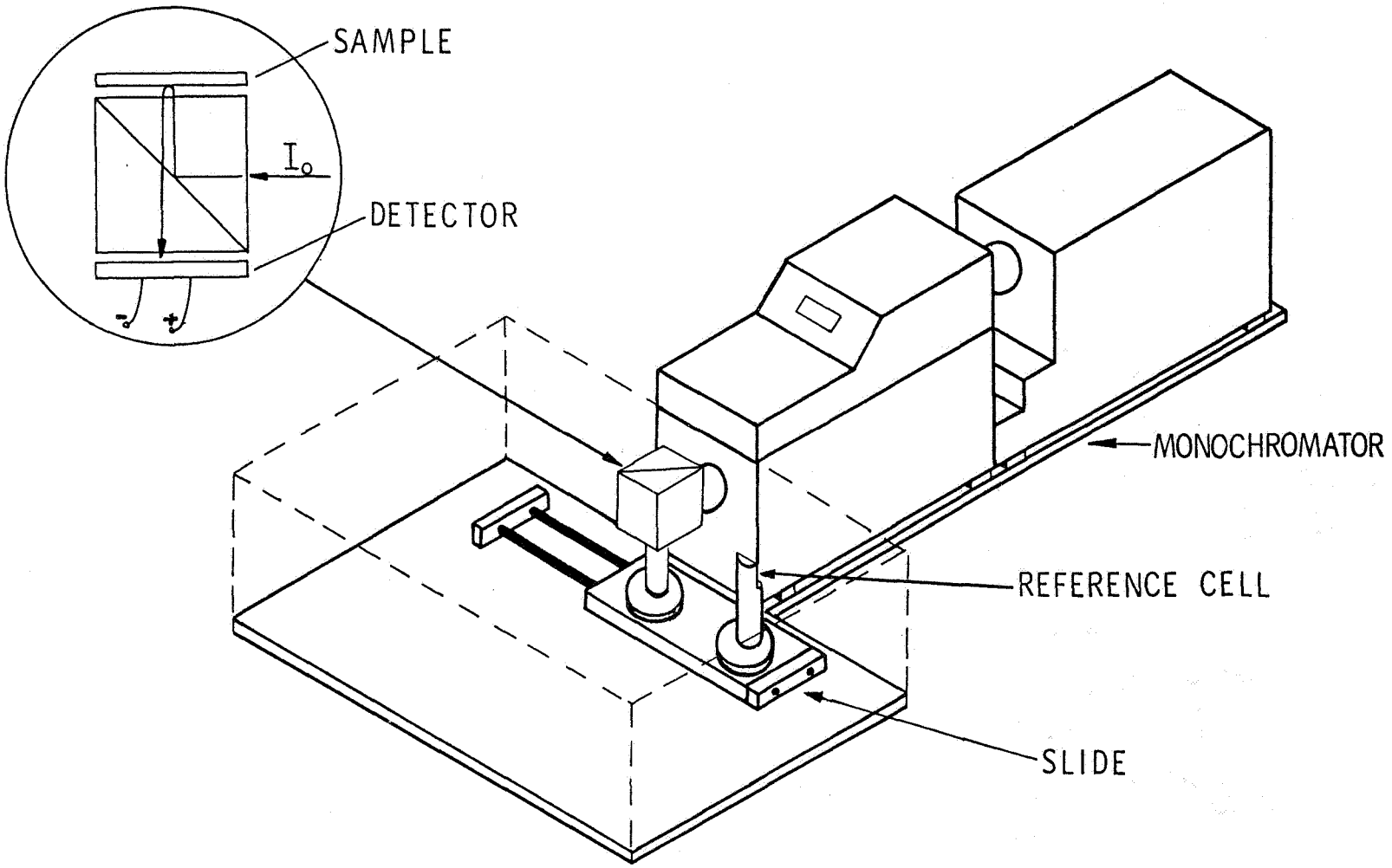


Figure 3. Approach for Normal Incidence Reflectivity Measurement.

# REFLECTIVITY MEASUREMENT

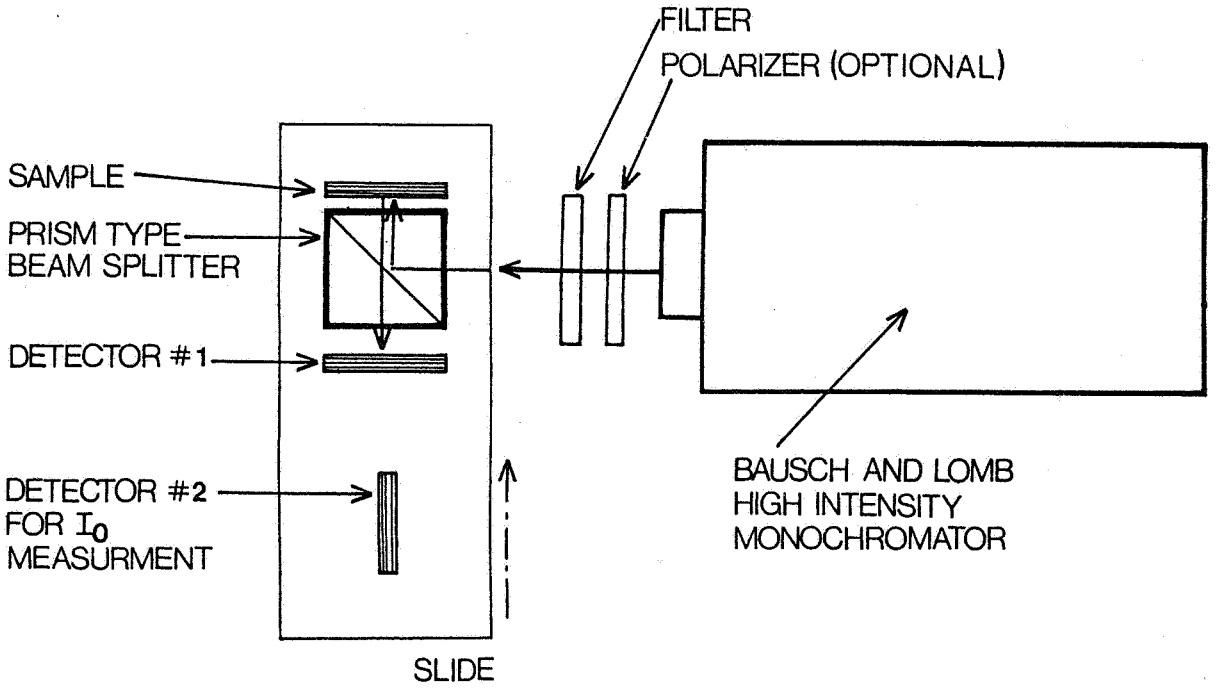


Figure 4. Illustration of How Two Detectors and a Beam Splitter Are Utilized to Measure Normal Incidence Reflectivity.

TRANSMISSION COEFFICIENTS FOR BEAM SPLITTER

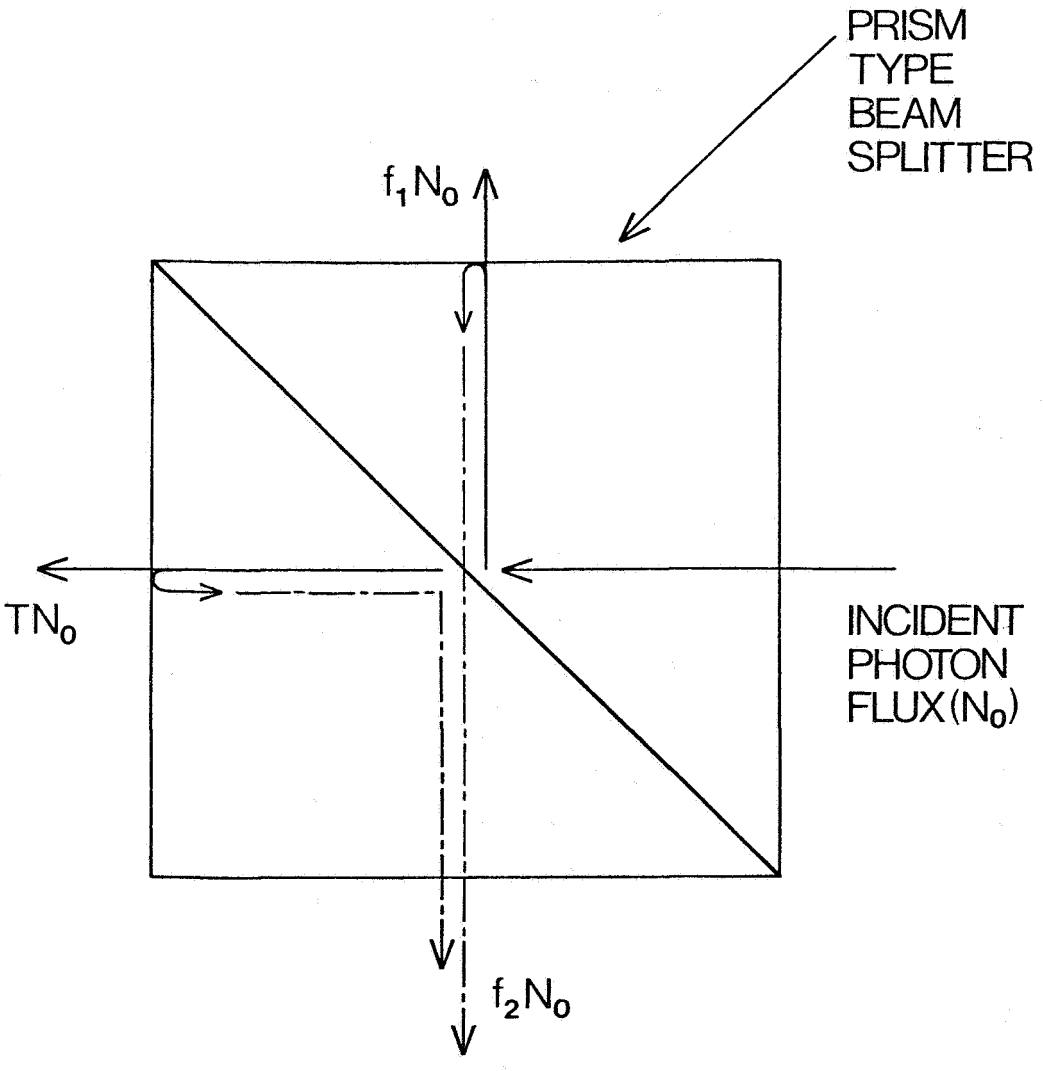


Figure 5. Definition of Transmission Coefficients of Prism-Type Beam Splitter.

MULTIPLE REFLECTIONS AT INTERFACE OF SAMPLE AND BEAM SPLITTER

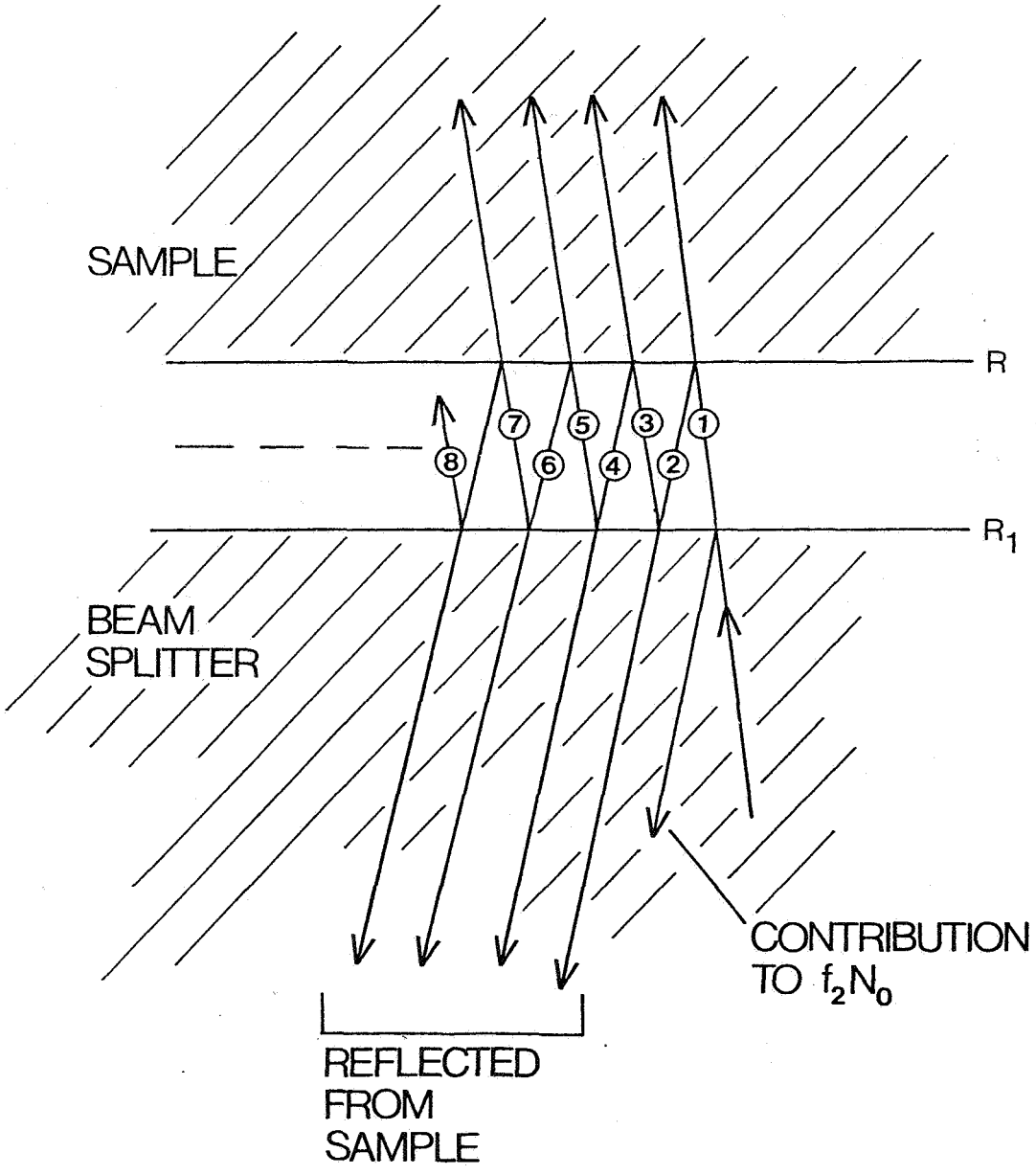


Figure 6. Multiple Reflections at Interface of Sample and Beam Splitter.

# SILICON SOLAR CELL COLLECTION EFFICIENCY

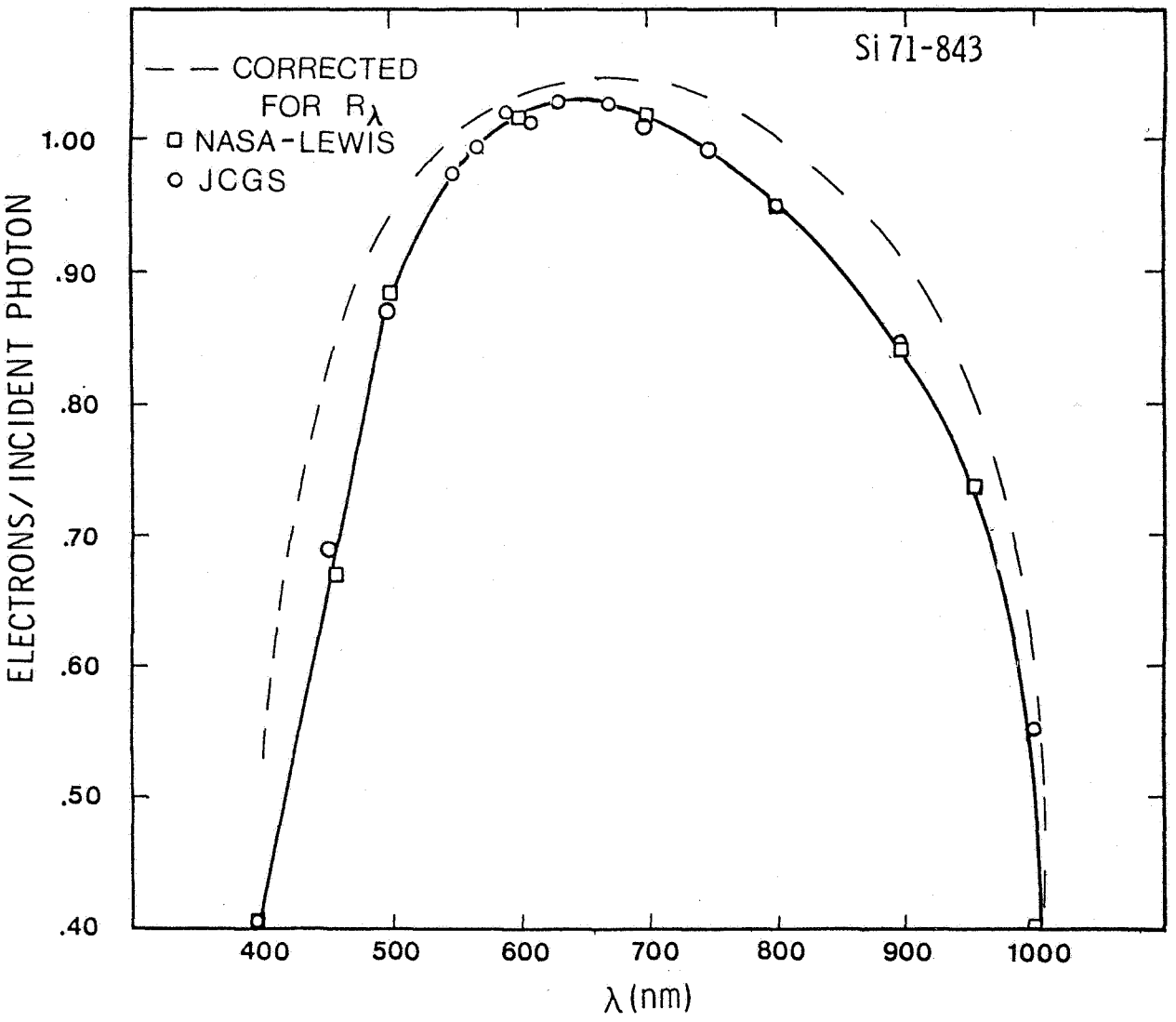

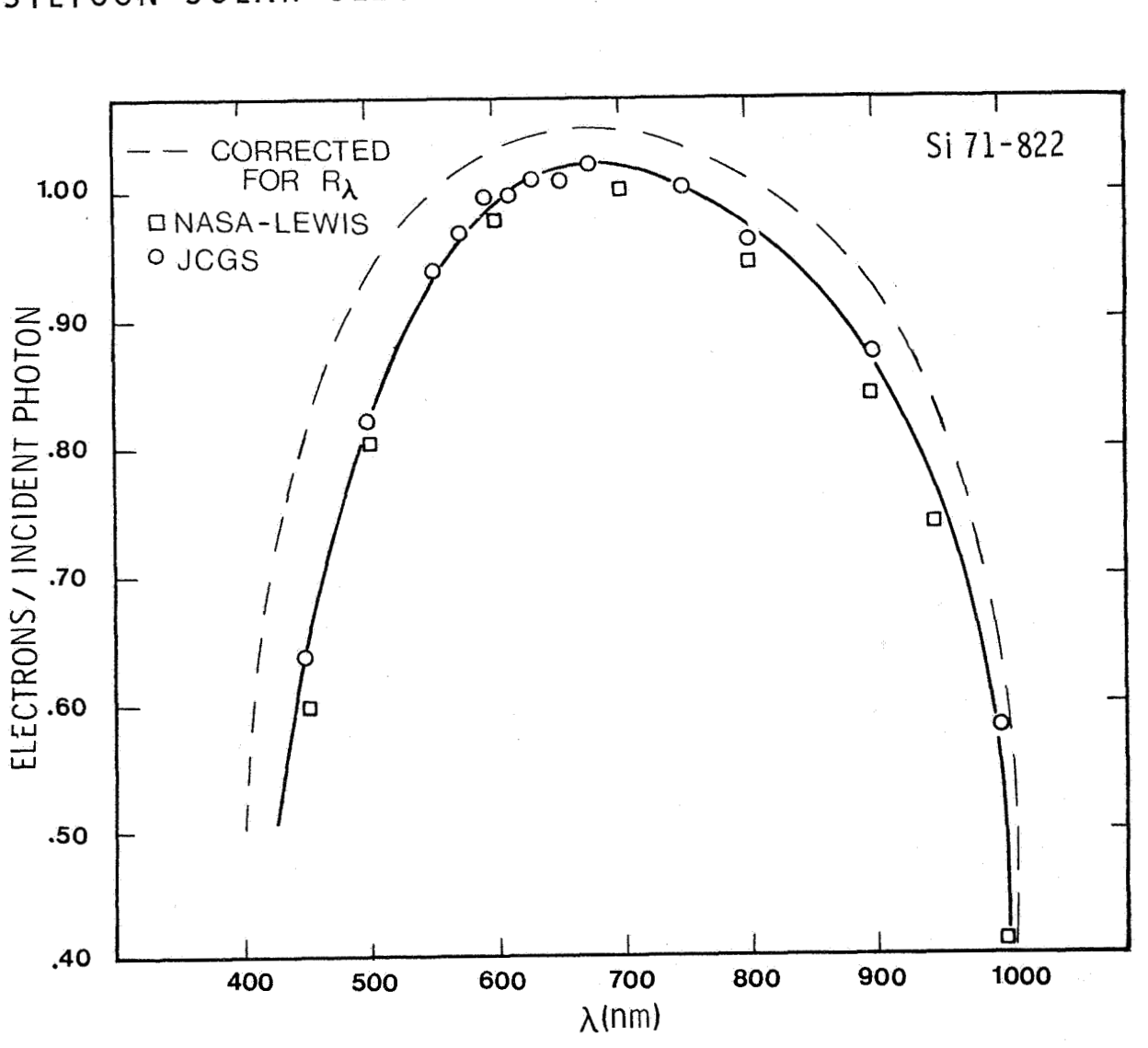


Figure 8. Quantum Yield Results for a 2 Ω-cm N/P Silicon Solar Cell(Si 71-822).

SPECTRAL COLLECTION EFFICIENCY FOR BACKWALL Cu / $Cu_2O$ CELLS

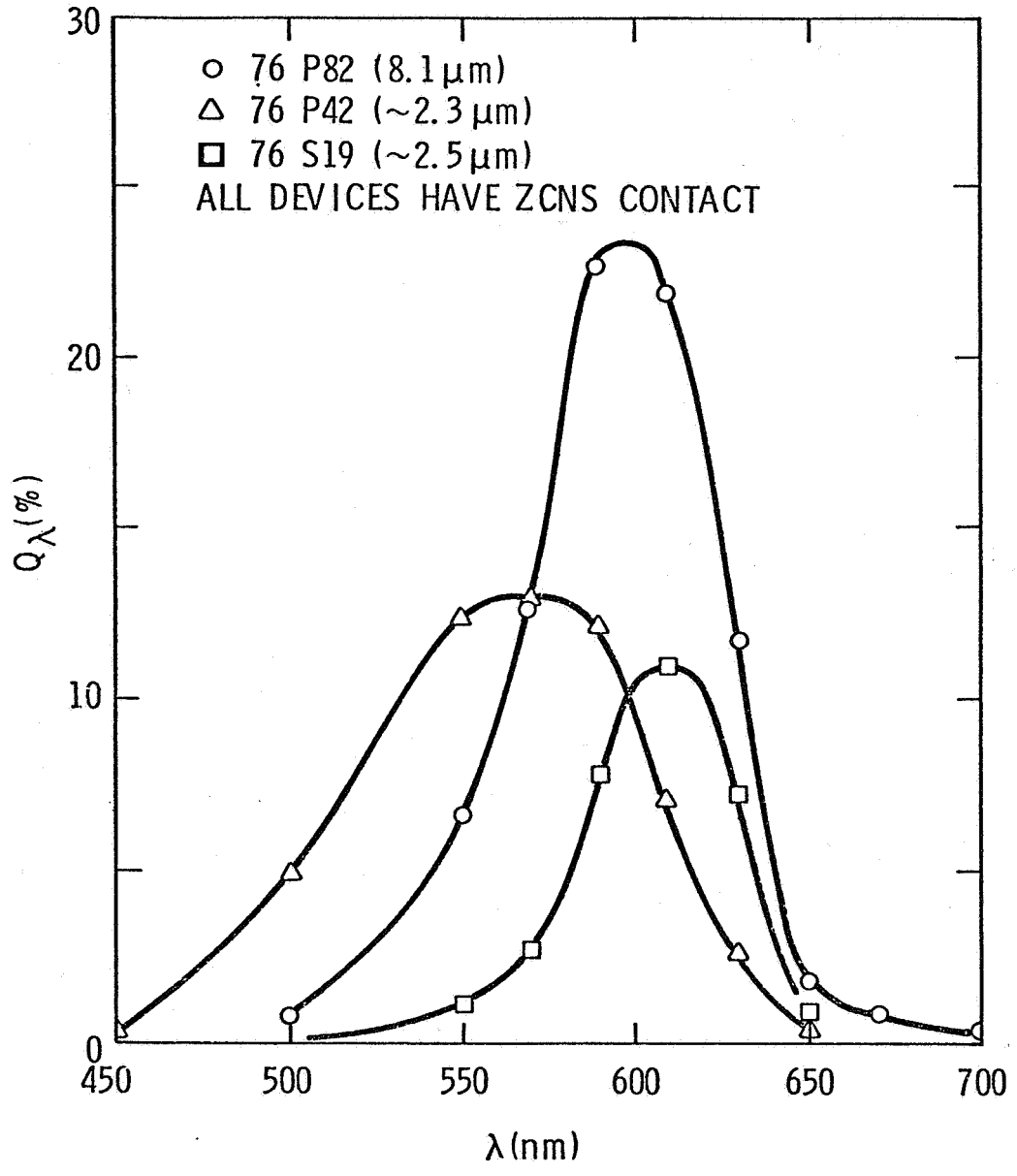


Figure 9. Collection Efficiency vs. Wavelength for Thin-Film Backwall, $Cu/Cu_2O$ Solar Cells.

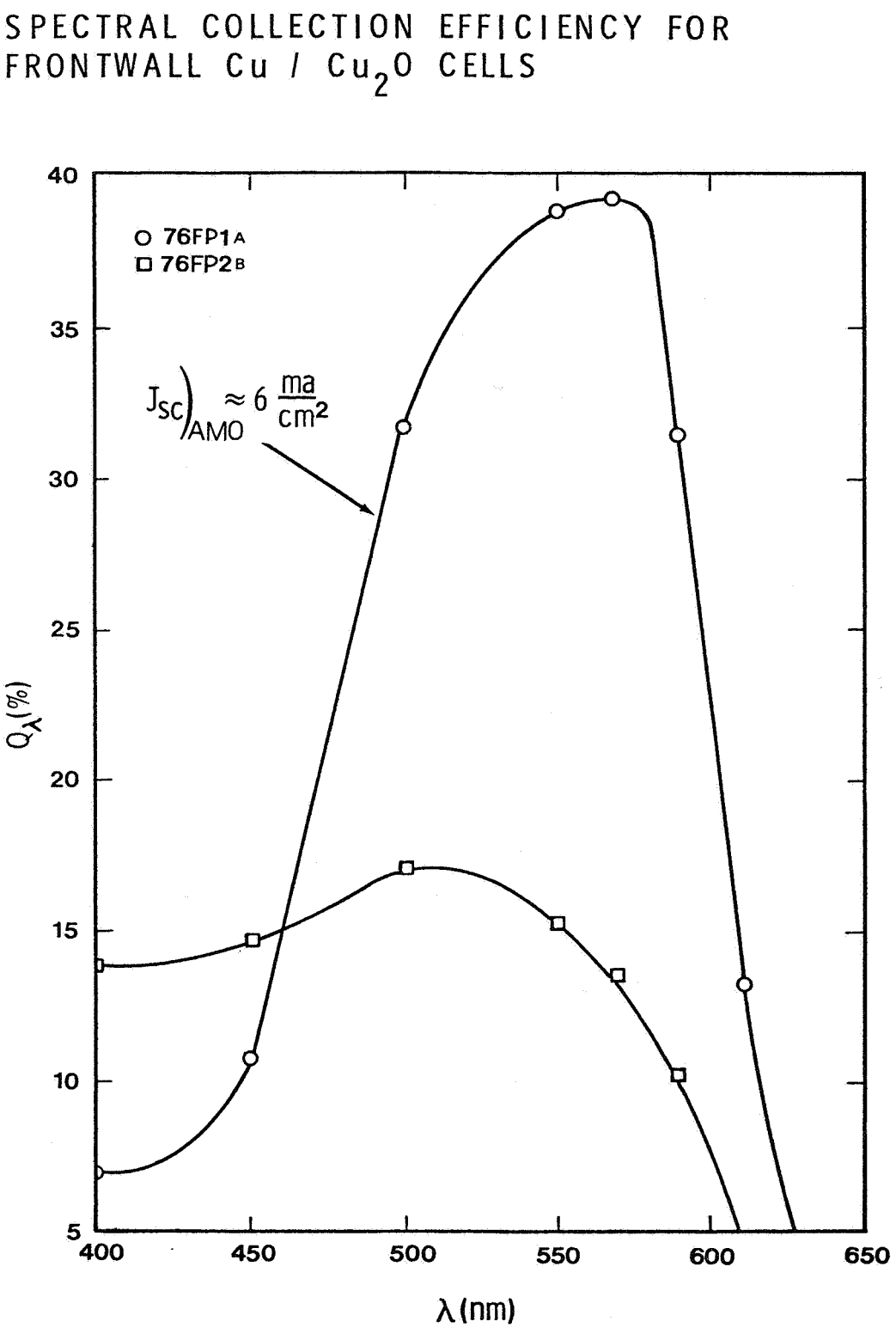


Figure 10. Collection Efficiency vs. Wavelength for Frontwall $Cu/Cu_2O$ Solar Cells.

# Spectral Response Measurements with White Light Bias*

W. Devaney, S. Lorenz, J. D. Meakin
Institute of Energy Conversion
University of Delaware
Newark, Delaware 19711

## ABSTRACT

The spectral response of certain solar cells such as the $CdS/Cu_2S$ cell is well known to be non-linear with distinct quenching and enhancement bands. One possible technique to produce standardized solar efficiencies is to fold in spectral response with a standard solar spectrum. It is therefore necessary to measure the spectral response of a cell in a way which will match cell behavior under white light illumination. A technique has been developed to measure the response of a cell to low intensity chopped monochromatic light while the cell is also illuminated with a white light bias corresponding to AM1.

*Supported in part by the National Science Foundation under Grant # NSF/RANN/AER72-03478 and the United States Energy Research and Development Administration Grant # ERDA E(49-18)-2538.

## Introduction

The natural variability of sunlight makes it difficult if not impossible to specify a standard for solar cell performance under natural insolation. This problem is not readily solved by utilizing simulated illumination because of the difficulty of simulating natural insolation and the practical difficulties in reproducing and maintaining a standard spectral distribution in a simulator. The main cell characteristic which varies with insolation is the short circuit current; over reasonable intensity and spectral ranges the fill factor and open circuit voltage are effectively constant. One possible technique for standardizing cell performance is to measure the spectral response of the cell over the active portion of the solar spectrum and to integrate the product of this with a standard tabulated spectrum. For cells typified by the single crystal silicon cell, the procedure is relatively straightforward as the short circuit current under white light is simply the integral of the response at each wavelength. Previous published work presents convincing evidence that the proposed technique for standardizing cell response is applicable to silicon cells.[1] In marked contrast, cells of the type typified by CdS/$Cu_2S$ show significantly non-additive behavior, with spectral regions that show current enhancement or quenching.[2-4] If a simple spectral scan is performed on such cells, the response versus wavelength shows extreme hysteresis[5] and the overall white light conversion efficiency computed from the apparent spectral response would be quite erroneous.

## Spectral Response with White Light Bias

In order to measure the effective spectral response of the CdS/$Cu_2S$ cell while illuminated by white light approximating the solar spectrum,

a technique has been developed to modulate a narrow band of the spectrum and to measure the incremental cell output from the modulating intensity. A chopped monochromatic beam is superposed on a constant white light bias and using synchronous detection techniques, the increment of cell output due to the chopped monochromatic input is detected and displayed. The monochromatic beam is chopped at 94Hz, the lowest frequency consistent with good signal to noise ratio. The white bias is adjusted to give a short circuit current equal to that recorded in a W-I simulator set to AM1 using a NASA-Lewis standard $CdS/Cu_2S$ cell. The selectivity of the synchronous amplification allows the use of a monochromatic component equivalent to less than 1% of the same wavelength band from the white light bias; the monochromatic flux is in the range $10^{13}$-$10^{14}/cm^2/sec$.

Figure 1 shows a block diagram of the experimental arrangements. The initial step is to replace the cell under test with the pyroelectric radiometer and to measure the intensity of the monochromatic source as a function of wavelength and store this in the mini-computer. The incremental short circuit current from the cell is then measured and the absolute quantum efficiency as a function of wavelength computed using the stored intensity calibration. The reduced data can be displayed graphically or printed in tabular form.

The absolute accuracy of the radiometer is given as 5% over the range of 0.23 + 3.2 μm. The stability and accuracy of the other system components ensure that the whole system accuracy is close to 5%.

## Experimental Results

For a cell of the silicon type, there should be no difference between the spectral response measured with or without the white light bias. Figure 2a shows this to be the case within the experimental accuracy. In marked contrast, a CdS/$Cu_2S$ cell shows a spectral response that changes considerably depending on the white light bias conditions. The no bias light condition (Fig. 2b, curve 1) is a non-stationary response and varies with the wavelength scan speed and direction. An unfiltered W-I bias (deficient in blue or rich in I-R) shows anomalous enhancement in the region of 500 nm (Figure 2b, curve 2). Using a filtered W-I source containing sufficient blue light to saturate the CdS depletion region a spectral response behavior is obtained which corresponds to cell behavior under illumination similar to natural sunlight (Figure 2b, curve 3).

## Conclusions

An experimental technique has been developed to measure the spectral response behavior of nonlinear solar cells in a manner which corresponds to cell performance under white light illumination. The technique would allow the computation of cell efficiency under a standard tabulated spectrum. Further experiments will be conducted to establish the degree to which the observed spectral response is sensitive to the specific nature of the white light bias. It is anticipated, but not as yet proved, that the observed spectral response will be relatively insensitive to the details of the white light bias as long as there is a sufficiently intense blue component.

The technique is considered to have the following advantages over previous procedures[6,7] for deriving spectral response under white light bias.

1. The direct output of absolute quantum efficiency as a function of wavelength makes the technique available as a standard analytical procedure.

2. Spectral response is measured at full AM1 or other illumination of interest.

3. Good accuracy is achievable as a consequence of the intensity callibration technique and the sensitivity of the synchronous detection ensures negligible perturbation of the white light behavior.

References


1. H. W. Brandhorst, Jr., Terrestrial Photovoltaic Measurements, NASA TMX-71802, p. 120, 1975.

2. W. D. Gill and R. H. Bube, J. Appl. Phys. 41, 3731, 1970.

3. P. F. Lindquist and R. H. Bube, J. Appl. Phys. 43, 2839, 1974.

4. J. Lindmayer and A. G. Revesz, Solid State Electronics 14, 647, 1971.

5. Research Directed to Stable High Efficiency CdS Solar Cells, NSF/RANN/AER72-03478 A04 PR75/4, p. 34.

6. A. E. Potter, Jr., and R. L. Schalla, 6th IEEE Photovoltaic Specialist Conference, p. 24, 1967.

7. L. R. Shiozawa, F. Augustine, G. A. Sullivan, J. M. Smith III and W. R. Cook, Jr., Research on the Mechanism of the Photovoltaic Effect in High Efficiency CdS Thin Film Solar Cells, ARL69-0155, p. 127, 1969.

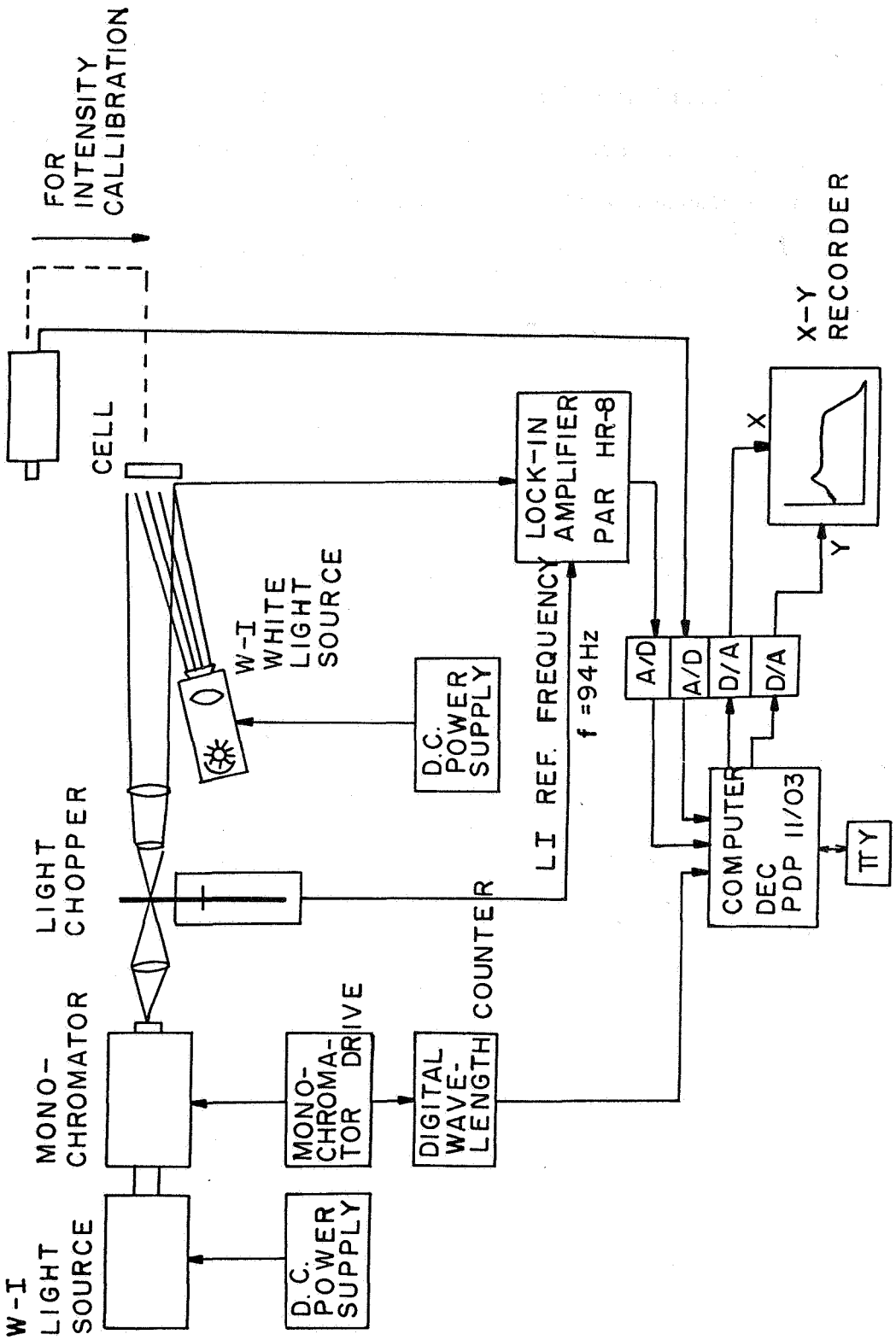


Figure 1. Block diagram of experimental arrangement.

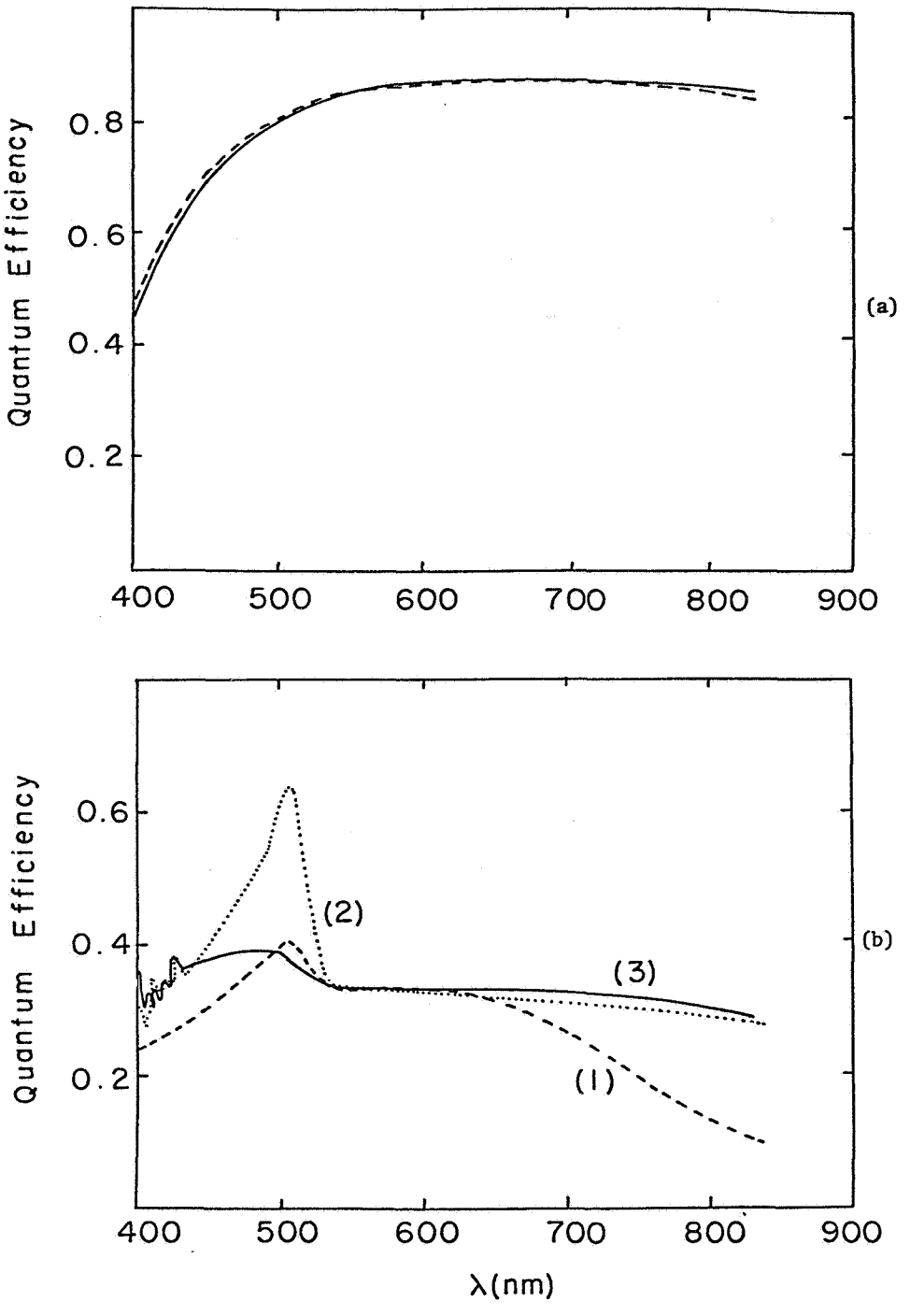


Figure 2. (a) Spectral response curve for a silicon cell ——— with AM1 white light bias ------- without bias light.
(b) Spectral response for a CdS/$Cu_2S$ cell. (1) without bias. (2) unfiltered W-I bias. (3) filtered W-I bias.

Henry Curtis/NASA-Lewis Research Center

This workshop session covered two main areas: cell measurements and array measurements. In the cell measurement area, discussions were limited to how to revise the procedures in the Interim Procedures Manual. The array measurement discussions covered a wide range of topics including indoor and outdoor measurements; cell temperature measurements in arrays, ambient conditions, etc. The main results of this session were:

1. The Interim Testing Procedures are generally in use. There should be some changes made in them, however. These changes included: (for all measurements)

   a. Outdoor measurements should be made at an irradiance level of 80 $mW/cm^2$ or greater as measured by a reference cell.

   b. The reference cell method is the only method acceptable for making measurements for reporting purposes. However if someone would want to take his own internal data, he could use the pyranometer method described in the Interim Procedures. This conclusion was not unanimous and several people felt that outdoor cell measurements based on total detector irradiance data should be allowed. However, the use of reference cells has an important advantage. The sensitivity of solar cells can vary by 5% or more due to the atmospheric composition. The use of a reference cell, calibrated at a set of standard

conditions, will nearly eliminate this source of error.

The discussion of array measurements started with the reasons for making I-V measurements. These include degradation analysis, system design and data needed for matching of modules in building arrays. Three definitions were suggested for module and array terminology. In all cases, an array includes internal wiring and any circuit protection devices. The definitions are:

Module: The smallest non-cell unit delivered by the manufacturer.

Sub-array: A specified size building block made up of modules.

Array: All the sub-arrays required to meet the particular power requirement.

It was felt that indoor measurements made using a flash simulator, would probably be the most accurate and the easiest to make. Outdoor measurements have significant problems involving cell temperature within the module or arrays, and the voltage-current transformations to convert the measured curve to same standard conditions. The suggestions concerning array (a module and sub-array) measurements were:

1. Measure the I-V curve near the standard temperature ($28^{o}C$) using either a flash simulator indoors or a shaded technique outdoors.

2. Determine the temperature coefficient of array performance.

3. Determine the equilibrium temperature which the array reaches under same ambient operating conditions and convert the data to this temperature using the temperature

coefficient of item 2 above. This procedure identifies the better thermal design modules.

4. All efficiency data to be based on total area of module, sub-array or array, not the total cell area.

5. Distinguish between $P_{max}$ and the power at a specified voltage.

## Report of Working Group on Concentrator Systems Measurements

Don Schueler/Sandia Laboratories

Summary

1. For concentrators, just as for flat plate arrays, solar cell performance characterization should be separated from system performance.

2. Interim test procedures for concentrator solar cell performance characterization should be developed and included in the next issue of the Terrestrial Measurement Procedures Manual.

3. Future work should be directed towards the development of system-level test procedures and the refinement of solar cell test procedures.

### Test Procedure Recommendations - Concentrator Cells

- Procedure should be similar to the standard method for 1-sun measurements except that the illumination intensity is treated as a measurement variable.
- Conversion efficiency should be calculated and reported on the basis of the area designed to be illuminated.
- Illumination intensity should be reported in units of power per unit area such as $W/cm^2$ or $kW/m^2$.
- The reference solar spectrum should be the same as that adopted for 1-sun measurements.
- Illumination uniformity is important and should be $\pm 10\%$ or better over the active area of the cell under test.
- Solar cell junction temperature is the temperature of interest that should be measured and reported. The temperature of reference should be $28^{o}C$ as for 1-sun measurements.

- The angle of incidence of illumination should be restricted to no greater than 30 degrees from normal incidence (a 60 degree full-angle cone).
- Both natural sunlight and simulated sunlight characterization is acceptable within the same limitations as applied to 1-sun measurements. A cautionary note is that the transmission or reflection characteristics of optical concentrators may alter the input spectrum. This must be accounted for in the measurement procedure:

Reference Standards

- Pyranometer methods are not applicable to high intensity measurements.
- Recommended method is the Standard Solar Cell Method. Standard cell must be same type as one under test and must have a known short circuit current-versus-intensity response over the range of use. Intensity is determined by the ratio of short circuit currents.

Recommended Future Work

1. NASA-Lewis should design a series of standard cells for concentrator measurements having:
    a. known variation of short circuit current with illumination
    b. a holder designed for 30 degree incidence angles and high input power density
2. Calorimetric methods for direct measurement of high solar intensities should be developed.
3. The adequacy of the recommended ±10% illumination uniformity requirement should be confirmed in practice.
4. System-level test and evaluation procedures need to be developed.

# Report of Working Group on Diagnostic Cell Measurements Including Spectral Response

John Meakin/Univ. of Delaware

## Summary of Main Recommendations

There should be a compilation of the various methods and techniques for measuring cell parameters other than I-V curves and spectral response. These include series and shunt resistances, diffusion length, diode quality factor etc. This compilation should be separate from the manual from this Workshop.

There will be a need in the future for additional diagnostic techniques and specifications that can be the subject of future workshops.

The technique used in measuring series resistance should always be reported along with the data.

There were several recommendations regarding spectral response measurements.

They included:

1. A better defined terminology is needed.
2. The cell active area is to be used in reporting collection efficiency.
3. Bias light should be used unless proven to be unnecessary.
4. AC (chopping) techniques were slightly favored over DC (steady state).
5. The NBS standard detector package should be used in a series of tests to determine uniformity of measurements among laboratories.

## ATTENDEES

Richard R. Addiss
Solar Power Corp.
5 Executive Park Drive
N. Billerica, MA 01862

Richard L. Anderson
Syracuse Univ.
Syracuse, NY 13210

William L. Bailey
Motorola Inc.
4039 East Raymond Street
Phoenix, AZ 85040

Richard O. Bell
Mobil Tyco
16 Hickory Drive
Waltham, MA 02154

Walter Bishop
Jet Propulsion Laboratory
4800 Oak Grove Drive
Pasadena, CA 91103

Norman A. Blum
Johns Hopkins University
Applied Physics Laboratory
Laurel, MD 20810

Karl W. Boer
University of Delaware
Institue of Energy Conversion
Newark, DE 19711

Eldon C. Boes
Sandia Laboratories
Albuquerque, NM 87115

Jack W. Bond
Meradcom
DXR FB--E
Fort Belvoir, VA 22307

Henry Brandhorst
NASA Lewis Research Center
21000 Brookpark Road
Cleveland, OH 44135

E. L. Burgess
ORG 5133
Sandia Laboratories
Albuquerque, NM 87115

An-Ti Chai
NASA Lewis Research Center
21000 Brookpark Road
Cleveland, OH 44135

Roy Crabb
ESA
ESTEC, Noordijk
Holland

Dennis J. Curtin
Communications Satellite Corp.
Comsat Labs
Clarksburg, MD 20734

Henry B. Curtis
NASA Lewis Research Center
21000 Brookpark Road
Cleveland, OH 44135

Robert De Violini
Pacific Missile Test Center
Geophysics Division, Code 3250
Point Mugu, CA 93042

Gil Downing
Jet Propulsion Laboratory
4800 Oak Grove Drive
Pasadena, CA 91103

Larry N. Dumas
Jet Propulsion Laboratory
4800 Oak Grove Drive
Pasadena, CA 91103

Henry L. Durand
Philips Research
Paris, France

Charles Fishman
Exxon Research Center
P. O. Box 51
Linden, NJ 07036

A. F. Forestieri
NASA Lewis Research Center
21000 Brookpark Road
Cleveland, OH 44135

Lewis M. Fraas
Hughes Research Laboratories
3011 Malibu Canyon Road
Malibu, CA 90265

Jon Geist
National Bureau Standards
Washington, DC 20234

John V. Goldsmith
Jet Propulsion Laboratory
4800 Oak Grove Drive
Pasadena, CA 91103

Henry C. Hadley
SES, Inc.
1 Tralee Industrial Park
Newark, DE 19711

Jack A. Hall
Rockwell International
3370 Miraloma Avenue
Anaheim, CA 92803

Harry L. Hampton
Joint Center for Graduate Study
100 Sprout Road
Richland, WA 99352

Russell E. Hart Jr.
NASA Lewis Research Center
21000 Brookpark Road
Cleveland, OH 44135

Thomas M. Klucher
NASA Lewis Research Center
21000 Brookpark Road
Cleveland, OH 44135

Curt M. Lampkin
Photon Power
1820 Mills Avenue
El Paso, TX 79901

Roger Little
Simulation Physics
41 B Street
Burlington, MA 01803

James N. Lovelady
Spectrolab
12500 Gladstone Avenue
Sylmar, CA 91342

Albert Lunde
Boeing Aerospace Co.
P. O. Box 3999
Seattle, WA 98124

Milo Macha
Sollos Inc.
11408 Sorrento Valley
San Diego, CA 92121

John D. Meakin
University of Delaware
Institute of Energy Conversion
Newark, DE 19711

Robert Mertens
University of Louvain
Kardinaal Mercierlaan 94
3030 Heverlee
Belgium

Shigekazu Minagawa
Hitachi, Ltd.
1-8-88 Higashikoigakubo,
Kokubunji
Tokyo, Japan

Edward B. Murphy
Lincoln Laboratories
Massachusetts Institute of
Technology
Lexington, MA 02173

Jack Posner
JARAH Consultants Inc.
1727 Ladd Street
Silver Spring, MD 20902

Eugene L. Ralph
Spectrolab
12500 Gladstone Avenue
Sylmar, CA 91342

Michael Riches
Energy Research and Development
Administration
20 Massachusetts Avenue, N. W.
Washington, DC 20545

Bernd Ross
Consultant
2154 Blackmore Court
San Diego, CA 92109

Steven B. Sacco
Lincoln Laboratories
Massachusetts Institute of
Technology
Lexington, MA 02173

Don Schuler
Sandia Laboratories
Alburquerque, NM 87115

A. Seck
Optical Coating Laboratory, Inc.
15251 E. Don Julian Road
City of Industry, CA 91746

Desmond P. Spittlehouse
McGraw Edison, Corp.
P. O. Box 237
Bristol, CT 06010

Everett D. Stokes
S. M. U.
333 Science Information Center
6425 Airline
Dallas, TX 75275

Jim Stultz
Jet Propulsion Laboratory
4800 Oak Grove Drive
Pasadena, CA 91103

Tsuji Takateru
Central Research Laboratories
Sharp Corporation
2613-1 Ichinomoto-Cho
Tenri-Shi
Nara 632 Japan

Fred Treble
Royal Aircraft Establishment
Farnsborough, England (Hants)

Douglas Warschauer
Energy Research and Development
Administration
20 Massachusetts Avenue N. W.
Washington, DC 20545

Otto K. Weber
Sensor Technology
21012 Lassen Street
Chatsworth, CA 91300

Kenneth Wilkes
Batelle Memorial Institute
505 King Avenue
Columbus, OH 43214

John A. Zoutendyk
Jet Propulsion Laboratory
4800 Oak Grove Drive
Pasadena, CA 91103

Solomon Zwerdling
Argonne National Laboratories
Argonne, IL 60439

## ORGANIZATIONS REPRESENTED

Applied Physics Lab
Argonne National Laboratories
Batelle Memorial Institute
Boeing Aerospace Co.
Communications Satellite Corp.
Energy Res. & Dev. Adm.
ESA (Holland)
Exxon Research Center
Hitachi, Ltd. (Japan)
Hughes Research Labs
JARAH Consultants, Inc.
Jet Propulsion Laboratory
Joint Center for Graduate Study
Lincoln Laboratories (MIT)
McGraw Edison Corp.
Meradcom (Ft. Belvoir)
Mobil Tyco
Motorola, Inc.
NASA Lewis Research Center
National Bureau of Standards
Optical Coating Laboratory
Pacific Missile Test Center
Philips Research (France)
Photon Power
Royal Aircraft Estab. (England)
Rockwell International
Sandia Laboratories
Sensor Technology
SES, Inc.
Sharp Corp. (Japan)
Simulation Physics
Solar Power Corp.
Sollos, Inc.
Southern Methodist University
Spectrolab
Syracuse University
University of Delaware
University of Louvain (Belgium)

☆ U. S. GOVERNMENT PRINTING OFFICE: 1977-757-070/6304 Region No. 5-11